SYNTHESIS AND APPLICATION OF STYRYL PHOSPHONIC AND CINNAMIC ACID DERIVATIVES

by

Brett William McNichols

A dissertation submitted to the Faculty and the Board of Trustees of the Colorado School of Mines in partial fulfillment of the requirements for the degree of Doctor of Philosophy (Applied Chemistry)

Golden, Colorado

Date _____

Signed: _____

Brett W. McNichols

Signed: _____

Dr. Alan Sellinger

Thesis Advisor

Golden, Colorado

Date _____

Signed: _____

Dr. Thomas Gennett

Professor and Head

Department of Chemistry

ABSTRACT

Styryl phosphonic and cinnamic acid derivatives have been gaining attention as key candidates to modulate specific electrode properties in organic electronic devices such as work function, surface energies, wettability, and electron charge transfer kinetics that lead to increased efficiency, operational range, and device lifetimes. Very few of these acids are commercially available. The driving factor behind this research is to explore simple, high yield, and inexpensive synthetic routes towards synthesis of these acids. Herein, the novel synthesis of vinyl phosphonic acids (VPAs) and their subsequent influence on interface properties compared to their phenyl phosphonic acids (PPAs) and benzyl phosphonic acids (BPAs) analogues are explored. This includes an in depth comparison of varying polar VPA, BPA, and PPA "families" attachment on conductive oxides as they allow for careful work function tuning of band edge energy and chemical properties on these surfaces

By leveraging similar techniques of VPA synthesis we can produce analogous cinnamic acids in which these same surface control concepts are applied on the surface of lead sulfide (PbS) colloidal semiconductor nano-crystals, or quantum dots (QDs). In order to do this, first a development of a simple solution-phase ligand exchange was necessary, from which we selectively replace native solubilizing ligands with these fictionalized cinnamic acids. This application achieved remarkable control allowing the band edge position to be tuned over an unprecedented 2.0 eV.

This cinnamic acid synthetic chemistry can then be extended to functionalize multi acrylate containing molecules creating organic linkers to be integrated into Metal Organic Frameworks (MOFs). MOFs have increasingly gained attention for many high impact applications including but not limited to catalysis, gas storage and release, sensors, energy harvesting, conductivity, and filtration. A great amount of research is presently being conducted in developing new MOFs from the same handful of commercially available linkers. We introduce synthetic techniques for 18 isoreticular series of linkers that can be formulated with similar, if not identical, conditions giving way to the formation of previously unknown frameworks. This technique led us to incorporate a number of these linkers into Ni-MOFs and investigate catalytic activity for conversion of oleic acid to liquid hydrocarbons.

TABLE OF CONTENTS

LIST OF FIGURES

LIST OF TABLES

LIST OF SCHEMES

ACKNOWLEDMENTS

First, I would like to thank the United States Air Force for this incredible opportunity. Next, to my advisor Dr. Alan Sellinger, thank you for being willing to take on my compressed timeline, and for providing the guidance, counseling, encouragement and wisdom along the way. To my committee members, Dr. Jeramy Zimmerman, Dr. Svitlana Pylypenko and Dr. Yongan Yang, thank you for your advice and scientific direction, especially over the last few months.

To the Sellinger group members past and present: Dr. Tinkham, Dr. Fernando, Dr. Senevirathna, Dr. Yemam, Ryan, Josh, Tracy, Allison, Griselda, Amy and Everett, who reviewed papers, conducted scientific discussion or just made graduate school life in both the office more entertaining, and the lab more enlightening, thank you.

Finally, to my family, thank you for all the love, support and guidance over my last 30 years.

DEDICATION

To my wife,

Thank you for your love, encouragement, and support, even through these long hours,
I would have never reached this point without you by my side,
nor would I want to be here without you.

CHAPTER 1
INTRODUCTION

1.1. Overview of Dissertation

Organic synthesis is an incredibly vast and exciting field that unlocks the understanding of the chemical properties of organic molecules by leveraging the fascinating power of forming bonds between atoms. Novel organic compounds are continually created utilizing the innumerable named organic reactions, catalysts and synthetic schemes. This dissertation concentrates on the design and synthesis of organic ligands with a theme exploring the most efficient conditions to produce the purest compounds while mitigating waste, excessive steps, and extreme reaction conditions. This dissertation takes a fundamental look at linking the chemical structure of a small molecule with its properties, which in turn have a direct effect on the application of these small molecules in optoelectronic devices. Specifically, discussed within this study is how the linking group between the binding site (carboxylic and phosphonic acid) and the dipole active aromatic group influence subsequent properties – i.e. work function of transparent conductive oxide (TCO) electrodes, optoelectronic properties of inorganic quantum dots (ODs), and metal organic frameworks (MOF). Also discussed is a new synthetic methodology to produce styryl phosphonic acids in high purity and yield.

Chapter 2 is an introduction and review of the principles of surface modification with the direct intent of altering electronic properties of TCOs and QDs. This chapter is primarily a review on the efficient synthesis of styryl phosphonic and cinnamic acids in their purest form and their applications on surfaces for tuning electronic devices. This chapter discusses the ability to fine tune the interface in these materials, which leads to vast improvement in adhesion, wettability, surface smoothness, work function, and bandgap tuning. Additionally, this chapter briefly discusses these improvements and how they have a profound effect on increasing organic electronic device lifetime and efficiency.

Chapter 3 presents a slightly deeper dive into organic synthesis with the introduction of a single step palladium-catalyzed Heck coupling of aryl halides with vinyl phosphonic acid to produce functionalized (*E*)-styryl phosphonic acids. This chapter discusses the exploration of a single step Heck coupling that utilizes a variety of commercially available aryl halides, vinyl phosphonic acid (VPA), and bis(tri-t-butylphosphine) palladium (0) [$Pd(P(t\text{-}Bu)_3)_2$] catalyst to

produce higher purities of VPAs. This chapter communicates this new method and comprehensively details the synthesis of two novel compounds, (*E*)-(3,5-difluoro-4-(trifluoromethyl) styryl) phosphonic acid and (*E*)-(4-(bis(4-methoxyphenyl) amino) styryl) phosphonic acid, which are complimented with complete NMR characterizations.

Chapter 4 combines the topics of the previous two chapters and explores synthesizing families of phosphonic acids for the modification of metal oxides. The synthetic mechanisms of Heck coupling, Hirao coupling, the Arbusov reaction, and phosphonic ester hydrolysis, which are briefly mentioned in the prior chapters, are explored in much greater detail to provide a deeper understanding of the synthetic effort required to construct and purify these acids. Two of the acids, (*E*)-(4-nitrostyryl) phosphonic acid and (*E*)-(4-cyanostyryl) phosphonic acid are novel compounds and an in-depth synthetic procedure and a full NMR characterization of these two acids are provided. All of the synthesized phenyl phosphonic acids, benzyl phosphonic acids, and styryl phosphonic acids that were functionalized with para-nitro, para-cyano, para-trifluoromethyl, and ortho-difluoro groups were then applied to indium tin oxide (ITO) TCOs. A comparison of the gas phase Density Functional Theory (DFT) calculated dipole moment to the change in work function is then explored and discussed in detail, and a correlation between these two factors are found supporting the work function surface modification examination covered in Chapter 1.

Chapter 5 is a change in approach, as we analyzed the analogues cinnamic acids and their effects on chemical binding to the surface of PbS quantum dots. Specifically, this chapter is a detailed experimental exploration of synthetic procedures and full characterization of several novel cinnamate ligands. This chapter further describes and details the application of these acids on the surface of PbS quantum dots through a simple ligand exchange method that resulted in remarkable work function tuning by an unprecedented 2.0 eV range.

Chapter 6 is an even further change in project approach by utilizing the synthetic techniques of cinnamic acid synthesis in Chapter 5, and modifying the synthesis with multi halogenated aromatic precursors to form novel di- and tri- acrylic acids. These novel acrylic acids can then be incorporated into metal organic frameworks (MOF). In this chapter we explore isoreticular series of linkers that can be formulated with similar, if not identical, conditions to their analogous benzoic acid derivatives. Several of these reported molecules are novel linkers.

Detailed descriptions of synthetic conditions are reported along with detailed characterization. An analysis of Brunauer–Emmett–Teller (BET) surface areas examines the porosity of the MOFs for potential candidates in various gas storage applications. In addition, Chapter 6 describes the successful synthesis of nickel-based MOFs using (E)-4-(2-carboxyvinyl) benzoic acid and (E)-3-(2-carboxyvinyl) benzoic acid). These resultant crystalline Ni-MOFs displayed BET surface areas as high as ~315 m^2/g. To investigate their catalytic activity for conversion of oleic acid to liquid hydrocarbons, Ni-MOFs were grown on zeolite 5A beads that served as catalytic supports. The catalytic activity was correlated to the concentration of acid sites

This dissertation concludes with Chapter 7, which is a consolidated summery and a general discussion of conclusions and future applications for exploration. A brief dialogue of future exploration and utilization of the synthesized small molecules from the previous experimental Chapters 3 - 6 are discussed to provide some basic research framework of interesting topics and applications. Many of these applications were envisioned at the commencement of this project but could not be achieved, due to the intensive preliminary work in the synthetic discovery alone.

1.2. Dissertation Attributions

Chapter 2 was solely authored by Brett W. McNichols and is a manuscript that has been prepared for submission to Organic and Biomolecular Chemistry, Professor Alan Sellinger provided supervision, and initial ideas.

Chapter 3 was solely authored by Brett W. McNichols and has been submitted for publication in Chemical Communications at the time of writing this work. Brett W. McNichols designed, synthesized, and characterized select phosphonic acid derivatives, and Professor Alan Sellinger provided supervision, funding for chemicals, and initial ideas.

Chapter 4 was authored by Brett W. McNichols who designed, synthesized, and characterized select phosphonic acid derivatives. Dr. Jonathan Tinkham and Joshua T. Koubek provided the computational results. Dr. Dan Kroupa, and Chloe Castaneda of the University of Colorado, Boulder conducted the Kelvin Probe work function measurements at the National Renewable Energy Laboratory (NREL). Professor Alan Sellinger provided supervision, funding for chemicals, and initial ideas.

Chapter 5 was authored by Brett W. McNichols who designed, synthesized, and characterized select cinnamic acid derivatives. Part of this chapter has been published, the work of Brett W McNichols has been selected and modified with permission from *Nature Communications* 8, Article number: 15257 (2017) doi:10.1038/ncomms15257. Dr. Dan Kroupa and Professors Matt Beard and Alan Sellinger conceived the original ideas and designed the experiment; Dr. Dan Kroupa carried out the ligand exchange experiments, characterized the ligand/QD complexes, and analyzed the experimental data and was the primary author of the publication; Dr. Elisa M. Miller performed the XPS measurements and analyzed the data. Dr. Jing Gu characterized select cinnamic acid derivatives and ligand/QD complexes; Márton Vörös, Nicholas P. Brawand and Professor Giulia Galli designed the computational study. Márton Vörös and Nicholas P. Brawand carried out the calculations and analyzed the data. Dr. Dan Kroupa, Márton Vörös, Professors Giulia Galli and Matt Beard wrote the manuscript. Professor Arthur J. Nozik assisted in the preparation of the manuscript. All authors discussed the results and commented on the manuscript.

Chapter 6 is a combination of two manuscripts: The first manuscript has been published in *Catalyst Science and Technology*, 2017, DOI: 10.1039/C7CY00564D). Liqiu Yang and Brett W. McNichols are co-first authors. Brett W. McNichols designed, synthesized, and characterized select carboxylic linker derivatives. Liqiu Yang conducted Ni-MOF synthesis, characterization, and catalysis. Malcolm Davidson provided Ni-MOF experimental analysis and surface characterization. Ben Schweitzer provided the computational results. Professors Diego Gómez-Gualdrón, Brian Trewyn, Alan Sellinger, and Moises Carreon provided supervision, funding for chemicals, and initial ideas. The second manuscript was authored by Brett W. McNichols who designed, synthesized, and characterized select cinnamic acid derivatives and will be prepared according to pending laboratory experimental results. Additional that have contributed to a future manuscript are J. Everett Baumann and Amy Keuhlen who designed, synthesized, and characterized select cinnamic acid derivatives, and MOFs under the supervision of Brett W. McNichols.

CHAPTER 2
STYRYL PHOSPHONIC AND CINNAMIC ACID DERIVATIVES FOR APPLICATION IN TUNING THE ELECTRONIC PROPERTIES OF ELECTRODES AND QUANTUM DOTS

Modified from a manuscript to be submitted to Organic and Biomolecular Chemistry

Brett W. McNichols [a], Alan Sellinger [a]

2.1. Abstract

Transparent conducting oxides (TCOs) and quantum dots (QDs) are important materials in many hybrid semiconductor applications. The ability to fine tune the interface in these materials leads to vast improvement in adhesion, wettability, smoothness, work function, and bandgap tuning. These improvements have a profound effect on increasing device lifetime, and efficiency. This review will focus upon the surface modification of TCOs via the attachment of organic ligands, such as styryl phosphonic and cinnamic acids, primarily for application of work function and bandgap tuning. Discussed within are efficient syntheses of ligands, anchor group binding characteristics, and a survey of state-of-the-art examples of interface tuning and surface modification of TCOs and QDs.

2.2. Introduction

Demand is ever growing for lightweight, flexible, low cost, organic/hybrid-based devices, such as organic light emitting diodes (OLEDs), organic/hybrid photovoltaics (OPVs), and most recently perovskite solar cells. Along with this demand there is a pressing desire for devices with increased efficiency, stability, and reliability in order to achieve longer lifetimes. One possible strategy to achieve these longer device lifetimes is by interface tuning of specific layers within the device such as the transparent conducting oxide (TCOs) electrode.[1]

---

[a] Department of Chemistry, Colorado School of Mines, Golden, CO 80401

The surface of these layers can be modified through one or a combination of several approaches: etching with an acid or base, plasma treatment, application of polymer thin film or inorganic layers, and attachment of small organic molecules. Specifically, this review will assess the attachment of organic surface ligands, as they allow for fine control of work function, band edge energy, and chemical properties on these surfaces.[2-3]

Interface tuning of TCOs and quantum dot (QD) surfaces via chemical modification is a diverse and rapidly growing field.[1] Styryl phosphonic acids (PAs) and cinnamic acids (CAs) have been gaining attention as key candidates to modulate key properties in organic electronic devices such as work function, surface energies, wettability, and electron charge transfer kinetics that lead to increased efficiency and operational range.[4-5] At this time, few of these acids are commercially available, and there is a demand for synthetic ease to produce molecules that push the properties to further extremes, which in turn will afford finer precision in the control of surface properties. Our goal here is to provide the community synthetic background for the most efficient syntheses and introduce current applications and future possibilities for the use of PAs and CAs on various device surfaces.

This chapter is divided into the following topics; Section 2.3 Characteristics of Anchor Groups and Surface Binding, is an overview of relevant carboxylic and phosphonic acids, their binding motifs on surfaces, and how each group is deposited onto a surface. Section 2.4 Acid Synthesis, will provide the most efficient synthetic methods for preparation of these molecules: in short, to best tailor the reaction conditions using a spacer group (Figure 2.1 blue, Page 7) with both the anchor group (Figure 2.1 red, Page 7), and the head group (Figure 2.1 green, Page 7) to produce the highest yield of the desired product. Finally, Section 2.5 Surface Modification examines the application of these acids as Self Assembled Monolayers (SAMs), their effects of work function tuning on the surface of electrodes, and as ligands for tuning the optoelectronic properties of quantum dots.

2.2.1. Anchor Groups

As illustrated in several other reviews, the chemical behavior of TiO_2, ZnO, SiO_2 In_2O_3-SNO_2 (ITO) and PbS QDs include multiple reactivity patterns when considering surface

modification chemistry.[6-12] These chemical interactions between the ligand and surface are typically dominated by reactions of the M^{n+} (metal) species of the surface and O^-, =O and/or -OH

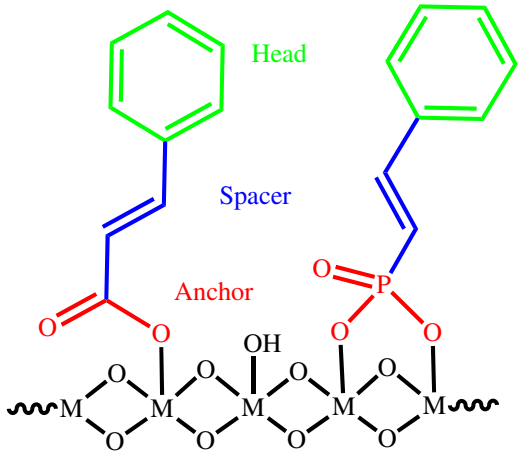

Figure 2.1 PA (right) and CA (left) ligand to metal oxide surface interaction depicting anchor group (red), spacer (blue), and head group (green).

2.3. Characteristics of Anchor Groups and Surface Binding

species of the ligand. To facilitate self-assembly or binding, an anchor group is essential at the terminus of the ligand. Anchor groups have a direct effect on packing density, stability of the SAMs, electrode work-function, and strength of interaction between the molecule and surface.[13] These interactions range from weak hydrogen bonding to covalent bonds that are stable up to 350°C.[14] This section addresses the anchor group chemistry and the best methods for their attachment to the desired surface.

It is generally agreed that attachment of an acid-based ligand to a metal oxide surface proceeds through a Lewis acid site on the metal-oxide surface followed by condensation with the surface hydroxyl groups. Examples of this attachment are shown in Figures 2.2 & 2.3(Page 8 & 9 respectively). This process can be accelerated based on the surface hydroxyl content, use of mild bases, and the temperature of the surface.[15-17] Surface attachment in hydroxyl-free surfaces is also possible.[18] However, high hydroxyl content is preferred as it is key for the rapid deposition of highly uniform, and dense coverage layers.[19] Strength of attachment is also an important factor to consider; the weaker the anchor group interaction to the surface, the more

likely the chance of dissociation, which leads to degradation of performance. Generally, the association strength of phosphonic acids are stronger than carboxylic acids.[20-21]

2.3.1. Phosphonic Acid Anchor

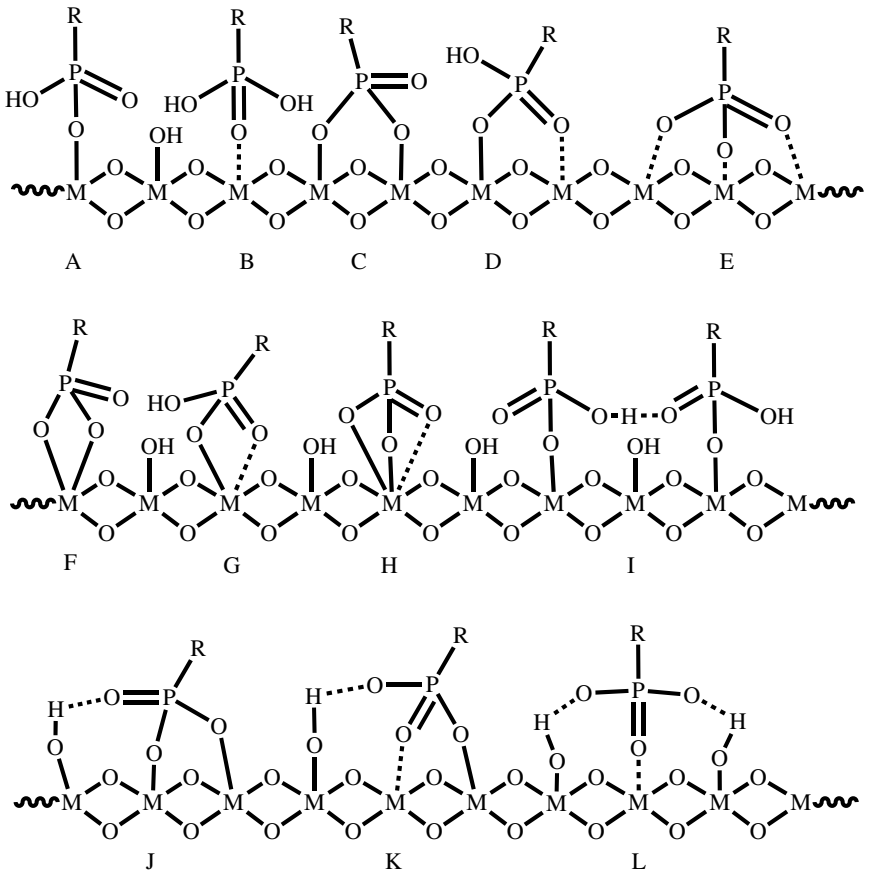

Figure 2.2 Binding modes of phosphonic acids on a metal oxide surface (M=metal): monodentate bridging (A and B), bidentate bridging (C and D), tridentate bridging (E), bidentate chelating (F and G), tridentate chelating (H), and additional hydrogen-bonding interactions (I – L). Recreated from reference [10]

Phosphonic anchor groups have become increasingly important in the field of organic electronics as they can be used in a plethora of applications for surface modification. A number of studies have evaluated phosphonic acids characterizing their binding motif on various metal oxides.[1, 19, 22-25] Phosphonic acids show a high compatibility with other organic functional groups and both ester (PO_3R_2) and acid (PO_3H_2) forms can generally be used for surface modifications, which can be carried out in many organic solvents and water.[1]

As illustrated in Figure 2.2 (Page 8) the presence of three oxygen atoms on the phosphorous allows for mono-, bi-, or tridentate binding to the metal oxide surfaces, or chelation of a single metal with two or three oxygen, in addition to the possibility of hydrogen bonding interactions originating from either the P-O-H or M-O-H hydrogen. Therefore phosphonic acid has a very strong affinity for oxophilic metal ions, which explains their ability to produce robust SAMs and well defined crystalline layers.[26]

Depending on the nature of the surface, phosphonic acid SAMs can form via two distinct mechanisms. On a strong Lewis acidic site phosphonic SAMs form through the phosphoryl oxygen to the metal oxide surface (Figure 2.2 B, Page 8), followed by a hetero condensation allowing mono, di or tridentate binding to the same or multiple metal centers (Figure 2.2 A, D-H, Page 8). In the case of a weak Lewis acidic surface the second phosphonic SAM formation is observed, the heterocondensation without phosphoryl coordination (Figure 2.2 A, C, Page 8), leading to mono- or bi-dentate binding and the possibility of phosphoryl hydrogen binding (Figure 2.2 A, C, J-L Page 8).[27]

2.3.2. Carboxylic Acid Anchor

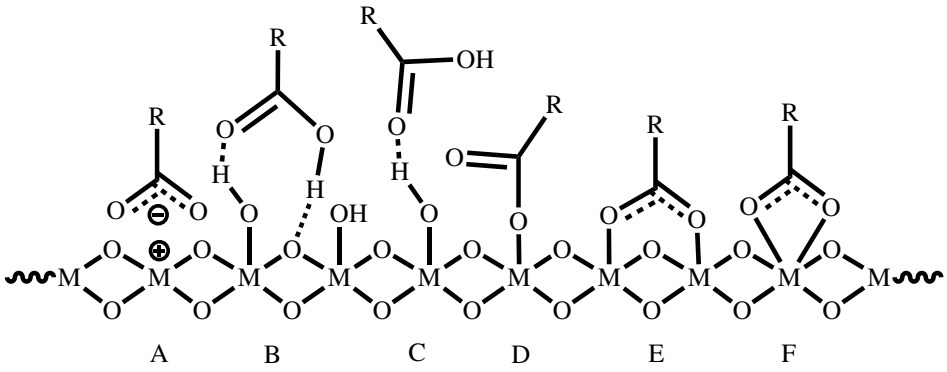

Figure 2.3. Binding modes of carboxylic acids on a metal oxide surface - Possible binding modes of COOH or COO- groups to metal oxide surfaces showing inner and out sphere adsorption. Hydrogen bonding interactions are generally outer sphere while electrostatic and metal to acid binding are inner sphere. Recreated from reference [10]

Carboxylic acids are the most systematically studied SAM anchor with a focus on spacer and head groups of long chain fatty acids; nonetheless, several surface to acid binding modes have been well reviewed.[15-16, 21, 28-29] As with phosphonic acids, hydroxyl content of the surface

has a great influence on the binding characteristics of carbocyclic anchors. Carboxylic acids are capable of two different types of adsorption mechanisms: "inner-sphere adsorption complexes," consisting primarily of covalent bonds formed through dehydration reactions (Figure 2.3 D), and "outer-sphere adsorption complexes," characterized by formation of hydrogen bonds in the hydroxide layer just above the surface (Figure 2.3 B, C, Page 9). Carboxylic acids participate in outer sphere adsorption with a high hydroxyl content metal oxide. This allows hydrogen bonding with both a bridging oxygen and the carboxylic oxygen. High hydroxyl content metal oxide surfaces also are capable of inner sphere adsorption covalent bonds, forming monodentate metal-ester coordination (Figure 2.3 D, Page 9) and mono- and bidentate chelating directly to metal centers (Figure 2.3 E, F, Page 9). Surfaces with minimal hydroxyl content only allow for inner sphere adsorption, monodentate metal-ester coordination and mono- and bidentate chelating and electrostatic attractions as show in Figure 2.3 A, D-F (Page 9).[10, 30]

2.3.3. SAM Anchoring Techniques

Three techniques are typically used for anchoring of these types of ligands to form a SAM on an oxide surface; the Langmuir Blodgett (LB) technique, solution processing, and gas phase processing. LB is the assembly of the monolayer at a water-gas interface by mechanical compression, and then the monolayer is transferred to the surface of interest. While this method has the advantage of producing highly ordered thin films, in contrast the process involves water that can interfere by creating a weak interaction between the monolayer and substrate.[31] Solution processing such as soaking, dip coating, spin coating, spray coating or tethering by aggregation (TBAG), seem to be the methods of choice throughout the literature, mainly due to being an inexpensive technique, easily scalable, and provides moderately uniform thin films.[10, 18, 32] These methods generally use organic solvents and require an annealing step that could create some limitation based on the surface compatibility with heat or solvents. Lastly, gas-phase processing such as vacuum vapor deposition or atomic layer deposition.[33-34] This method is used throughout the literature however, issues include a limit to substrate size and creating non-uniform or multi-layers that must be rinsed with methods similar to those found in solution processing.[35]

2.4. Acid Synthesis

2.4.1. Design of Acids

The following section is a review of general methods for synthesizing commonly used phosphonic ligands. Each example provides a synthetic route to best produce the desired product with high yields under mild conditions. It is also important to note that not all synthetic routes allow conditions that are applicable to both the head group, which may have sensitive functional groups and/or the acid anchor group, and that care must be taken in selecting a process that provides the desired product. While this is not a comprehensive list of phosphonic and carboxylic ligand synthetic schemes, it will describe the common synthetic routes.

Another important factor that should be considered in acid design is the molecular orientation and the magnitude of the dipole moment relative to the surface. As discussed in Section 2.3 above, the orientation of the dipole relative to the surface has significant implications, and thus special consideration must be given to the sterics, molecular geometry, bound molecule tilt angle and SAM stacking to best fit the desired application. The position of electron withdrawing or donating groups in any combination of ortho-, meta- or para- positions can create an array of dipoles that will effect the dipole relative to the surface and binding strength of the ligand.

2.4.2. Phosphonic Ligand Reagents and Methods

As indicated above in Section 2.3, phosphonic acid ligands have recently gained interest for the purpose of surface modification, and particular attention has been given to the modification of ITO.[3] With a relative ease of synthesis, simple purification, formation of shelf stable products, and strength of surface binding, phosphonic acid ligands have many attractive qualities that make their use ideal for electrode and QD energetic tuning. Commercial sources of styryl phosphonic acids (Ar-$(CH)_2$-P) (PAs) are extremely limited and can be costly when found. For example, at the time of writing this dissertation the only commercially available styryl phosphonic acid was from Sigma-Aldrich (product # PH002029-1MG) for $128.75/mg, which translates to $128,750/g. As will be shown throughout in this dissertation, we are able to synthesize a variety of functional styryl PA's with high yield and in multi-gram quantities. The following sections will help define some of the common routes for synthesis of PA esters and acids. However, currently the most commonly used acids are phenyl phosphonic (Ar-P) acids

(PPA), and benzyl phosphonic (Ar-CH_2-P) acids (BPA), the syntheses of these will be briefly reviewed to elucidate the state of the art.[3]

2.4.2.1. PPA and BPA - Michaelis-Arbusov Reagents and Similar Methods

Michaelis discovered one of the most versatile P-C bond formation reactions, termed the Michaelis-Arbusov method. This reaction between an alkyl halide and trialkyl phosphite is accomplished by their mixing with moderate heat, resulting in a phosphonic ester as shown in Scheme 2.1, a more thorough discussion of the mechanism for this reaction is presented in Chapter 5. It has also been reported that milder conditions (i.e. room temperature) with a Lewis acid can be achieved in high yields, even with alkyl chlorides and alcohols.[36] While the two following reactions do not form styryl phosphonates, they do form benzyl phosphonates (Ar-CH_2-P bridge) or phenyl phosphonate (Ar-P bridge), which come into consideration due to their relative ease of synthesis, leading to a direct effect in their usage as reported in the literature.[35, 37-38]

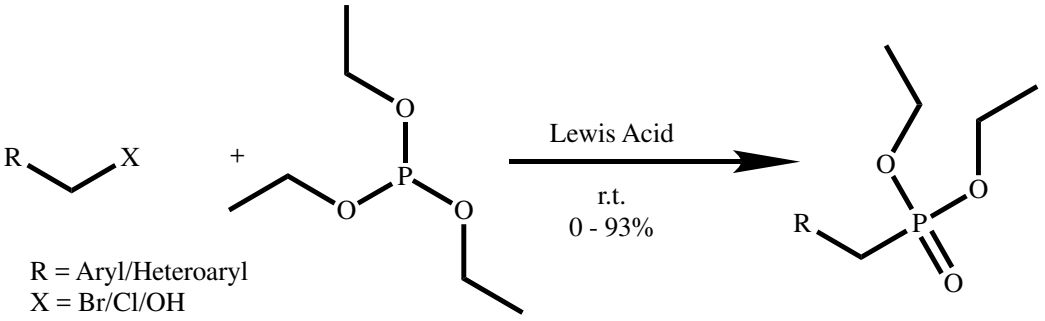

Scheme 2.1 Michaelis-Arbusov method - phosphorus to carbon bond formation utilizing a halide species with triethyl phosphite in the presence of a Lewis base. Figure recreated from reference [36]

Keglevich et al. reported a microwave assisted Arbuzov reaction where aryl bromides could be combined with triethyl phosphite in the presence anhydrous $NiCl_2$ catalyst with direct microwave heating yielding 70-90% (Scheme 2.2a, Page13).[39] In contrast, Villemin et al. (Scheme 2.2b, Page 13) reported catalyst-free microwave condition at 150°C for 3 min producing good to high yields of 75-99%.[39-40] Additionally Goossen and Dezfuli (Scheme 2.2c, Page 13) determined that coupling with palladium catalyst systems could be used at 2 mol% to

obtain yields as high as 98%. However with highly deactivating precursors yields may be significantly lower.[41]

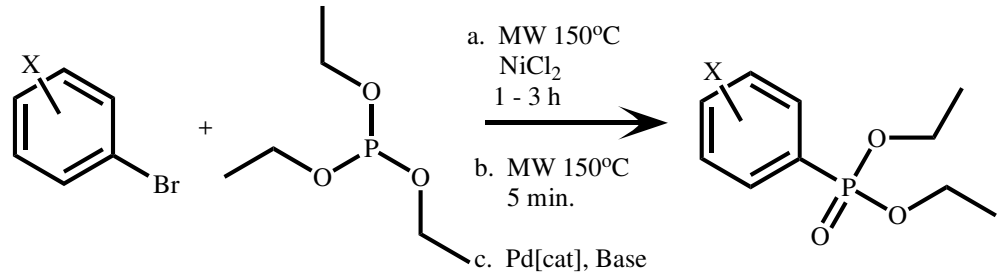

Scheme 2.2 Arbuzov reaction - aryl bromides combined with triethyl phosphite (a.) shown by Keglevich et al. were $NiCl_2$ catalyst and microwave heating leads resulting in 70-90% yield of benzylphosphonates. And (b.) shown by Villemin et al. were catalyst free direct microwave heating leads to 75-99% yields of desired benzylphosphonates. Recreated from reference (c.) Goossen and Dezfuli determined that Heck Coupling with 2 mol % palladium and base yielded up to 98%. Figure recreated from references [39-41]

2.4.3. PA Reagents and Methods

2.4.3.1. Palladium Catalyzed Additions

In the early 1980s, Hirao et al. reported the synthesis of vinyl phosphonates via palladium catalyzed cross coupling of vinyl halides with dialkyl phosphites.[42] The reactions are conducted at relatively mild conditions of 90°C in toluene under inert atmosphere, with $Pd(PPh_3)_4$ as the optimal catalyst system yielding 69 - 90% desired products. (Scheme 2.3) In Chapter 4 a detailed discussion and analysis of the mechanism of the Pd catalytic cycle is fully explored.

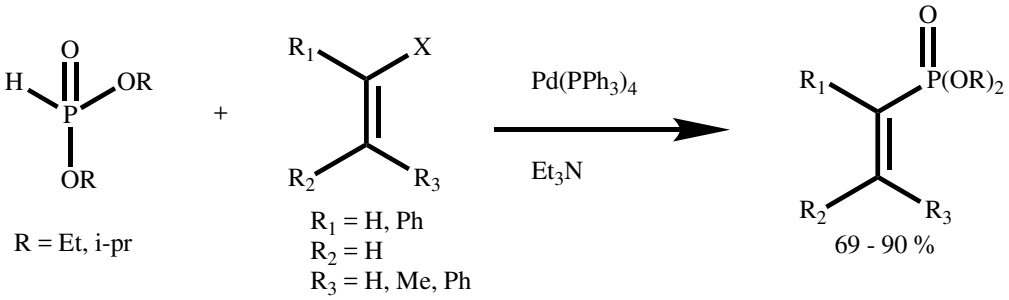

Scheme 2.3 Hirao cross coupling - coupling of vinyl halide with phosphites utilizing Pd catalysts resulting in 69 - 90% yields. Recreated from reference. [1]

Another route by Kabalka and Guchhait was introduced where vinyl boronates are substituted for the vinyl halides, leading to greater control of the stereospecific (E)- and (Z)-alkenyl phosphonates. The stereospecific products of this reaction are resultant of a direct coupling of the corresponding (E)- or (Z)-boronate starting material. In Scheme 2.4, yields of 60-84% were reported with the conditions of 95°C, O_2 atmosphere, and $Pd(OAc)_2$ being the optimized catalyst system making this an attractive reaction when considering the highly diverse number of commercially available boronic acid derivatives.[45]

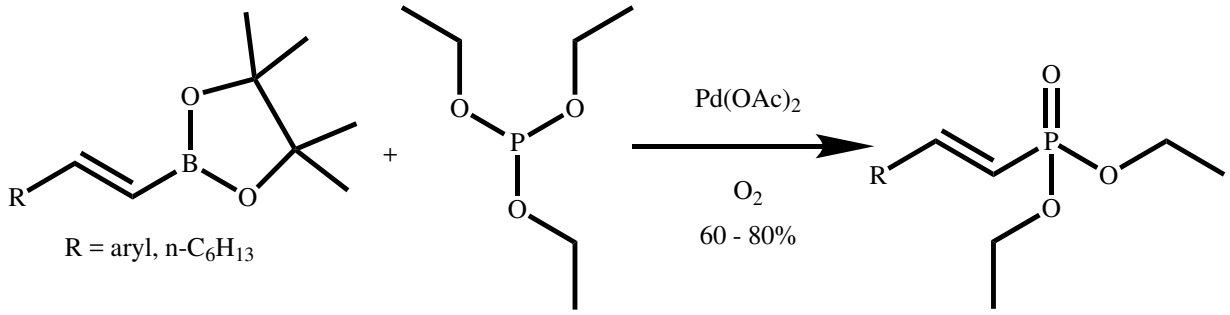

Scheme 2.4 Suzuki Coupling of vinyl phosphonate cross coupling reaction with vinylboronic acids. Figure recreated from reference [1]

Even though these methods show good yields, the high cost of palladium catalysts should be a consideration. Also, the resultant products are still in the ester form and need to be converted to the acid to ensure more uniform surface coverage.

2.4.3.2. Nickel-Catalyzed Addition of Dimethyl Phosphonate on Alkyne Derivatives

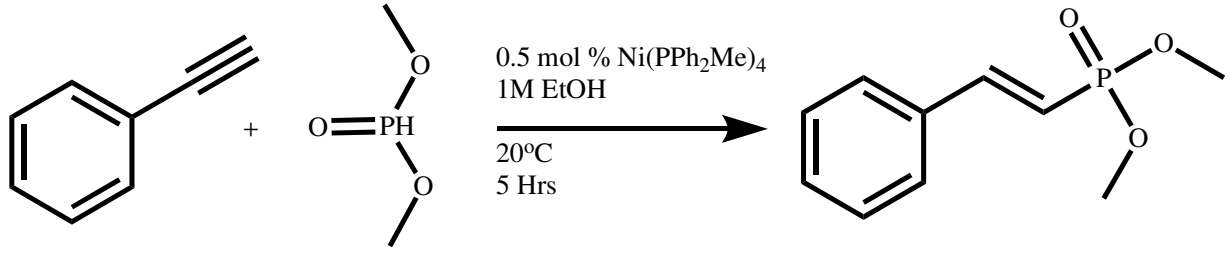

Scheme 2.5 Nickel-Catalyzed Addition - Nickel-mediated selective P-H addition to alkynes. Recreated from reference [43.]

As shown by Han et al. Ni catalysts are more reactive than the corresponding noble metal catalysts in the additions of a variety of P(O)−H bonds to alkynes, affording regio- and stereo selectivity both in the Markovnikov and anti-Markovnikov adducts in high yields.[43] In Scheme 2.5, the Ni catalyst leads to a high yield of dimethyl (E)-styryl phosphonate from ethynylbenzene under mild conditions of 20°C for 5 hours in THF catalyzed by 0.5 mol % $Ni(PPh_2Me)_4$.

Although small mixtures of regioisomers are observed in the product, it is reported the production of diethyl (E)-styryl phosphonate formed 99% to 1% (Z)-styryl phosphonate. It is well documented that modification of alkyl- and aryl- substituted phosphines can be substituted in the ligand system in which the steric hindrance on the phosphine is a key factor in tuning the catalytic results.[43] This reaction is limited to the ethynylbenzene derivatives that are commercially available or the limited ethynylbenzene derivatives synthesized in the lab. It should also be noted the resultant products are still in the ester form and will need to be converted to the acid.

2.4.3.3. Copper Iodide Catalysis

Thielges et al. reported an Arbusov-like synthesis of styryl phosphonic esters by using copper (I) iodide and tetramethylethylenediamine (TEMDA) with K_2CO_3 as a base in THF/DMF that resulted in an 80% yield of the expected vinyl phosphonate (Scheme 2.6).[44] Additionally, this synthesis is highly stereo-selective in creation of the desired (E)-styryl phosphonate (Scheme 2.6).[44]

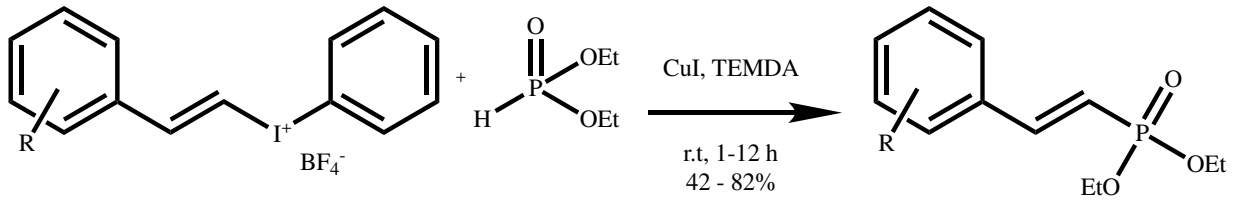

Scheme 2.6 Copper iodide catalyzed Arbusov - Preparation of 2-aryl-vinylphosphonates based on the coupling of hypervalent vinyliodonium salts to H-phosphonates. Recreated from reference [44]

This reaction is limited to the commercially available idodotetrafluoroborate precursors that are or that can be prepared from the modified Ochiai method of reacting alkenylsilanes with

iodosylbenzene and triethyloxonium tetrafluoroborate. An advantage of this Ochiai preparation is that only (*E*)- isomers reacted and lead to stereo chemically pure (*E*)- iodonium salts for the precursor.[45] However, it has been reported that some of these iodonium salts are unstable and difficult to purify or handle.[44]

2.4.3.4. Palladium Catalysis

As shown in Scheme 2.7 a large number of styryl phosphonic esters can be synthesized through palladium-catalyzed Heck coupling using both electron rich and electron deficient aryl halides as substrates with diethyl vinyl phosphonate resulting in product yields of 40 - 78%.[46] Lower yields of non-activated aryl halides were reported however, modifications of the catalyst system, solvents, and base have dramatic effects on the specific product yield. It should be noted the resultant products are still in the ester form and will need to be converted to the acid as discussed earlier in this paper.

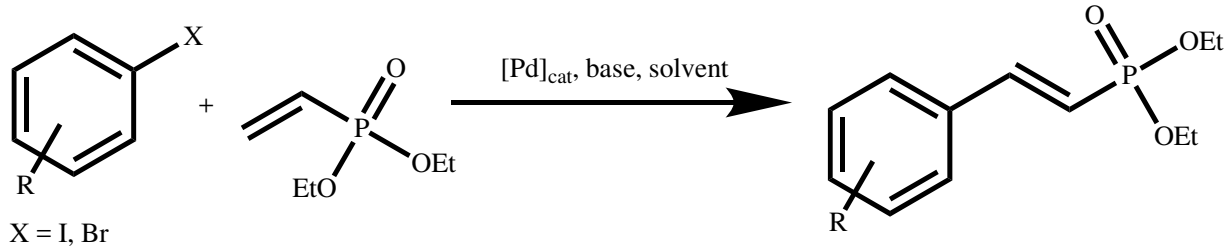

X = I, Br
R = Simple and condensed aryl and heteroaryl nuclei

Scheme 2.7 Palladium catalyzed Heck coupling of phosphonic esters - Heck arylation of diethyl vinylphosphonate with various aryl and heteroaryl bromides, recreated from reference [46]

The Michaelis-Arbusov and related methods are limited to the availability of commercial precursors and the resultant products are still in the ester form and will need to undergo further conversion to the acid as discussed next.

2.4.4. Hydrolysis of Dialkyl Phosphonates

All the syntheses discussed thus far produce dialkyl phosphonate groups that must undergo hydrolysis to provide the corresponding phosphonic acids. As described in the previous section, esters can be used for surface modification however the acid derivative is better suited for the application in SAMs forming more stable, and uniform surface mono-layers. Shown in

Scheme 2.8 (Page 17) are two general methods that facilitate high yield hydrolysis of the phosphonic esters: inorganic acids and trimethylsilyl (TMS) halides. Inorganic acids such as HCl or HBr, in polar solvents afford the corresponding acid in high yield (91–94%). Refluxing HCl or room temperature HBr is usually sufficient to achieve hydrolysis, however other functional groups within the molecule may not be stable under these highly acidic conditions. (Scheme 2.8 upper) [47]

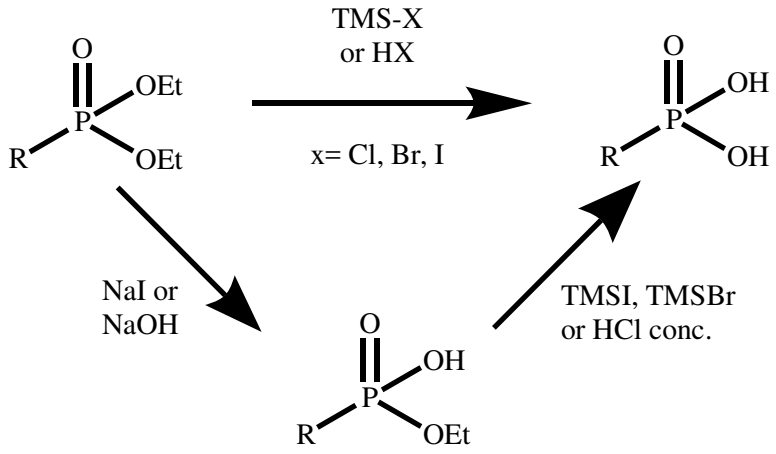

Scheme 2.8 Hydrolysis of esters - phosphonic ester hydrolysis into the free phosphonic acid or via mono-deprotected phosphonic acid undergoing treatment with iodo- bromo- trimethylsilyl-X(TMS) hydrolysis to render the desired product. Figure recreated from reference [47]

Trimethylsilyl halides, (TMS-X) (e.g.-chloride, -bromide, or –iodide) and NaI in a polar aprotic solvent, such as dichloromethane or acetone, readily undergo hydrolysis with the introduction of water or alcohols and afford the desired phosphonic acid in good yields (72-89%). This method is limited in scope as the hydrolysis of other labile protection groups, such as acetals, may occur under these conditions. (Scheme 2.8 lower) [47] The specific mechanism for these processes are discussed in much greater detail in Chapter 4.

2.4.5. Single Step PA Synthesis

2.4.5.1. Direct Phosphonation

As reported by Maranescu et al. the synthesis of PAs can be carried out by the addition of phosphorus pentachloride to styrene in toluene under inert gas at 60°C (Scheme 2.9, Page 18). The reaction goes through an intermediate chlorophosphane, which is then hydrolyzed with water to give the resultant phosphonic acid. Yields were not reported for any of the styryl products.[48]

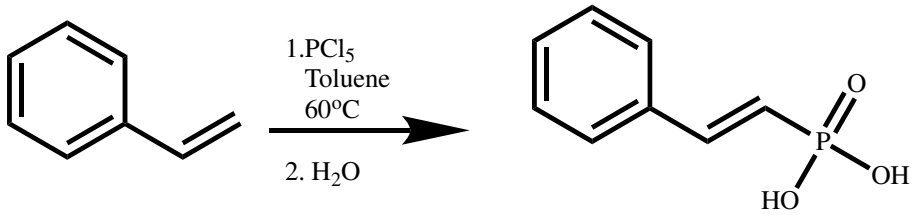

Scheme 2.9 Styrene phosphonation - Direct phosphonation of styrene using phosphorus pentachloride, Recreated from reference [48]

2.4.5.2. Palladium Catalysis

As thoroughly discussed in Chapter 4, we have developed conditions that allow for a single step coupling of vinyl phosphonic acid with aryl halides affording a wide array of PAs. This step utilizes bis (tri-*tert*-butylphosphine) palladium catalyst, acetonitrile as the solvent, and dicyclohexylmethylamine (NCy_2Me) as the base (Scheme 2.10). Reaction times range from 6-24 hours at 80°C with traditional heating, and utilizing microwave, reaction times decrease to 5 min. at 180°C with similar yield. This single pot microwave method has been very successful for increasing overall reaction yield as compared to two step processes, with the exception of very deactivating groups (e.g. -CN or $-NO_2$) in the para- and ortho- positions.

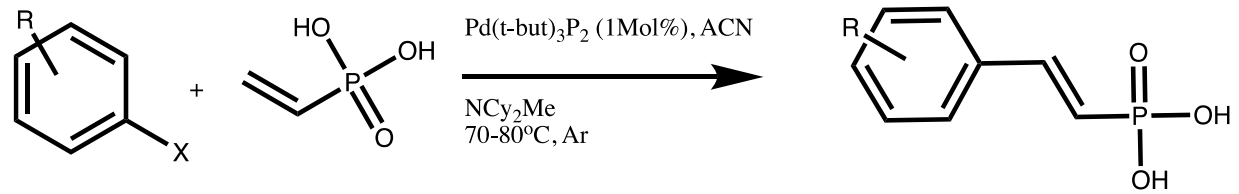

Scheme 2.10 Palladium catalyzed Heck coupling of PAs - Direct Heck coupling of vinyl phosphonic acid with aryl halide in a single step reaction to produce phosphonic acid.

These palladium catalyzed methods are ideal when considering the sizeable number of iodo-, bromo-, and chloro- benzene derivatives that are commercially available in addition to the mild reaction conditions that may favor sensitive functional groups however, the high cost of palladium catalyst must be considered. Furthermore, vinyl phosphonic acid is an inexpensive reagent and readily available from several commercial suppliers.

2.4.6. Carboxylic Reagents and Methods

In general, a fair number of CAs (or styryl carboxylic acids, and also known as cinnamic acids) are readily commercially available from multiple vendors. However, should a suitable acid not be available, the following should give an understanding of simple synthetic routes with commercially available precursors.

2.4.6.1. Condensation Reactions

The oldest and simplest synthesis of CAs is via the Knoevenagel condensation reaction, an aldol condensation between an aldehyde or ketone with subsequent dehydration in the presence of a base.[49] Facilitated with the Doebner modification, as shown in Scheme 2.11 condensation of benzaldehyde and malonic acid mediated by pyridine gives the trans unsaturated cinnamic acid in high yield (90%).[50]

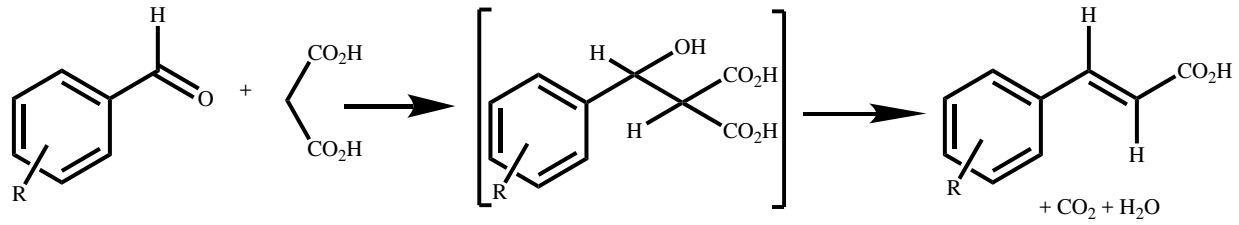

Scheme 2.11 Doebner modification on condensation of benzaldehyde and malonic acid mediated by pyridine. Figure recreated from reference [50]

One of the earliest reported condensation reactions producing a di-cinnamate derivative was by Ziegler and Lüttringhaus in 1934.[51] Here, isophthalaldehyde and malonic acid in pyridine are stirred for two hours at 50°C. The high yield product m-phenylene diacrylacid is then

precipitated and filtered and washed with warm acidic water to obtain a pure product (Scheme 2.11).

2.4.6.2. Palladium Catalyzed Additions

Bumagin et al. reported mild conditions for Heck coupling with palladium catalyzed arylation of acrylic acid with aryl halides in aqueous media for the synthesis of substituted cinnamic acids (Scheme 2.12, Page 20).[52] A thorough review by Beletskaya and Cheprakov notes the customizability of this synthetic route, and "often a small variation of substrate structure, nature of base, ligands, temperature, pressure, etc., leads to unpredictable results." [53]

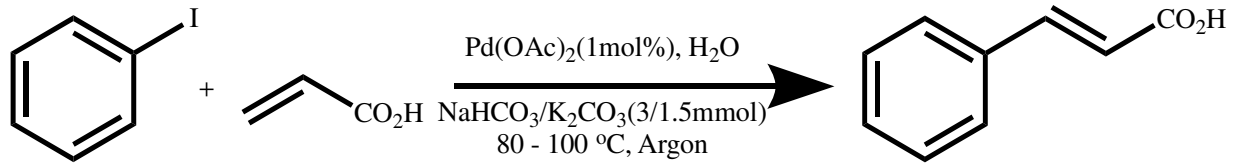

Scheme 2.12 Palladium catalyzed Heck coupling of CAs - Heck coupling with palladium catalyzed arylation of acrylic acid with aryl halides. Figure recreated from reference [52]

2.5. Surface Modification

2.5.1. Work Function Tuning

The work function of an electrode is an important property to consider in electronic applications. Total work function change ($\Delta\phi$) can be attributed to three characteristics: first, the interface dipole, which is a change in the electrostatic potential energy caused by the charge redistribution from the covalently attached monolayer ($\Delta V_{int.dip.}$); second, the possible geometry relaxation upon the ligand monolayer bonding ($\Delta V_{geom.rel.}$); and third, the modifier molecular dipole moment perpendicular to the surface ($\Delta V_{mol.}$). These three terms allow for the modification of work function to be written as $\Delta\phi = \Delta V_{int.dip} + \Delta V_{geom.rel.} + \Delta V_{mol.}$.[37, 54-55]

However, the sum of $\Delta V_{int.dip.} + \Delta V_{geom.rel.}$ induced by a SAM has a very small relative value. In addition, acids of the same anchor group induce equivalent changes; for example, $\Delta_{V int.dip}$, $+ \Delta V_{geom.rel.}$ for all phosphonic acid ligands have the same small impact on $\Delta\phi$. Therefore, $\Delta V_{int.dip} + \Delta V_{geom.rel.}$ are very minor contributors and the major source of $\Delta\phi$ is derived from $\Delta V_{mol.}$ However, the $\Delta V_{mol.}$ of a ligand is amplified by both the total dipole magnitude of

the molecule and by orienting the dipole perpendicular to the surface. This is most efficiently achieved by orienting polar groups in specified locations on the ligand head. Specifically, a ligand bound to the surface capped with an electron-withdrawing group in the ortho or para positions will pull charge from the surface. This results in a net positive charge density away from the surface and pulls more electrons at the surface.

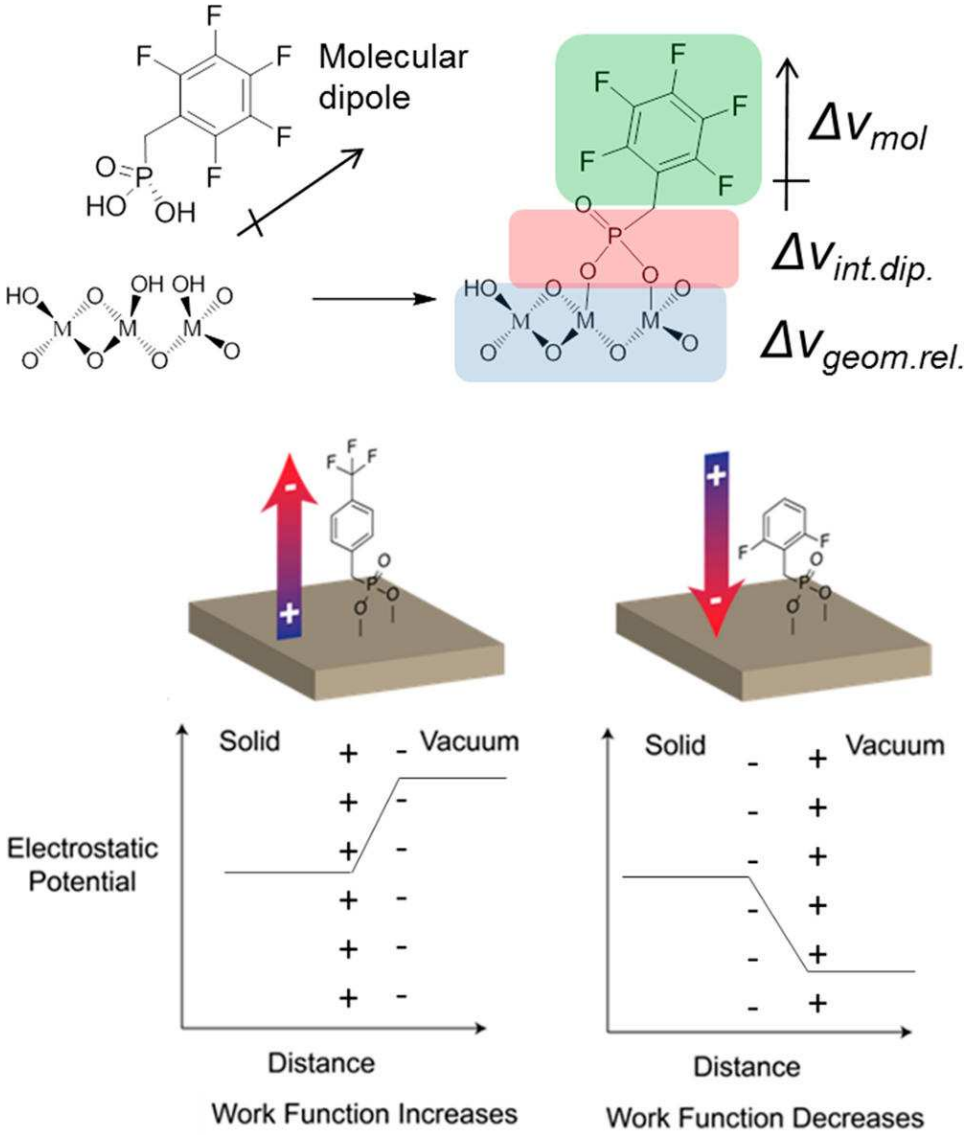

Figure 2.4 Dipole correlation of work function – (Top) Schematic representation of a phosphonic acid attaching to ITO and the work-function changes attributed to molecular dipole ($\Delta V_{mol.}$), interface dipole ($\Delta V_{int.dip.}$), and geometry relaxation($\Delta V_{geom.rel.}$). (Bottom) Illustration of the variation in electrostatic potential caused by (opposing) molecular dipoles. Taken directly with permission from reference.[37]

The importance of understanding the molecular tilt angle relative to the surface has only recently gained consideration.[37] As the $\Delta V_{mol.}$ is measured perpendicular relative to the surface, it can be predicted that the more rigid and parallel a molecule binds to the surface the greater effect of the molecule dipole on $\Delta V_{mol.}$ For example, PPAs have a tilt angle of ~19° ±5° on ITO, while BPAs have a tilt angle of ~47° ±5° on ITO.[56] The increased tilt angle can both reduce $\Delta V_{mol.}$ and significantly impact the electron transfer kinetics at the layer interface, with negative effect on the device performance.[57] This suggests that rational design of conjugated molecules with fewer flexible bonds such as phenyl or styryl derivatives would lead to optimizing the interface of a device.

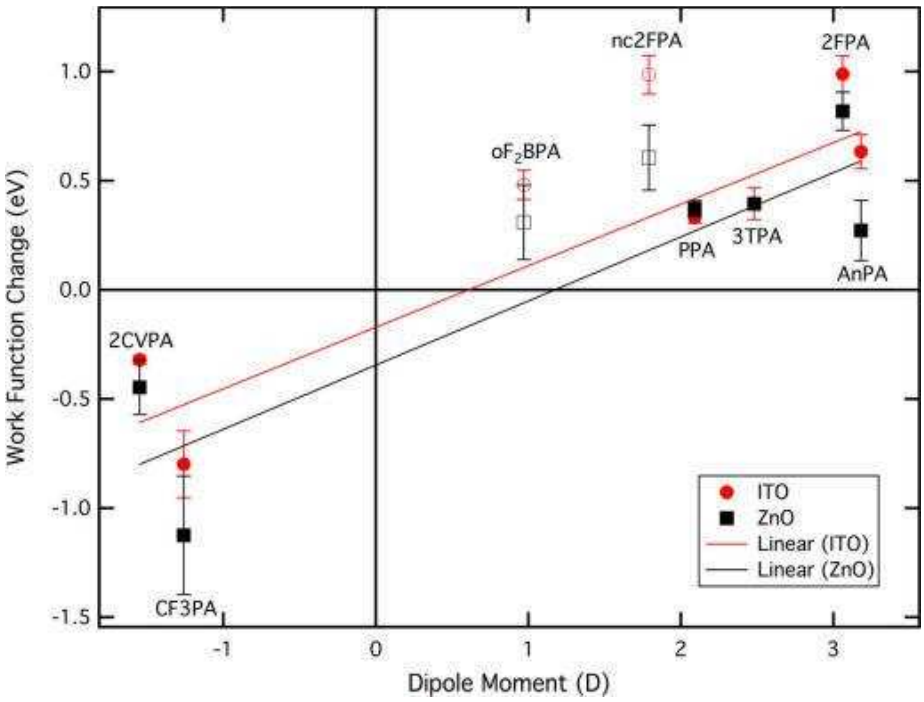

Figure 2.5 Modification of ITO and ZnO - Values of the dipole moment magnitudes along the phosphorus−carbon bond of phosphonic acids versus the work function change of modified ZnO (black squares) and ITO (red circles) with respect to unmodified oxides. Hollow points indicate unconjugated molecules, which have been excluded from the linear fits. Taken directly with permission from reference [23].

It is important to note that the double bond between the two carbon atoms promotes π-electron delocalization into the anchor group. As hypothesized by Braid et al., this facilitates an increase in molecular dipole as well as an improved charge transport between the molecule and

In turn, the induced electrostatic potential facilitates easier electron removal from the surface to vacuum, i.e., reducing the work function (Figure 2.4 lower left, Page 21). In opposition, ligands capped with functional groups oriented to push charge into the surface, such as an electron donating group in the ortho or para positions, results in a net negative charge density above the surface and fewer electrons at the surface. This makes it more difficult to move electrons from the surface to vacuum, i.e., increasing the work function (Figure 2.4 lower right, Page 21).[37]

the surface. Better energy alignment at the interface reduces the energy lost due to inefficient electron extraction and/or injection at the interface. In the case of OPVs, this leads to increased voltage onset current (Voc) and built in field, increasing the fill factor of the device and ultimately increasing performance and efficiency of the device. [22 58 59]

This effect is further illustrated by Koldemir et al., who examined the tuning effect of molecular dipole on work function of ITO and ZnO with vinyl PAs, BPA, and ethyl bridged phosphonic acids. They found that electrode work function tuning could be directly correlated to the strength of the dipole (Figure 2.5, Page 22). In addition, they observed an unprecedented work function tuning range of 2 eV, the most reported in the literature. Nonetheless, they reported that the non-conjugated 2FPA had similar results to the conjugated 2FPA on ITO (~1 eV); however, there was a notable difference of ~0.25 eV on ZnO. This result suggests these surface oxides will have varied responses, e.g. ITO modified with two different SAMs produced a similar response, while ZnO showed a larger modification in work function when the same two different SAMs were applied. This varied response dictates that some experimentation will be required to find a suitable modification of a surface. Overall, there is a general trend that could allow for predictive tuning of the surface via Density Functional Theory (DFT) gas phase dipole calculation for optimal device operation.

2.5.2. Quantum Dot

As described in Section 2.3, and in Chapter 5, QDs have been shown to have highly tunable electronic and optical properties that are of interest to a number of researchers. QD surface modification has long been examined to modulate surfaces, electronically activate or quench surface states, and to electronically couple QDs allowing for enhanced charge transport in thin films. All QDs share a common feature of having large surface to volume ratios; thus,

their surfaces play a dominate role in many of the physical and chemical processes in which they are utilized.[11] Modification of the QD surfaces has several effects. First, the ligands introduce surface molecules that can alter the energy and reactivity of the QD surface.[60] Second, the ligands form a capping layer that saturate dangling bonds.[61] Third, the ligands themselves can play a vital role in synthesis with targeted species to interact with clustering or polymeric organic reactions.[62-66]

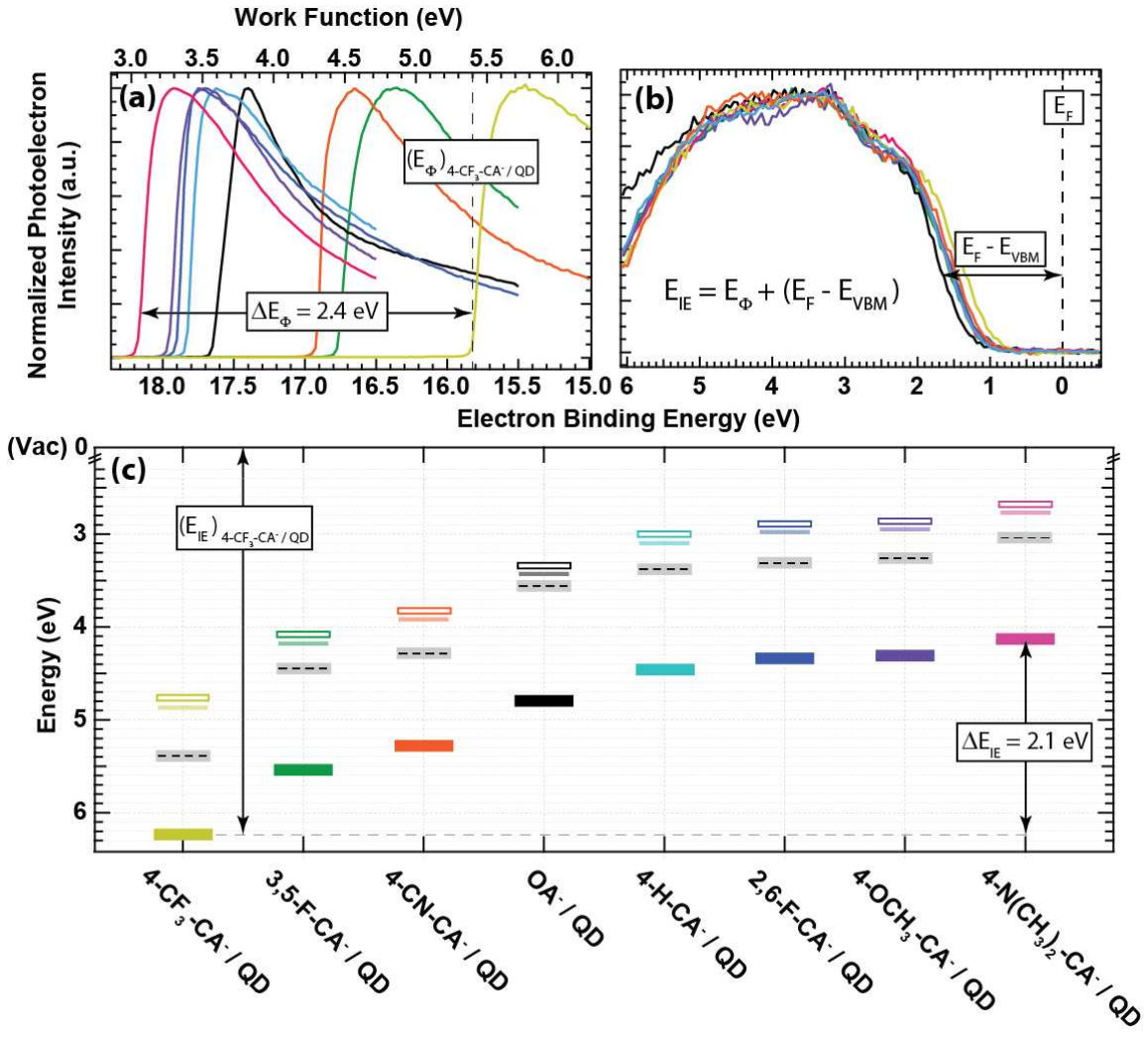

Figure 2.6 Photoelectron spectroscopy measurements of ligand/QD complexes. (a) Photoelectron cutoff region of XPS spectra used to determine ligand/QD film work function. (b) Valence band edge region of XPS spectra used to extract the ligand/QD film valence band maximum (VBM) with respect to the Fermi energy ($E_F - E_{VBM}$). The dashed black line represents the instrument equilibrated Fermi energy at an electron binding energy of 0 eV. (c) Band edge energies of films fabricated from OA- and R-CA- terminated 3.2 nm diameter PbS QDs; ionization energy (solid rectangles) and work function (dashed black lines). Also included the conduction band minimum

(E_{CBM}, open rectangles) that is determined from summing the optical gap determined from absorbance measurements (opaque lines) and calculated exciton binding energy. Figure taken directly with permission from reference [67]

Furthermore, band edge positions and optical absorption tuning determine the functionality of semiconductors in many QD opto-electronic applications, such as QD-PVs, QD-photo-electrochemical cells, and QD-OLEDs. Specifically, Kroupa et al. show that using CAs has led to unprecedented and precise tuning of PbS QD work function by a total range of 2.4 eV through surface modification (Figure 2.6, Page 24).[67]

Figure 2.6 (Page 24) illustrates that ligand dipole is a critical parameter in aiding in prediction of the overall magnitude of band edge shifting in QD films. Traditionally, QDs are deposited into a thin film, then modification is performed on the solid state QDs surface. Interestingly, Kroupa et al. developed and demonstrated a highly sought after method for solution phase ligand exchange prior to deposition of the QDs on the substrate, which leads to many desired constructive effects. This exchange method allows for precise control of the surface energy of the QD in addition to interactions with the organic layer in which the QDs are co-deposited. Additionally, this exchange method allows for purification of the modified QDs solution prior to their incorporation in the thin film, exclusion of displaced native oleate ligands allowed for a finer control of the thin film, potentially leading to more uniform and controlled thin films with increased device longevity, output and efficiency. This topic is further explored, in much greater detail in Chapter 5.

2.6. Conclusion and Summary

The examples of surface modification science in this chapter provide an overview of this exciting and quickly evolving field. Surface modification with styryl phosphonic acids and cinnamic acids is a technique that has gained popularity in applications of tuning interface properties and electronics of electrodes, and quantum dots. Once tuned for optimum characteristics, these surfaces can then be integrated into optoelectronic devices that, in theory, could result in higher efficiencies and lifetimes. The underlying purpose of this review is to document the synthetic methods of producing ligands with styryl spacer groups and functionalized phenyl head groups to optimize both attachment and modification to the surface of study. It is clear from our review of the literature that phosphonic and carboxylic acid groups are highly stable and extremely versatile.

Introduced above is a selection of modern methods for synthesizing styryl dialkyl phosphonates, which are subsequently hydrolyzed to form the corresponding acid group, and two methods for single step synthesis. Some of these reactions and techniques will be further described in mechanistic detail in Chapter 4. To the organic synthetic chemist, we hope this provides a thorough review of efficient syntheses of these acids. Cinnamic acids also have significant effects in similar applications, and, while diverse selections of these acids are readily commercially available, some unique derivatives may require synthesis, a few of these are discussed in Chapter 5. These corresponding synthetic routes are discussed to provide some general schematics of how to derive the desired product.

Finally, we have reviewed recent state-of-the-art work on the surface modification of metals, metal oxide, and metal quantum dots, which is a rapidly expanding area of research. Advances in modification of electrodes and thin films are a driving force for creating highly efficient, multilayered optoelectronic devices. The ability to fine-tune the effective work function of a semiconductor substrate to be ideally optimized for the desired application opens doors for higher efficiencies, new materials, and new technologies.

2.7. References Cited

1. Queffélec, C. m.; Petit, M.; Janvier, P.; Knight, D. A.; Bujoli, B., Surface modification using phosphonic acids and esters. *Chemical Reviews* **2012,** *112* (7), 3777-3807.

2. Bulliard, X.; Ihn, S.-G.; Yun, S.; Kim, Y.; Choi, D.; Choi, J.-Y.; Kim, M.; Sim, M.; Park, J.-H.; Choi, W.; Cho, K., Enhanced Performance in Polymer Solar Cells by Surface Energy Control. *Advanced Functional Materials* **2010,** *20* (24), 4381-4387.

3. Hotchkiss, P. J.; Malicki, M.; Giordano, A. J.; Armstrong, N. R.; Marder, S. R., Characterization of phosphonic acid binding to zinc oxide. *Journal of Materials Chemistry* **2011,** *21* (9), 3107.

4. Sharma, A.; Hotchkiss, P. J.; Marder, S. R.; Kippelen, B., Tailoring the work function of indium tin oxide electrodes in electrophosphorescent organic light-emitting diodes. *Journal of Applied Physics* **2009,** *105* (8), 084507.

5. Guo, L.-H.; Facci, J. S.; McLendon, G., Distance dependence of electron transfer rates in bilayers of a ferrocene Langmuir-Blodgett monolayer and a self-assembled monolayer on gold. *The Journal of Physical Chemistry* **1995,** *99* (21), 8458-8461.

6. Diebold, U., The surface science of titanium dioxide. *Surface Science Reports* **2003,** *48* (5–8), 53-229.

7. Woll, C., The chemistry and physics of zinc oxide surfaces. *Progress in Surface Science* **2007,** *82* (2-3), 55-120.

8. E.F. Vansant, P. V. D. V.; Vrancken, K. C., Chapter 2 Physical characterization of the silica surface. In *Studies in Surface Science and Catalysis*, E.F. Vansant, P. V. D. V.; Vrancken, K. C., Eds. Elsevier: 1995; Vol. Volume 93, pp 31-58.

9. Calzolari, A.; Ruini, A.; Catellani, A., Anchor Group versus Conjugation: Toward the Gap-State Engineering of Functionalized ZnO(10$\bar{1}$0) Surface for Optoelectronic Applications. *Journal of the American Chemical Society* **2011,** *133* (15), 5893-5899.

10. Pujari, S. P.; Scheres, L.; Marcelis, A. T. M.; Zuilhof, H., Covalent Surface Modification of Oxide Surfaces. *Angewandte Chemie International Edition* **2014,** *53* (25), 6322-6356.

11. Boles, M. A.; Ling, D.; Hyeon, T.; Talapin, D. V., The surface science of nanocrystals. *Nat Mater* **2016,** *15* (2), 141-153.

12. Hoel, C. A.; Mason, T. O.; Gaillard, J.-F.; Poeppelmeier, K. R., Transparent Conducting Oxides in the ZnO-In2O3-SnO2 System. *Chemistry of Materials* **2010,** *22* (12), 3569-3579.

13. Klauk, H., *Organic Electronics: Materials, Manufacturing, and Applications*. John Wiley & Sons: 2006; p 449.

14. Vuillaume, D., Organic Insulating Films at Nanometer Scale. *MRS Proceedings* **1996,** *446*.

15. Bauer, T.; Schmaltz, T.; Lenz, T.; Halik, M.; Meyer, B.; Clark, T., Phosphonate- and Carboxylate-Based Self-Assembled Monolayers for Organic Devices: A Theoretical Study of Surface Binding on Aluminum Oxide with Experimental Support. **2013**.

16. Giza, M.; Thissen, P.; Grundmeier, G., Adsorption Kinetics of Organophosphonic Acids on Plasma-Modified Oxide-Covered Aluminum Surfaces. *Langmuir* **2008,** *24* (16), 8688-8694.

17. Hotchkiss, P. J.; Jones, S. C.; Paniagua, S. A.; Sharma, A.; Kippelen, B.; Armstrong, N. R.; Marder, S. R., The modification of indium tin oxide with phosphonic acids: mechanism of binding, tuning of surface properties, and potential for use in organic electronic applications. *Accounts of Chemical Research* **2011,** *45* (3), 337-346.

18. Hanson, E. L.; Schwartz, J.; Nickel, B.; Koch, N.; Danisman, M. F., Bonding Self-Assembled, Compact Organophosphonate Monolayers to the Native Oxide Surface of Silicon. *Journal of the American Chemical Society* **2003,** *125* (51), 16074-16080.

19. Ra, H. W.; Khan, R.; Kim, J. T.; Kang, B. R.; Bai, K. H.; Im, Y. H., Effects of surface modification of the individual ZnO nanowire with oxygen plasma treatment. *Materials Letters* **2009,** *63* (28), 2516-2519.

20. Yu, X.; Ci, Z.; Liu, T.; Feng, X.; Wang, C.; Ma, T.; Bao, M., Influence of different electron acceptors in organic sensitizers on the performance of dye-sensitized solar cells. *Dyes and Pigments* **2014,** *102*, 126-132.

21. Brennan, B. J.; Llansola Portoles, M. J.; Liddell, P. A.; Moore, T. A.; Moore, A. L.; Gust, D., Comparison of silatrane, phosphonic acid, and carboxylic acid functional groups for attachment of porphyrin sensitizers to TiO2 in photoelectrochemical cells. *Phys Chem Chem Phys* **2013,** *15* (39), 16605-14.

22. Braid, J. L.; Koldemir, U.; Sellinger, A.; Collins, R. T.; Furtak, T. E.; Olson, D. C., Conjugated Phosphonic Acid Modified Zinc Oxide Electron Transport Layers for Improved Performance in Organic Solar Cells. *ACS Applied Materials & Interfaces* **2014,** *6* (21), 19229-19234.

23. Koldemir, U.; Braid, J. L.; Morgenstern, A.; Eberhart, M.; Collins, R. T.; Olson, D. C.; Sellinger, A., Molecular Design for Tuning Work Functions of Transparent Conducting Electrodes. *The Journal of Physical Chemistry Letters* **2015,** *6* (12), 2269-2276.

24. Guerrero, G.; Mutin, P. H.; Vioux, A., Anchoring of Phosphonate and Phosphinate Coupling Molecules on Titania Particles. *Chemistry of Materials* **2001,** *13* (11), 4367-4373.

25. Gawalt, E. S.; Lu, G.; Bernasek, S. L.; Schwartz, J., Enhanced Bonding of Alkanephosphonic Acids to Oxidized Titanium Using Surface-Bound Alkoxyzirconium Complex Interfaces. *Langmuir* **1999,** *15* (26), 8929-8933.

26. Thompson, M. E., Use of Layered Metal Phosphonates for the Design and Construction of Molecular Materials. *Chemistry of Materials* **1994,** *6* (8), 1168-1175.

27. Guerrero, G.; Mutin, P. H.; Vioux, A., Organically modified aluminas by grafting and sol-gel processes involving phosphonate derivatives. *Journal of Materials Chemistry* **2001,** *11* (12), 3161-3165.

28. Chernyshova, I. V.; Ponnurangam, S.; Somasundaran, P., Adsorption of fatty acids on iron (hydr)oxides from aqueous solutions. *Langmuir* **2011,** *27* (16), 10007-18.

29. Miller, D. J.; Sun, L.; Walzak, M. J.; McLntyre, N. S.; Chvedov, D.; Rosenfeld, A., Static SIMS studies of carboxylic acids on gold and aluminium–magnesium alloy surfaces. *Surface and Interface Analysis* **2003,** *35* (5), 463-476.

30. Gulley-Stahl, H.; Hogan, P. A.; Schmidt, W. L.; Wall, S. J.; Buhrlage, A.; Bullen, H. A., Surface Complexation of Catechol to Metal Oxides: An ATR-FTIR, Adsorption, and Dissolution Study. *Environmental Science & Technology* **2010,** *44* (11), 4116-4121.

31. Dubois, L. H.; Zegarski, B. R.; Nuzzo, R. G., Spontaneous organization of carboxylic acid monolayer films in ultrahigh vacuum. Kinetic constraints to assembly via gas-phase adsorption. *Langmuir* **1986,** *2* (4), 412-417.

32. Raman, A.; Gawalt, E. S., Self-Assembled Monolayers of Alkanoic Acids on the Native Oxide Surface of SS316L by Solution Deposition. *Langmuir* **2007,** *23* (5), 2284-2288.

33. Martz, J.; Zuppiroli, L.; Nüesch, F., Benzoic and Aliphatic Carboxylic Acid Monomolecular Layers on Oxidized GaAs Surface as a Tool for Two-Dimensional Photonic Crystal Infiltration. *Langmuir* **2004,** *20* (26), 11428-11432.

34. Buckholtz, G. A.; Gawalt, E. S., Effect of Alkyl Chain Length on Carboxylic Acid SAMs on Ti-6Al-4V. *Materials* **2012,** *5* (7), 1206.

35. Bulusu, A.; Paniagua, S. A.; MacLeod, B. A.; Sigdel, A. K.; Berry, J. J.; Olson, D. C.; Marder, S. R.; Graham, S., Efficient Modification of Metal Oxide Surfaces with Phosphonic Acids by Spray Coating. *Langmuir* **2013,** *29* (12), 3935-3942.

36. Rajeshwaran, G. G.; Nandakumar, M.; Sureshbabu, R.; Mohanakrishnan, A. K., Lewis Acid-Mediated Michaelis−Arbuzov Reaction at Room Temperature: A Facile Preparation of Arylmethyl/Heteroarylmethyl Phosphonates. *Organic Letters* **2011,** *13* (6), 1270-1273.

37. Paniagua, S. A.; Giordano, A. J.; Smith, O. N. L.; Barlow, S.; Li, H.; Armstrong, N. R.; Pemberton, J. E.; Brédas, J.-L.; Ginger, D.; Marder, S. R., Phosphonic Acids for Interfacial Engineering of Transparent Conductive Oxides. *Chemical Reviews* **2016**.

38. Bhattacharya, A. K.; Thyagarajan, G., Michaelis-arbuzov rearrangement. *Chemical Reviews* **1981,** *81* (4), 415-430.

39. Keglevich, G.; Grün, A.; Bölcskei, A.; Drahos, L.; Kraszni, M.; Balogh, G. T., Synthesis and Proton Dissociation Properties of Arylphosphonates: A Microwave-Assisted Catalytic Arbuzov Reaction with Aryl Bromides. *Heteroatom Chemistry* **2012,** *23* (6), 574-582.

40. Villemin, D.; Simeon, F.; Decreus, H.; Jaffres, P.-A., RAPID AND EFFICIENT ARBUZOV REACTION UNDER MICROWAVE IRRADIATION. *Phosphorus, Sulfur, and Silicon and the Related Elements* **1998,** *133* (1), 209-213.

41. Goossen, L. J.; Dezfuli, M. K., Practical protocol for the palladium-catalyzed synthesis of arylphosphonates from bromoarenes and diethyl phosphite. *SYNLETT* **2005,** *2005* (03), 445-448.

42. Hirao, T.; Masunaga, T.; Ohshiro, Y.; Agawa, T., Stereoselective synthesis of vinylphosphonate. *Tetrahedron Letters* **1980,** *21* (37), 3595-3598.

43. Han, L.-B.; Zhang, C.; Yazawa, H.; Shimada, S., Efficient and Selective Nickel-Catalyzed Addition of H−P(O) and H−S Bonds to Alkynes. *Journal of the American Chemical Society* **2004,** *126* (16), 5080-5081.

44. Thielges, S.; Bisseret, P.; Eustache, J., Copper-Mediated Cross-Coupling of H-Phosphonates with Vinyliodonium Salts: A Novel Very Mild Synthesis of 2-Arylvinylphosphonates. *Organic Letters* **2005,** *7* (4), 681-684.

45. Ochiai, M.; Sumi, K.; Takaoka, Y.; Kunishima, M.; Nagao, Y.; Shiro, M.; Fujita, E., Reactions of vinylsilanes with lewis acid-activated iodosylbenzene: stereospecific syntheses of vinyliodonium tetrafluoroborates and their reactions as highly activated vinyl halides. *Tetrahedron* **1988,** *44* (13), 4095-4112.

46. Al-Maksoud, W.; Mesnager, J.; Jaber, F.; Pinel, C.; Djakovitch, L., Synthesis of diethyl 2-(aryl)vinylphosphonates by the Heck reaction catalysed by well-defined palladium complexes. *Journal of Organometallic Chemistry* **2009,** *694* (20), 3222-3231.

47. Demmer, C. S.; Krogsgaard-Larsen, N.; Bunch, L., Review on modern advances of chemical methods for the introduction of a phosphonic acid group. *Chem Rev* **2011,** *111* (12), 7981-8006.

48. Maranescu, B.; Visa, A.; Ilia, G.; Simon, Z.; Demadis, K. D.; Colodrero, R. M. P.; Cabeza, A.; Vallcorba, O.; Rius, J.; Choquesillo-Lazarte, D., Synthesis and structural characterization of 2-D layered copper(II) styrylphosphonate coordination polymers. *Journal of Coordination Chemistry* **2014,** *67* (9), 1562-1572.

49. Knoevenagel, E., Condensation von Malonsäure mit aromatischen Aldehyden durch Ammoniak und Amine. *Berichte der deutschen chemischen Gesellschaft* **1898,** *31* (3), 2596-2619.

50. Doebner, O., Ueber die der Sorbinsäure homologen, ungesättigten Säuren mit zwei Doppelbindungen. *Berichte der deutschen chemischen Gesellschaft* **1902,** *35* (1), 1136-1147.

51. Ziegler, K.; Luttringhaus, A., Uber vielgliedridge Ringsysteme III. Meta- u. Para Rinschlusse in der Benzolreihe. *Annalen Der Chemie* **1934,** *511* (1), 1-12.

52. Bumagin, N. A.; More, P. G.; Beletskaya, I. P., Synthesis of substituted cinnamic acids and cinnamonitriles via palladium catalyzed coupling reactions of aryl halides with acrylic acid and acrylonitrile in aqueous media. *Journal of Organometallic Chemistry* **1989,** *371* (3), 397-401.

53. Beletskaya, I. P.; Cheprakov, A. V., The Heck Reaction as a Sharpening Stone of Palladium Catalysis. *Chemical Reviews* **2000,** *100* (8), 3009-3066.

54. Paniagua, S. A.; Hotchkiss, P. J.; Jones, S. C.; Marder, S. R.; Mudalige, A.; Marrikar, F. S.; Pemberton, J. E.; Armstrong, N. R., Phosphonic Acid Modification of Indium−Tin Oxide Electrodes: Combined XPS/UPS/Contact Angle Studies. *The Journal of Physical Chemistry C* **2008,** *112* (21), 7809-7817.

55. Li, H.; Paramonov, P.; Bredas, J.-L., Theoretical study of the surface modification of indium tin oxide with trifluorophenyl phosphonic acid molecules: impact of coverage density and binding geometry. *Journal of Materials Chemistry* **2010,** *20* (13), 2630.

56. Gliboff, M.; Sang, L.; Knesting, K. M.; Schalnat, M. C.; Mudalige, A.; Ratcliff, E. L.; Li, H.; Sigdel, A. K.; Giordano, A. J.; Berry, J. J.; Nordlund, D.; Seidler, G. T.; Brédas, J.-L.; Marder, S. R.; Pemberton, J. E.; Ginger, D. S., Orientation of Phenylphosphonic Acid Self-Assembled Monolayers on a Transparent Conductive Oxide: A Combined NEXAFS, PM-IRRAS, and DFT Study. *Langmuir* **2013,** *29* (7), 2166-2174.

57. Lin, H.-C.; MacDonald, G. A.; Shi, Y.; Polaske, N. W.; McGrath, D. V.; Marder, S. R.; Armstrong, N. R.; Ratcliff, E. L.; Saavedra, S. S., Influence of Molecular Orientation on Charge-Transfer Processes at Phthalocyanine/Metal Oxide Interfaces and Relationship to Organic Photovoltaic Performance. *The Journal of Physical Chemistry C* **2015,** *119* (19), 10304-10313.

58. Brenner, T. M.; Chen, G.; Meinig, E. P.; Baker, D. J.; Olson, D. C.; Collins, R. T.; Furtak, T. E., Tuning zinc oxide/organic energy level alignment using mixed triethoxysilane monolayers. *Journal of Materials Chemistry C* **2013,** *1* (37), 5935-5943.

59. Gosselink, R. W.; Hollak, S. A. W.; Chang, S.-W.; van Haveren, J.; de Jong, K. P.; Bitter, J. H.; van Es, D. S., Reaction Pathways for the Deoxygenation of Vegetable Oils and Related Model Compounds. *ChemSusChem* **2013,** *6* (9), 1576-1594.

60. Laibinis, P. E.; Whitesides, G. M.; Allara, D. L.; Tao, Y. T.; Parikh, A. N.; Nuzzo, R. G., Comparison of the structures and wetting properties of self-assembled monolayers of n-alkanethiols on the coinage metal surfaces, copper, silver, and gold. *Journal of the American Chemical Society* **1991,** *113* (19), 7152-7167.

61. Chadi, D. J., Atomic and Electronic Structures of Reconstructed Si(100) Surfaces. *Physical Review Letters* **1979,** *43* (1), 43-47.

62. Nag, A.; Kovalenko, M. V.; Lee, J.-S.; Liu, W.; Spokoyny, B.; Talapin, D. V., Metal-free Inorganic Ligands for Colloidal Nanocrystals: S2–, HS–, Se2–, HSe–, Te2–, HTe–, TeS32–,

OH–, and NH2– as Surface Ligands. *Journal of the American Chemical Society* **2011,** *133* (27), 10612-10620.

63. Llordes, A.; Garcia, G.; Gazquez, J.; Milliron, D. J., Tunable near-infrared and visible-light transmittance in nanocrystal-in-glass composites. *Nature* **2013,** *500* (7462), 323-326.

64. Pellegrino, T.; Manna, L.; Kudera, S.; Liedl, T.; Koktysh, D.; Rogach, A. L.; Keller, S.; Rädler, J.; Natile, G.; Parak, W. J., Hydrophobic Nanocrystals Coated with an Amphiphilic Polymer Shell: A General Route to Water Soluble Nanocrystals. *Nano Letters* **2004,** *4* (4), 703-707.

65. Liu, Y.; Tolentino, J.; Gibbs, M.; Ihly, R.; Perkins, C. L.; Liu, Y.; Crawford, N.; Hemminger, J. C.; Law, M., PbSe Quantum Dot Field-Effect Transistors with Air-Stable Electron Mobilities above 7 cm2 V–1 s–1. *Nano Letters* **2013,** *13* (4), 1578-1587.

66. Anderson, N. C.; Hendricks, M. P.; Choi, J. J.; Owen, J. S., Ligand Exchange and the Stoichiometry of Metal Chalcogenide Nanocrystals: Spectroscopic Observation of Facile Metal-Carboxylate Displacement and Binding. *Journal of the American Chemical Society* **2013,** *135* (49), 18536-18548.

67. Kroupa, D. M.; Vörös, M.; Brawand, N. P.; McNichols, B. W.; Miller, E. M.; Gu, J.; Nozik, A. J.; Sellinger, A.; Galli, G.; Beard, M. C., Tuning colloidal quantum dot band edge positions through solution-phase surface chemistry modification. *Nature Communications* **2017,** *8*, 15257.

CHAPTER 3
SINGLE STEP STYRYL PHOSPHONIC ACIDS SYNTHESIS: PALLADIUM-CATALYZED HECK COUPLING OF VINYL PHOSPHONIC ACID WITH ARYL HALIDE

A modified manuscript submitted to Chemical Communications

of The Royal Society of Chemistry

Brett W. McNichols [a], and Alan Sellinger [a]

3.1. Abstract

We have developed a single step palladium-catalyzed Heck coupling of aryl halides with vinyl phosphonic acid to produce functionalized (E)-styryl phosphonic acids. This pathway utilizes a variety of commercially available aryl halides, vinyl phosphonic acid and $Pd(P(t\text{-}Bu)_3)_2$ as catalyst. These conditions produce a wide range of styryl phosphonic acids with good to excellent yields (42-80%).

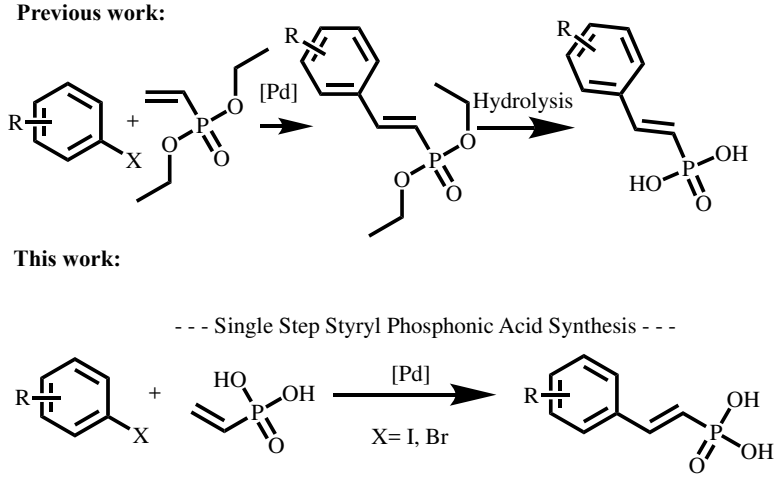

Scheme 3.1 Palladium-catalyzed styryl phosphonic acid general synthesis

[a] Department of Chemistry, Colorado School of Mines, Golden, CO 80401

3.2. Introduction

The palladium catalyzed Heck reaction is a powerful synthetic tool in both simple and complex organic syntheses, the topic of thousands of publications, and part of the 2010 Nobel prize in chemistry.[1-3] Recently the Heck coupling of aryl halides with acrylic acid to produce functionalized cinnamic acid derivatives for applications in tuning electrode interfacial surface energetics have been reported.[4-7] However, a thorough survey of the literature reveals that styryl phosphonic acid analogues of cinnamic acids are quite rare. [8-11]

The broad utility of phosphonic acid ligands have been studied and reviewed for the tuning of electrode work function, surface energies, and electron charge transfer kinetics.[12-13] These modifications with phosphonic acid ligands have led to increased efficiency and operational range in organic-based devices, such as organic light emitting diodes (OLEDs), organic photovoltaic (OPVs), and most recently perovskite solar cells.[8-11, 14-20] Much of this effect is attributed to the conjugated linkage between the acid group (i.e. binding site) and the functional aromatic ring. For example, upon binding to a surface through the phosphonic acid group the dipole on the aromatic ring can better communicate to the surface through the conjugated linkage. Thus, when the acid is bound to the surface of an electrode a rather large tuning of the electrode has been observed which has been shown to have modest improvement in the power conversion efficiency of inverted P3HT:ICBA solar cells.[6, 21]

Despite these promising results very few of these acids are commercially available, which has led us to explore a route for their simple, high yield, and cost-effective synthesis. In general, the current synthetic route of synthesizing these styryl phosphonic acid ligands is a two-step mechanism. First, the Heck coupling of aromatic halide with diethyl vinylphosphonate yielding the intermediate diethyl (*E*)-styryl phosphonate followed by column chromatography purification, and second, the hydrolysis of the dialkyl esters which requires harsh conditions utilizing reagents such as trimethylsilyl halides or refluxing in inorganic strong acids. These rather harsh conditions are not tolerant of functional groups and often lead to poor yields (Scheme 3.1- previous work, Page 32).[10, 16, 22-23] In addition, final products were often slightly discolored, indicating the possibility of impurities despite characterization showing high purity, i.e. NMR, GCMS. It has been well established that the slightest impurities could lead to reduced performance or lifetime of OLED, OPV or perovskite devices.[24-25] Thus, there is a need to

develop efficient methods for the direct high yield synthesis of highly pure and functionalized styryl phosphonic acids. Thus, there is an opportunity to develop efficient methods for the direct high yield synthesis of highly pure and functionalized styryl phosphonic acids. Herein we report the highly stereo-selective Heck coupling of vinyl phosphonic acid with commercially available aryl halides to form styryl phosphonic acids in good yields. (Scheme 3.1 – this work Page 32)

3.3. Experimental Section

3.3.1. Experimental Methods

All chemicals were used as received without further purification unless noted. Acetonitrile (ACN, ACS) dichloromethane (DCM, ACS), anhydrous tetrahydrofuran (THF, ≥99.9%), N,N-dicyclohexylmethylamine (NCy_2Me, 97%), and anhydrous magnesium sulfate ($MgSO_4$), were obtained from Sigma Aldrich. Sodium hydroxide (NaOH, Pearl 97%) was obtained from Fisher Scientific. Bis(tri-tert-butylphosphine)palladium ($Pd[P(t\text{-}Bu)_3]_2$, 98%) was obtained from Strem Chemical. Vinyl phosphonic acid (95%) was obtained from TCI chemicals. Chemicals. Hydrochloric acid (HCl, ACS) was obtained from Macron Fine Chemicals. All glassware was base, acid, and water washed then oven dried. ^{1}H. ^{13}C, ^{19}F, and ^{31}P NMR, spectra were obtained on a JEOL ECA 500 liquid-state NMR spectrometer and data obtained was manipulated in MestReNova NMR processor software. Microwave synthesis was performed on a Biotage Initiator+ microwave system. Flash chromatography was performed on a Biotage Isolara Prime flash chromatography system with Biotage Snap Ultra or Biotage Snap Kp-sil cartridges.

3.3.2. Phosphonic Acid synthesis

Microwave phosphonic acid synthesis - A 20 mL Biotage microwave vial equipped with a magnetic stir bar was charged with the aromatic halide, Vinyl phosphonic Acid, N,N-dicyclohexylmethylamine, $Pd[P(t\text{-}Bu)_3]_2$ (catalyst used at 1 mol % level), and THF. The mixture was heated to 180°C at 12 Bar for 15 min, upon completion and cooling workup followed crude PA purification below.

Traditional PA synthesis - A Schlenk flask equipped with a magnetic stir bar under argon was charged with the aromatic halide, Vinyl phosphonic acid, N,N-dicyclohexylmethylamine, $Pd[P(t\text{-}Bu)_3]_2$ (catalyst used at 1 mol % level), and THF. The mixture

was heated to 70°C for 24 h and periodically tested via TLC for reaction completion, upon completion and cooling followed crude PA purification below.

Crude PA purification - The crude product mixture was extracted three times with Ethyl acetate and acidic water (5% HCl). The organic layer was dried with $MgSO_4$, filtered, and the solvent removed using a rotary evaporator. The resultant product was then further purified by recrystallization in ACN or precipitation in DCM.

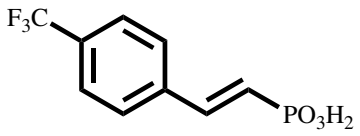

BM01 – CF_3VPA - (E)-(4-(trifluoromethyl)styryl)phosphonic acid -

Synthesis followed microwave PA synthesis procedure above, utilizing 4-(trifluoromethyl) bromobenzene as the aromatic halide. However as noted in article text, purification of the reaction crude was first treated in an acidic aqueous (5% HCl/vol) organic EA extraction. The organic fraction was then dried with magnesium sulfate, and the solvent was concentrated under rotor evaporation to a volume of only a few milliliters. Finally, CF_3VPA was isolated by precipitation into DCM and filtration producing a white powder. This compound has been previously synthesized and reported[16, 21], and ^{1}H NMR characterization matches appropriately. The following NMR spectrum is located in Appendix A.

^{1}H NMR (500 MHz, DMSO-d_6) δ 7.80 (s, 2H), 7.71 (s, 2H), 7.26 (dd, 1H), 6.65 (dd, 1H), 5.72 (s, 2H).

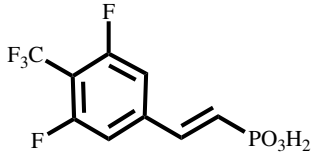

BM05 – m$F_2C F_3$VPA - (E)-(3,5-difluoro-4-(trifluoromethyl)styryl)phosphonic acid

Synthesis followed the microwave PA synthesis procedure above, utilizing (3,5-difluoro-4-(trifluoromethyl) bromobenzene as the aromatic halide. However as noted in article text, purification of the reaction crude was first treated in an acidic aqueous (5% HCl/vol) organic EA extraction. The organic fraction was then dried with magnesium sulfate, and the solvent was

concentrated under rotor evaporation to a volume of only a few milliliters. Finally, mF_2CF_3VPA was isolated by precipitation into DCM and filtration yielding white flakes. To our knowledge this is a novel compound. The following NMR spectra are located in Appendix A.

^{1}H NMR (500 MHz, DMSO-d_6) δ 7.71 (d, J = 11.6 Hz, 2H), 7.14 (dd, J = 21.2 Hz, 1H), 6.84 (dd, J = 17.4, 14.7 Hz, 1H), 5.72 (s, 2H).

^{13}C NMR (126 MHz, DMSO-D_6) δ 167.37, 160.68-158.64 (D J_{C-P} =160Hz 1C), 142.52, 140.36, 125.54 (2C), 123.10-120.93 (d, J_{C-P} 122Hz 1C) 113.27, 113.08, 39.92.

^{19}F NMR (471 MHz, DMSO-D_6) δ -55.20, -112.07.

^{31}P NMR (202 MHz, DMSO-D_6) δ 11.85.

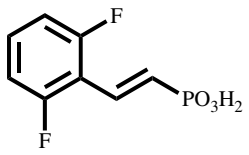

BM02 – oF_2VPA - (E)-(2,6-difluorostyryl)phosphonic acid

Synthesis followed the microwave PA synthesis procedure above utilizing 2,6-difluoroiodobenzene as the aromatic halide, However as noted in article text, purification of the reaction crude was first treated in an acidic aqueous (5% HCl/vol) organic EA extraction. Then, the organic fraction was dried with magnesium sulfate, and the solvent was concentrated under rotor evaporation to a volume of only a few milliliters. Finally, oF_2VPA was isolated by precipitation into DCM and filtration yielding brilliantly white flakes. This compound has been previously synthesized and reported[16, 21], and characterization matches appropriately. The following NMR spectrum is located in Appendix A.

^{1}H NMR (500 MHz, DMSO-d_6) δ 10.06 (s, 1H), 7.43 (t, J = 9.6 Hz, 1H), 7.21 – 7.07 (m, 3H), 6.54 (t, J = 17.5 Hz, 1H).

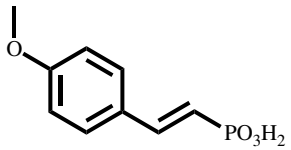

BM41 - AnVPA - (E)-(4-methoxystyryl) phosphonic acid

Synthesis followed the microwave PA synthesis procedure above utilizing 4-bromoanisole as the aromatic halide. This compound has been previously synthesized and reported[16, 21], and ^{1}H NMR characterization matches appropriately. The following NMR spectrum is located in Appendix A.

^{1}H NMR (500 MHz, DMSO-d_6) δ 7.51 (d, J = 8.7 Hz, 2H), 7.09 (dd, J = 21.9, 17.4 Hz, 1H), 6.91 (d, J = 8.7 Hz, 2H), 6.27 (t, J = 16.9 Hz, 1H), 3.74 (s, 3H).

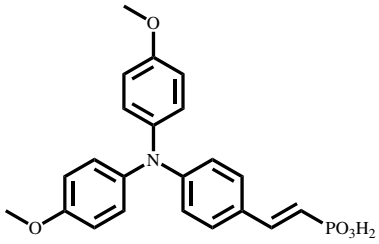

BM25 - TPAVPA - (E)-(4-(bis(4-methoxyphenyl) amino) styryl) phosphonic acid

Synthesis followed the traditional PA synthesis procedure above utilizing 4-iodo-4',4''-dimethoxytriphenylamine as the aromatic halide, with the exception that once the crude was isolated after extraction and flash chromatography isolated 130mg (31% yield) of bright yellow, highly fluorescent product. To our knowledge this is a novel compound. The following NMR spectra are located in Appendix A.

^{1}H NMR (500 MHz, DMSO-d_6) δ 7.15 – 6.98 (m, 2H), 6.97 – 6.84 (m, 4H), 6.79 (d, J = 14.0 Hz, 4H), 6.69 (d, J = 27.2 Hz, 2H), 6.27 – 6.07 (m, 1H), 3.71 – 3.63 (m, 6H).

^{13}C NMR (126 MHz, DMSO-D_6) δ 156.04, 155.74, 147.82, 146.94, 141.18, 140.71, 138.55, 133.46, 129.97, 128.89, 128.58, 128.18, 127.72, 127.30, 126.98, 126.76, 126.43, 126.34, 121.31, 120.42, 115.35, 115.28, 55.69, 55.67, 40.05, 21.80.

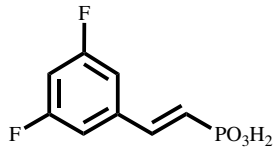

BM07 – mF$_2$VPA - (*E*)-(3,5-difluorostyryl) phosphonic acid

Synthesis followed microwave PA synthesis procedure above utilizing 3,5-difluorobromobenzene as the aromatic halide, this compound has been previously synthesized and reported[16, 21], and ^{1}H NMR characterization matches appropriately. The following NMR spectrum is located in Appendix A.

^{1}H NMR (500 MHz, DMSO-d_6) δ 7.42 – 7.33 (m, 2H), 7.20 – 7.16 (m, 1H), 7.11 (dd, J = 20.2 Hz, 1H), 6.63 (dd, J = 16.5 Hz, 1H).

3.4. Discussion

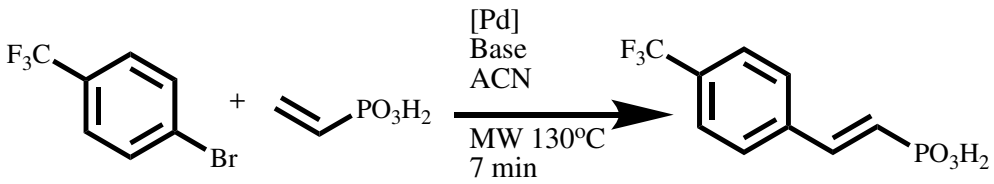

Scheme 3.2 Model reaction of CF_3VPA

We began our investigation with a model reaction of 4-bromobenzotrifluoride (**1**) and vinyl phosphonic acid (**2**), which were coupled under microwave conditions to form product (**3**) (*E*)-(4-(trifluoromethyl) styryl) phosphonic acid, CF_3VPA (Scheme 3.2). The CF_3VPA product was selected as the model reaction because we found in our previous work that the workup and purification is relatively simple. Upon reaction completion, the product mixture was first treated in a standard acidic aqueous (5% HCl/vol) organic (ethyl acetate - EA) extraction. Then, the organic fraction was dried with magnesium sulfate, filtered, and the filtrate was concentrated under rotary evaporation to a volume of only a few milliliters. Finally, CF_3VPA was isolated by precipitation into dichloromethane (DCM) and recovered by filtration producing a brilliant white powder, which was found to be sufficiently pure based on NMR.

To find a suitable catalytic system for the coupling of VPA, we evaluated various Pd catalysts (e.g., Pd(P(*t-Bu*)$_3$)$_2$, Pd(PPh$_3$)$_4$, Pd(dba)/TPP, Herrmann's palladacycle, and Pd(OAc)$_2$). Results showed that only Pd(P(*t*-Bu)$_3$)$_2$ provided any measurable yield of the desired product, so we moved forward with this particular catalyst to prepare more acids.[26] We found that all other catalysts led to no recoverable yield, specifically no product was formed in any detectable quantity (e.g. TLC, GCMS, NMR).

In tandem, we investigated the influences of various bases on the reaction. As shown in Table 3.1, the selected bases did not have any effect on the reactivity of the Pd catalyst systems. In addition, we noted a slight increase in yield (Table 3.1, Entry 1) when utilizing NCy$_2$Me, over TEA or Cs$_2$CO$_3$ with Pd(P(*t*-Bu)$_3$)$_2$.

Table 3.1 Catalyst selection of vinyl phosphonic acid with 4-bromobenzotrifluoride

Entry	Catalyst	Solvent	Base (TEA)	Base Cs_2CO_3	Base (NCy_2Me)
1	Pd(P(*t*-Bu)$_3$)$_2$	ACN	63%	65%	66%
2	Pd(PPh$_3$)$_4$	ACN	NR	NR	-
3	Pd(dba)/TPP	ACN	NR	NR	-
4	Herrmann's	ACN	NR	NR	-
5	Pd(Oac)$_2$/TPP	ACN	NR	NR	-

Reaction conditions; 4-bromobenzotrifluoride (1mmol), vinyl phosphonic acid (1.1mmol), Pd cat. (10 mol%), base (1.1 mmol) under dry conditions and 3 ml of solvent, *for Pd (II) systems TPP was introduced at 2 equivalents. Percentages are based on an average of two reactions. Reaction was microwaved for 7 minutes and 130°C with stirring.

Finally, to fully optimize reaction conditions, we investigated the influence of various polar solvents (e.g. ACN, dioxane, THF) on the reaction yield. For this reaction optimization we considered only polar solvents, as VPA does not readily dissolve in non-polar solvents such as toluene. Although ACN, dioxane, and THF all performed similarly, we selected THF as it was the best solvent with regard to solubilizing a wide variety of aromatic halides. After evaluating many reaction conditions we selected microwave conditions of 7 minutes at 130°C.

We then studied the Heck coupling reaction (this mechanism is discussed in detail in Chapter 4) as a consequence of electron withdrawing and donating groups on the aromatic halides. As shown in Figure 3.2 (Page 38) products were prepared in moderate to good yields.

With the exception of products NO_2VPA, CNVPA and t-MeOxVPA, products were confirmed via GCMS; however, they were inseparable from the crude reaction. Details for successful synthesis of NO_2VPA, and CNVPA can be found in detail in Chapter 4.

Table 3.2 Solvent optimization in microwave conditions

Entry	Catalyst	Base	Solvent	Yield
6	$Pd(P(t\text{-}Bu)_3)_2$	NCy_2Me	ACN	66%
7	$Pd(P(t\text{-}Bu)_3)_2$	NCy_2Me	Dioxane	67%
8	$Pd(P(t\text{-}Bu)_3)_2$	NCy_2Me	THF	68%

Reaction conditions; 4-bromobenzotrifluoride (1mmol), vinyl phosphonic acid (1.1mmol), $Pd(P(t\text{-}Bu)_3)_2$. (10 mol%), NCy2Me (1.1 mmol) under dry conditions and 3 ml of solvent, Reaction was microwaved for 7 minutes and 130°C with stirring.

The highly fluorinated products CF_3VPA, 35F4CF_3VPA, and oF_2VPA were easily separated through a precipitation process as described in detail in Experimental Section 3.3.2 Phosphonic Acid Synthesis. Furthermore, these isolated products were magnificently white powders, indicating a higher purity when compared to the hydrolysis products of Scheme 3.1 - previous work (Page 32), which were reported to have slight off white characteristics.[16, 21]

Product mF_2VPA and AnVPA were obtained from extraction and ultimately recrystallized in ACN; further purification details and information can also be found in the Experimental Section 3.3.2 Phosphonic Acid Synthesis. Notably, in all of the purified products a trace amount of the (*Z*)-isomer is detectable (See Appendix A NMR spectra). Generally, the $Pd(P(t\text{-}Bu)_3)_2$ combined with NCy_2Me yield the (E)-isomer, however we do note a consistent 20/1 E/Z ratio. This potentially could be improved with minor changes to the base or solvent systems, but this high E/Z stereoisomer selectivity is consistent with similar cinnamic derivatives and these reaction conditions, and seen in Chapters 4-7.[4, 7, 27]

Additionally, products CF_3VPA, mF_2VPA, and oF_2VPA were scaled up to 10 gram reactions using traditional hotplate and Schlenk line techniques, as this amount exceeded the capability of our microwave reactor. Here, a 50 mL flask was evacuated and purged with argon 3x, and then the solid reactants were added to the flask.

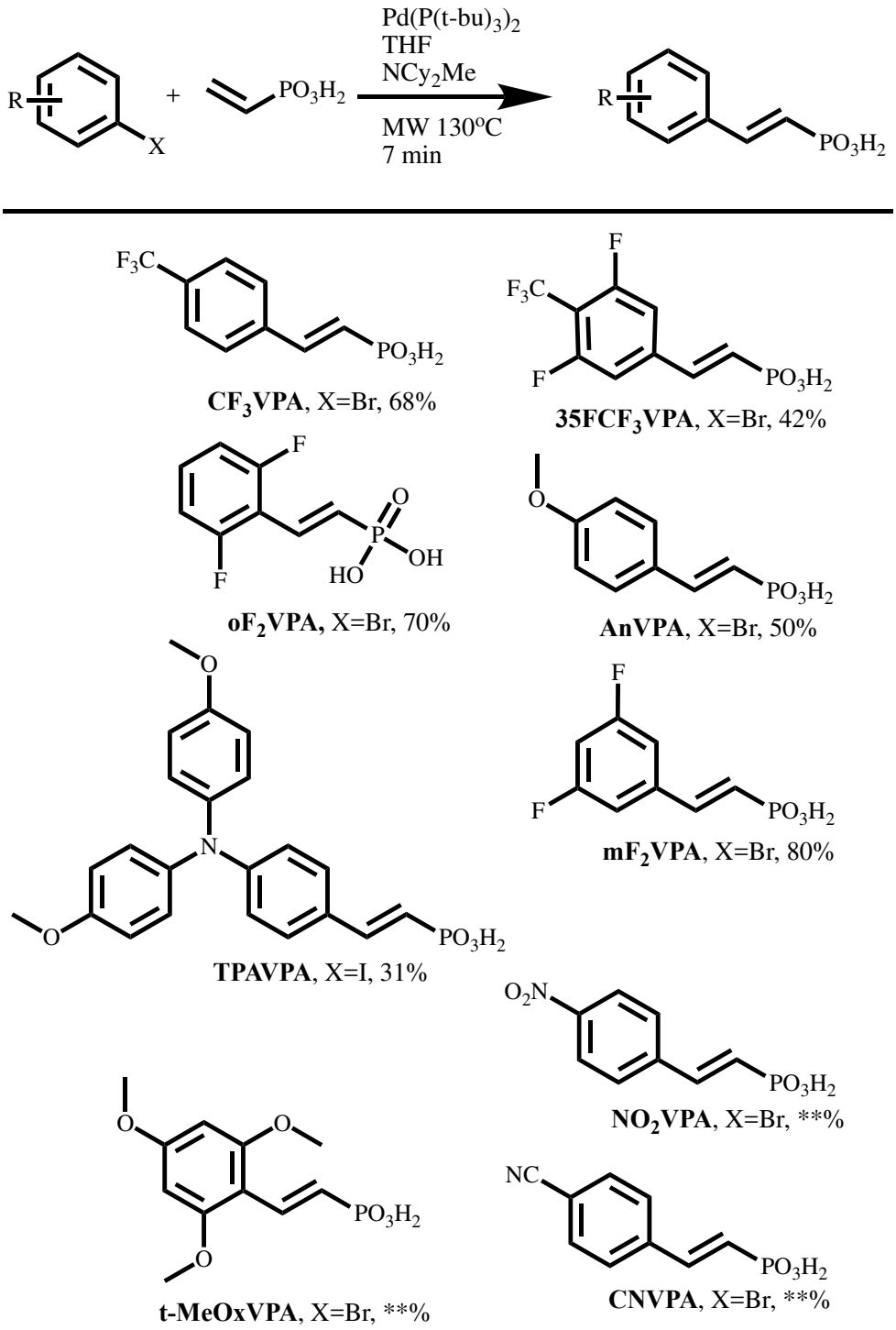

Figure 3.1 Optimized single step Heck coupling with substrate (top) and scope of synthesized styryl phosphonic acids using VPA and aromatic halides. (bottom) Reaction conditions; aromatic halide (1mmol), vinyl phosphonic acid (1.1mmol), Pd(P(*t*-Bu)$_3$)$_2$ (10 mol%), NCy$_2$Me (1.1 mmol) and 3 mL of anhydrous THF were microwaved for 7 minutes at 12 bar and 130°C with stirring. Yield is the average of two reactions. **Products were inseparable from reaction crude

3.5. Conclusions

In conclusion, we have developed a practical and original set of conditions for the direct palladium-catalyzed coupling of aromatic halides with vinyl phosphonic acid to form new (*E*)-styryl phosphonic acids. This method results in moderate to good yields from a one-pot reaction using a variety of electron donating or withdrawing aromatic halides resulting in excellent purity when compared to other methods. Our reaction conditions can be achieved using both traditional or microwave heating and are fully scalable to gram size reactions with high purity and product yields. We anticipate that our protocol has a number of applications where introduction of the vinyl phosphonic acid group may be desired.

In the following Chapter 4, we will utilize this synthetic technique for the production of CF_3VPA**,** along with a few other techniques to produce families of phosphonic acids. This method has provided a powerful single step process that not only produces what looks to be a cleaner, purer product, but also greatly reduces the time requirement for synthesis and purification of the final product.

3.6. Acknowledgment

B.W.M. respectfully acknowledges the sponsorship and support of the United States Air Force Institute of Technology (AFIT). A.S. acknowledges the U.S. Department of Energy under Contract DE-AC36− 08-GO28308 with the National Renewable Energy Laboratory (NREL) through the DOE SETP program, and start-up funds from the Colorado School of Mines.

3.7. References Cited

1. Stille, J. K., The Palladium-Catalyzed Cross-Coupling Reactions of Organotin Reagents with Organic Electrophiles [New Synthetic Methods (58)]. *Angewandte Chemie International Edition in English* **1986,** *25* (6), 508-524.

2. Karimi, B.; Behzadnia, H.; Elhamifar, D.; Akhavan, P. F.; Esfahani, F. K.; Zamani, A., Transition-metal-catalyzed oxidative Heck reactions. *Synthesis* **2010,** *2010* (09), 1399-1427.

3. Heck, R. F.; Nolley, J. P., Palladium-catalyzed vinylic hydrogen substitution reactions with aryl, benzyl, and styryl halides. *The Journal of Organic Chemistry* **1972,** *37* (14), 2320-2322.

4. Beletskaya, I. P.; Cheprakov, A. V., The Heck Reaction as a Sharpening Stone of Palladium Catalysis. *Chemical Reviews* **2000,** *100* (8), 3009-3066.

5. Bumagin, N. A.; More, P. G.; Beletskaya, I. P., Synthesis of substituted cinnamic acids and cinnamonitriles via palladium catalyzed coupling reactions of aryl halides with acrylic acid

and acrylonitrile in aqueous media. *Journal of Organometallic Chemistry* **1989,** *371* (3), 397-401.

6. Kroupa, D. M.; Vörös, M.; Brawand, N. P.; McNichols, B. W.; Miller, E. M.; Gu, J.; Nozik, A. J.; Sellinger, A.; Galli, G.; Beard, M. C., Tuning colloidal quantum dot band edge positions through solution-phase surface chemistry modification. *Nature Communications* **2017,** *8*, 15257.

7. Littke, A. F.; Fu, G. C., Heck Reactions in the Presence of P(t-Bu)3: Expanded Scope and Milder Reaction Conditions for the Coupling of Aryl Chlorides. *The Journal of Organic Chemistry* **1999,** *64* (1), 10-11.

8. Paniagua, S. A.; Giordano, A. J.; Smith, O. N. L.; Barlow, S.; Li, H.; Armstrong, N. R.; Pemberton, J. E.; Brédas, J.-L.; Ginger, D.; Marder, S. R., Phosphonic Acids for Interfacial Engineering of Transparent Conductive Oxides. *Chemical Reviews* **2016**.

9. Pujari, S. P.; Scheres, L.; Marcelis, A. T. M.; Zuilhof, H., Covalent Surface Modification of Oxide Surfaces. *Angewandte Chemie International Edition* **2014,** *53* (25), 6322-6356.

10. Queffélec, C. m.; Petit, M.; Janvier, P.; Knight, D. A.; Bujoli, B., Surface modification using phosphonic acids and esters. *Chemical Reviews* **2012,** *112* (7), 3777-3807.

11. Kalek, M.; Ziadi, A.; Stawinski, J., Microwave-Assisted Palladium-Catalyzed Cross-Coupling of Aryl and Vinyl Halides with H-Phosphonate Diesters. *Organic Letters* **2008,** *10* (20), 4637-4640.

12. Gliboff, M.; Sang, L.; Knesting, K. M.; Schalnat, M. C.; Mudalige, A.; Ratcliff, E. L.; Li, H.; Sigdel, A. K.; Giordano, A. J.; Berry, J. J.; Nordlund, D.; Seidler, G. T.; Brédas, J.-L.; Marder, S. R.; Pemberton, J. E.; Ginger, D. S., Orientation of Phenylphosphonic Acid Self-Assembled Monolayers on a Transparent Conductive Oxide: A Combined NEXAFS, PM-IRRAS, and DFT Study. *Langmuir* **2013,** *29* (7), 2166-2174.

13. Hotchkiss, P.; Marder, S.; Giordano, A.; Anthopoulos, T. D., Electronic devices comprising novel phosphonic acid surface modifiers. Google Patents: 2014.

14. Sharma, A.; Hotchkiss, P. J.; Marder, S. R.; Kippelen, B., Tailoring the work function of indium tin oxide electrodes in electrophosphorescent organic light-emitting diodes. *Journal of Applied Physics* **2009,** *105* (8), 084507.

15. Guo, L.-H.; Facci, J. S.; McLendon, G., Distance dependence of electron transfer rates in bilayers of a ferrocene Langmuir-Blodgett monolayer and a self-assembled monolayer on gold. *The Journal of Physical Chemistry* **1995,** *99* (21), 8458-8461.

16. Koldemir, U.; Braid, J. L.; Morgenstern, A.; Eberhart, M.; Collins, R. T.; Olson, D. C.; Sellinger, A., Molecular Design for Tuning Work Functions of Transparent Conducting Electrodes. *The Journal of Physical Chemistry Letters* **2015,** *6* (12), 2269-2276.

17. Demmer, C. S.; Krogsgaard-Larsen, N.; Bunch, L., Review on modern advances of chemical methods for the introduction of a phosphonic acid group. *Chem Rev* **2011,** *111* (12), 7981-8006.

18. Diebold, U., The surface science of titanium dioxide. *Surface Science Reports* **2003,** *48* (5–8), 53-229.

19. Hoel, C. A.; Mason, T. O.; Gaillard, J.-F.; Poeppelmeier, K. R., Transparent Conducting Oxides in the ZnO-In2O3-SnO2 System. *Chemistry of Materials* **2010,** *22* (12), 3569-3579.

20. Leijtens, T.; Giovenzana, T.; Habisreutinger, S. N.; Tinkham, J. S.; Noel, N. K.; Kamino, B. A.; Sadoughi, G.; Sellinger, A.; Snaith, H. J., Hydrophobic Organic Hole Transporters for Improved Moisture Resistance in Metal Halide Perovskite Solar Cells. *ACS Applied Materials & Interfaces* **2016,** *8* (9), 5981-5989.

21. Braid, J. L.; Koldemir, U.; Sellinger, A.; Collins, R. T.; Furtak, T. E.; Olson, D. C., Conjugated Phosphonic Acid Modified Zinc Oxide Electron Transport Layers for Improved Performance in Organic Solar Cells. *ACS Applied Materials & Interfaces* **2014,** *6* (21), 19229-19234.

22. Wu, Y.; Liu, L.; Yan, K.; Xu, P.; Gao, Y.; Zhao, Y., Nickel-Catalyzed Decarboxylative C–P Cross-Coupling of Alkenyl Acids with P(O)H Compounds. *The Journal of Organic Chemistry* **2014,** *79* (17), 8118-8127.

23. Han, L.-B.; Zhang, C.; Yazawa, H.; Shimada, S., Efficient and Selective Nickel-Catalyzed Addition of H−P(O) and H−S Bonds to Alkynes. *Journal of the American Chemical Society* **2004,** *126* (16), 5080-5081.

24. Becker, H.; Spreitzer, H.; Kreuder, W.; Kluge, E.; Schenk, H.; Parker, I.; Cao, Y., Soluble PPVs with Enhanced Performance—A Mechanistic Approach. *Advanced Materials* **2000,** *12* (1), 42-48.

25. Xia, S.; Kwong, R.; Adamovich, V.; Weaver, M.; Brown, J. In *OLED Device Operational Lifetime: Insights and Challenges*, 2007 IEEE International Reliability Physics Symposium Proceedings. 45th Annual.

26. He, L.-Y., Bis(tri-tert-butylphosphine)palladium(0) [Pd(t-Bu3P)2]. *SYNLETT* **2015,** *26* (06), 851-852.

27. Littke, A. F.; Fu, G. C., A Versatile Catalyst for Heck Reactions of Aryl Chlorides and Aryl Bromides under Mild Conditions. *Journal of the American Chemical Society* **2001,** *123* (29), 6989-7000.

CHAPTER 4
SYNTHESIS AND CHARACTERIZATION OF PHOSPHONIC ACID FAMILIES FOR SURFACE MODIFICATION

4.1. Introduction

In this chapter we hypothesize that a phosphonic acid that includes a specific linker and functional head group will create a desired ligand dipole. In turn, deposition of these PAs on the surface of ITO will allow for a specific engineered energetic effect of the surface (i.e. work function modification ($\Delta\Phi$)). As described in Chapter 2, there are several synthetic pathways to prepare phosphonic acids, of which many utilize the dialkyl phosphonate as an intermediate. In addition, Chapter 3 described that the direct synthesis of phosphonic acids is also a viable route to prepare of a select number of these acids. This chapter will build upon these examples covered in the previous two and examine the preparation of these acids with more detail. This chapter will cover the synthesis of BPAs, PPAs, and VPAs with oF_2-, pCF_3-, pNO_2-, and pCN- head groups to create "families" of phosphonic acids with varying dipoles. From there we explore various methods of application of these acids onto ITO surfaces and the resultant work function modification. In addition, Density Functional Theory (DFT) is utilized to help calculate the gas phase dipole moments and HOMO energy orbitals, which assist in the prediction of work function modification. Finally, a study of the surface monolayers with polarization modulation infrared absorption reflection spectroscopy (PM-IRRAS) to assist in the interpretation of the mixed and unexpected results of the surface modification and work function experiments will be described.

The anchor of this chapter is distilled down to one element, phosphorus, which is an incredibly versatile and complex element. Phosphorus has an ability to form a variety of covalent bonds, transition metal complexes, salts, and most importantly for this dissertation, organophosphorus compounds. Much of the interesting chemistry comes from its ability to tap into d orbitals and oxidation states that range from -3 to +5. As shown in Figure 4.1 (Page 46), phosphorus is usually found in it's tri- (+3) or pentavalent (+5) state.[1] Specifically, the phosphine oxide species, has back donation of vacant d orbitals that overlap with oxygen lone pairs to form

a 2pπ-3dπ bond, which is shown in the following sections, and can be highly exploited in organic synthetic chemistry.[2]

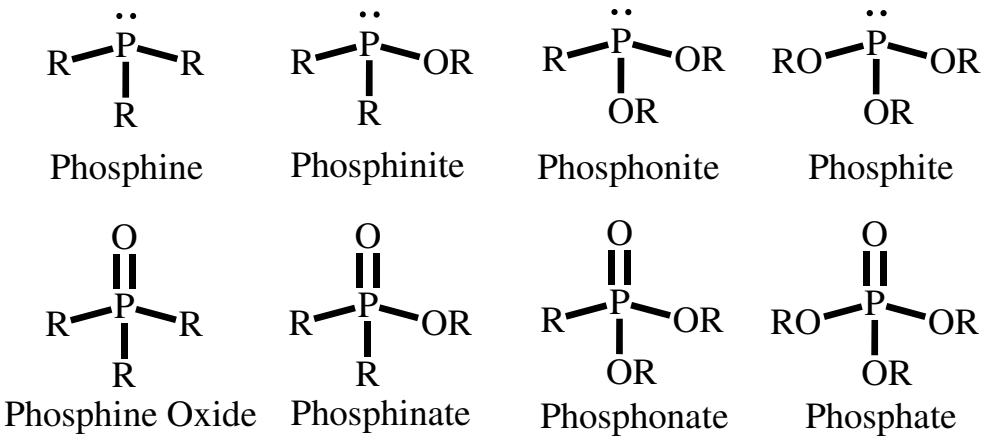

Figure 4.1 Organophosphorus in its many forms (R = H, C, halide, or ion).

4.2. General Synthetic Techniques of Phosphonic Acids

4.2.1. VPA Production

As described in the previous two chapters, VPAs are very difficult to synthesize. Specifically, the comprehensive discussion of this topic in Chapter 2 reveals a number of conditions and reactions to produce VPAs. Heck coupling was the primary focus for this dissertation mainly for the mild conditions and high yield of products. The following is a brief review of the Heck mechanism however, much more in-depth reviews and seminal publications of the reaction can be found in the literature.[3-7].

4.2.1.1. The Heck Mechanism

Shown in Scheme 4.1 (Page 47), this mechanism can be broken down into five simple steps: preactivation, oxidative addition, insertion, elimination, and reductive elimination.

First is preactivation, which is a requirement for entry of the catalyst into the cycle. This step requires Pd to first be in a Pd (0) oxidative state. Due to the reactivity of the Pd (0) with water and O_2, these catalysts are generally commercially available in a much more stable Pd(II) form and must be reduced to Pd (0) in order to proceed. The primary reducing agents are generally phosphine compounds, although reductions with hydroxide, alkoxide, acetate, and even

water have been reported.[8-11] These reducing agents are generally added stoichiometrically at two equivalents to the Pd(II) catalyst. Specifically in phosphine systems, the selection of phosphine agents can highly affect the activity of the catalyst and should be carefully considered.[4]

Second is oxidative addition, which is a concerted process in which the R-X bond breaking is simultaneously synchronized with the formation of the Pd-R and Pd-X bonds, or the insertion of the Pd between the R-X bond. This step is generally less sensitive to the substituents attached to the carbon side of the bond, but is highly sensitive to the R-X and Pd-X bond strength and nature of the nucleofuge, which generally the order of reactivity follows Cl < Br < OTf < I.

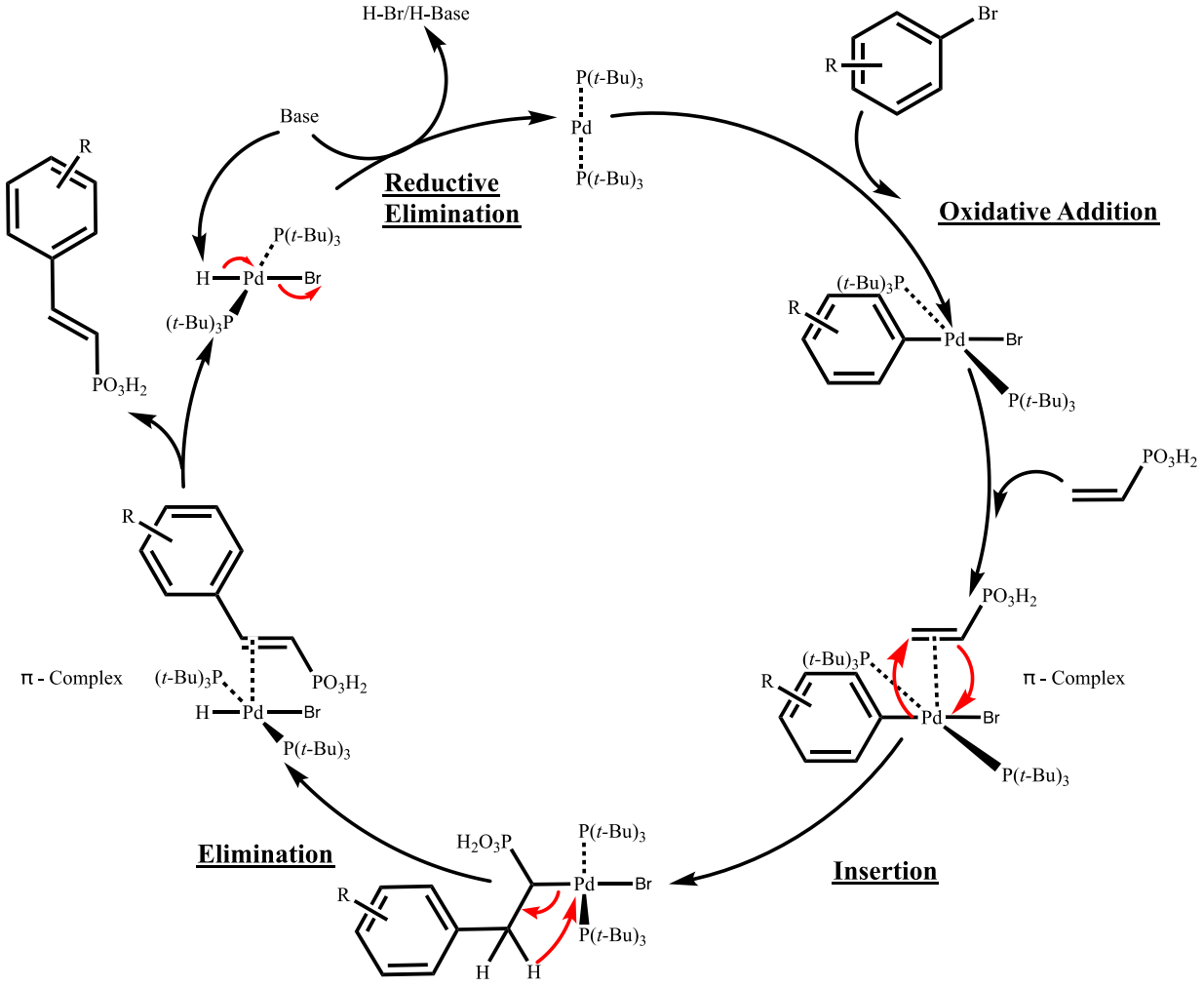

Scheme 4.1 Heck mechanism of vinyl phosphonic acid coupling

The third step is insertion, which is the product-forming step of the catalytic cycle where the first C-C bond is formed. The specific mechanism for this interaction is highly disputed, in which those specifics are outside the scope of this this dissertation.[4] Nonetheless, there is a general alignment and coordination of the C=C alkene bonds with the Pd center and a C-C bond formation with the transfer of C=C alkene carbon to Pd-R, forming the Pd-C-C-R intermediate.

Fourth is elimination where the Pd-H releases the newly formed (*E*) C=C product through the mechanism of a hydride shift with the breaking of the Pd-C bond and transfer to form the C=C bond.

The fifth and last step is reductive elimination, which proceeds after the elimination the newly formed alkene bond is still coordinated to the Pd-H, the product liberation occurs as the base scavenges the proton from HBr (to form $R_3NH^+Br^-$) in order to regenerate the Pd (0) catalyst. This regenerated catalyst is now free to continue the catalytic cycle over and over again.

4.2.2. BPA Production

BPAs can be produced through a number of different mechanisms. This section discusses mainly the Michaelis-Arbuzov reaction, but will also cover methods for thermal, UV, and catalytic synthesis. It should also be pointed out that the catalyst free microwave conditions below are a "green" reaction as a result of the triethyl phosphite being both the solvent of the aryl halide and a reactant.

4.2.2.1. The Michaelis-Arbuzov Reaction

As briefly introduced in Chapter 2, the most well-known P-C bond forming reaction is the Michaelis-Arbuzov reaction (hereon referred to as the Arbuzov reaction). The Arbuzov reaction mechanism can be broken down into two S_N2 steps. Step 1, (Scheme 4.2 step 1, Page 48) the first S_N2 reaction where the lone pair of the phosphorus attacks a carbon with a good leaving group (predominantly halides), generating an intermediate quasi-phosphonium salt. Step 2, (Scheme 4.2 step 2, Page 48) the second S_N2 reaction where the previously displaced anion attacks the carbon bound to the oxygen attached to the positively charged phosphorus. This results in breaking of the O-C bond and the transfer of electrons to form the P=O double bond resulting in the phosphoryl group and by-product alkyl halide.[12]

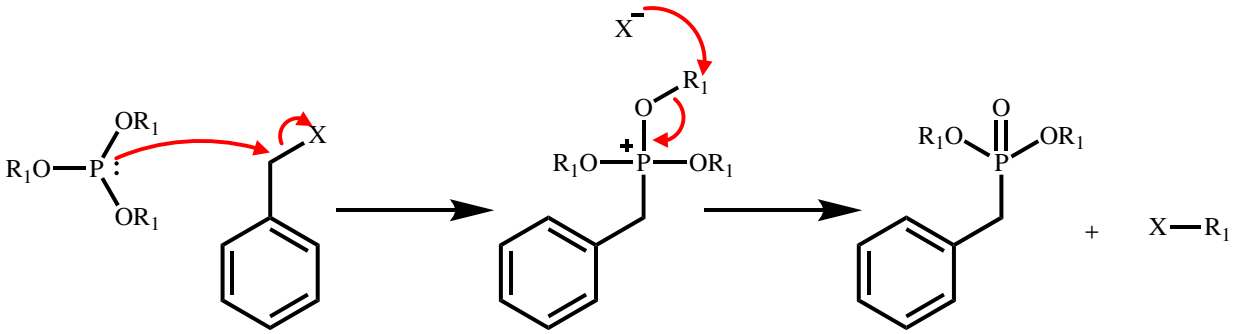

Scheme 4.2 Arbusov Reaction Mechanism to produce BPAs

It is important to note that the resultant by-product alkyl halide can now act as a competing participant in this reaction. To avoid this side product formation two approaches exist: first, removal of the alkyl halide by-product in a process such as evaporation, and second, using an excess of the trivalent phosphite to stoichiometrically quench the competing reaction. Heating near reflux is generally sufficient to provide the activation energy needed to initiate the reaction. These reaction temperatures also promote the escape of the more volatile alkyl halide, thus removing it from the reaction. In addition, these conditions can also be considered "green" as it can be performed "neat", in which the excess trivalent phosphite is also utilized as the solvent for the system. This reaction can also be successfully carried out under microwave heating, which reduces the reaction time from several hours to only a few minutes.[13-14]

4.2.2.2. BPA Synthesis

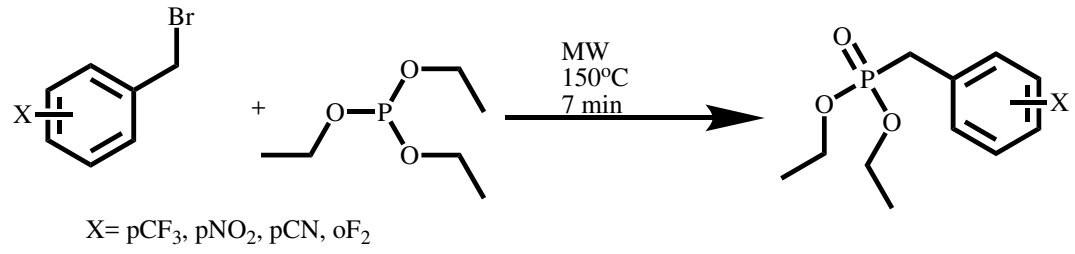

Scheme 4.3 Microwave assisted Arbusov reaction and hydrolysis to produce BPAs

For this study, and as illustrated in Scheme 4.3, the BPA precursors were all prepared via microwave activated Arbusov reaction generally yielding 90% or higher of the desired diethyl

benzyl phosphonate. The only side product detected was the triethyl ethyl phosphate, which was easily removed via flash chromatography in a gradient of hexanes to ethyl acetate. The product was then concentrated under rotary evaporation, and the acid product was produced by utilizing the hydrolysis procedure discussed in Chapter 1. This mechanism is discussed in further detail in Section 4.2.6, and the specific characterization of these products is found in Section 4.3.3.

4.2.3. PPA Production

As shown above, the Arbusov reactions are a very simple yet powerful way to create phosphonates in "neat" reaction conditions. However, when the initial S_N2 pathway is not available, alternative methods utilizing other activation pathways or transition metal catalysts must be employed. Specifically, in synthesizing PPAs, alternative methods must be used due to the steric hindrance of the aryl ring. The following sub-sections will cover the photo-initiated Arbusov reaction and Hirao cross coupling to produce the diethyl phenyl phosphonates that are discussed and characterized Section 4.3.4

4.2.3.1. Photo initiated Arbuzov Reaction

Substituted aryl halide rings contain a number of groups that cause steric hindrance and block the initial S_n2 Arbusov reaction step. In order to utilize fluoro-iodo-benzene precursors in an Arbusov reaction, an alternative activation energy such as UV light is required. In a "neat" solution of trialkyl phosphate and an aryl-iodide, under the presence of UV light, the aryl-iodide can dissociate to form two species, an aryl radical and an iodide radical (Scheme 4.4, step 1, Page 51). The trialkyl phosphite can then trap the aryl radical to form the radical-neutral phosphorus intermediate (Scheme 4.4 step 2, Page 51). Next, the radical phosphorus is converted to a quasi phosphonium salt by the single-electron transfer to the iodide radical (Scheme 4.4, step 3, Page 51). Then, a similar S_N2 reaction as seen in the Arbusov reaction occurs (Scheme 4.2, Page 49), where the previously displaced anion attacks the carbon bound to the oxygen attached to the positively charged phosphorus (Scheme 4.4 step 4, Page 51). This results in the breaking of the C-O bond and the transfer of electrons to form the P=O double bond, resulting in the phosphoryl group and alkyl halide (Scheme 4.4, step 4, Page 51).[15-16]

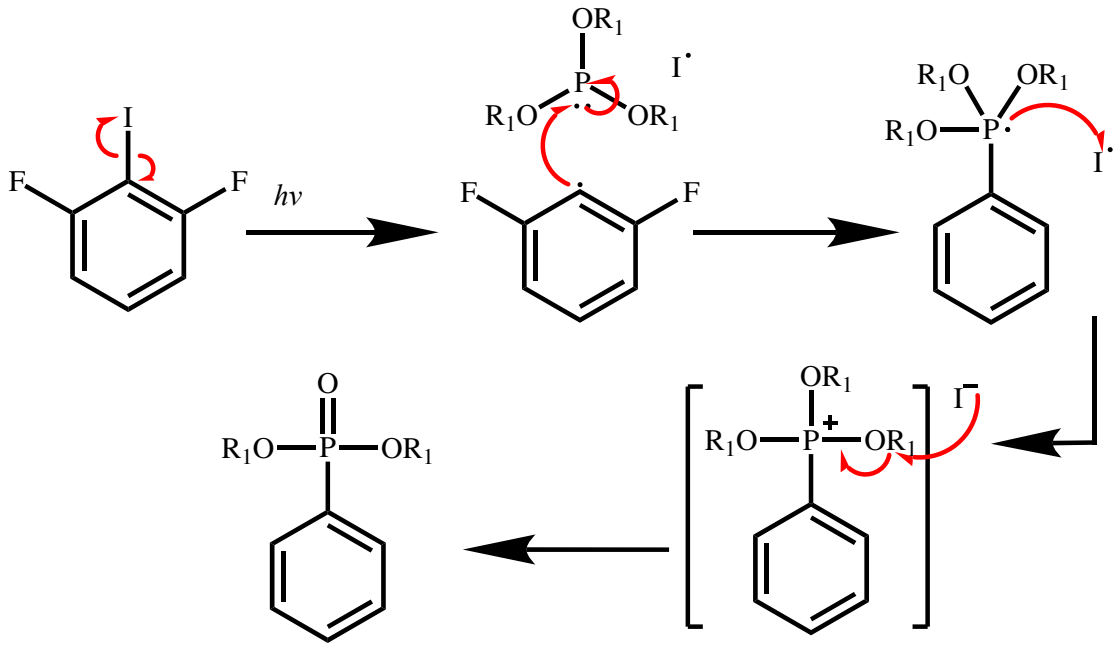

Scheme 4.4 Photo initiated Arbusov reaction mechanism to produce PPAs

4.2.3.2. Hirao Coupling

The use of Pd catalyst for the formation of aryl C-P bonds was first published by Hirao et al in the early 1980's.[17] This catalytic mechanism is nearly analogous to the Heck mechanism in Scheme 4.1 (Page 47). The Pd catalyst undergoes similar oxidative additions with aryl halides to give an aryl-Pd-halide complex. The one difference in the Hirao coupling is that instead of insertion of an alkene, we observe the P=O π complex of a dialkylphosphite to this newly formed aryl-Pd-halide complex, which then leads to the aryl phosphonate. The catalyst is then regenerated by the amine base, which can then repeat the catalytic cycle (Scheme 4.5).[13, 18-19]

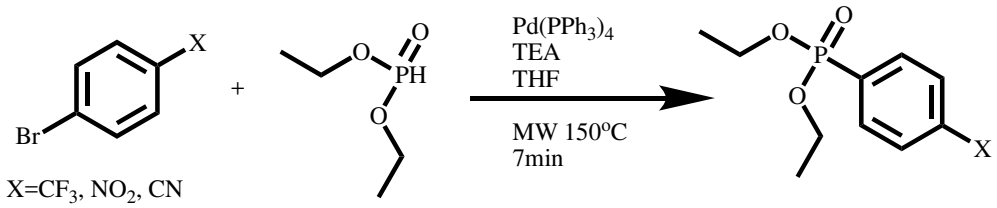

Scheme 4.5 Hirao Cross Coupling

This reaction can also be further optimized by the use of microwave heating. Yields in the c.a. 80% for formation of aryl phosphonates were reported by Villemin et. al[13], and were successfully recreated for this study, these conditions are listed in Section 4.3.4 (Page 51).

4.2.4. Hydrolysis of Phosphonates to Phosphonic Acids

Once the desired phosphonate ester has been synthesized it must undergo hydrolysis to the phosphonic acid, as briefly discussed in Chapter 1, which is the best form to be utilized for surface modification. The most common and simple route to obtain these acids is through acid catalyzed de-alkylation. As illustrated in Scheme 4.6, refluxing the phosphonate in concentrated inorganic acids (6M or higher) for 2 - 12 hours is generally sufficient to hydrolyze the ester to the acid. Cooling or removal of the water and inorganic acid under rotary evaporation is sufficient to precipitate the acid, which can then be isolated via filtration. A number of sources reported that sensitive functional groups may be damaged by strong acids, however we found that groups such as nitro- and cyano- are robust enough to withstand these conditions with only a slight degradation of yield.

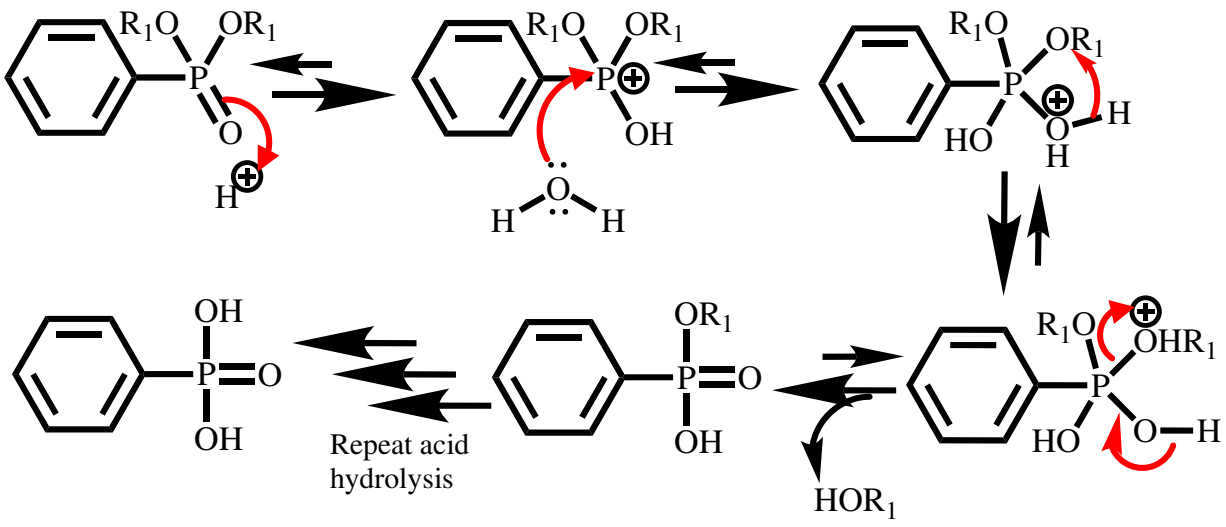

Scheme 4.6 Mechanism of Acid Catalyzed Hydrolysis of Phosphonic ester

As reported by Hotchkiss et. al, a milder approach for hydrolysis utilizes trimethyl silyl halides (TMS-X).[20] The mechanism for TMS hydrolysis is an S_N2 process that is very similar to the Arbusov reaction covered in Section 4.4.1. The TMS hydrolysis reaction starts with the

phosphoryl oxygen attack on the silicon, displacing the halogen (Scheme 4.7 step 1). Next, the halogen ion through S_N2 attacks one of the alkoxy groups, creating the intermediate TMS-phosphonate compound (Scheme 4.7 step 2). These last two steps are then repeated to form the bis-(TMS) phosphonate (Scheme 4.7 Step 3 multi arrow). Next, is the quenching of the reaction with ethanol and water, which has a two-part outcome. First, upon contact with water and methanol or ethanol, the TMS readily undergoes hydrolysis to the respective acid (Scheme 4.7 lower). Second, the excess TMS-X readily reacts with water and is deactivated.

The order of reactivity for TMS-X is dependent of the halogen (e.g. I > Br > Cl,), TMS-I, while it is commercially available, is so highly reactive it is best used by generation in-situ. Much less reactive TMS-Br is easier to work with however it must be stored under cold and inert atmosphere. Finally, TMS-Cl is lab shelf stable, and while it is significantly less reactive still can be used to convert phosphonates although needs long periods of time and elevated temperature and pressure.

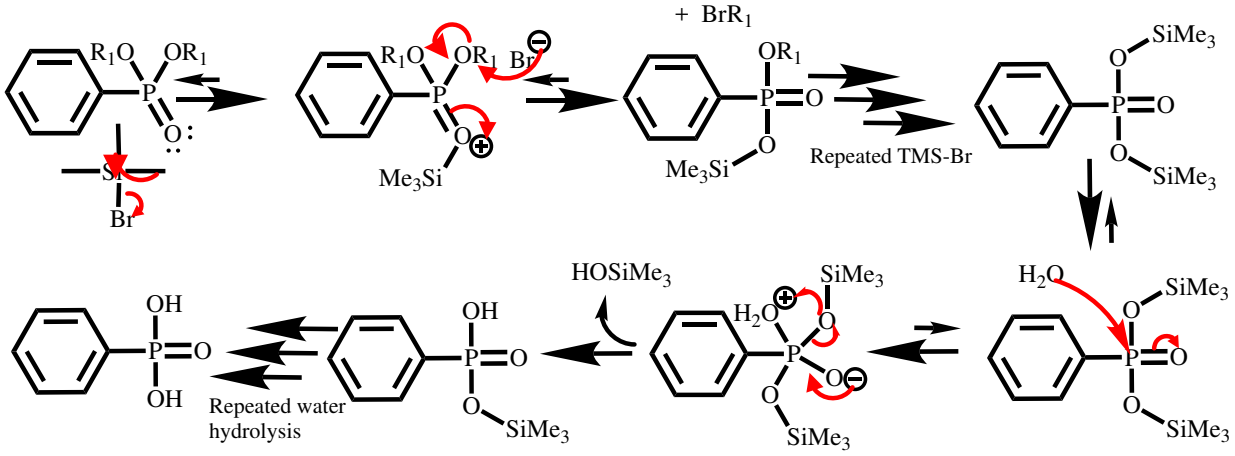

Scheme 4.7 TMS-Br Hydrolysis of Phosphonic Esters

Within our lab successful results were obtained by the addition of stoichiometric amounts of KI, allowing for the formation of TMS-I in-situ, greatly increasing the reactivity and decreasing the reaction time from days to only a few hours. TMS-Br also was successfully utilized, both with and without KI at 80°C.

4.3. Phosphonic Acid and Surface Modification Experimental

4.3.1. Experimental Methods

All chemicals were used as received without further purification unless noted. Acetonitrile (ACN, ACS) dichloromethane (DCM, ACS), anhydrous tetrahydrofuran (THF, ≥99.9%), N,N-dicyclohexylmethylamine (NCy_2Me, 97%), anhydrous magnesium sulfate ($MgSO_4$), triethylphosphine, 4-bromobenzonitrile (99%), 4-(bromomethyl) benzonitrile, diethyl vinyl phosphonate were obtained from Sigma Aldrich. Sodium hydroxide (NaOH, Pearl 97%) was obtained from Fisher Scientific. Bis(tri-tert-butylphosphine) palladium ($Pd[P(t\text{-}Bu)_3]_2$, 98%) was obtained from Strem Chemical. Vinyl phosphonic acid (95%) was obtained from TCI chemicals. Hydrochloric acid (HCl, ACS) was obtained from Macron Fine Chemicals. 2,6-Difluoroiodobenzene, (98%), 1-bromo-4-nitrobenzene (95+%), (4-nitrobezyl) bromide, 2,6-difluorobenzyl bromide, 4-(trifluoromethyl) benzyl bromide were obtained from Matrix scientific. All glassware was base, acid, and water washed then oven dried. ^{1}H. ^{13}C, ^{19}F, and ^{31}P NMR, spectra were obtained on a JEOL ECA 500 liquid-state NMR spectrometer and data obtained was manipulated in MestReNova NMR processor software.

4.3.2. Vinyl Phosphonic Acid synthesis

A Schlenk flask equipped with a magnetic stir bar under argon was charged with the aromatic halide, diethyl vinyl phosphonate, N,N-dicyclohexylmethylamine, $Pd[P(t\text{-}Bu)_3]_2$ (catalyst used at 1 mol % level), and THF or ACN. The mixture was heated to 70°C for 24 h and periodically tested via TLC for reaction completion. The crude product mixture was extracted three times with DCM and acidic water (5% HCl). The organic layer was dried with $MgSO_4$, filtered, and the solvent removed using a rotary evaporator. The resultant crude product was then further purified by flash chromatography and excess was solvent removed using a rotary evaporator. The ester precursor was then converted to VPA by refluxing overnight in 12M HCl. The VPA precipitated from solution upon cooling and then the pure acid product was collected by filtration and washing with DI water. All products were checked for purity and characterized via 1H NMR, and ^{13}C NMR, and for novel compounds ^{31}P NMR and for fluorine products ^{19}F NMR, these spectra can be found in Appendix A.

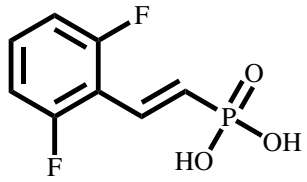

oF$_2$VPA

Synthesis and characterization for this molecule can be found in Chapter 3 and NMR spectra in Appendix A.

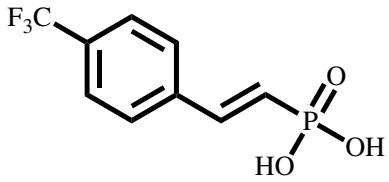

CF$_3$VPA

Synthesis and characterization for this molecule can be found in Chapter 3 and NMR spectra in Appendix A.

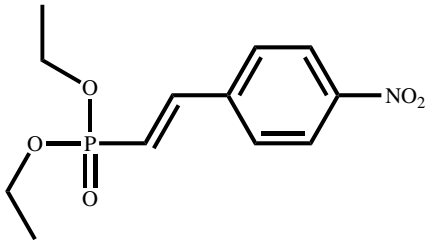

NO$_2$VPE - diethyl (*E*)-(4-nitrostyryl) phosphonate

Diethyl (E)-(4-nitrostyryl) phosphonate utilized 1-bromo-4-nitrobenzene, 95+% and followed the general synthesis above, resulting in a light yellow oil. This compound has been previously synthesized and reported[21] and the ^{1}H NMR characterization matches appropriately. The following NMR spectra are located in Appendix A.

^{1}H NMR (500 MHz, DMSO-d_6) δ 8.20 (d, J = 9.6 Hz, 2H), 7.95 (d, J = 9.0 Hz, 2H), 7.52 – 7.40 (m, 1H), 6.85 (t, J = 16.0 Hz, 1H), 4.01 (q, J = 9.1, 7.6 Hz, 4H), 1.23 (s, 6H).

^{13}C NMR (126 MHz, DMSO-D_6) δ 148.49, 145.45, 145.40, 141.61, 141.42, 129.59, 124.43, 121.45, 119.98, 62.04, 40.04, 16.79.

^{31}P NMR (202 MHz, DMSO-D_6) δ 19.83.

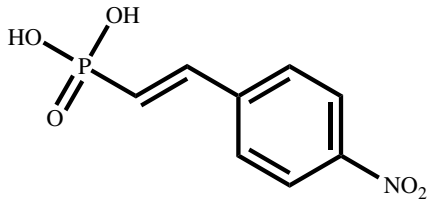

NO_2VPA - (*E*)-(4-nitrostyryl) phosphonic acid

(*E*)-(4-Nitrostyryl) phosphonic acid followed the general hydrolysis above yielding white needle like crystals that turned pink upon further drying. To our knowledge this is a novel compound and the following NMR spectra are located in Appendix A.

^{1}H NMR (500 MHz, DMSO-d_6) δ 10.87 (s, 2H), 8.16 (d, $^{3}J_{HH}$ = 9.0 Hz, 2H), 7.85 (d, $^{3}J_{HH}$=9.0 Hz, 2H), 7.26 (dd, $^{3}J_{HH}$=17.5 Hz, $^{3}J_{HP}$=21.6Hz 1H), 6.75 (dd, $^{3}J_{HH}$ 17.5 Hz, $^{2}J_{HP}$ 15.5 Hz)

^{13}C NMR (126 MHz, DMSO-D_6) δ 148.03, 142.42-142.24 (d, $^{4}J_{C\text{-}P}$=22.4 1C) 141.03, 129.03 (2C), 127.00-125.57(d, $^{1}J_{C\text{-}P}$=180Hz, 1C), 124.44 (2C).

^{31}P NMR (202 MHz, DMSO-D_6) δ 12.57(dd, $^{2}J_{PH}$=15.5 Hz, $^{3}J_{PH}$=21.6 Hz)

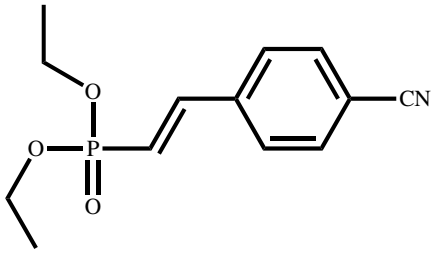

CNVPE - diethyl (*E*)-(4-cyanostyryl) phosphonate

Diethyl (*E*)-(4-cyanostyryl) phosphonate, utilized 4-bromobenzonitrile and followed the general synthesis above, resulting in a light yellow oil. This compound has been previously synthesized and reported[21] and the ^{1}H NMR characterization matches appropriately. The following NMR spectra are located in Appendix A.

^{1}H NMR (500 MHz, DMSO-d_6) δ 7.85 (q, J = 8.5 Hz, 4H), 7.41 (dd, J = 22.5, 17.5 Hz, 1H), 6.80 (dd, J = 17.3 Hz, 1H), 3.99 (dt, J = 14.8, 7.2 Hz, 4H), 1.21 (t, J = 7.0 Hz, 6H).

^{13}C NMR (126 MHz, DMSO-d_6) δ 146.02 (d, J = 6.8 Hz), 139.63 (d, J = 24.0 Hz), 133.23, 129.15, 120.47, 119.05 (d, J = 10.2 Hz), 112.69, 62.00 (d, J = 5.5 Hz), 16.72 (d, J = 6.3 Hz).

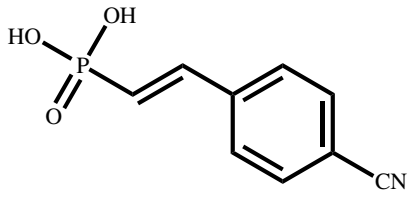

CNVPA - (*E*)-(4-cyanostyryl) phosphonic acid

(*E*)-(4-Cyanostyryl) phosphonic acid followed the general hydrolysis above yielding a white powder. To our knowledge this is a novel compound. The following NMR spectra are located in Appendix A.

^{1}H NMR (500 MHz, DMSO-d_6) δ 9.88 (s, 2H), 8.15 (d, $^{3}J_{HH}$= 8.5 Hz, 2H), 7.85 (d, $^{3}J_{HH}$= 8.5 Hz, 2H), 7.26 (dd, $^{3}J_{HP}$= 21.5, $^{3}J_{HH}$17.5 Hz, 1H), 6.74 (dd, $^{3}J_{HH}$= 17.5, $^{2}J_{HP}$=15.9 Hz, 1H).

^{13}C NMR (126 MHz, DMSO-D_6) δ 148.02, δ 142.33 (d, $^{3}J_{CP}$ = 23.2 Hz, 1C), 141.03, 140.98, 129.03(2C), 126.28 (d, $^{2}J_{CP}$= 180.3 Hz, 1C), 124.44 (2C).

4.3.3. Benzyl Phosphonic Acid Synthesis

BPE were all prepared via microwave activated Arbuzov reaction (Scheme 4.2, Page 49) according to reference [14], where benzyl bromide (0.025 mol) and triethylphosphine (0.025 mol) were sealed in a Biotage 20 mL microwave vial with a magnetic stir bar. The reaction was then microwaved with active cooling at 150°C for 7 minutes. The crude was then purified via flash chromatography with hexanes eluting at 40-60% EA generally yielding < 90% of the desired diethyl benzyl phosphate. The acid form was obtained by refluxing the purified diethyl benzyl phosphate in excess concentrated HCl (12M) for 4-24 hours. The benzyl phosphonic acid precipitated upon cooling and was collected under vacuum filtration.

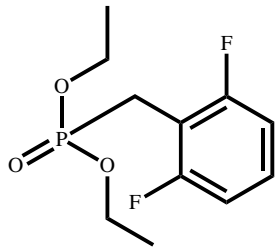

oF$_2$BPE - diethyl (2,6-difluorobenzyl) phosphonate

Diethyl (2,6-difluorobenzyl) phosphonate utilized 2,6-difluorobenzyl bromide and followed the general BPE synthesis above, resulting in a clear liquid product with a 91% yield. The product was confirmed via GCMS and sufficiently pure to proceeded to the next step of hydrolysis.

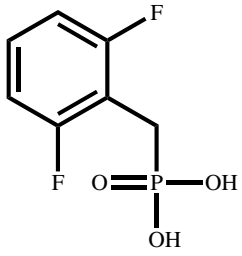

oF$_2$BPA - (2,6-difluorobenzyl) phosphonic acid

(2,6-Difluorobenzyl) phosphonic acid followed the hydrolysis procedure above with a quantitative yield of a white powder after 12 hours of reflux. The following NMR spectra are located in Appendix A.

^{1}H NMR (500 MHz, DMSO-d_6) δ 7.31 - 7.22 (m, 1H), 7.01 (t, J = 8.9 Hz, 2H), 2.94 (d, J = 21.0 Hz, 2H).

^{13}C NMR (126 MHz, DMSO-d_6) δ 162.30 (dd, J = 8.6, 5.7 Hz), 160.33 (dd, J = 8.4, 5.5 Hz), 128.80 (td, J = 10.2, 3.7 Hz), 111.72 (ddd, J = 20.2, 5.9, 3.4 Hz), 111.10 (td, J = 20.2, 9.7 Hz), 23.55 (d, J = 134.6 Hz).

^{31}P NMR (202 MHz, DMSO-D_6) δ 19.15.

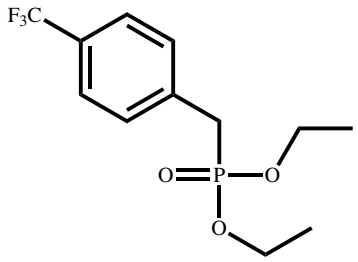

CF_3BPE - diethyl (4-(trifluoromethyl)benzyl) phosphonate

Diethyl (4-(trifluoromethyl) benzyl) phosphonate utilized 4-(trifluoromethyl) benzyl bromide and followed the general BPE synthesis above, resulting in a clear liquid product with a 90% yield. The product was confirmed via GCMS and sufficiently pure to proceeded to the next step of hydrolysis.

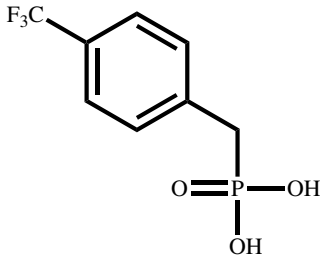

CF_3BPA (4-(trifluoromethyl)benzyl) phosphonic acid

(4-(trifluoromethyl) benzyl) phosphonic acid followed the hydrolysis procedure above with a quantitative yield of a white powder after 12 hours of reflux. The following NMR spectra are located in Appendix A.

^{1}H NMR (500 MHz, DMSO-d_6) δ 7.60 (d, J = 8.1 Hz, 2H), 7.42 (d, J = 6.7 Hz, 2H), 3.04 (d, J = 21.6 Hz, 2H).

^{13}C NMR (126 MHz, DMSO-d_6) δ 140.09, 130.99 (d, J = 6.0 Hz), 125.33 (p, J = 3.9 Hz), 35.90 (d, J = 130.3 Hz). ^{31}P NMR (202 MHz, DMSO-D_6) δ 20.58.

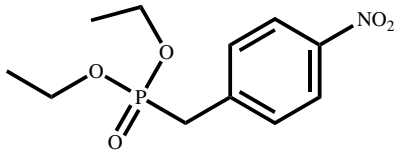

NO_2BPE - diethyl (4-nitrobenzyl) phosphonate

Diethyl (4-nitrobenzyl) phosphonate utilized (4-nitrobezyl) bromide and followed the general BPE synthesis above, resulting in a clear liquid product with a 95% yield. The following NMR spectra are located in Appendix A.

^{1}H NMR (500 MHz, DMSO-d_6) δ 8.14 (d, J = 8.1 Hz, 2H), 7.52 (dd, J = 8.6, 1.8 Hz, 2H), 3.96 - 3.91 (m, 4H), 3.42 (d, J = 22.3 Hz, 2H), 1.13 (d, J = 12.9 Hz, 6H).

^{13}C NMR (126 MHz, DMSO-D_6) δ 146.80, 146.77, 141.57, 141.50, 131.53, 123.81, 123.78, 63.60, 63.55, 62.18, 62.12, 61.30, 61.25, 40.02, 33.31, 32.26, 16.40.

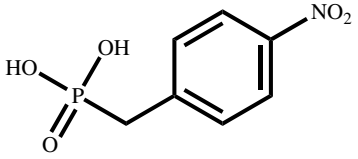

NO_2BPA - (4-nitrobenzyl) phosphonic acid

(4-Nitrobenzyl) phosphonic acid followed the hydrolysis procedure above with a quantitative yield after 4 hours of reflux. The following NMR spectrum is located in Appendix A.

^{1}H NMR (500 MHz, DMSO-d_6) δ 8.12 (d, J = 9.0 Hz, 2H), 7.51 - 7.44 (m, 2H), 3.11 (d, J = 22.1 Hz, 2H).

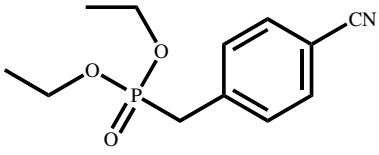

CNBPE - diethyl (4-cyanobenzyl) phosphonate

Diethyl (4-cyanobenzyl) phosphonate utilized 4-(Bromomethyl) benzonitrile and followed the general BPE synthesis above, resulting in a clear liquid product with a 96% yield. The following NMR spectra are located in Appendix A.

^{1}H NMR (500 MHz, DMSO-d_6) δ 7.75 (s, 2H), 7.44 (dd, J = 8.3, 2.3 Hz, 2H), 3.99 - 3.86 (m, 5H), 3.32 (s, 2H), 1.12 (t, J = 7.1 Hz, 6H).

^{13}C NMR (126 MHz, DMSO-D_6) δ 139.28, 139.21, 132.60, 131.33, 131.28, 119.35, 119.33, 109.90, 63.61, 63.56, 62.12, 62.07, 61.31, 61.26, 40.03, 33.51, 32.45, 16.68, 16.63, 6.97, 6.91.

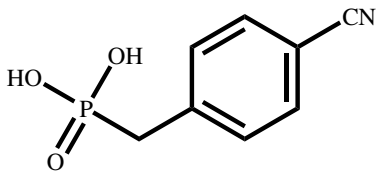

CNBPA (4-cyanobenzyl) phosphonic acid

(4-cyanobenzyl) phosphonic acid followed the hydrolysis procedure above with a quantitative yield after 24 hours of reflux. The following NMR spectra are located in Appendix A.

^{1}H NMR (500 MHz, DMSO-d_6) δ 8.12 (d, J = 9.0 Hz, 2H), 7.51 - 7.44 (m, 2H), 3.11 (d, J = 22.1 Hz, 2H).

^{13}C NMR (126 MHz, DMSO-D_6) δ 146.80, 146.77, 141.57, 141.50, 131.53, 123.81, 123.78, 62.18, 62.12, 40.02, 33.31, 32.26, 16.67, 16.62.

4.3.4. Phenyl Phosphonic Acid Synthesis

PPE synthesis - A Schlenk flask under argon and equipped with a magnetic stir bar was charged with the aromatic halide (0.01 mol), diethyl phosphonate (0.01 mol), triethyl amine, and $Pd(PPh_3)_4$ (catalyst used at 1 mol % level), and 25 ml THF. The mixture was heated to 65°C for 24 h and periodically tested via TLC for reaction completion. The crude product mixture was extracted three times with DCM and acidic water (5% HCl). The organic layer was then dried with $MgSO_4$, filtered, and the solvent removed using a rotary evaporator. The resultant crude product was then further purified by flash chromatography and excess was solvent removed using a rotary evaporator. The phenyl phosphonic acid was obtained by refluxing the purified diethyl phenyl phosphonate in excess concentrated HCl (12M) for 12-24 hours. The benzyl phosphonic acid precipitated upon cooling and was collected under vacuum filtration.

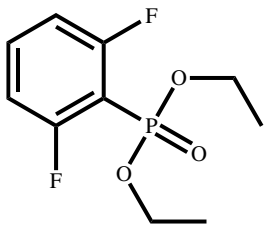

oF$_2$PPE diethyl (2,6-difluorophenyl) phosphonate

(2,6-Difluorophenyl) phosphonate required a unique synthesis, where the photo initiated abusive reaction was used (Scheme 4.4, Page 51). Here triethylphosphine (0.0175 mol) and 2,6-difluoroiodobenzene (0.0175) were mixed together and degassed then put into a sealed quartz cuvette and placed on top of a 256 nm hand lamp then encased in mirrors for 48 hours. This process was repeated 4 times, the crude products were combined and the volatiles were removed under rotary evaporation. The condensed crude was then purified with flash chromatography affording a clear liquid product (1.02 g, 5% yield). The procedure described by references [15-16, 22] call for the utilization of a photo-reactor and has a much greater reaction yield of 40 - 75%. The product was confirmed via GCMS and sufficiently pure to proceeded to the next step of hydrolysis.

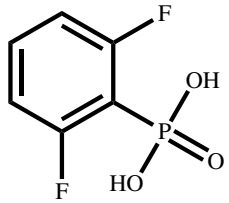

$_O$F$_2$PPA - (2,6-difluorophenyl) phosphonic acid

(2,6-Difluorophenyl) phosphonic acid followed the hydrolysis procedure above with the only change that upon cooling the product did not precipitate. In order to collect the product, the water and HCl were removed under rotary evaporation leading to a quantitative yield of a white solid, which was found to be sufficiently pure. The following NMR spectra are located in Appendix A.

^{1}H NMR (500 MHz, DMSO-d_6) δ 11.32 (s, 2H), 7.53 (t, J = 7.8 Hz, 1H), 7.05 (tot, J = 8.4, 3.9 Hz, 2H).^{13}C NMR (126 MHz, DMSO-D_6) δ 163.99, 161.99, 134.46, 112.73, 112.56, 112.04, 110.66, 39.95.

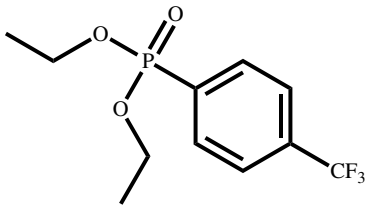

CF_3PPE - diethyl (4-(trifluoromethyl)phenyl) phosphonate

Diethyl (4-(trifluoromethyl) phenyl) phosphonate utilized 4-bromo benzotrifluoride and followed the general PPE synthesis above, resulting in a clear liquid product with a 95% yield. The following NMR spectrum is located in Appendix A.

^{1}H NMR (500 MHz, DMSO-d_6) δ 7.95 - 7.82 (m, 4H), 4.07 - 3.96 (m, 4H), 1.19 (t, J = 7.0 Hz, 6H).

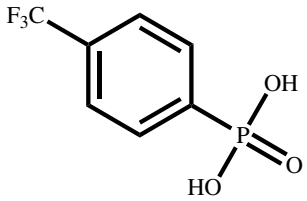

CF_3PPA - (4-(trifluoromethyl)phenyl) phosphonic acid

(4-(Trifluoromethyl) phenyl) phosphonic acid followed the hydrolysis procedure above with a quantitative yield of a white powder after 12 hours of reflux. The following NMR spectra are located in Appendix A.

^{1}H NMR (500 MHz, DMSO-d_6) δ 7.79 (dd, J = 12.4, 7.9 Hz, 2H), 7.69 (d, J = 6.3 Hz, 2H).

^{31}P NMR (202 MHz, DMSO-D_6) δ 10.25.

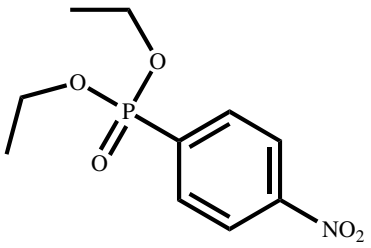

NO_2PPE - diethyl (4-nitrophenyl) phosphonate

Diethyl (4-nitrophenyl) phosphonate utilized 1-Bromo-4-nitrobenzene and followed the general PPE synthesis above, resulting in a clear liquid product with a 92% yield. The following NMR spectrum is located in Appendix A.

^{1}H NMR (500 MHz, DMSO-d_6) δ 8.40 - 8.29 (m, 2H), 8.07 - 7.91 (m, 2H), 4.07 (dt, J = 15.3, 7.6 Hz, 4H), 1.31 - 1.22 (m, 6H).

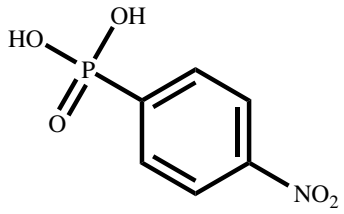

NO_2PPA - (4-nitrophenyl) phosphonic

(4-Nitrophenyl) phosphonic acid followed the hydrolysis procedure above with a quantitative yield after 12 hours of reflux. The following NMR spectra are located in Appendix A.

^{1}H NMR (500 MHz, DMSO-d_6) δ 8.12 (s, 1H), 7.48 (s, 1H).

^{13}C NMR (126 MHz, DMSO-D_6) δ 146.48, 143.65, 131.47, 123.64, 40.01.

^{31}P NMR (202 MHz, DMSO-D_6) δ 19.83.

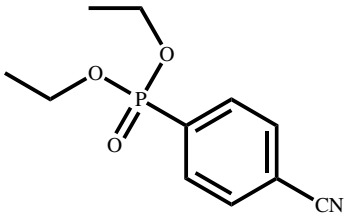

CNPPE - diethyl (4-cyanophenyl) phosphonate

Diethyl (4-cyanophenyl) phosphonate utilized 4-bromo benzonitrile and followed the general PPE synthesis above, resulting in a clear liquid product with a 90% yield. The following NMR spectra are located in Appendix A.

^{1}H NMR (500 MHz, DMSO-d_6) δ 7.93 (d, J = 23.0 Hz, 2H), 7.79 (d, J = 12.1 Hz, 2H), 3.97 (d, J = 12.1 Hz, 4H), 1.24 - 1.10 (m, 6H).

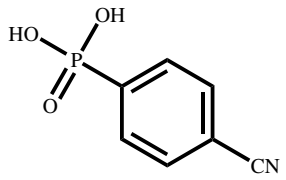

CNPPA - (4-cyanophenyl) phosphonic acid

(4-Cyanophenyl) phosphonic acid followed the hydrolysis procedure above with a quantitative yield after 12 hours of reflux. The following NMR spectrum is located in Appendix A.

^{1}H NMR (500 MHz, DMSO-d_6) δ 10.49 (s, 2H), 7.97 (d, J = 10.6 Hz, 2H), 7.79 - 7.71 (m, 2H).

4.3.5. ITO Preparation and Kelvin Probe Measurements.

Glass/ITO substrate are cleaned and prepared by first being cut to 1" squares then scrubbed with Micro-90 detergent then given a deionized water rinse. Then the substrate was sonicated in acetone and then isopropanol for 15 min each, followed by 5 min in a 100 °C oven and 15 min in a UV-ozone cleaner (Jelight Company, Inc.). PA films were either spun, soaked or T-BAG coated then annealed at 150 C rinsed and annealed again. A KPTechnology SKP/SVP/LE 450 system is utilized for Kelvin probe measurements of the work function and calibrated with Al and Au reference samples in air. All work function measurements are then calculated as change (ΔΦ) from the ITO control.

4.3.6. DFT Dipole Calculations

The DFT z-dipole computations for the BPAs, PPAs and VPAs, were done using Amsterdam Density Functional Package (ADF) version 2016.107 and Microsoft Excel 2013. All calculations were done in accordance with reference[23-24] conformational analysis using the RDFKit, followed by geometry optimization using the LDA:DZP functional-basis, followed by single point using a hybrid 80% B3LYP 20% HF with a TZP basis. The only modifications that were made were only the lowest 10 conformers were geometry optimized, the lowest 5 geometries were analyzed via single point, and a straight average dipole moment of the 5 single points was then calculated. These changes were made in the interest of computational time and

possibility of non-uniform global ground state configuration. The average values of these calculations are located in Table 4.2 (Page 70).

4.3.7. Polarization Modulated Infrared Reflection Absorbance Spectroscopy (PM-IRRAS)

A Nicolet 6700 FTIR spectrometer coupled to a tabletop optical module was used to collect PM-IRRAS data. Polarization modulation is provided by Hinds instruments PM-90 Modulator with a ZnSe 50 kHz optical head. The optical signal was obtained with a MCT-A detector. PM-IRRAS data was collected using an incident angle of 81.5° with respect to the surface normal with an average of 800 scans with 4 cm^{-1} resolution and a maximum de-phasing at 1500 cm^{-1}. Reference spectra were acquired on a "wet blank" ITO sample that was identically cleaned and placed in methanol for the same duration of the TBAG period.

4.4. Results and Discussion

4.4.1. Dipole and HOMO Analysis

As shown in Figure 4.6 (Page 71) and Table 4.1 (Page 67), we observe an increase in dipole with increased conjugation from BPAs to PPAs. However, with these more precise calculations performed by Joshua T. Koubek we observe general stagnation (if not reduction) in dipole strength as we compare the PPAs to VPAs. In light of this, when we compare the HOMO orbitals we can see that for all the vinyl species (Figures 4.2-4.5 left, Pages 67-69) orbital density does extend down into the phosphorus atom from the vinyl bond. Additionally, these VPAs show a larger presence of HOMO orbital density on the oxygen atoms, which would support the hypothesis of Braid et. al where they examined the conjugation linkage effects on device efficiencies.[25] The exception to this correlation is shown in Figure 4.5 middle (Page 70), where the CNPPA does show HOMO orbital overlap into phosphorus. LUMO and Dipole direction projections were also calculated for all of the acids in this study and those illustrations can be found in Appendix D.

Table 4.1 Calculated molecular dipole (μ_{mol}) and dipole along the P-C bond (μ_z)

Acid	μ_{mol} (D)	μ_z (D)
NO_2BPA	1.7646	-1.42
NO_2PPA	1.632	-3.63
NO_2VPA	1.6784	-3.58
CNBPA	1.933	-1.72
CNPPA	1.5782	-3.44
CNVPA	1.484	-3.29
CF_3BPA	0.7422	1.22
CF_3PPA	1.0508	-1.72
CF_3VPA	0.7988	-1.36
oF_2BPA	1.1858	1.03
oF_2PPA	2.048	4.94
oF_2VPA	1.3832	3.02

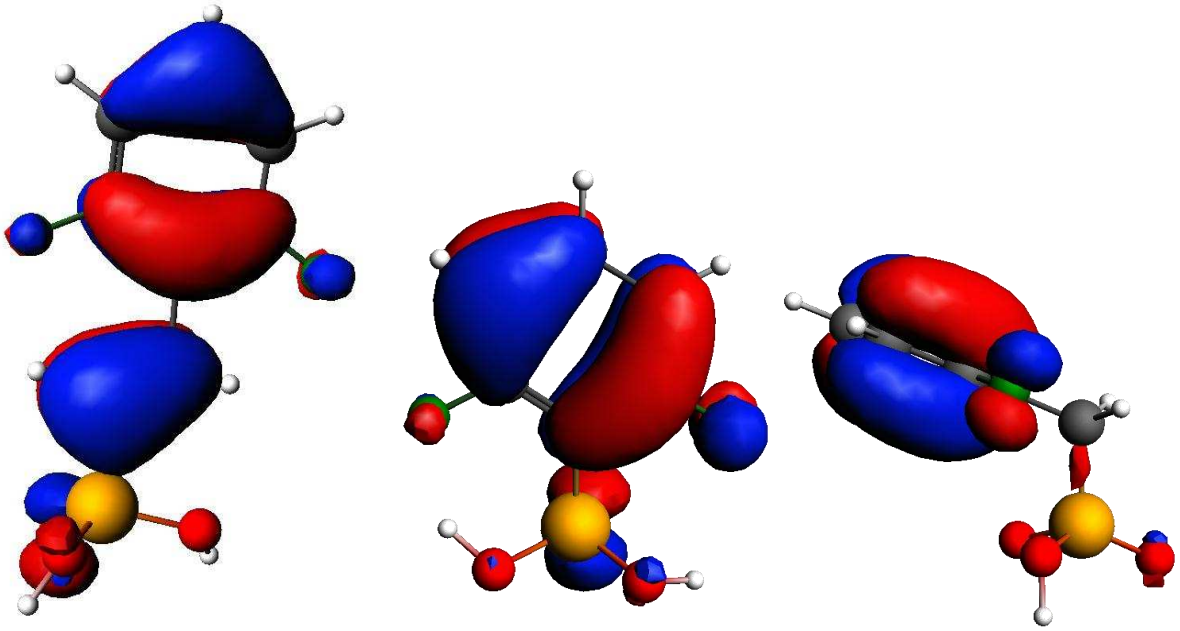

Figure 4.2 HOMO Orbitals of oF_2VPA (left), oF_2PPA (middle), and oF_2BPA

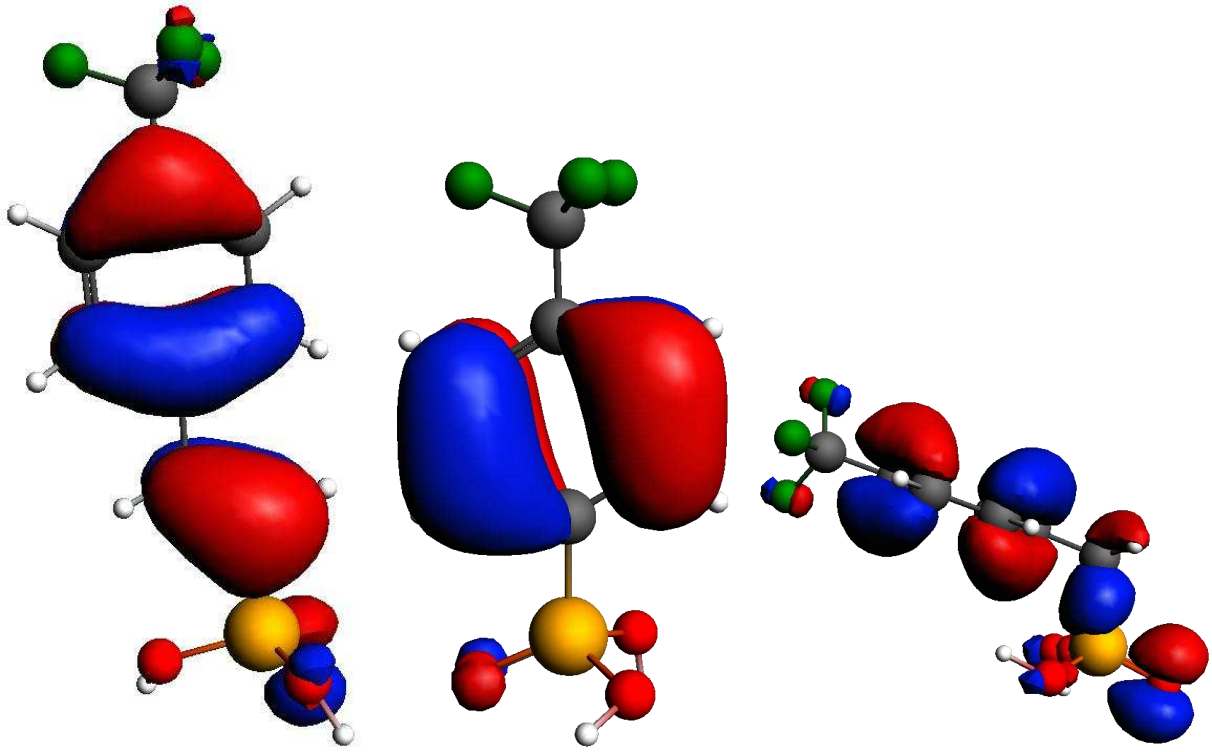

Figure 4.3 HOMO Orbitals of CF_3VPA (left), CF_3PPA (middle), and CF_3BPA (right).

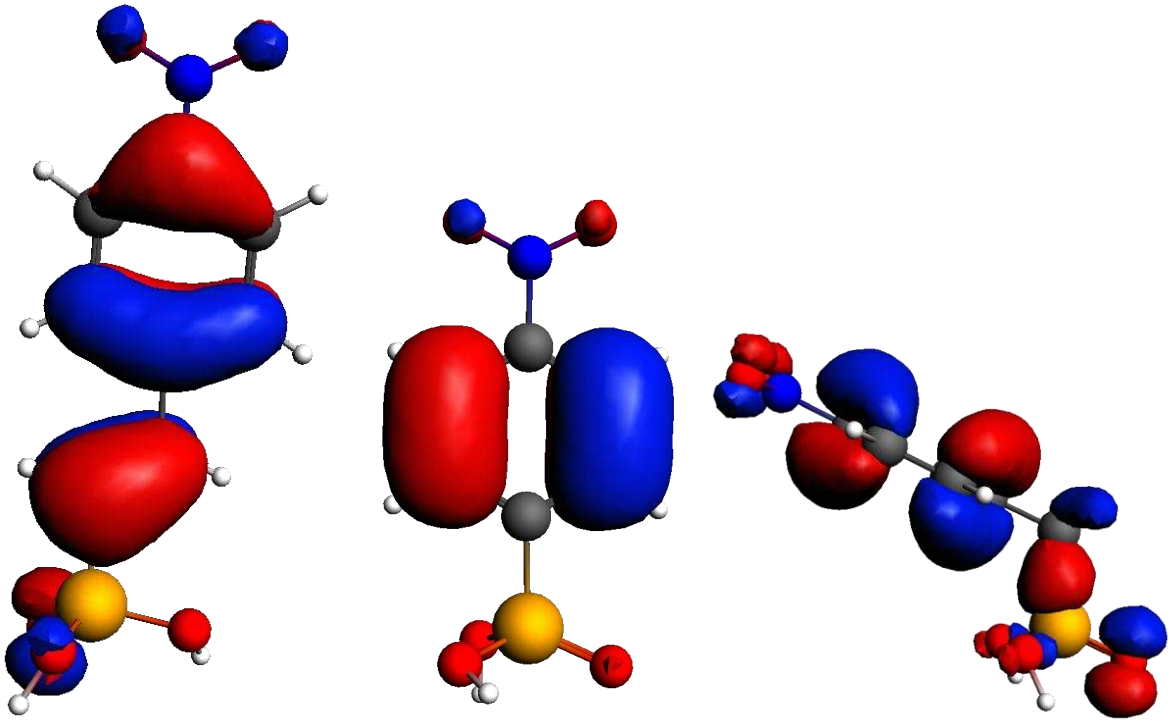

Figure 4.4 HOMO Orbitals of NO_2VPA (left), NO_2PPA (middle), and NO_2BPA (right).

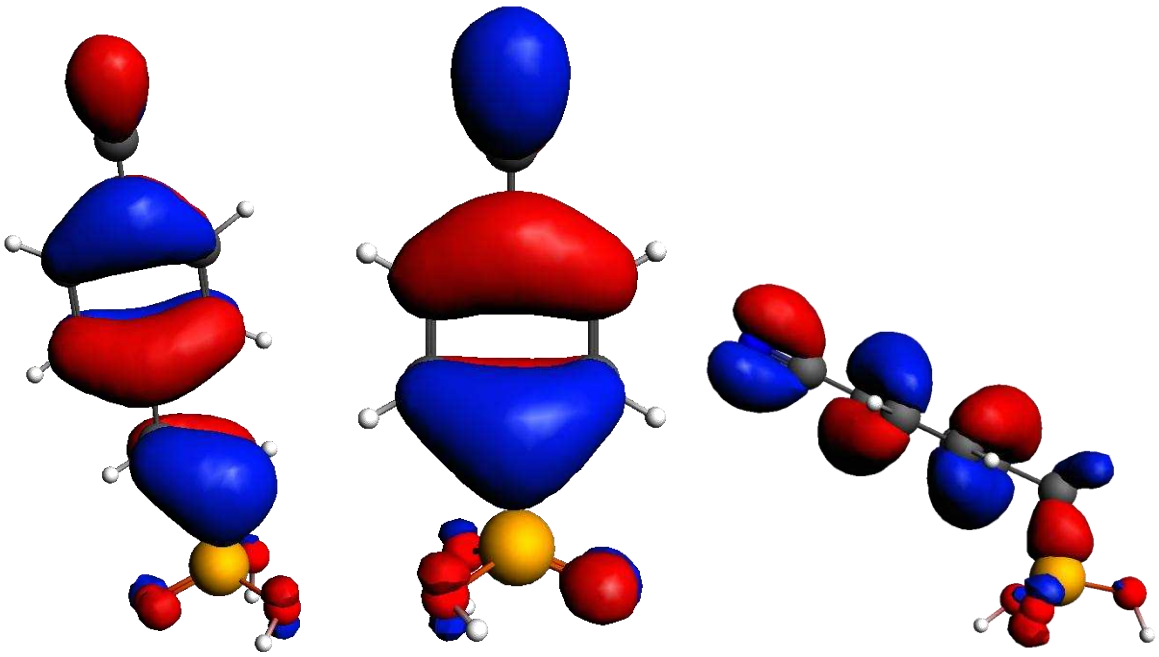

Figure 4.5 HOMO Orbitals of CNVPA (left), CNPPA (middle), and CNBPA (right).

4.4.1.1. Phosphonic Acid Work Function Change (ΔΦ) on ITO

For this surface modification study 1" x 1" ITO substrates were subjected to three different monolayer deposition techniques. Generally, the acid was deposited, annealed at 150°C for 15 minutes, rinsed with a stream of methanol, annealed at 150°C for another 15 min, and then the samples were measured under the kelvin probe. The first sets of samples were subjected to an 84-hour soak. The cleaned ITO was soaked in a 10mmol solution of methanol and phosphonic acid. The total contact time, suggested by Paniaguia et. al, of over 72 hours would be sufficient to form a uniform monolayer on the surface of the metal oxide.[26] The results are shown in Figure 4.6 (red bars, Page 71). We were unable to recreate the same ΔΦ for CF_3VPA, oF_2BPA, and oF_2VPA reported by Braid et. al, which was defined to be our experimental reference control.[27] In addition the unknown component of this study, CNVPA, and NO_2VPA had insignificant ΔΦ (Figure 4.2 red bars Page 71).

Our second surface deposition technique was spin coating, where 6-10 drops of 10 mmol solution were dropped onto the ITO surface while spinning at 6000RPM then spun for 60 seconds. The resulting samples were then rinsed and annealed as described above, and measured for ΔΦ. This process was repeated in accordance to Braid et. al, and we did find similar results in

regard to ΔΦ, of CF_3VPA, oF_2BPA and oF_2VPA[25]. However, the unknown component of this study, CNVPA, and NO_2VPA had insignificant ΔΦ (Figure 4.6 green bars Page 71).

Our third and final surface deposition technique was TBAG (as discussed in Chapter 2), where the ITO samples were vertically positioned in 10mmol solutions and then placed in a fume hood where the solvent was allowed to evaporate over 6 days. Interestingly, during this process, the phosphonic acids crystalized in sheets on only the ITO surface, not the SiO_2 side of the sample. Once all the solvent had evaporated the samples were rinsed and annealed according to the procedure above and measured for ΔΦ. In accordance to Braid et. al, we found similar results in regard to ΔΦ, of CF_3VPA, oF_2BPA and oF_2VPA[25]. Again, the unknown component of this study, CNVPA, and NO_2VPA had insignificant ΔΦ (Figure 4.6 purple bars Page 71). We also found it interesting that oF_2PPA had the strongest μ_z however, it's ΔΦ was measured to be completely opposite of all the predicted trends and outcomes of this experiment.

Acid	Dipole (D)	Soak	Standard deviation	Spin	Standard deviation	TBAG	Standard deviation
		ΔΦ eV	ΔΦ eV	ΔΦ eV	ΔΦ eV	ΔΦ eV	ΔΦ eV
NO_2BPA	-1.42	0.069	0.005	-0.089	0.004	-0.202	0.003
NO_2PPA	-3.63	-0.149	0.003	-0.150	0.005	0.036	0.004
NO_2VPA	-3.58	-0.185	0.004	-0.061	0.005	-0.236	0.002
CNBPA	-1.72	0.019	0.004	0.069	0.005	0.194	0.003
CNPPA	-3.44	0.092	0.005	0.031	0.005	-0.251	0.003
CNVPA	-3.29	-0.159	0.004	-0.256	0.005	-0.009	0.003
CF_3BPA	1.22	-0.663	0.005	-0.581	0.004	-0.844	0.003
CF_3PPA	-1.72	-0.624	0.005	-0.206	0.005	0.033	0.004
CF_3VPA	-1.36	-0.627	0.005	-0.663	0.003	-0.902	0.004
oF_2BPA	1.03	0.131	0.004	0.964	0.005	0.989	0.003
oF_2PPA	4.94	0.205	0.003	-0.680	0.004	-0.676	0.002
oF_2VPA	3.02	0.500	0.005	1.469	0.004	1.142	0.003

Table 4.2 Values of calculated dipole of selected acids, and ΔΦ eV on ITO using soak coating, spin coating, and TBAG.

We hypothesized the lack of CNVPA and NO_2VPA ΔΦ had two possible reasons; First, as the strength of the dipole increases and a greater negative charge is put onto the phosphorus, the weaker the conjugate base, and the weaker the binding group directly leading to a less stable and uniform monolayer. Second, the increased dipole strength allows for an inverted stacking effect where one acid molecule binds to the surface, and the strength of its dipole overcomes the strength of the interaction of the acid group to the surface, repelling this incoming molecule and

attracting another to align its dipole opposite of its own (with the acid group sticking "up"), effectively negating the effect of di-polarity on the surface and eliminating the effect on ΔΦ.

Testing of hypothesis one was accomplished in two different ways. First we attempted three techniques for creating a more ordered monolayer. Attempted first, dip soaking allows for random assortment of acids to bind to the surface, in a non-organized way, which resulted in unsuccessfully modifying the surface. Attempted second, spin casting is better at forcing a random monolayer or multilayer to the surface than dip soaking, but does not force uniform surface coverage, uniform binding, and promotes random multilayers. Finally, TBAG allows for some more uniform monolayer formation than dip or spin casting because more uniformity and alignment of the layer is generated as the solvent evaporates it is expected that the molecules aggregate at the solvent, air, ITO interface. We found that the spin coating and TBAG methods for the positive control groups of CF_3VPA, oF_2BPA, and oF_2VPA were sufficient.[25]

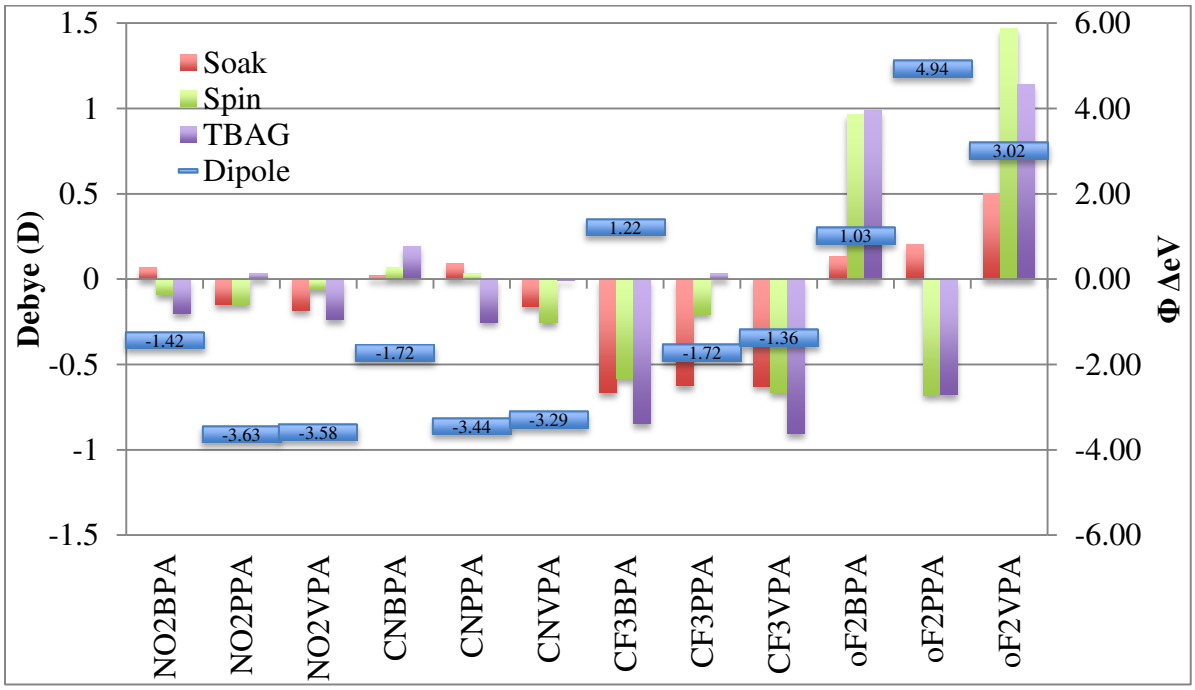

Figure 4.6 Surface modification experiments measured work function values with calculated μ_z dipoles

However, it cannot be determined if the unbound acids or inverted acids of the second hypothesis are contributing to this effect or if we simply did not form a monolayer. In order to

differentiate this, we need a powerful spectroscopic technique- PM-IRRAS, which is discussed in detail in section 4.4.2 below.

4.4.2. PM-IRRAS Measurements

Analyzing ITO PM-IRRAS data provides significant advantages over just IR or even an IRRAS system. PM-IRRAS measurements probe only the specific orientation of bonds associated with IR excitation of specific molecular vibrational modes normal to the plane of reflection.[28] The polarization modulation can eliminate the signals from ambient conditions (i.e. water and CO_2) and increase signal from poorly reflective surfaces (i.e. ITO). This provides a spectra with higher resolution and better signal to noise ratio than what is capable from other systems. However, if a monolayer of these acids is oriented on the surface such that the transition dipole is parallel to the surface, the molecules will not be detected. In general, PM-IRRAS is highly sensitive at detecting monolayers of adsorbed species because most monolayers will have some fraction of the transition dipole moment projected normal to the surface. For this experiment each family of phosphonic acids were probed with PM-IRRAS to determine if the PAs formed a detectable layer on the surface of ITO, this data is located below in Figures 4.7 - 4.10.

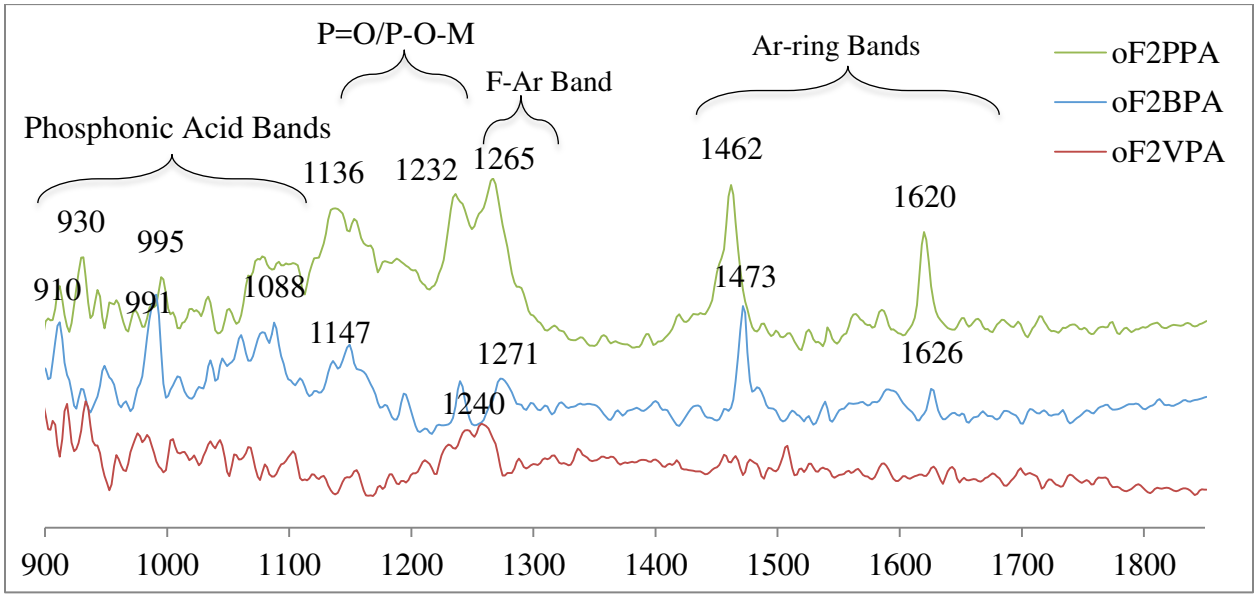

Figure 4.7 PM IRRAS spectra of TBAG oF_2 phosphonic acid family on ITO

As illustrated in Figure 4.7, the oF_2 family spectra show a number of bands for the oF_2PPA and oF_2BPA, however with oF_2VPA only one band at 1240 cm^{-1} is potentially detected. While we did measure the largest ΔΦ with oF_2VPA and can safely say a monolayer is present, we suspect two factors for this result; First, the strength of the oF_2VPA acid may be strong enough to have etched and altered the surface of ITO, potentially rendering the surface less reflective and making these acids bound to the surface much more difficult to observe. Second, because the polarization modulation only probes the orientation of bonds associated with IR excitation of specific molecular vibrational modes in the plane of radiation, a randomly dispersed layer of acids may be present. Nonetheless, for oF_2PPA and oF_2BPA we see phosphonic acid (P-O-H) bands assigned to the ca 930-1000 cm^{-1} region, and P=O/P-O-M bands attributed to the ca. 1140 cm^{-1} and 1230 cm^{-1} regions respectively. [29-30] While broad, the P-O-M band at 1240 cm^{-1} for oF_2VPA is present, however the signal to noise ratio for this sample is poor and additional samples and experiments are required to get a better idea of specific binding and monolayer characteristics. This data supports the second hypothesis, since we do observe both a ΔΦ and IR signals from all the oF_2 family, we can safely assert that monolayers of acids are bound to the surface of ITO.

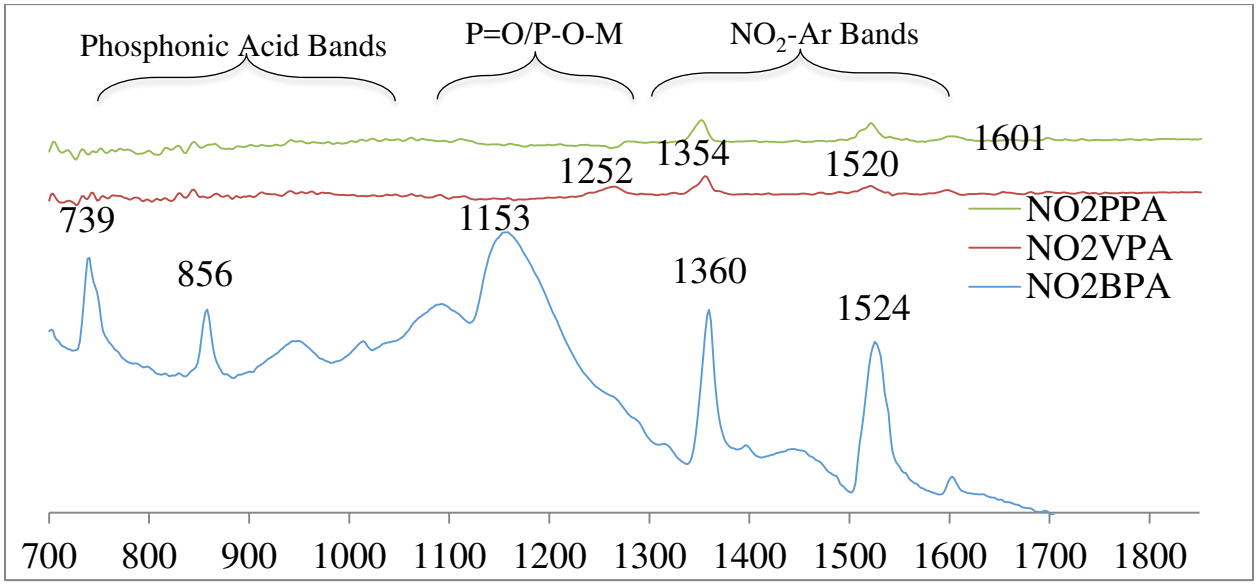

Figure 4.8 PM IRRAS spectra of TBAG NO_2 phosphonic acid family on ITO

For the NO_2 family, (Figure 4.8 below) we observe that bands at ca.1355 and 1520 cm^{-1} are assigned to aromatic NO_2- stretches,[31] and while subtle, the aromatic ring bending bands can

also be observed as minor peaks in that region also. For NO_2PPA, no other bands are discernable, suggesting that we have a layer of ligands on the surface, but little more. In the NO_2VPA spectrum, a small band at 1052 cm^{-1} is assigned as a P-O-M, indicating a monolayer is bound to the surface, but not much more information is apparent from this spectrum. The spectra of NO_2BPA shows a very strong P-O-H band at 856 cm^{-1}, a strong P-C band at 739 cm^{-1}, and in comparison to the large P=O band at1153 cm^{-1} suggests that a distribution of unbound acids are present.[32] This potentially leads to supporting the second hypothesis that inverted stacking is present and the phosphonic acid is strongly absorbing IR in conjunction to the NO_2-neighboring groups of the monolayer.

In Figure 4.9 we observe that both CNVPA and CNPPA show multiple absorption peaks. For CNBPA the lack of IR signal and no measurable ΔΦ suggest the possibility that no acids were bound to the surface. This would support the hypothesis that the weaker conjugate base is a poor binding group. It is also possible that the surface was etched and its reflective nature was degraded, rendering this spectroscopic technique impractical. However, to further explore this we performed a contact angle measurement on these substrates and found that the surface hydrophobicity was altered from the native ITO, suggesting that and layer of CN- acids are present on the surface of the modified ITO.

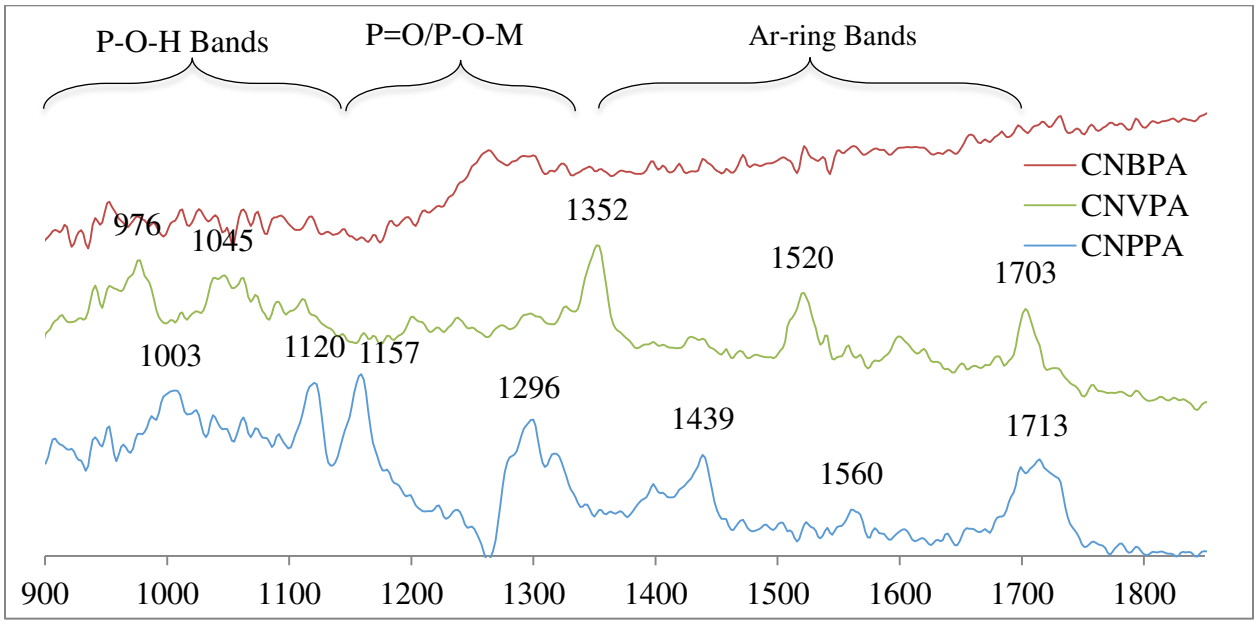

Figure 4.9 PM IRRAS spectra of TBAG CN phosphonic acid family on ITO

In Figure 4.10 (Page 76), the most apparent peak can be attributed to the Ar-CF_3 bands at 1336 and 1263 cm^{-1}.[31] In addition, a well-defined peak at 1070 cm^{-1} correlates to an asymmetric PO^{-2} band. For PPA, the ratio of this band in comparison to the P=O/P-O-M suggest that we can observe a strong bidentate binding of this acid to the surface of ITO.[33]

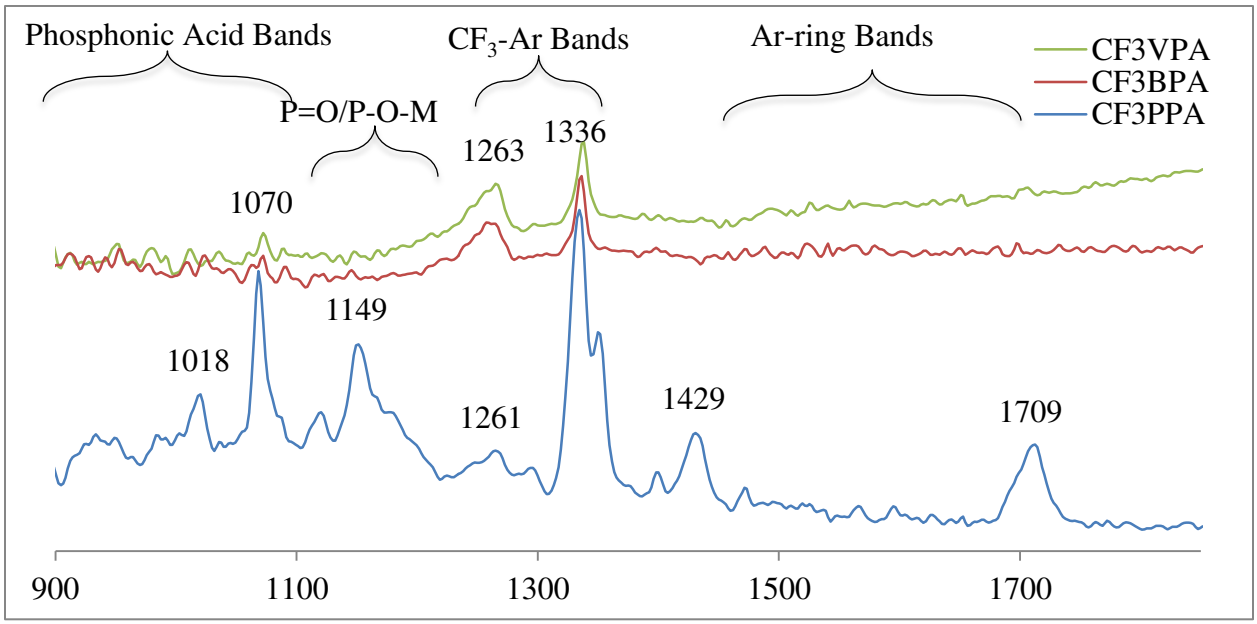

Figure 4.10 PM IRRAS spectra of TBAG CF_3 phosphonic acid family on ITO

4.5. Conclusions and Future Direction

BPA, PPA, and VPA phosphonic acid synthetic techniques for forming C-P bonds or C-C bonds and subsequent deposition techniques of these acids on ITO have been discussed. The most common and simplest method for production of phosphonic acids is the Arbuzov reaction. However, other important mechanisms were discussed, specifically Pd catalyzed Heck or Hirao coupling. The hydrolysis of these esters into their acid form was also a topic that carries a considerable consequence on the final purity of the desired acid. While utilization of chloro- or bromo- trimethylsilane to form the intermediate bis (trimethylsilyl) phosphonates is a milder approach, significant issues arise when trying to purify some of these products. Refluxing in concentrated HCl has been the hydrolysis method of choice for the phosphonic acid synthesis in this chapter and most of the compounds throughout future and previous chapters.

As many of these phosphonic acids are not commercially available, we needed to design and development efficient synthetic pathways for their production. For this study we hypothesized the ability to tailor make an acid that includes a specific linker and functional group would create a desired ligand dipole and allow for a specific engineered energetic effect on a modified surface. In total, 10 phosphonic esters and 12 phosphonic acids were synthesized in this study. The CN- and NO_2- VPA are believed to be novel compounds, interestingly in their synthesis, which against common synthetic organic practice, survived the hydrolysis in refluxing HCl.[34] This phenomenon was also observed in both the BPA and PPA variants, this is an interesting point and has a potential for a deeper fundamental computational and organic synthetic research project of the survival of these aromatic groups in the given conditions.

The gas phase dipole moments of these 12 acids were computed to determine if there is a correlating trend with increased conjugation, HOMO orbital overlap increase, and dipole increase. We observed that the functional group on the aromatic ring moiety and its ability to pull or donate election density with or against the phosphonic acid moiety can greatly change the HOMO orbitals and dipole. In the case of strong withdrawing ligands (i.e., NO_2, CN) in this study we observed in a few compounds that the increased electronegative strengths overpower the phosphonic acid and a trendless mixed batch of outcomes with the dipoles.

These results were even more diverse when comparing molecular dipole to the $\Delta\Phi$ of ITO. While our control groups of oF_2VPA and oF_2BPA matched previous studies for $\Delta\Phi$ on ITO, we found we were unable to consistently predict how $\Delta\Phi$ would correlate with other acids. We were able to observe through PM-IRRAS that we did successfully bind acids to the surface of ITO. However, due to a phenomenon that is not yet known at this time, we could not connect molecular dipole to $\Delta\Phi$ of all of the phosphonic acids in this study. Future directions for this work are further discussed in Chapter 7 of this dissertation.

4.6. References Cited

1. Emsley, J.; Hall, D., *The chemistry of phosphorus: environmental, organic, inorganic, biochemical, and spectroscopic aspects*. Wiley: 1976.

2. Corbridge, D. E. C., *Phosphorus: an outline of its chemistry, biochemistry, and uses*. Elsevier: 1995.

3. Heck, R. F.; Nolley, J. P., Palladium-catalyzed vinylic hydrogen substitution reactions with aryl, benzyl, and styryl halides. *The Journal of Organic Chemistry* **1972,** *37* (14), 2320-2322.

4. Beletskaya, I. P.; Cheprakov, A. V., The Heck Reaction as a Sharpening Stone of Palladium Catalysis. *Chemical Reviews* **2000,** *100* (8), 3009-3066.

5. Prakash, G. K.; Jog, P. V.; Krishnan, H. S.; Olah, G. A., A domino approach (hydrolysis/dehydrohalogenation/Heck coupling) for the synthesis of styrene sulfonate salts. *J Am Chem Soc* **2011,** *133* (7), 2140-3.

6. Littke, A. F.; Fu, G. C., Heck Reactions in the Presence of P(t-Bu)3: Expanded Scope and Milder Reaction Conditions for the Coupling of Aryl Chlorides. *The Journal of Organic Chemistry* **1999,** *64* (1), 10-11.

7. Karimi, B.; Behzadnia, H.; Elhamifar, D.; Akhavan, P. F.; Esfahani, F. K.; Zamani, A., Transition-metal-catalyzed oxidative Heck reactions. *Synthesis* **2010,** *2010* (09), 1399-1427.

8. Amatore, C.; Jutand, A.; M'Barki, M. A., Evidence of the formation of zerovalent palladium from Pd(OAc)2 and triphenylphosphine. *Organometallics* **1992,** *11* (9), 3009-3013.

9. Ioele, M.; Ortaggi, G.; Scarsella, M.; Sleiter, G., A rapid and convenient synthesis of tetrakis(triphenylphosphine)palladium(O) and -platinum(O) complexes by phase-transfer catalysis. *Polyhedron* **1991,** *10* (20), 2475-2476.

10. Grushin, V. V., Catalysis for Catalysis: Synthesis of Mixed Phosphine−Phosphine Oxide Ligands via Highly Selective, Pd-Catalyzed Monooxidation of Bidentate Phosphines. *Journal of the American Chemical Society* **1999,** *121* (24), 5831-5832.

11. Roffia, P.; Gregorio, G.; Conti, F.; Pregaglia, G. F.; Ugo, R., Catalysis by palladium salts VIII: an easy synthesis of zerovalent palladium and platinum triphenylphos phine catalysts by reduction with alkaline alkoxides. *Journal of Molecular Catalysis* **1977,** *2* (3), 191-201.

12. Bhattacharya, A. K.; Thyagarajan, G., Michaelis-arbuzov rearrangement. *Chemical Reviews* **1981,** *81* (4), 415-430.

13. Villemin, D.; Simeon, F.; Decreus, H.; Jaffres, P.-A., RAPID AND EFFICIENT ARBUZOV REACTION UNDER MICROWAVE IRRADIATION. *Phosphorus, Sulfur, and Silicon and the Related Elements* **1998,** *133* (1), 209-213.

14. Keglevich, G.; Grün, A.; Bölcskei, A.; Drahos, L.; Kraszni, M.; Balogh, G. T., Synthesis and Proton Dissociation Properties of Arylphosphonates: A Microwave-Assisted Catalytic Arbuzov Reaction with Aryl Bromides. *Heteroatom Chemistry* **2012,** *23* (6), 574-582.

15. Wolf, W.; Kharasch, N., Photolysis of Iodoaromatic Compounds in Benzene1. *The Journal of Organic Chemistry* **1965,** *30* (8), 2493-2498.

16. Plumb, J. B.; Obrycki, R.; Griffin, C. E., Phosphonic Acids and Esters. XVI. Formation of Dialkyl Phenylphosphonates by the Photoinitiated Phenylation of Trialkyl Phosphites1,2. *The Journal of Organic Chemistry* **1966,** *31* (8), 2455-2458.

17. Hirao, T.; Masunaga, T.; Ohshiro, Y.; Agawa, T., Stereoselective synthesis of vinylphosphonate. *Tetrahedron Letters* **1980,** *21* (37), 3595-3598.

18. Hirao, T.; Masunaga, T.; Ohshiro, Y.; Agawa, T., A Novel Synthesis of Dialkyl Arenephosphonates. *Synthesis* **1981,** *1981* (01), 56-57.

19. Goossen, L. J.; Dezfuli, M. K., Practical protocol for the palladium-catalyzed synthesis of arylphosphonates from bromoarenes and diethyl phosphite. *SYNLETT* **2005,** *2005* (03), 445-448.

20. McKenna, C. E.; Higa, M. T.; Cheung, N. H.; McKenna, M.-C., The facile dealkylation of phosphonic acid dialkyl esters by bromotrimethylsilane. *Tetrahedron Letters* **1977,** *18* (2), 155-158.

21. Al-Maksoud, W.; Mesnager, J.; Jaber, F.; Pinel, C.; Djakovitch, L., Synthesis of diethyl 2-(aryl)vinylphosphonates by the Heck reaction catalysed by well-defined palladium complexes. *Journal of Organometallic Chemistry* **2009,** *694* (20), 3222-3231.

22. Hotchkiss, P. J.; Malicki, M.; Giordano, A. J.; Armstrong, N. R.; Marder, S. R., Characterization of phosphonic acid binding to zinc oxide. *Journal of Materials Chemistry* **2011,** *21* (9), 3107.

23. Kroupa, D. M.; Vörös, M.; Brawand, N. P.; McNichols, B. W.; Miller, E. M.; Gu, J.; Nozik, A. J.; Sellinger, A.; Galli, G.; Beard, M. C., Tuning colloidal quantum dot band edge positions through solution-phase surface chemistry modification. *Nature Communications* **2017,** *8*, 15257.

24. Koldemir, U.; Braid, J. L.; Morgenstern, A.; Eberhart, M.; Collins, R. T.; Olson, D. C.; Sellinger, A., Molecular Design for Tuning Work Functions of Transparent Conducting Electrodes. *The Journal of Physical Chemistry Letters* **2015,** *6* (12), 2269-2276.

25. Braid, J. L. Understanding efficiency improvement in organic photovoltaics with molecular modifiers. Colorado School of Mines. Arthur Lakes Library, 2016.

26. Paniagua, S. A.; Giordano, A. J.; Smith, O. N. L.; Barlow, S.; Li, H.; Armstrong, N. R.; Pemberton, J. E.; Brédas, J.-L.; Ginger, D.; Marder, S. R., Phosphonic Acids for Interfacial Engineering of Transparent Conductive Oxides. *Chemical Reviews* **2016**.

27. Braid, J. L.; Koldemir, U.; Sellinger, A.; Collins, R. T.; Furtak, T. E.; Olson, D. C., Conjugated Phosphonic Acid Modified Zinc Oxide Electron Transport Layers for Improved Performance in Organic Solar Cells. *ACS Applied Materials & Interfaces* **2014,** *6* (21), 19229-19234.

28. Gliboff, M.; Sang, L.; Knesting, K. M.; Schalnat, M. C.; Mudalige, A.; Ratcliff, E. L.; Li, H.; Sigdel, A. K.; Giordano, A. J.; Berry, J. J.; Nordlund, D.; Seidler, G. T.; Brédas, J.-L.; Marder, S. R.; Pemberton, J. E.; Ginger, D. S., Orientation of Phenylphosphonic Acid Self-Assembled Monolayers on a Transparent Conductive Oxide: A Combined NEXAFS, PM-IRRAS, and DFT Study. *Langmuir* **2013,** *29* (7), 2166-2174.

29. Thomas, L. C., *Interpretation of the infrared spectra of organophosphorus compounds [by] LC Thomas*. 1974.

30. Hotchkiss, P. J., *The design, synthesis, and use of phosphonic acids for the surface modification of metal oxides*. Georgia Institute of Technology: 2009.

31. Larkin, P., *Infrared and Raman spectroscopy: principles and spectral interpretation*. Elsevier: 2011.

32. Barja, B. C.; Tejedor-Tejedor, M. I.; Anderson, M. A., Complexation of Methylphosphonic Acid with the Surface of Goethite Particles in Aqueous Solution. *Langmuir* **1999,** *15* (7), 2316-2321.

33. Sang, L.; Mudalige, A.; Sigdel, A. K.; Giordano, A. J.; Marder, S. R.; Berry, J. J.; Pemberton, J. E., PM-IRRAS Determination of Molecular Orientation of Phosphonic Acid Self-Assembled Monolayers on Indium Zinc Oxide. *Langmuir* **2015,** *31* (20), 5603-13.

34. Dewick, P. M., *Essentials of organic chemistry: for students of pharmacy, medicinal chemistry and biological chemistry*. John Wiley & Sons: 2006.

CHAPTER 5
TUNING COLLOIDAL QUANTUM DOT BAND EDGE POSITIONS THROUGH SOLUTION-PHASE SURFACE CHEMISTRY MODIFICATION

Modified from reference [1] with permission from Nature Publishing Group

Daniel M. Kroupa,[1,2] Márton Vörös,[3,4] Nicholas P. Brawand,[4] Brett W. McNichols,[5] Elisa M. Miller,[1] Jing Gu,[1] Arthur J. Nozik,[1,2] Alan Sellinger,[1,5*] Giulia Galli,[3,4*] and Matthew C. Beard[1*]

5.1. Abstract

Band edge positions of semiconductors determine their functionality in many optoelectronic applications such as photovoltaics, photoelectrochemical cells and light emitting diodes. Here we show that band edge positions of lead sulfide (PbS) colloidal semiconductor nanocrystals, specifically quantum dots (QDs), can be tuned over 2.0 eV through surface chemistry modification. We achieved this remarkable control through the development of simple, robust and scalable solution-phase ligand exchange methods, which completely replace native ligands with functionalized cinnamate ligands, allowing for well-defined, highly tunable chemical systems. By combining experiments and *ab initio* simulations, we establish clear relationships between QD surface chemistry and the band edge positions of ligand/QD hybrid systems. We find that in addition to ligand dipole, inter-QD ligand shell inter-digitization contributes to the band edge shifts. We expect that our established relationships and principles can help guide future optimization of functional organic/inorganic hybrid nanostructures for diverse optoelectronic applications.

---

[1] Chemical and Material Sciences Center, National Renewable Energy Laboratory, Colorado 80401, United States.
[2] Department of Chemistry and Biochemistry, University of Colorado, Boulder, Colorado 80309.
[3] Materials Science Division, Argonne National Laboratory, Argonne, Illinois 60439.
[4] Institute for Molecular Engineering, University of Chicago, Chicago, Illinois 60637.
[5] Department of Chemistry, Colorado School of Mines, Colorado 80401, United States.
[*] Corresponding Author

5.2. Authors Attribution Note

In addition to the attributions declared in Section 1.2 it is important to note that the majority of the content of reference [1] while an outstanding article is out of the scope specifically for this dissertation. The contributions of Brett W. McNichols have been appropriately selected and modified from the original document and have been reprinted with permission here. In addition, the synthetic work for other cinnamic acid and related compounds have been included here that have not yet been captured in publication.

5.3. Introduction

As introduced in Chapter 2, cinnamic acids (CAs) are the carboxylic acid equivalent of the phosphonic acids discussed in the previous chapters. Like PAs, CAs optoelectronic properties are highly tunable through the functionalization of the aromatic ring. In addition, the vinyl linkage provides a conjugated connection allowing electronic coupling of the dipole and functionalized aromatic ring to the surface.[1-2] In order to promote solubility, solution processability, and prevent coagulation, PbS QDs are generally coated with a native ligand (i.e. oleic acid for this investigation). [3-6] This study required the development of a simple yet robust solution phase ligand exchange where the native oleate ligands are replaced with the CA ligands of interest and measured in situ (Figure 5.1, Page 86).[7-8]

Herein, we explore the synthesis of CAs for the utilization in modifying optoelectronic properties of QDs. CAs have generally a less intensive synthetic process however, contain individual challenges as described in the following Section 5.4 Experimental Methods. The synthetic methods for CA production were first introduced in Section 2.4.6, and are also analogous to the single step phosphonic acid synthesis described in Chapter 3. Using the Heck coupling mechanism discussed in Section 4.2.1.1 with the substitution of acrylic acid or methyl acrylate in place of vinyl phosphonic acid will produce a number of CAs. Purification of CAs is also slightly less of a problem. Generally, CAs are highly soluble in ethyl acetate and flash or column chromatography methods and are sufficient to purify the desired product, in addition to the recrystallization method used below.

5.4. Experimental Methods

All chemicals were used as received without further purification unless noted. Anhydrous tetrahydrofuran (THF, ≥99.9%) 4-bromobenzaldehyde (99%), 4-bromobenzonitrile (99%), anhydrous acrylic acid (99%), N,N-dicyclohexylmethylamine (97%) anhydrous magnesium sulfate($MgSO_4$), malononitrile (≥99) were obtained from Sigma Aldrich. Bis(tri-tert-butylphosphine) palladium (98%) was obtained from Strem Chemicals. Hydrochloric acid (HCl, ACS) was obtained from Macron Fine Chemicals.

5.4.1. Functionalized Cinnamic Acid Synthesis

General Synthesis. A 20 mL Biotage microwave reaction vial equipped with a Teflon magnetic stir bar was charged with aromatic bromide (10 mmol), acrylic acid (11 mmol), N,N-dicyclohexylmethylamine (11 mmol), bis(tri-tert-butylphosphine) palladium (1.0 mol %) and THF (10 mL). The vial was capped and the mixture irradiated with a ceiling temperature of 180°C for 15 minutes.[9] The crude product was then extracted three times with 200 mL dichloromethane and 200 mL acidic aqueous (5% vol HCl) solution. The organic layer was dried with $MgSO_4$ and the solvent removed using a rotary evaporator. The crude product was further purified by recrystallization in ethanol

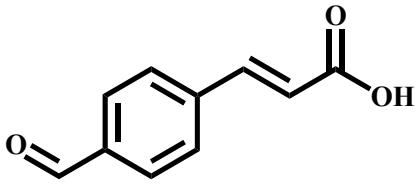

BM04 Precursor - (*E*)-3-(4-formylphenyl) acrylic acid

(E)-3-(4-formylphenyl) acrylic acid Following the general synthesis procedure from above, the product was obtained after recrystallization from ethanol resulting in a pale yellow powder (72% yield). The following NMR spectra are located in Appendix B.

^{1}H NMR (500 MHz, DMSO-d_6) δ 12.59 (s, 1H), 9.98 (s, 1H), 7.88 (s, 4H), 7.62 (d, J = 15.6 Hz, 1H), 6.66 (d, J = 15.4 Hz, 1H).

^{13}C NMR (126 MHz, DMSO-d_6) δ 193.22, 167.80, 142.92, 137.33, 130.42, 129.34, 123.01.

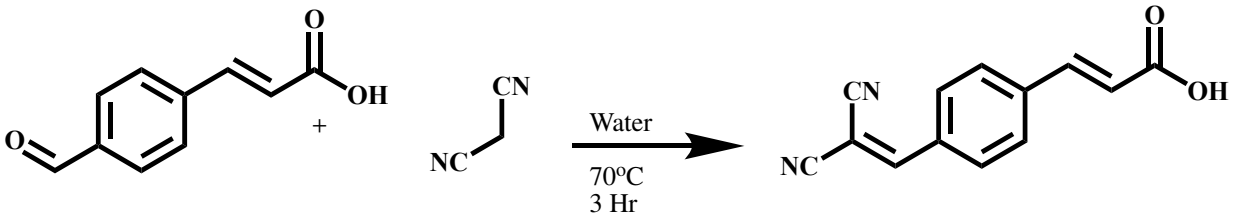

Scheme 5.1 Synthesis of 2CVCA (trans-4-formylcinnamic acid)

BM04 - Trans-4-(2,2-dicyanovinyl) cinnamic acid

Trans-4-formylcinnamic acid (10 mmol), and malononitrile (10 mmol) were added to 25 mL of distilled water and heated to 70°C with stirring for 3 hours, then cooled to 0°C and the solid dark yellow powder precipitate was filtered and air dried (quantitative yield). The product was sufficiently pure after this step to use directly as a ligand for the oleate exchange process. The following NMR spectra are located in Appendix B.

^{1}H NMR (500 MHz, DMSO-d_6) δ 12.62 (s, 1H), 8.51 (s, 1H), 7.92 (q, J = 10.7, 8.4, 6.1 Hz, 4H), 7.60 (d, J = 16.6 Hz, 1H), 6.70 (d, J = 16.3 Hz, 1H).

^{13}C NMR (126 MHz, DMSO-d_6) δ 167.74, 160.93, 142.60, 140.21, 132.90, 131.48, 129.56, 123.33, 114.76, 113.80, 82.47.

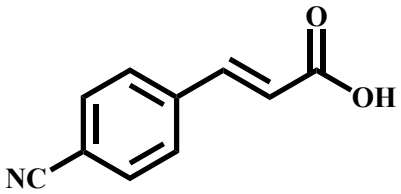

BM43 - (*E*)-3-(4-cyanophenyl) acrylic acid

(*E*)-3-(4-cyanophenyl) acrylic acid conditions were similar to the trans-4-formylcinnamic acid synthesis. The product was purified by recrystallization from ethanol affording white needle like crystals (92% yield). The product was sufficiently pure after this step to use directly as a ligand for the oleate exchange process. The following NMR spectra are located in Appendix B.

^{1}H NMR (500 MHz, DMSO-d_6) δ 12.63 (s, 1H), 7.89 – 7.81 (m, 4H), 7.60 (d, J = 15.9 Hz, 1H), 6.67 (d, J = 15.9 Hz, 1H). ^{13}C NMR (126 MHz, DMSO-d_6) δ 167.70, 142.46, 139.35, 133.25, 123.34, 119.15, 112.61.

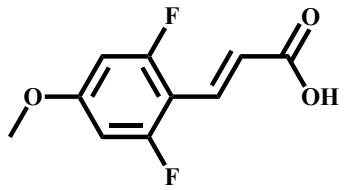

BM13 - 4An26FCA - (*E*)-3-(2,6-difluoro-4-methoxyphenyl) acrylic acid

(*E*)-3-(2,6-difluoro-4-methoxyphenyl) acrylic acid followed the general synthesis procedure from above, the product was obtained after recrystallization from ACN resulting in a white powder (65% yield). The following NMR spectra are located in Appendix B.

^{1}H NMR (500 MHz, DMSO-d_6) δ 14.03 (s, 1H), 7.68 (d, J = 20.1 Hz, 1H), 6.92 (d, J = 13.8 Hz, 2H), 6.31 (d, J = 21.4 Hz, 1H), 3.10 (s, 3H).

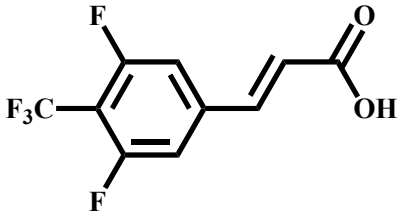

BM16 - 35F4CF$_3$CA - (*E*)-3-(3,5-difluoro-4-(trifluoromethyl)phenyl) acrylic acid

(*E*)-3-(3,5-difluoro-4-(trifluoromethyl) phenyl) acrylic acid followed the general synthesis procedure from above, the product was obtained by precipitating the concentrated crude into DCM (52% Yield). The following NMR spectra are located in Appendix B.

^{1}H NMR (500 MHz, DMSO-d_6) δ 7.75 (d, J = 11.3 Hz, 2H), 7.54 (d, J = 16.4 Hz, 1H), 6.78 (d, J = 16.0 Hz, 1H).

^{13}C NMR (126 MHz, DMSO-D_6) δ 167.37, 160.72, 158.65, 142.52, 140.37, 125.54, 120.94, 113.28, 113.26, 113.09, 39.92.

^{19}F NMR (471 MHz, DMSO-D_6) δ -55.28, -112.10.

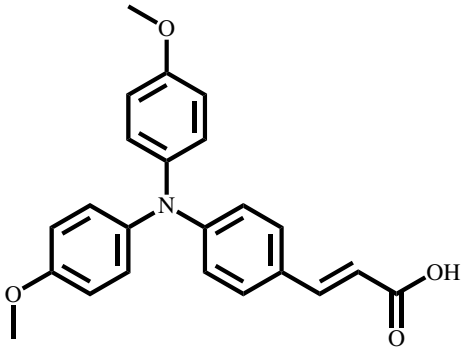

BM18 - TPACA - (*E*)-3-(4-(bis(4-methoxyphenyl) amino) phenyl) acrylic acid

(*E*)-3-(4-(bis(4-methoxyphenyl) amino) phenyl) acrylic acid utilized 4-iodo-*N*, *N*-bis(4-methoxyphenyl) aniline and followed the general synthesis procedure from above, the product was purified with flash chromatography producing a fluorescent yellow solid (42% yield). The following NMR spectra are located in Appendix B.

^{1}H NMR (500 MHz, DMSO-D_6) δ 12.14, 7.42, 7.41, 7.41, 7.38, 7.18, 7.06, 7.05, 6.95, 6.92, 6.90, 6.63, 6.61, 6.23, 6.20, 3.71, 3.29, 2.46.

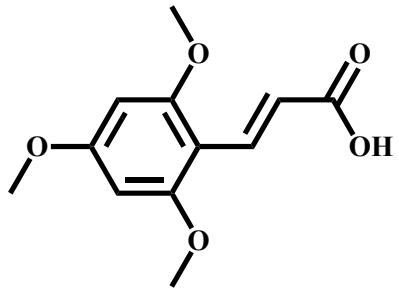

BM17 - tMeOxCA - (*E*)-3-(2,4,6-trimethoxyphenyl) acrylic acid

(*E*)-3-(2,4,6-trimethoxyphenyl) acrylic acid utilized 2-bromo-1,3,5-trimethoxybenzene and followed the general synthesis procedure from above, the product was purified by precipitation into 5% HCl water then filtration producing a white solid (50% yield). The following NMR spectra are located in Appendix B.

^{1}H NMR (500 MHz, DMSO-d_6) δ 11.90 (s, 1H), 7.83 (d, J = 16.1 Hz, 1H), 6.51 (d, J = 16.1 Hz, 1H), 6.24 (s, 2H), 3.87 – 3.72 (m, 9H).

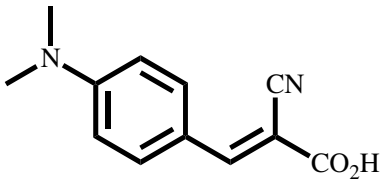

BM82 - (*E*)-2-cyano-3-(4-(dimethylamino)phenyl) acrylic acid

(*E*)-2-cyano-3-(4-(dimethylamino)phenyl)acrylic acid was synthesized using a Knoevenagel condensation where 4-(dimethylamino)benzaldehyde(5 mmol) and 2-cyanoacetic acid (5 mmol) and piperidine (6 mol %) were mixed in ethanol and heated to 60 °C for 3 hours.[10] The reaction vessel was then cool in an ice water bath where a bright orange precipitate formed. The product was filtered and rinsed with excess cold methanol, producing bright orange solid (10% yield) The following NMR spectra are located in Appendix B.

^{1}H NMR (500 MHz, DMSO-d_6) δ 8.03 (s, 1H), 7.90 (d, J = 9.1 Hz, 2H), 6.79 (d, J = 9.1 Hz, 2H), 3.03 (s, 6H).

^{13}C NMR (126 MHz, DMSO-D_6) δ 165.36, 154.35, 154.04, 134.03, 118.93, 118.47, 112.20, 94.00, 40.54, 40.37, 40.20, 40.12, 40.04, 39.87, 39.70, 39.54.

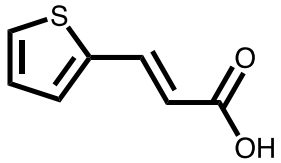

BM103 - ThioCA - (E)-3-(thiophen-2-yl) acrylic acid

(E)-3-(thiophen-2-yl) acrylic acid initially was attempted with the general synthesis above, however was unsuccessful. To produce the desired acid, 2-bromothiophene and methyl acrylate were coupled using the general conditions above to create the methyl ester, which was then purified by flash chromatography. The ester intermediate was then refluxed in concentrated HCl overnight, after cooling the dark purple precipitate was filtered (80% yield). The following NMR spectra are located in Appendix B.

^{1}H NMR (500 MHz, DMSO-d_6) δ 12.35 (s, 1H), 7.77 – 7.64 (m, 2H), 7.47 (s, 1H), 7.10 (t, J = 4.6 Hz, 1H), 6.13 (d, J = 15.7 Hz, 1H).^{13}C NMR (126 MHz, DMSO-D_6) δ 167.79, 139.42, 137.29, 132.24, 130.06, 129.03, 117.93, 40.03.

5.5. Discussion

The results of the ligand exchange can be found in Figure 5.1(a) and Figure 2.6 (a) (Page 24). In this experiment, Kroupa et. al found a general agreement between using *ab initio* calculations and the experimental results of the ligand exchange.[1] We found that the calculated ligand dipole is a critical parameter for prediction of the upper limit of the magnitude of band edge shift of PbS QD thin films.[11] This validates that a reasonable prediction of the absorption enhancement can be made computationally, and the desired ligand can be purchased or synthesized and exchanged to obtain the desired effect. [12-15]

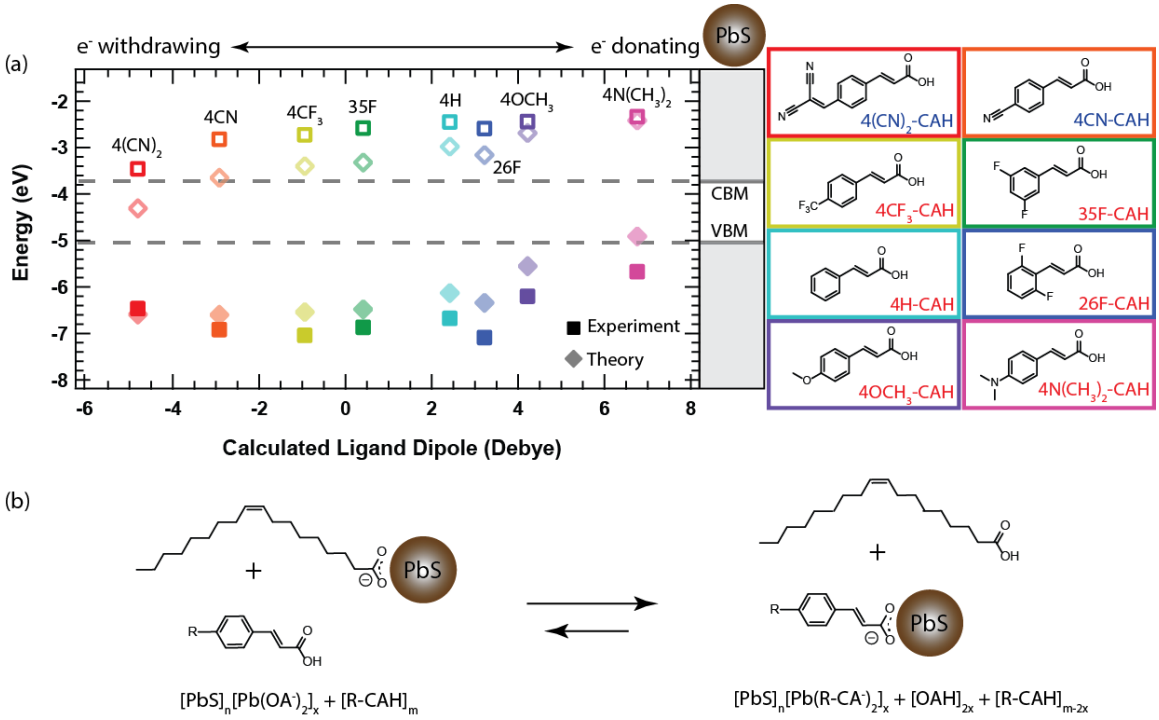

Figure 5.1 The model ligand/QD system utilized in this study. (a) Chemical structures, computed vacuum electronic dipoles and labels used throughout this work of the molecules in our ligand library. (b) The X-type ligand exchange in which surface bound oleate is displaced by functionalized cinnamic acid molecules.

As previously stated, a great number of CAs are commercially available and moderately inexpensive. However, this study required the synthesis of (BM43) CNCA (shown in Figure 2.6 Page 24, and Figure 5.1) and BM04 (shown as "4(CN)$_2$.CAH" in Figure 5.1). These synthesized CAs introduced larger work function and bandgap modification then what could be obtained from commercial sources alone. As mentioned in Section 5.3, Heck coupling is the primary

synthetic route utilized for producing these acids (also see Section 4.2.1.1), however, some other synthetic schemes were also employed to introduce additional ligand functionality. Specifically, for BM82, the introduction of the α-cyano group is the result of a piperidine catalyzed Knoevenagel condensation with 2-cyanoacetic acid and 4-(dimethylamino) benzaldehyde. We hypothesized that introduction of the α-cyano group would provide some enhanced optoelectronic properties when compared to the standard cinnamic acid.

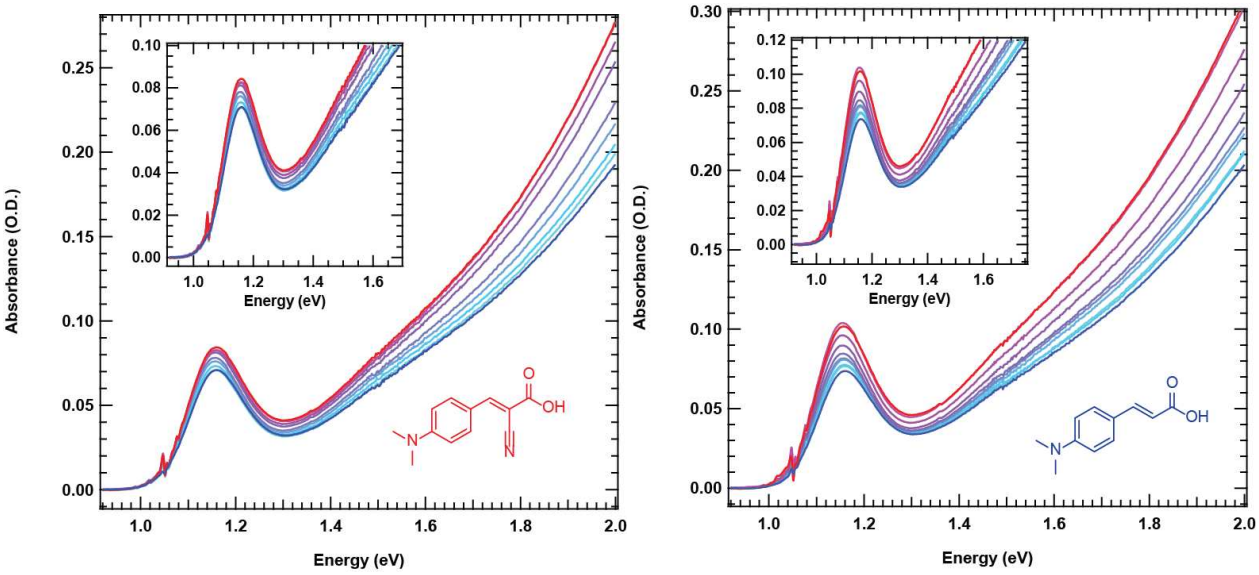

Figure 5.2 Absorption enhancement comparison of alpha-cyano CA to standard CA on PbS QDs.

However, as shown in Figure 5.2, the absorbance enhancement of the α-cyano ligand is less intense than the cinnamic ligand. We suspect that even though the calculated dipole is stronger for the α-cyano ligand, the strength of acidity could be less than that of the cinnamic ligand and at the point of saturation fewer α-cyano ligands are bound to the surface of the QD. We also suspect that the α-cyano group could interrupt the conjugation seen in the cinnamic acids, which would also interfere with the "hybridization" between the ligand and QD core energy levels introduced by Kroupa et. al.

5.6. Conclusion

We introduced the synthetic route and conditions of 9 CAs, of which one (CNCA) was used in the study performed by Kroupa et. al.[1] In addition to this, a comparison of BM82 with 4-(dimethylamino) cinnamic acid showed that the α-cyano group is a non-ideal ligand that suppresses the absorption enhancement. We believe that these surface modification principles

can also be explored with a number of other ligands, perhaps coupling the QD to cinnamate hybridization with ligands that have much higher optical absorbance. These ligands could then possibly enhance the absorption of desired bands in the visible light spectrum, specifically where some QD systems may not have the best absorbance. [16] This potentially would allow for these QDs to increase broadband spectrum absorption, ultimately leading to a more efficient uv-vis light harvesting. [17] We would also like to see exploration into other QD systems that could benefit from similar results described here.

In addition to this, in Chapter 6 we introduce a number of di- and tri- acrylic acids that we incorporate into MOFs. However, we believe that these bi and tri functional ligands could be incorporated into a QD thin film. The multi-functionality of these linkers would allow for bridging between QDs that perhaps would allow for this hybridization to extend from one QD to another, in effect electronically coupling a network of QDs together. This potentially would allow for some future studies in QD thin film functionality and applications.

5.7. References Cited

1. Kroupa, D. M.; Vörös, M.; Brawand, N. P.; McNichols, B. W.; Miller, E. M.; Gu, J.; Nozik, A. J.; Sellinger, A.; Galli, G.; Beard, M. C., Tuning colloidal quantum dot band edge positions through solution-phase surface chemistry modification. *Nature Communications* **2017,** *8*, 15257.

2. Giansante, C.; Infante, I.; Fabiano, E.; Grisorio, R.; Suranna, G. P.; Gigli, G., "Darker-than-Black" PbS Quantum Dots: Enhancing Optical Absorption of Colloidal Semiconductor Nanocrystals via Short Conjugated Ligands. *Journal of the American Chemical Society* **2015,** *137* (5), 1875-1886.

3. Hendricks, M. P.; Campos, M. P.; Cleveland, G. T.; Jen-La Plante, I.; Owen, J. S., A tunable library of substituted thiourea precursors to metal sulfide nanocrystals. *Science* **2015,** *348* (6240), 1226-1230.

4. Boles, M. A.; Ling, D.; Hyeon, T.; Talapin, D. V., The surface science of nanocrystals. *Nat Mater* **2016,** *15* (2), 141-153.

5. Harris, R. D.; Bettis Homan, S.; Kodaimati, M.; He, C.; Nepomnyashchii, A. B.; Swenson, N. K.; Lian, S.; Calzada, R.; Weiss, E. A., Electronic Processes within Quantum Dot-Molecule Complexes. *Chemical Reviews* **2016,** *116* (21), 12865-12919.

6. Yang, S.; Prendergast, D.; Neaton, J. B., Tuning Semiconductor Band Edge Energies for Solar Photocatalysis via Surface Ligand Passivation. *Nano Letters* **2012,** *12* (1), 383-388.

7. Giansante, C.; Carbone, L.; Giannini, C.; Altamura, D.; Ameer, Z.; Maruccio, G.; Loiudice, A.; Belviso, M. R.; Cozzoli, P. D.; Rizzo, A.; Gigli, G., Colloidal Arenethiolate-Capped PbS Quantum Dots: Optoelectronic Properties, Self-Assembly, and Application in Solution-Cast Photovoltaics. *The Journal of Physical Chemistry C* **2013,** *117* (25), 13305-13317.

8. Kroupa, D. M.; Anderson, N. C.; Castaneda, C. V.; Nozik, A. J.; Beard, M. C., In situ spectroscopic characterization of a solution-phase X-type ligand exchange at colloidal lead sulphide quantum dot surfaces. *Chemical Communications* **2016,** *52* (96), 13893-13896.

9. Stadler, A.; Yousefi, B. H.; Dallinger, D.; Walla, P.; Van der Eycken, E.; Kaval, N.; Kappe, C. O., Scalability of Microwave-Assisted Organic Synthesis. From Single-Mode to Multimode Parallel Batch Reactors. *Organic Process Research & Development* **2003,** *7* (5), 707-716.

10. Fioravanti, S.; Pellacani, L.; Tardella, P. A.; Vergari, M. C., Facile and Highly Stereoselective One-Pot Synthesis of Either (E)- or (Z)-Nitro Alkenes. *Organic Letters* **2008,** *10* (7), 1449-1451.

11. Liu, Y.; Tolentino, J.; Gibbs, M.; Ihly, R.; Perkins, C. L.; Liu, Y.; Crawford, N.; Hemminger, J. C.; Law, M., PbSe Quantum Dot Field-Effect Transistors with Air-Stable Electron Mobilities above 7 cm2 V−1 s−1. *Nano Letters* **2013,** *13* (4), 1578-1587.

12. Brown, P. R.; Kim, D.; Lunt, R. R.; Zhao, N.; Bawendi, M. G.; Grossman, J. C.; Bulović, V., Energy Level Modification in Lead Sulfide Quantum Dot Thin Films through Ligand Exchange. *ACS Nano* **2014,** *8* (6), 5863-5872.

13. Chuang, C.-H. M.; Brown, P. R.; Bulović, V.; Bawendi, M. G., Improved performance and stability in quantum dot solar cells through band alignment engineering. *Nat Mater* **2014,** *13* (8), 796-801.

14. Santra, P. K.; Palmstrom, A. F.; Tanskanen, J. T.; Yang, N.; Bent, S. F., Improving Performance in Colloidal Quantum Dot Solar Cells by Tuning Band Alignment through Surface Dipole Moments. *The Journal of Physical Chemistry C* **2015,** *119* (6), 2996-3005.

15. Crisp, R. W.; Kroupa, D. M.; Marshall, A. R.; Miller, E. M.; Zhang, J.; Beard, M. C.; Luther, J. M., Metal Halide Solid-State Surface Treatment for High Efficiency PbS and PbSe QD Solar Cells. **2015,** *5*, 9945.

16. Yang, J.; Wise, F. W., Effects of Disorder on Electronic Properties of Nanocrystal Assemblies. *The Journal of Physical Chemistry C* **2015,** *119* (6), 3338-3347.

17. Ning, Z.; Dong, H.; Zhang, Q.; Voznyy, O.; Sargent, E. H., Solar Cells Based on Inks of n-Type Colloidal Quantum Dots. *ACS Nano* **2014,** *8* (10), 10321-10327.

CHAPTER 6
NOBLE METAL-FREE CATALYTIC DECARBOXYLATION OF OLEIC ACID TO N-HEPTADECANE ONNICKEL-BASED METAL-ORGANIC FRAMEWORKS (MOFS)

Modified from reference [1] with permission from The Royal Society of Chemistry

Liqiu Yang,[a]† Brett. W. McNichols,[b]† Malcolm Davidson,[c] Benjamin Schweitzer,[a] Diego A. Gómez-Gualdrón,[a] Bryan G. Trewyn,[bc] Alan Sellinger*[bc] and Moises A. Carreon*[ac]

An additional manuscript is currently in preparation and to be submitted shortly, additional authors include J. Everett Baumann and Amy E. Keuhlen

6.1. Abstract

Nickel based metal organic frameworks (Ni-MOFs) were successfully synthesized using new conjugated carboxylic acid linkers. These conjugated carboxylic acid linkers were synthesized using mild Heck coupling that led to the incorporation of functional groups not possible by traditional synthetic methods. Control of linker size allows for porosity tuning of the crystalline network and high surface area that in theory, results in the increased accessibility to Ni metal centers for catalysis. The resultant crystalline Ni-MOFs displayed BET surface areas as high as ~314 m_2/g. To investigate their catalytic activity for conversion of oleic acid to liquid hydrocarbons, Ni-MOFs were grown on zeolite 5A beads that served as catalytic supports. The resultant catalysts displayed heptadecane yields as high as ~77% at mild reaction conditions, one of the highest yields for non-noble metal containing catalysts. The catalytic activity correlated to the concentration of acid sites. A slight decrease in catalytic activity was observed after catalysts recycling.

---

[a] Dept. of Chemical & Biological Engineering, Colorado School of Mines, Golden, CO 80401
[b] Dept. of Chemistry, Colorado School of Mines, Golden, CO 80401
[c] Materials Science Program, Colorado School of Mines, Golden, CO 80401
* Corresponding authors: aselli@mines.edu; mcarreon@mines.edu
† Authors are co-first author

6.2. Introduction

Low-cost, readily available lipid-based biomass is an attractive feedstock for catalytic conversion into renewable alternative fuels. Recent research efforts have focused on converting triglycerides and fatty acids into linear, paraffinic hydrocarbons that can be potentially used as precursors for the production of liquid fuels, lubricants and/or other valuable petrochemicals.[2-7] Decarboxylation is an effective route for the conversion of carboxylic acids to linear, paraffinic hydrocarbons. Compared to biodiesel, alternative liquid fuels produced by catalytic decarboxylation are higher quality and more stable due to lower content or absence of oxygen.

Decarboxylation of carboxylic acids over various catalysts have received considerable attention. However, since many of the catalysts employ noble metals (Pd, Pt, Rh, Ru, Ir, Os) as the active species to attain good catalytic performance, industrial application is currently far from feasible due to limitations in cost and scale-up.[8-10] Few reports exist on non-noble metal catalysts such as nickel bimetallic sulfide phases and other metal oxides.[11-13] Non-noble metal catalysts are significantly lower cost, but have so far displayed limited catalytic performance in comparison to supported, noble metal catalysts. Another drawback of non-noble bimetallic sulfide catalysts is the sulfide contamination of resultant products. Therefore, it is important to design effective non-noble metal catalysts that display enhanced catalytic conversion of lipid-based biomass into clean alternative fuel hydrocarbon feedstock. This could be potentially achieved using metal organic frameworks (MOFs), that have emerged as a promising type of highly-tunable (chemically and topologically) crystalline microporous material.[14] MOFs combine desirable properties that make them ideal candidates for catalytic applications,[15] such as uniform micro-porosity, high surface area,[16] and (increasingly so) high thermal and chemical stability.[17-18] In principle, the metal cations or metal-based-clusters can act as the catalytic active species, and the ordered microporous structure can provide the pathway for guest and product molecules to diffuse with enhanced mass transfer. [19-21]

In this chapter, we report the synthesis of nickel based metal organic frameworks (Ni-MOFs) based on our new di- and tri-cinnamic acid derivatives, and their improved catalytic activity (as compared to Pd and Pt) for the decarboxylation reaction of fatty acids. Nickel was chosen as the inorganic metal cation due to its promising catalytic activity for deoxygenation of fatty acids,[8] and its low cost (compared to Pd and Pt, the price of Ni is roughly 2,500X lower), that makes it appealing for decarboxylation and/or deoxygenation reactions. Supported nickel

catalysts can afford reasonable yields of hydrocarbons in the catalytic deoxygenation of fatty acids even in the absence of hydrogen.[22-23] Our conjugated carboxylic acid linkers allow for new MOF structures to be prepared and tested for catalytic activity. These Ni-based MOFs were grown on the surface of zeolite 5A beads to form Ni-MOF membrane/zeolite5A bead phases, which were then used as catalysts to convert oleic acid to liquid hydrocarbons.

In the following section 6.3 we report the detailed synthesis and characterization of 17 organic linkers containing acrylate links for the incorporation into MOFs. Inherent of these mild synthetic techniques, we are able to produce functionalized linkers, which allow for interesting side chain or group incorporation into the lattice of the resultant MOFs, which could enhance adsorption of H_2, N_2, CO_2, and CH_4. Additionally, we report the XRD, porosity, and SEM of multiple zinc based MOFs. One member of this series, BM53 has previously been determined to have ca. 3500 m^2/g,[24] however as discussed in previous chapter the method that follows utilizes mild conditions and fairly inexpensive precursors.

6.3. Experimental methods

All chemicals were used as received without further purification unless noted. Dichloromethane (DCM, ACS), anhydrous tetrahydrofuran (THF, ≥99.9%), methyl acrylate (>99%), N,N-dicyclohexylmethylamine (NCy_2Me, 97%) and anhydrous magnesium sulfate ($MgSO_4$), were obtained from Sigma-Aldrich. Sodium hydroxide (NaOH, Pearl 97%) was obtained from Fisher Scientific. Bis(tri-tert-butylphosphine) palladium ($Pd[P(t\text{-}Bu)_3]_2$, 98%) was obtained from Strem Chemicals. Hydrochloric acid (HCl, ACS) was obtained from Macron Fine Chemicals. All glassware was base, acid, and water washed then oven-dried. ^1H and ^{13}C NMR spectra were obtained on a JEOL ECA 500 liquid-state NMR spectrometer and data obtained was manipulated in MestReNova NMR processor software.

6.3.1. Carboxylic linkers synthesis and characterization

General carboxylic acid synthesis. A Schlenk flask under argon and equipped with a magnetic stir bar was charged with the aromatic halide, methyl acrylate, N,N-dicyclohexylmethylamine, $Pd[P(t\text{-}Bu)_3]_2$ (catalyst used at 1 mol % level), and THF. The mixture was heated to 70°C for 24 h and periodically tested via TLC for reaction completion. The crude product mixture was extracted three times with DCM and acidic water (5% HCl). The organic

layer was dried with $MgSO_4$, filtered, and the solvent removed using a rotary evaporator. The resultant crude product was then further purified by flash chromatography and excess was solvent removed using a rotary evaporator. The ester precursor was then converted to the corresponding acid by refluxing for 4 h in a NaOH (x10 mol equivalents) and methanol solution followed by cooling, acidification to >2 pH with HCl, then the pure acid product was collected by vacuum filtration.

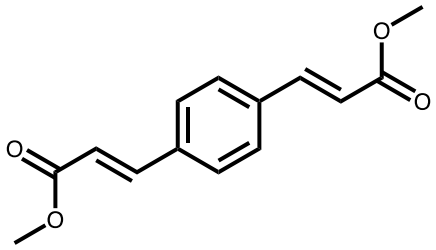

BM45 - precursor - dimethyl 3,3'-(1,4-phenylene) (2*E*,2'*E*)-diacrylate

Dimethyl 3,3'-(1,4-phenylene) (2*E*,2'*E*)-diacrylate followed the general synthesis above with the only change of adding 5% DCM additive in the flash chromatography. Resulting in an off white powder (87% yield). The following NMR spectra are located in Appendix C.

^{1}H NMR (500 MHz, DMSO-d_6) δ 7.73 (s, 4H), 7.63 (d, J = 15.7 Hz, 2H), 6.68 (d, J = 15.2 Hz, 2H), 3.69 (s, 6H). ^{13}C NMR (126 MHz, DMSO-D_6) δ 167.11, 144.13, 136.38, 129.38, 119.43, 52.08.

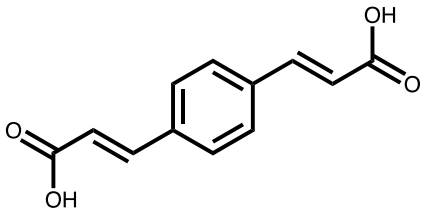

BM45 - (2*E*,2'*E*)-3,3'-(1,4-phenylene) diacrylic acid

(2*E*,2'*E*)-3,3'-(1,4-phenylene) diacrylic acid followed the general synthesis above resulting in an off white powder (80% yield). The following NMR spectra are located in Appendix C.

^{1}H NMR (500 MHz, DMSO-d_6) δ 7.69 (s, 4H), 7.56 (d, J = 16.0 Hz, 2H), 6.56 (d, J = 16.0 Hz, 2H). ^{13}C NMR (126 MHz, DMSO-D_6) δ 168.04, 143.55, 136.40, 129.22, 120.77.

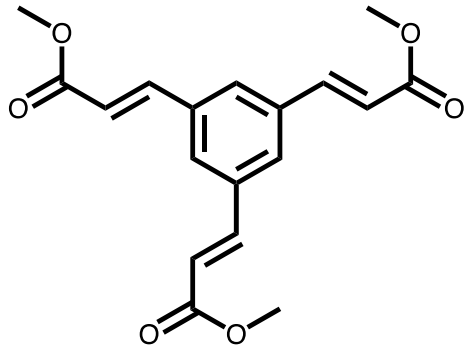

BM53 Precursor- trimethyl 3,3',3''-(benzene-1,3,5-triyl) (2*E*,2'*E*,2''*E*)-triacrylate

Trimethyl 3,3',3''-(benzene-1,3,5-triyl) (2*E*,2'*E*,2''*E*)-triacrylate followed the general synthesis above resulting in a slight yellow liquid product. (83%) The following NMR spectra are located in Appendix C.

^{1}H NMR (500 MHz, DMSO-d_6) δ 8.12 (s, 1H), 7.63 (d, J = 16.1 Hz, 1H), 6.86 (d, J = 15.2 Hz, 1H), 3.71 (s, 3H).

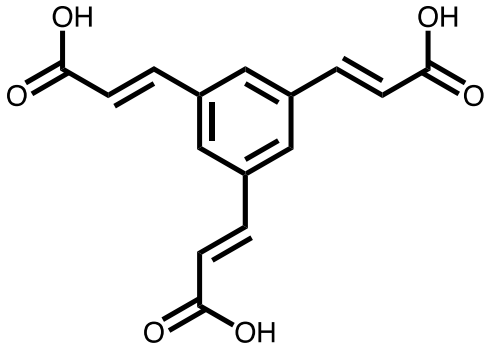

BM53 - (2*E*,2'*E*,2''*E*)-3,3',3''-(benzene-1,3,5-triyl) triacrylic acid

(2E,2'E,2''E)-3,3',3''-(benzene-1,3,5-triyl) triacrylic acid followed the general synthesis above resulting in an off white powder (80% yield). The following NMR spectra are located in Appendix C.

^{1}H NMR (500 MHz, DMSO-d_6) δ 12.46 (s, 3H), 8.05 (s, 3H), 7.56 (d, J = 16.0 Hz, 3H), 6.74 (d, J = 15.9 Hz, 3H).^{13}C NMR (126 MHz, DMSO-D_6) δ 168.06, 143.26, 136.11, 129.73, 121.49

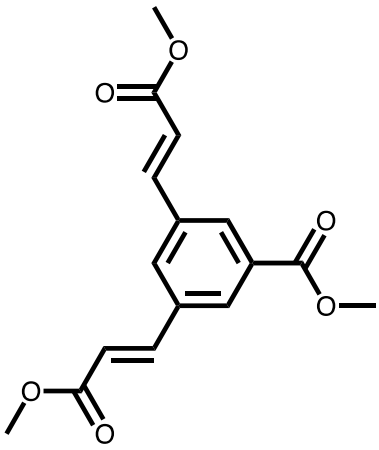

BM74 Precursor - dimethyl 3,3'-(5-(methoxycarbonyl)-1,3-phenylene) (2*E*,2'*E*)-diacrylate

Dimethyl 3,3'-(5-(methoxycarbonyl)-1,3-phenylene) (2*E*,2'*E*)-diacrylate diacrylate followed the general synthesis above resulting in an off white powder (85%% yield). The following NMR spectra are located in Appendix C.

^{1}H NMR (500 MHz, DMSO-d_6) δ 8.41 (s, 1H), 8.16 (s, 2H), 7.68 (d, J = 16.1 Hz, 2H), 6.84 (d, J = 16.1 Hz, 2H), 3.84 (s, 3H), 3.71 (s, 6H).

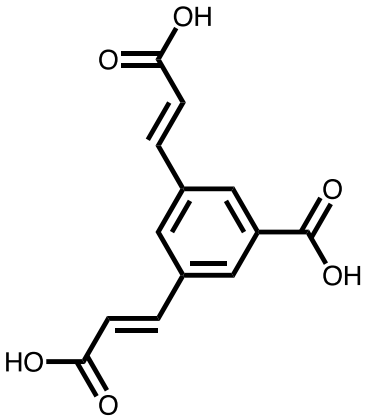

BM74 - (2*E*,2'*E*)-3,3'-(5-carboxy-1,3-phenylene) diacrylic acid

(2*E*,2'*E*)-3,3'-(5-carboxy-1,3-phenylene) diacrylic acid followed the general synthesis above resulting in an off white powder (82% yield). The following NMR spectra are located in Appendix C.

^{1}H NMR (500 MHz, DMSO-d_6) δ 8.32 (s, 1H), 8.11 (s, 2H), 7.62 (d, J = 16.0 Hz, 2H), 6.71 (d, J = 16.1 Hz, 2H).^{13}C NMR (126 MHz, DMSO-D_6) δ 167.86, 167.04, 142.85, 135.98, 132.83, 131.24, 130.84, 121.89, 40.00.

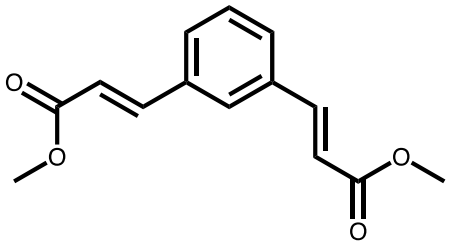

BM57 precursor - dimethyl 3,3'-(1,3-phenylene) (2*E*,2'*E*)-diacrylate

Dimethyl 3,3'-(1,3-phenylene) (2*E*,2'*E*)-diacrylate followed the general synthesis above resulting in an off white powder (91% yield). The following NMR spectra are located in Appendix C.

^{1}H NMR (500 MHz, DMSO-d_6) δ 8.12 (s, 1H), 7.72 (d, J = 9.2 Hz, 2H), 7.64 (d, J = 16.1 Hz, 2H), 7.43 (s, 1H), 6.76 (d, J = 16.1 Hz, 2H), 3.70 (s, 6H).

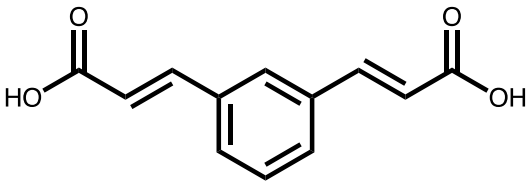

BM57 - (2*E*,2'*E*)-3,3'-(1,3-phenylene) diacrylic acid

(2*E*,2'*E*)-3,3'-(1,3-phenylene) diacrylic acid diacrylate followed the general synthesis above resulting in an off white powder (82% yield). The following NMR spectra are located in Appendix C.

^{1}H NMR (500 MHz, DMSO-d_6) δ 12.43 (s, 2H), 8.03 (s, 1H), 7.69 – 7.65 (m, 2H), 7.57 (d, J = 15.8 Hz, 2H), 7.44 – 7.37 (m, 1H), 6.63 (d, J = 15.9 Hz, 2H). ^{13}C NMR (126 MHz, DMSO-D_6) δ 168.09, 143.81, 135.45, 130.41, 129.97, 128.18, 120.69.

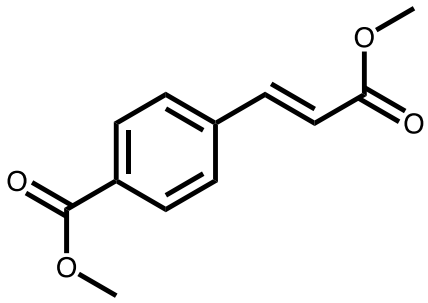

BM65 precursor - methyl (*E*)-4-(3-methoxy-3-oxoprop-1-en-1-yl) benzoate

Methyl (*E*)-4-(3-methoxy-3-oxoprop-1-en-1-yl) benzoate followed the general synthesis above with the only change of 1.1 equivalents of methyl acrylate was utilized resulting in a white powder (92% yield). The following NMR spectra are located in Appendix C.

^{1}H NMR (500 MHz, DMSO-d_6) δ 7.93 (s, 2H), 7.84 (s, 2H), 7.68 (d, J = 16.0 Hz, 1H), 6.75 (d, J = 16.0 Hz, 1H), 3.82 (s, 3H), 3.70 (s, 3H).

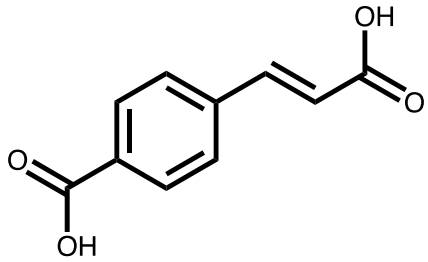

BM65 - (*E*)-4-(2-carboxyvinyl) benzoic acid

(*E*)-4-(2-carboxyvinyl) benzoic acid followed the general synthesis above resulting in a white powder (96% yield). The following NMR spectra are located in Appendix C.

^{1}H NMR (500 MHz, DMSO-d_6) δ 12.83 (s, 2H), 7.91 (d, J = 7.6 Hz, 2H), 7.77 (d, J = 7.8 Hz, 2H), 7.60 (d, J = 16.1 Hz, 1H), 6.61 (d, J = 16.2 Hz, 1H). ^{13}C NMR (126 MHz, DMSO-D_6) δ 167.83, 167.35, 143.17, 138.88, 132.34, 130.25, 128.82, 122.11.

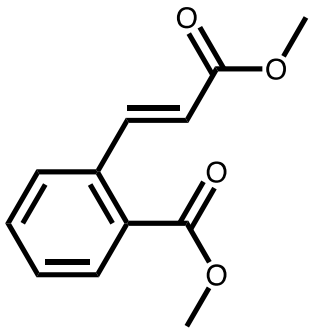

BM66 precursor - methyl (*E*)-2-(3-methoxy-3-oxoprop-1-en-1-yl) benzoate

Methyl (*E*)-2-(3-methoxy-3-oxoprop-1-en-1-yl) benzoate followed the general synthesis above with the only change of 1.1 equivalents of methyl acrylate was utilized resulting in a clear liquid product (83% yield). The following NMR spectra are located in Appendix C.

^{1}H NMR (500 MHz, DMSO-d_6) δ 8.26 (d, J = 15.2 Hz, 1H), 7.84 (dd, J = 13.5, 7.8 Hz, 2H), 7.60 (t, J = 7.6 Hz, 1H), 7.51 (t, J = 7.6 Hz, 1H), 6.50 (d, J = 15.9 Hz, 1H), 3.82 (s, 3H), 3.70 (s, 3H). ^{13}C NMR (126 MHz, DMSO-D_6) δ 167.19, 166.92, 143.24, 135.37, 133.12, 130.82, 130.53, 130.25, 128.52, 120.93, 52.97, 52.13.

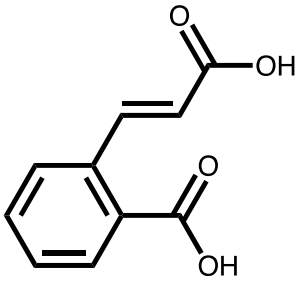

BM66 - (E)-2-(2-carboxyvinyl) benzoic acid

(E)-2-(2-Carboxyvinyl) benzoic acid benzoate followed the general synthesis above resulting in a white powder (70% yield). The following NMR spectra are located in Appendix C.

^{1}H NMR (500 MHz, DMSO-d_6) δ 12.85 (s, 4H), 8.27 (d, J = 16.0 Hz, 2H), 7.83 (s, 2H), 7.77 (s, 2H), 7.55 (s, 2H), 7.47 (s, 2H), 6.37 (d, J = 16.0 Hz, 2H). ^{13}C NMR (126 MHz, DMSO-D_6) δ 168.69, 167.96, 143.06, 135.37, 132.63, 131.57, 130.84, 130.23, 128.27, 121.89.

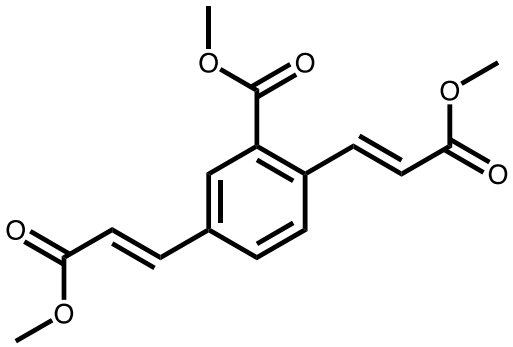

BM67 Precursor - dimethyl 3,3'-(2-(methoxycarbonyl)-1,4-phenylene) (2*E*,2'*E*)-diacrylate

Dimethyl 3,3'-(2-(methoxycarbonyl)-1,4-phenylene) (2*E*,2'*E*)-diacrylate followed the general synthesis above resulting in a white powder (92% yield). The following NMR spectra are located in Appendix C.

^{1}H NMR (500 MHz, DMSO-d_6) δ 8.19 (d, J = 15.9 Hz, 2H), 8.11 (s, 2H), 7.94 (s, 2H), 7.89 (s, 2H), 7.67 (d, J = 15.5 Hz, 2H), 6.74 (d, J = 15.7 Hz, 2H), 6.60 (d, J = 15.9 Hz, 2H), 3.84 (s, 5H), 3.73 (s, 1H). ^{13}C NMR (126 MHz, DMSO-D_6) δ 166.90, 166.90, 166.86, 143.09, 142.13, 136.47, 136.06, 131.96, 131.13, 130.77, 129.02, 121.75, 120.54, 53.13, 52.21, 52.18, 40.02.

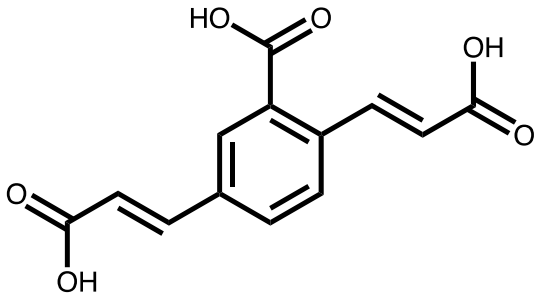

BM67 - (2*E*,2'*E*)-3,3'-(2-carboxy-1,4-phenylene) diacrylic acid

(2*E*,2'*E*)-3,3'-(2-Carboxy-1,4-phenylene) diacrylic acid followed the general synthesis above resulting in a white powder (80% yield). The following NMR spectra are located in Appendix C.

^{1}H NMR (500 MHz, DMSO-d_6) δ 8.22 (d, J = 15.8 Hz, 1H), 8.05 (d, J = 1.9 Hz, 1H), 7.91 – 7.81 (m, 2H), 7.60 (d, J = 16.0 Hz, 1H), 6.60 (d, J = 16.0 Hz, 1H), 6.47 (d, J = 16.0 Hz, 1H), 3.12 (s, 2H), 2.04 (s, 1H).^{13}C NMR (126 MHz, DMSO-D_6) δ 167.89, 142.70, 141.99, 136.29, 136.03, 132.52, 131.32, 130.57, 128.78, 122.66, 121.68, 49.12, 39.98, 31.22.

BM68 precursors - dimethyl 2,5-bis((*E*)-3-methoxy-3-oxoprop-1-en-1-yl) terephthalate

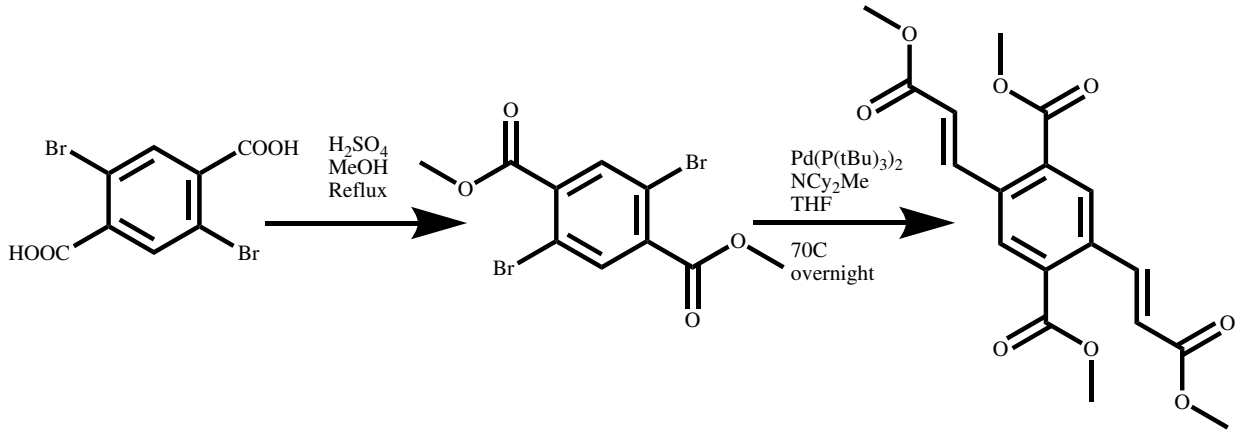

Scheme 6.1 Synthesis of BM68 precursor Dimethyl 2,5-bis((*E*)-3-methoxy-3-oxoprop-1-en-1-yl) terephthalate

Dimethyl 2,5-bis((*E*)-3-methoxy-3-oxoprop-1-en-1-yl) terephthalate was synthesized from 7 g 2,5-dibromoterephthalic acid that was dissolved in 80 mL methanol and 1 mL sulfuric acid and allowed to reflux for 24 hours. The resultant product was then precipitated overnight in the freezer and collected via filtration resulting in quantitative yield of 7.5g of white needle-like crystals (characterization follows). The dimethyl 2,5-dibromoterephthalate was sufficiently pure to proceed with Heck coupling. Dimethyl 2,5-bis((E)-3-methoxy-3-oxoprop-1-en-1-yl) terephthalate followed the general synthesis above resulting in a greasy white solid (60% yield). The following NMR spectra are located in Appendix C.

Dimethyl 2,5-dibromoterephthalate

^{1}H NMR (500 MHz, DMSO-d_6) δ 8.06 (s, 2H), 3.84 (s, 6H).

Dimethyl 2,5-bis((E)-3-methoxy-3-oxoprop-1-en-1-yl) terephthalate

^{1}H NMR (500 MHz, DMSO-d_6) δ 8.21 (d, J = 15.0 Hz, 2H), 8.12 (d, J = 16.0 Hz, 2H), 6.65 (dd, J = 53.5, 15.7 Hz, 2H), 3.70 (s, 6H), 3.58 (s, 6H).

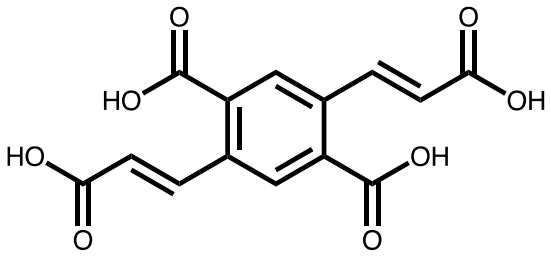

BM68 - 2,5-bis((*E*)-2-carboxyvinyl) terephthalic acid

2,5-Bis((E)-2-carboxyvinyl) terephthalic acid benzoate followed the general synthesis above resulting in a white powder (49% yield). The following NMR spectra are located in Appendix C.

^{1}H NMR (500 MHz, DMSO-d_6) δ 8.26 (d, J = 15.9 Hz, 2H), 7.95 (s, 2H), 6.41 (d, J = 16.1 Hz, 2H).

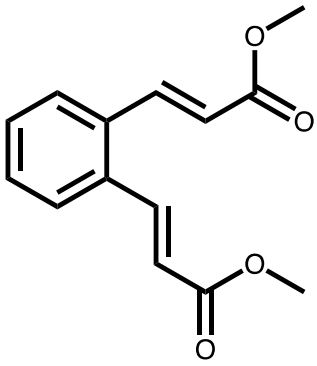

BM70 precursor - dimethyl 3,3'-(1,2-phenylene) (2*E*,2'*E*)-diacrylate

2,5-Bis((*E*)-2-carboxyvinyl) terephthalic acid followed the general synthesis above resulting in a light yellow liquid product (81% yield). The following NMR spectra are located in Appendix C.

^{1}H NMR (500 MHz, DMSO-d_6) δ 7.89 (dd, J = 15.7, 2.8 Hz, 2H), 7.75 – 7.69 (m, 2H), 7.44 – 7.39 (m, 2H), 6.47 (dd, J = 15.8, 2.9 Hz, 2H), 3.70 (d, J = 2.8 Hz, 6H). ^{13}C NMR (126 MHz, DMSO-D_6) δ 166.80, 141.20, 133.97, 130.93, 128.24, 121.65, 52.19, 39.99.

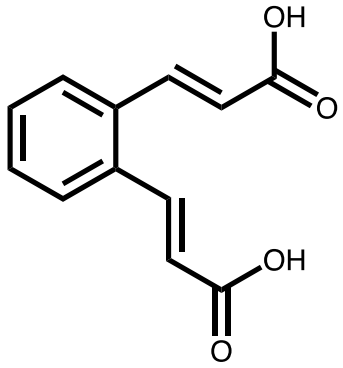

BM70 - (2*E*,2'*E*)-3,3'-(1,2-phenylene) diacrylic acid

(2E,2'E)-3,3'-(1,2-Phenylene) diacrylic acid followed the general synthesis above upon dissolution and addition of NaOH while refluxing the reaction turned milky pastel blue then turned into a white powder upon acidification (80% yield). The following NMR spectra are located in Appendix C.

^{1}H NMR (500 MHz, DMSO-d_6) δ 12.59 (s, 2H), 7.86 (d, J = 15.9 Hz, 2H), 7.73 (s, 2H), 7.42 (s, 2H), 6.40 (d, J = 15.9 Hz, 2H). ^{13}C NMR (126 MHz, DMSO-D_6) δ 167.73, 140.70, 134.07, 130.74, 128.17, 123.02, 40.02.

BM72 – precursor – methyl (*E*)-5-(3-methoxy-3-oxoprop-1-en-1-yl) thiophene-2-carboxylate

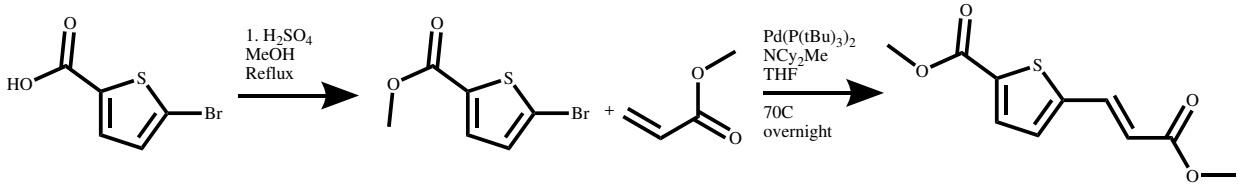

Scheme 6.2 synthesis of BM72 precursors 5-bromothiophene-2-carboxylate and methyl (E)-5-(3-methoxy-3-oxoprop-1-en-1-yl)thiophene-2-carboxylate

Methyl (E)-5-(3-methoxy-3-oxoprop-1-en-1-yl) thiophene-2-carboxylate was synthesized from 5-bromothiophene-2-carboxylic acid that was dissolved in 80 mL methanol and 1 mL sulfuric acid and allowed to reflux for 24 hours. The resultant product was then precipitated overnight in the freezer and collected via filtration resulting in a white powder with quantitative

yield. The resultant product methyl 5-bromothiophene-2-carboxylate was sufficiently pure to proceed to with the Heck coupling step as listed above. The resultant product formed a white powder (73% yield). The following NMR spectra are located in Appendix C.

5-bromothiophene-2-carboxylate

^{1}H NMR (500 MHz, DMSO-d_6) δ 7.61 (s, 1H), 7.33 (s, 1H), 3.78 (s, 3H). ^{13}C NMR (126 MHz, DMSO-D_6) δ 66.19, 39.96, 39.46, 37.49, 25.17, -42.05, -55.07.

(E)-5-(3-methoxy-3-oxoprop-1-en-1-yl) thiophene-2-carboxylate

^{1}H NMR (500 MHz, DMSO-d_6) δ 7.79 (d, J = 15.9 Hz, 1H), 7.75 (d, J = 3.9 Hz, 1H), 7.60 (d, J = 4.0 Hz, 1H), 6.49 (d, J = 15.9 Hz, 1H), 3.80 (s, 3H), 3.69 (s, 3H). ^{13}C NMR (126 MHz, DMSO-D_6) δ 166.56, 162.01, 145.31, 136.86, 134.91, 134.89, 132.44, 119.93, 53.07, 52.26, 40.03.

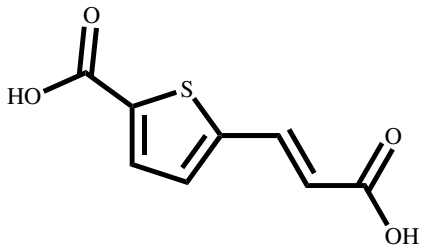

BM72 - methyl (*E*)-5-(3-methoxy-3-oxoprop-1-en-1-yl) thiophene-2-carboxylate

Methyl (*E*)-5-(3-methoxy-3-oxoprop-1-en-1-yl) thiophene-2-carboxylate followed the general synthesis resulting in an off white powder. The following NMR spectra are located in Appendix C.

^{1}H NMR (500 MHz, DMSO-d_6) δ 7.68 (d, J = 15.8 Hz, 2H), 7.64 (d, J = 3.9 Hz, 2H), 7.49 (d, J = 3.9 Hz, 2H), 6.33 (d, J = 16.0 Hz, 2H). ^{13}C NMR (126 MHz, DMSO-D_6) δ 167.43, 163.01, 145.06, 136.70, 136.46, 134.33, 131.99, 121.01, 39.99.

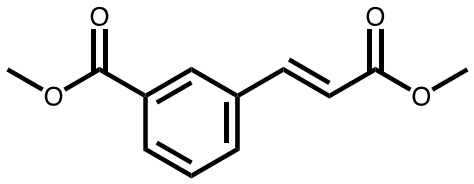

BM73 – precursor - methyl (*E*)-3-(3-methoxy-3-oxoprop-1-en-1-yl) benzoate

Methyl (*E*)-3-(3-methoxy-3-oxoprop-1-en-1-yl) benzoate followed the general synthesis above with the only change of 1.1 equivalents of methyl acrylate was utilized resulting in a white solid (92% yield). The following NMR spectra are located in Appendix C.

^{1}H NMR (500 MHz, DMSO-d_6) δ 8.16 (s, 1H), 7.95 (dd, *J* = 21.6, 7.8 Hz, 2H), 7.69 (d, *J* = 16.1 Hz, 1H), 7.53 (t, *J* = 7.8 Hz, 1H), 6.67 (d, *J* = 16.1 Hz, 1H), 3.83 (s, 3H), 3.69 (s, 3H). ^{13}C NMR (126 MHz, DMSO-D_6) δ 166.96, 166.30, 143.87, 135.14, 132.98, 131.28, 130.91, 129.94, 129.57, 119.76, 52.82, 52.10, 40.04.

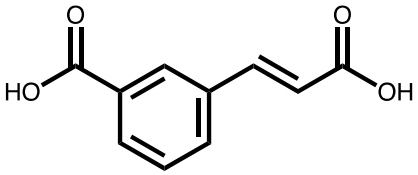

BM73 - (*E*)-3-(2-carboxyvinyl) benzoic acid

(*E*)-3-(2-carboxyvinyl) benzoic acid followed the general synthesis resulting in a white powder (95% yield). The following NMR spectra are located in Appendix C.

^{1}H NMR (500 MHz, DMSO-d_6) δ 8.12 (s, 1H), 7.93 (d, *J* = 4.6 Hz, 2H), 7.62 (d, *J* = 15.5 Hz, 1H), 7.51 (d, *J* = 10.8 Hz, 1H), 6.55 (d, *J* = 15.6 Hz, 1H). ^{13}C NMR (126 MHz, DMSO-D_6) δ 167.88, 167.42, 143.45, 135.20, 132.52, 132.06, 131.28, 129.80, 129.52, 120.97, 40.02.

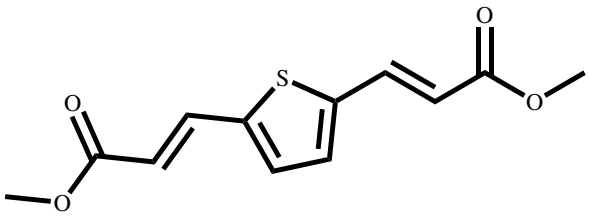

JB03- precursor - dimethyl 3,3'-(thiophene-2,5-diyl) (2E,2'E)-diacrylate

Dimethyl 3,3'-(thiophene-2,5-diyl) (2E,2'E)-diacrylate followed the general synthesis above with the only change being that a manual column was performed with 10% ethyl acetate, 5% DCM and 85% hexanes. Resulting in a matte yellow powder (85% yield). The following NMR spectra are located in Appendix C.

^{1}H NMR (500 MHz, DMSO-d_6) δ 7.75 (d, *J* = 16.0 Hz, 2H), 7.53 (s, 2H), 6.30 (d, *J* = 15.4 Hz, 2H), 3.68 (s, 6H).^{13}C NMR (126MHz, DMSO-D_6) δ 166.66, 141.89, 137.16, 118.34, 52.17.

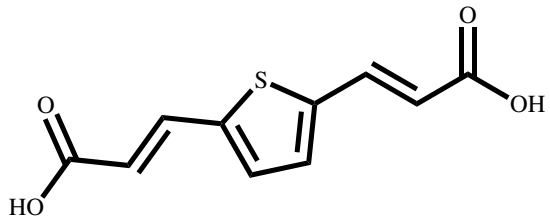

JB03 - (2*E*,2'*E*)-3,3'-(thiophene-2,5-diyl) diacrylic acid

(2*E*,2'*E*)-3,3'-(thiophene-2,5-diyl) diacrylic acid followed the general synthesis above resulting in a matte yellow powder (86% yield). The following NMR spectra are located in Appendix C.

^{1}H NMR (500 MHz, DMSO-d_6) δ 7.75 (d, J = 16.0 Hz, 2H), 7.53 (s, 2H), 6.30 (d, J = 15.4 Hz, 2H), 3.68 (s, 6H). ^{13}C NMR (126MHz, DMSO-D_6) δ 167.52, 141.80, 136.65, 133.15, 119.78.

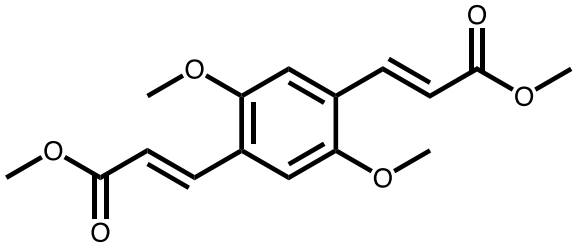

JB04-precursor - dimethyl 3,3'-(2,5-dimethoxy-1,4-phenylene) (2*E*,2'*E*)-diacrylate

Dimethyl 3,3'-(2,5-dimethoxy-1,4-phenylene) (2*E*,2'*E*)-diacrylate followed the general synthesis above, but instead of an extraction with DCM and acidic water the crude was stirred in acid water overnight and then filtered through a silica plug. In addition, trimethylamine was used instead of the N,N-dicyclohexylmethylamine. Resulting in a yellow powder (73% yield). The following NMR spectra are located in Appendix C.

^{1}H NMR (500 MHz, DMSO-d_6) δ 7.83 (d, J = 15.6 Hz, 1H), 7.39 (s, 1H), 6.77 (d, J = 15.9 Hz, 1H), 3.84 (s, 3H), 3.69 (s, 3H).

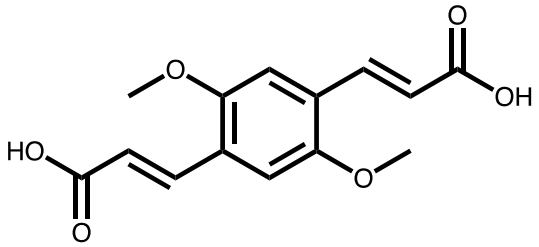

JB04 - (2*E*,2'*E*)-3,3'-(2,5-dimethoxy-1,4-phenylene) diacrylic acid

(2*E*,2'*E*)-3,3'-(2,5-Dimethoxy-1,4-phenylene) diacrylic acid followed the general synthesis above. Resulting in a bright yellow powder (86% yield). The following NMR spectra are located in Appendix C.

^{1}H NMR (500 MHz, DMSO-d_6) δ 12.38 (s, 1H), 7.78 (d, J = 16.0 Hz, 1H), 7.34 (s, 1H), 6.65 (d, J = 16.1 Hz, 1H), 3.83 (s, 3H). ^{13}C NMR (126MHz, DMSO-D_6) δ 168.33, 152.40, 138.25, 125.73, 121.14, 111.61 56.80.

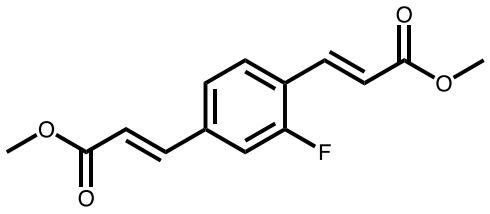

JB05-precursor - dimethyl 3,3'-(2-fluoro-1,4-phenylene) (2*E*,2'*E*)-diacrylate

Dimethyl 3,3'-(2-fluoro-1,4-phenylene) (2*E*,2'*E*)-diacrylate followed the general synthesis above, but instead of an extraction with DCM and acidic water the crude was stirred in acid water overnight and then filtered through a silica plug. Resulting in a shiny white powder (82% yield). The following NMR spectra are located in Appendix C.

^{1}H NMR (500 MHz, DMSO-d_6) δ 7.85 (s, 1H), 7.72 – 7.53 (m, 4H), 6.79 – 6.66 (m, 2H), 3.70 (s, 6H). ^{13}C NMR (126 MHz, DMSO-D_6) δ 166.89, 162.16, 160.16, 142.90, 138.81, 136.05, 130.19, 125.61, 123.74, 121.75, 120.99, 115.90, 115.72, 52.24, 52.16, 40.05.

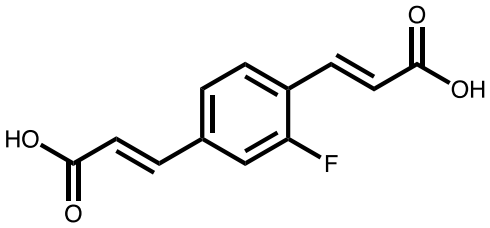

JB05 - (2*E*,2'*E*)-3,3'-(2-fluoro-1,4-phenylene) diacrylic acid

(2*E*,2'*E*)-3,3'-(2-Fluoro-1,4-phenylene) diacrylic acid followed the general synthesis above. Resulting in a white powder (76% yield). The following NMR spectra are located in Appendix C.

^{1}H NMR (500 MHz, DMSO-d_6) δ 7.81 (s, 1H), 7.69 – 7.46 (m, 4H), 6.62 (t, J = 13.9 Hz, 2H). ^{13}C NMR (126 MHz, DMSO-D6) δ 167.80, 167.73, 162.09, 160.10, 142.32, 138.80, 138.73, 135.51, 130.04, 125.39, 123.74, 123.64, 123.11, 123.07, 122.31, 115.74, 115.56, 40.27.

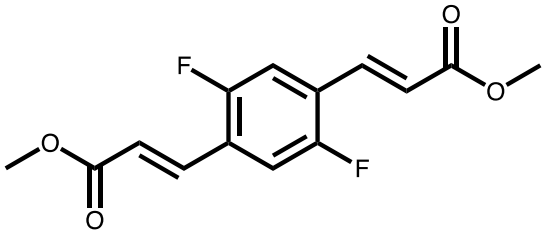

JB07-precursor - dimethyl 3,3'-(2,5-difluoro-1,4-phenylene) (2*E*,2'*E*)-diacrylate

Dimethyl 3,3'-(2,5-difluoro-1,4-phenylene) (2*E*,2'*E*)-diacrylate followed the general synthesis above, but instead of an extraction with DCM and acidic water the crude was stirred in acid water overnight and then filtered through a silica plug. In addition, two separate columns were run, the second using pure DCM. Resulting in a white powder (60% yield). The following NMR spectra are located in Appendix C.

^{1}H NMR (500MHz, DMSO-d_6) δ 7.88 (t, 2H), δ 7.59 (d, 2H), δ 6.79 (d, 2H), δ 3.71 (s, 6H).

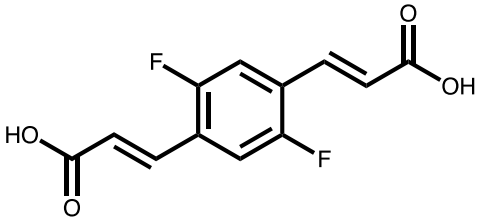

JB07 - (2*E*,2'*E*)-3,3'-(2,5-difluoro-1,4-phenylene) diacrylic acid

(2*E*,2'*E*)-3,3'-(2,5-Difluoro-1,4-phenylene) diacrylic acid followed the general synthesis above. Resulting in a white powder (83% yield). The following NMR spectra are located in Appendix C.

1H NMR (500 MHz, DMSO-d6) δ 7.84 (t, J = 8.6 Hz, 2H), 7.53 (d, J = 16.1 Hz, 2H), 6.68 (d, J = 16.1 Hz, 2H). 13C NMR (126 MHz, DMSO-D6) δ 167.51, 158.04, 156.09, 134.38, 125.50, 125.41, 125.31, 124.45, 116.24, 116.16, 116.09, 116.01, 115.95, 39.91.

6.3.2. Ni-MOF synthesis and characterization

All Ni-MOF crystals were prepared via a solvothermal approach.[25] The employed inorganic source was nickel nitrate hexahydrate (Alfa Aesar, ≥97%) and the employed organic linkers were BM 65 and BM 73, and, for comparison, the conventional BTC linker, benzene-1,3,5-tricarboxylic acid. The molar ratio of the nickel source to organic linker was kept constant at 4.08:1. In a typical synthesis, 2.0 g of nickel nitrate hexahydrate was dissolved in 15 mL of deionized water. In a separate beaker, 0.3 g of linker was dissolved in a solution mixture of 7.5 mL deionized water and 7.5 mL ethanol. The two solutions were combined and the resultant mixture was stirred thoroughly for 2 h. The mixture was transferred into a 45 mL Teflon-lined stainless steel autoclave and heated at 180 °C for 24 h. Then, the autoclave was cooled down to room temperature, and the resultant crystals at the bottom of the autoclave were washed with methanol three times. The crystals were dried overnight in the oven at 80 °C and used for subsequent characterization.

6.3.3. Ni-MOF/5A bead catalyst synthesis and characterization

Ni-MOF/zeolite 5A bead catalysts were prepared by solvothermally growing Ni-MOF on zeolite 5A beads (Grace Company) as described in our recent studies.[26-27] This zeolite displays LTA topology and has uniform micropores of ~0.5 nm. A similar Ni/organic linker mixture as described above was used and transferred into a 45 mL Teflon-lined stainless steel autoclave containing 5 g of pure zeolite 5A. The autoclave was then heated at 180 °C for 24 h. The resultant layered 5A beads were dried overnight at 80 °C. A second layer of Ni-MOF was applied repeating the procedure described above.

All samples were characterized by X-ray diffraction (XRD), field emission scanning electron microscopy with energy dispersive X-ray spectroscopy (FESEM-EDX), nitrogen sorption (BET), temperature programmed desorption (TPD), and thermal gravimetric analysis (TGA). XRD patterns were collected on a Kristalloflex 800 by Siemens at 25 mA and 30 kV with Cu Kα radiation. Before measurements, the Ni-MOF/zeolite 5A bead catalysts were ground by mortar and pestle into very fine powders. FESEM images were taken on JEOL ISM-7000F using a field emission gun and an accelerating voltage of 5 kV. N_2 isotherms were collected in a Micromeritics Tristar-3000 porosimeter at 77 K using liquid nitrogen as coolant. Before

measurements, the samples were degassed at 180 °C for 6 h under vacuum. TPD plots were acquired on a Micrometrics Autochem 2920 instrument. Samples were pretreated under helium at 120 °C for 1 h and then up to 300 °C for 1 h. The samples were then exposed to 10 % NH_3 gas in He, followed by a temperature ramp to 100 °C to remove any physisorbed species. The samples were then ramped at 30 °C min-1 from 120 to 300 °C to obtain the TPD curve. Data was normalized to sample mass, and integrated using Micrometrics software suite to obtain the quantity of NH3 adsorbed, which was equated to acid site density using a 1:1 stoichiometry. TGA profiles were obtained on a TGA Q50 under a constant flow of carbon dioxide, which is the gas atmosphere employed during the decarboxylation reactions.

6.3.4. Reaction procedures

Oleic acid (90%, Alfa Aesar) was used as the model fatty acid molecule. Before the reaction, the catalysts were pre-activated in an oven for 3 h at 150 °C. The reactions were conducted in a 100 mL stainless steel, high pressure batch reactor (Parr model 4560). Oleic acid and the catalyst were loaded into the reactor (mass ratio 1:1). Before the reaction was initiated, the air in the reactor was removed by flowing CO_2, followed by a pressure increase to 20 bar. Then the reactor was heated to 340 °C under constant stirring, and the temperature was kept constant during the duration of the reaction. After the reaction, the catalyst was separated from the product and washed with n-hexane 3 times, then with methanol 3 times, and finally heated at 300 °C overnight to remove the carbonaceous species formed during reaction.

6.3.5. Product analysis

The liquid product was collected and analyzed with a gas chromatograph (GC, 6980N) equipped with a HP-5 MS column (with dimensions of 30 m × 250 µm × 0.25 µm) and a 5973N MSD detector. Before the GC analysis, samples were silylated with N,O-bis(trimethylsilyl)trifluoroacetamide (BSTFA) (Sigma-Aldrich, ≥ 99.0%) and kept at 60 °C for 1 h. The sample (0.2 µL) was injected into the GC column (250 °C, 10.52 psi) with a 100:1 split ratio. The carrier gas was helium with a flow rate of 1.0 mL/min. The following gas chromatograph temperature program was used for the study: 100 °C for 5 min, 300 °C (1 °C/min for 2 min). The product identification was confirmed with a gas chromatograph-mass spectrometer (GC-MS).

Similar to our previous reports, the decarboxylation conversion of the oleic acid was estimated from the reduction in the number of oleic acid carboxylic acid groups during the reaction.[25-27] The amount of carboxylic acid groups remaining in the products after the reaction was evaluated by quantifying the acid number (ASTMD974). This acid number can be estimated with the mass of potassium hydroxide (KOH) in milligrams that is required to neutralize one gram of chemical substance. To quantify the acid number, a known amount of sample was dissolved in a solvent (ethanol and petroleum ether), then titrated with a solution of sodium hydroxide (NaOH, 0.1 N) using phenolphthalein as a color indicator.

The acid number was calculated from this equation where N=0.1 (N); V=volume of NaOH consumed (mL); W=mass of the sample (g).

$$\text{Acid number} = 56.1\frac{\text{NV}}{\text{W}}$$

The percent decarboxylation was calculated using the acid number of oleic acid and acid number of the product using the following relation: % Decarboxylation = (acid number of oleic acid – acid number of the product) / acid number of oleic acid × 100%.

6.3.6. Results and Discussion

Figure 6.1 (Page 112) shows representative SEM images of all synthesized Ni-MOF crystals. Ni-BM 65 and Ni-BM-73 crystals (Figure 6.1(b,c), Page 112) showed porous sphere-like structures with "raspberry" morphology, whereas Ni-BTC crystals (Figure 1(a)) showed irregular plate-like morphology with average widths of c.a. 10 μm and lengths of varying size over 100 μm. The average size of Ni-BM 65 crystals (Figure 6.1(b) Page 112) was 9.0 μm. Two different particle sizes for Ni-BM 73 crystals (Figure 6.1(c), Page 112) were observed: 3.1 μm and 8.3 μm. To confirm the crystalline character of the synthesized materials, XRD patterns of all prepared Ni-MOFs were collected and shown in Figure 6.2. The materials do present crystallinity, although the

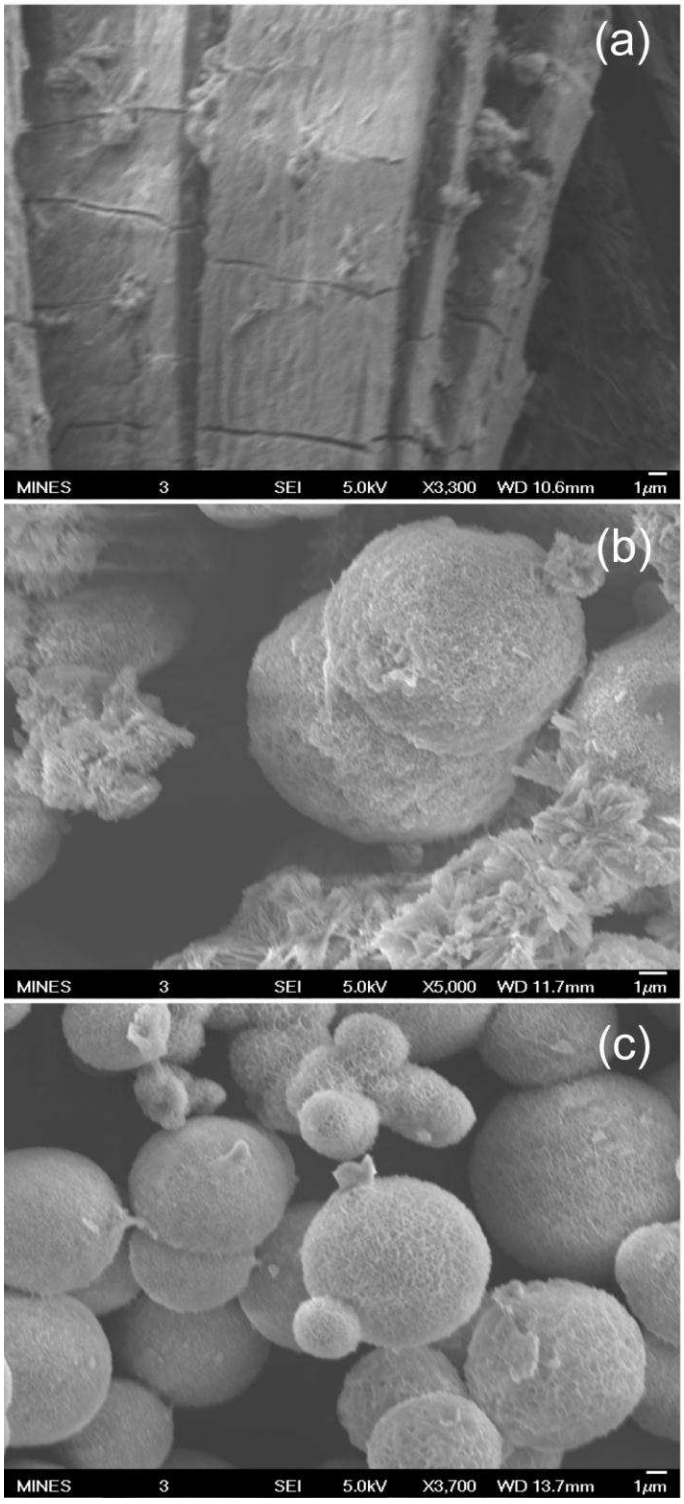

Figure 6.1 Representative SEM images for Ni-MOF crystals (a) Ni-BTC MOF; (b) Ni-BM 65 MOF and (c) Ni-BM 73 MOF.

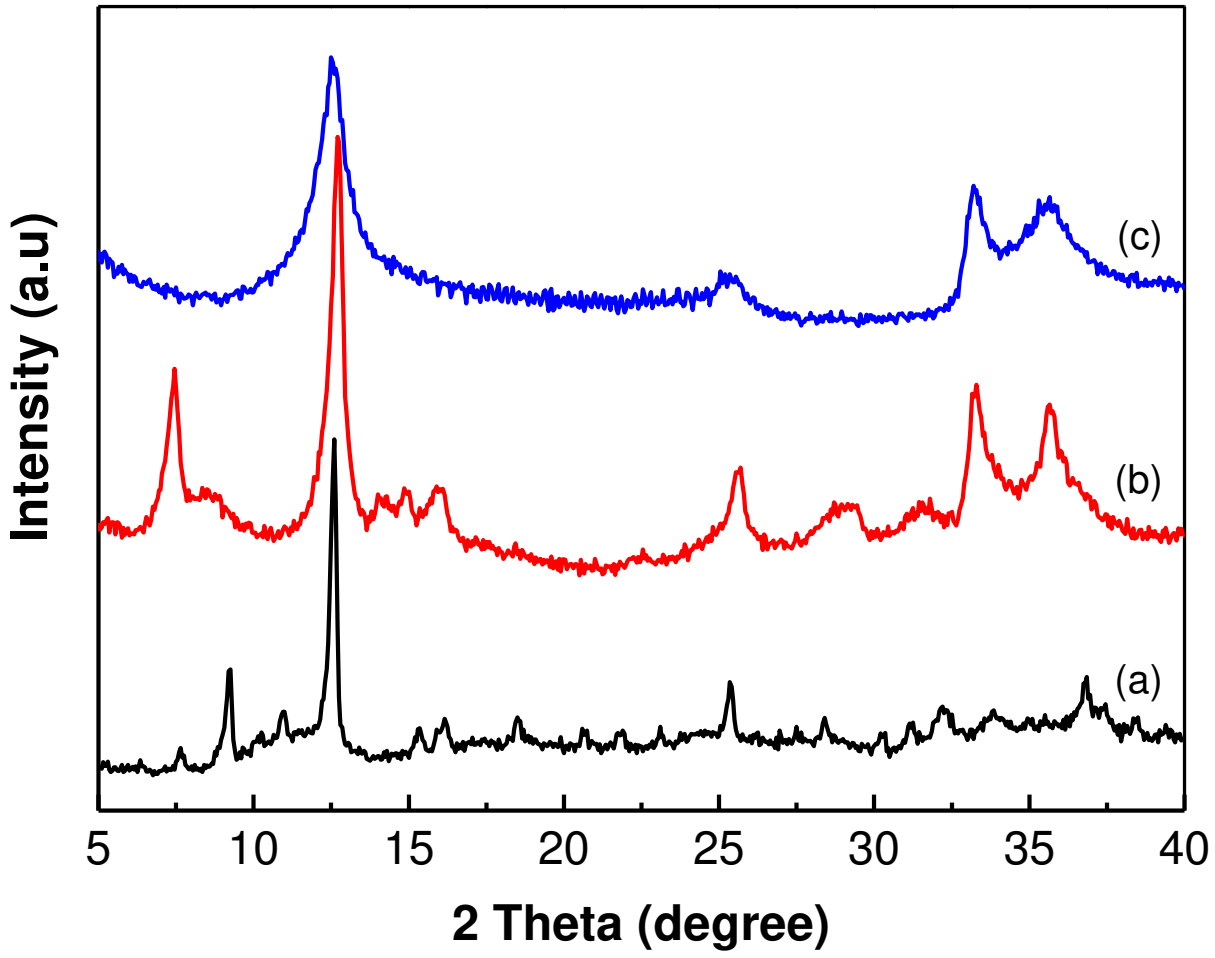

Figure 6.2 XRD patterns for Ni-MOF crystals (a) Ni-BTC; (b) Ni-BM 65 and (c) Ni-BM 73

varied "sharpness" of the XRD patterns for the three materials suggest varied degree of crystallinity. In particular, the relative sharpness of the patterns suggests that the larger molecule structure of the BM 65 and BM 73 linkers (as compared to BTC) led to overall lower crystallinity. PXRDs for MOFs based on these two linker present distinctive peaks at 2θ ~33˚ and ~36˚. Although, it was not possible to experimentally solve the structure of the MOFs synthesized here to unequivocally assign the origin of these peaks, inspection of simulated XRD patterns in over 200 Ni-MOFs obtained from the computation-ready, experimental (CoRE) MOF database,[28] clearly suggest that these peaks are indicative of short range features such as Ni-Ni distances (Figure S7 in reference [29] presents typical arrangements of Ni atoms in CoRE MOFs).

The CoRE MOFs as a subset of structures identified as MOFs derived from the Cambridge Structural Database (CSD)[30] are a good representation of MOFs synthesized to date.

By inspecting the linkers and crystallographic structures of the over 200 Ni-based CoRE MOFs, it is clear that Ni-BM 65 and Ni-BM 73 had not been previously synthesized. The CoRE MOFs, on the other hand, revealed around 15 different Ni-MOFs that have been synthesized based on the BTC linkers. Thus, we proceeded to compare simulated XRD patterns for these CoRE MOFs with the pattern measured here for Ni-BTC to determine whether our obtained Ni-BTC had been previously synthesized and possibly determine the crystallographic structure. This comparison discarded our Ni-BTC having the (3,4)-connected tbo topological network of the well-known Cu-BTC MOF,[31] or having a two dimensional structure. The closest match was obtained with the Ni-BTC MOF synthesized by Prior and Rosseinsky.[32]

To confirm the porosity of the synthesized materials, the surface areas of all studied Ni-MOFs were estimated applying BET theory to measured N_2 isotherms and listed in Table 6.1. To be certain of a meaningful comparison of BET areas for the synthesized is MOFs, we guided the BET area calculation with four consistency criteria as detailed in reference[33]. The BET areas ranged from 12 to 303 m^2/g, with Ni-BTC presenting the lowest BET area. Given the presumed small pore size of the three synthesized MOFs, the BET area correlates well with pore volume as expected.[29, 33] The thermal stability of the synthesized MOFs was determined via TGA. As shown in Figure 6.3 (Page 115), it is confirmed that the Ni-MOF crystals are thermally stable up to (at least) 360 °C.

After the described characterization of the MOFs was completed, we proceeded to grow the resultant Ni-MOFs on the surface of zeolite 5A beads, and to evaluate their catalytic ability to decarboxylate oleic acid into liquid hydrocarbons. Zeolite 5A is an aluminosilicate medium-pore-size molecular sieve with acidic sites that is commercially available at a relatively low cost.

Table 6.1 BET area of studied Ni-MOFs

MOF Sample	BET area (m^2/g)	Pore volume (cm^3/g)
Ni-BTC	12	0.02
Ni-BM 65	175	0.45
Ni-BM 73	303	0.89

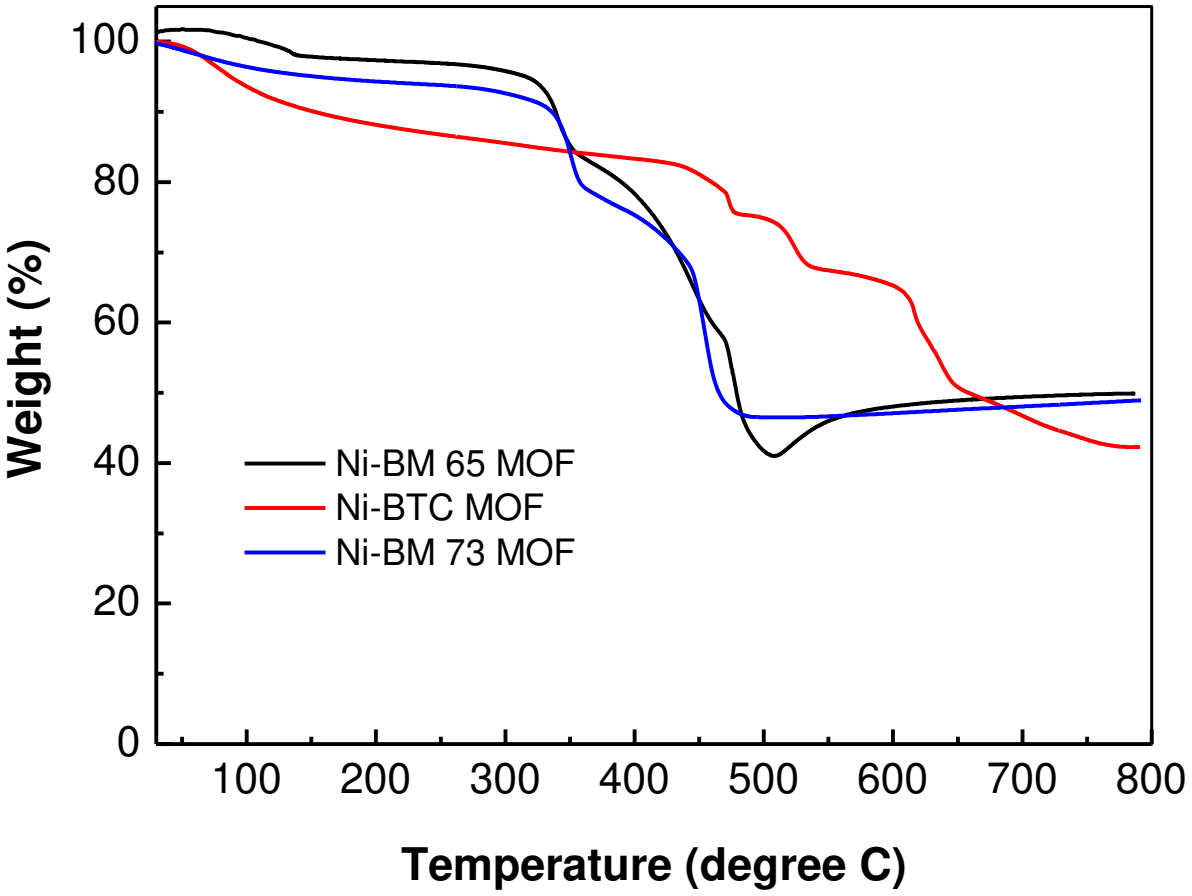

Figure 6.3 Three TGA profiles for the studied Ni-MOF crystals

It is well known that acidic supports play an important role in the decarboxylation reaction to obtain improved heptadecane selectivities.[34-35] In addition, as compared to powders, beads are much easier to recycle and can be fully recovered, and are therefore more amenable for potential scale-up in catalytic applications.

Figure 6.4 (Page 115) shows representative SEM images of the Ni-MOF/zeolite 5A bead catalysts. The images show continuous Ni-MOF layers of 375, 538 and 415 μm thickness, respectively, for Ni-BTC, Ni-BM 65 and Ni-BM 73, respectively. XRD characterization for all catalysts showed the typical structure of zeolite 5A, which crystallizes in the LTA topology. Figures 6.5 c-h (Page 118) specifically confirm that the crystalline structure of zeolite 5A was preserved after Ni-MOF deposition and recycling, indicating structural stability of the 5A bead supports.

The catalysts shown in Figure 6.4 (Page 117) were evaluated for the decarboxylation of oleic acid to liquid hydrocarbons. High conversion was observed (as high as 90% for decarboxylation) for all catalysts employed (fresh and spent) under the reaction conditions. The observed liquid product distribution for all the studied catalysts is summarized in Table 6.2 (Page 118). To clearly appreciate the role of the Ni-MOF catalysts, it is important to note that pure zeolite 5A beads provided heptadecane yields of only ~14%. Indeed, mainly short chain hydrocarbons (C7-C12) were observed in the presence of pure zeolite 5A beads, which are generated through cracking of oleic acid and/or long chain hydrocarbons.[36-37] Furthermore, the selectivity to heptadecane increased when zeolite 5A beads were coated with the Ni-MOFs, with the highest selectivity to n-heptadecane obtained with the Ni-BM 65/zeolite 5A catalyst. Other components in the liquid product included branched paraffins formed by isomerization of the initially formed heptadecane, and lower molecular weight hydrocarbons (mostly C7-C16 paraffins) formed by cracking of the heptadecane. The observed products were: octadecane, heptadecane, dodecane, undecane, decane, nonane, octane, and heptane.

A decrease of selectivity to n-heptadecane was observed for the spent catalysts (Table 6.2, Page 119) likely the result of surface carbon deposited on the catalysts thus lowering subsequent activity. This observation is consistent with decreases in pore volume for all studied catalysts (Table 6.3, Page 120) which may prevent access of oleic acid into the active sites. The Ni content of fresh and spent Ni-MOF/zeolite 5A bead catalysts were estimated by EDX. Importantly, the EDX results confirmed that there was negligible Ni leaching for all recycled spent catalysts after decarboxylation reactions (Table 6.4, Page 120).

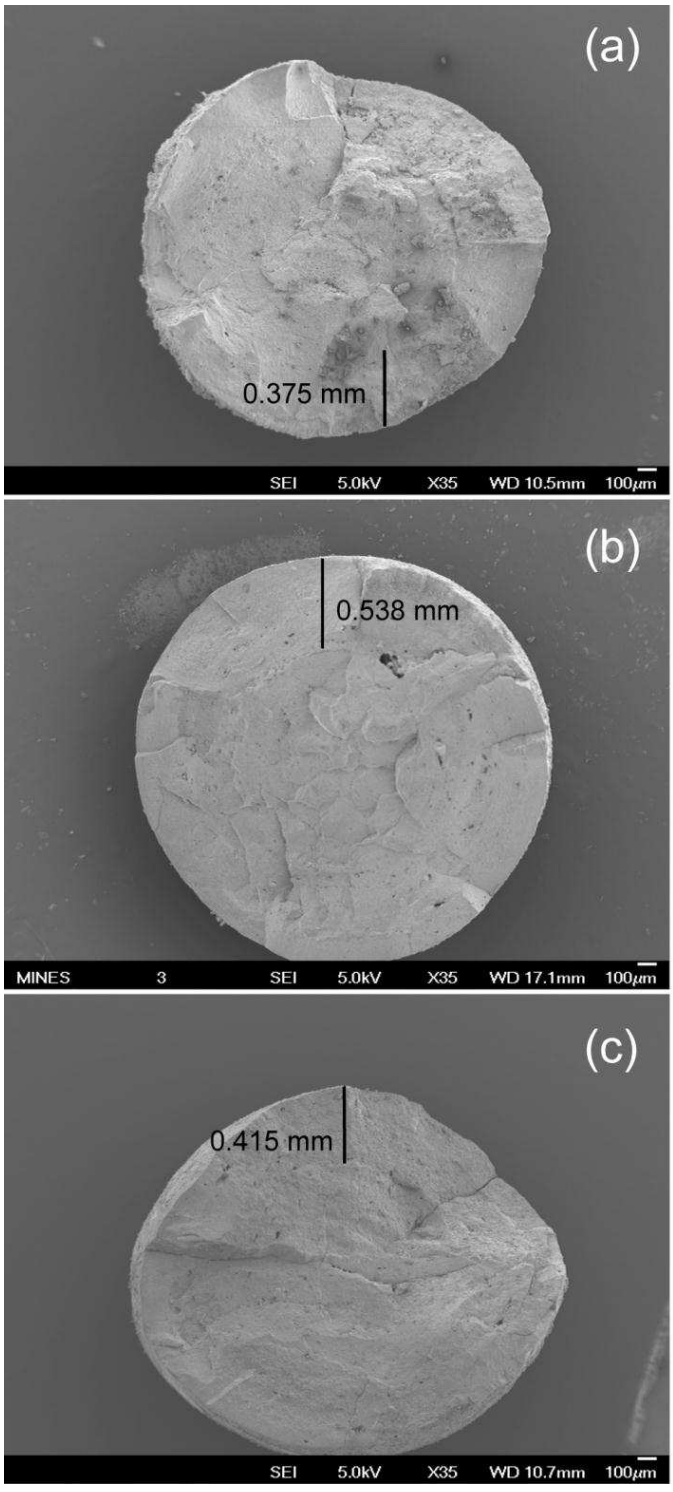

Figure 6.4 SEM images for Ni-MOF/zeolite 5A bead catalysts (a) Ni-BTC MOF/zeolite 5A; (b) Ni-BM 65 MOF/zeolite 5A and (c) Ni-BM 73 MOF/zeolite 5A.

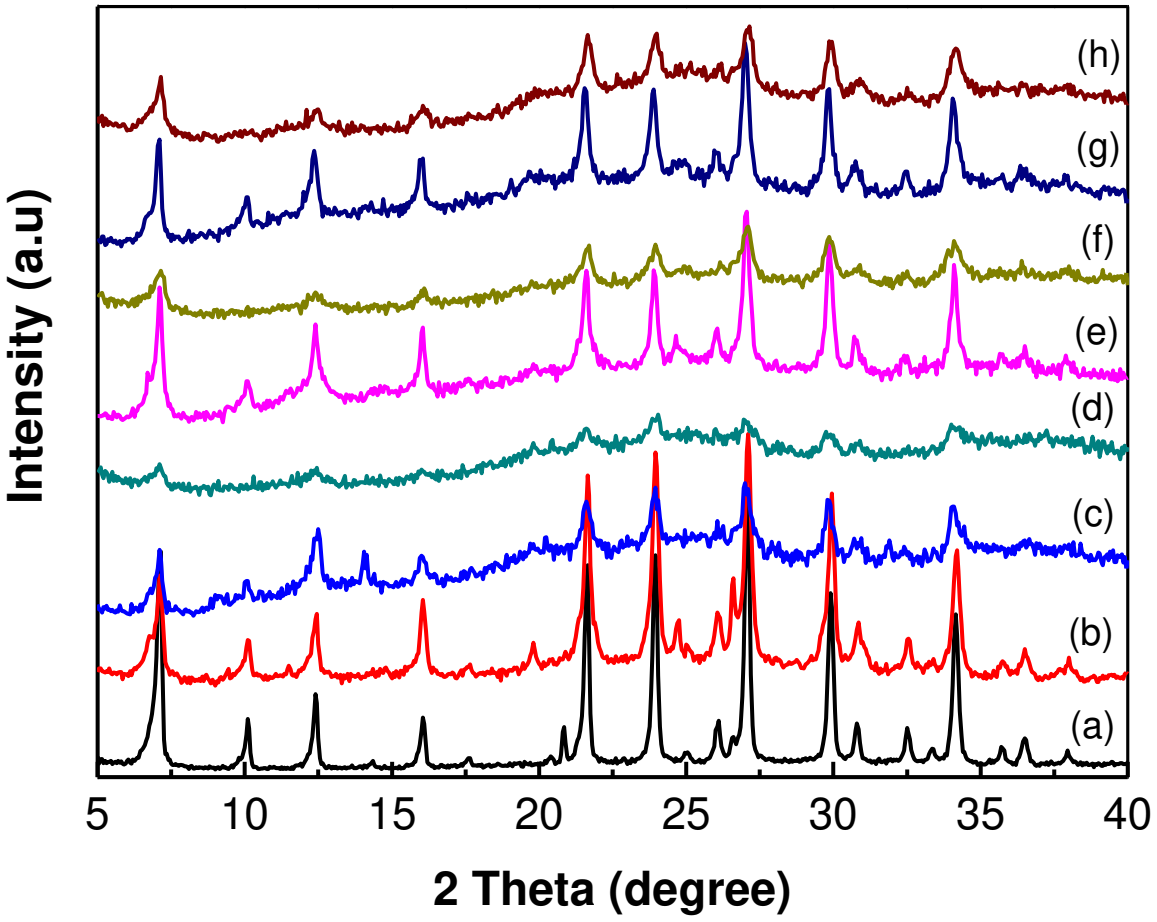

Figure 6.5 XRD patterns for catalysts (a) fresh zeolite 5A; (b) spent zeolite 5A; (c) fresh Ni-BTC MOF/zeolite 5A; (d) spent Ni-BTC MOF/zeolite 5A; (e) fresh Ni-BM 65 MOF/zeolite 5A; (f) spent Ni-BM 65 MOF/zeolite 5A; (g) fresh Ni-BM 73 MOF/zeolite 5A and (h) spent Ni-BM 73 MOF/zeolite 5A.

Table 6.2 Liquid product distribution for all studied catalysts

Catalysts	**Hydrocarbon distribution (%)**						
	Octadecane	Heptadecane	Hexadecane	Pentadecane	Tetradecane	Tridecane	
Zeolite 5A	8.18	13.91	2.12	3.56	2.75	3.84	
fresh Ni-BTC MOF/zeolite 5A	1.64	70.11	2.21	3.17	0.95	1.39	
spent Ni-BTC MOF/zeolite 5A	3.18	49.37	2.16	3.68	2.06	3.05	
fresh Ni-BM65 MOF/zeolite 5A	2.57	76.74	1.48	2.80	0.89	1.21	
spent Ni-BM65 MOF/zeolite 5A	1.79	56.19	1.43	3.03	1.20	1.50	
fresh Ni- BM73 MOF/zeolite 5A	2.22	71.97	1.58	2.65	1.06	1.58	
spent Ni- BM 73 MOF/zeolite 5A	2.64	52.92	1.53	3.16	1.44	2.09	
Catalysts	Hydrocarbon distribution (%)						
	Dodecane	Undecane	Decane	Nonane	Octane	Heptane	Unknown
zeolite 5A	7.43	9.16	9.90	11.36	12.91	11.79	3.06
fresh Ni-BTC MOF/zeolite 5A	2.25	2.81	2.30	4.24	4.67	3.04	1.22
spent Ni-BTC MOF/zeolite 5A	4.19	5.27	5.65	7.03	7.84	5.31	1.21
fresh Ni-BM65 MOF/zeolite 5A	1.67	2.30	2.06	2.48	2.85	1.92	1.03
spent Ni-BM65 MOF/zeolite 5A	2.50	3.54	4.06	7.51	9.20	6.83	1.21
fresh Ni-BM73 MOF/zeolite 5A	2.28	3.03	2.40	3.39	4.07	2.65	1.12
spent Ni-BM73 MOF/zeolite 5A	3.45	4.42	4.99	7.08	8.13	6.41	1.74

Table 6.3 BET areas and pore volumes for fresh and spent Ni-MOF/zeolite 5A bead catalysts

Catalysts	BET area (m^2/g)	Pore volume (cm^3/g)	Micropore volume (cm^3/g)
fresh Ni-BTC MOF/zeolite 5A	188	0.20	0.032
spent Ni-BTC MOF/zeolite 5A	139	0.19	0.024
fresh Ni-BM 65 MOF/zeolite 5A	264	0.24	0.083
spent Ni- BM 65 MOF/zeolite 5A	170	0.18	0.047
fresh Ni- BM 73 MOF/zeolite 5A	164	0.15	0.050
spent Ni- BM 73 MOF/zeolite 5A	129	0.14	0.033

Table 6.4 Ni content for all studied Ni-MOF/zeolite 5A bead catalysts

Catalysts	Averaged Ni content (wt%)
fresh Ni-BTC MOF/zeolite 5A	27.49±1.46
spent Ni-BTC MOF/zeolite 5A	27.07±2.73
fresh Ni-BM 65 MOF/zeolite 5A	27.67±2.79
spent Ni- BM 65 MOF/zeolite 5A	27.23±1.55
fresh Ni- BM 73 MOF/zeolite 5A	28.21±2.94
spent Ni- BM 73 MOF/zeolite 5A	27.20±2.06

The acid sites on the as-prepared and spent MOF/zeolite 5A catalysts are summarized in Table6.5. Fresh catalyst exhibited significantly higher acidity than the corresponding spent catalyst. Post-catalysis samples show approximately a 50% decrease in acid site content, except for Ni-BM 73 MOF/zeolite 5A, which shows negligible change. Ni-BM 73 also shows a reduction in the temperature of the peak desorption. The higher temperature desorption peak observed for Ni-BM73 is likely associated to free carboxylic acids of the linker that have not crystalized into the MOF framework due to the asymmetry of the linker. [38]

Table 6.5 Summary of acid site density data from TPD of NH_3 post catalysis

Catalysts	**T_{max} (°C)**	**Acid site density (µmol/g)**
zeolite 5A	255	1451
fresh Ni-BTC MOF/zeolite 5A	213	952
spent Ni-BTC MOF/zeolite 5A	206	494
fresh Ni-BM 65 MOF/zeolite 5A	205	1382
spent Ni- BM 65 MOF/zeolite 5A	196	423
fresh Ni- BM 73 MOF/zeolite 5A	300	456
spent Ni- BM 73 MOF/zeolite 5A	196	441

The high aptitude towards selective oleic acid decarboxylation to heptadecane of these structurally disordered MOFs does not correlate with the density of sites. The zeolite 5A support shows comparable acidity with Ni-BTC and Ni-BM 65, but minimal heptadecane yield. Therefore, Ni must play a key role in the catalytic decarboxylation of oleic acid. Interestingly, heptadecane yield scaled with micropore volume. As we move from BTC to BM 73 to BM 65 the length of the linker increases leading to progressively larger micropore volumes. Larger linkers can facilitate mass transport of the substrate and the product increasing observed yield.

Table 6.6 Comparison of the catalytic conversion of oleic acid to heptadecane through different catalysts*

Entry	Catalyst	Reaction conditions	Mass ratio of metal to oleic acid	Conversion (%)	Heptadecane selectivity (%)	Ref
1	Activated carbon	T=370 °C, t=3 h	-	80±4	7±1	[2]
2	$Co_{0.5}Mo_{0.5}$	T=300 °C, t=3 h	1:40	88.1	6.1	[6]
3	5CoAl	T=330 °C, P=50 bar, LHSV=2 h^{-1}	-	100.0	47.0	[10]
4	5NiAl	T=330 °C, P=50 bar, LHSV=2 h^{-1}	-	93.0	25.5	[10]
5	Sulfide Mo/P/Al_2O_3	T=320 °C	-	81.9	76.0	[11]
6	Sulfide NiW/Al_2O_3	T=340 °C	-	85.7	75.5	[11]
7	MgO-Al_2O_3	T=400 °C	1:42	98	6.93	[12]
8	$Ce_{0.6}Zr_{0.4}O_2$	T=300 °C, t=6 h	1:40	94.6	11	[13]
9	Mo/Zeol	T=360 °C, P=20 bar, t=1 h	-	-	19	[39]
10	SnAlMg-2	T=300 °C, t=6 h	1:75	71.1	3.7	[40]
11	Ni/Al_2O_3	T=360 °C, P=20 bar, t=0.75 h	1:21505	-	10	[41]
12	Fe-MSN	T=290 °C, P=30 bar, t=6 h	1:4.7	100	12	[42]
13	NiWC/Al-SBA-15	4 h in super-critical water	1:44	97.3	5.2	[43]
14	Activated carbon	T=370±2 °C, P=241 bar	-	99.4±0.5	80.6±4	[44]
15	Mo_2N/γ-Al_2O_3	T=380 °C, P=71.5 bar, LHSV=0.45 h^{-1}	-	99.9	12	[45]
16	Ni/ZnO-Al_2O_3	T=280 °C, P=30 bar, t=6 h	1:100	100	95.1	[46]
17	Ni-BM 65 MOF/zeolite 5A	T=340 °C, P=20 bar, t=2 h	1:33	91.1	76.7	this study

*Only the best catalytic performance of each reference is shown. Note: in entries 8, 9, 11, 12, 15 and 16, hydrogen is used.

We ran a reaction with a homogeneous catalyst consisting of nickel nitrate hexahydrate and BM-65 MOF linker (reaction conditions: T=340 °C, P=20 bar, CO_2 atmosphere, t=2 h) and mass ratio of catalyst to oleic acid 1:1. The conversion was ~94%, with much lower selectivity to heptadecane (47.7%). These results suggest that indeed the presence of a MOF structure (and porosity) is needed to observe higher heptadecane selectivity (Table 6.6, Page 122).

In addition, we evaluated the catalytic activity of Ni-BM 65 MOF powders. The Ni-MOF powders displayed good catalytic ability (~90% conversion and ~73% heptadecane selectivity). This performance was slightly lower than the Ni-BM 65 MOF/zeolite 5A (Table 6.6 entry 17 Page 122). We have demonstrated previously that acid supports[25, 34] including zeolite 5A[26] help to improve heptadecane selectivity. Therefore, both Ni- BM 65 MOF and zeolite 5A play an important role as active sites for the decarboxylation of oleic acid to heptadecane. Further studies are needed to elucidate the specific role of each of them for this particular reaction. It is important to mention that only ~50% of the Ni-BM 65 powders were recovered after reaction, while 100% of the Ni-BM 65 MOF/zeolite 5A was recovered after reaction.

Table 6.6 (Page 122) compares the state-of-the-art non-noble metal catalysts that have been employed specifically for the catalytic conversion of oleic acid to heptadecane. Sulfide Mo/P and NiW supported on Al_2O_3 had similar catalytic performance (76% selectivity to heptadecane) as Ni-BM 65 MOF/zeolite 5A bead catalyst.[11] However, the use of sulfur based catalysts may result in sulfide contamination leading to serious environmental issues. Activated carbon shows high selectivity to heptadecane 80%). However, to achieve this the pressure as high as 241 bar and temperature of 370 °C are needed.[44] Ni supported on ZnO and Al_2O_3 has displayed heptadecane selectivities higher than 95%, but the reaction requires higher pressure and longer reaction times (30 bar and 6 hours).[46] Importantly, in our study we did not employ hydrogen (we employed CO_2, a lower cost renewable feedstock), that has higher potential as a viable commercial process. The benefit of using CO_2 gas atmosphere was reported in our previous research.[27]

6.4. Conclusions

We have demonstrated the successful synthesis of nickel based metal organic frameworks (Ni-MOFs) employing novel carboxylic acid linkers. Furthermore, the deposition of these MOFs on zeolite 5A beads was illustrated and shown to produce catalytically active materials for the

conversion of oleic acid into liquid hydrocarbons. The resultant Ni-MOF/zeolite 5A bead catalysts displayed heptadecane selectivity as high as ~77%. All of the studied catalysts displayed a loss in catalytic activity after recycling. This is likely due to surface carbon that deposited during the reaction, resulting in the loss of surface area and pore volume. Our efforts demonstrate that it is possible to obtain effective catalytic decarboxylation of fatty acid with non-noble metal-based catalysts. Indeed, to the best of our knowledge the catalytic performance of Ni-BM 65 MOF/zeolite 5A bead catalyst is superior to all non-noble metal state-of-the-art catalysts at mild reaction conditions. We also show that the use of CO_2 during reaction may lead to a more viable and cost effective route to catalytically convert fatty acid methyl esters into alternative liquid fuels. We envision the presented work will encourage synthesis and study of MOFs based on earth-abundant metals for catalytic applications.

6.5. Acknowledgements

This research was supported by the Renewable Energy Materials Research Science and Engineering Center (REMRSEC) under Award Number DMR-0820518, and by startup funds from Colorado School of Mines (CSM).

6.6. References Cited

1. Yang, L.; McNichols, B. W.; Davidson, M.; Schweitzer, B.; Gomez-Gualdron, D. A.; Trewyn, B. G.; Sellinger, A.; Carreon, M. A., Noble metal-free catalytic decarboxylation of oleic acid to n-heptadecane on nickel-based metal-organic frameworks (MOFs). *Catalysis Science & Technology* **2017**.

2. Fu, J.; Shi, F.; Thompson, L. T.; Lu, X.; Savage, P. E., Activated Carbons for Hydrothermal Decarboxylation of Fatty Acids. *ACS Catalysis* **2011,** *1* (3), 227-231.

3. De, S.; Saha, B.; Luque, R., Hydrodeoxygenation processes: advances on catalytic transformations of biomass-derived platform chemicals into hydrocarbon fuels. *Bioresour Technol* **2015,** *178*, 108-18.

4. Vardon, D. R.; Sharma, B. K.; Jaramillo, H.; Kim, D.; Choe, J. K.; Ciesielski, P. N.; Strathmann, T. J., Hydrothermal catalytic processing of saturated and unsaturated fatty acids to hydrocarbons with glycerol for in situ hydrogen production. *Green Chemistry* **2014,** *16* (3), 1507.

5. Hengst, K.; Arend, M.; Pfützenreuter, R.; Hoelderich, W. F., Deoxygenation and cracking of free fatty acids over acidic catalysts by single step conversion for the production of diesel fuel and fuel blends. *Applied Catalysis B: Environmental* **2015,** *174–175*, 383-394.

6. Shim, J.-O.; Jeong, D.-W.; Jang, W.-J.; Jeon, K.-W.; Kim, S.-H.; Jeon, B.-H.; Roh, H.-S.; Na, J.-G.; Oh, Y.-K.; Han, S. S.; Ko, C. H., Optimization of unsupported CoMo catalysts for decarboxylation of oleic acid. *Catalysis Communications* **2015,** *67*, 16-20.

7. Striebich, R. C.; Smart, C. E.; Gunasekera, T. S.; Mueller, S. S.; Strobel, E. M.; McNichols, B. W.; Ruiz, O. N., Characterization of the F-76 diesel and Jet-A aviation fuel hydrocarbon degradation profiles of Pseudomonas aeruginosa and Marinobacter hydrocarbonoclasticus. *International Biodeterioration & Biodegradation* **2014,** *93*, 33-43.

8. Snåre, M.; Kubičková, I.; Mäki-Arvela, P.; Eränen, K.; Murzin, D. Y., Heterogeneous Catalytic Deoxygenation of Stearic Acid for Production of Biodiesel. *Industrial & Engineering Chemistry Research* **2006,** *45* (16), 5708-5715.

9. Berenblyum, A. S.; Shamsiev, R. S.; Podoplelova, T. A.; Danyushevsky, V. Y., The influence of metal and carrier natures on the effectiveness of catalysts of the deoxygenation of fatty acids into hydrocarbons. *Russian Journal of Physical Chemistry A* **2012,** *86* (8), 1199-1203.

10. Srifa, A.; Faungnawakij, K.; Itthibenchapong, V.; Assabumrungrat, S., Roles of monometallic catalysts in hydrodeoxygenation of palm oil to green diesel. *Chemical Engineering Journal* **2015,** *278*, 249-258.

11. Szarvas, T.; Eller, Z.; Kasza, T.; Ollár, T.; Tétényi, P.; Hancsók, J., Radioisotopic investigation of the oleic acid-1-14C HDO reaction pathways on sulfided Mo/P/Al2O3 and NiW/Al2O3 catalysts. *Applied Catalysis B: Environmental* **2015,** *165*, 245-252.

12. Na, J.-G.; Yi, B. E.; Kim, J. N.; Yi, K. B.; Park, S.-Y.; Park, J.-H.; Kim, J.-N.; Ko, C. H., Hydrocarbon production from decarboxylation of fatty acid without hydrogen. *Catalysis Today* **2010,** *156* (1–2), 44-48.

13. Shim, J.-O.; Jeong, D.-W.; Jang, W.-J.; Jeon, K.-W.; Jeon, B.-H.; Cho, S. Y.; Roh, H.-S.; Na, J.-G.; Ko, C. H.; Oh, Y.-K.; Han, S. S., Deoxygenation of oleic acid over Ce(1–x)Zr(x)O2 catalysts in hydrogen environment. *Renewable Energy* **2014,** *65*, 36-40.

14. Gómez-Gualdrón, D. A.; Colón, Y. J.; Zhang, X.; Wang, T. C.; Chen, Y.-S.; Hupp, J. T.; Yildirim, T.; Farha, O. K.; Zhang, J.; Snurr, R. Q., Evaluating topologically diverse metal–organic frameworks for cryo-adsorbed hydrogen storage. *Energy & Environmental Science* **2016,** *9* (10), 3279-3289.

15. Gascon, J.; Corma, A.; Kapteijn, F.; Llabrés i Xamena, F. X., Metal Organic Framework Catalysis: Quo vadis? *ACS Catal.* **2014,** *4*, 361.

16. Farha, O. K.; Shultz, A. M.; Sarjeant, A. A.; Nguyen, S. T.; Hupp, J. T., Active-site-accessible, porphyrinic metal-organic framework materials. *Journal of the American Chemical Society* **2011,** *133*, 5652.

17. Cavka, J. H.; Jakobsen, S.; Olsbye, U.; Guillou, N.; Lamberti, C.; Bordiga, S.; Lillerud, K. P., A new zirconium inorganic building brick forming metal organic frameworks with exceptional stability. *Journal of the American Chemical Society* **2008,** *130* (42), 13850-13851.

18. Mondloch, J. E.; Bury, W.; Fairen-Jimenez, D.; Kwon, S.; DeMarco, E. J.; Weston, M. H.; Sarjeant, A. A.; Nguyen, S. T.; Stair, P. C.; Snurr, R. Q.; Farha, O. K.; Hupp, J. T., Vapor-Phase Metalation by Atomic Layer Deposition in a Metal–Organic Framework. *Journal of the American Chemical Society* **2013,** *135*, 10294.

19. Park, K. S.; Ni, Z.; Cote, A. P.; Choi, J. Y.; Huang, R.; Uribe-Romo, F. J.; Chae, H. K.; O'Keeffe, M.; Yaghi, O. M., Exceptional chemical and thermal stability of zeolitic imidazolate frameworks. *Proc Natl Acad Sci U S A* **2006,** *103* (27), 10186-91.

20. Férey, G.; Mellot-Draznieks, C.; Serre, C.; Millange, F.; Dutour, J.; Surblé, S.; Margiolaki, I., A Chromium Terephthalate-Based Solid with Unusually Large Pore Volumes and Surface Area. *Science* **2005,** *309*, 2040.

21. MacGillivray, L. R., *Metal-organic frameworks: design and application*. John Wiley & Sons: 2010.

22. Gosselink, R. W.; Hollak, S. A. W.; Chang, S.-W.; van Haveren, J.; de Jong, K. P.; Bitter, J. H.; van Es, D. S., Reaction Pathways for the Deoxygenation of Vegetable Oils and Related Model Compounds. *ChemSusChem* **2013,** *6* (9), 1576-1594.

23. Wu, J.; Shi, J.; Fu, J.; Leidl, J. A.; Hou, Z.; Lu, X., Catalytic Decarboxylation of Fatty Acids to Aviation Fuels over Nickel Supported on Activated Carbon. *Scientific Reports* **2016,** *6*, 27820.

24. Jiang, J.; Furukawa, H.; Zhang, Y.-B.; Yaghi, O. M., High Methane Storage Working Capacity in Metal–Organic Frameworks with Acrylate Links. *Journal of the American Chemical Society* **2016,** *138* (32), 10244-10251.

25. Yang, L.; Ruess, G. L.; Carreon, M. A., Cu, Al and Ga based metal organic framework catalysts for the decarboxylation of oleic acid. *Catalysis Science & Technology* **2015,** *5* (5), 2777-2782.

26. Yang, L.; Tate, K. L.; Jasinski, J. B.; Carreon, M. A., Decarboxylation of Oleic Acid to Heptadecane over Pt Supported on Zeolite 5A Beads. *ACS Catalysis* **2015,** *5* (11), 6497-6502.

27. Yang, L.; Carreon, M. A., Effect of reaction parameters on the decarboxylation of oleic acid over Pt/ZIF-67membrane/zeolite 5A bead catalysts. *Journal of Chemical Technology & Biotechnology* **2017,** *92* (1), 52-58.

28. Chung, Y. G.; Camp, J.; Haranczyk, M.; Sikora, B. J.; Bury, W.; Krungleviciute, V.; Yildirim, T.; Farha, O. K.; Sholl, D. S.; Snurr, R. Q., Computation-Ready, Experimental Metal–Organic Frameworks: A Tool To Enable High-Throughput Screening of Nanoporous Crystals. *Chemistry of Materials* **2014,** *26*, 6185.

29. Yang, L.; McNichols, B. W.; Davidson, M.; Schweitzer, B.; Gomez-Gualdron, D. A.; Trewyn, B. G.; Sellinger, A.; Carreon, M. A., Noble metal-free catalytic decarboxylation of oleic acid to n-heptadecane on nickel-based metal-organic frameworks (MOFs). *Catalysis Science & Technology* **2017,** *7* (14), 3027-3035.

30. Groom, C. R.; Bruno, I. J.; Lightfoot, M. P.; Ward, S. C., The Cambridge Structural Database. *Acta Crystallographica Section B* **2016,** *72* (2), 171-179.

31. Chui, S. S. Y.; Lo, S. M. F.; Charmant, J. P. H.; Orpen, A. G.; Williams, I. D., *Science* **1999,** *283*, 1148.

32. Prior, T.; Rosseinsky, M., Chiral direction and interconnection of helical three-connected networks in metal-organic frameworks. *Inorganic Chemistry* **2003,** *42* (5), 1564-1575.

33. Gomez-Gualdron, D. A.; Moghadam, P. Z.; Hupp, J. T.; Farha, O. K.; Snurr, R. Q., Application of Consistency Criteria To Calculate BET Areas of Micro- And Mesoporous Metal-Organic Frameworks. *Journal of the American Chemical Society* **2016,** *138*, 215.

34. Ahmadi, M.; Nambo, A.; Jasinski, J. B.; Ratnasamy, P.; Carreon, M. A., Decarboxylation of oleic acid over Pt catalysts supported on small-pore zeolites and hydrotalcite. *Catal. Sci. Technol.* **2015,** *5* (1), 380-388.

35. Ahmadi, M.; Macias, E. E.; Jasinski, J. B.; Ratnasamy, P.; Carreon, M. A., Decarboxylation and further transformation of oleic acid over bifunctional, Pt/SAPO-11 catalyst and Pt/chloride Al2O3 catalysts. *Journal of Molecular Catalysis A: Chemical* **2014,** *386*, 14-19.

36. Černý, R.; Kubů, M.; Kubička, D., The effect of oxygenates structure on their deoxygenation over USY zeolite. *Catalysis Today* **2013,** *204*, 46-53.

37. Mo, N.; Tandar, W.; Savage, P. E., Aromatics from saturated and unsaturated fatty acids via zeolite catalysis in supercritical water. *The Journal of Supercritical Fluids* **2015,** *102*, 73-79.

38. Xia, W.; Wang, Y.; Bergsträßer, R.; Kundu, S.; Muhler, M., Surface characterization of oxygen-functionalized multi-walled carbon nanotubes by high-resolution X-ray photoelectron spectroscopy and temperature-programmed desorption. *Applied Surface Science* **2007,** *254* (1), 247-250.

39. Ayodele, O. B.; Farouk, H. U.; Mohammed, J.; Uemura, Y.; Daud, W. M. A. W., Hydrodeoxygenation of oleic acid into n- and iso-paraffin biofuel using zeolite supported fluoro-oxalate modified molybdenum catalyst: Kinetics study. *Journal of the Taiwan Institute of Chemical Engineers* **2015,** *50*, 142-152.

40. Tong, D. S.; Zhou, C. H.; Li, M. Y.; Yu, W. H.; Beltramini, J.; Lin, C. X.; Xu, Z. P., Structure and catalytic properties of Sn-containing layered double hydroxides synthesized in the presence of dodecylsulfate and dodecylamine. *Applied Clay Science* **2010,** *48* (4), 569-574.

41. Ayodele, O. B.; Lethesh, K. C.; Gholami, Z.; Uemura, Y., Effect of ethanedioic acid functionalization on Ni/Al2O3 catalytic hydrodeoxygenation and isomerization of octadec-9-enoic acid into biofuel: kinetics and Arrhenius parameters. *Journal of Energy Chemistry* **2016,** *25* (1), 158-168.

42. Kandel, K.; Anderegg, J. W.; Nelson, N. C.; Chaudhary, U.; Slowing, I. I., Supported iron nanoparticles for the hydrodeoxygenation of microalgal oil to green diesel. *Journal of Catalysis* **2014,** *314*, 142-148.

43. Al Alwan, B.; Salley, S. O.; Ng, K. Y. S., Biofuels production from hydrothermal decarboxylation of oleic acid and soybean oil over Ni-based transition metal carbides supported on Al-SBA-15. *Applied Catalysis A: General* **2015,** *498*, 32-40.

44. Popov, S.; Kumar, S., Rapid Hydrothermal Deoxygenation of Oleic Acid over Activated Carbon in a Continuous Flow Process. *Energy & Fuels* **2015,** *29* (5), 3377-3384.

45. Monnier, J.; Sulimma, H.; Dalai, A.; Caravaggio, G., Hydrodeoxygenation of oleic acid and canola oil over alumina-supported metal nitrides. *Applied Catalysis A: General* **2010,** *382* (2), 176-180.

46. Li, G.; Zhang, F.; Chen, L.; Zhang, C.; Huang, H.; Li, X., Highly Selective Hydrodecarbonylation of Oleic Acid into n-Heptadecane over a Supported Nickel/Zinc Oxide–Alumina Catalyst. *ChemCatChem* **2015,** *7* (17), 2646-2653.

CHAPTER 7
GENERAL CONCLUSIONS AND FUTURE DIRECTIONS

The synthesis, characterization, and applications of a number of phosphonic and carboxylic acids have been reported in this dissertation. As mentioned in the introductory chapter, organic synthesis is an incredibly vast and exciting field that unlocks the understanding of the chemical properties by leveraging the captivating power of bond formation between atoms. This body of work was aimed at understanding and improving the synthesis and applications of these compounds, in which we addressed several key limitations and advances that will allow for further expansion and utilization of the compounds synthesized and characterized within.

7.1. General Conclusions and Future Directions

Chapter 2 provided a broad overview of the application of the phosphonic and carboxylic acids and their application in photovoltaics. Discussed here were the application of these acids for work function modification of TCOs and QDs. Specifically, this chapter surveyed the literature aimed at synthetic pathways for production of styryl phosphonic and cinnamic acids.

In Chapters 3 & 4, the discovery of a novel synthetic route of styryl phosphonic acids and the subsequent surface modification of those acids on ITO were studied. This work aimed to continue and improve upon the surface modification work of Braid et. al[1] however, fell short in our predictions. We found that our best efforts led to the synthesis and characterization of 2 novel compounds, yet fell short with the application of these acids onto ITO in which we didn't see the predicted trend when comparing molecular dipole and a measured correlation of work function modification. While we were able to deposit these phosphonic acids and show through PMIRRAS measurements that the surface was functionalized, the results of the novel compounds were dismal at best. We suspect that monolayer uniformity and orientation onto the surface are major factors that must be controlled in order to get the desired surface effects.

The work in Chapter 4 provides multiple avenues for future explorations. First, the precise deposition and analysis of a true SAM (opposed to the random oriented thin film of this

study) could potently validate the initial hypothesis of this chapter. In addition, a number of these acids, or acid families have yet to be studied on other types of TCOs. We suspect that novel studies of these acids may lead to exciting result and applications. Ultimately, we imagine the incorporation of these acids into a photovoltaic device to drive new efficiencies would be the end goal of future applications.

In Chapter 5, we explored the synthesis of a number of cinnamic acids. These acids were then utilized in a development of simple, robust, and scalable solution-phase ligand exchange methods, which completely replace native ligands allowing for well-defined, highly tunable chemical systems on the surface of PbS QDs. Here, we show that band edge positions of PbS QDs can be tuned over 2.0 eV through this surface chemistry modification. We also explored the synthesis and applications of functionalized α-cyano ligands compared to the cinnamic equivalent. Here, we found that the α-cyano group interferes with acid to metal binding and hybridization to the QD core, ultimately diminishing the band edge absorption enhancement effect when compared to the cinnamic counterpart.

The cinnamic acids in Chapter 5 have an excess of applications yet to be explored. Specifically, for PbS systems we would like to continue exploration of the application of new ligands with stronger dipoles and stronger electron withdrawing/donating groups. In addition to this, the synthesis of photo donor-acceptor type motifs could enhance the visible light absorption of PbS QDs which could optimize a QD-PV device. We also believe that a number of other QD systems could be modified to show similar or better absorption enhancement. Finally, as mentioned in the conclusion of this chapter, the introduction of the di- and tri- acrylate linkers synthesized in Chapter 6 could couple networks of QDs together and improve absorption, charge transfer, and a number of other characteristics to make more efficient QD devices.

Finally, in Chapter 6, we explored the synthesis of 16 novel linkers and their incorporation into MOFs where the catalysis of oleic acid to heptadecane was studied. We found that our novel Ni-MOF systems are ideal candidates for efficient selectivity of heptadecane with the mildest conditions reported. The metal centers in these MOFs are Ni, a non-noble metal that is earth abundant and inexpensive, making these Ni-MOFs ideal candidates for scale up into inexpensive industrial biomass conversion catalytic systems.

The work here in Chapter 6 seems to have the most abundant future applications. Over the last decade MOFs have increasingly gained attention for many high impact applications, including but not limited to catalysis,[2-4] gas storage and release,[5-7] sensors,[8-10] energy harvesting,[11-14] conductivity,[15] and filtration.[16-19] The driving force behind this rapidly growing field of study is the highly modular and tunable nature of the components of MOFs. However, MOFs are complicated by state-of-the-art methods for synthesis, which include solvothermal,[20] electrochemical,[21-22] mechanochemical,[23] and microwave assisted growth.[24] A number of systematic parameters (i.e. time, temperature, concentration, pH,) can be modified to effect the topology, crystal size, and phase purity. This demands that strategies to control and direct formation of the framework are highly valuable. We believe that a number of the linkers introduced here could be integrated into a highly ordered MOF, and then integrated into the aforementioned applications.

A related point in controlling the formation of a crystalline framework is the relationship between the linker and its resultant MOF topology.[25] Wherein, isoreticular series of linkers can be formulated with similar, if not identical, conditions giving way to the formation of similar framework topologies.[26] Eddaoudi et. al were able to systematically design porous structures in which they demonstrated systematic control of pore size and functionality through isoreticular extension of the organic linker.[27] This introduces the idea of systematic design and synthesis with mild conditions of these linkers, which allows for the rapid screening and exploration of new MOFs. Jiang et. al were able to use this theory and build upon 1,3,5-benzene tricarboxylate (BTC) with the introduction of acrylate links to create benzene-1,3,5-tri-acrylate (BTAC- BM56) and expand pore size of the crystal lattice and create MOFs with c.a. 3000 m^2g^{-1}.[6] We believe the integration a few of the linkers introduced here, or integration of functional groups into new likers using synthetic routes introduce here, could lead to the formation of new MOF systems leading to a number of new exciting research projects.

7.2. References Cited

1. Braid, J. L. Understanding efficiency improvement in organic photovoltaics with molecular modifiers. Colorado School of Mines. Arthur Lakes Library, 2016.

2. Yang, L.; Ruess, G. L.; Carreon, M. A., Cu, Al and Ga based metal organic framework catalysts for the decarboxylation of oleic acid. *Catalysis Science & Technology* **2015,** *5* (5), 2777-2782.

3. Yang, L.; McNichols, B. W.; Davidson, M.; Schweitzer, B.; Gomez-Gualdron, D. A.; Trewyn, B. G.; Sellinger, A.; Carreon, M. A., Noble metal-free catalytic decarboxylation of oleic acid to n-heptadecane on nickel-based metal-organic frameworks (MOFs). *Catalysis Science & Technology* **2017**.

4. Falcaro, P.; Hill, A. J.; Nairn, K. M.; Jasieniak, J.; Mardel, J. I.; Bastow, T. J.; Mayo, S. C.; Gimona, M.; Gomez, D.; Whitfield, H. J.; Riccò, R.; Patelli, A.; Marmiroli, B.; Amenitsch, H.; Colson, T.; Villanova, L.; Buso, D., A new method to position and functionalize metal-organic framework crystals. **2011,** *2*, 237.

5. Li, J. R.; Kuppler, R. J.; Zhou, H. C., Selective gas adsorption and separation in metal-organic frameworks. *Chemical Society Reviews* **2009,** *38*, 1477.

6. Jiang, J.; Furukawa, H.; Zhang, Y.-B.; Yaghi, O. M., High Methane Storage Working Capacity in Metal–Organic Frameworks with Acrylate Links. *Journal of the American Chemical Society* **2016,** *138* (32), 10244-10251.

7. Alezi, D.; Belmabkhout, Y.; Suyetin, M.; Bhatt, P. M.; Weseliński, Ł. J.; Solovyeva, V.; Adil, K.; Spanopoulos, I.; Trikalitis, P. N.; Emwas, A.-H.; Eddaoudi, M., MOF Crystal Chemistry Paving the Way to Gas Storage Needs: Aluminum-Based soc-MOF for CH4, O2, and CO2 Storage. *Journal of the American Chemical Society* **2015,** *137* (41), 13308-13318.

8. Hu, Z.; Deibert, B. J.; Li, J., Luminescent metal-organic frameworks for chemical sensing and explosive detection. *Chemical Society Reviews* **2014,** *43*, 5815.

9. Moreira, N. H.; Rosa, A. L. d.; Frauenheim, T., Covalent functionalization of ZnO surfaces: A density functional tight binding study. *Applied Physics Letters* **2009,** *94* (19), 193109.

10. Shiozawa, H.; Bayer, B. C.; Peterlik, H.; Meyer, J. C.; Lang, W.; Pichler, T., Doping of metal–organic frameworks towards resistive sensing. *Scientific Reports* **2017,** *7* (1), 2439.

11. So, M. C.; Wiederrecht, G. P.; Mondloch, J. E.; Hupp, J. T.; Farha, O. K., Metal-organic framework materials for light-harvesting and energy transfer. *Chem. Commun.* **2015,** *51*, 3501.

12. Wang, J. L.; Wang, C.; Lin, W., Metal–Organic Frameworks for Light Harvesting and Photocatalysis. *ACS Catal.* **2012,** *2*, 2630.

13. Williams, D. E.; Shustova, N. B., Metal–Organic Frameworks as a Versatile Tool To Study and Model Energy Transfer Processes. *Chem. - Eur. J.* **2015,** *21*, 15474.

14. Duan, J.; Chen, S.; Zhao, C., Ultrathin metal-organic framework array for efficient electrocatalytic water splitting. **2017,** *8*, 15341.

15. Sun, L.; Campbell, M. G.; Dincă, M., Electrically Conductive Porous Metal–Organic Frameworks. *Angew. Chem., Int. Ed.* **2016,** *55*, 3566.

16. Zhao, X.; Bu, X.; Wu, T.; Zheng, S. T.; Wang, L.; Feng, P., Selective anion exchange with nanogated isoreticular positive metal-organic frameworks. *Nat. Commun.* **2013,** *4*, 2344.

17. DeCoste, J. B.; Peterson, G. W., Metal-organic frameworks for air purification of toxic chemicals. *Chemical Reviews* **2014,** *114*, 5695.

18. Howarth, A. J.; Liu, Y.; Hupp, J. T.; Farha, O. K., Metal-organic frameworks for applications in remediation of oxyanion/cation-contaminated water. *CrystEngComm* **2015,** *17*, 7245.

19. Denny Jr, M. S.; Moreton, J. C.; Benz, L.; Cohen, S. M., Metal–organic frameworks for membrane-based separations. **2016,** *1*, 16078.

20. Yaghi, O. M.; Li, H., Hydrothermal Synthesis of a Metal-Organic Framework Containing Large Rectangular Channels. *Journal of the American Chemical Society* **1995,** *117*, 10401.

21. Al-Kutubi, H.; Gascon, J.; Sudhölter, E. J. R.; Rassaei, L., Electrosynthesis of Metal-Organic Frameworks: Challenges and Opportunities. *ChemElectroChem* **2015,** *2*, 462.

22. Li, M.; Dincă, M., Reductive Electrosynthesis of Crystalline Metal–Organic Frameworks. *Journal of the American Chemical Society* **2011,** *133*, 12926.

23. Klimakow, M.; Klobes, P.; Thünemann, A. F.; Rademann, K.; Emmerling, F., Mechanochemical Synthesis of Metal–Organic Frameworks: A Fast and Facile Approach toward Quantitative Yields and High Specific Surface Areas. *Chemistry of Materials* **2010,** *22*, 5216.

24. Klinowski, J.; Paz, F. A.; Silva, P.; Rocha, J., Microwave-assisted synthesis of metal-organic frameworks. *Dalton Trans.* **2011,** *40*, 321.

25. Lee, S. J.; Doussot, C.; Telfer, S. G., Architectural Diversity in Multicomponent Metal–Organic Frameworks Constructed from Similar Building Blocks. *Crystal Growth & Design* **2017,** *17* (6), 3185-3191.

26. Furukawa, H.; Go, Y. B.; Ko, N.; Park, Y. K.; Uribe-Romo, F. J.; Kim, J.; O'Keeffe, M.; Yaghi, O. M., Isoreticular Expansion of Metal–Organic Frameworks with Triangular and Square Building Units and the Lowest Calculated Density for Porous Crystals. *Inorg. Chem.* **2011,** *50*, 9147.

27. Eddaoudi, M.; Kim, J.; Rosi, N.; Vodak, D.; Wachter, J.; O'Keeffe, M.; Yaghi, O. M., Systematic Design of Pore Size and Functionality in Isoreticular MOFs and Their Application in Methane Storage. *Science* **2002,** *295* (5554), 469-472.

APPENDIX A

SELECTED NMR FOR CHAPTERS 3 & 4

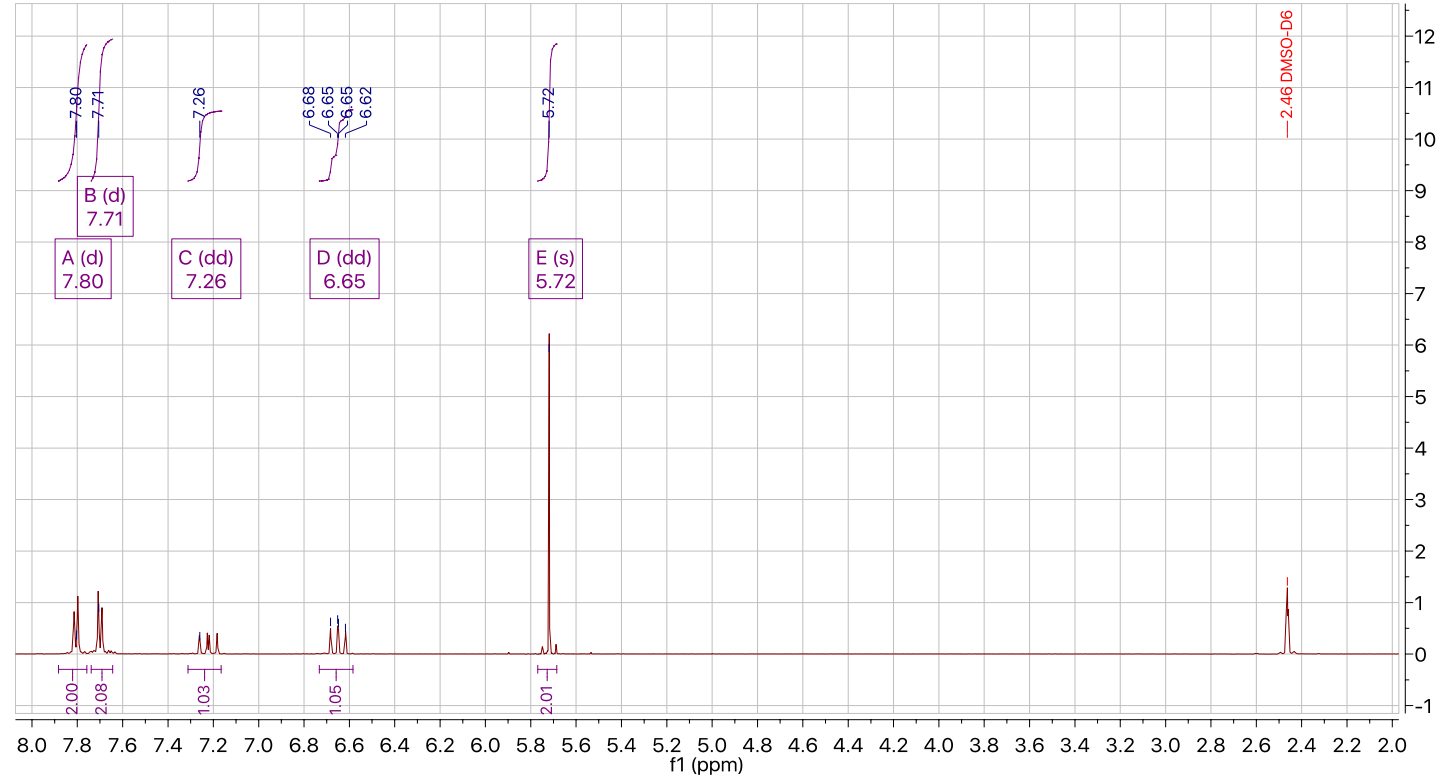

^{1}H NMR (500 MHz, DMSO-d_6) δ 7.80 (s, 2H), 7.71 (s, 2H), 7.26 (dd, 1H), 6.65 (dd, 1H), 5.72 (s, 2H).

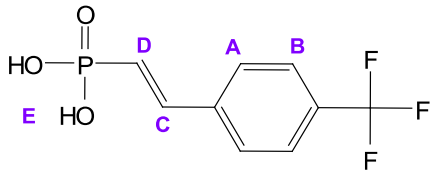

Figure A.1 ^{1}H NMR of BM01 - CF_3PA- (E)-(4-(trifluoromethyl)styryl) phosphonic acid

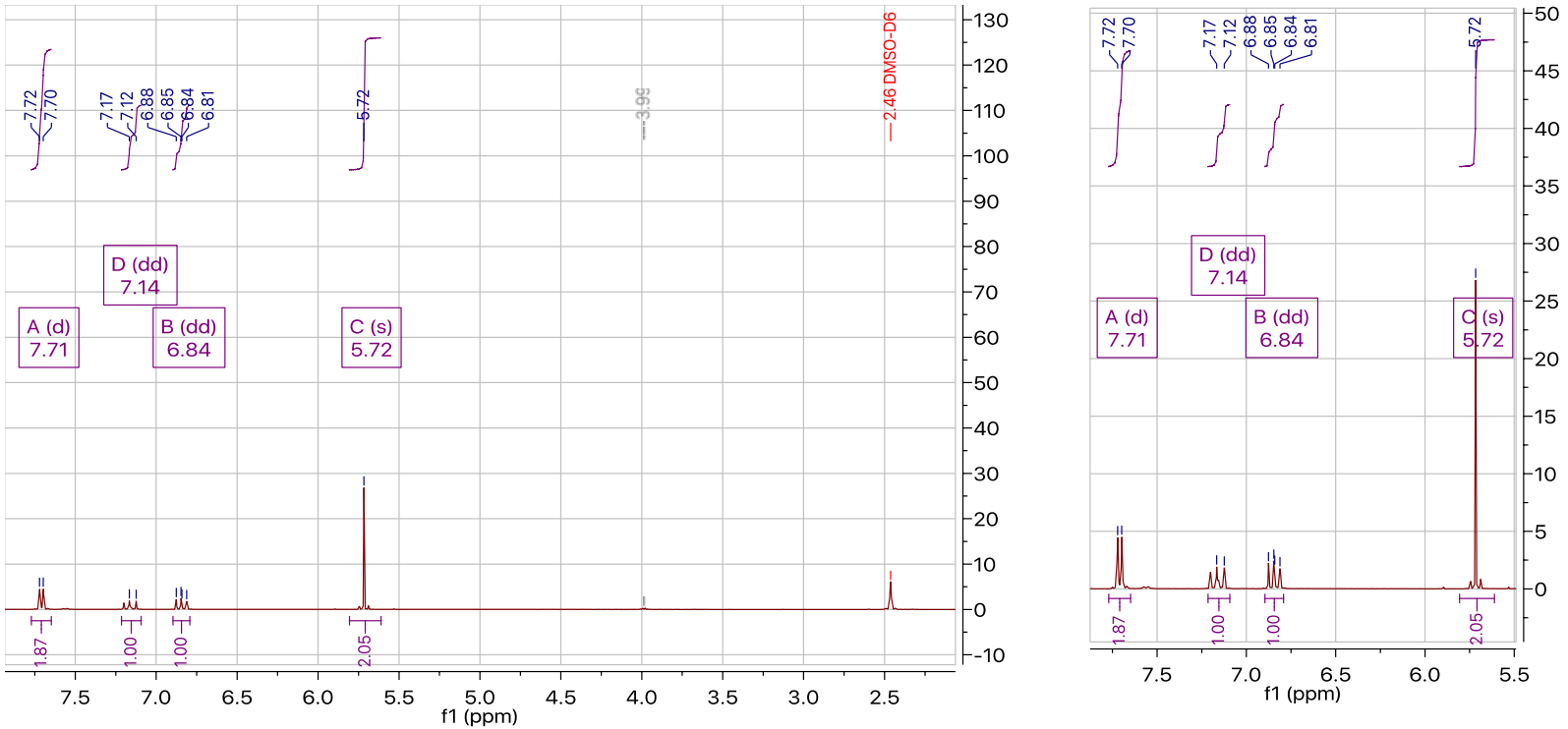

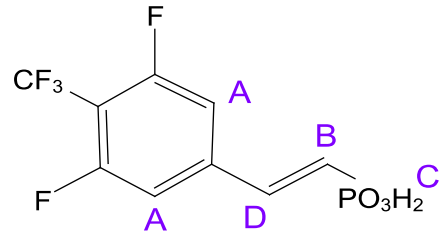

^{1}H NMR (500 MHz, DMSO-d_6) δ 7.71 (d, J = 11.6 Hz, 2H), 7.14 (dd, J = 21.2 Hz, 1H), 6.84 (dd, J = 17.4, 14.7 Hz, 1H), 5.72 (s, 2H).

Figure A.2 ^{1}H NMR of BM05 - (E)-(3,5-difluoro-4-(trifluoromethyl)styryl) phosphonic acid

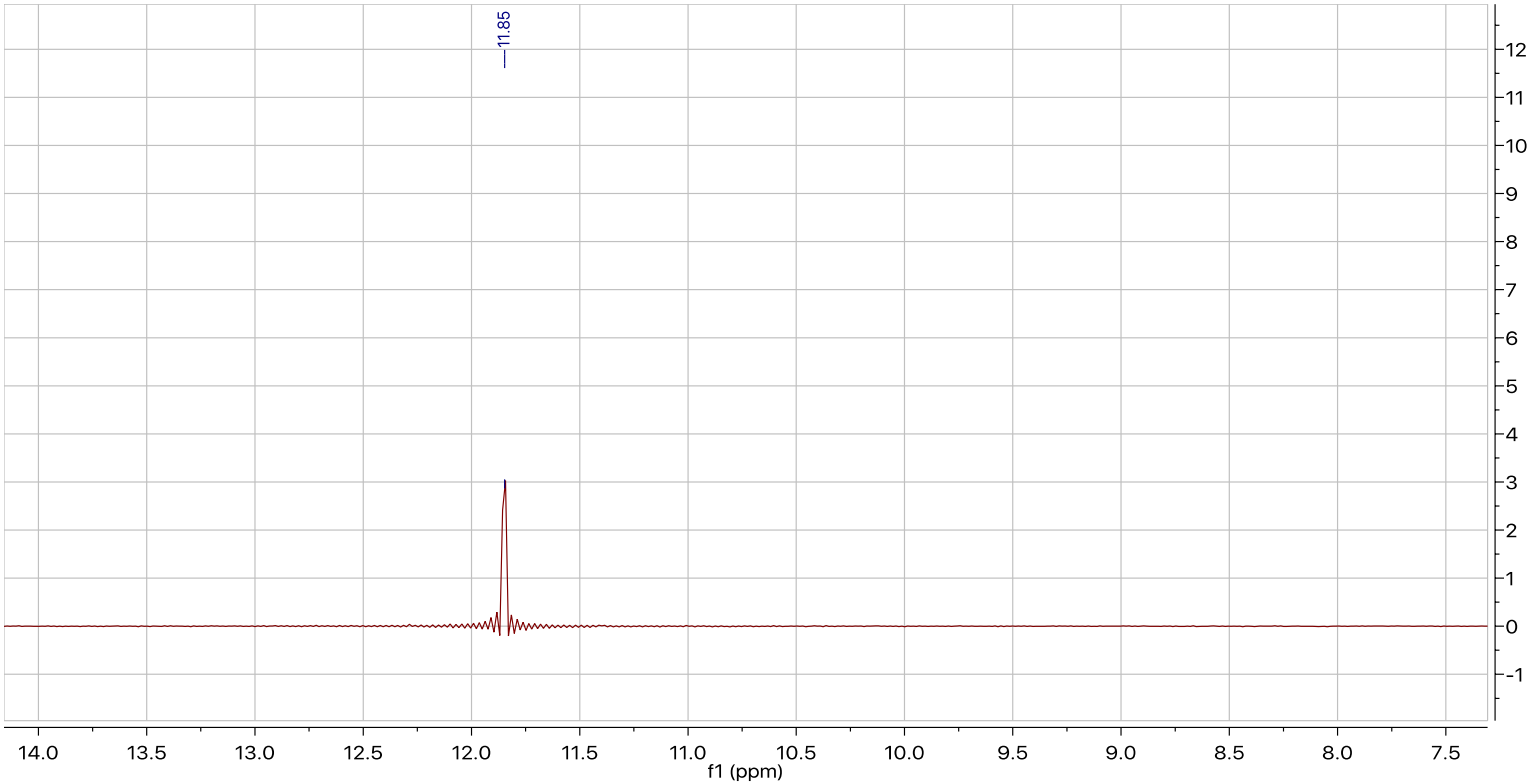

^{31}P NMR (202 MHz, DMSO-D_6) δ 11.85.

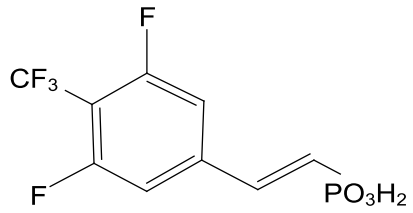

Figure A.3 ^{31}P NMR of BM05 - (E)-(3,5-difluoro-4-(trifluoromethyl)styryl) phosphonic acid

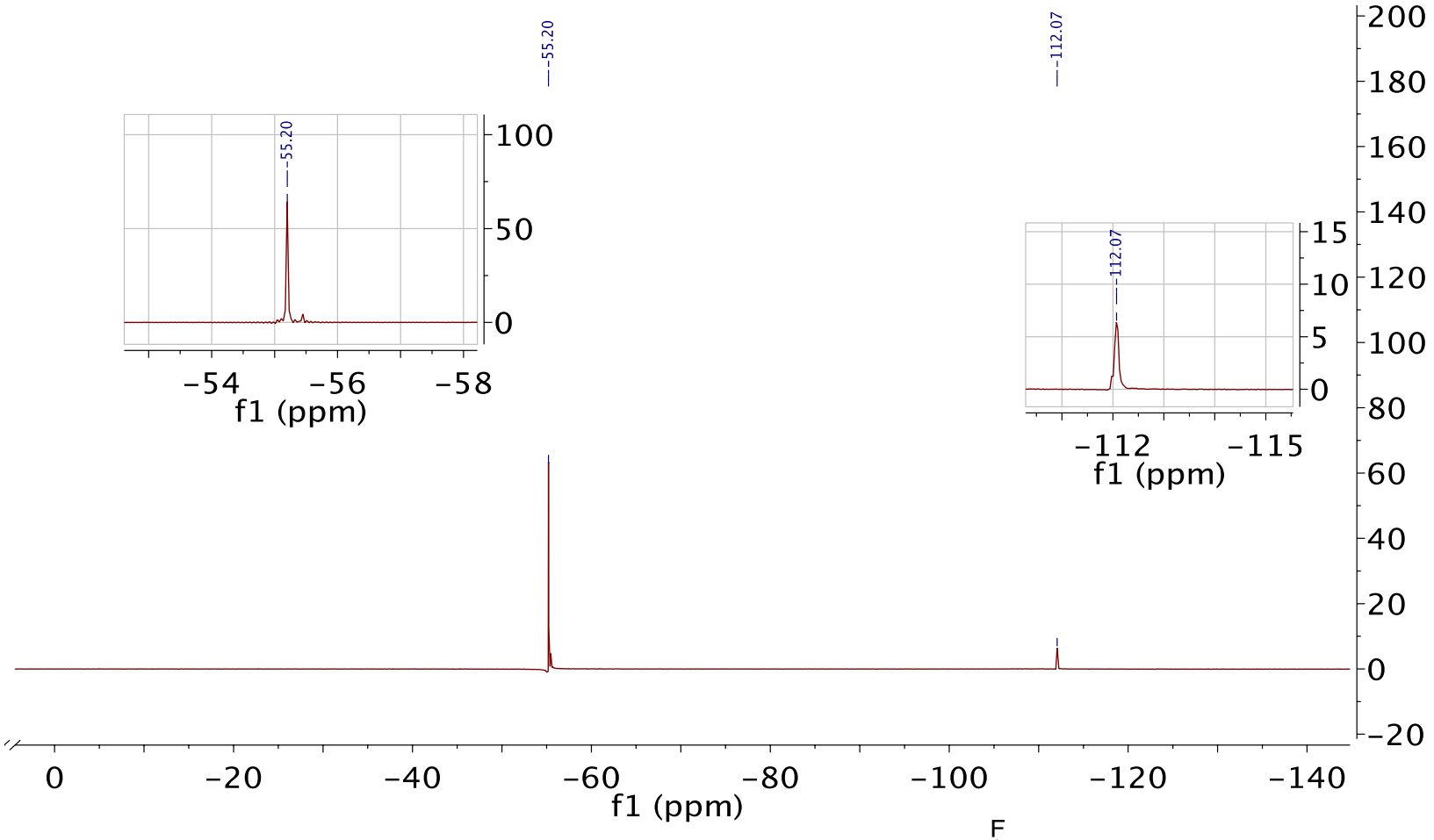

^{19}F NMR (471 MHz, DMSO-D_6) δ -55.20, -112.07.

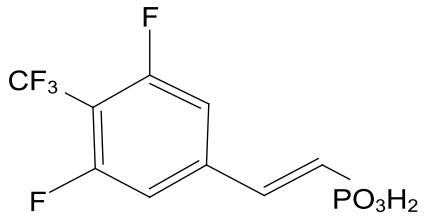

Figure A.4 ^{19}F NMR of BM05 - (E)-(3,5-difluoro-4-(trifluoromethyl)styryl) phosphonic acid

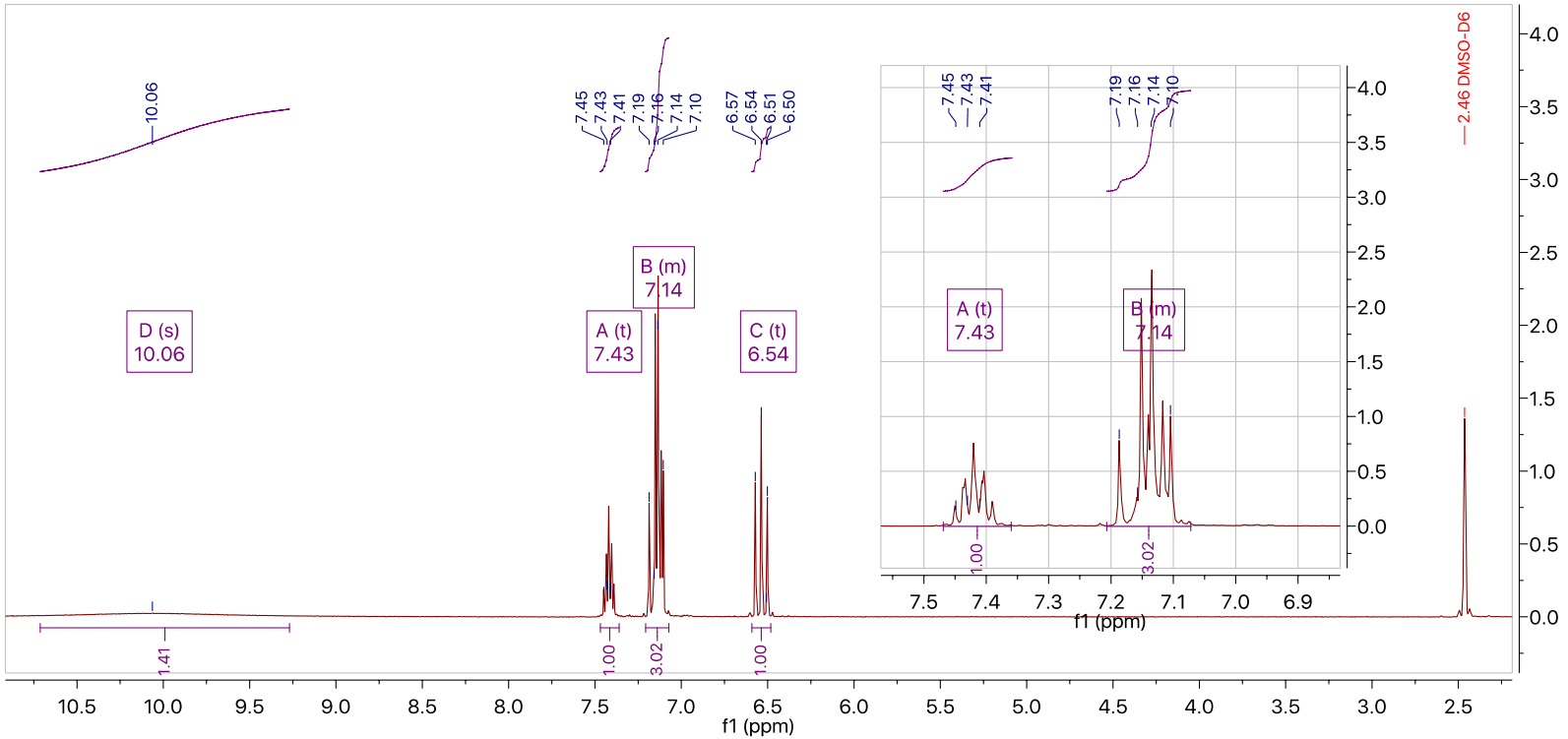

^{1}H NMR (500 MHz, DMSO-d_6) δ 10.06 (s, 1H), 7.43 (t, J = 9.6 Hz, 1H), 7.21 – 7.07 (m, 3H), 6.54 (t, J = 17.5 Hz, 1H).

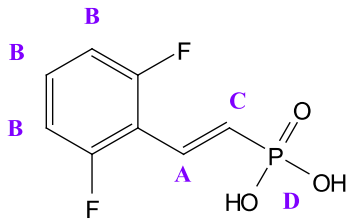

Figure A.5 ^{1}H NMR of BM02 - (E)-(2,6-difluorostyryl) phosphonic acid

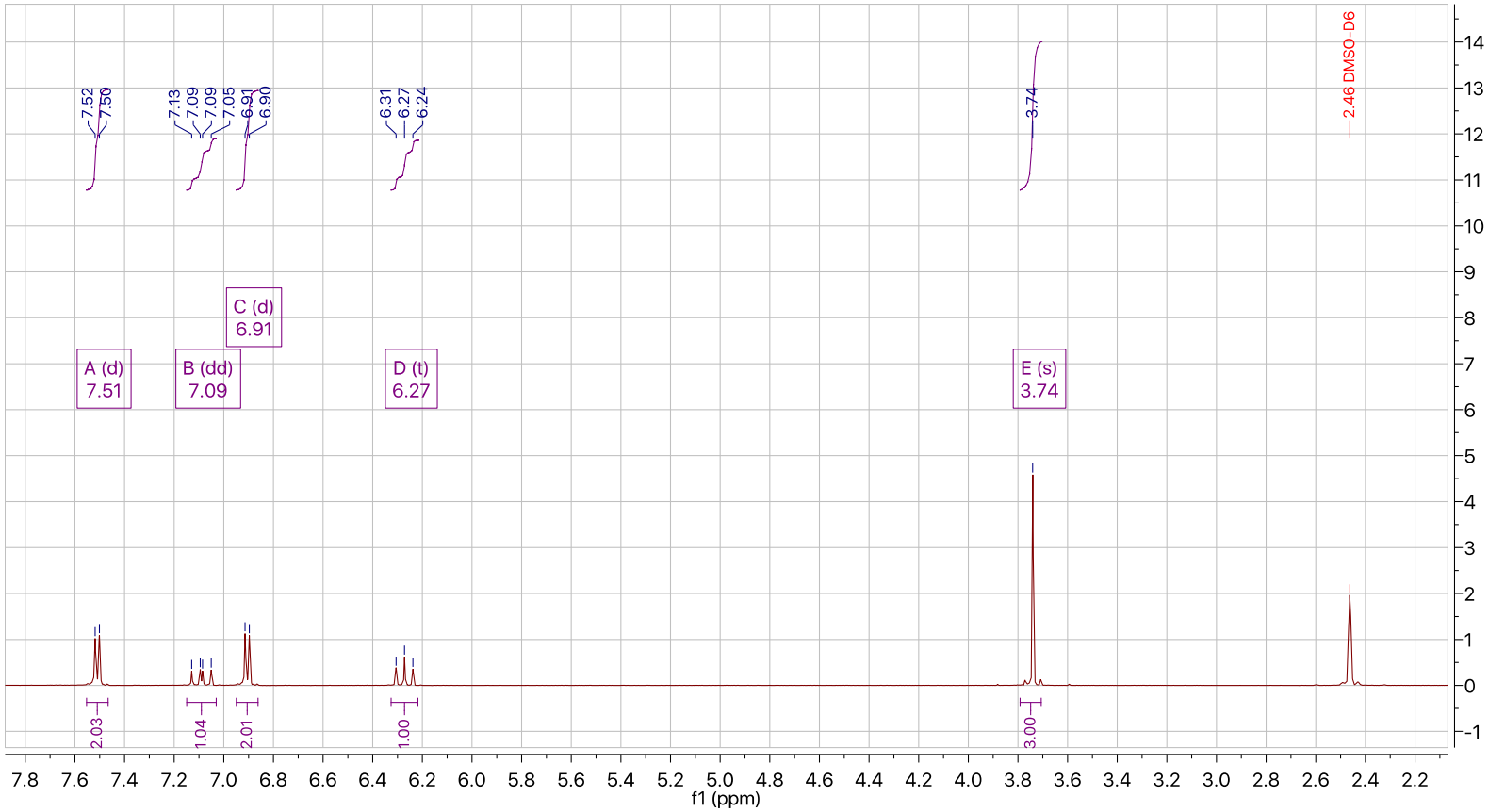

^{1}H NMR (500 MHz, DMSO-d_6) δ 7.51 (d, J = 8.7 Hz, 2H), 7.09 (dd, J = 21.9, 17.4 Hz, 1H), 6.91 (d, J = 8.7 Hz, 2H), 6.27 (t, J = 16.9 Hz, 1H), 3.74 (s, 3H).

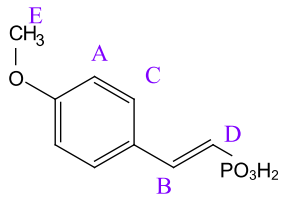

Figure A.6 ^{1}H NMR of BM41 (E)-(4-methoxystyryl) phosphonic acid

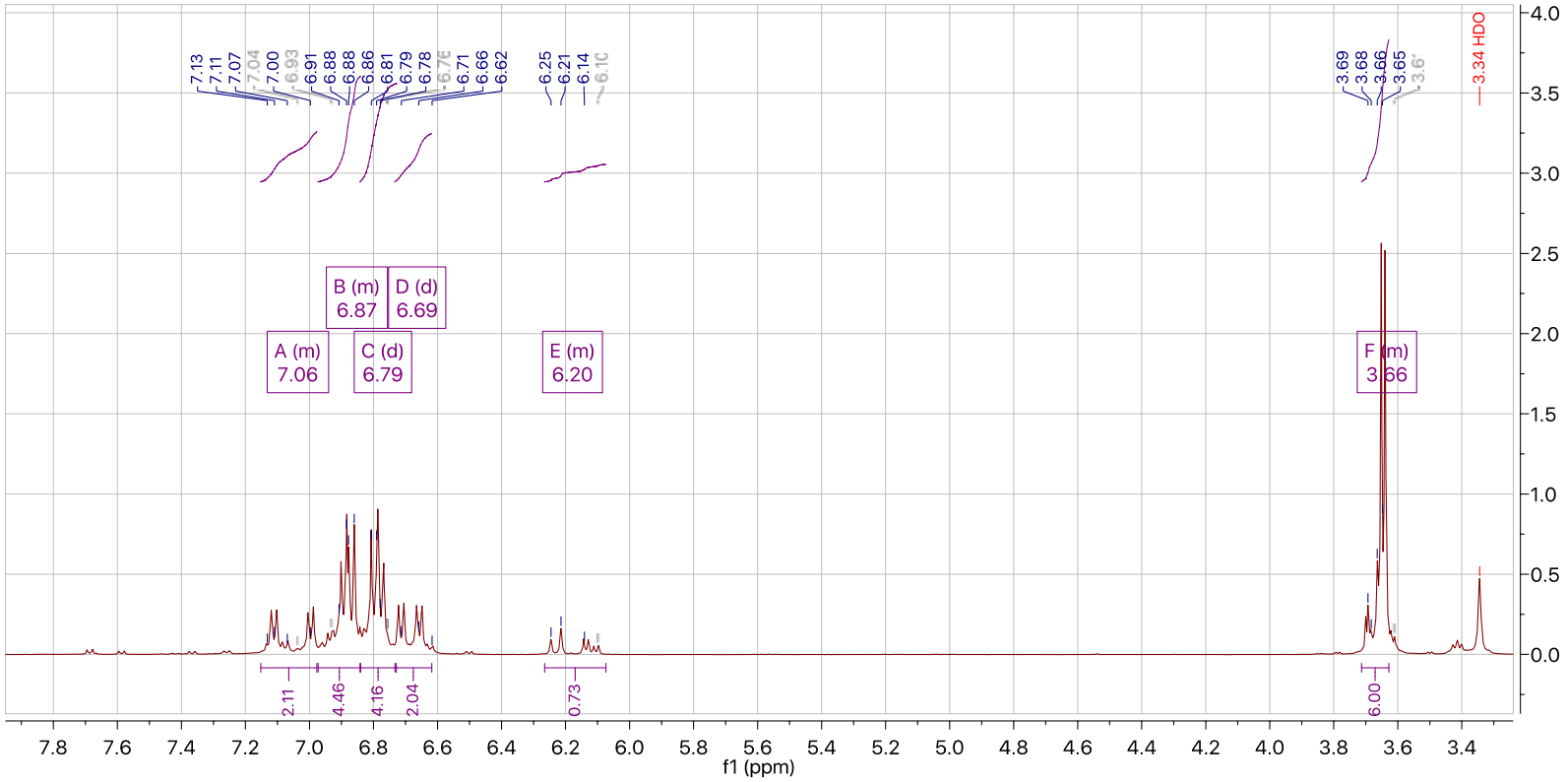

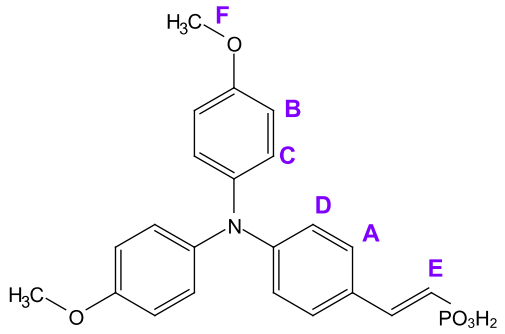

^{1}H NMR (500 MHz, DMSO-d_6) δ 7.15 – 6.98 (m, 2H), 6.97 – 6.84 (m, 4H), 6.79 (d, J = 14.0 Hz, 4H), 6.69 (d, J = 27.2 Hz, 2H), 6.27 – 6.07 (m, 1H), 3.71 – 3.63 (m, 6H).

Figure A.7 ^{1}H NMR of BM25 (E)-(4-(bis(4-methoxyphenyl)amino)styryl) phosphonic acid

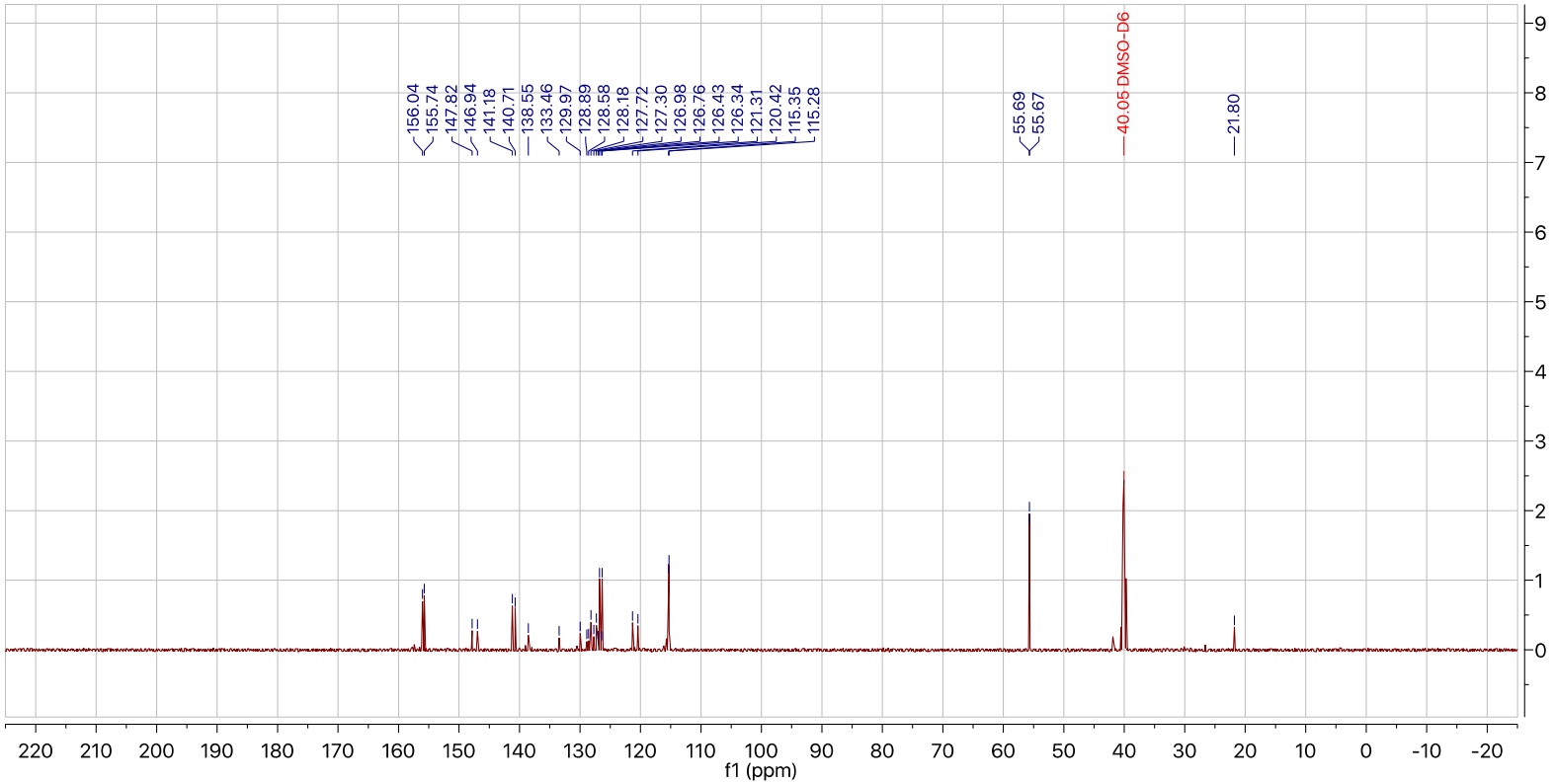

^{13}C NMR (126 MHz, DMSO-D_6) δ 156.04, 155.74, 147.82, 146.94, 141.18, 140.71, 138.55, 133.46, 129.97, 128.89, 128.58, 128.18, 127.72, 127.30, 126.98, 126.76, 126.43, 126.34, 121.31, 120.42, 115.35, 115.28, 55.69, 55.67, 40.05, 21.80.

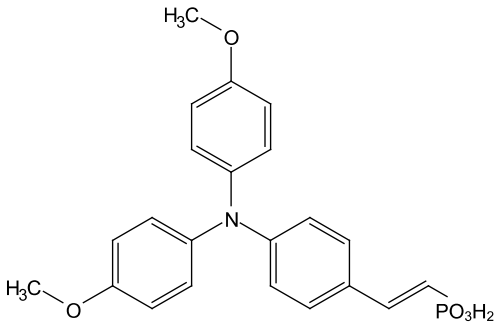

Figure A.8 ^{13}C NMR of BM25 (E)-(4-(bis(4-methoxyphenyl)amino)styryl) phosphonic acid

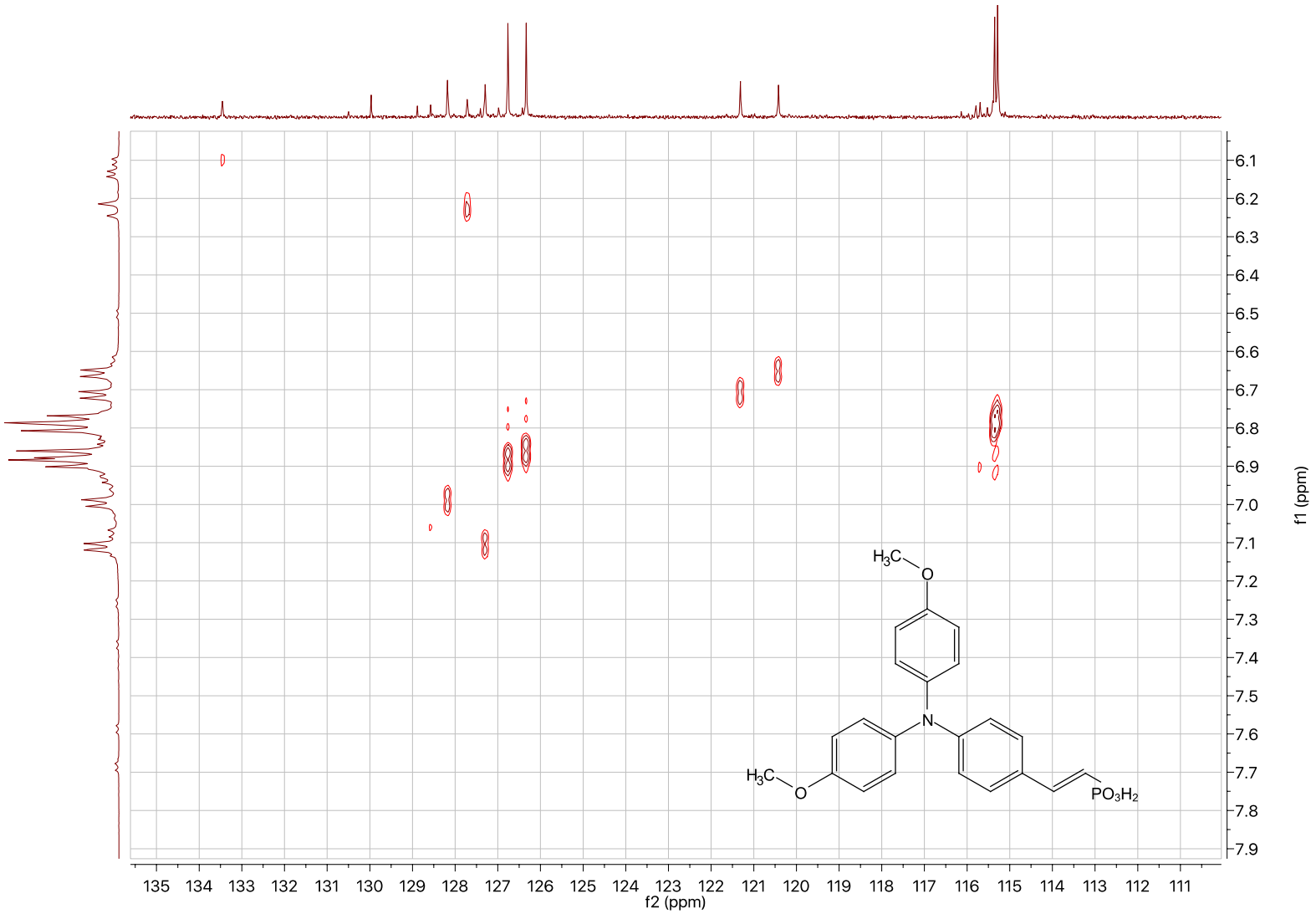

Figure A.9 Two dimensional heteronuclear correlation (HETCOR) of BM25 (E)-(4-(bis(4-methoxyphenyl)amino)styryl) phosphonic acid

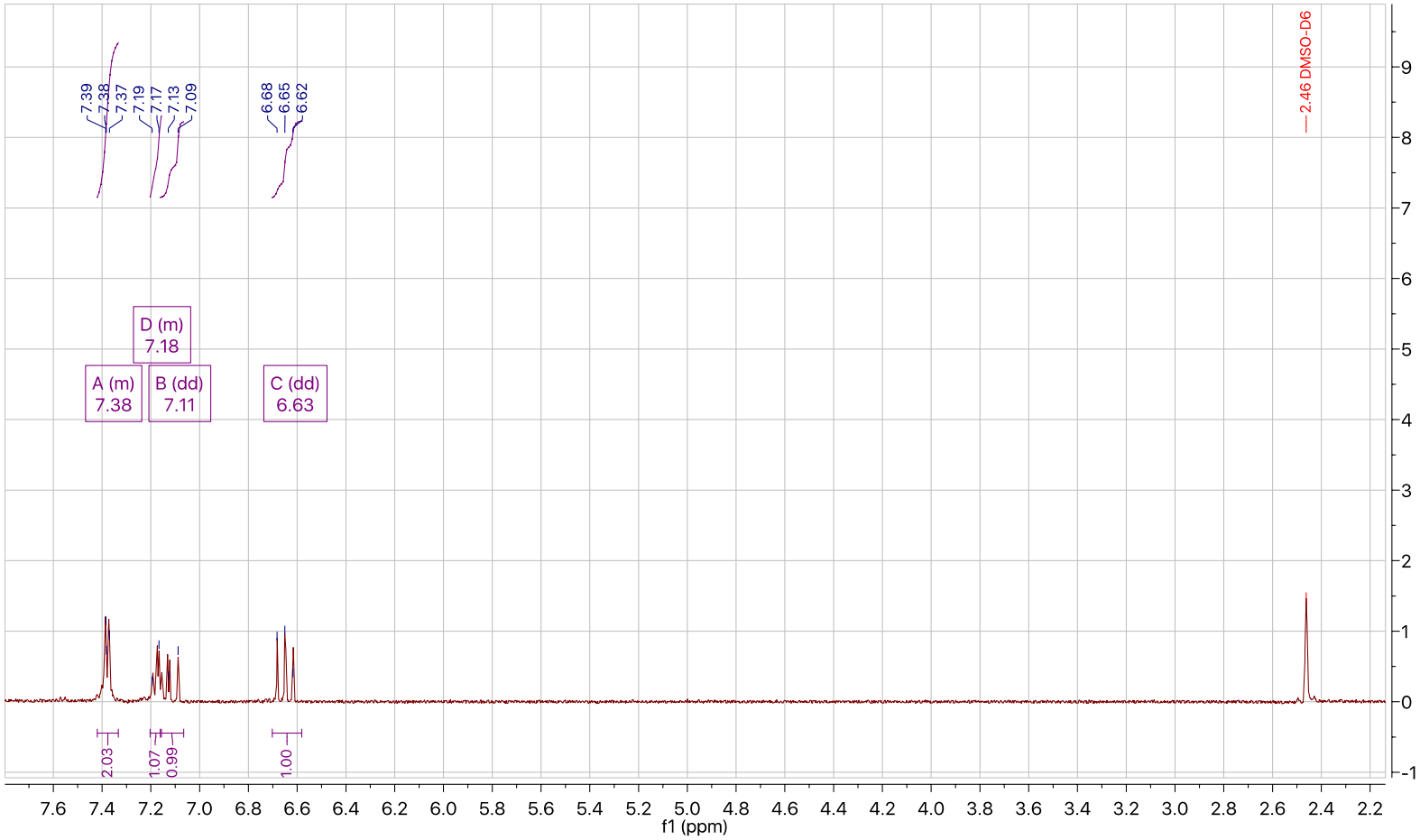

^{1}H NMR (500 MHz, DMSO-d_6) δ 7.42 – 7.33 (m, 2H), 7.20 – 7.16 (m, 1H), 7.11 (dd, J = 20.2 Hz, 1H), 6.63 (dd, J = 16.5 Hz, 1H).

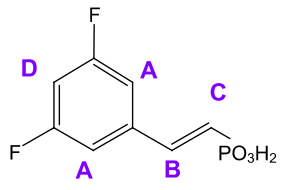

Figure A.10 ^{1}H NMR of BM07 - (*E*)-(3,5-difluorostyryl) phosphonic acid

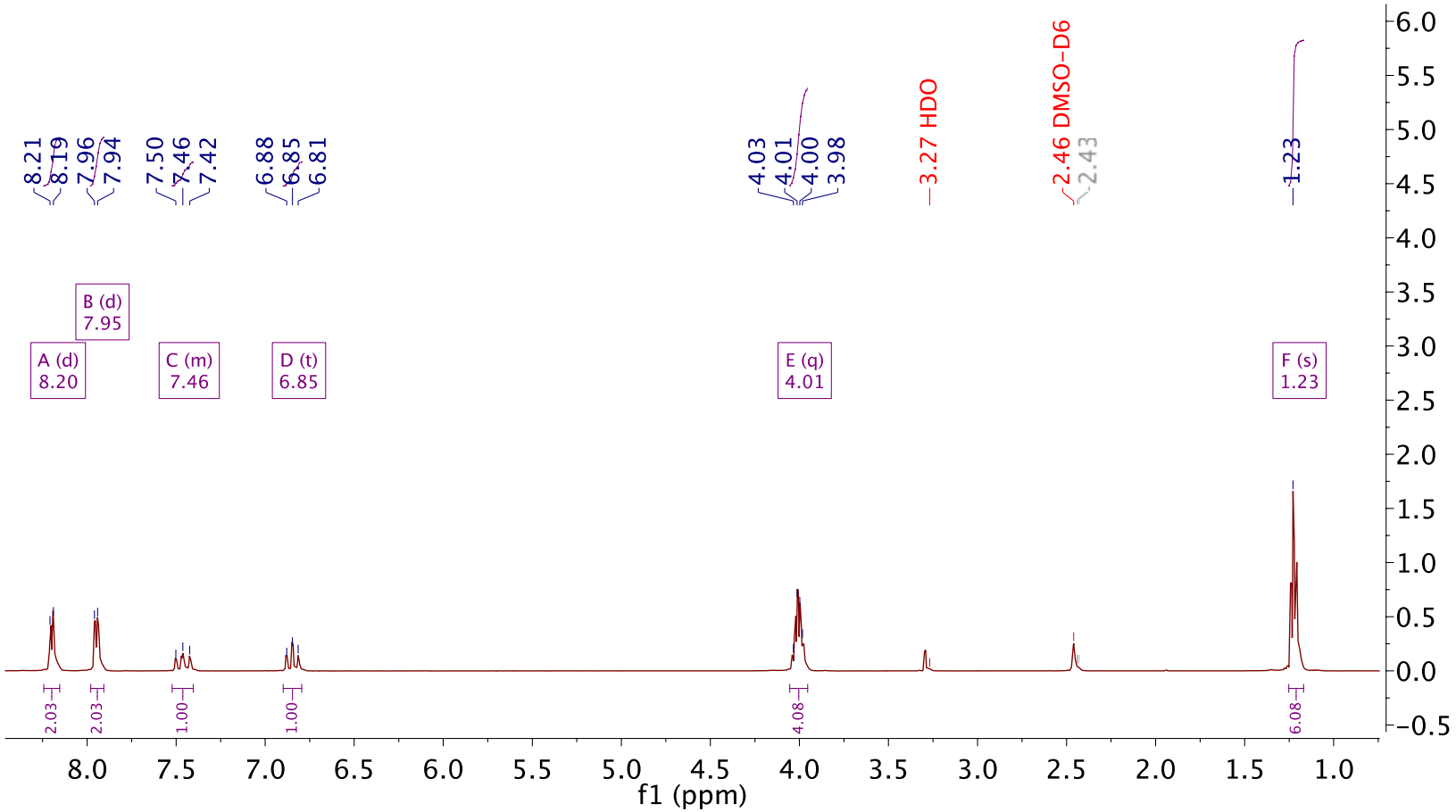

^{1}H NMR (500 MHz, DMSO-d_6) δ 8.20 (d, J = 9.6 Hz, 2H), 7.95 (d, J = 9.0 Hz, 2H), 7.52 – 7.40 (m, 1H), 6.85 (t, J = 16.0 Hz, 1H), 4.01 (q, J = 9.1, 7.6 Hz, 4H), 1.23 (s, 6H).

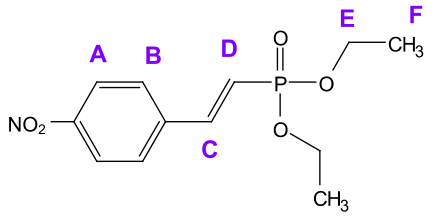

Figure A.11 ^{1}H NMR of NO_2VPE - diethyl (*E*)-(4-nitrostyryl) phosphonate

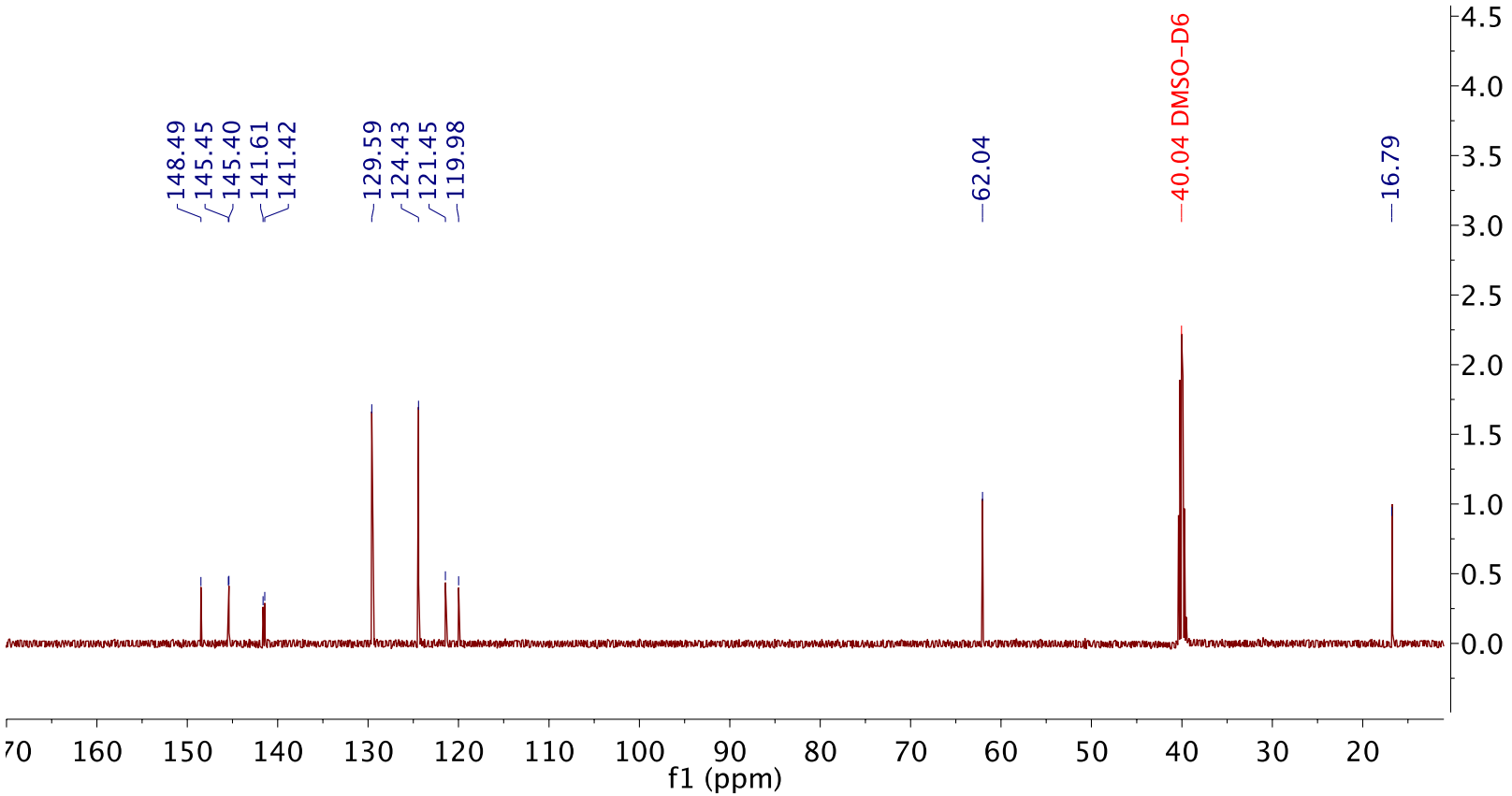

^{13}C NMR (126 MHz, DMSO-D_6) δ 148.49, 145.45, 145.40, 141.61, 141.42, 129.59, 124.43, 121.45, 119.98, 62.04, 40.04, 16.79.

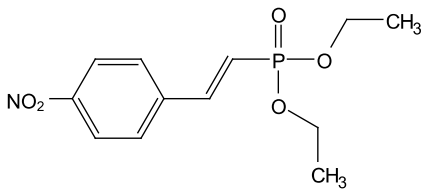

Figure A.12 ^{13}C NMR of NO_2VPE - diethyl (*E*)-(4-nitrostyryl) phosphonate

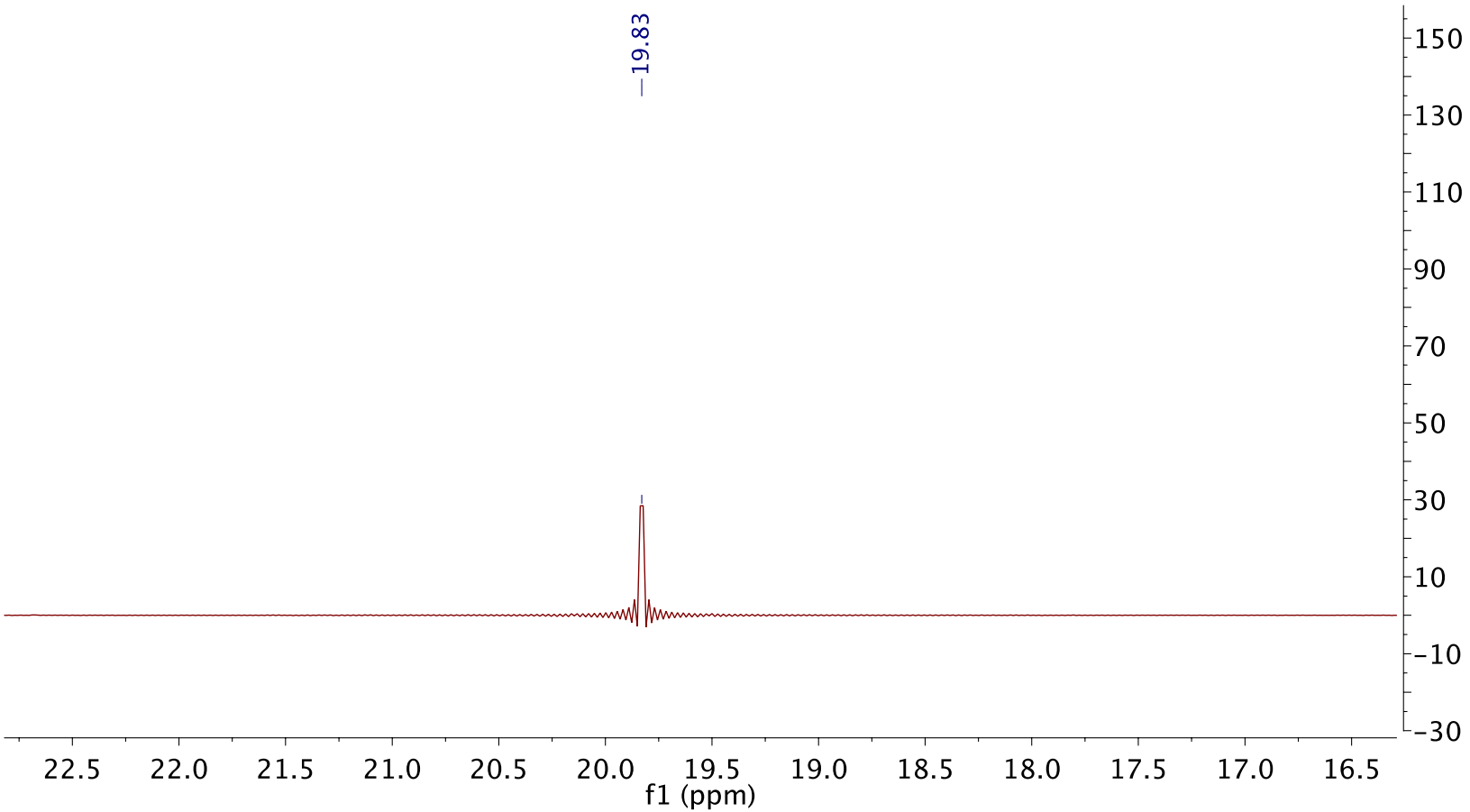

^{31}P NMR (202 MHz, DMSO-D_6) δ 19.83.

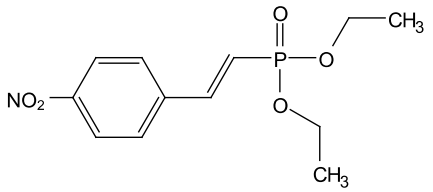

Figure A.13 ^{31}P NMR of NO_2VPE - diethyl (*E*)-(4-nitrostyryl) phosphonate

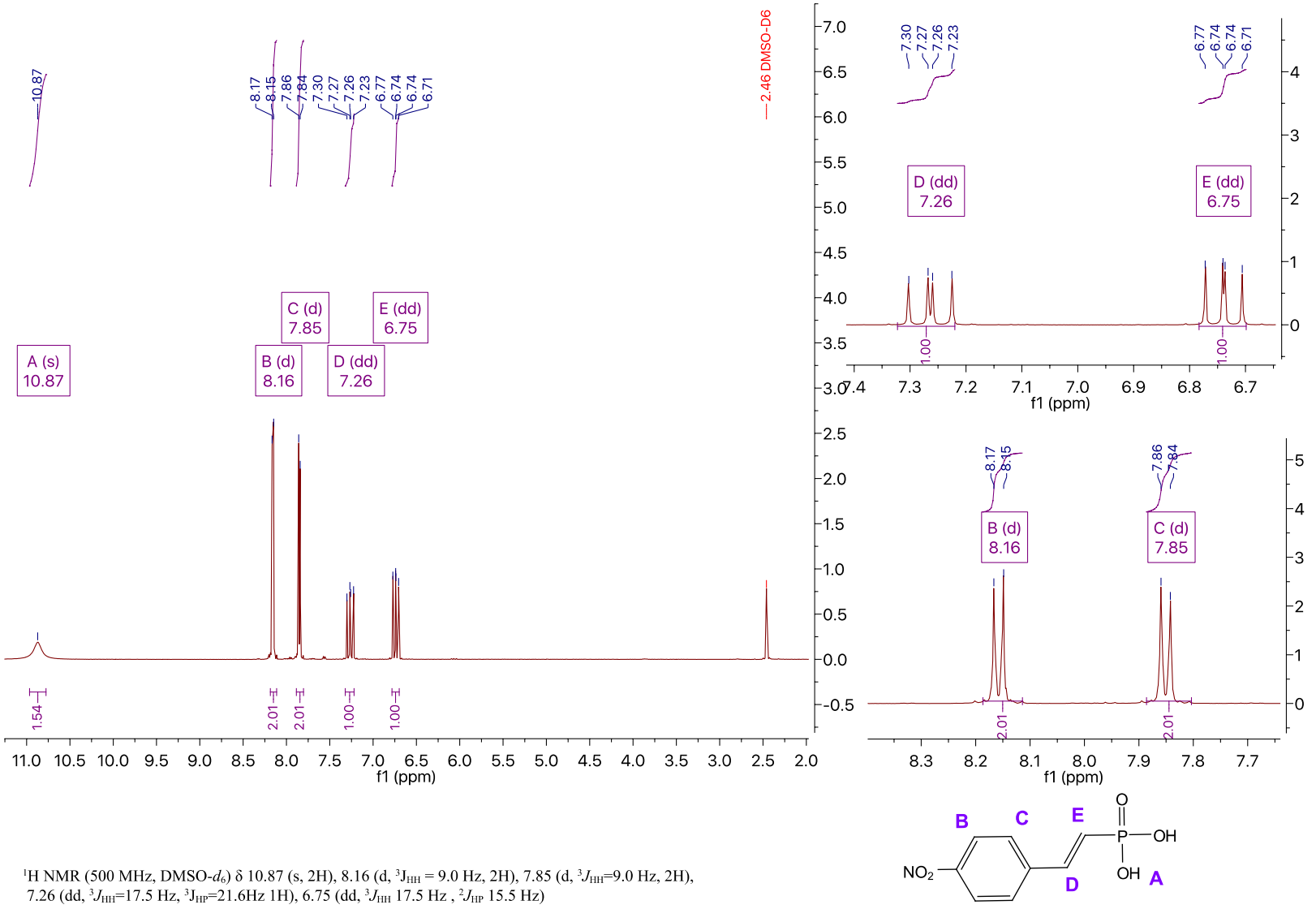

^{1}H NMR (500 MHz, DMSO-d_6) δ 10.87 (s, 2H), 8.16 (d, $^{3}J_{HH}$ = 9.0 Hz, 2H), 7.85 (d, $^{3}J_{HH}$=9.0 Hz, 2H), 7.26 (dd, $^{3}J_{HH}$=17.5 Hz, $^{3}J_{HP}$=21.6Hz 1H), 6.75 (dd, $^{3}J_{HH}$ 17.5 Hz , $^{2}J_{HP}$ 15.5 Hz)

Figure A.14 ^{1}H NMR of NO_2VPA - (*E*)-(4-nitrostyryl) phosphonic acid

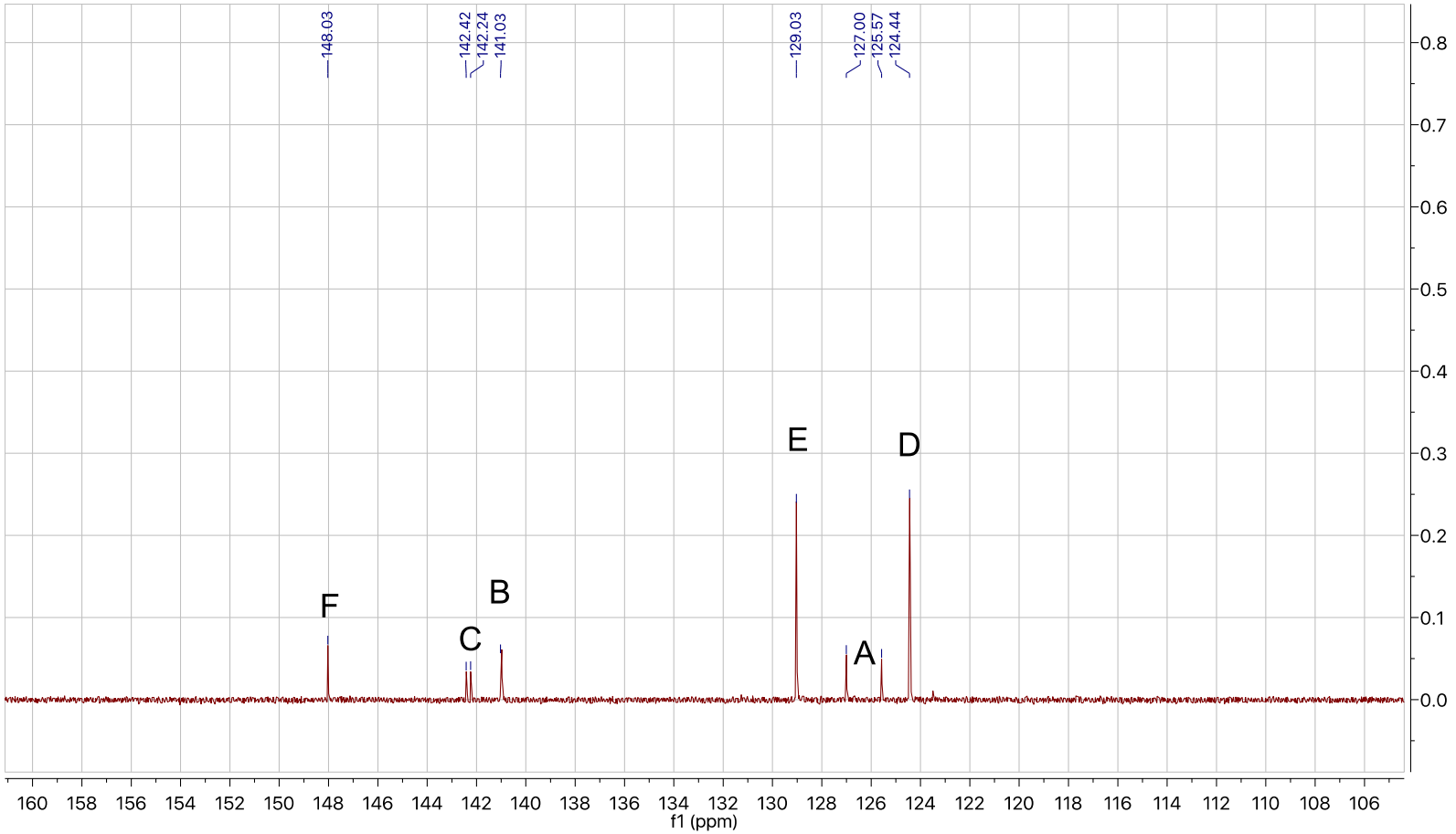

^{13}C NMR (126 MHz, DMSO-D_6) δ 148.03, 142.42-142.24 (d, $^{4}J_{C\text{-}P}$=22.4 1C) 141.03, 129.03 (2C), 127.00-125.57(d, $^{1}J_{C\text{-}P}$=180Hz, 1C) , 124.44 (2C).

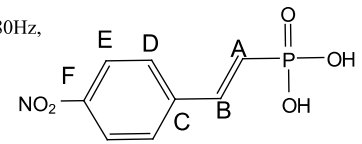

Figure A.15 ^{13}C NMR of NO_2VPA - (*E*)-(4-nitrostyryl) phosphonic acid

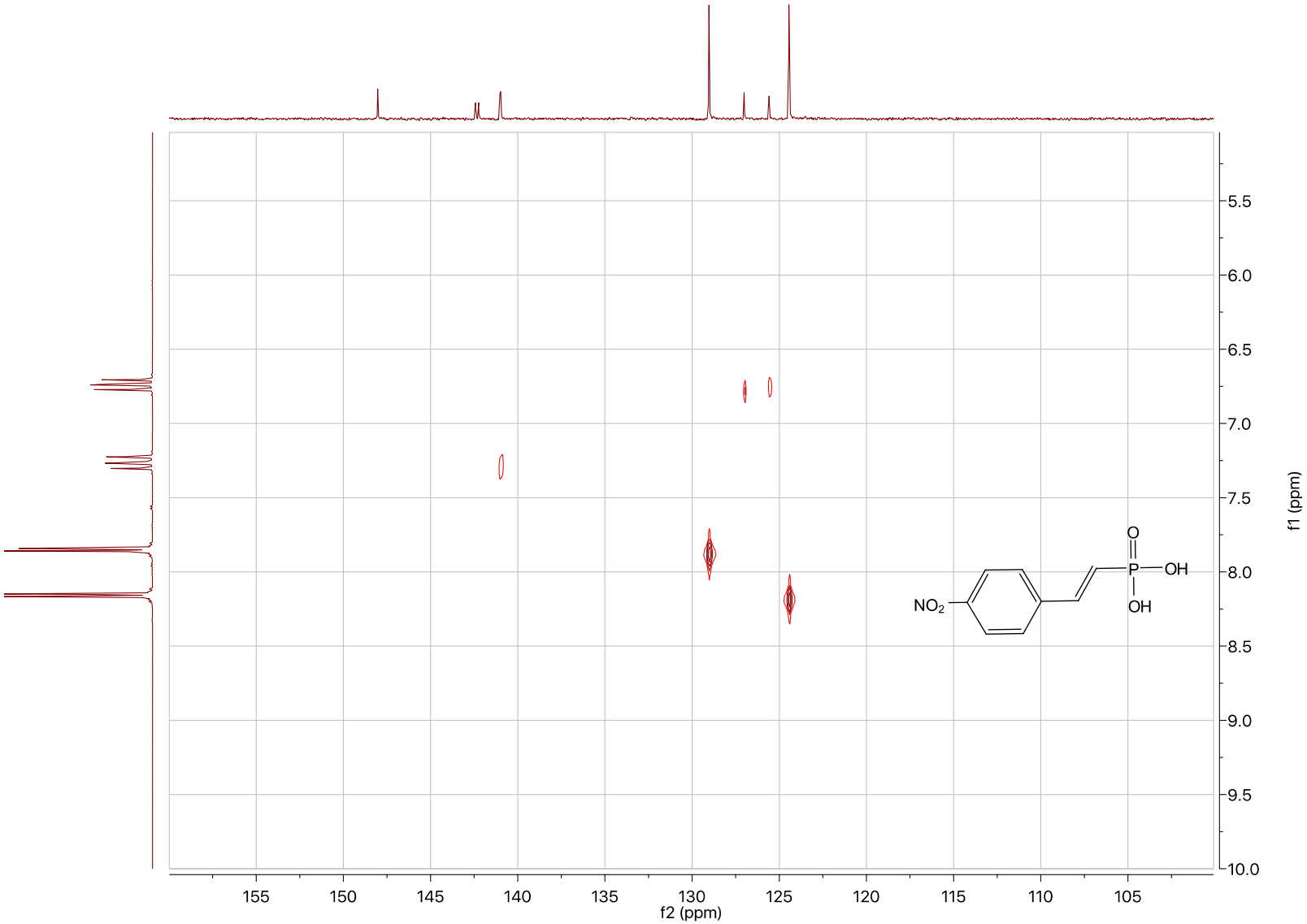

Figure A.16 Two dimensional heteronuclear correlation (HETCOR) of NO_2VPA - (*E*)-(4-nitrostyryl) phosphonic acid

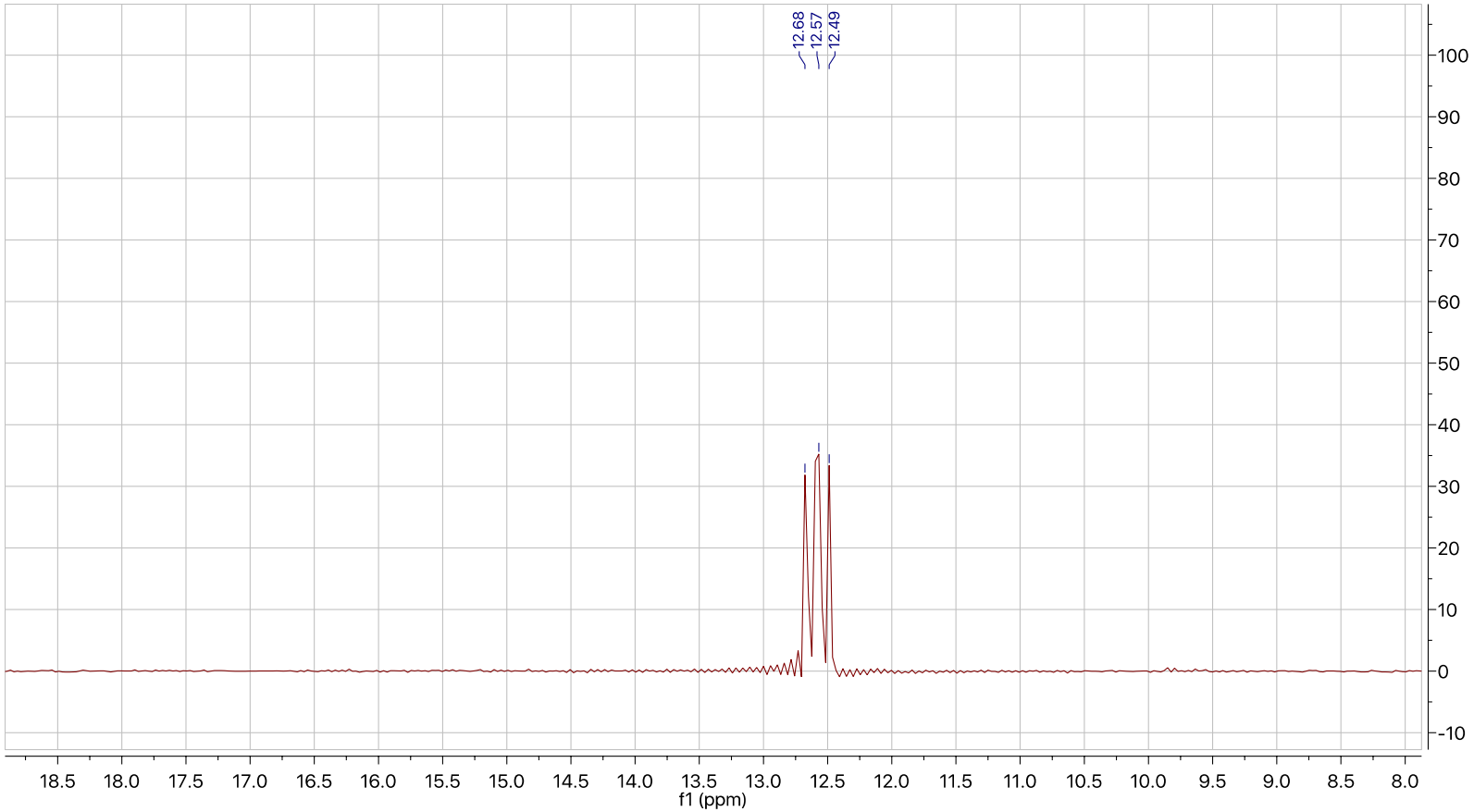

^{31}P NMR (202 MHz, DMSO-D_6) δ 12.57(dd, $^{2}J_{PH}$=15.5 Hz, $^{3}J_{PH}$=21.6 Hz)

Figure A.17 ^{31}P NMR of NO_2VPA - (*E*)-(4-nitrostyryl) phosphonic acid

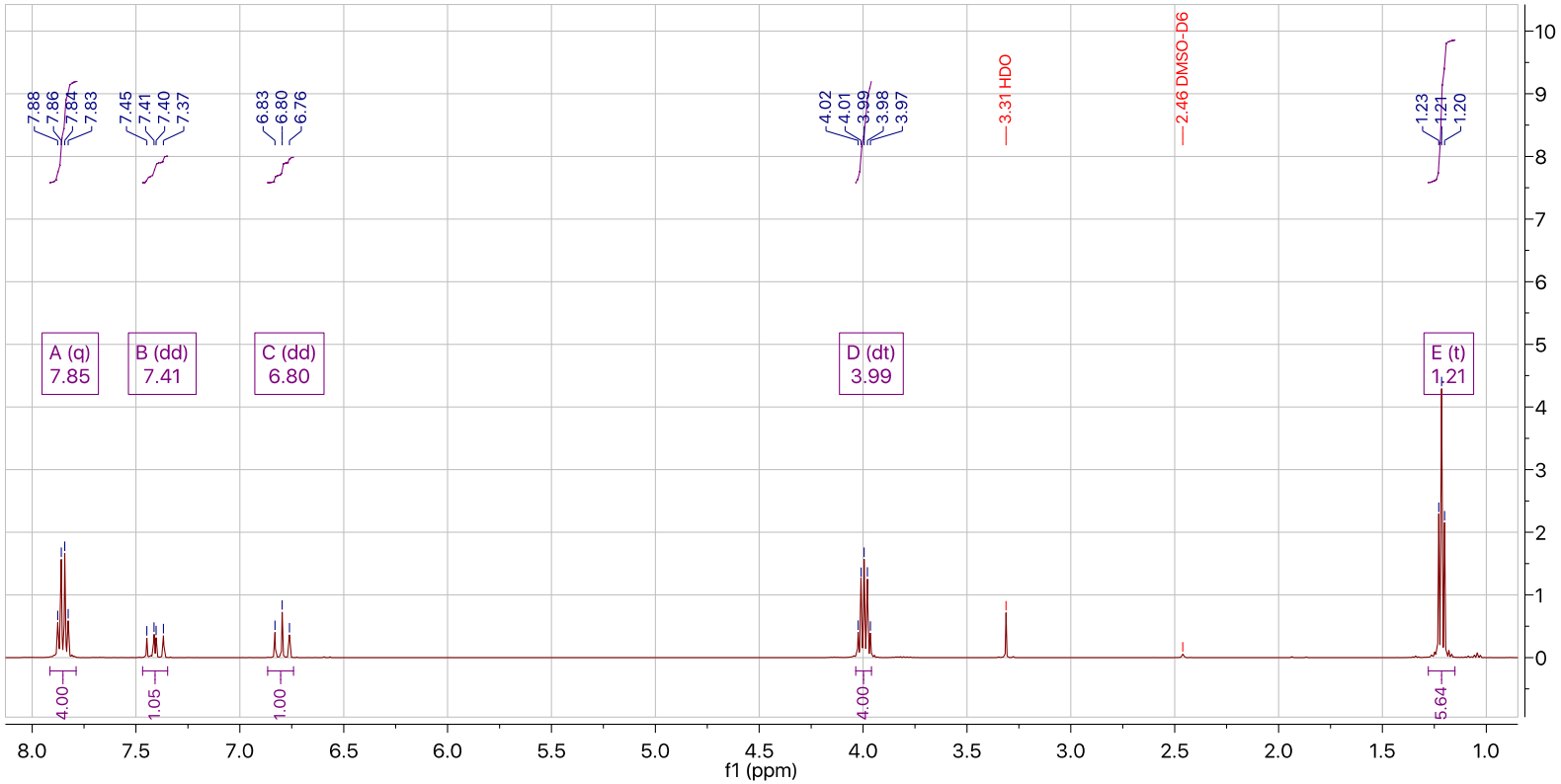

^{1}H NMR (500 MHz, DMSO-d_6) δ 7.85 (q, J = 8.5 Hz, 4H), 7.41 (dd, J = 22.5, 17.5 Hz, 1H), 6.80 (dd, J = 17.3 Hz, 1H), 3.99 (dt, J = 14.8, 7.2 Hz, 4H), 1.21 (t, J = 7.0 Hz, 6H).

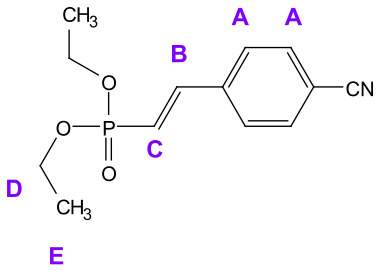

Figure A.18 ^{1}H NMR of CNVPE - diethyl (*E*)-(4-cyanostyryl) phosphonate

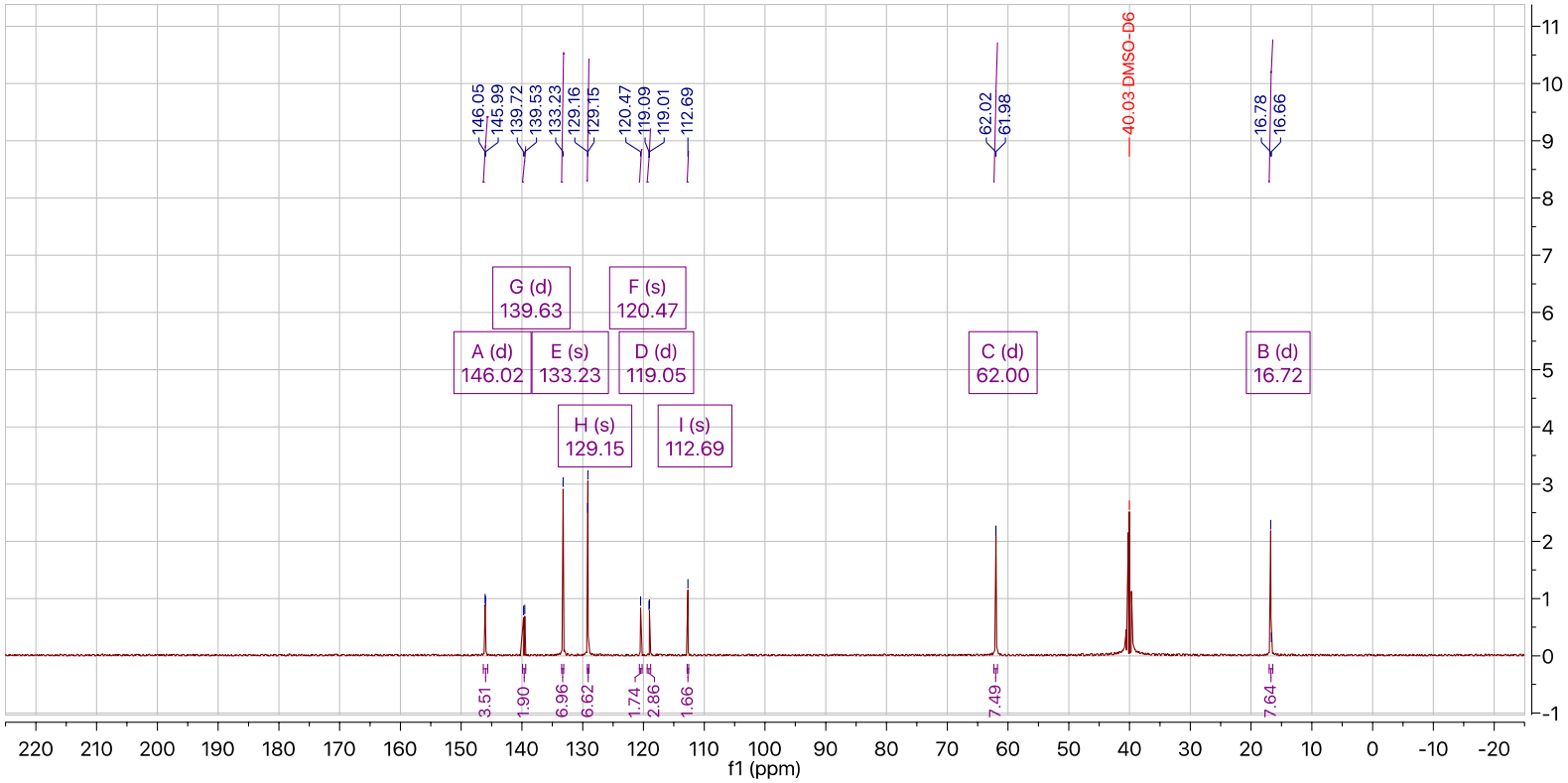

^{13}C NMR (126 MHz, DMSO-d_6) δ 146.02 (d, J = 6.8 Hz), 139.63 (d, J = 24.0 Hz), 133.23, 129.15, 120.47, 119.05 (d, J = 10.2 Hz), 112.69, 62.00 (d, J = 5.5 Hz), 16.72 (d, J = 6.3 Hz).

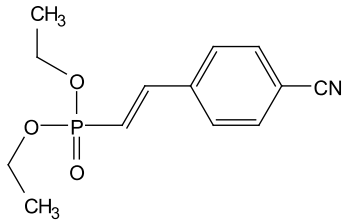

Figure A.19 ^{13}C NMR of CNVPE - diethyl (*E*)-(4-cyanostyryl) phosphonate

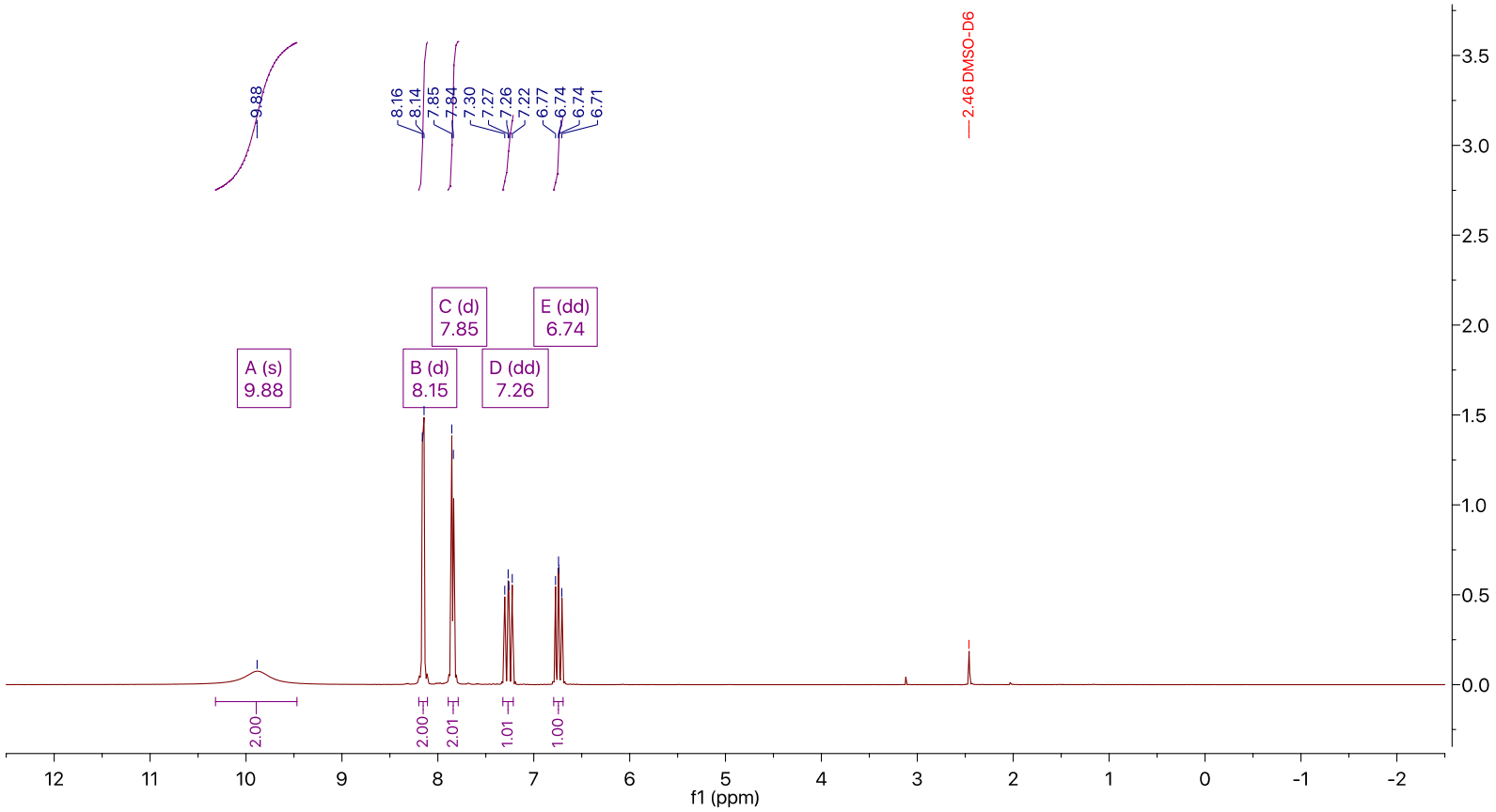

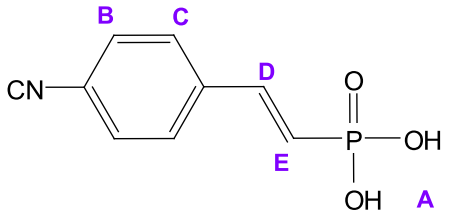

^{1}H NMR (500 MHz, DMSO-d_6) δ 9.88 (s, 2H), 8.15 (d, $^{3}J_{HH}$= 8.5 Hz, 2H), 7.85 (d, $^{3}J_{HH}$= 8.5 Hz, 2H), 7.26 (dd, $^{3}J_{HP}$= 21.5, $^{3}J_{HH}$17.5 Hz, 1H), 6.74 (dd, $^{3}J_{HH}$= 17.5, $^{2}J_{HP}$=15.9 Hz, 1H).

Figure A.20 ^{1}H NMR of CNVPA - (E)-(4-cyanostyryl) phosphonic acid

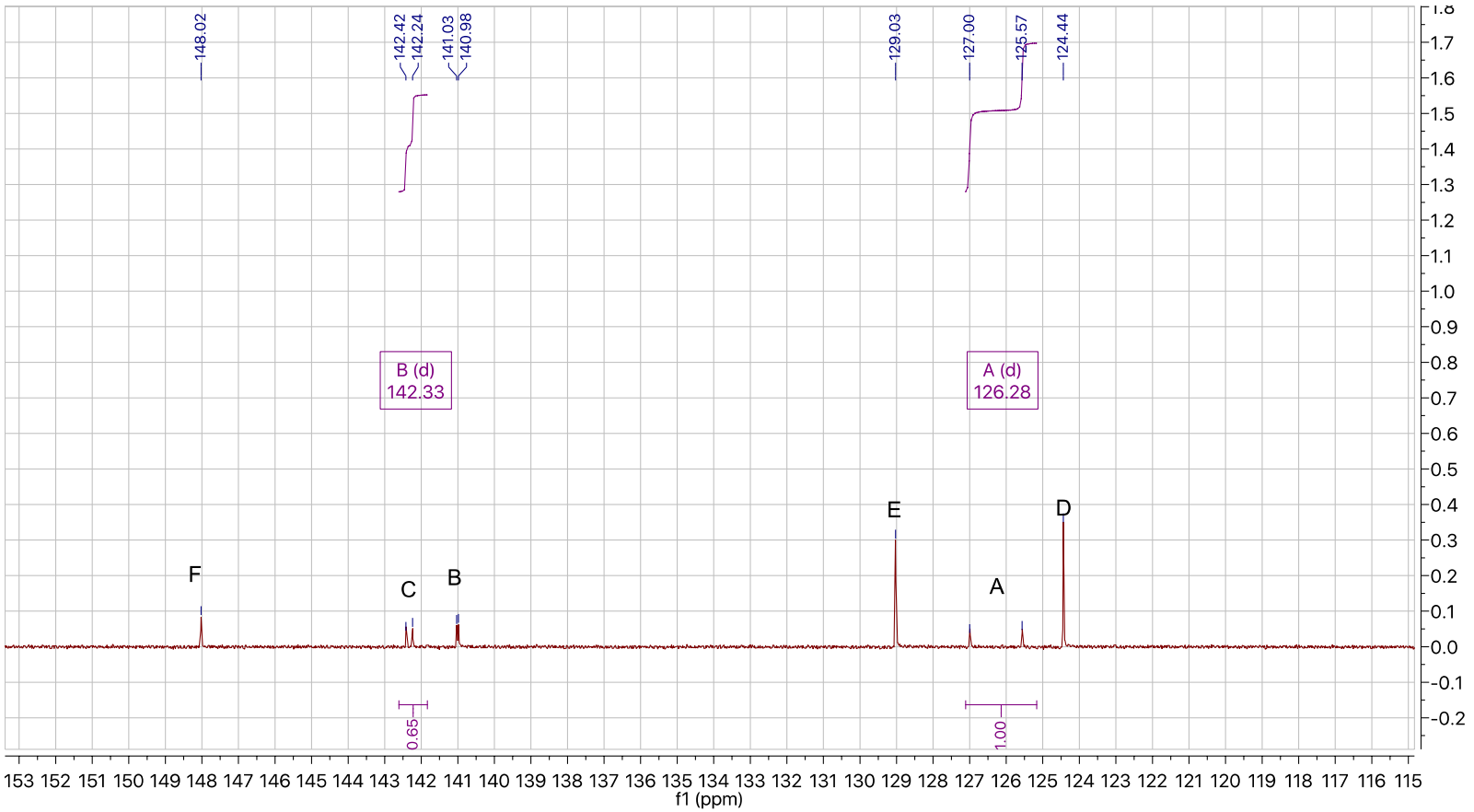

^{13}C NMR (126 MHz, DMSO-D_6) δ 148.02, 142.42, 142.24, 141.03, 140.98, 129.03, 127.00, 125.57, 124.44,.

^{13}C NMR (126 MHz, DMSO-d_6) δ 142.33 (d, J = 23.2 Hz), 126.28 (d, J = 180.3 Hz).

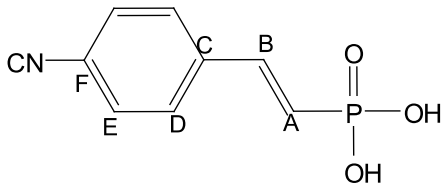

Figure A.21 ^{13}C NMR of CNVPA - (E)-(4-cyanostyryl) phosphonic acid

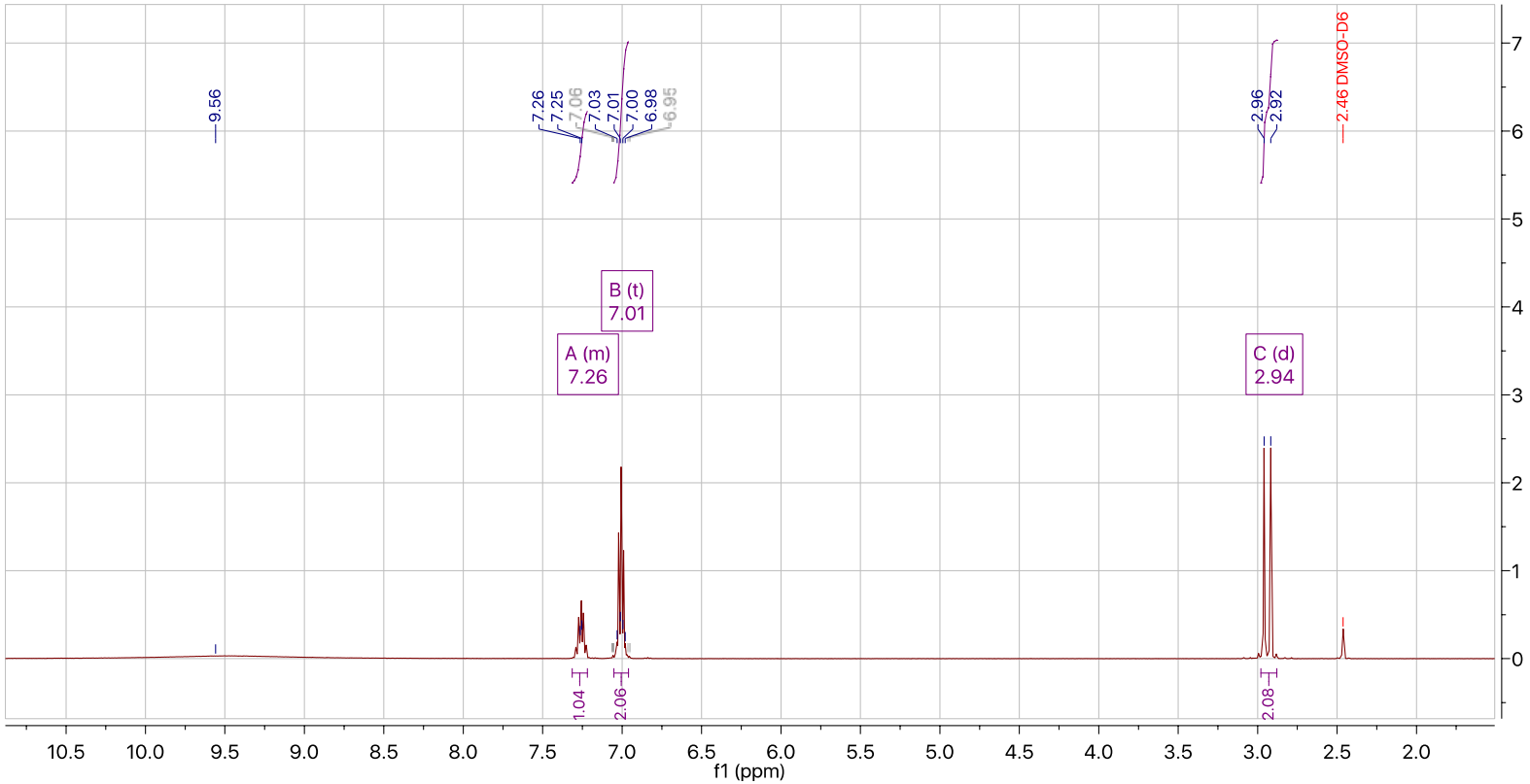

[1]H NMR (500 MHz, DMSO-d_6) δ 7.31 – 7.22 (m, 1H), 7.01 (t, J = 8.9 Hz, 2H), 2.94 (d, J = 21.0 Hz, 2H).

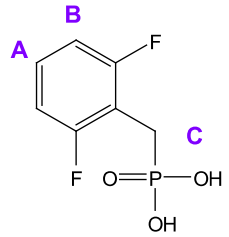

Figure A.22 [1]H NMR of oF_2BPA - (2,6-difluorobenzyl) phosphonic acid

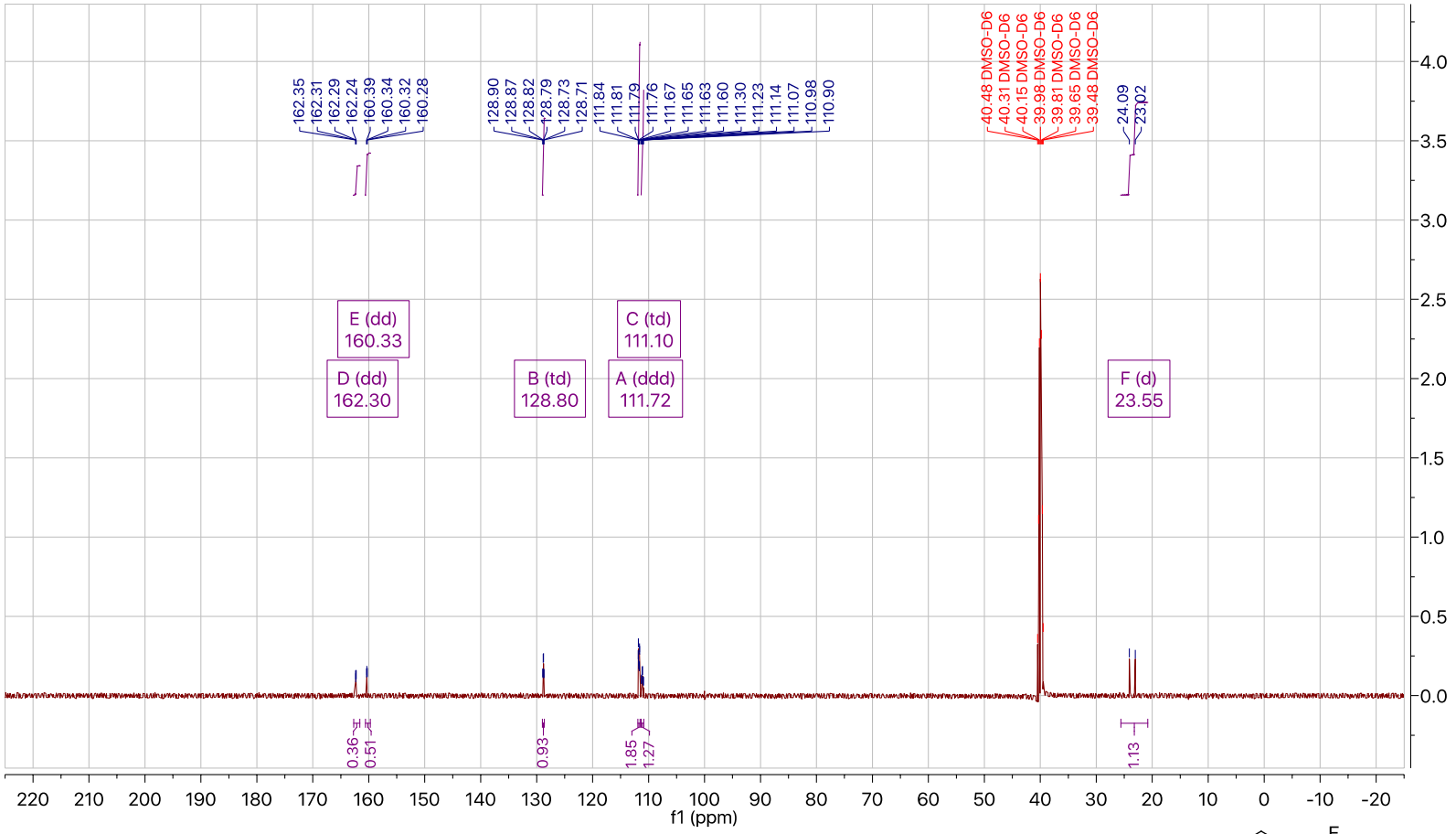

^{13}C NMR (126 MHz, DMSO-d_6) δ 162.30 (dd, J = 8.6, 5.7 Hz), 160.33 (dd, J = 8.4, 5.5 Hz), 128.80 (td, J = 10.2, 3.7 Hz), 111.72 (ddd, J = 20.2, 5.9, 3.4 Hz), 111.10 (td, J = 20.2, 9.7 Hz), 23.55 (d, J = 134.6 Hz).

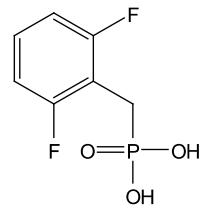

Figure A.23 ^{13}C NMR of oF_2BPA - (2,6-difluorobenzyl) phosphonic acid

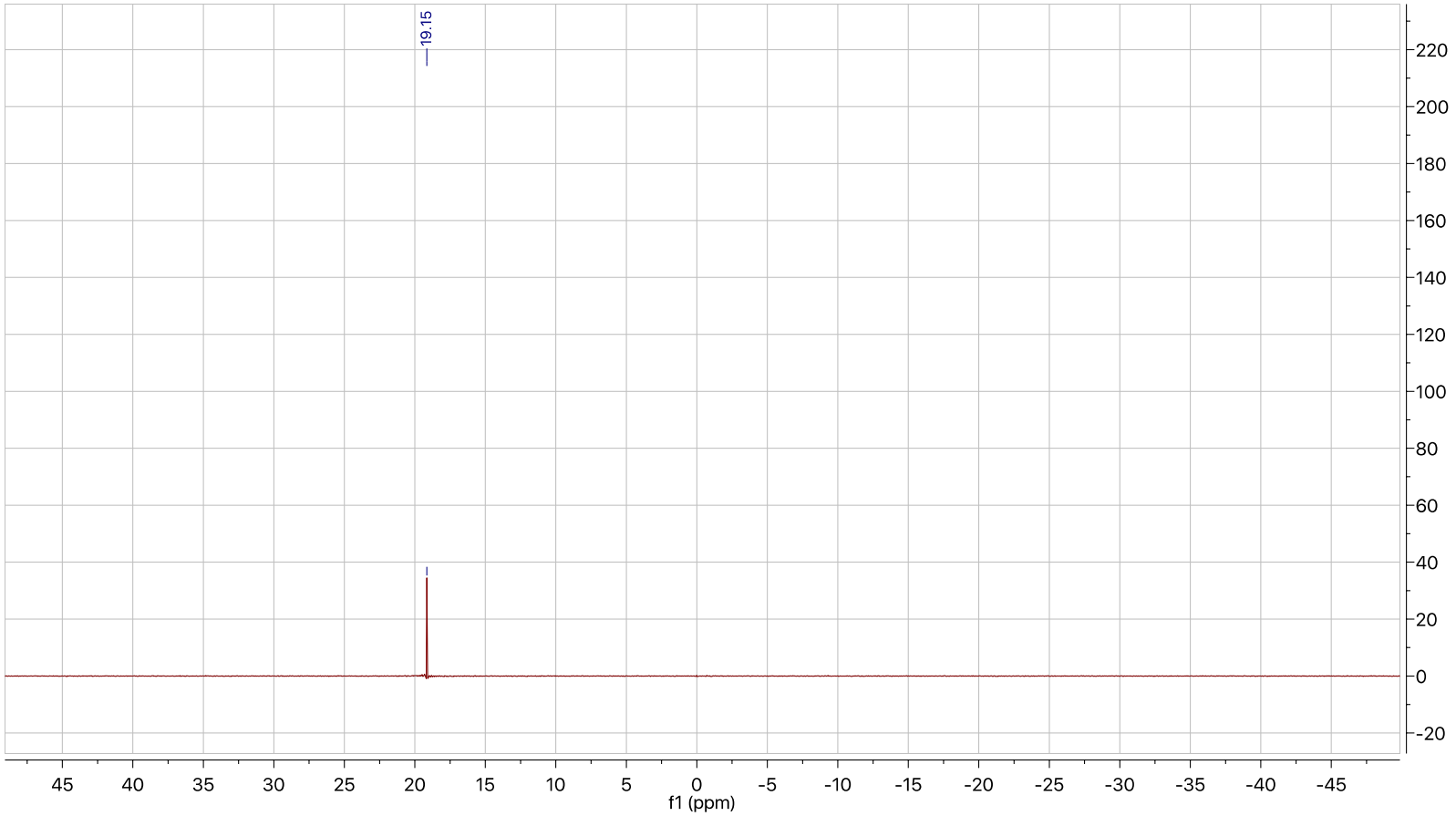

^{31}P NMR (202 MHz, DMSO-D_6) δ 19.15,

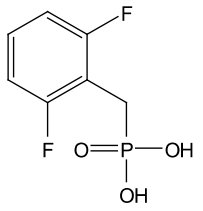

Figure A.24 ^{31}P NMR of oF_2BPA - (2,6-difluorobenzyl) phosphonic acid

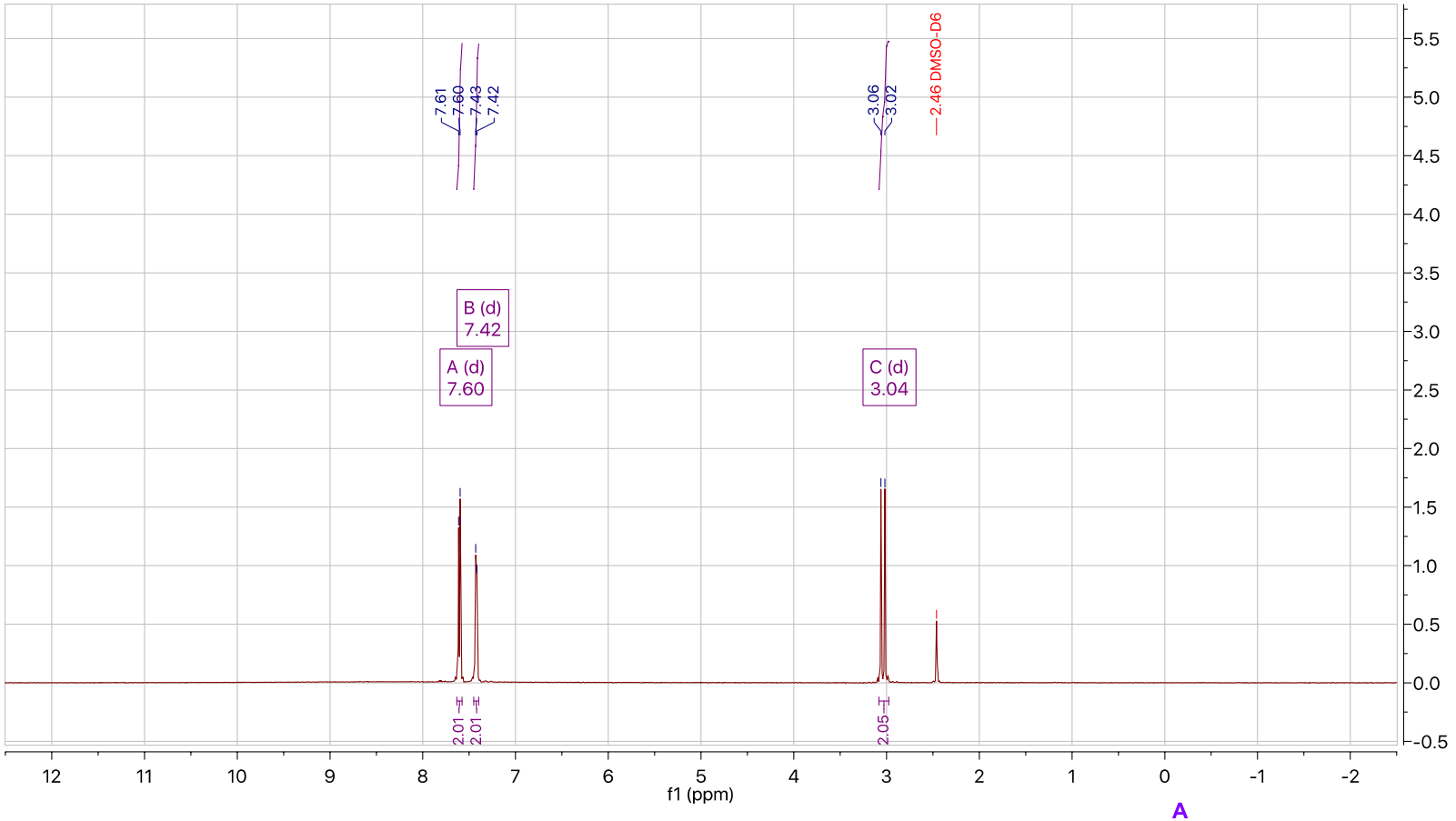

^{1}H NMR (500 MHz, DMSO-d_6) δ 7.60 (d, J = 8.1 Hz, 2H), 7.42 (d, J = 6.7 Hz, 2H), 3.04 (d, J = 21.6 Hz, 2H).

Figure A.25 ^{1}H NMR of CF_3BPA (4-(trifluoromethyl)benzyl) phosphonic acid

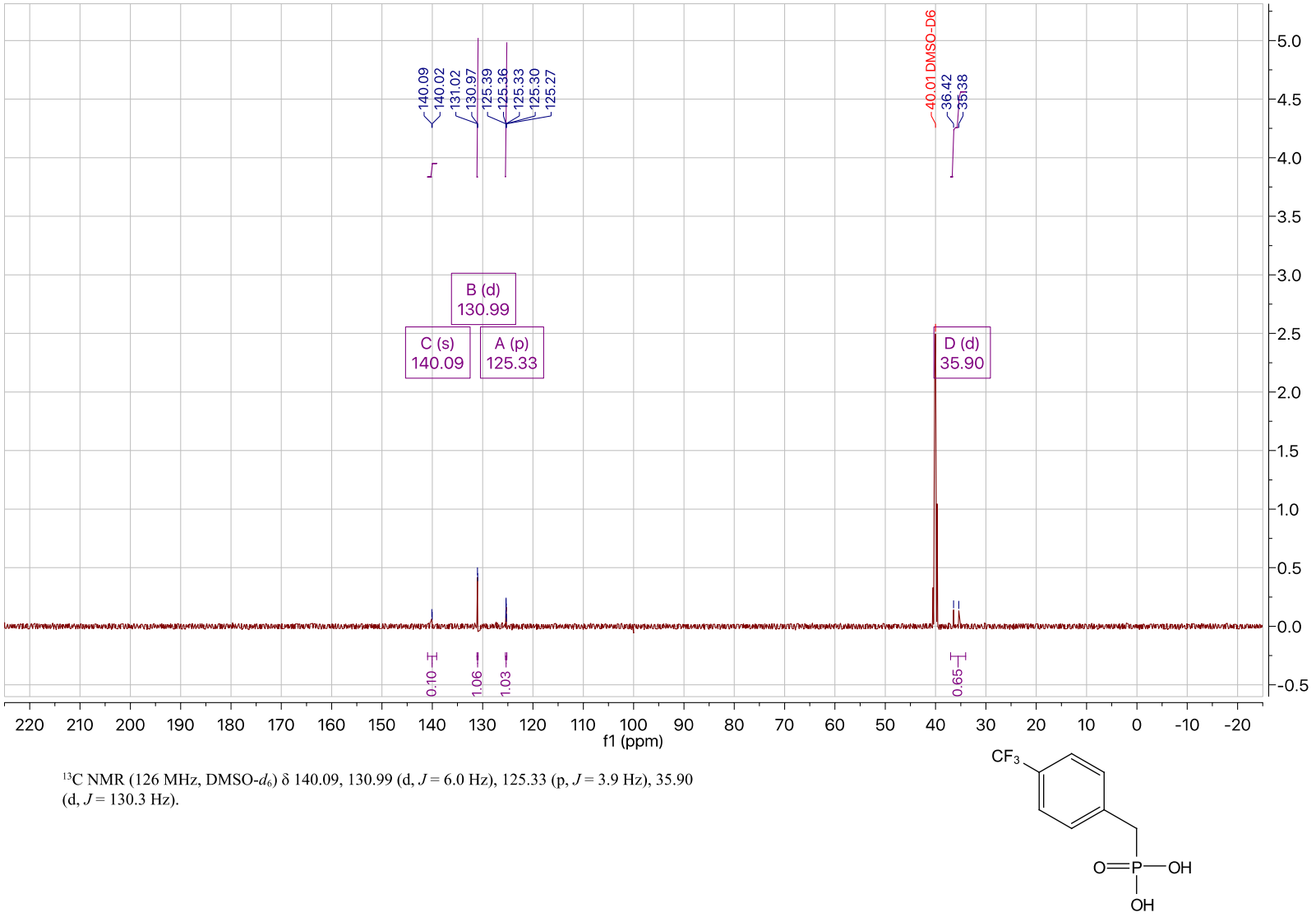

^{13}C NMR (126 MHz, DMSO-d_6) δ 140.09, 130.99 (d, J = 6.0 Hz), 125.33 (p, J = 3.9 Hz), 35.90 (d, J = 130.3 Hz).

Figure A.26 ^{13}C NMR of CF_3BPA (4-(trifluoromethyl)benzyl) phosphonic acid

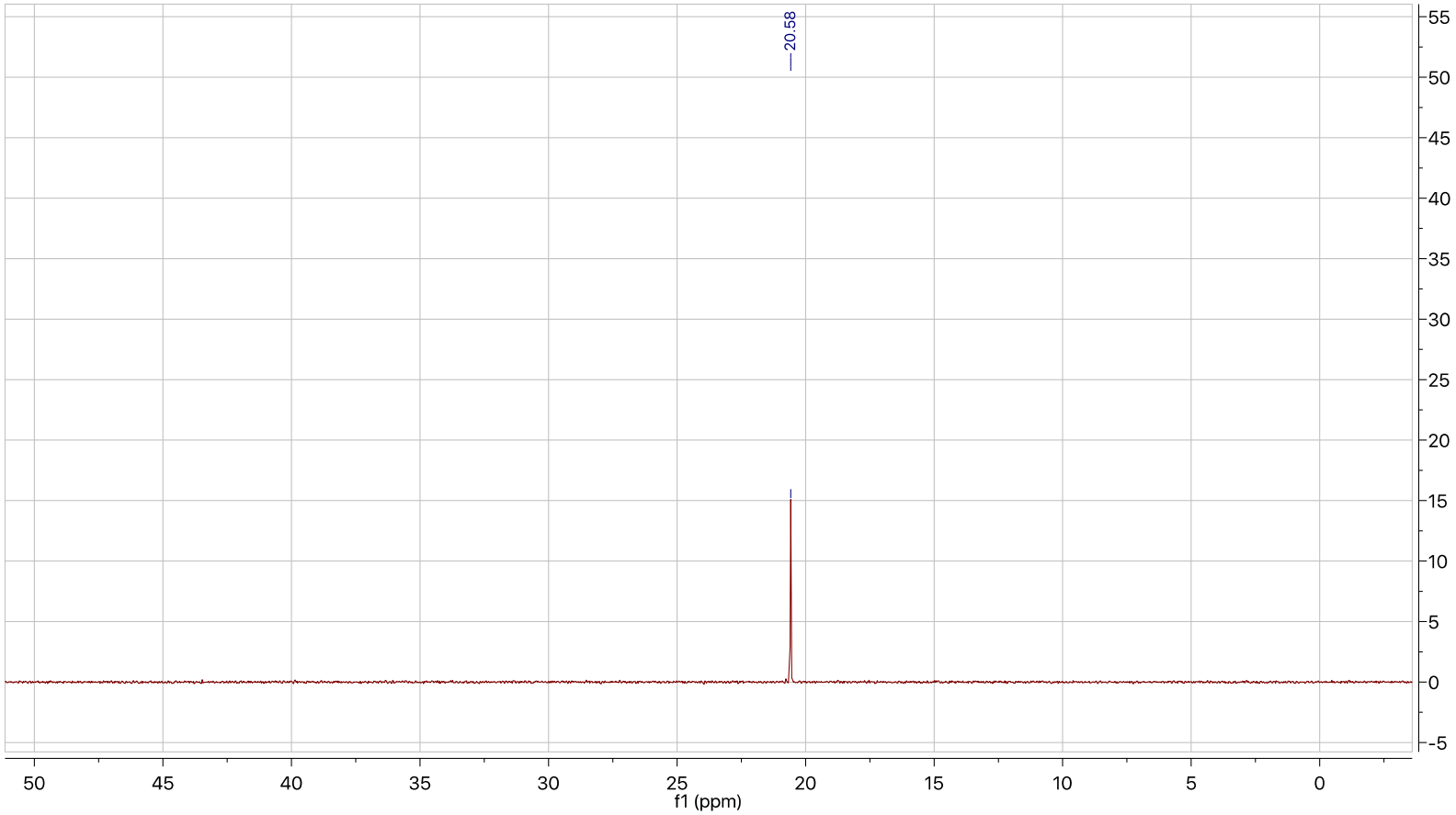

^{31}P NMR (202 MHz, DMSO-D_6) δ 20.58.

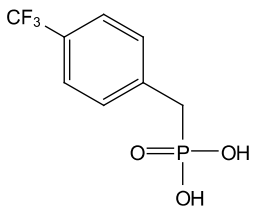

Figure A.27 ^{31}P NMR of CF_3BPA (4-(trifluoromethyl)benzyl) phosphonic acid

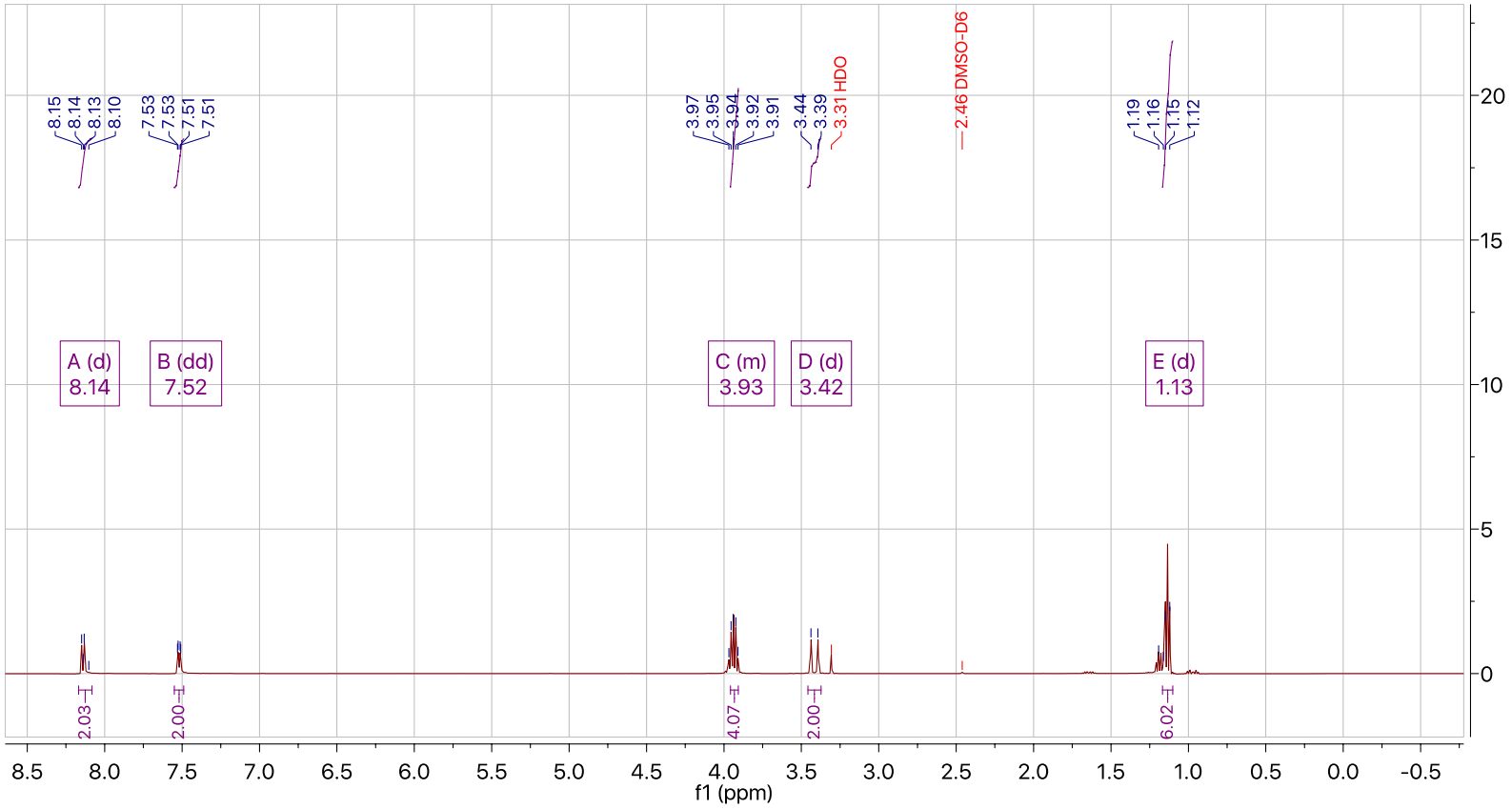

^{1}H NMR (500 MHz, DMSO-d_6) δ 8.14 (d, J = 8.1 Hz, 2H), 7.52 (dd, J = 8.6, 1.8 Hz, 2H), 3.96 – 3.91 (m, 4H), 3.42 (d, J = 22.3 Hz, 2H), 1.13 (d, J = 12.9 Hz, 6H).

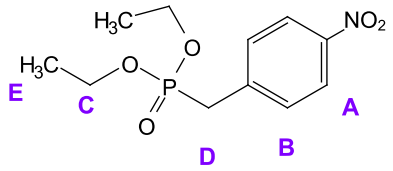

Figure A.28 ^{1}H NMR of NO_2BPE - diethyl (4-nitrobenzyl) phosphonate

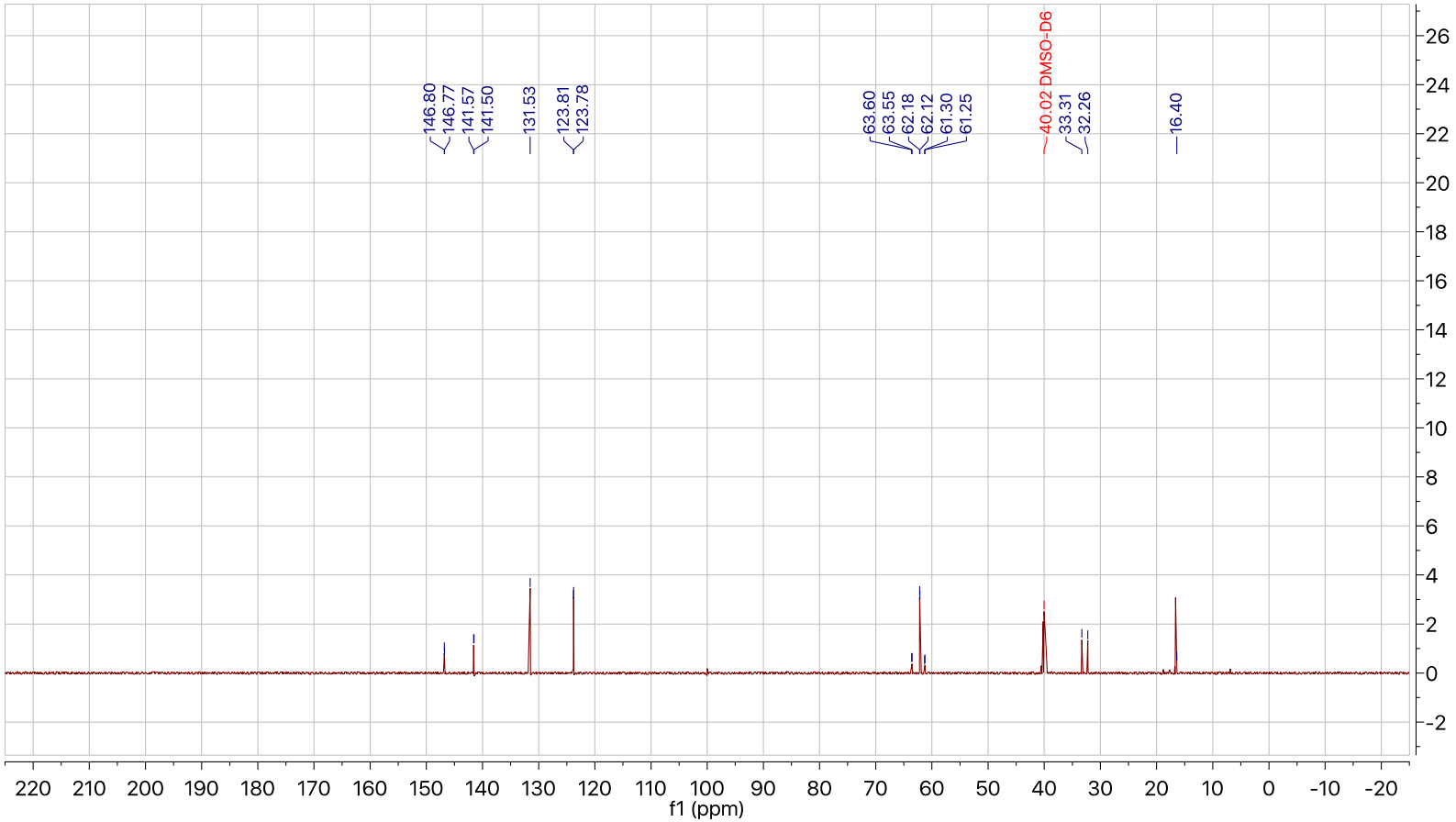

^{13}C NMR (126 MHz, DMSO-D_6) δ 146.80, 146.77, 141.57, 141.50, 131.53, 123.81, 123.78, 63.60, 63.55, 62.18, 62.12, 61.30, 61.25, 40.02, 33.31, 32.26, 16.40.

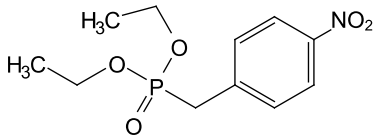

Figure A.29 ^{13}C NMR of NO_2BPE - diethyl (4-nitrobenzyl) phosphonate

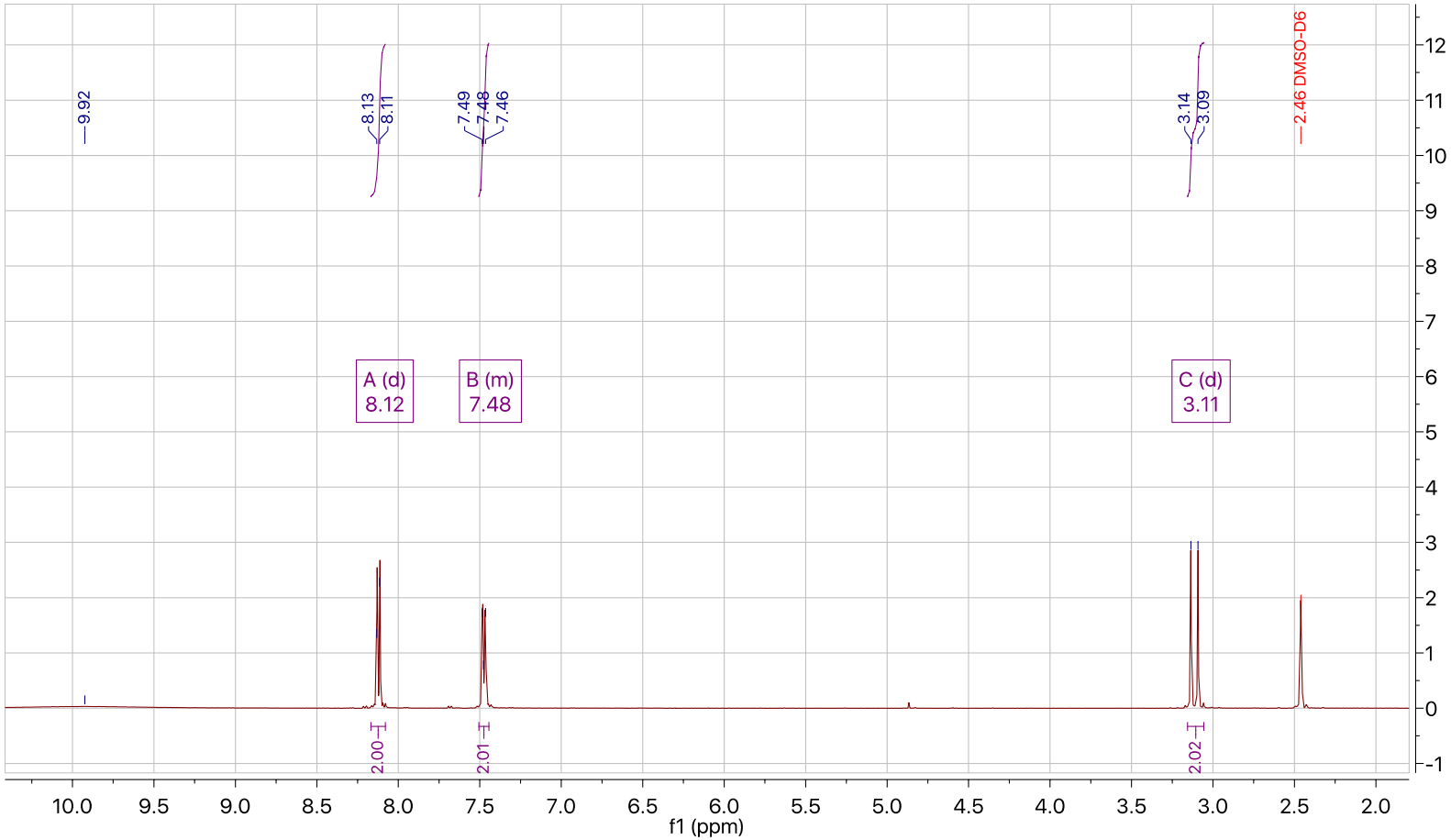

^{1}H NMR (500 MHz, DMSO-d_6) δ 8.12 (d, J = 9.0 Hz, 2H), 7.51 – 7.44 (m, 2H), 3.11 (d, J = 22.1 Hz, 2H).

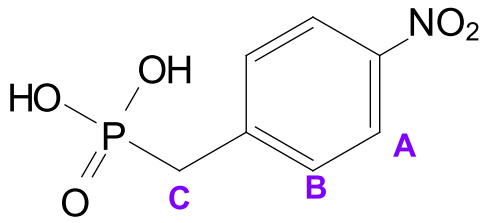

Figure A.30 ^{1}H NMR of NO_2BPA - (4-nitrobenzyl) phosphonic acid

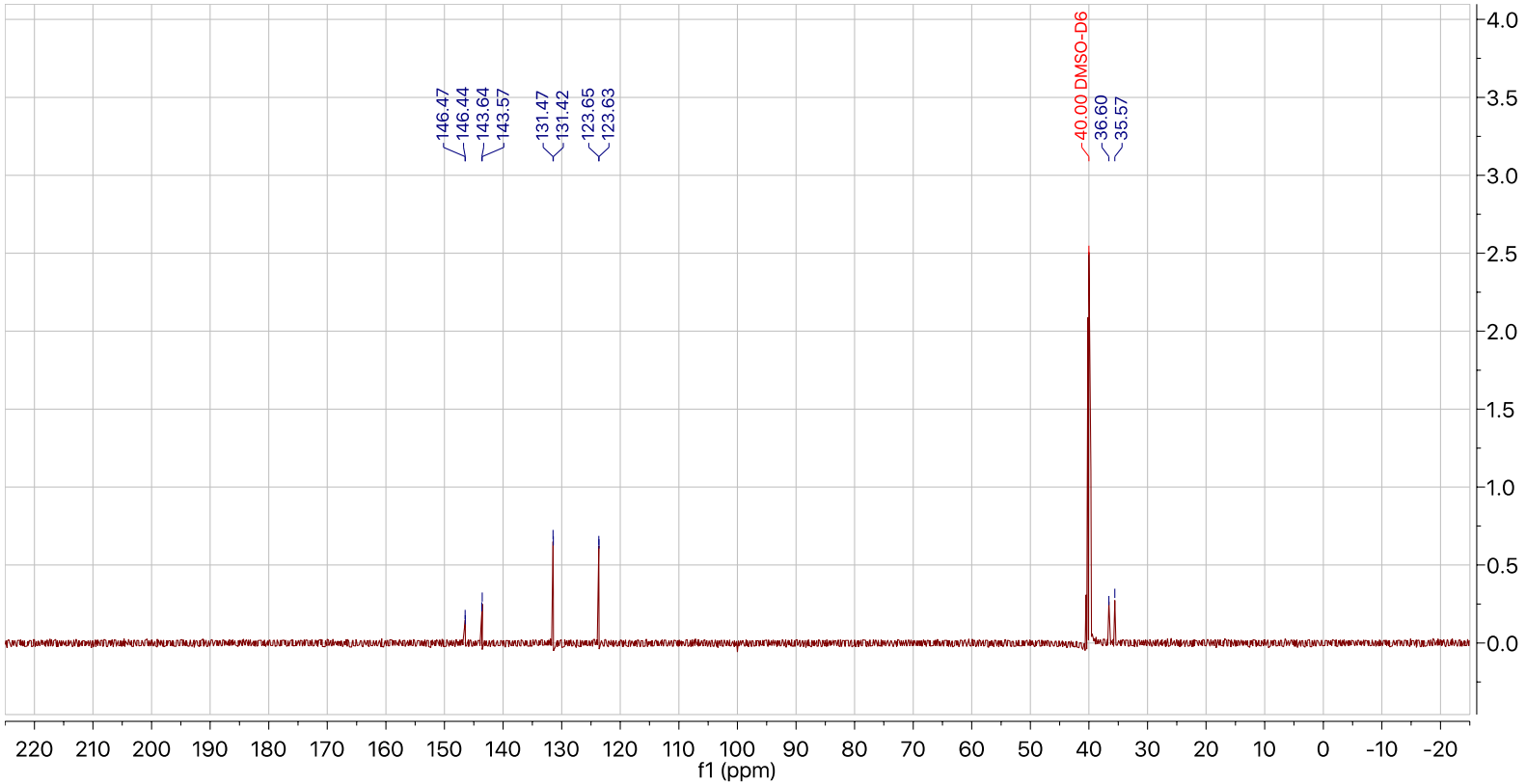

^{13}C NMR (126 MHz, DMSO-D_6) δ 146.47, 146.44, 143.64, 143.57, 131.47, 131.42, 123.65, 123.63, 40.00, 36.60, 35.57.

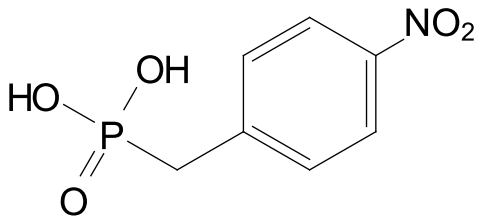

Figure A.31 ^{13}C NMR of NO_2BPA - (4-nitrobenzyl) phosphonic acid

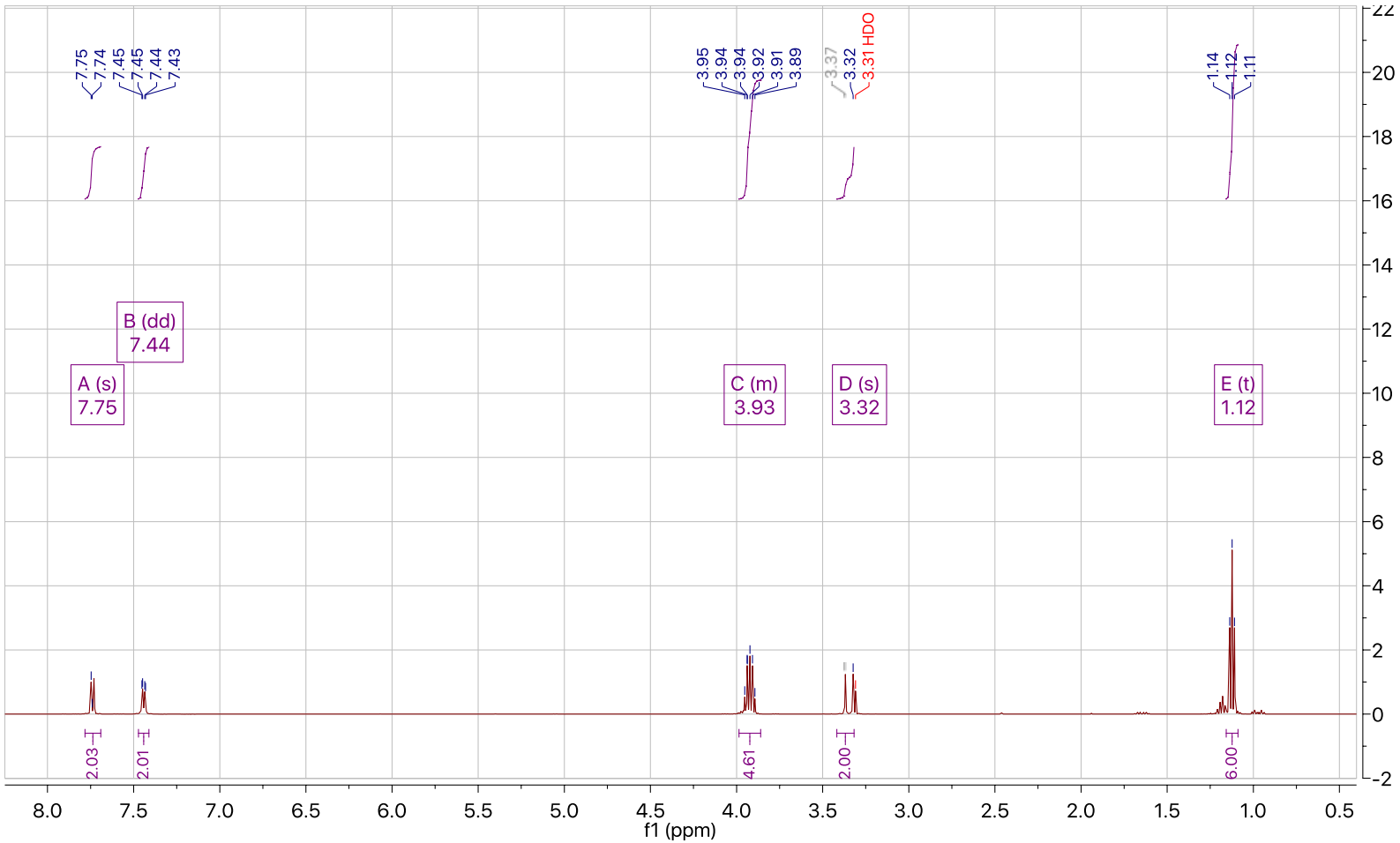

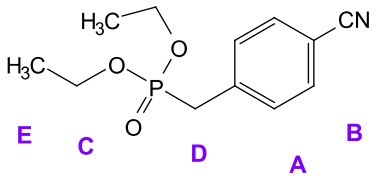

^{1}H NMR (500 MHz, DMSO-d_6) δ 7.75 (s, 2H), 7.44 (dd, J = 8.3, 2.3 Hz, 2H), 3.99 – 3.86 (m, 5H), 3.32 (s, 2H), 1.12 (t, J = 7.1 Hz, 6H).

Figure A.32 ^{1}H NMR of CNBPE - diethyl (4-cyanobenzyl) phosphonate

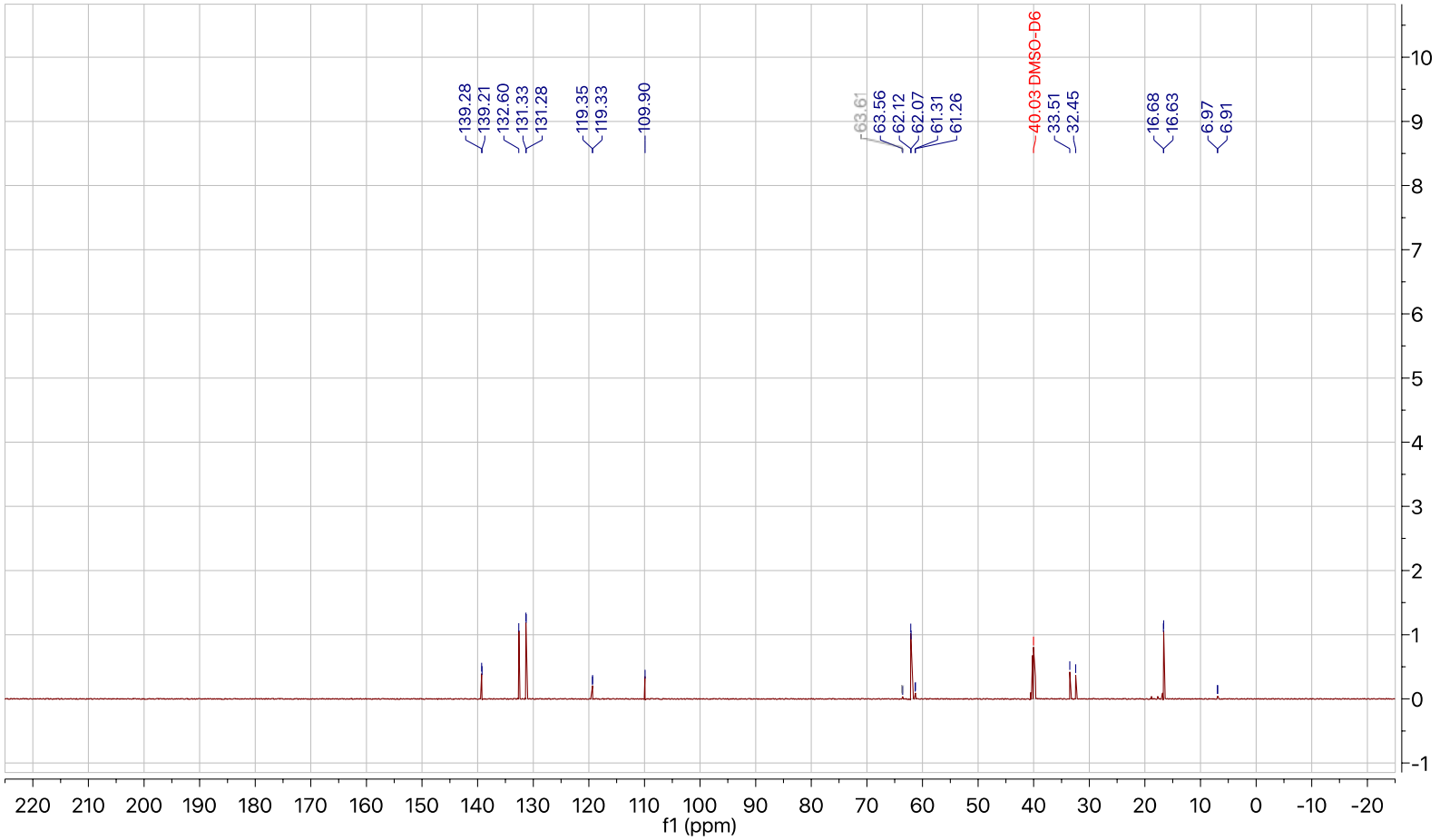

^{13}C NMR (126 MHz, DMSO-D_6) δ 139.28, 139.21, 132.60, 131.33, 131.28, 119.35, 119.33, 109.90, 63.61, 63.56, 62.12, 62.07, 61.31, 61.26, 40.03, 33.51, 32.45, 16.68, 16.63, 6.97, 6.91.

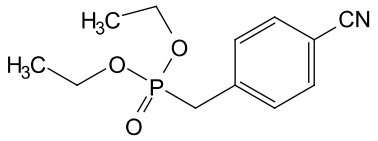

Figure A.33 ^{13}C NMR of CNBPE - diethyl (4-cyanobenzyl) phosphonate

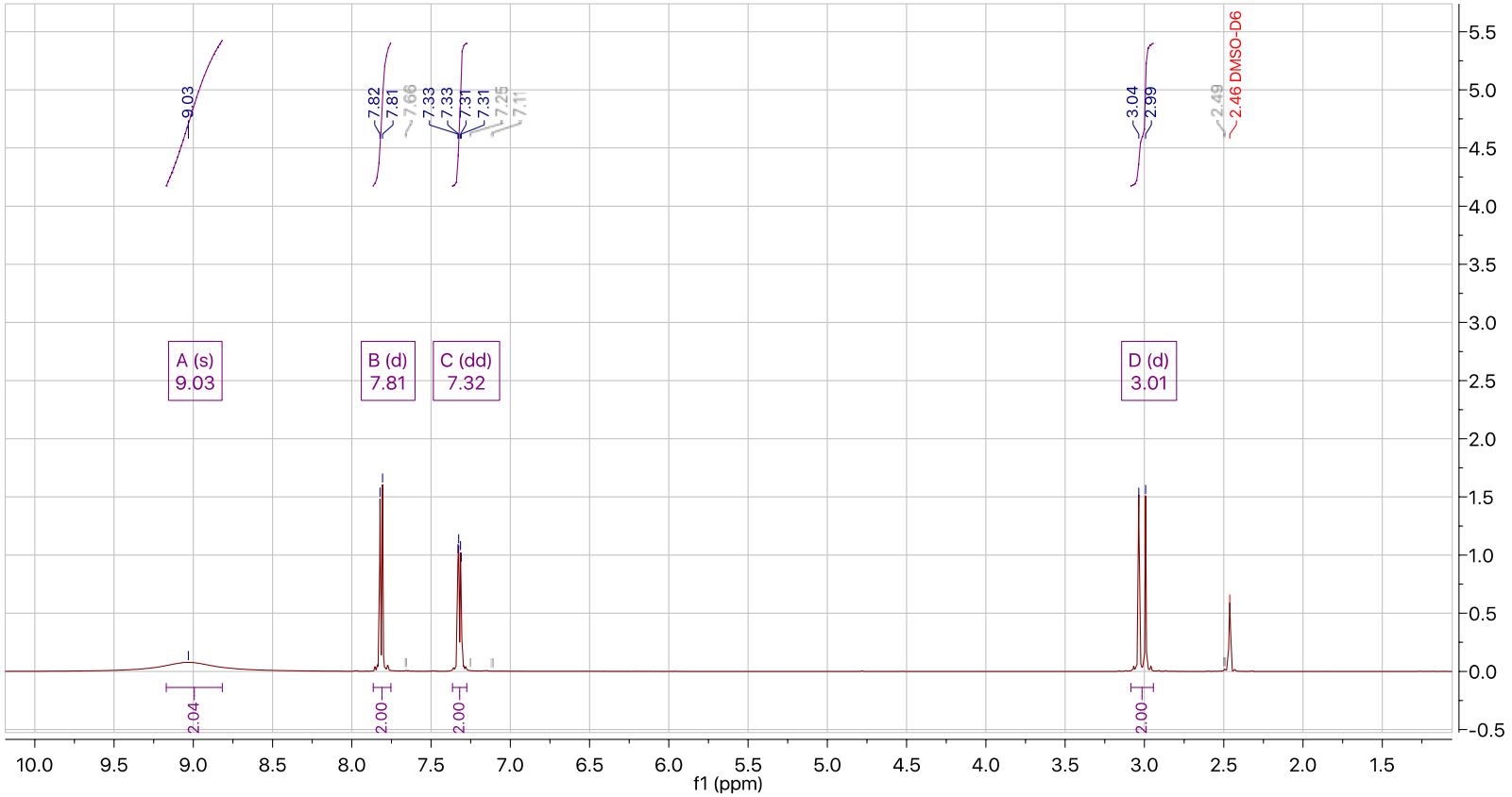

^{1}H NMR (500 MHz, DMSO-d_6) δ 9.03 (s, 2H), 7.81 (d, J = 8.2 Hz, 2H), 7.32 (dd, J = 8.2, 2.1 Hz, 2H), 3.01 (d, J = 21.6 Hz, 2H).

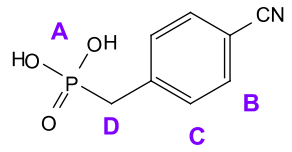

Figure A.34 ^{1}H NMR of CNBPA (4-cyanobenzyl) phosphonic acid

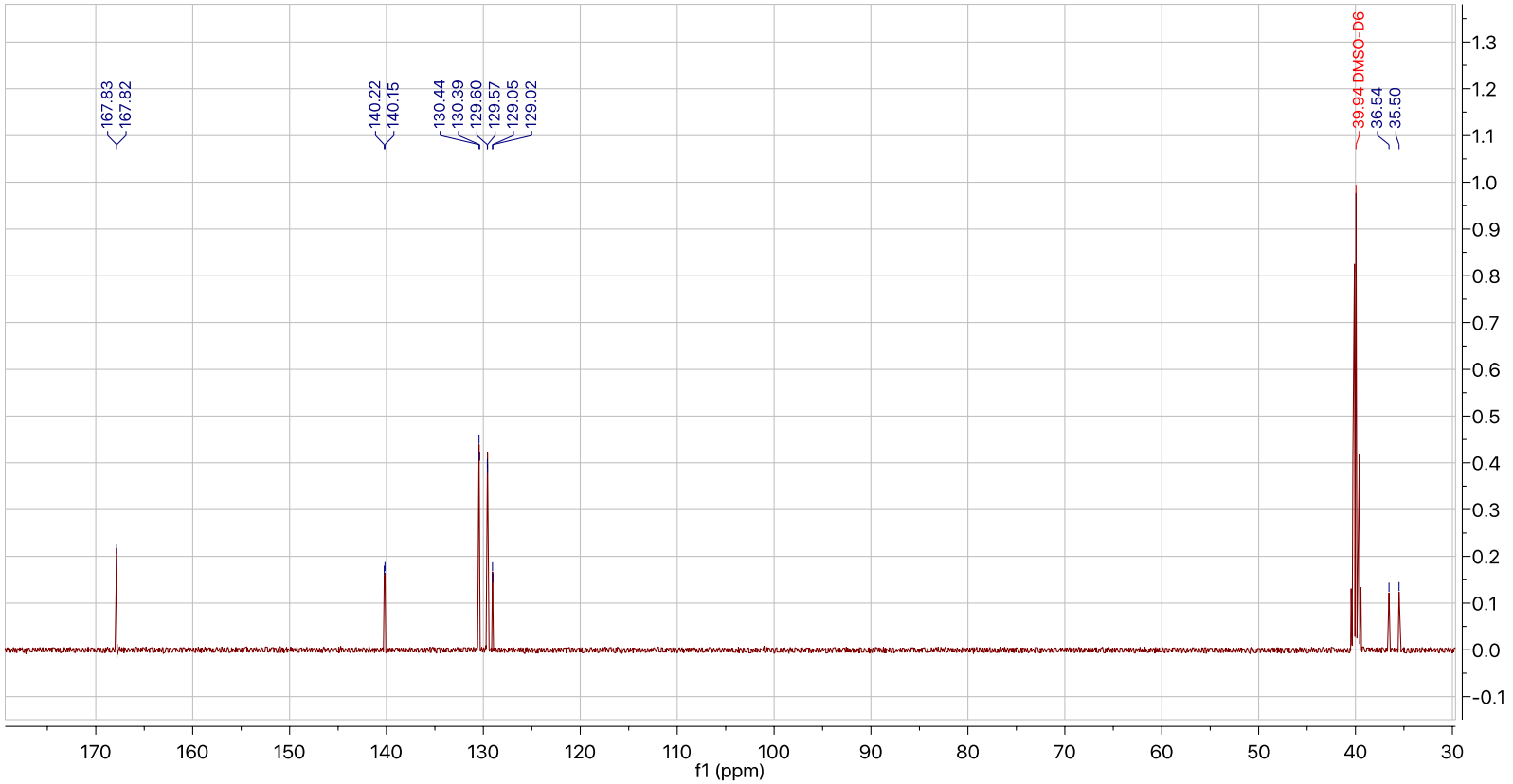

^{13}C NMR (126 MHz, DMSO-D_6) δ 167.83, 167.82, 140.22, 140.15, 130.44, 130.39, 129.60, 129.57, 129.05, 129.02, 39.94, 36.54, 35.50.

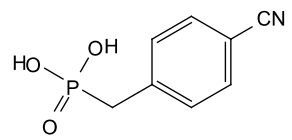

Figure A.35 ^{13}C NMR of CNBPA - (4-cyanobenzyl) phosphonic acid

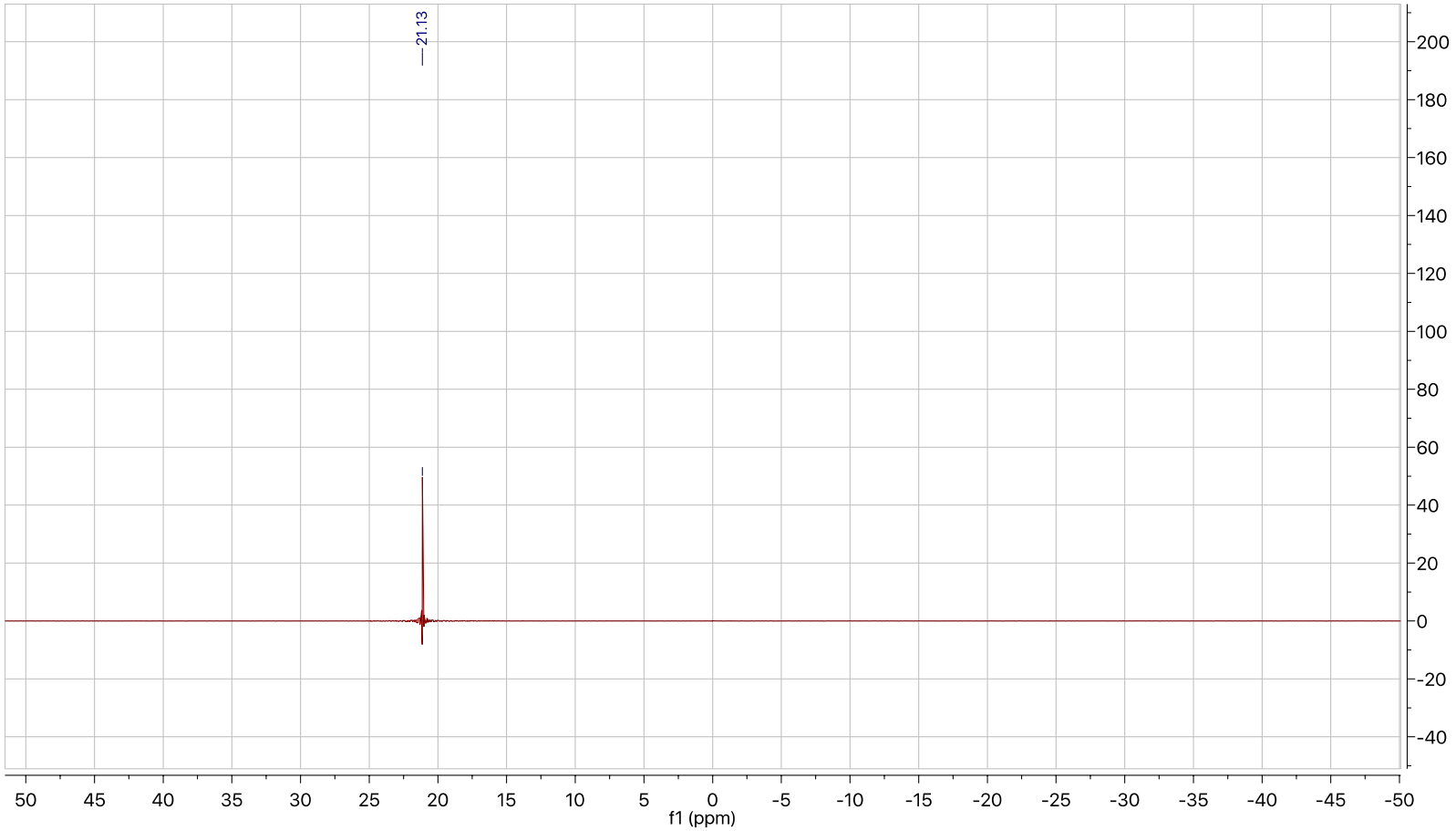

^{31}P NMR (202 MHz, DMSO-D_6) δ 21.13.

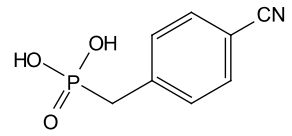

Figure A.36 ^{31}P NMR of CNBPA - (4-cyanobenzyl) phosphonic acid

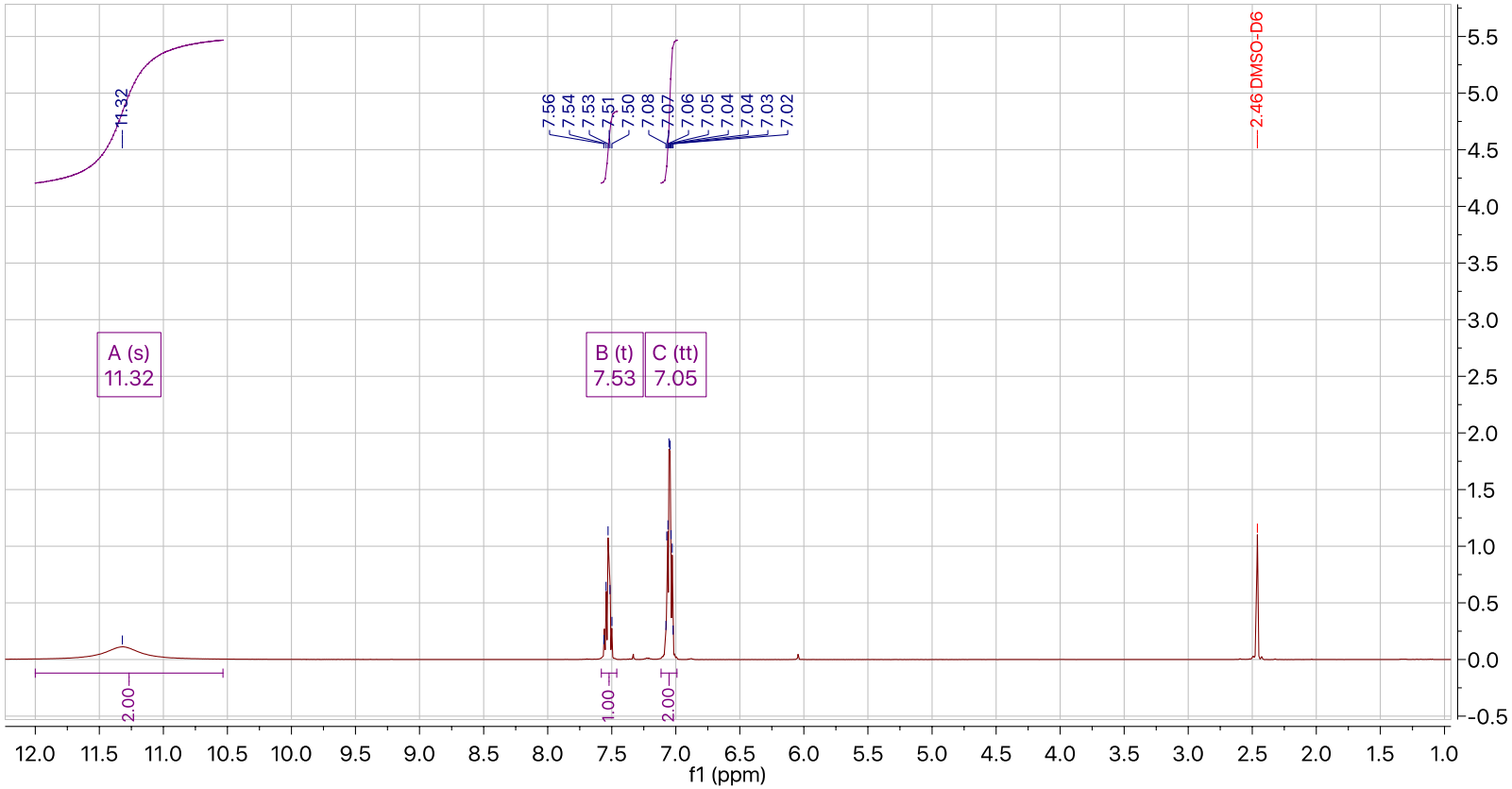

^{1}H NMR (500 MHz, DMSO-d_6) δ 11.32 (s, 2H), 7.53 (t, J = 7.8 Hz, 1H), 7.05 (tt, J = 8.4, 3.9 Hz, 2H).

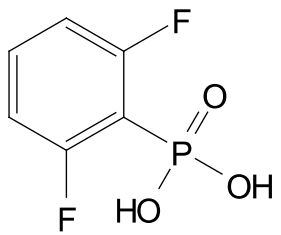

Figure A.37 ^{1}H NMR of oF$_2$PPA - (2,6-difluorophenyl) phosphonic acid

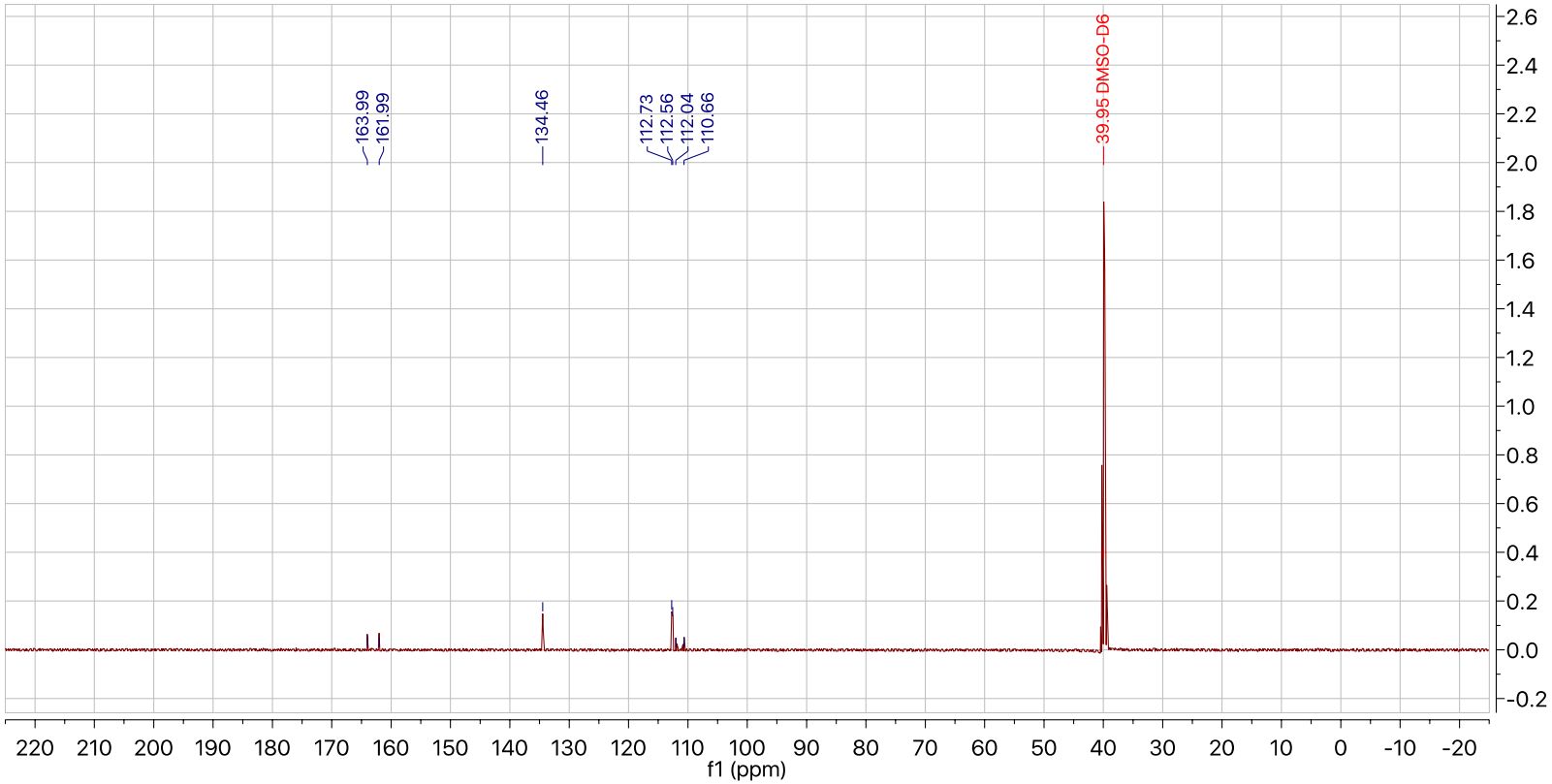

^{13}C NMR (126 MHz, DMSO-D_6) δ 163.99, 161.99, 134.46, 112.73, 112.56, 112.04, 110.66, 39.95.

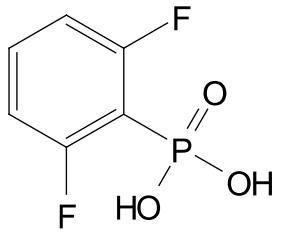

Figure A.38 ^{13}C NMR of oF_2PPA - (2,6-difluorophenyl) phosphonic acid

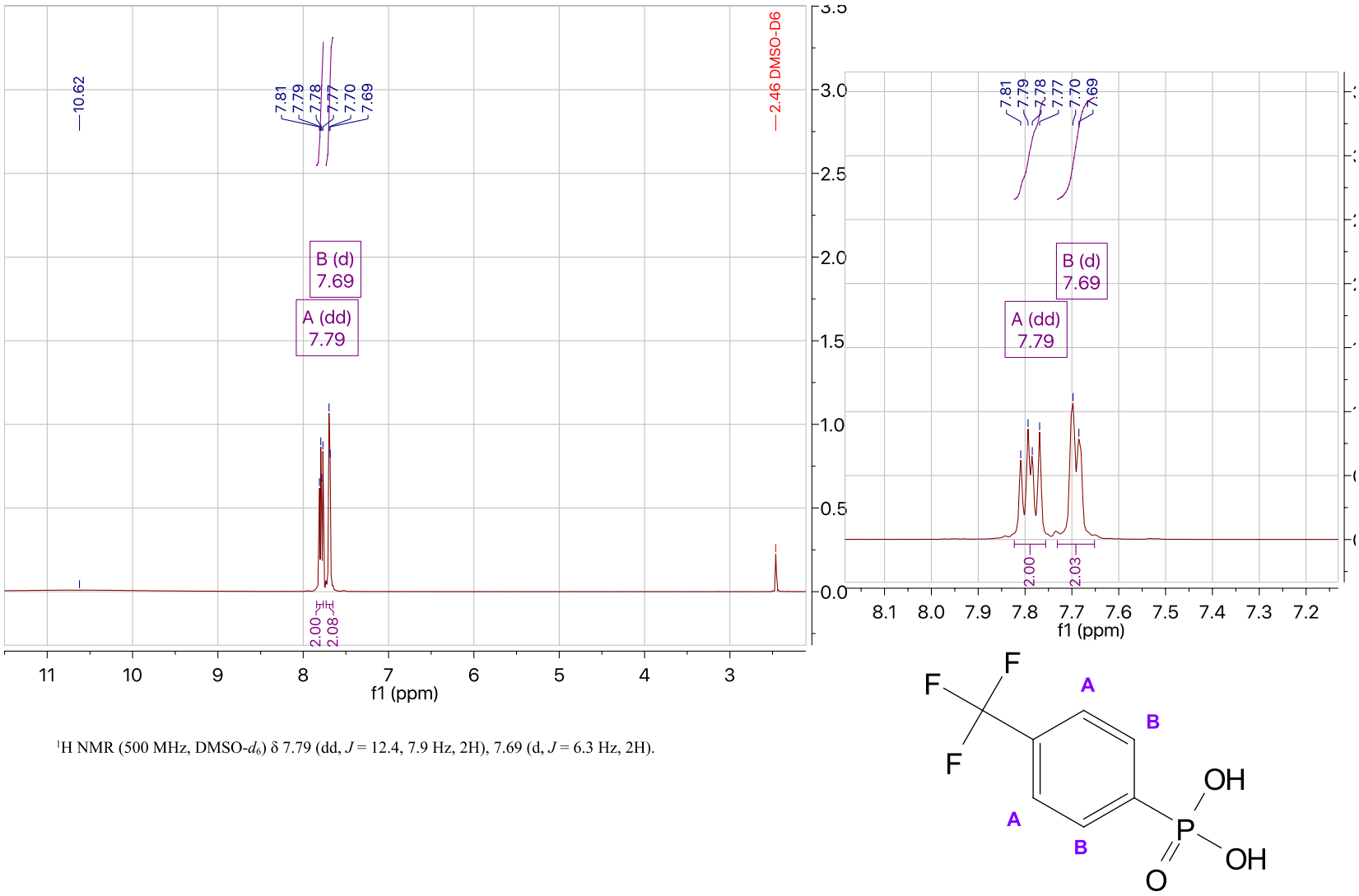

[1]H NMR (500 MHz, DMSO-d_6) δ 7.79 (dd, J = 12.4, 7.9 Hz, 2H), 7.69 (d, J = 6.3 Hz, 2H).

Figure A.39 [1]H NMR of CF_3PPA - (4-(trifluoromethyl)phenyl) phosphonic acid

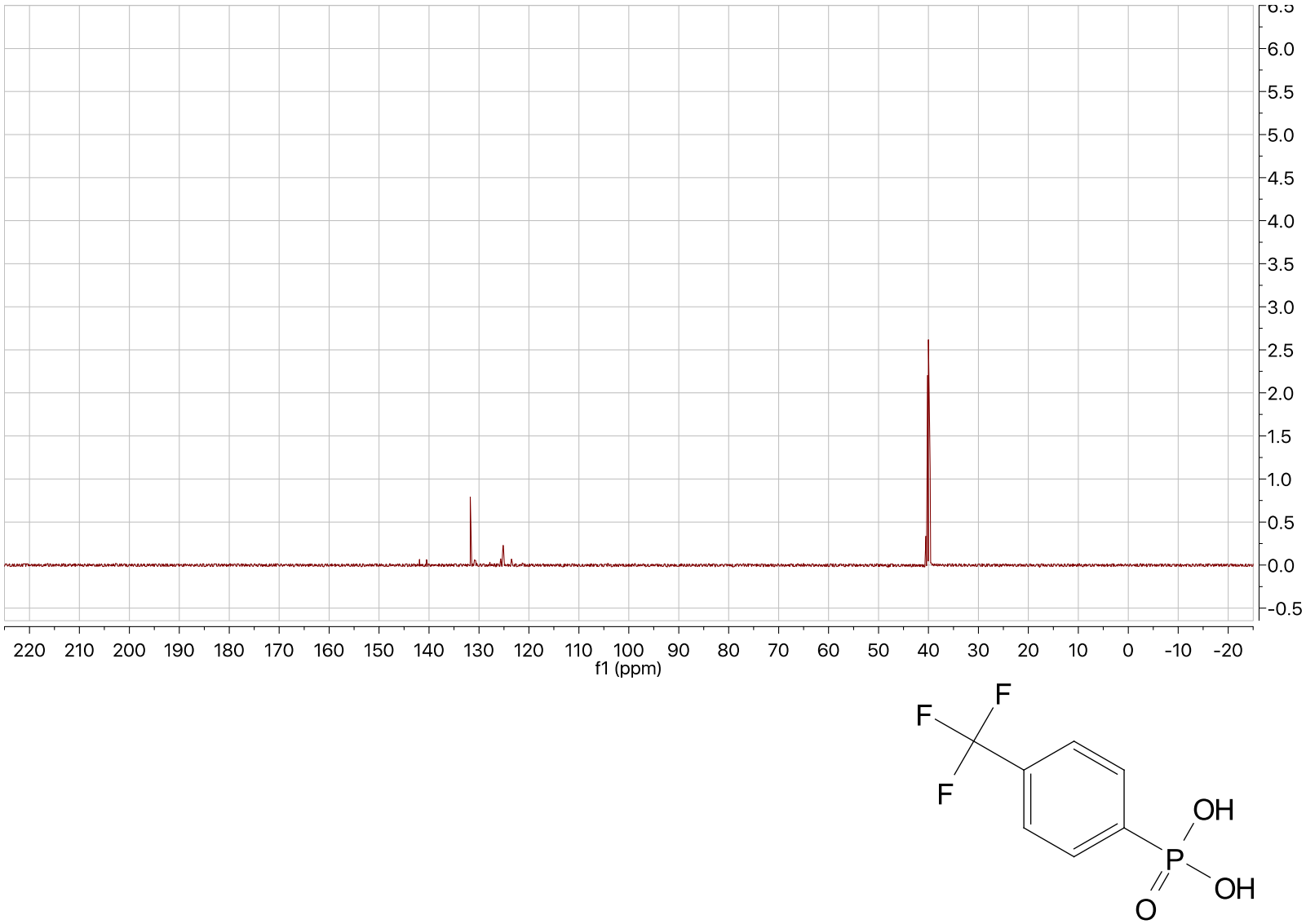

Figure A.40 ^{13}C NMR of CF_3PPA - (4-(trifluoromethyl)phenyl) phosphonic acid

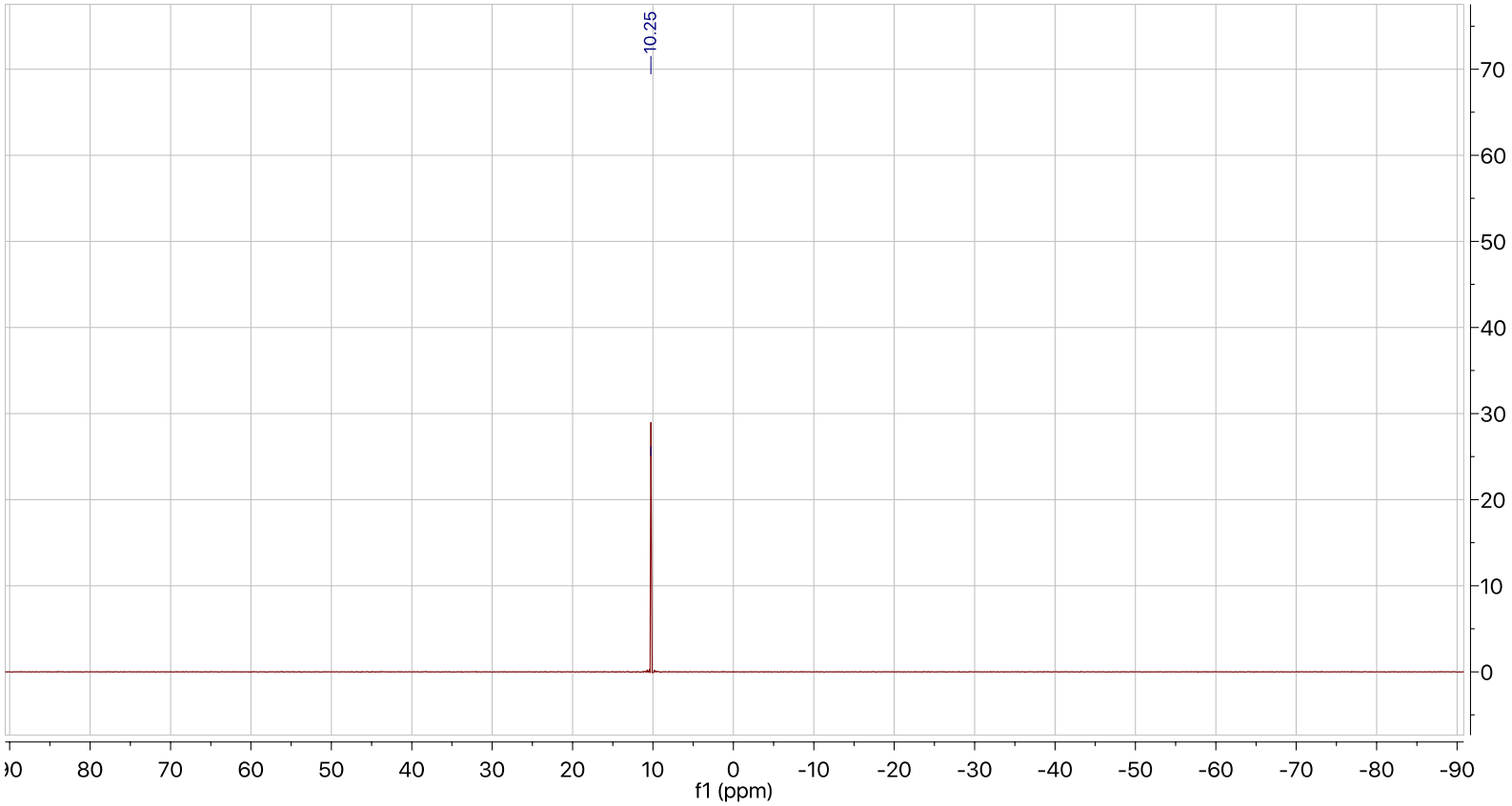

^{31}P NMR (202 MHz, DMSO-D_6) δ 10.25.

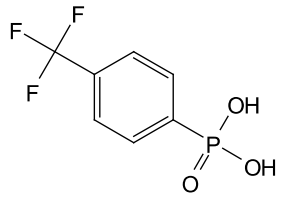

Figure A.41 ^{31}P NMR of CF_3PPA - (4-(trifluoromethyl)phenyl) phosphonic acid

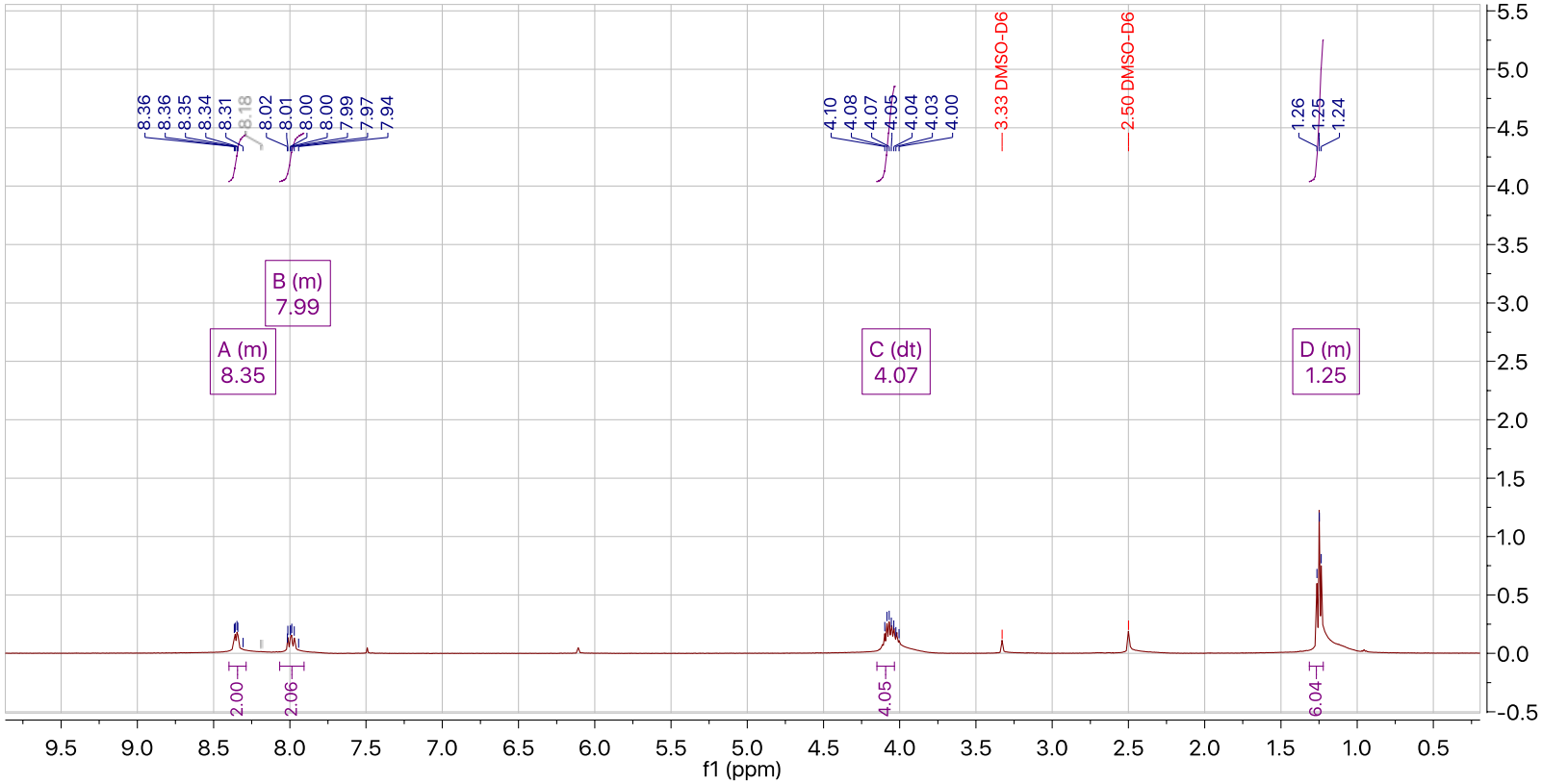

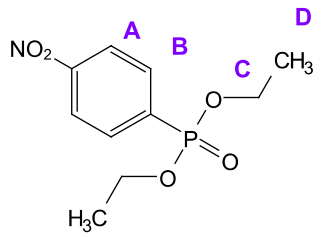

^{1}H NMR (500 MHz, DMSO-d_6) δ 8.40 – 8.29 (m, 2H), 8.07 – 7.91 (m, 2H), 4.07 (dt, J = 15.3, 7.6 Hz, 4H), 1.31 – 1.22 (m, 6H).

Figure A.42 ^{1}H NMR of NO_2PPE - diethyl (4-nitrophenyl) phosphonate

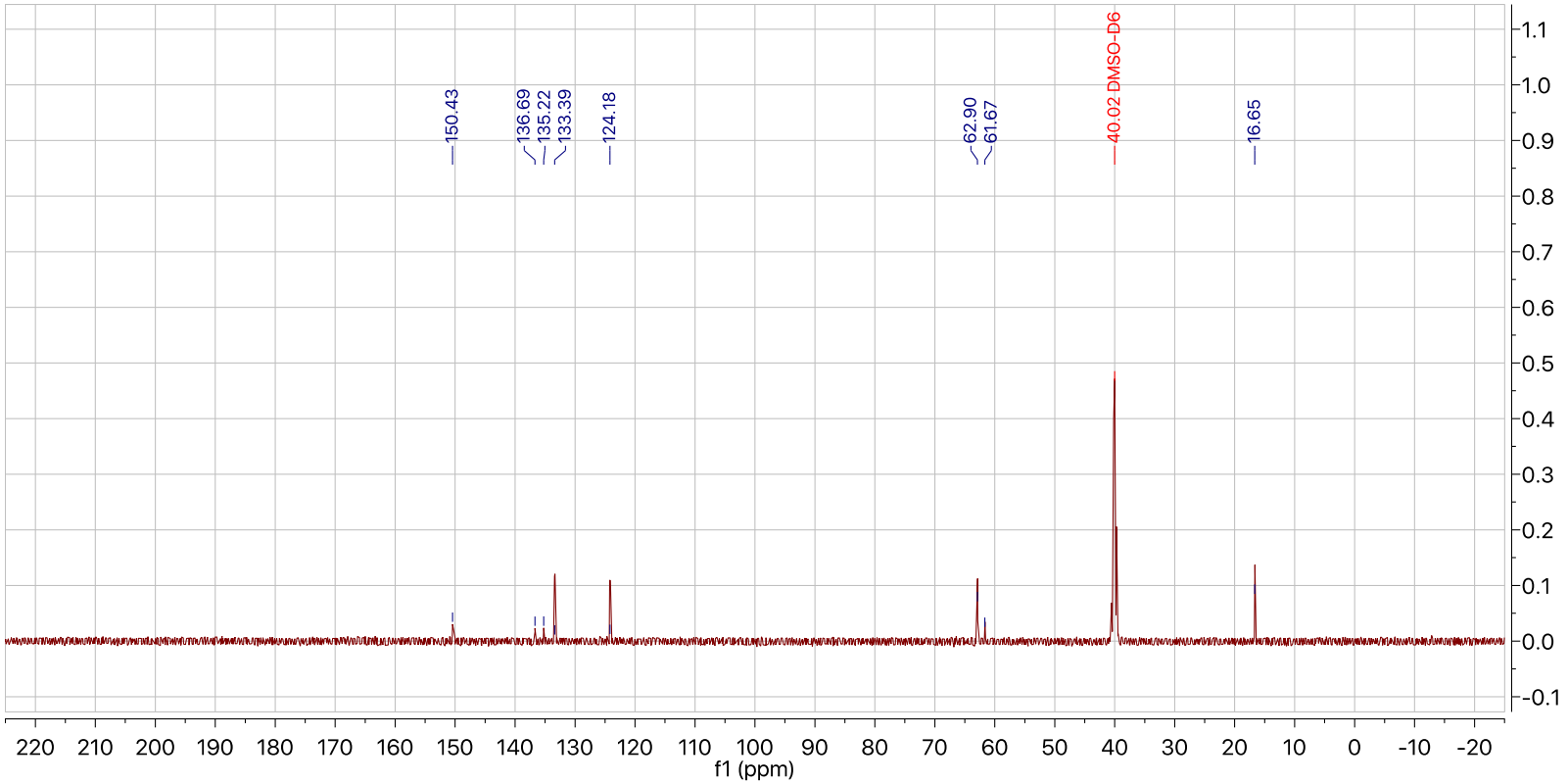

^{13}C NMR (126 MHz, DMSO-D_6) δ 150.43, 136.69, 135.22, 133.39, 124.18, 62.90, 61.67, 40.02, 16.65.

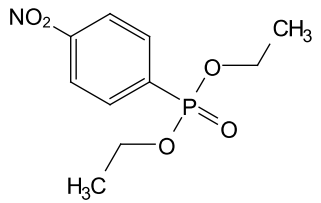

Figure A.43 ^{13}C NMR of NO_2PPE - diethyl (4-nitrophenyl) phosphonate

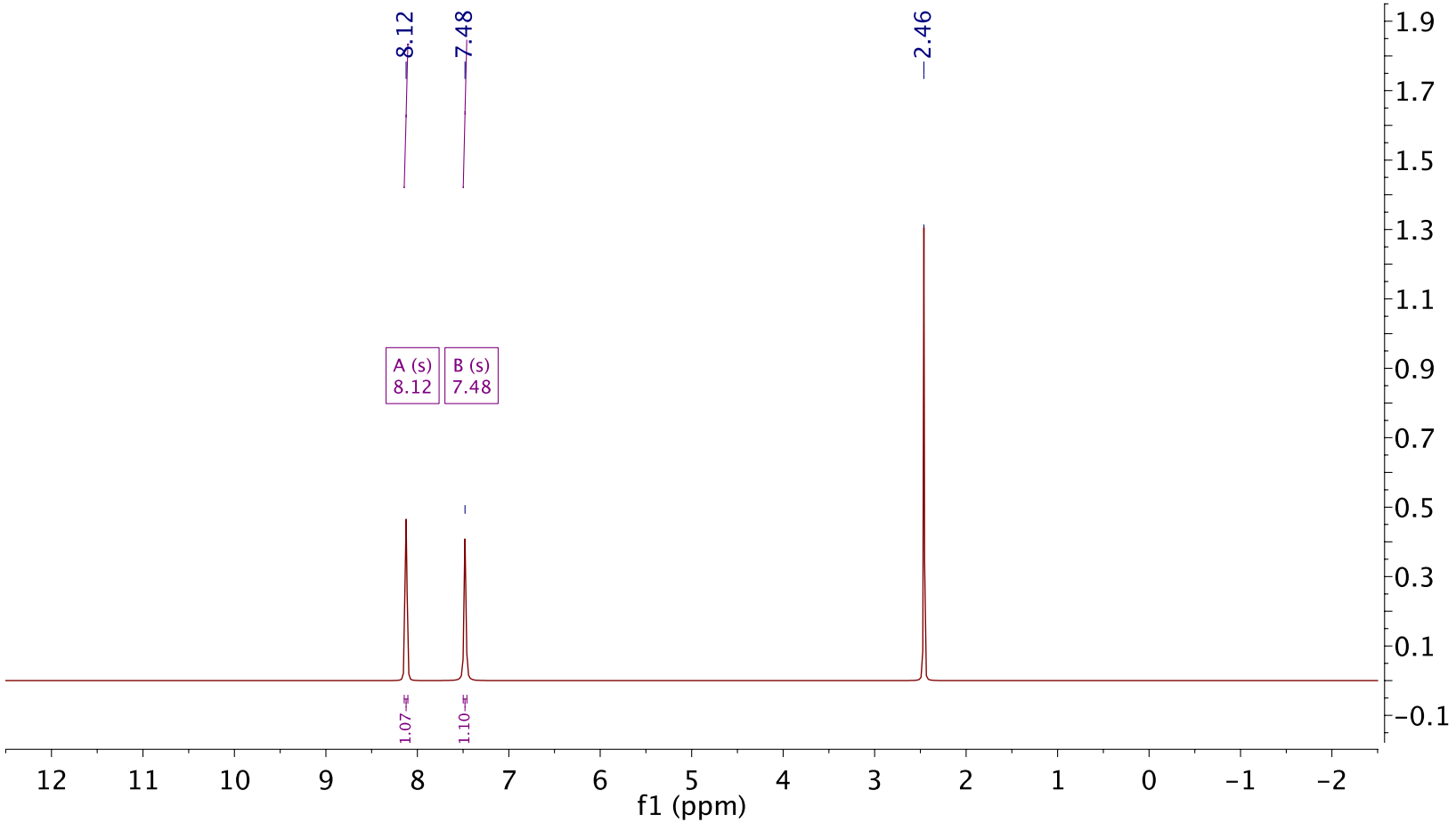

^{1}H NMR (500 MHz, DMSO-d_6) δ 8.12 (s, 1H), 7.48 (s, 1H).

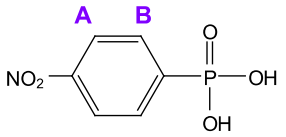

Figure A.44 ^{1}H NMR of NO_2PPA - (4-nitrophenyl) phosphonic acid

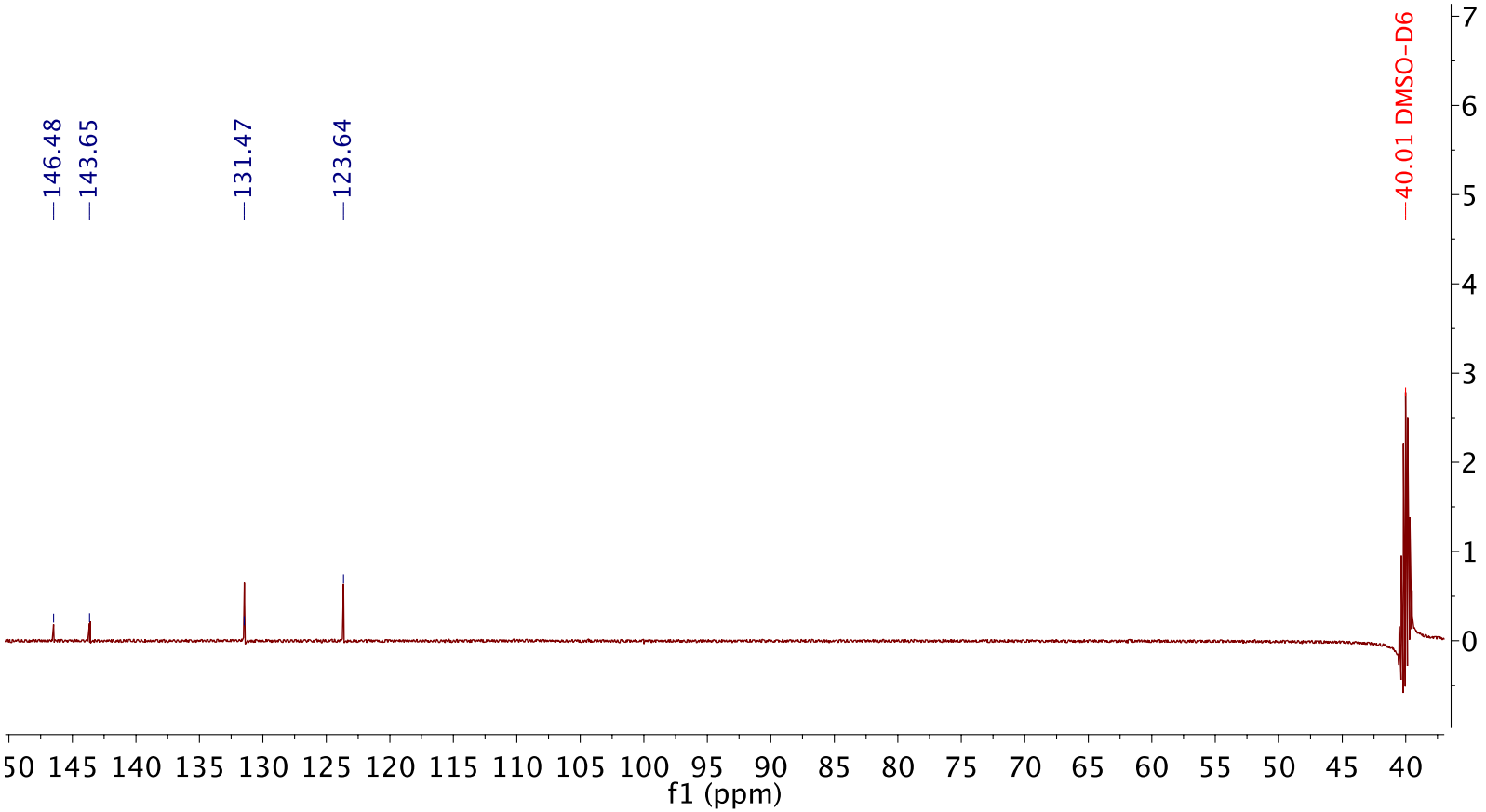

^{13}C NMR (126 MHz, DMSO-D_6) δ 146.48, 143.65, 131.47, 123.64, 40.01.

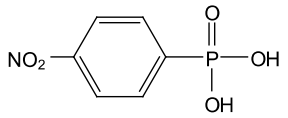

Figure A.45 ^{13}C NMR of NO_2PPA - (4-nitrophenyl) phosphonic acid

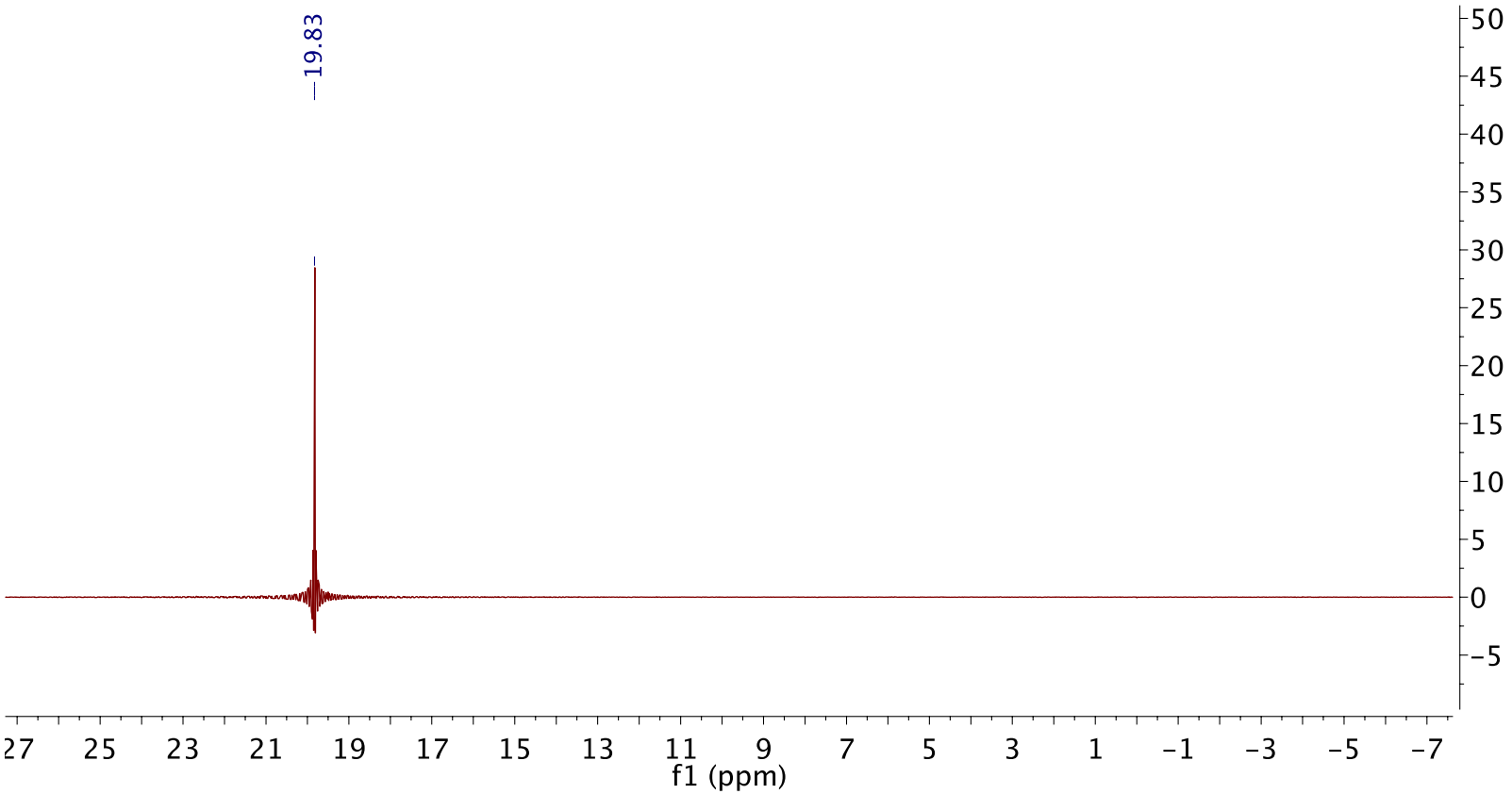

^{31}P NMR (202 MHz, DMSO-D_6) δ 19.83.

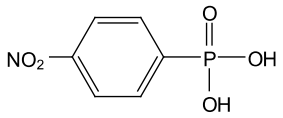

Figure A.46 ^{31}P NMR of NO_2PPA - (4-nitrophenyl) phosphonic acid

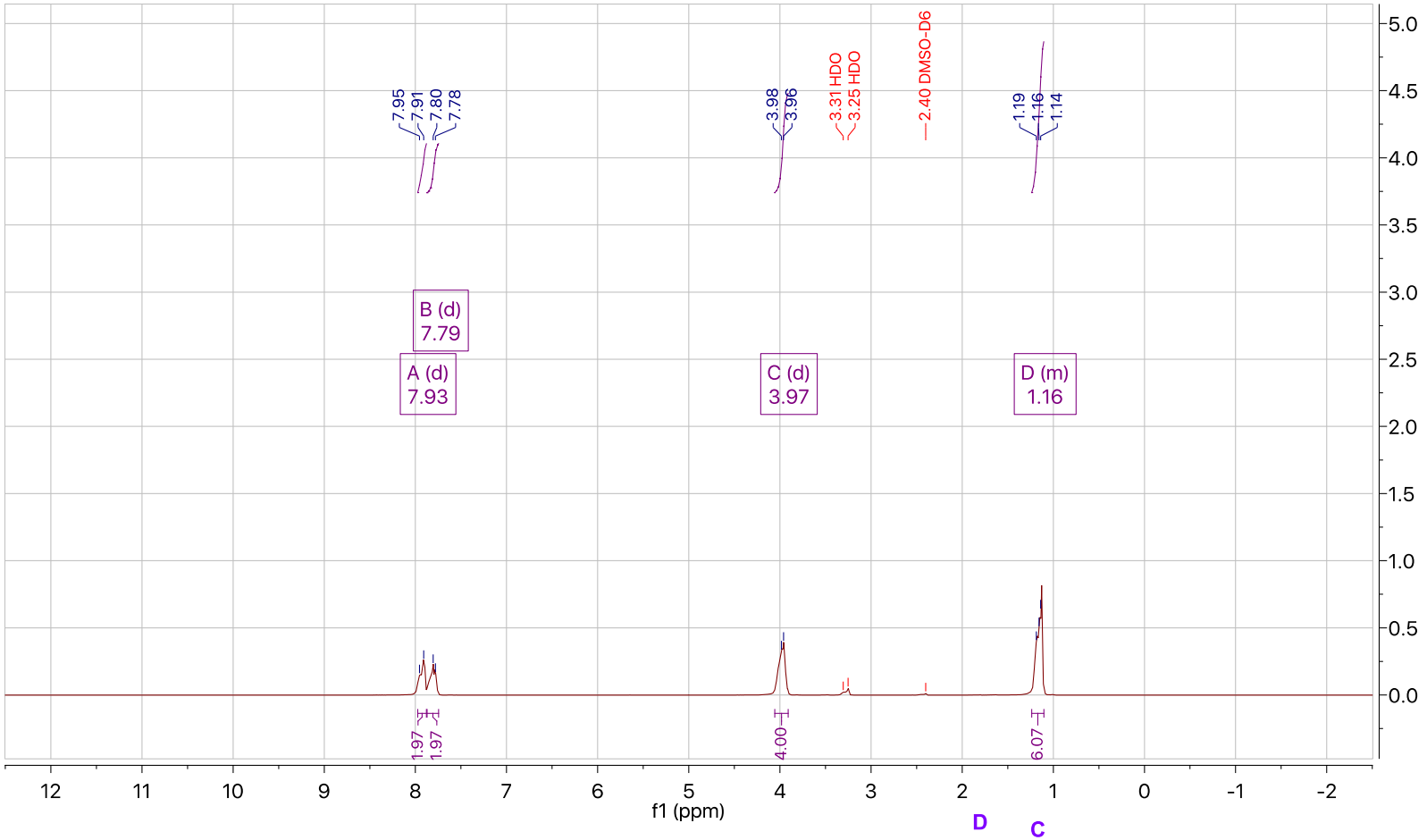

^{1}H NMR (500 MHz, DMSO-d_6) δ 7.93 (d, J = 23.0 Hz, 2H), 7.79 (d, J = 12.1 Hz, 2H), 3.97 (d, J = 12.1 Hz, 4H), 1.24 – 1.10 (m, 6H).

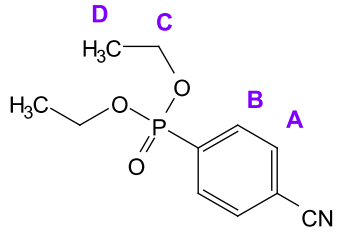

Figure A.47 1H NMR of CNPPE - diethyl (4-cyanophenyl) phosphonate

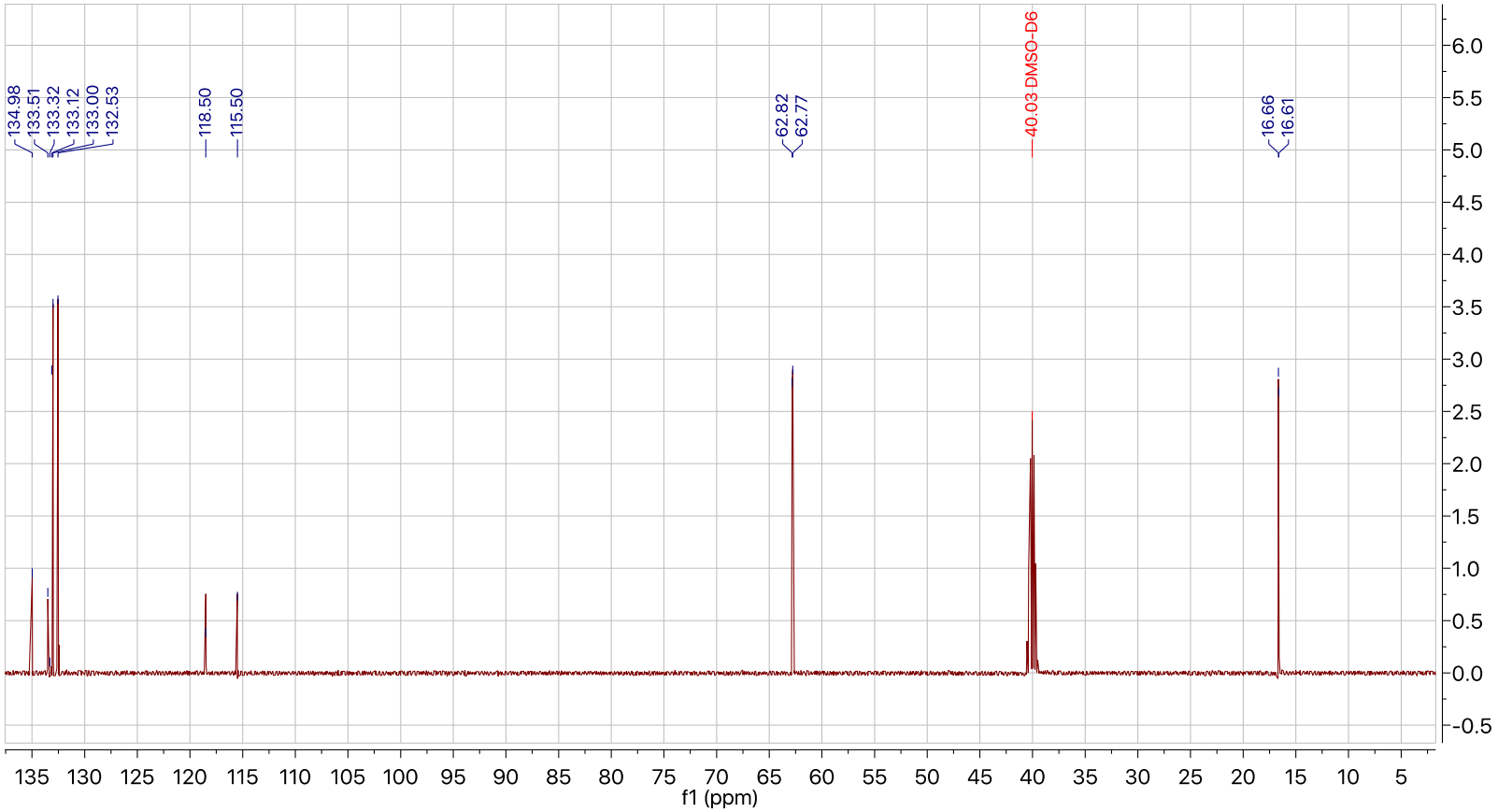

^{13}C NMR (126 MHz, DMSO-D_6) δ 134.98, 133.51, 133.32, 133.12, 133.00, 132.53, 118.50, 115.50, 62.82, 62.77, 40.03, 16.66, 16.61.

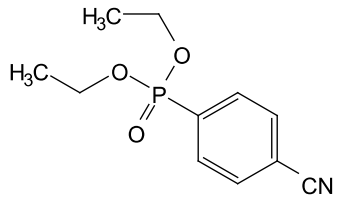

Figure A.48 ^{13}C NMR of CNPPE - diethyl (4-cyanophenyl) phosphonate

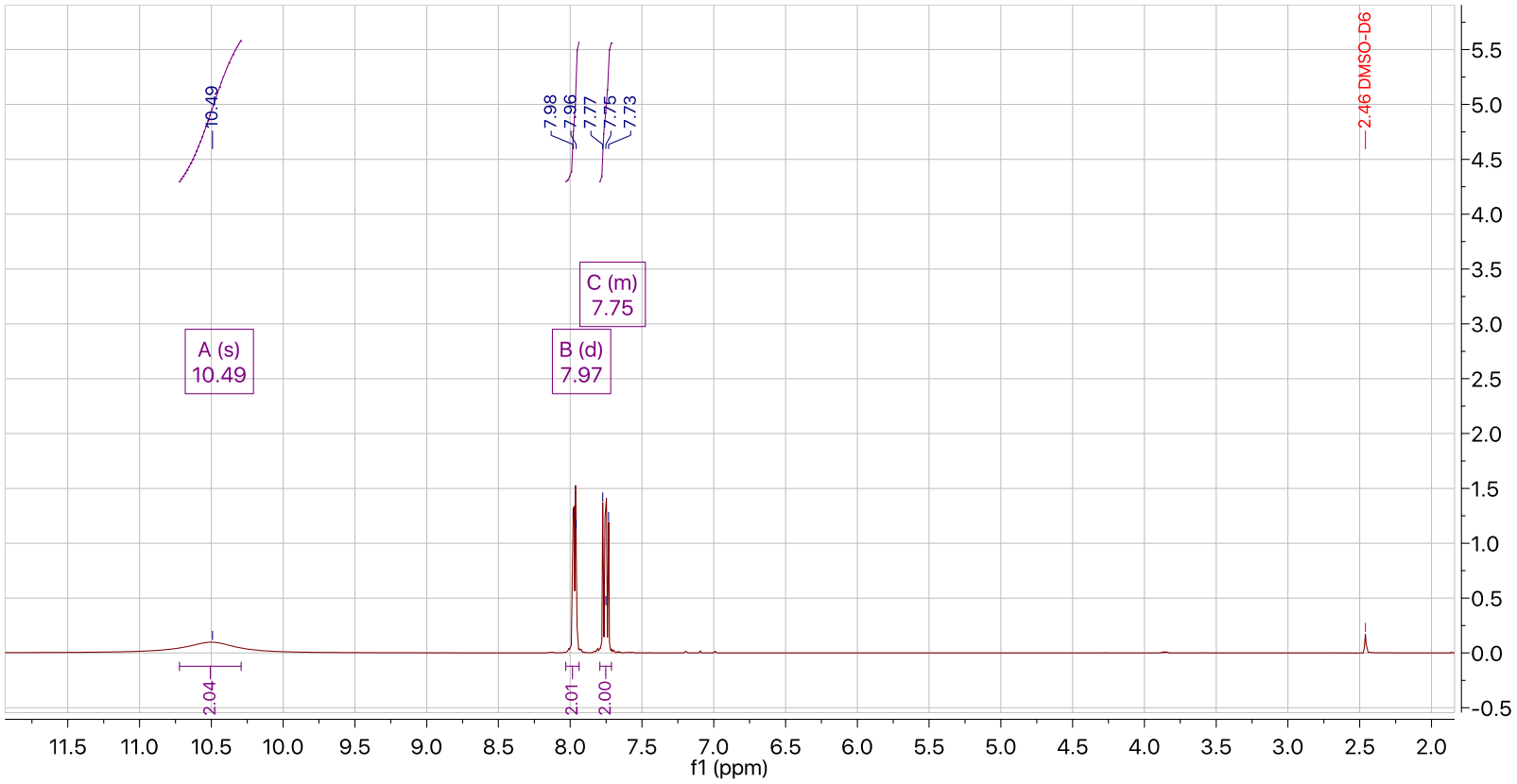

^{1}H NMR (500 MHz, DMSO-d_6) δ 10.49 (s, 2H), 7.97 (d, J = 10.6 Hz, 2H), 7.79 – 7.71 (m, 2H).

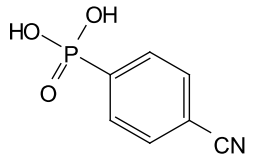

Figure A.49 ^{1}H NMR of CNPPA - (4-cyanophenyl) phosphonic acid

APPENDIX B

SELECTED NMR FOR CHAPTER 5

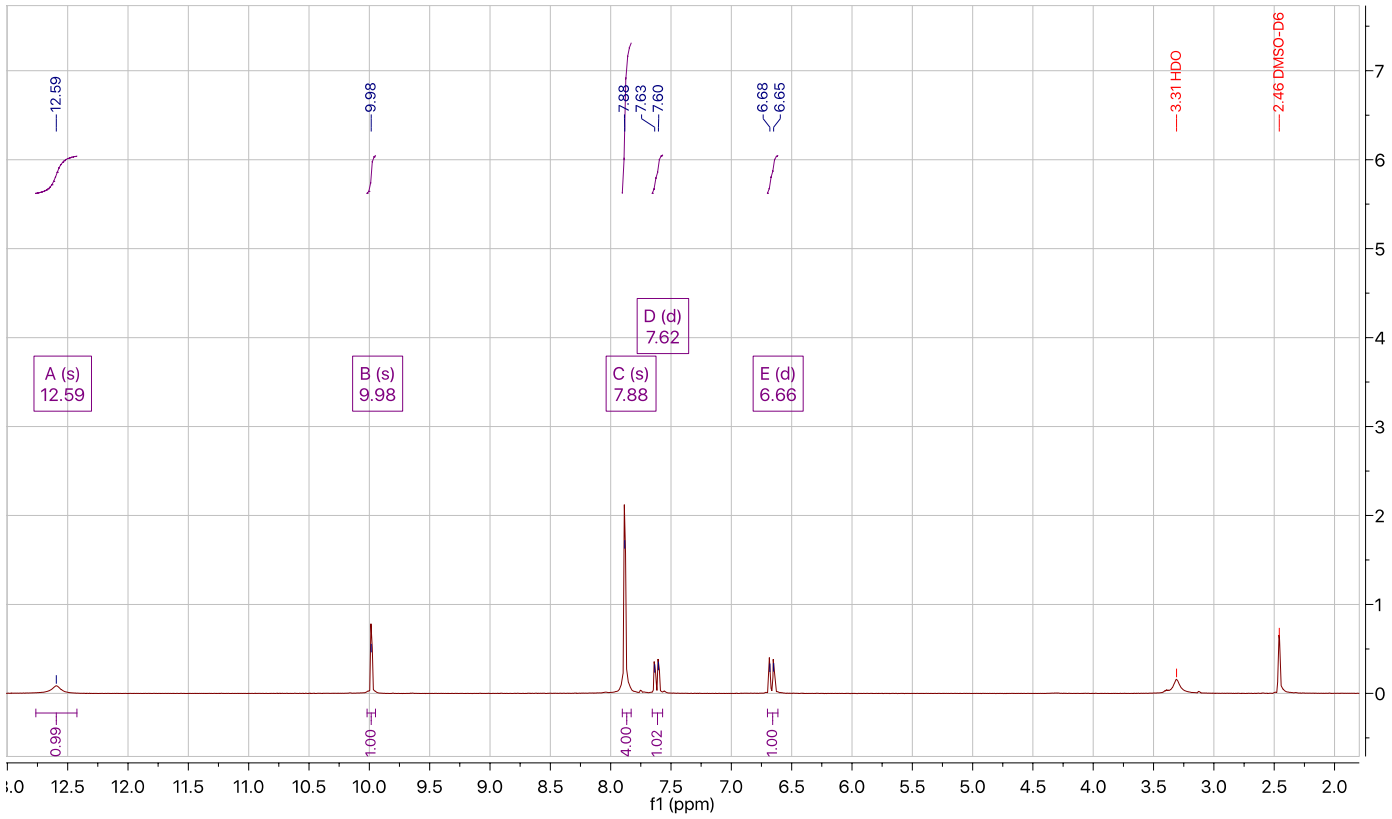

^{1}H NMR (500 MHz, DMSO-d_6) δ 12.59 (s, 1H), 9.98 (s, 1H), 7.88 (s, 4H), 7.62 (d, J = 15.6 Hz, 1H), 6.66 (d, J = 15.4 Hz, 1H).

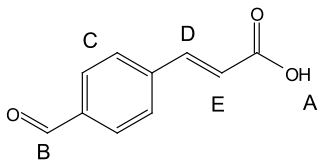

Figure B.1 ^{1}H NMR of BM04 precursor - *(E)*-3-(4-formylphenyl) acrylic acid

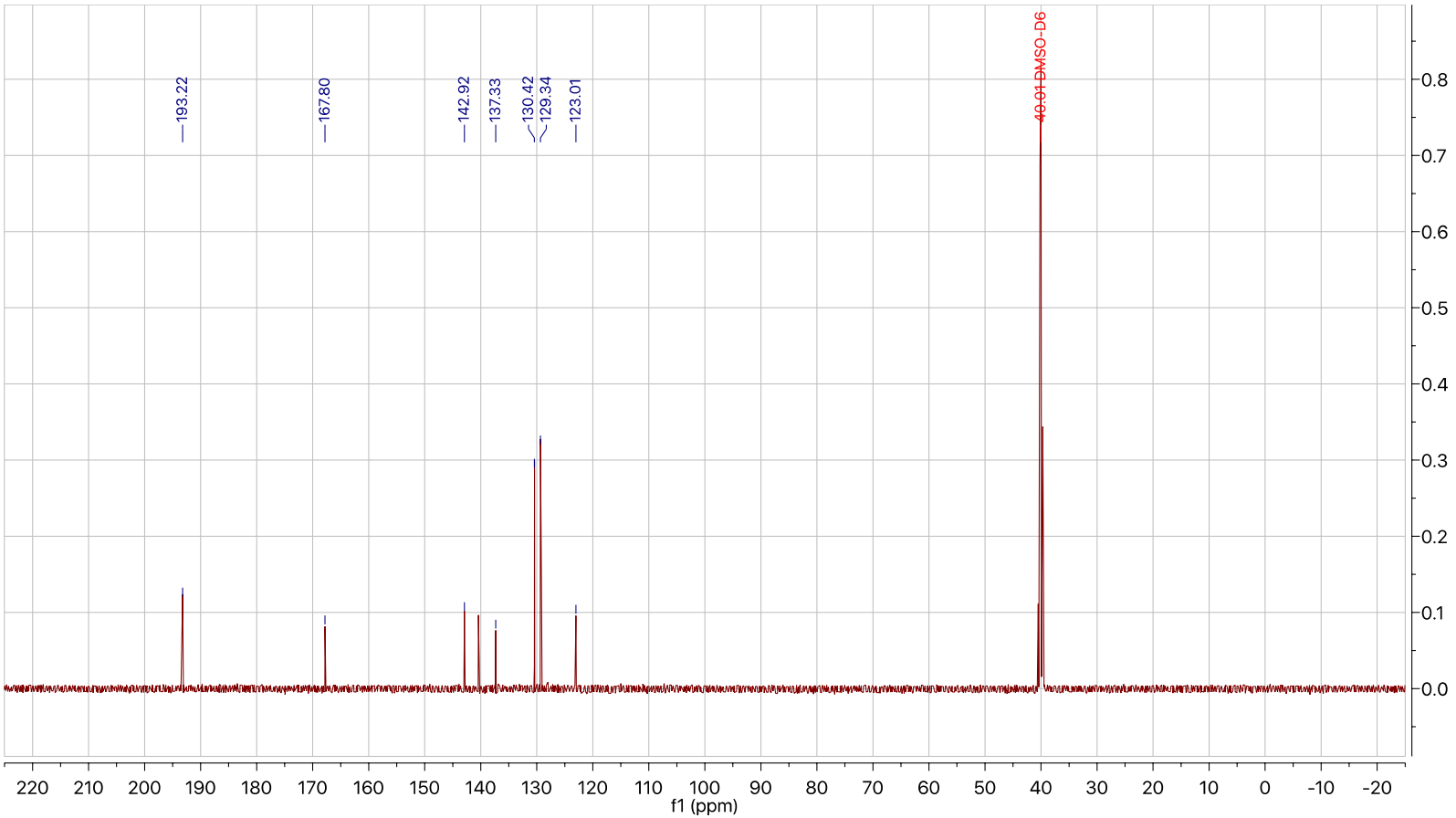

^{13}C NMR (126 MHz, DMSO-D_6) δ 193.22, 167.80, 142.92, 137.33, 130.42, 129.34, 123.01.

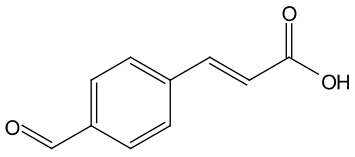

Figure B.2 ^{13}C NMR of BM04 precursor - *(E)*-3-(4-formylphenyl) acrylic acid

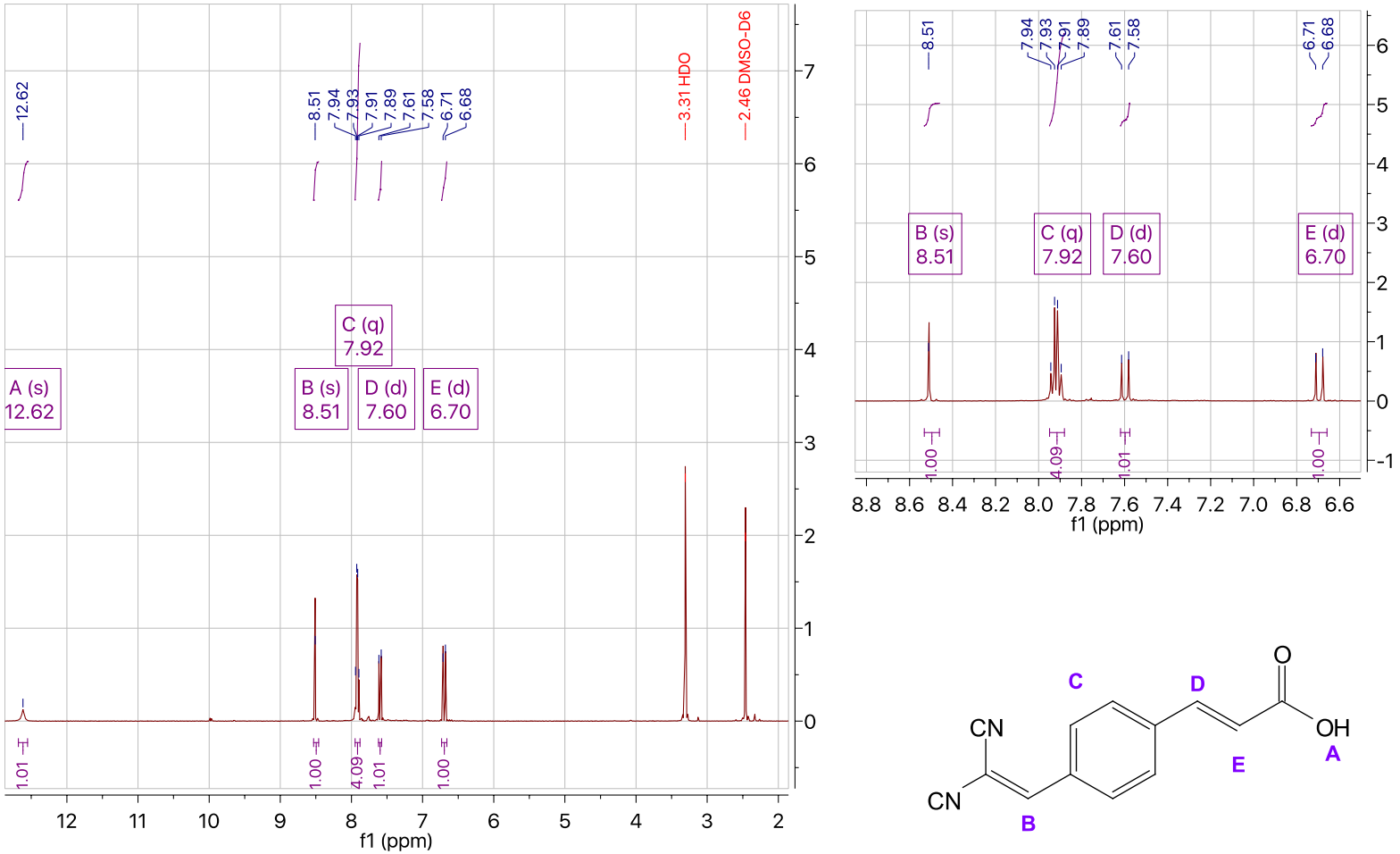

^{1}H NMR (500 MHz, DMSO-d_6) δ 12.62 (s, 1H), 8.51 (s, 1H), 7.92 (q, J = 10.7, 8.4, 6.1 Hz, 4H), 7.60 (d, J = 16.6 Hz, 1H), 6.70 (d, J = 16.3 Hz, 1H).

Figure B.3 ^{1}H NMR of BM04 - trans-4-(2,2-dicyanovinyl) cinnamic acid

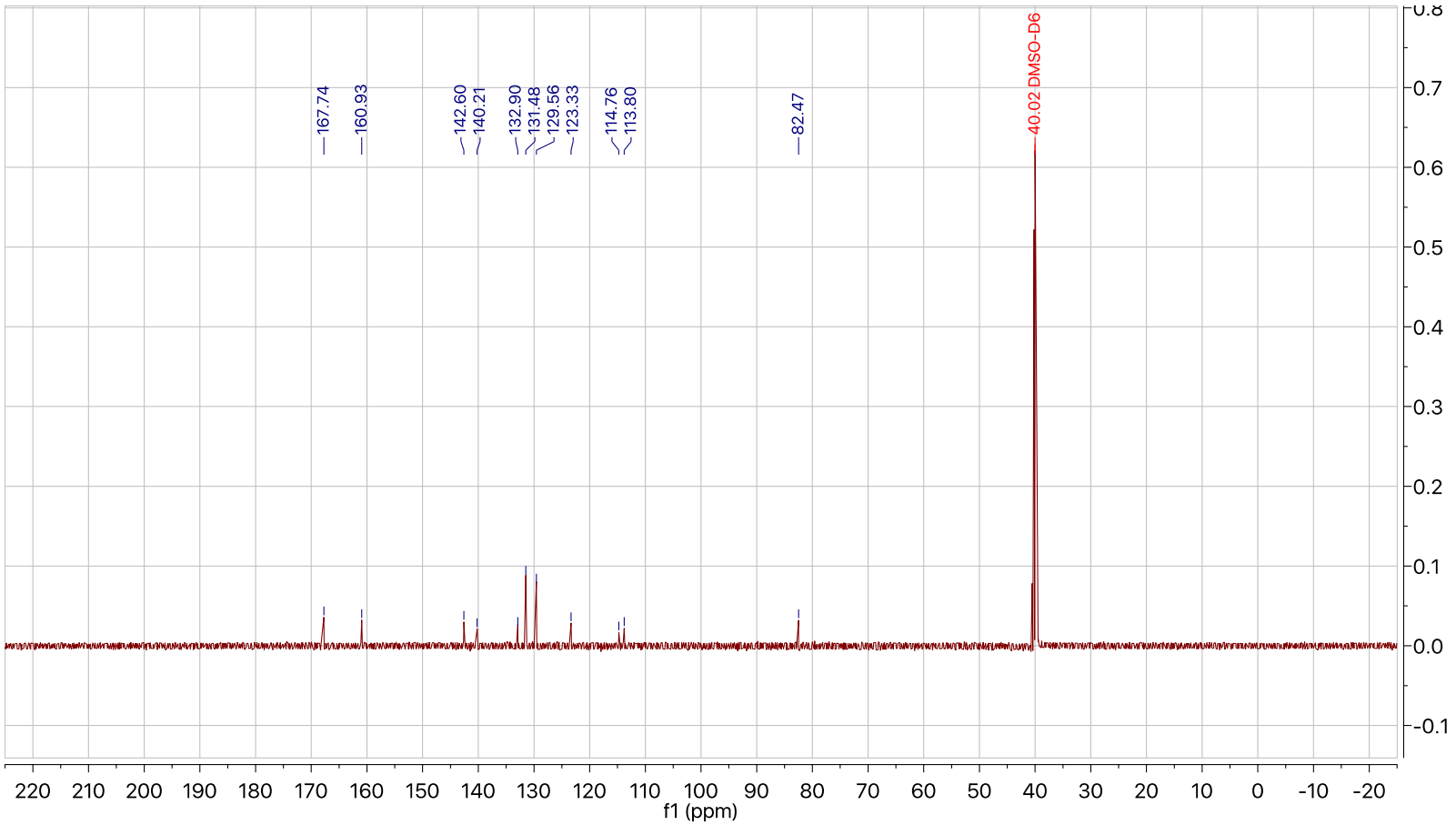

^{13}C NMR (126 MHz, DMSO-D_6) δ 167.74, 160.93, 142.60, 140.21, 132.90, 131.48, 129.56, 123.33, 114.76, 113.80, 82.47.

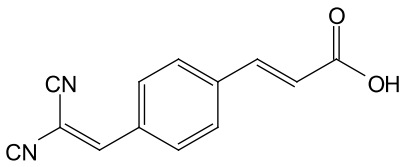

Figure B.4 ^{13}C NMR of BM04 - Trans-4-(2,2-dicyanovinyl)cinnamic acid

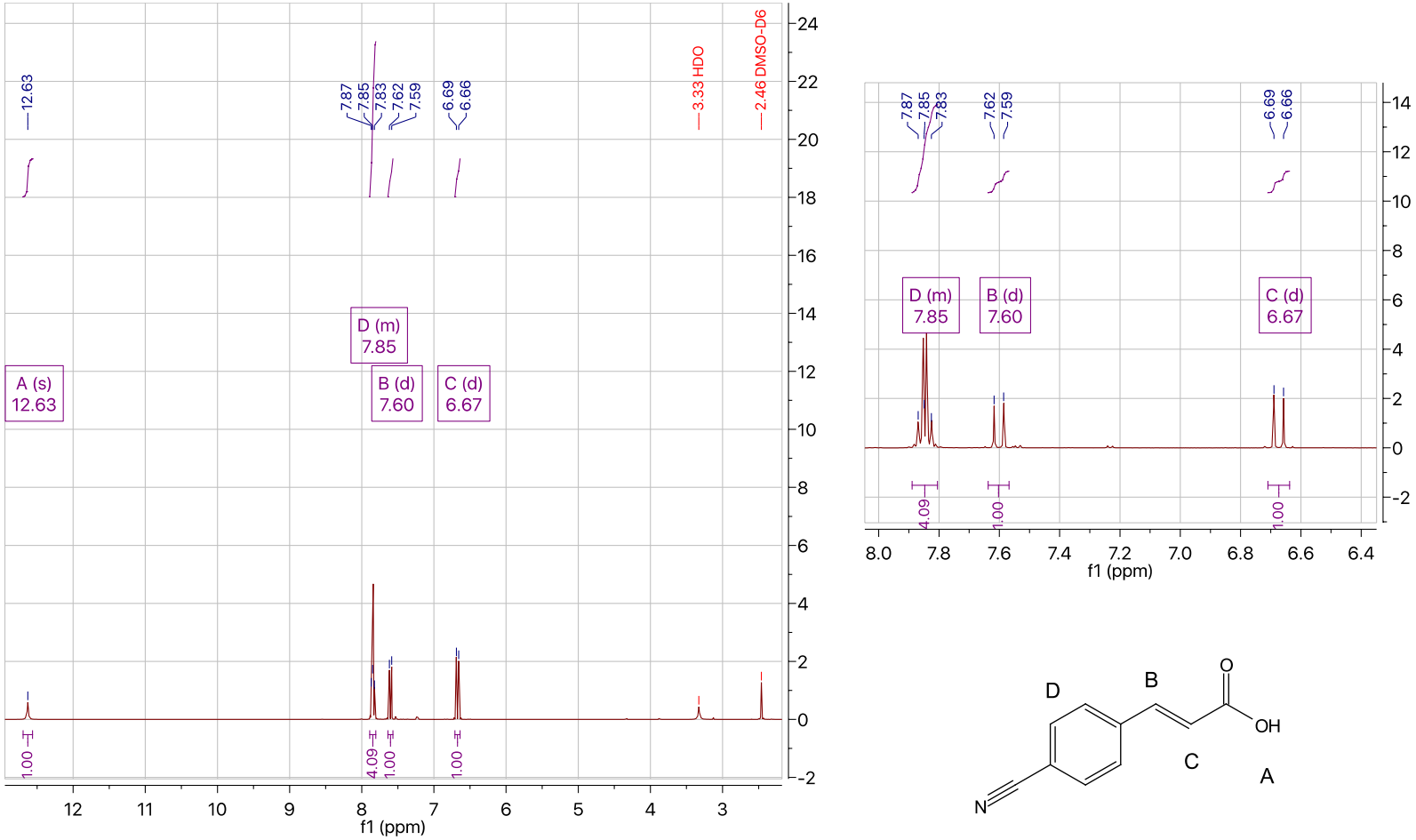

^{1}H NMR (500 MHz, DMSO-d_6) δ 12.63 (s, 1H), 7.89 – 7.81 (m, 4H), 7.60 (d, J = 15.9 Hz, 1H), 6.67 (d, J = 15.9 Hz, 1H).

Figure B.5 ^{1}H NMR of BM43 - (*E*)-3-(4-cyanophenyl) acrylic acid

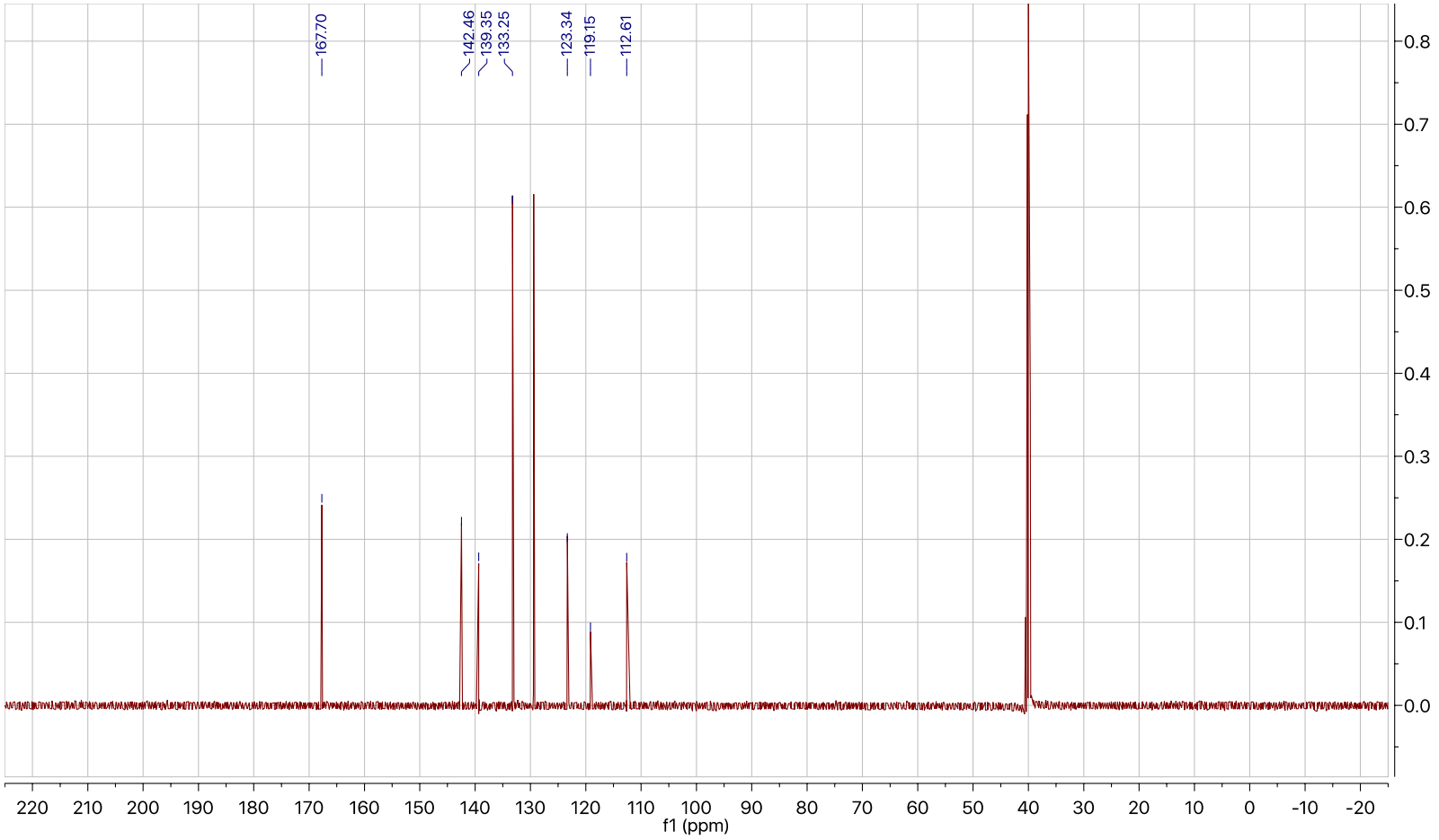

^{13}C NMR (126 MHz, DMSO-D_6) δ 167.70, 142.46, 139.35, 133.25, 123.34, 119.15, 112.61.

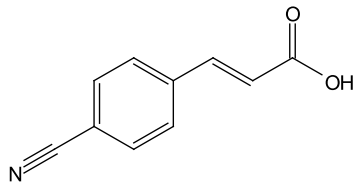

Figure B.6 ^{13}C NMR of BM43 - (*E*)-3-(4-cyanophenyl) acrylic acid

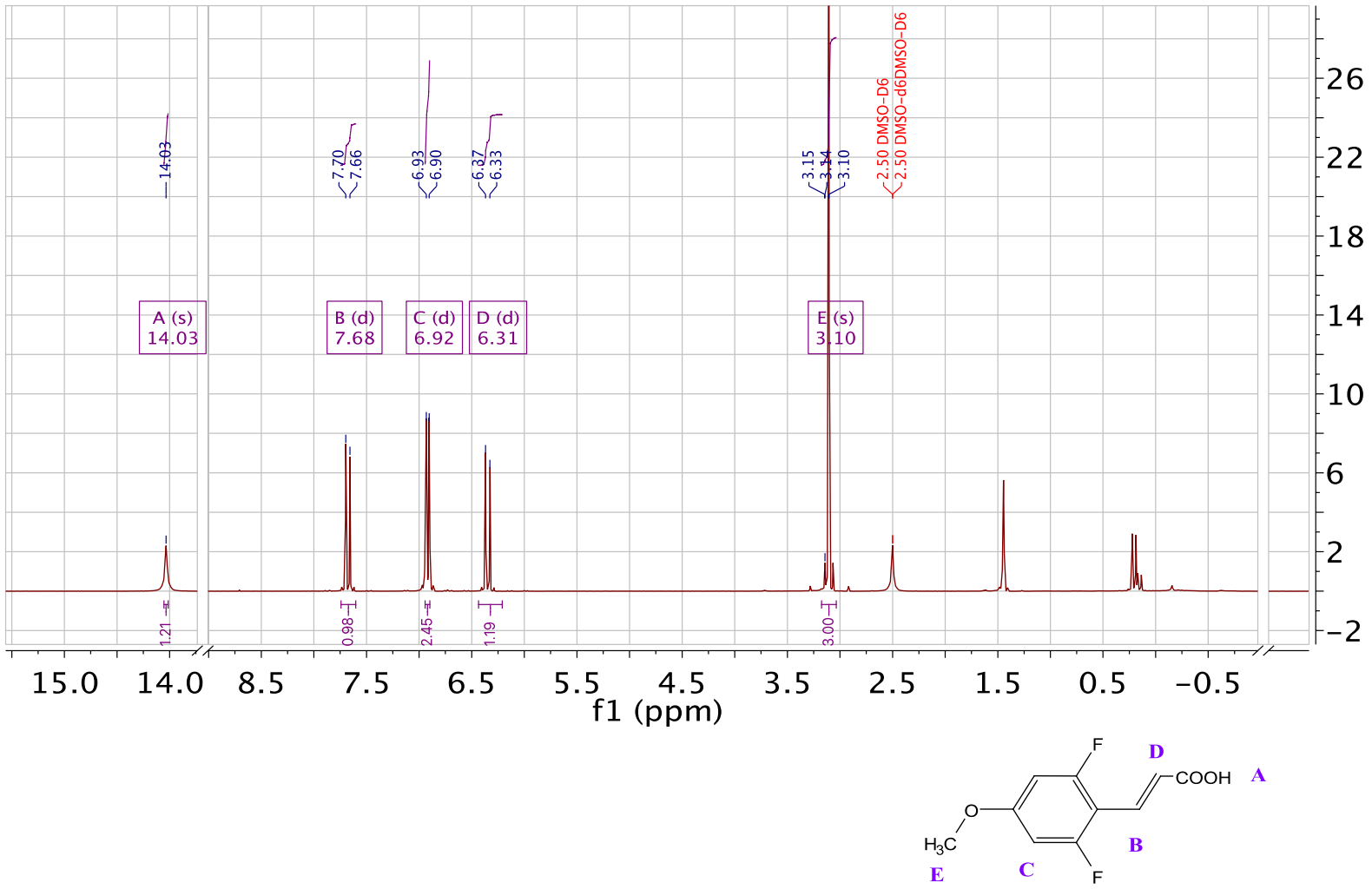

Figure B.7 [1]H NMR of BM13 - 4An26FCA - (*E*)-3-(2,6-difluoro-4-methoxyphenyl) acrylic acid

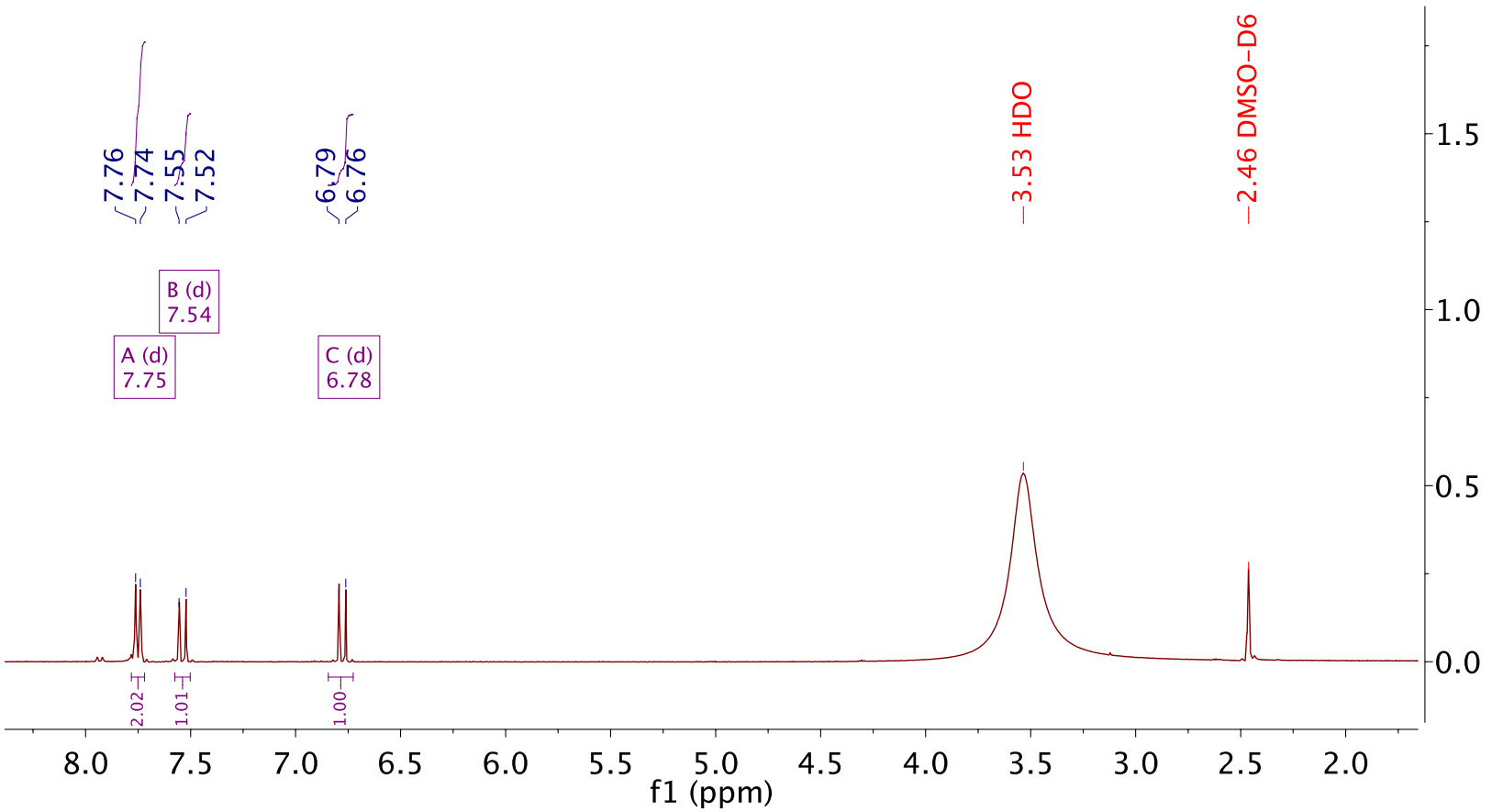

^{1}H NMR (500 MHz, DMSO-d_6) δ 7.75 (d, J = 11.3 Hz, 2H), 7.54 (d, J = 16.4 Hz, 1H), 6.78 (d, J = 16.0 Hz, 1H).

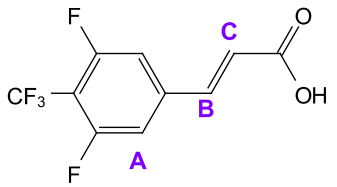

Figure B.8 ^{1}H NMR of BM16 – 35F4CF$_3$CA - (*E*)-3-(3,5-difluoro-4-(trifluoromethyl)phenyl) acrylic acid

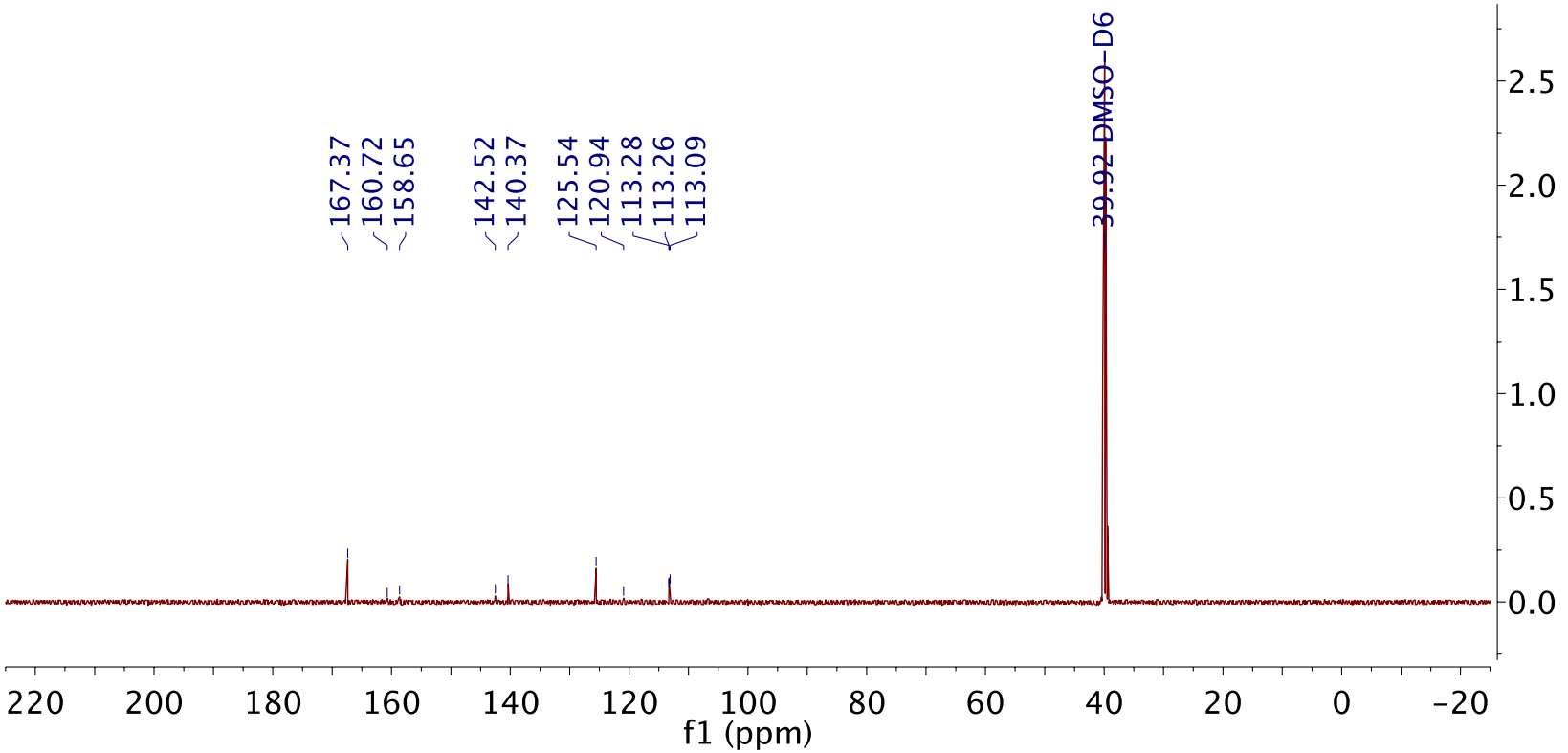

^{13}C NMR (126 MHz, DMSO-D_6) δ 167.37, 160.72, 158.65, 142.52, 140.37, 125.54, 120.94, 113.28, 113.26, 113.09, 39.92.

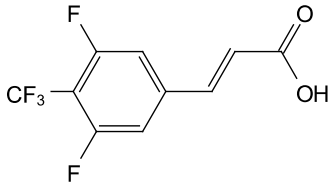

Figure B.9 ^{13}C NMR of BM16 – 35F4CF$_3$CA - (*E*)-3-(3,5-difluoro-4-(trifluoromethyl)phenyl) acrylic acid

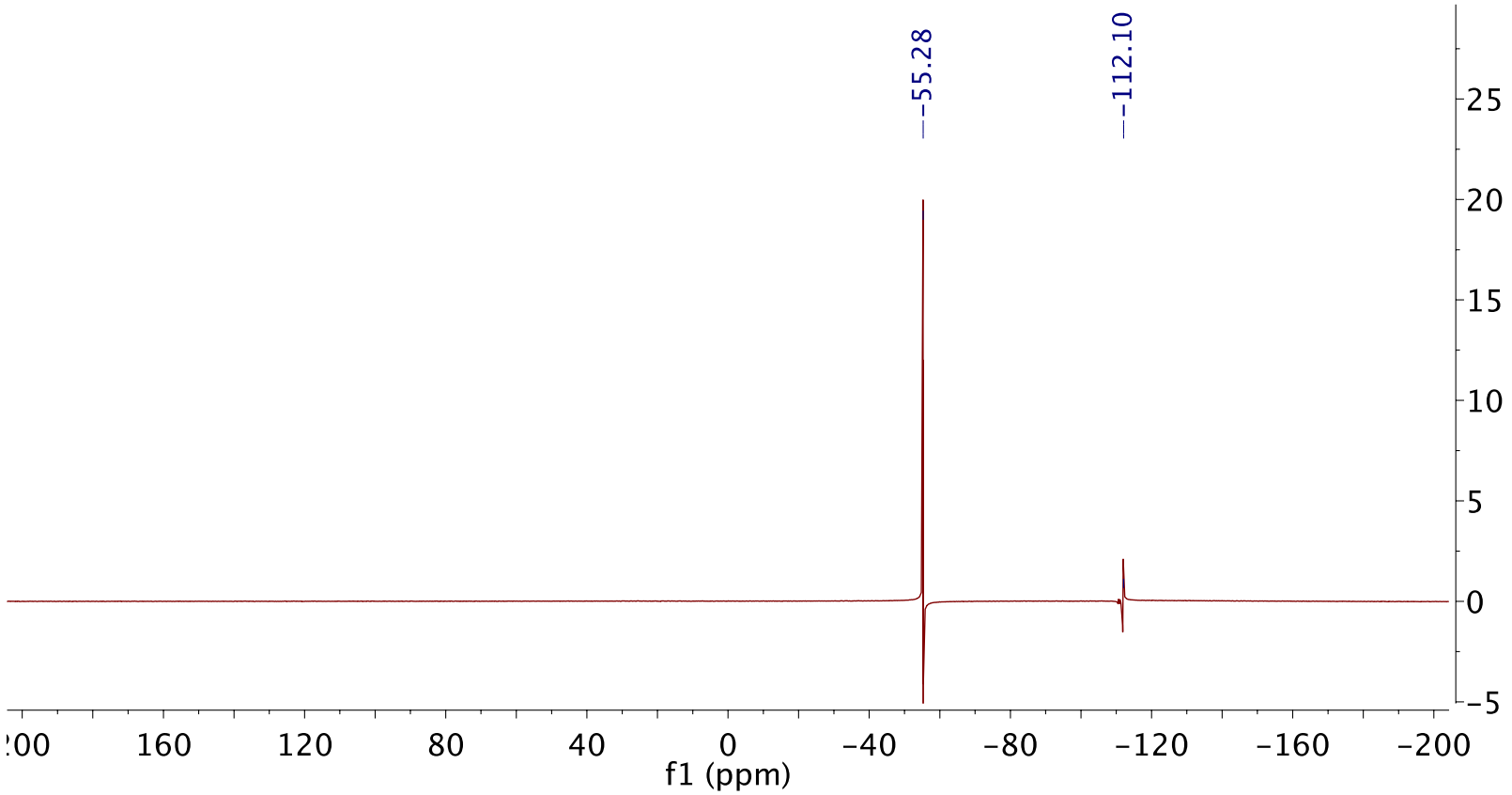

^{19}F NMR (471 MHz, DMSO-D_6) δ -55.28, -112.10.

Figure B.10 ^{19}F NMR of BM16 – 35F4CF$_3$CA - (*E*)-3-(3,5-difluoro-4-(trifluoromethyl)phenyl) acrylic acid

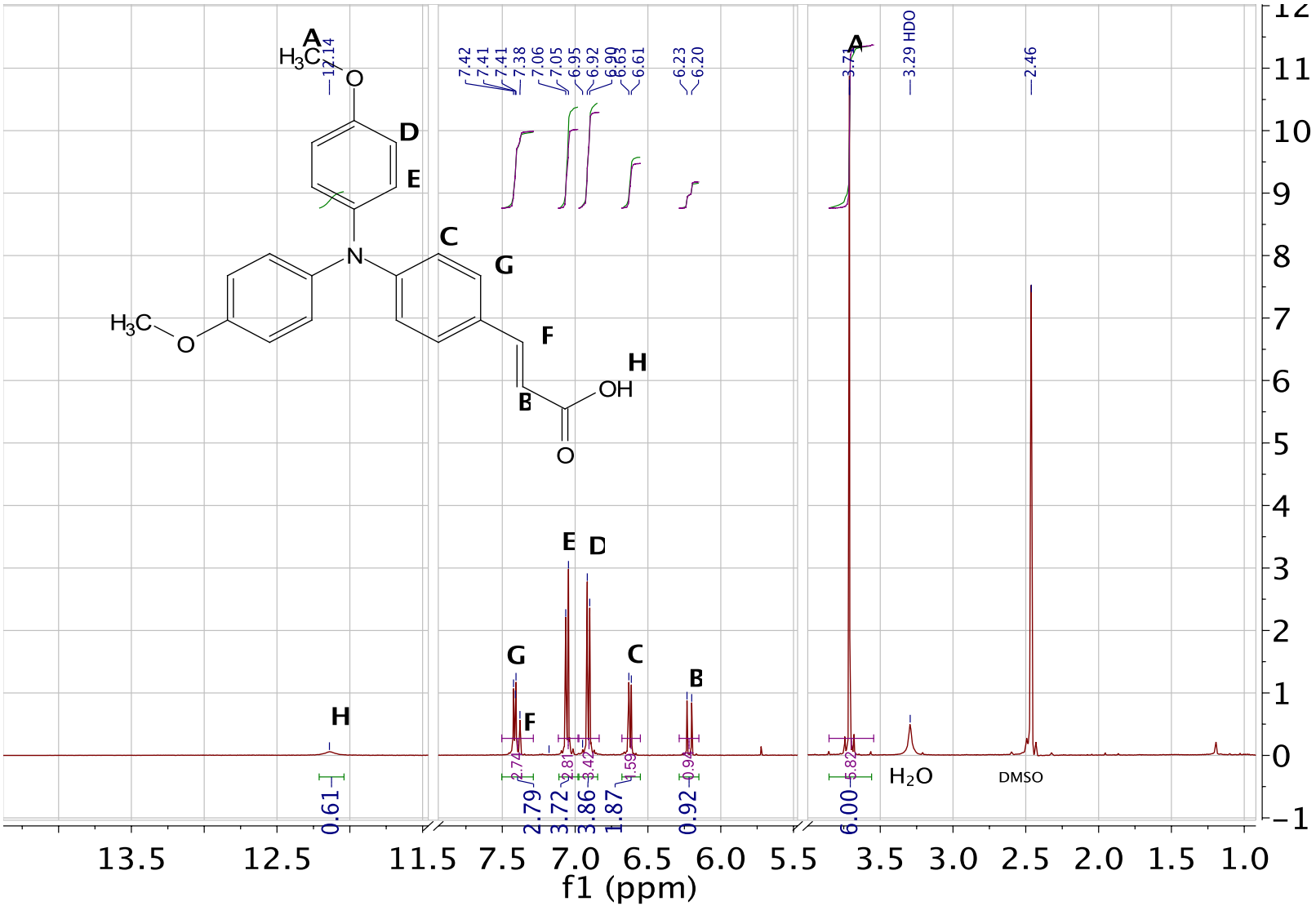

^{1}H NMR (500 MHz, DMSO-D$_6$) δ 12.14, 7.42, 7.41, 7.41, 7.38, 7.18, 7.06, 7.05, 6.
6.92, 6.90, 6.63, 6.61, 6.23, 6.20, 3.71, 3.29, 2.46.

Figure B.11 ^{1}H NMR of BM18 – TPACA - (*E*)-3-(4-(bis(4-methoxyphenyl)amino)phenyl) acrylic acid

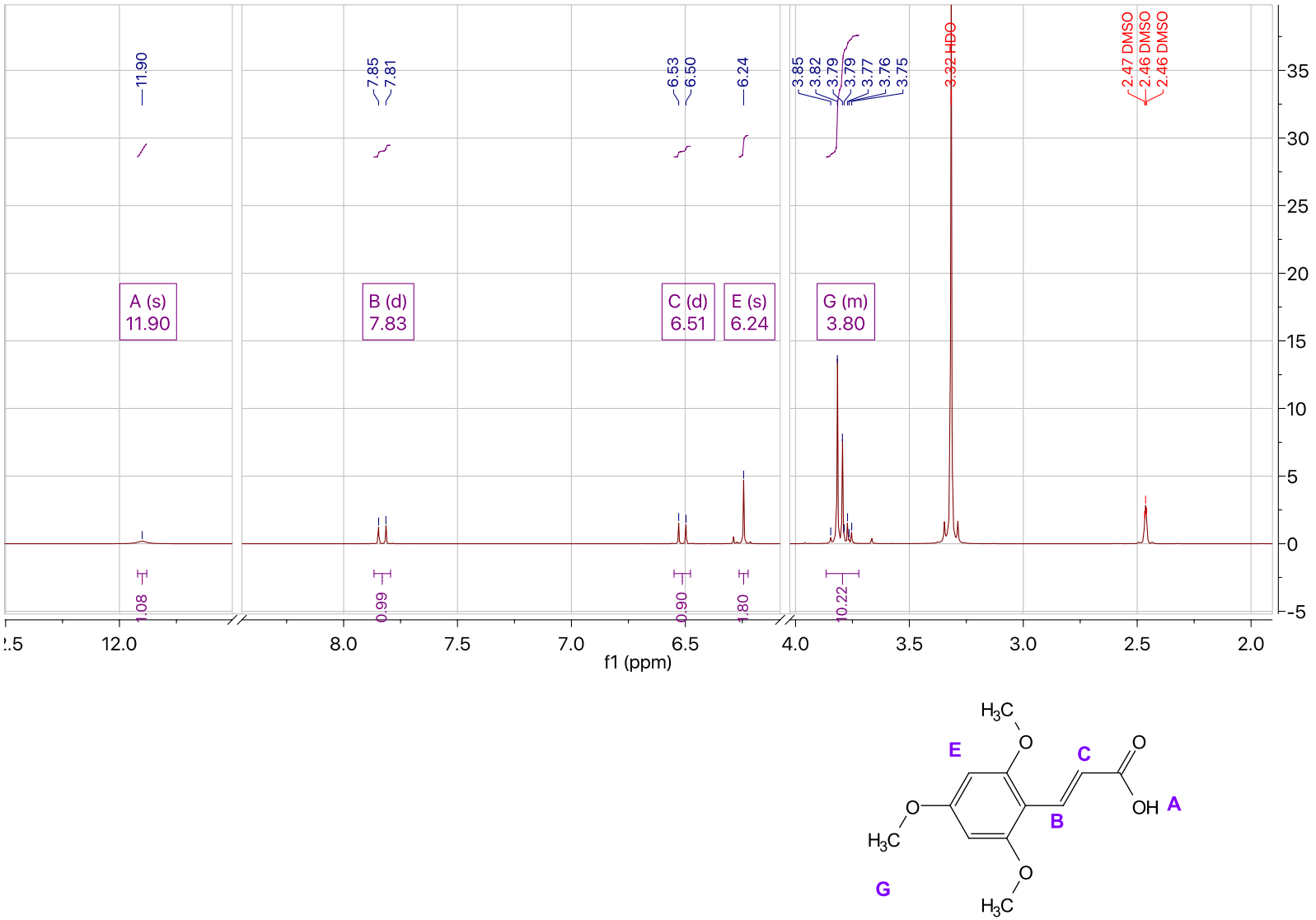

Figure B.12 ^{1}H NMR of BM17 - tMeOxCA - (*E*)-3-(2,4,6-trimethoxyphenyl) acrylic acid

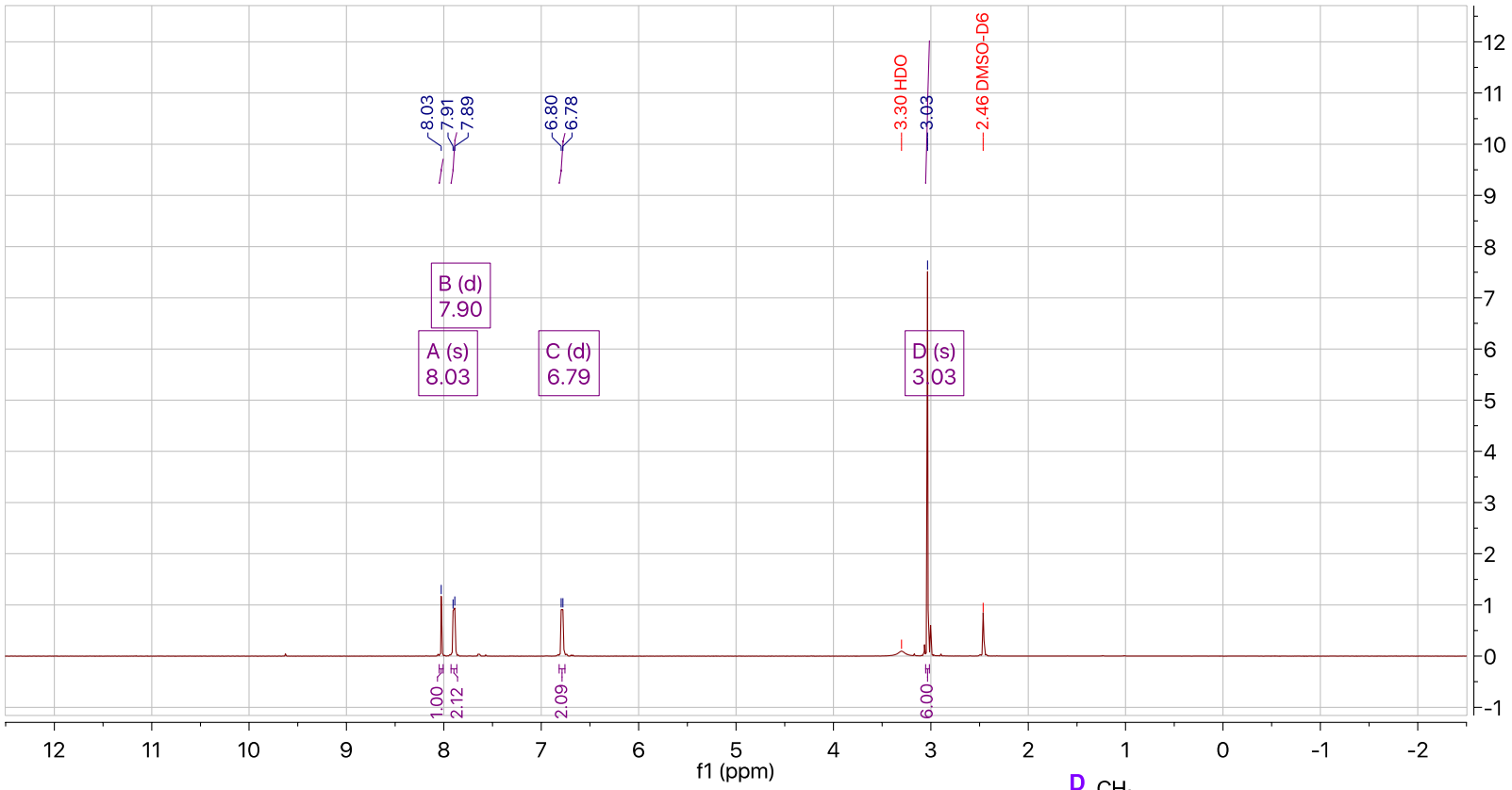

^{1}H NMR (500 MHz, DMSO-d_6) δ 8.03 (s, 1H), 7.90 (d, J = 9.1 Hz, 2H), 6.79 (d, J = 9.1 Hz, 2H), 3.03 (s, 6H).

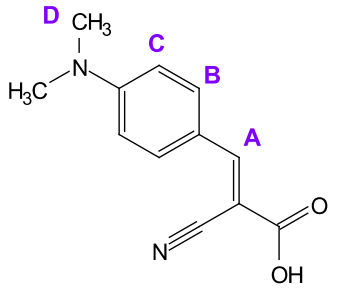

Figure B.13 ^{1}H NMR of BM82 - (*E*)-2-cyano-3-(4-(dimethylamino)phenyl) acrylic acid

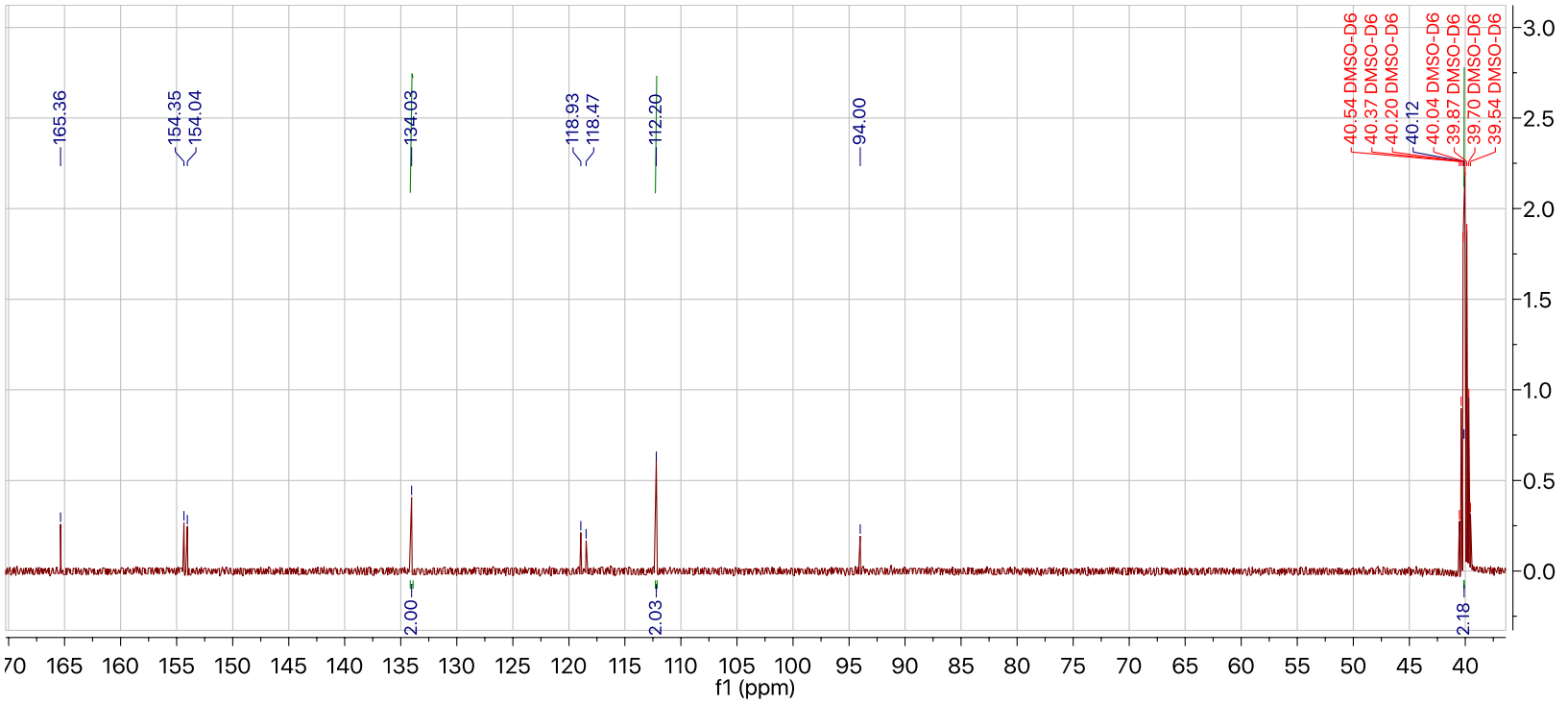

^{13}C NMR (126 MHz, DMSO-D_6) δ 165.36, 154.35, 154.04, 134.03, 118.93, 118.47, 112.20, 94.00, 40.54, 40.37, 40.20, 40.12, 40.04, 39.87, 39.70, 39.54.

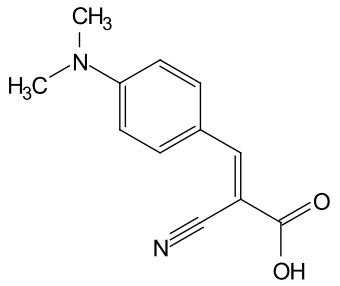

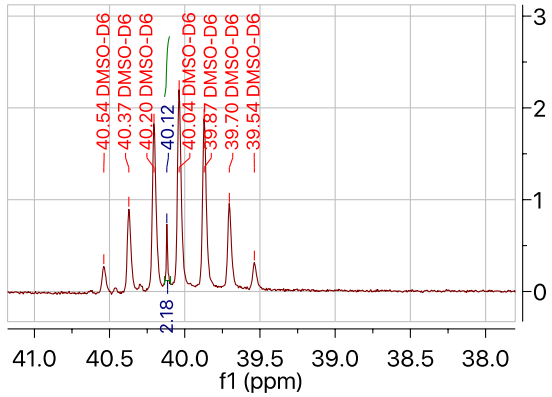

Figure B.14 ^{13}C NMR of BM82 - (*E*)-2-cyano-3-(4-(dimethylamino)phenyl) acrylic acid

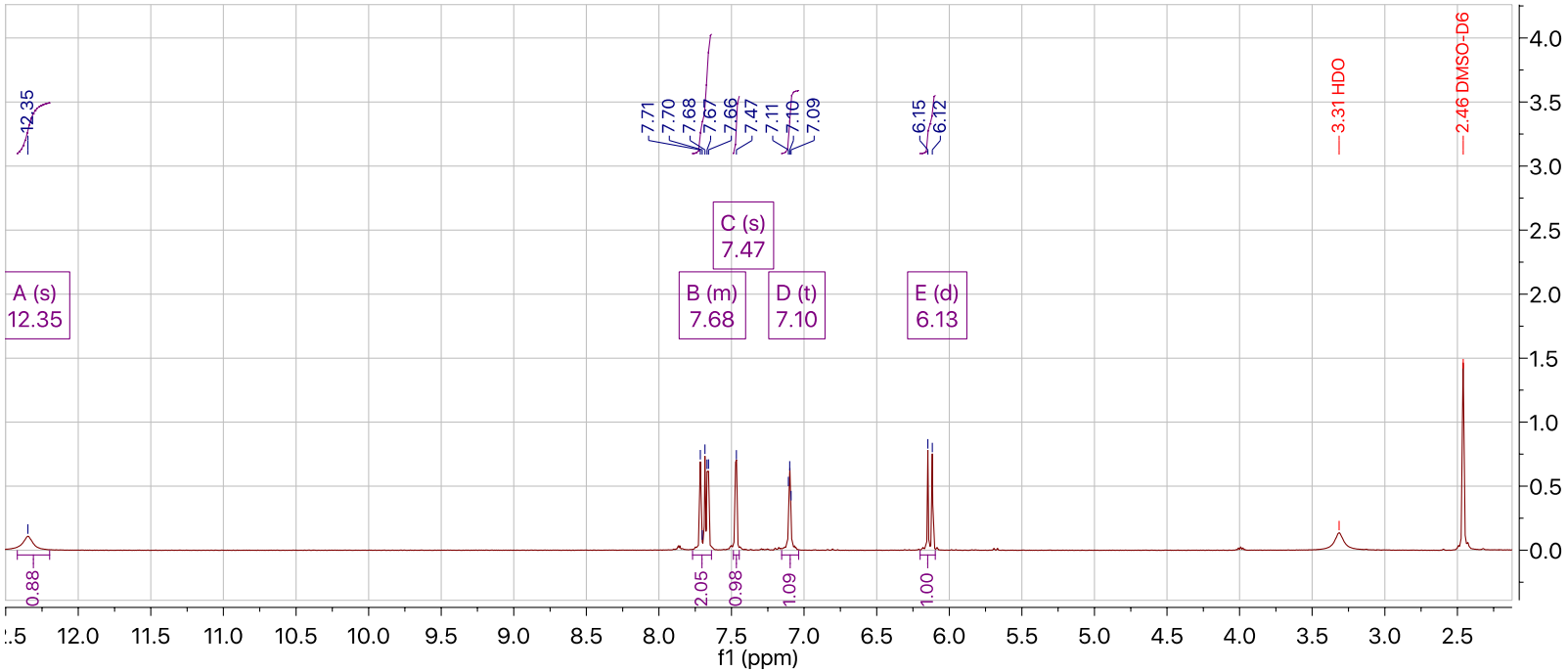

^{1}H NMR (500 MHz, DMSO-d_6) δ 12.35 (s, 1H), 7.77 – 7.64 (m, 2H), 7.47 (s, 1H), 7.10 (t, J = 4.6 Hz, 1H), 6.13 (d, J = 15.7 Hz, 1H).

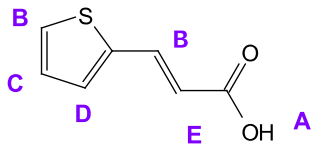

Figure B.15 ^{1}H NMR of BM103 - ThioCA - (E)-3-(thiophen-2-yl) acrylic acid

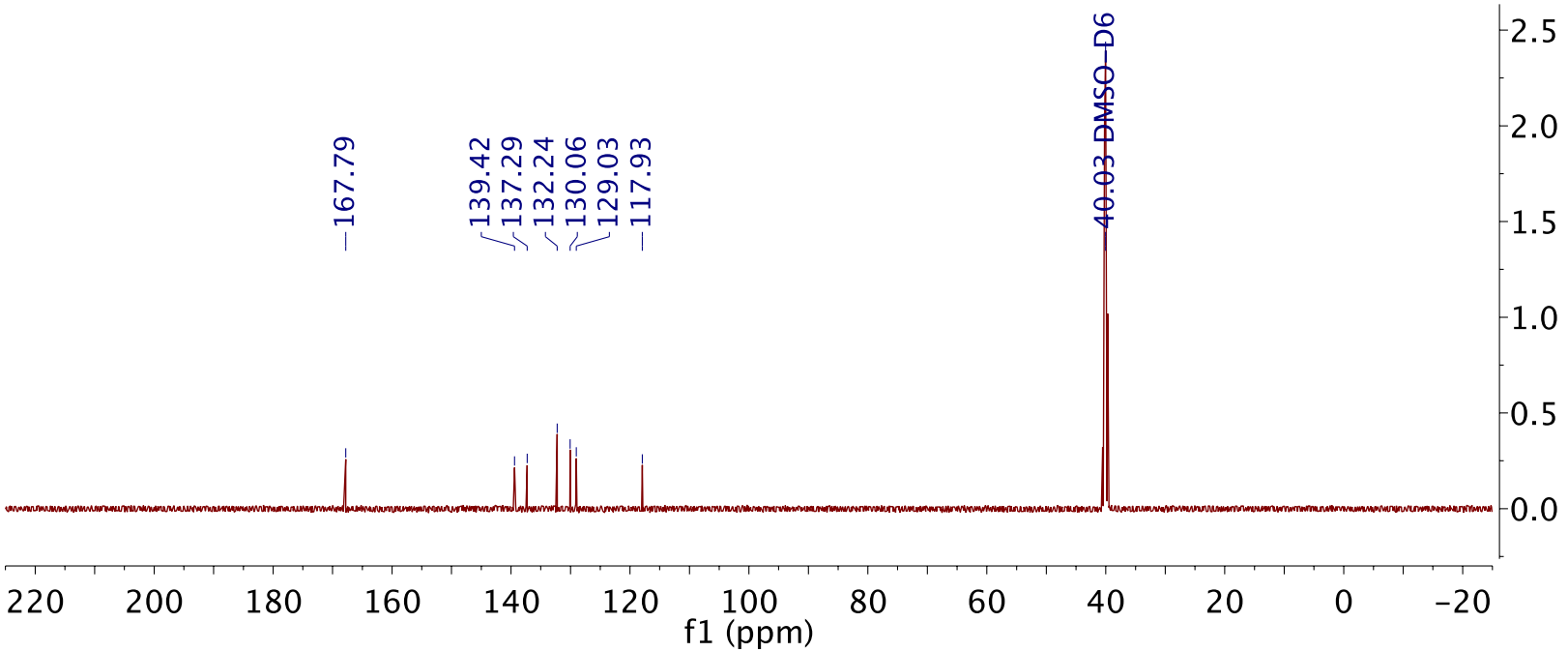

^{13}C NMR (126 MHz, DMSO-D_6) δ 167.79, 139.42, 137.29, 132.24, 130.06, 129.03, 117.93, 40.03.

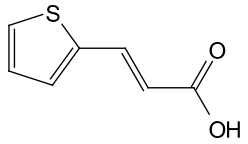

Figure B.16 ^{1}H NMR of BM103 - ThioCA - (E)-3-(thiophen-2-yl) acrylic acid

APPENDIX C

SELECTED NMR FOR CHAPTER 7

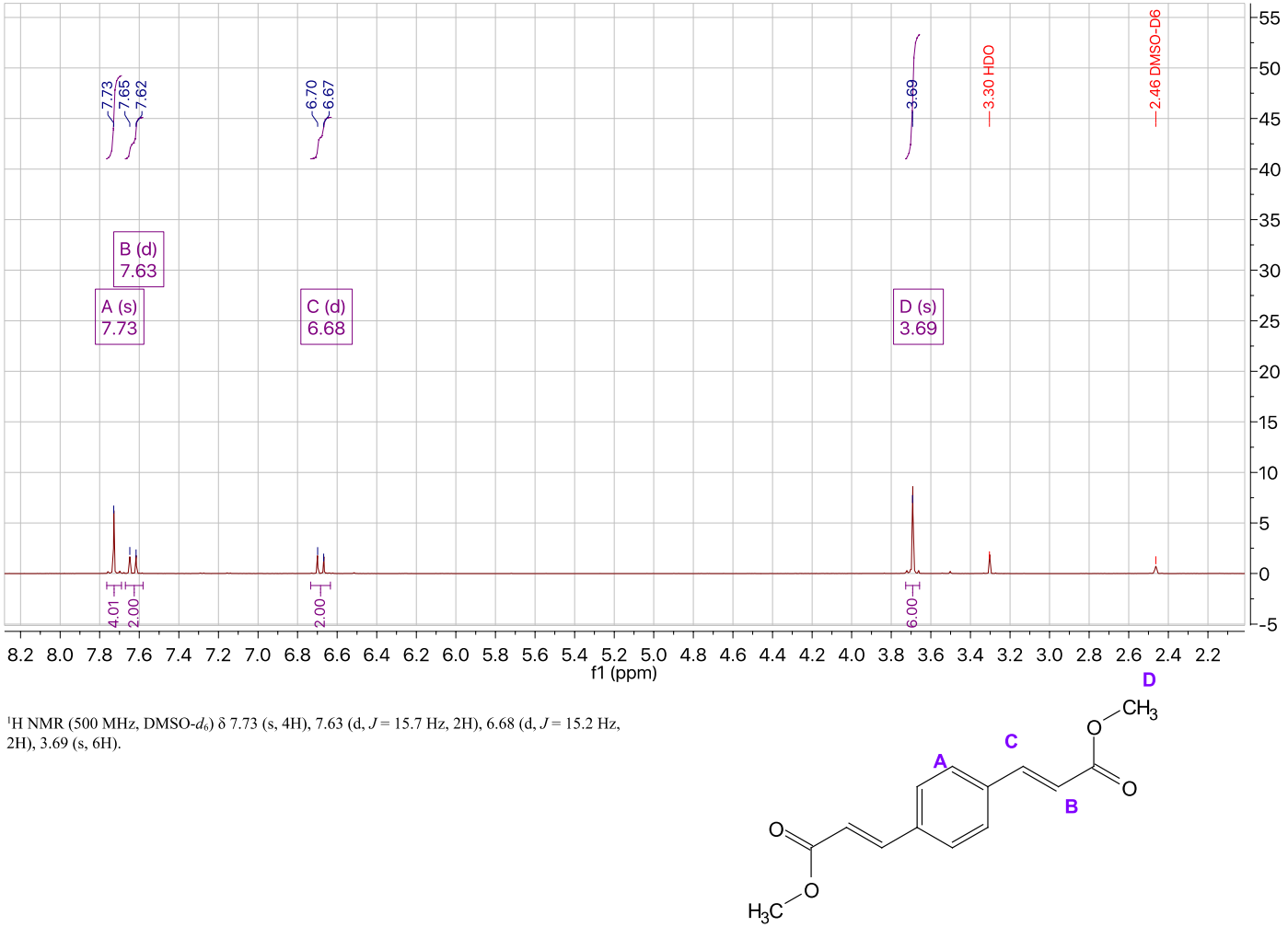

^{1}H NMR (500 MHz, DMSO-d_6) δ 7.73 (s, 4H), 7.63 (d, J = 15.7 Hz, 2H), 6.68 (d, J = 15.2 Hz, 2H), 3.69 (s, 6H).

Figure C.1 ^{1}H NMR of BM45 precursor - dimethyl 3,3'-(1,4-phenylene)(2*E*,2'*E*)-diacrylate

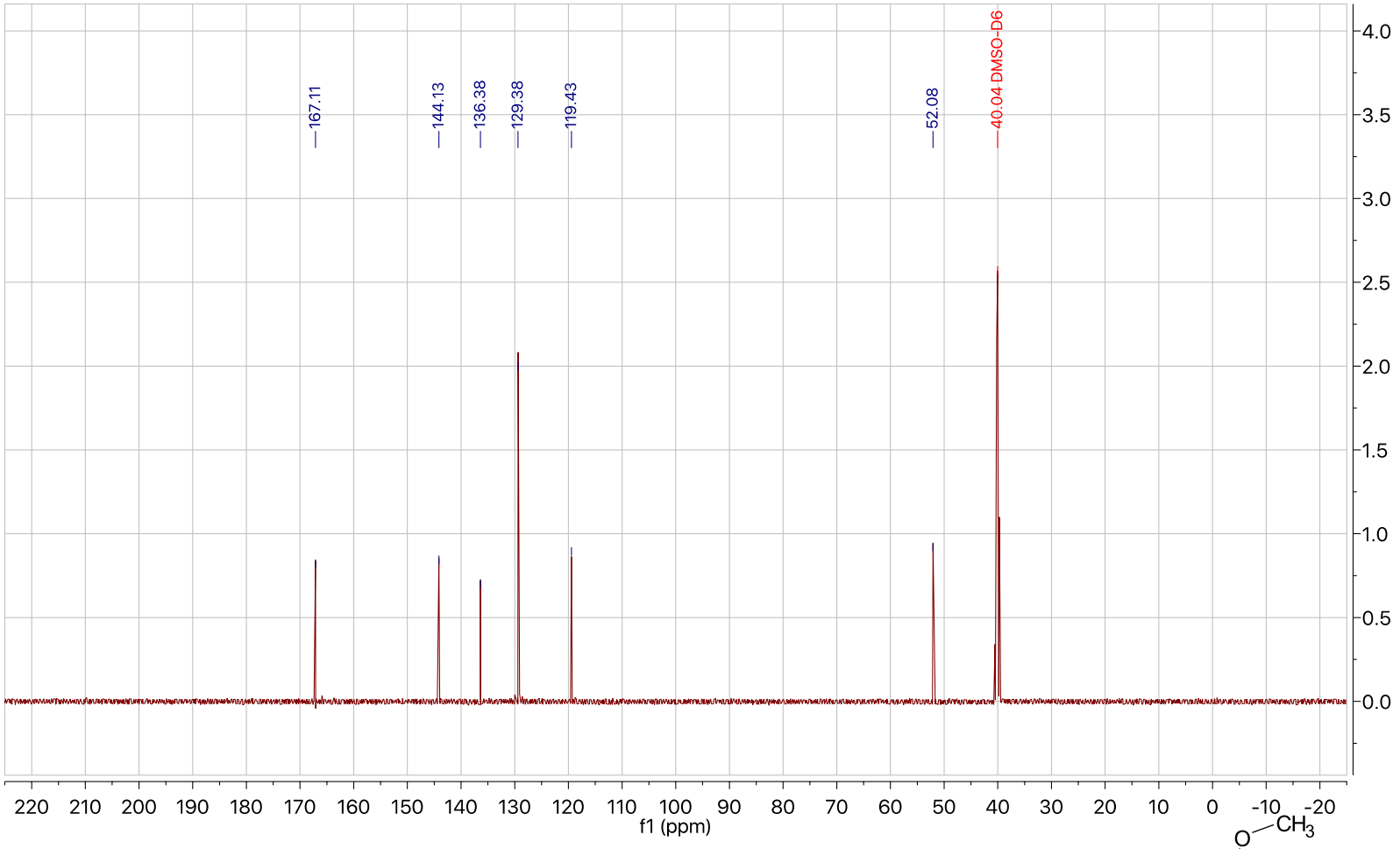

^{13}C NMR (126 MHz, DMSO-D_6) δ 167.11, 144.13, 136.38, 129.38, 119.43, 52.08, 40.04.

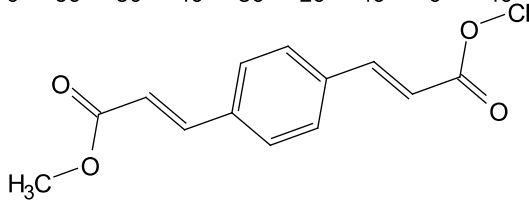

Figure C.2 ^{13}C of BM45 precursor - dimethyl 3,3'-(1,4-phenylene)(2*E*,2'*E*)-diacrylate

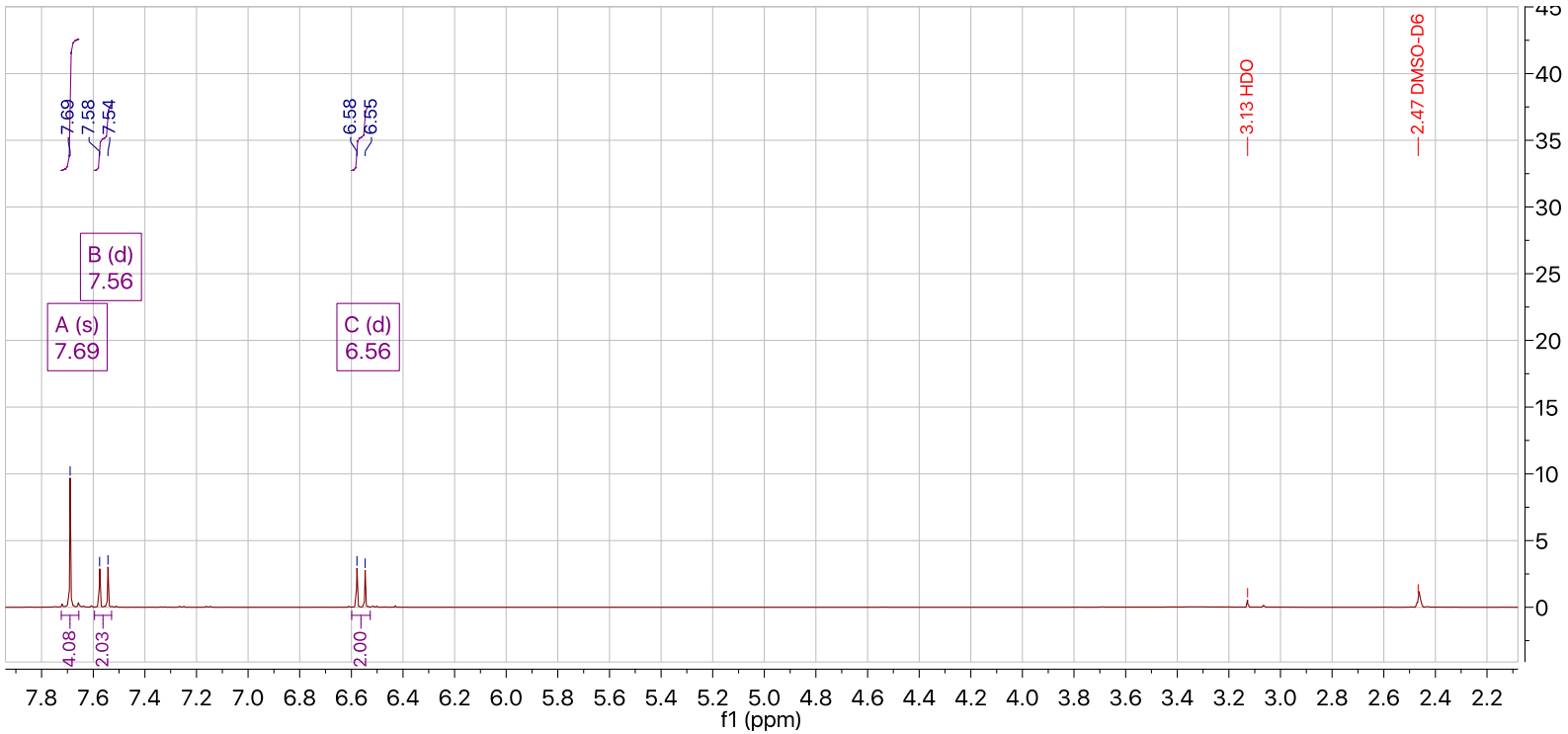

^{1}H NMR (500 MHz, DMSO-d_6) δ 7.69 (s, 4H), 7.56 (d, J = 16.0 Hz, 2H), 6.56 (d, J = 16.0 Hz, 2H).

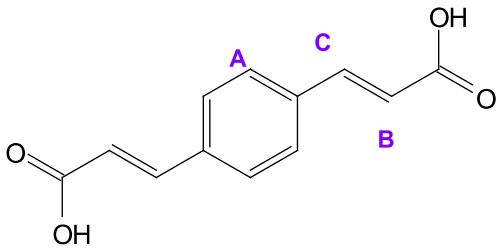

Figure C.3 ^{1}H NMR of BM45 - (2*E*,2'*E*)-3,3'-(1,4-phenylene) diacrylic acid

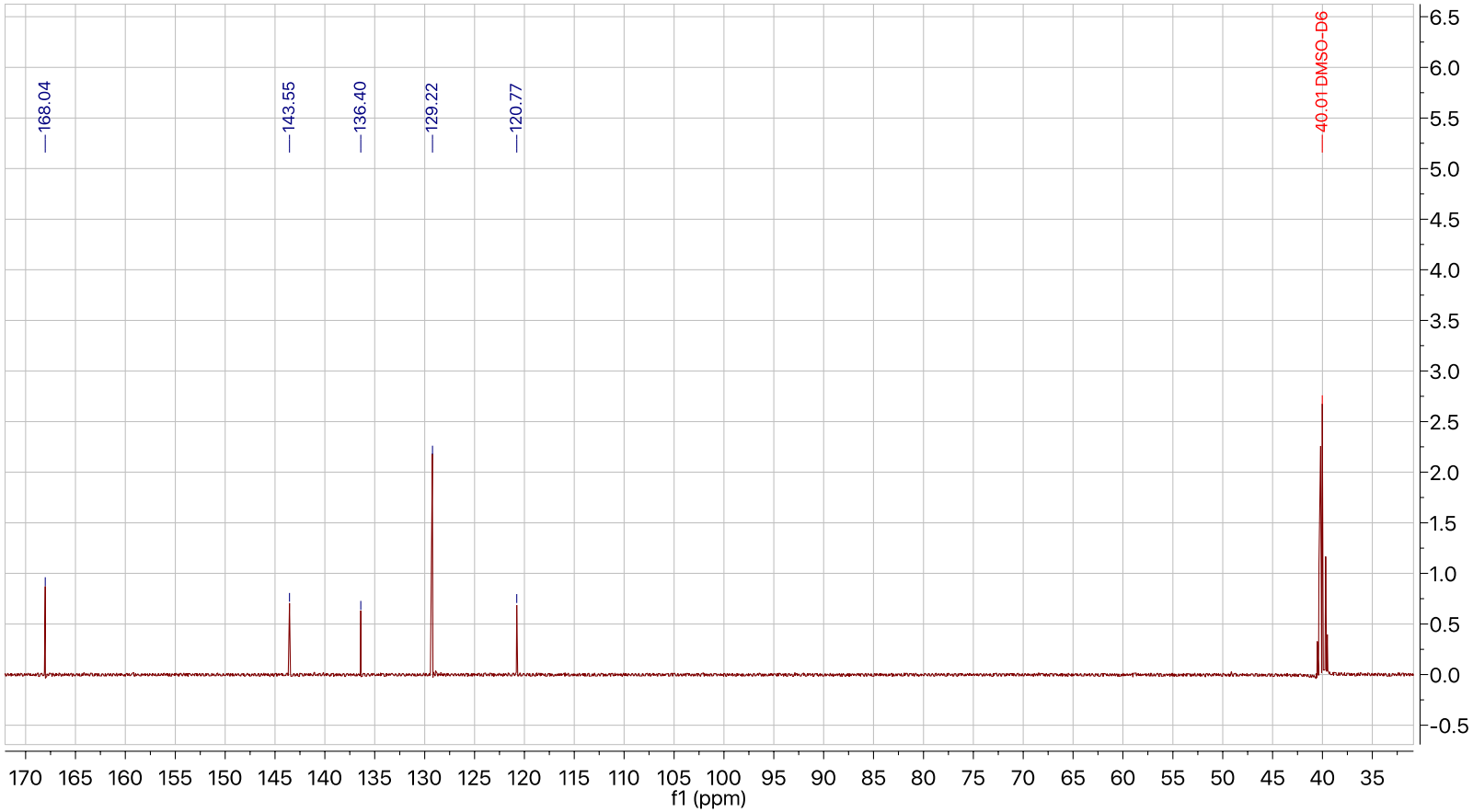

^{13}C NMR (126 MHz, DMSO-D_6) δ 168.04, 143.55, 136.40, 129.22, 120.77, 40.01.

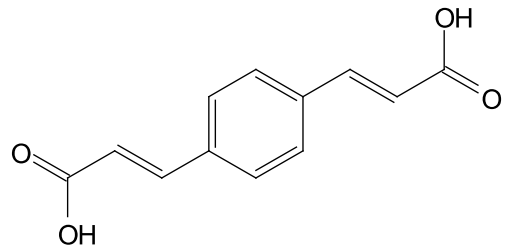

Figure C.4 ^{13}C NMR of BM45 - (2*E*,2'*E*)-3,3'-(1,4-phenylene) diacrylic acid

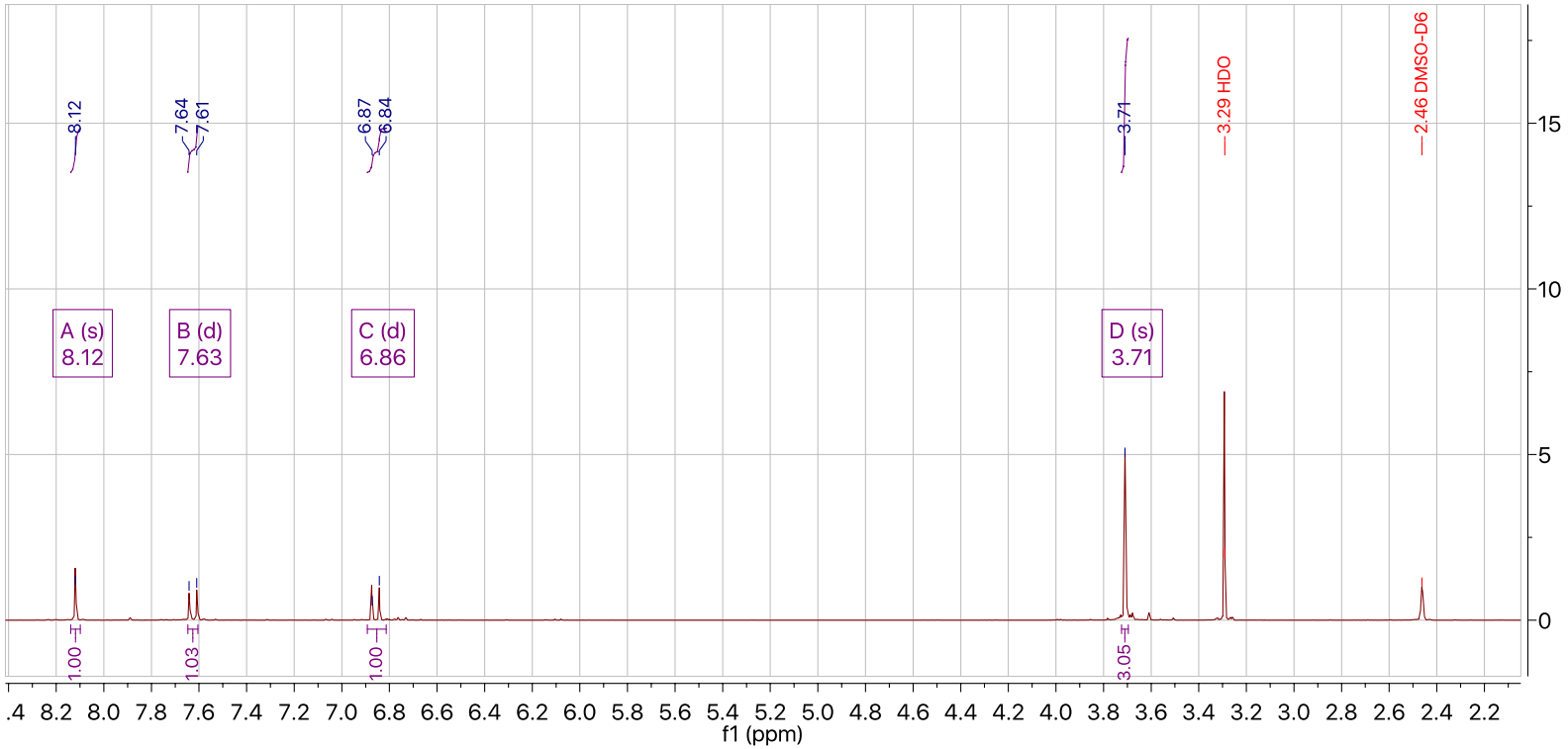

[1]H NMR (500 MHz, DMSO-d_6) δ 8.12 (s, 1H), 7.63 (d, J = 16.1 Hz, 1H), 6.86 (d, J = 15.2 Hz, 1H), 3.71 (s, 3H).

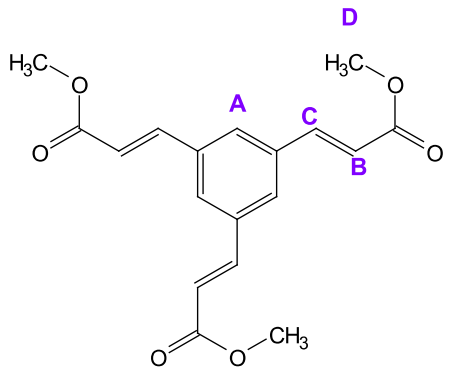

Figure C.5 [1]H NMR of BM53 Precursor- trimethyl 3,3',3''-(benzene-1,3,5-triyl)(2*E*,2'*E*,2''*E*)-triacrylate

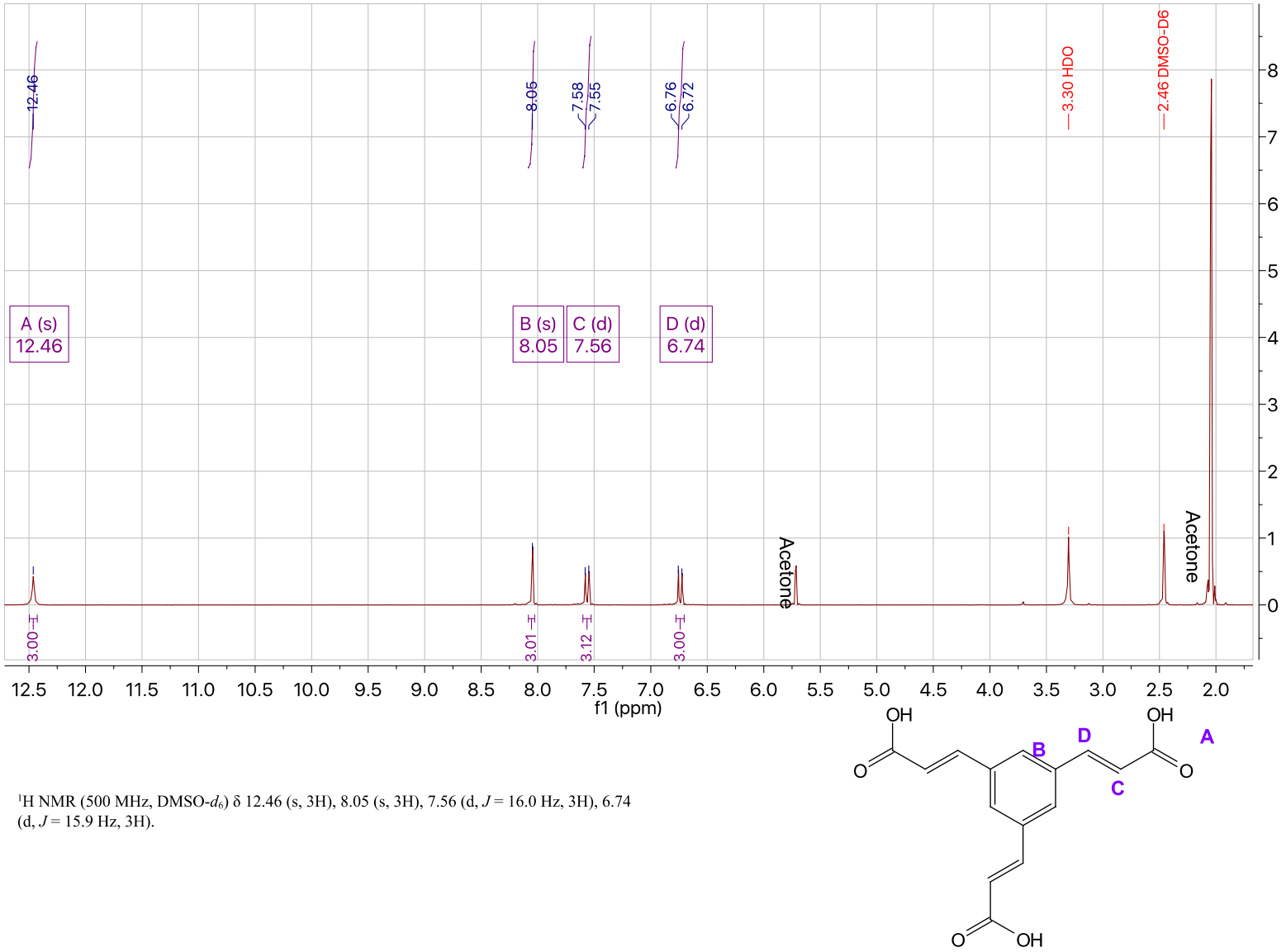

^{1}H NMR (500 MHz, DMSO-d_6) δ 12.46 (s, 3H), 8.05 (s, 3H), 7.56 (d, J = 16.0 Hz, 3H), 6.74 (d, J = 15.9 Hz, 3H).

Figure C.6 ^{1}H NMR of BM53 - (2*E*,2'*E*,2''*E*)-3,3',3''-(benzene-1,3,5-triyl) triacrylic acid

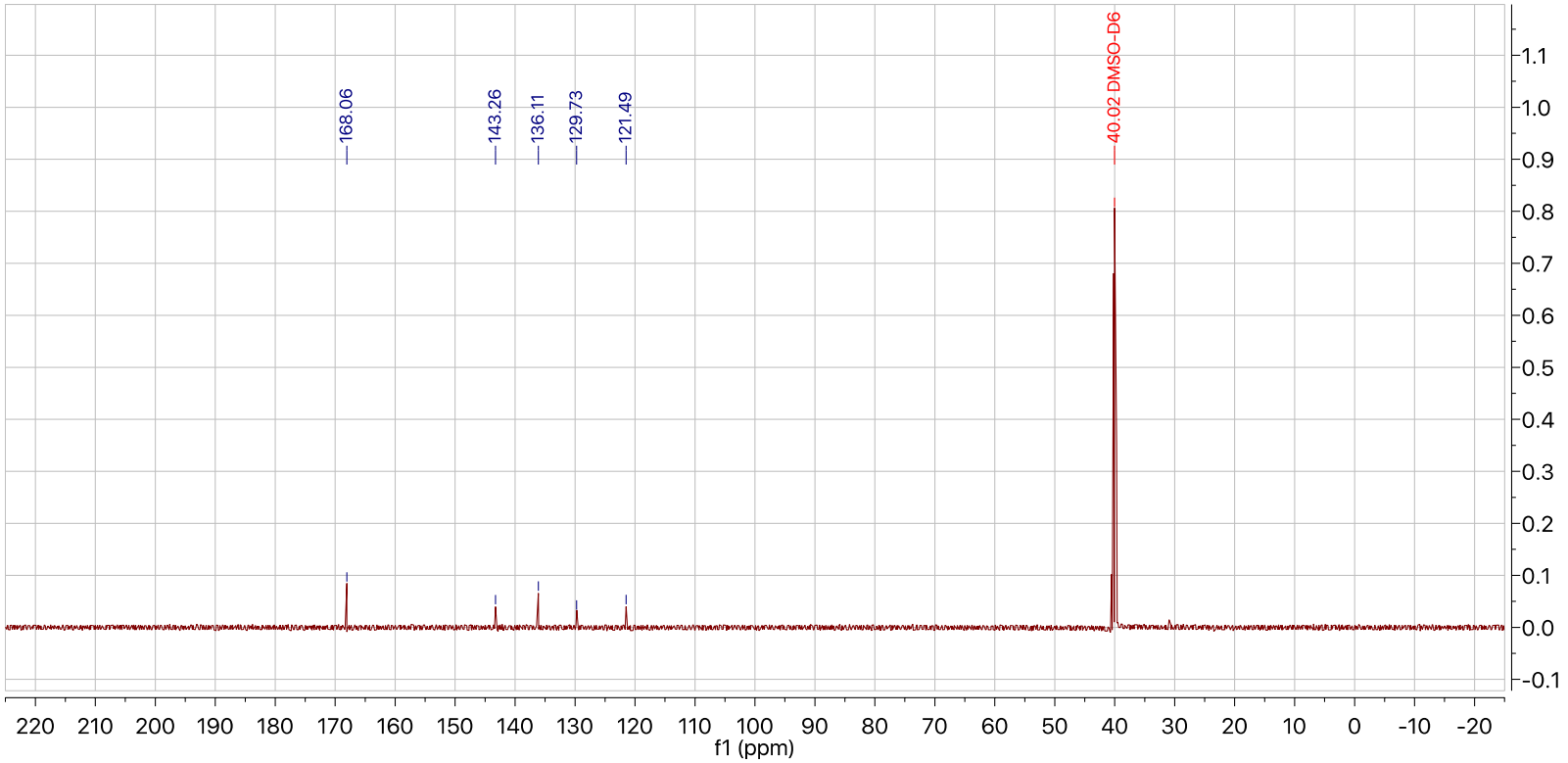

^{13}C NMR (126 MHz, DMSO-D_6) δ 168.06, 143.26, 136.11, 129.73, 121.49

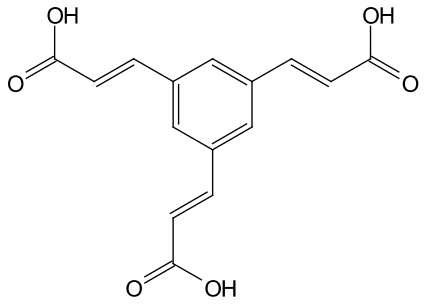

Figure C.7 ^{13}C NMR of BM53 - (2*E*,2'*E*,2''*E*)-3,3',3''-(benzene-1,3,5-triyl) triacrylic acid

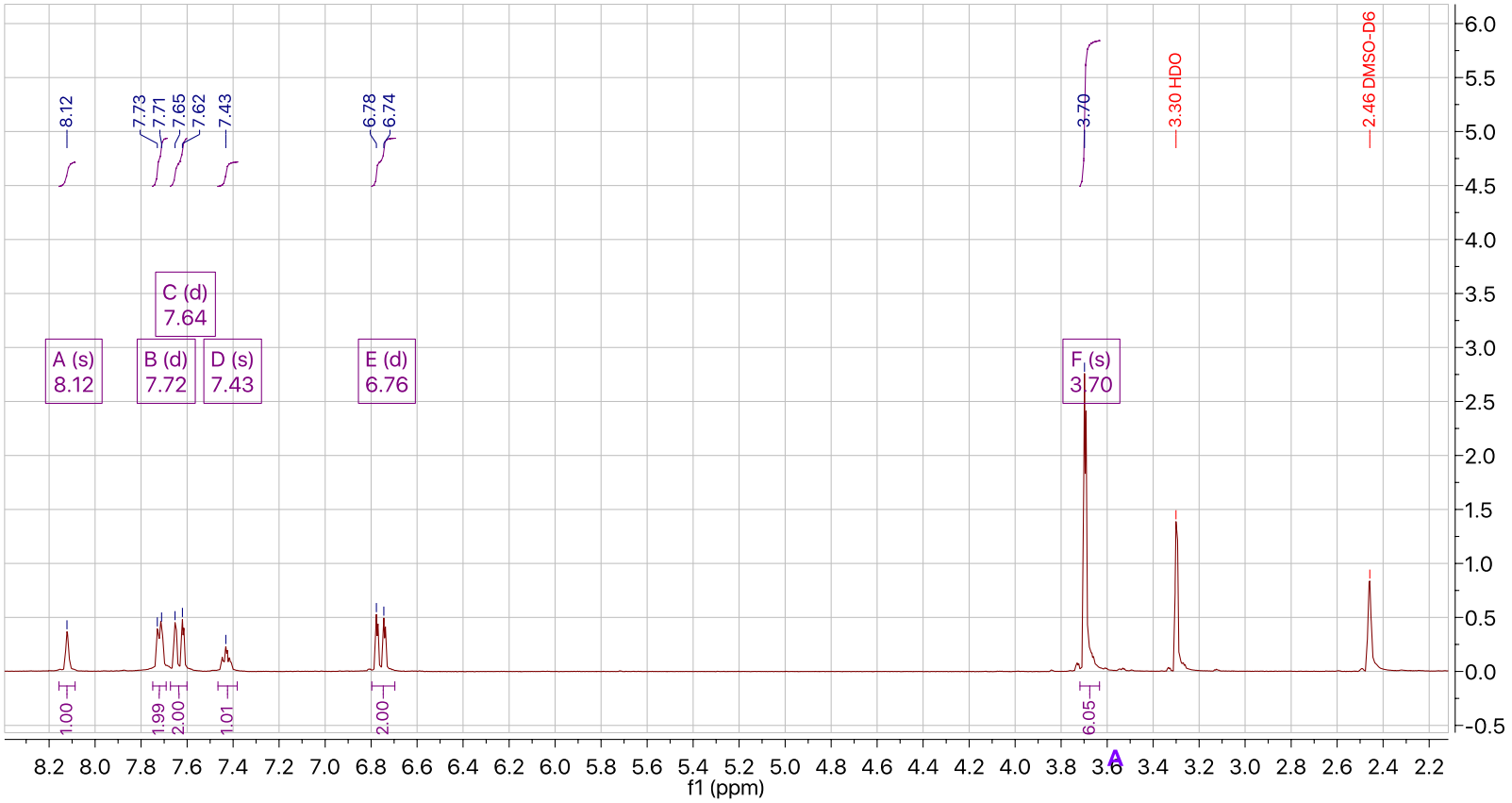

[1]H NMR (500 MHz, DMSO-d_6) δ 8.12 (s, 1H), 7.72 (d, J = 9.2 Hz, 2H), 7.64 (d, J = 16.1 Hz, 2H), 7.43 (s, 1H), 6.76 (d, J = 16.1 Hz, 2H), 3.70 (s, 6H).

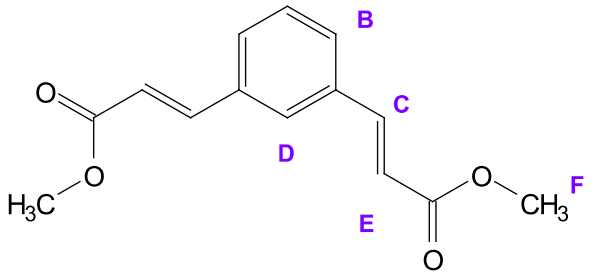

Figure C.8 [1]H NMR of BM57 precursor - dimethyl 3,3'-(1,3-phenylene)(2*E*,2'*E*)-diacrylate

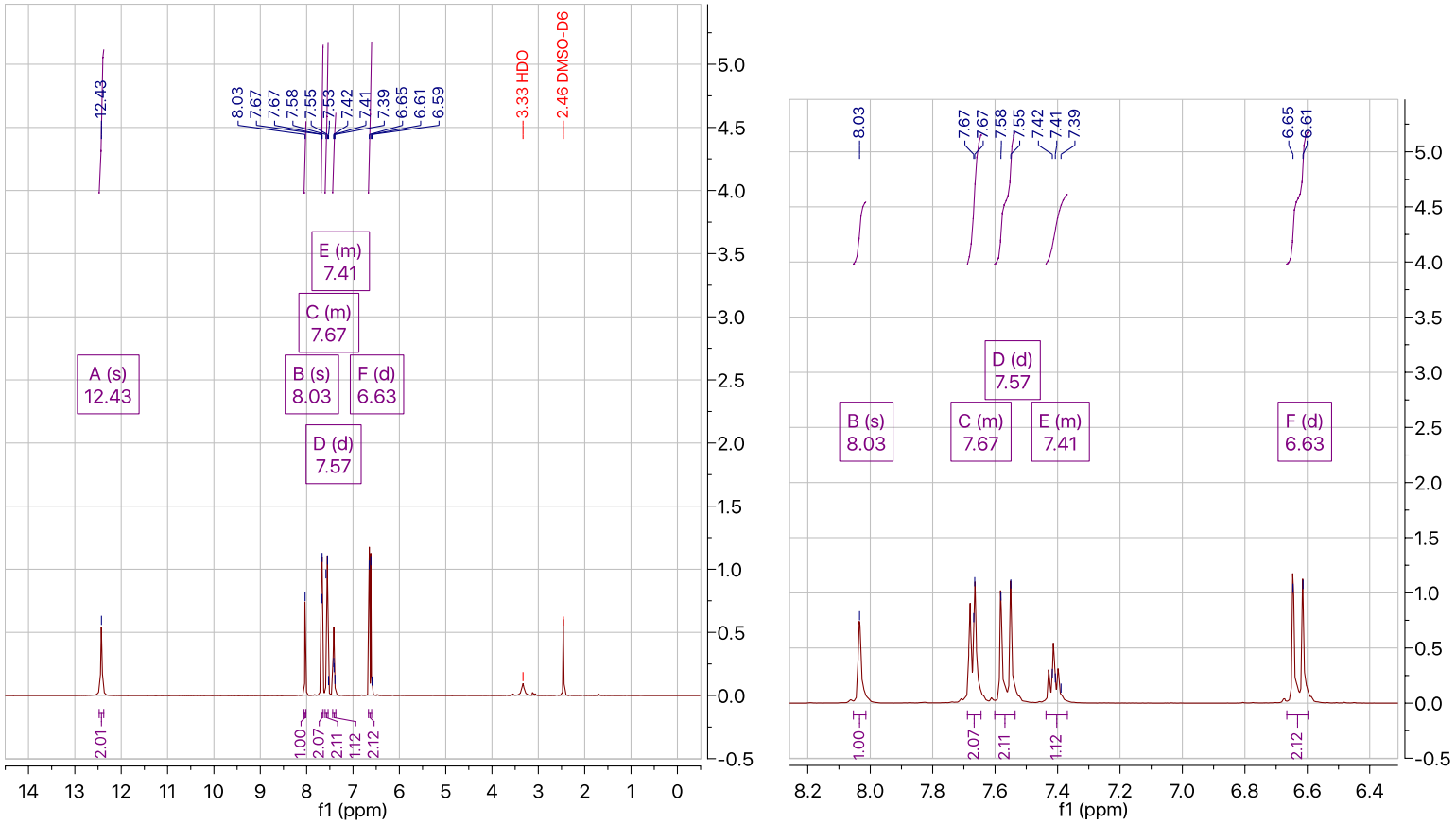

^{1}H NMR (500 MHz, DMSO-d_6) δ 12.43 (s, 2H), 8.03 (s, 1H), 7.69 – 7.65 (m, 2H), 7.57 (d, J = 15.8 Hz, 2H), 7.44 – 7.37 (m, 1H), 6.63 (d, J = 15.9 Hz, 2H).

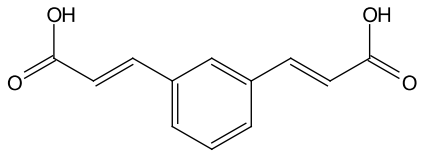

Figure C.9 ^{1}H NMR of BM57 - (2*E*,2'*E*)-3,3'-(1,3-phenylene) diacrylic acid

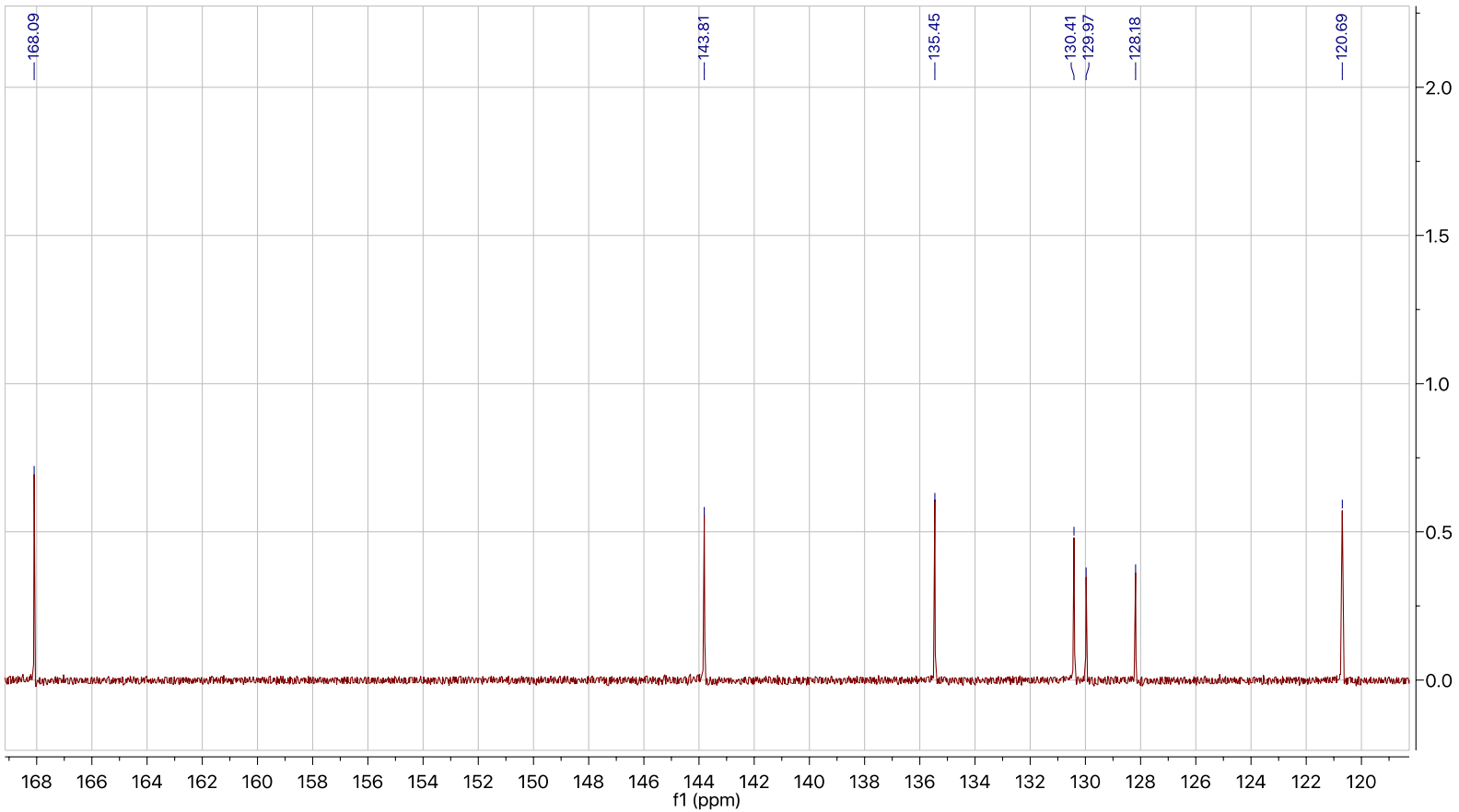

^{13}C NMR (126 MHz, DMSO-D_6) δ 168.09, 143.81, 135.45, 130.41, 129.97, 128.18, 120.69.

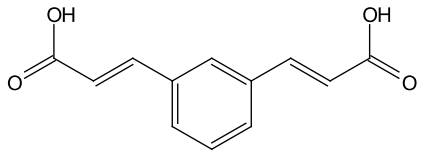

Figure C.10 ^{13}C NMR of BM57 - (2*E*,2'*E*)-3,3'-(1,3-phenylene) diacrylic acid

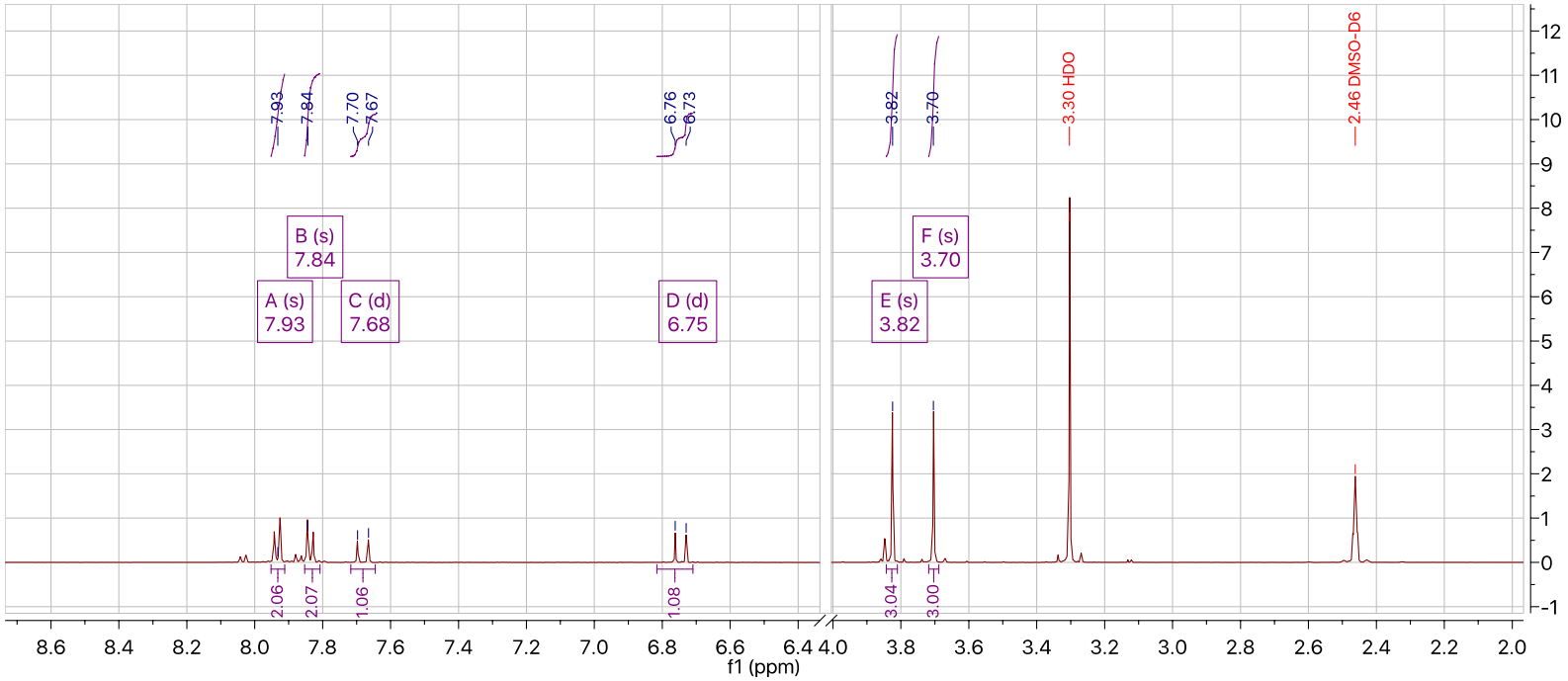

^{1}H NMR (500 MHz, DMSO-d_6) δ 7.93 (s, 2H), 7.84 (s, 2H), 7.68 (d, J = 16.0 Hz, 1H), 6.75 (d, J = 16.0 Hz, 1H), 3.82 (s, 3H), 3.70 (s, 3H).

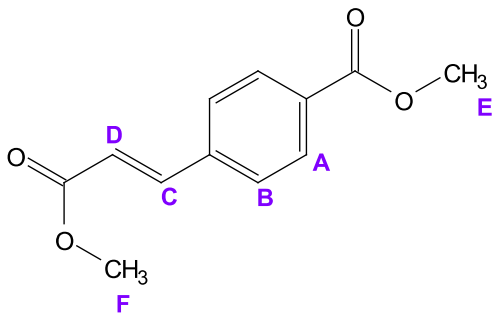

Figure C.11 ^{1}H NMR of BM65 precursor - methyl (*E*)-4-(3-methoxy-3-oxoprop-1-en-1-yl)benzoate

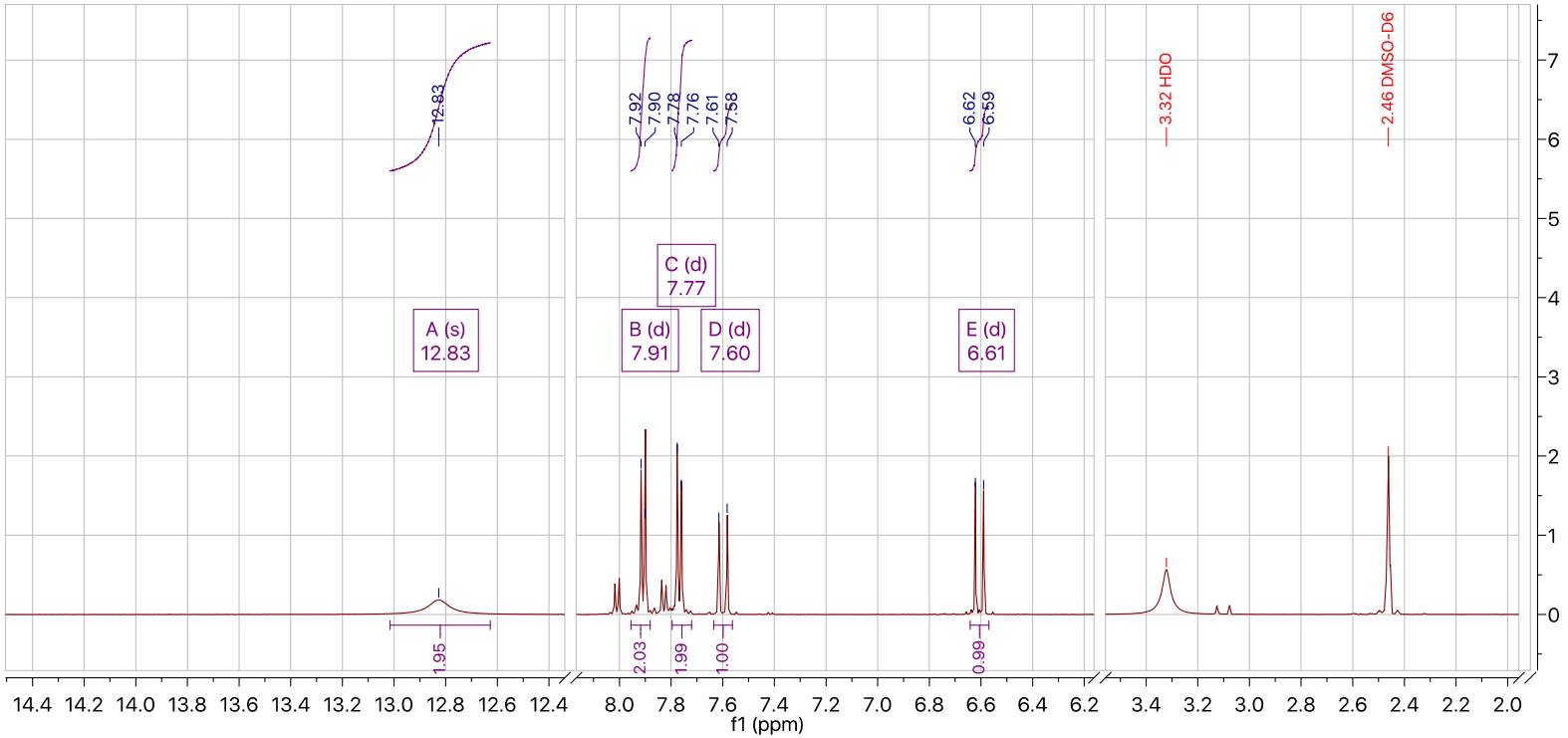

^{1}H NMR (500 MHz, DMSO-d_6) δ 12.83 (s, 2H), 7.91 (d, J = 7.6 Hz, 2H), 7.77 (d, J = 7.8 Hz, 2H), 7.60 (d, J = 16.1 Hz, 1H), 6.61 (d, J = 16.2 Hz, 1H).

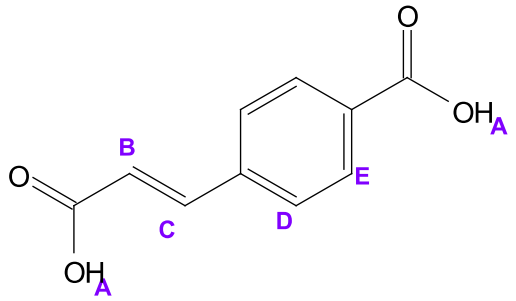

Figure C.12 ^{1}H NMR of BM65 - (*E*)-4-(2-carboxyvinyl) benzoic acid

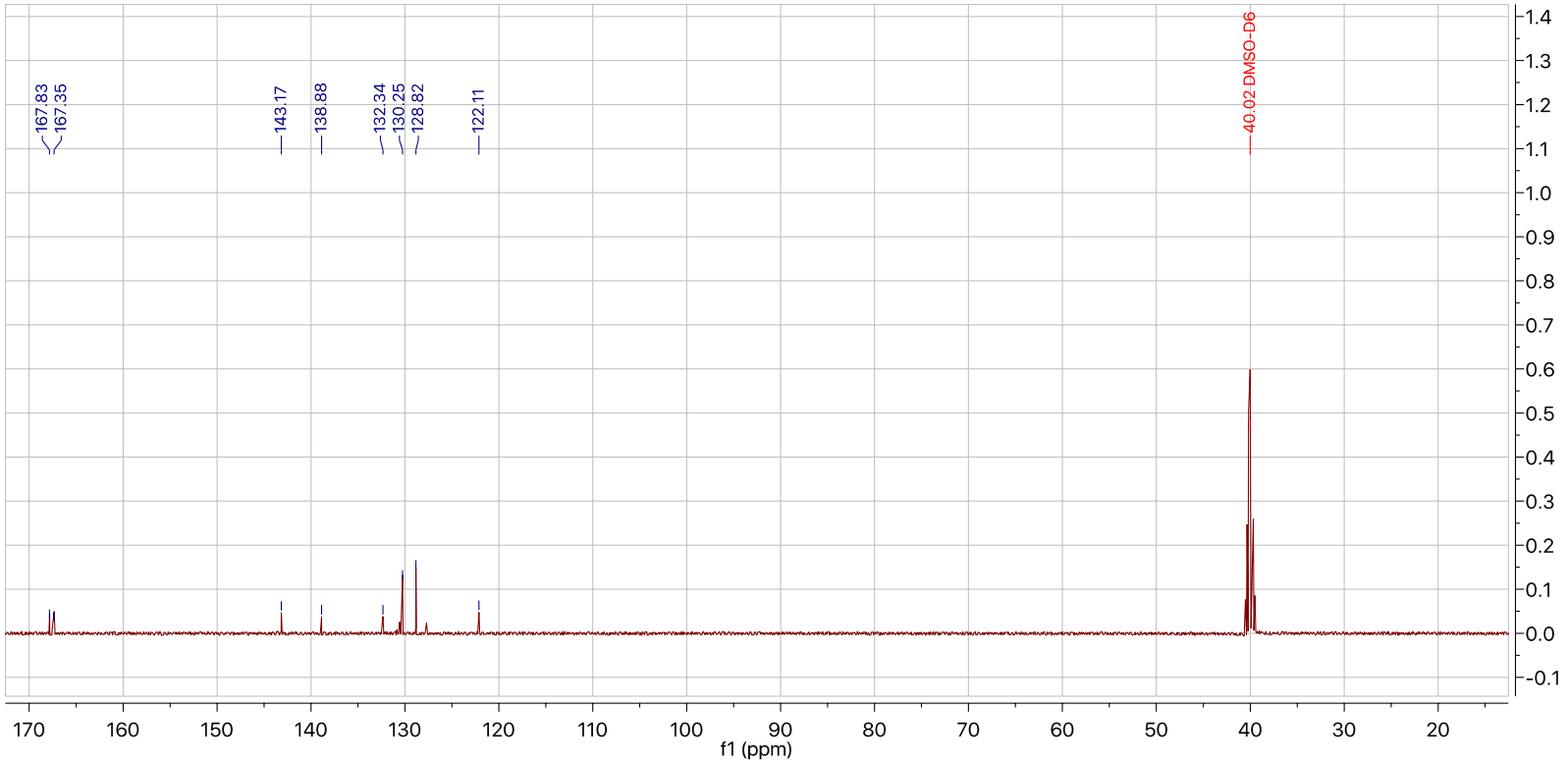

^{13}C NMR (126 MHz, DMSO-D_6) δ 167.83, 167.35, 143.17, 138.88, 132.34, 130.25, 128.82, 122.11, 40.02.

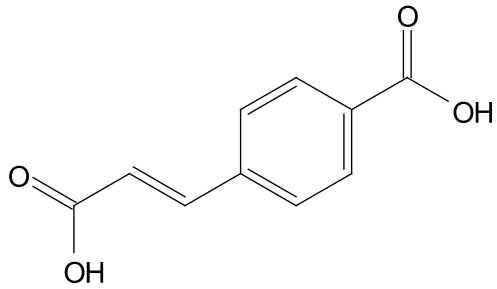

Figure C.13 ^{13}C of BM65 - (*E*)-4-(2-carboxyvinyl) benzoic acid

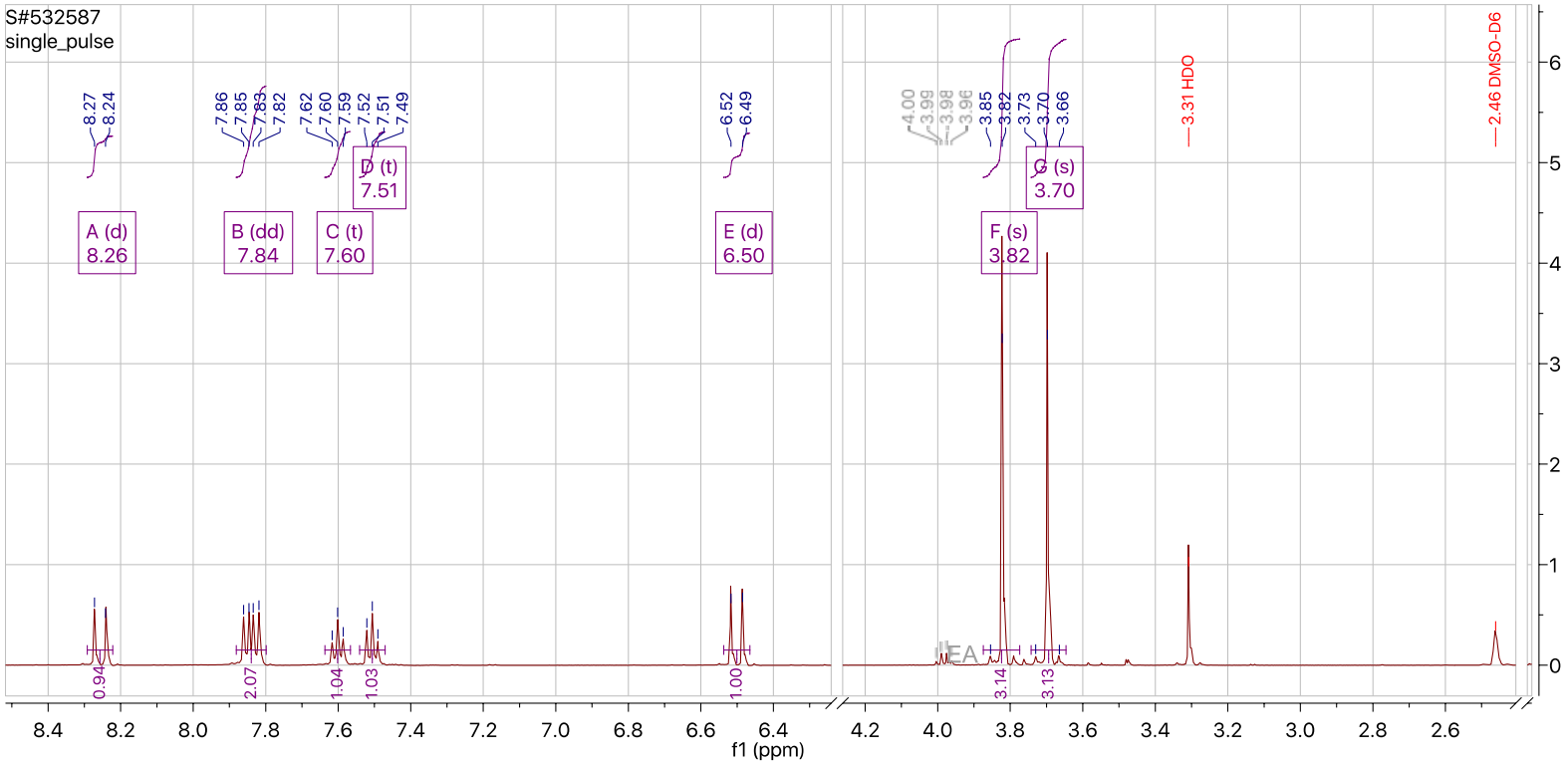

^{1}H NMR (500 MHz, DMSO-d_6) δ 8.26 (d, J = 15.2 Hz, 1H), 7.84 (dd, J = 13.5, 7.8 Hz, 2H), 7.60 (t, J = 7.6 Hz, 1H), 7.51 (t, J = 7.6 Hz, 1H), 6.50 (d, J = 15.9 Hz, 1H), 3.82 (s, 3H), 3.70 (s, 3H).

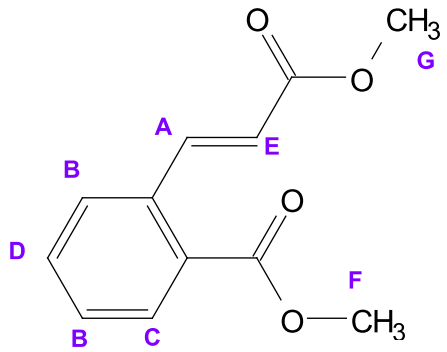

Figure C.14 ^{1}H NMR of BM66 precursor - methyl (*E*)-2-(3-methoxy-3-oxoprop-1-en-1-yl) benzoate

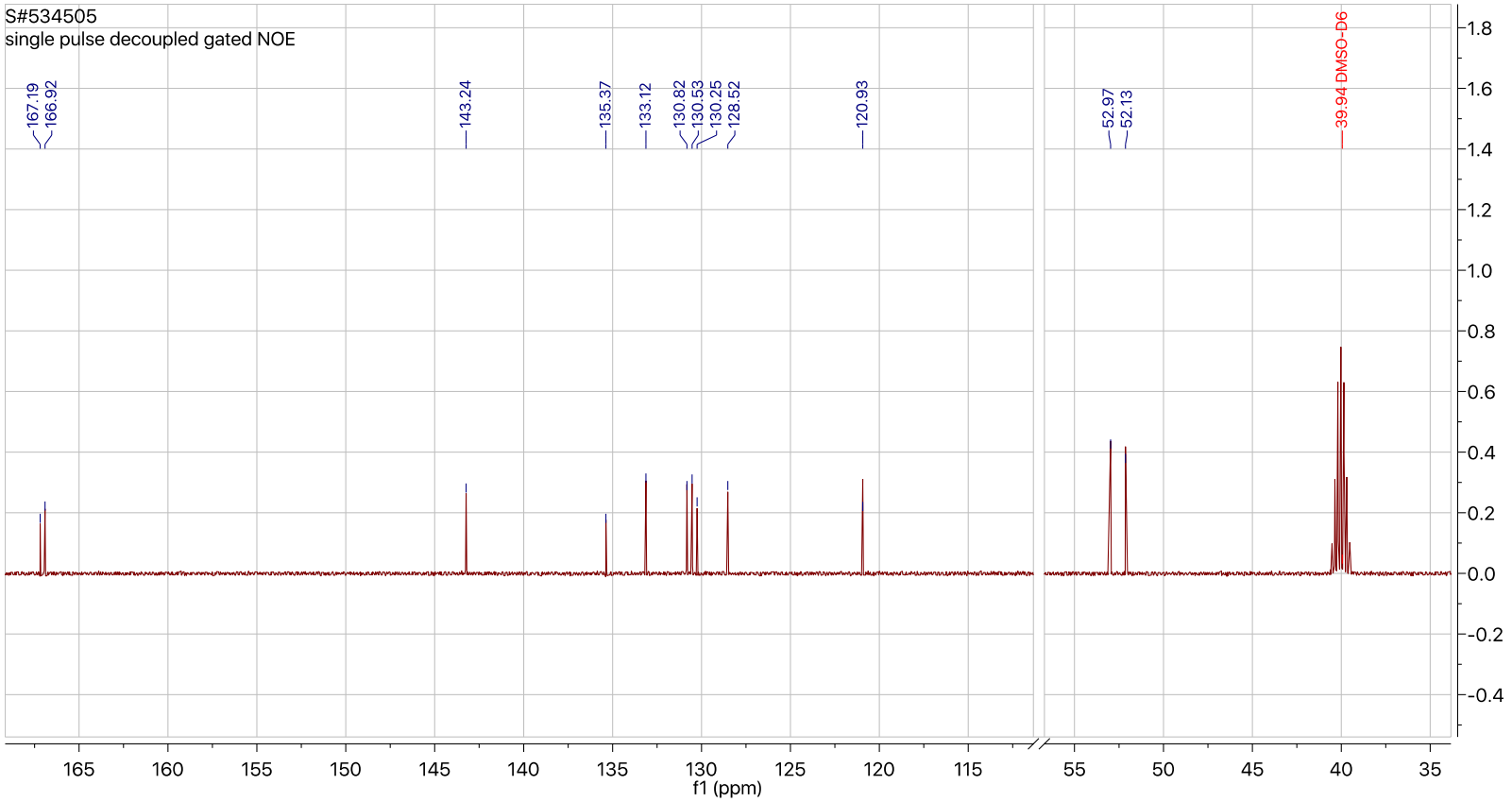

^{13}C NMR (126 MHz, DMSO-D_6) δ 167.19, 166.92, 143.24, 135.37, 133.12, 130.82, 130.53, 130.25, 128.52, 120.93, 52.97, 52.13, 40.53,

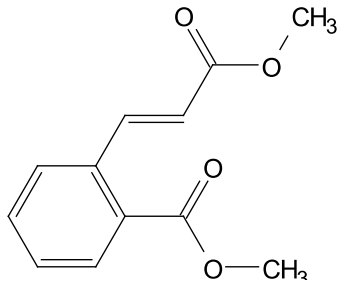

Figure C.15 ^{13}C NMR of BM66 precursor - methyl (*E*)-2-(3-methoxy-3-oxoprop-1-en-1-yl) benzoate

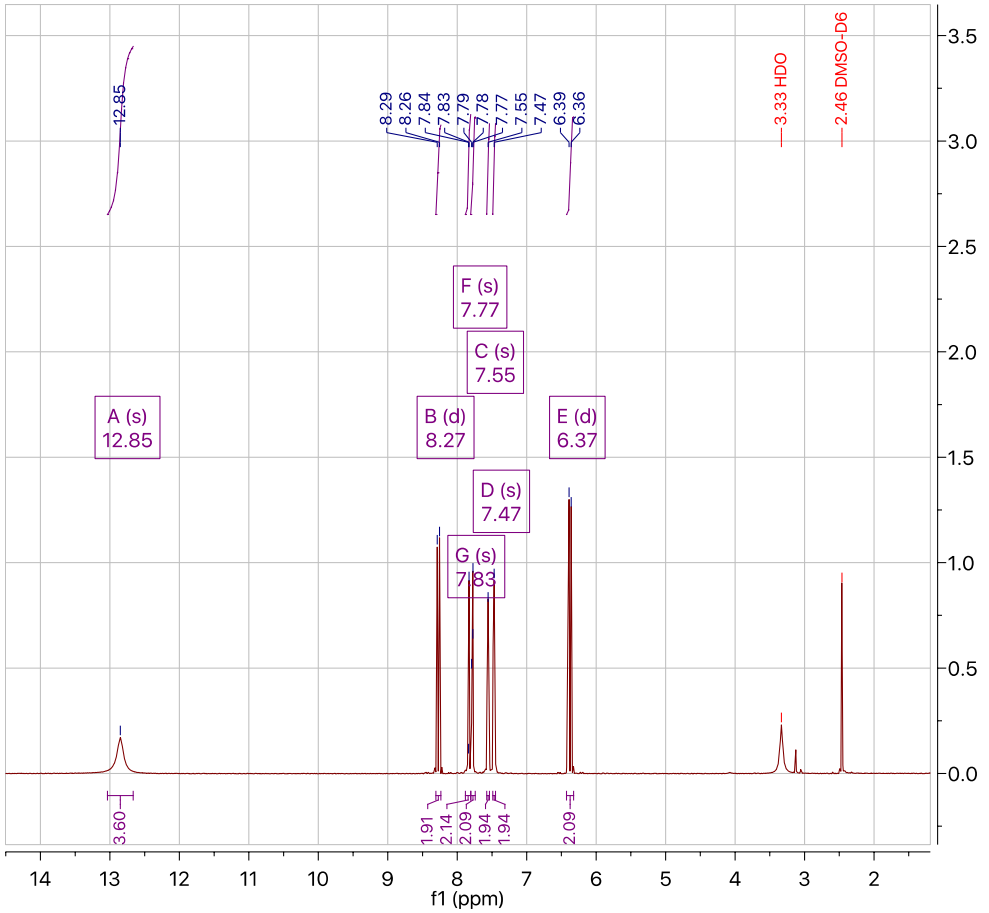

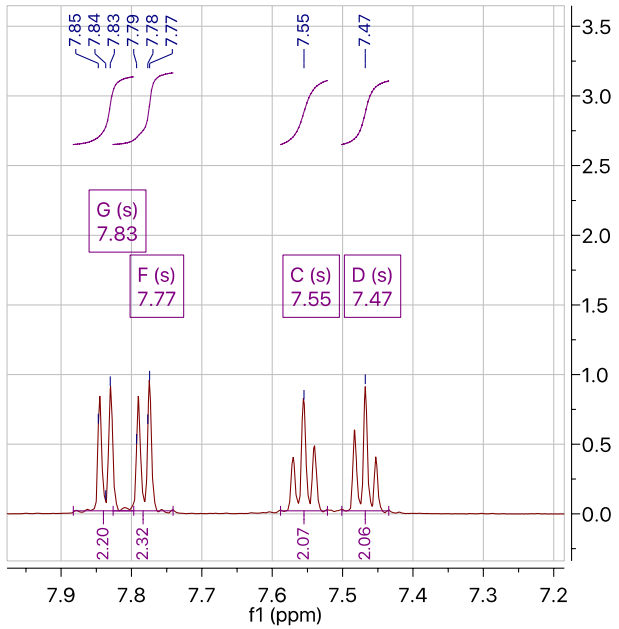

[1]H NMR (500 MHz, DMSO-d_6) δ 12.85 (s, 4H), 8.27 (d, J = 16.0 Hz, 2H), 7.83 (s, 2H), 7.77 (s, 2H), 7.55 (s, 2H), 7.47 (s, 2H), 6.37 (d, J = 16.0 Hz, 2H).

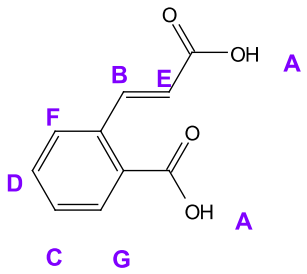

Figure C.16 [1]H NMR of BM66 - (E)-2-(2-carboxyvinyl) benzoic acid

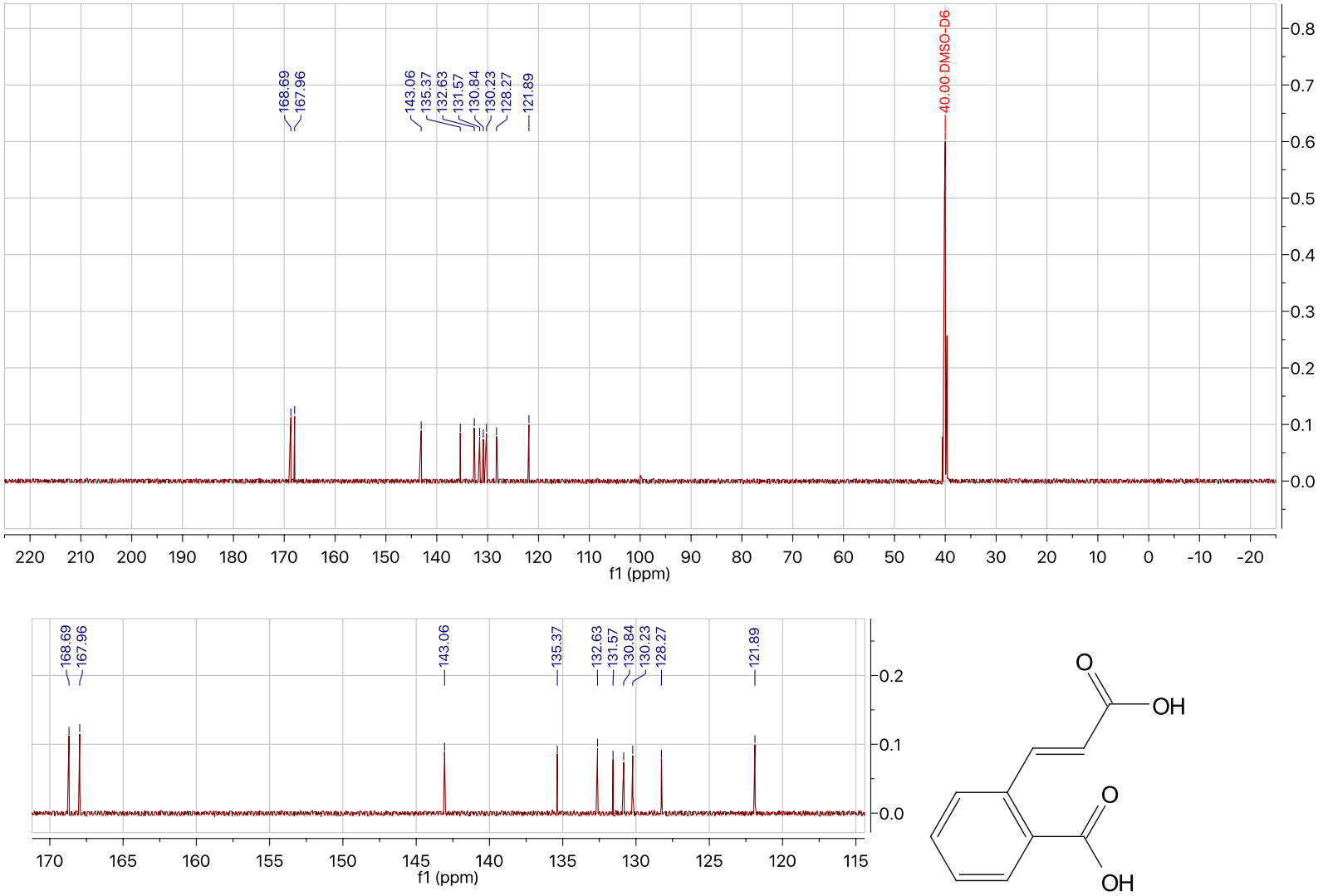

^{13}C NMR (126 MHz, DMSO-D_6) δ 168.69, 167.96, 143.06, 135.37, 132.63, 131.57, 130.84, 130.23, 128.27, 121.89, 40.00.

Figure C.17 ^{13}C NMR of BM66 - (E)-2-(2-carboxyvinyl) benzoic acid

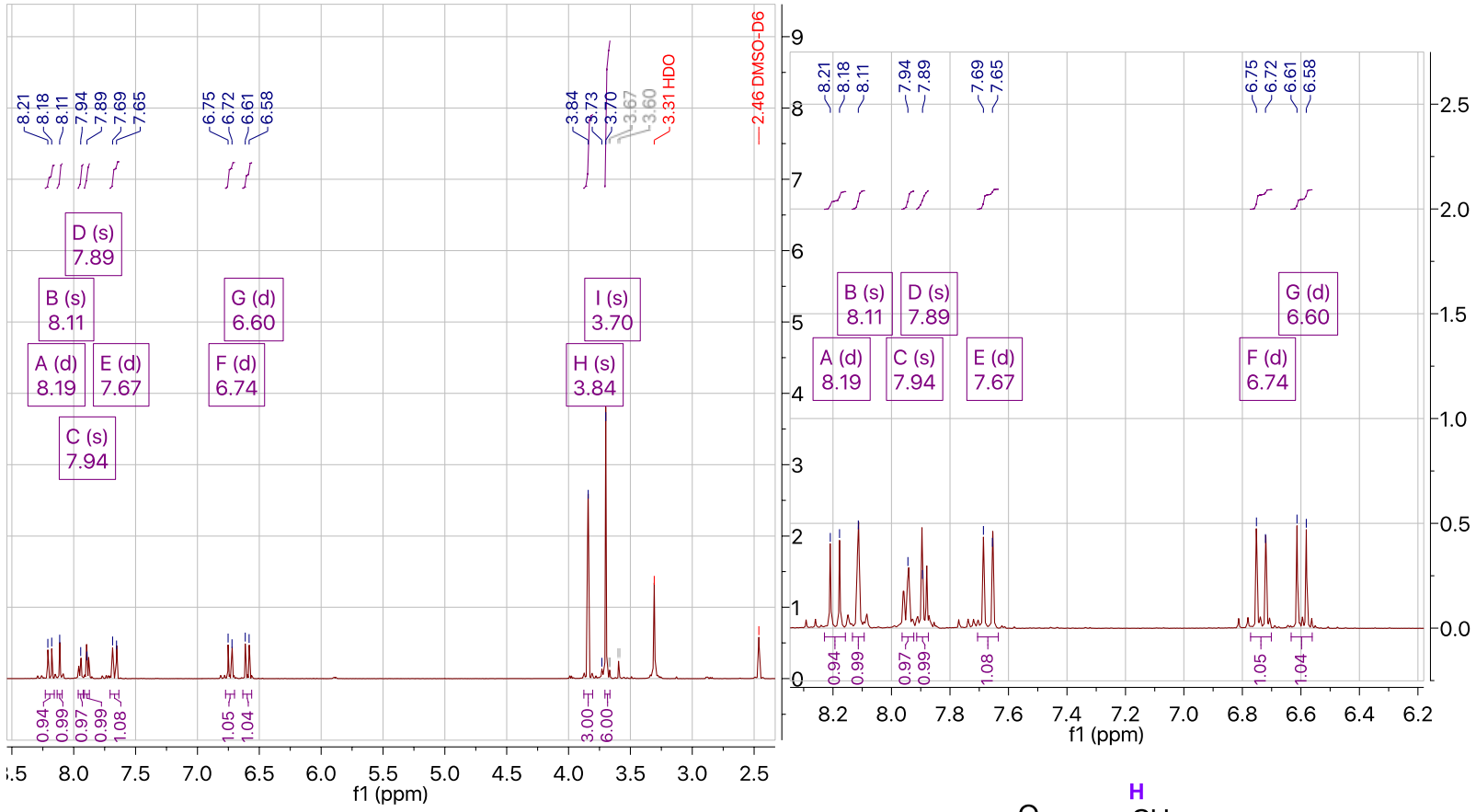

[1]H NMR (500 MHz, DMSO-d_6) δ 8.19 (d, J = 15.9 Hz, 2H), 8.11 (s, 2H), 7.94 (s, 2H), 7.89 (s, 2H), 7.67 (d, J = 15.5 Hz, 2H), 6.74 (d, J = 15.7 Hz, 2H), 6.60 (d, J = 15.9 Hz, 2H), 3.84 (s, 5H), 3.73 (s, 1H).

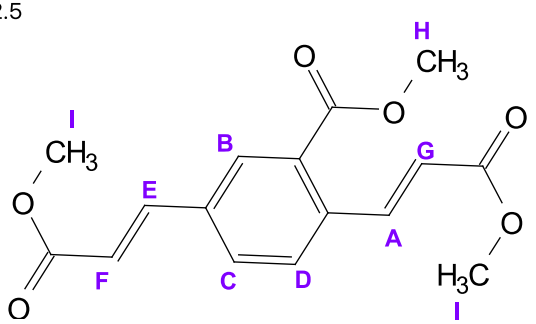

Figure C.18 [1]H NMR of BM67 precursor - dimethyl 3,3'-(2-(methoxycarbonyl)-1,4-phenylene) (2*E*,2'*E*)-diacrylate

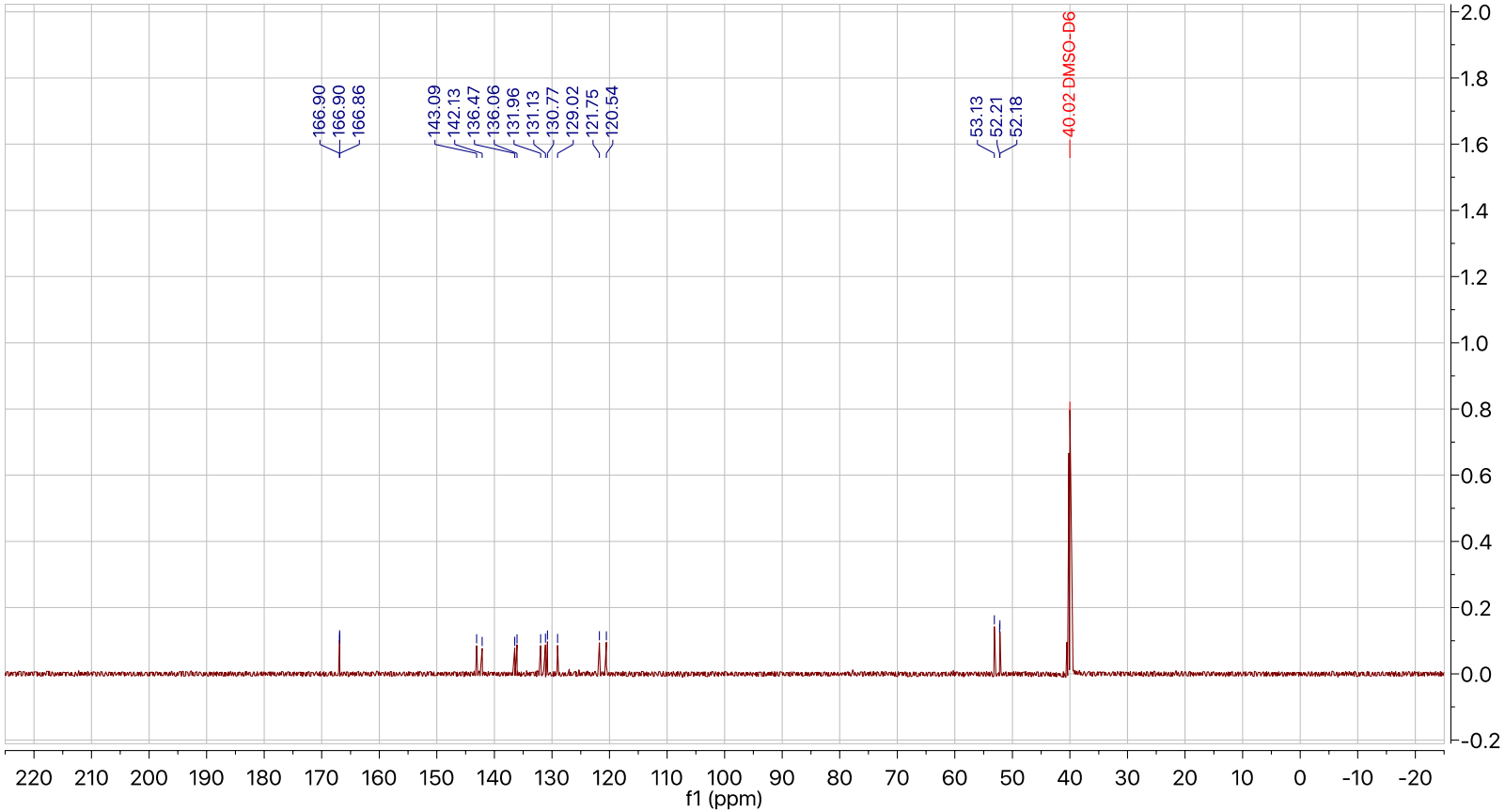

^{13}C NMR (126 MHz, DMSO-D_6) δ 166.90, 166.90, 166.86, 143.09, 142.13, 136.47, 136.06, 131.96, 131.13, 130.77, 129.02, 121.75, 120.54, 53.13, 52.21, 52.18, 40.02.

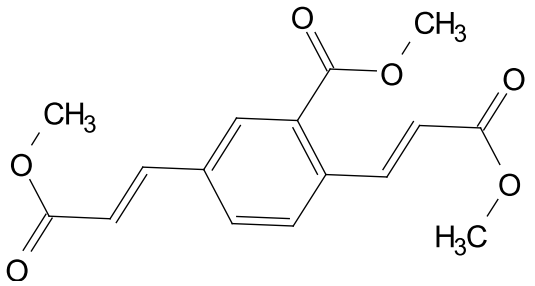

Figure C.19 ^{13}C NMR of BM67 precursor - dimethyl 3,3'-(2-(methoxycarbonyl)-1,4-phenylene) (2*E*,2'*E*)-diacrylate

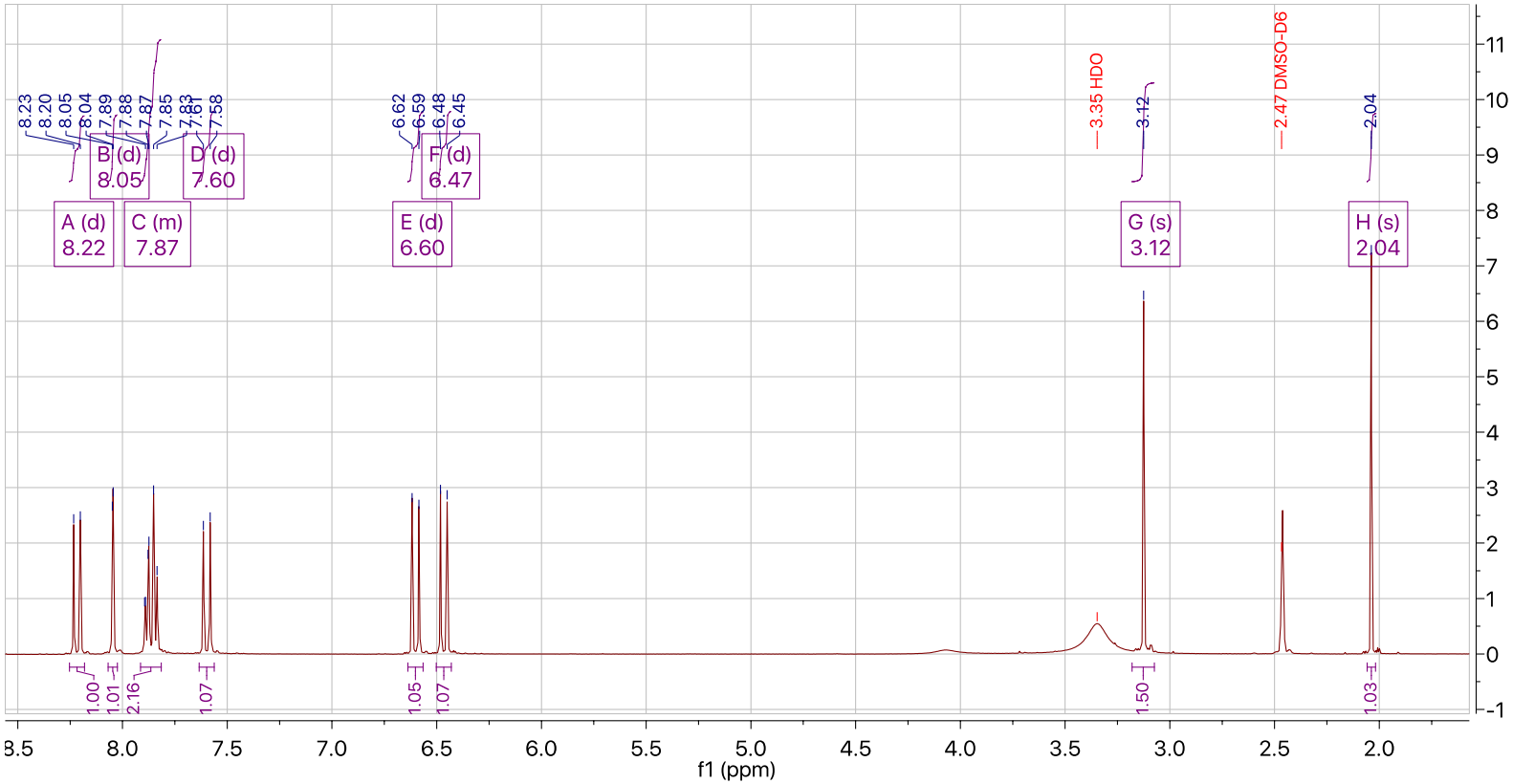

^{1}H NMR (500 MHz, DMSO-d_6) δ 8.22 (d, J = 15.8 Hz, 1H), 8.05 (d, J = 1.9 Hz, 1H), 7.91 – 7.81 (m, 2H), 7.60 (d, J = 16.0 Hz, 1H), 6.60 (d, J = 16.0 Hz, 1H), 6.47 (d, J = 16.0 Hz, 1H), 3.12 (s, 2H), 2.04 (s, 1H).

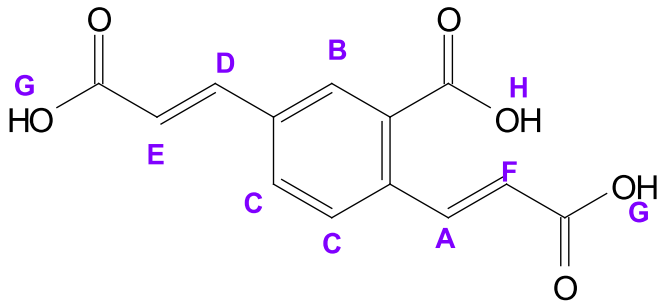

Figure C.20 ^{1}H NMR of BM67 - (2*E*,2'*E*)-3,3'-(2-carboxy-1,4-phenylene) diacrylic acid

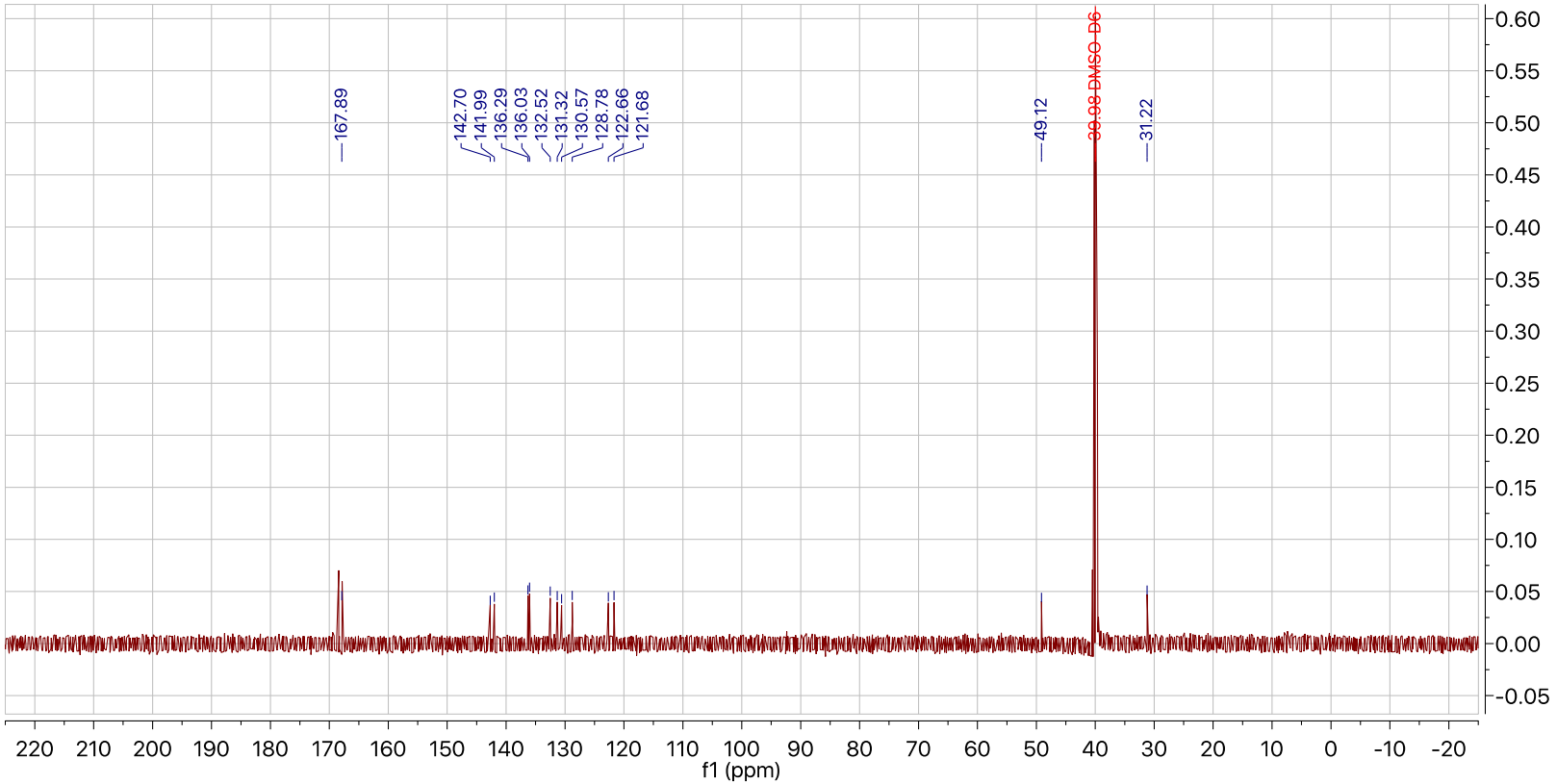

^{13}C NMR (126 MHz, DMSO-D_6) δ 167.89, 142.70, 141.99, 136.29, 136.03, 132.52, 131.32, 130.57, 128.78, 122.66, 121.68, 49.12, 39.98, 31.22.

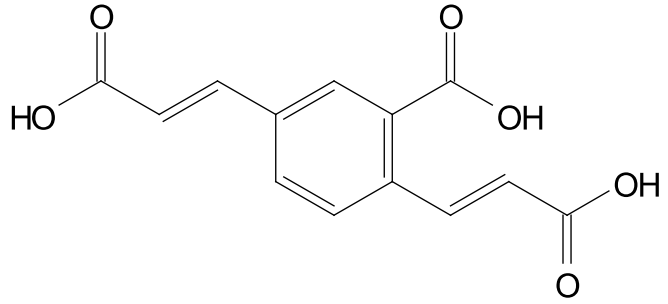

Figure C.21 ^{13}C NMR of BM67 - (2*E*,2'*E*)-3,3'-(2-carboxy-1,4-phenylene) diacrylic acid

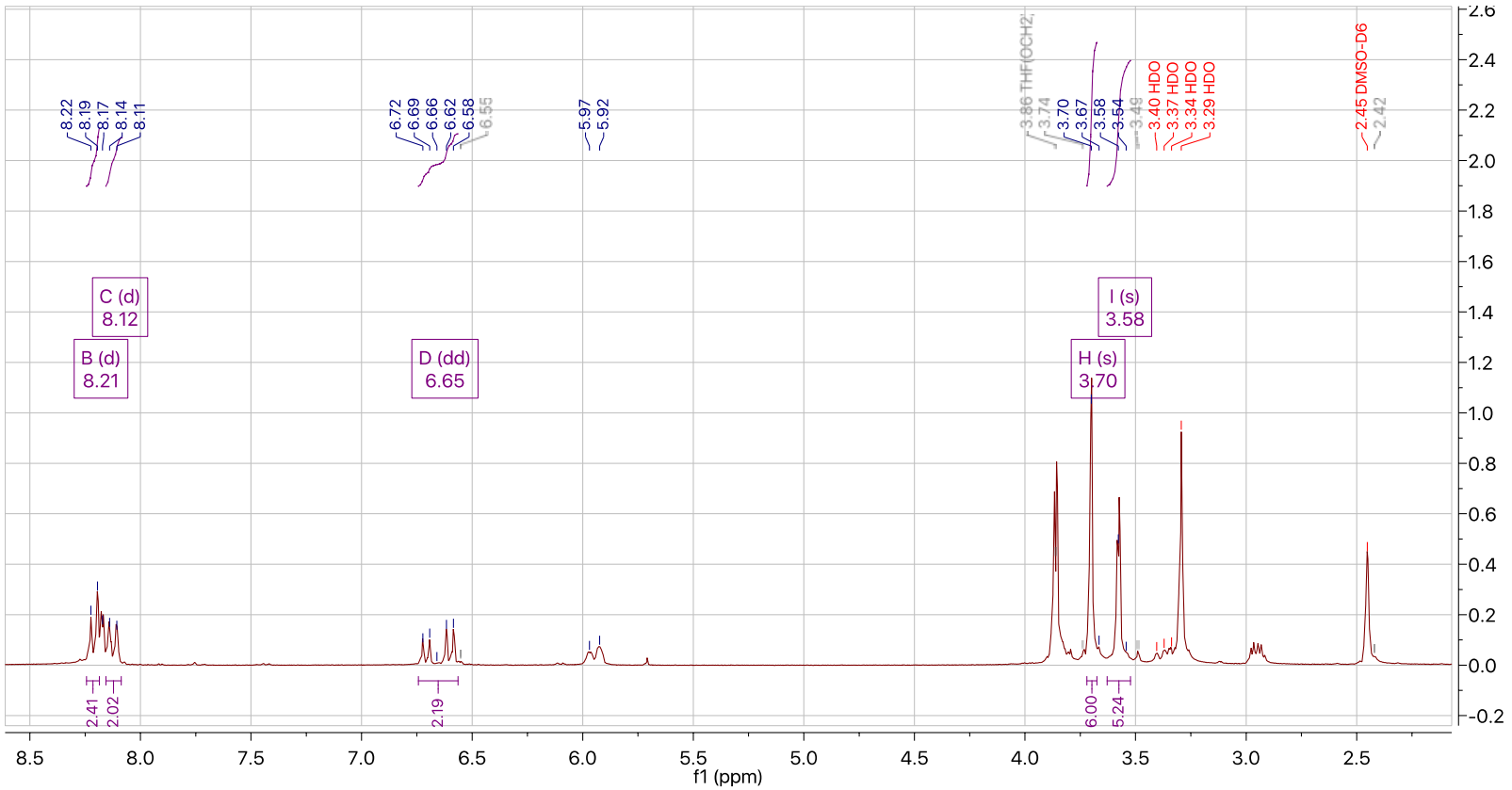

^{1}H NMR (500 MHz, DMSO-d_6) δ 8.21 (d, J = 15.0 Hz, 2H), 8.12 (d, J = 16.0 Hz, 2H), 6.65 (dd, J = 53.5, 15.7 Hz, 2H), 3.70 (s, 6H), 3.58 (s, 6H).

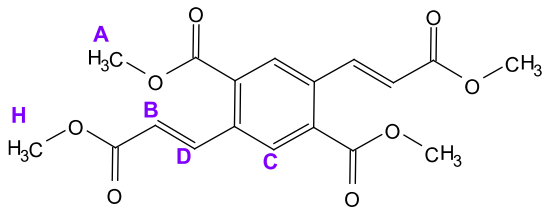

Figure C.22 ^{1}H NMR of BM68 precursors - dimethyl 2,5-bis((*E*)-3-methoxy-3-oxoprop-1-en-1-yl) terephthalate

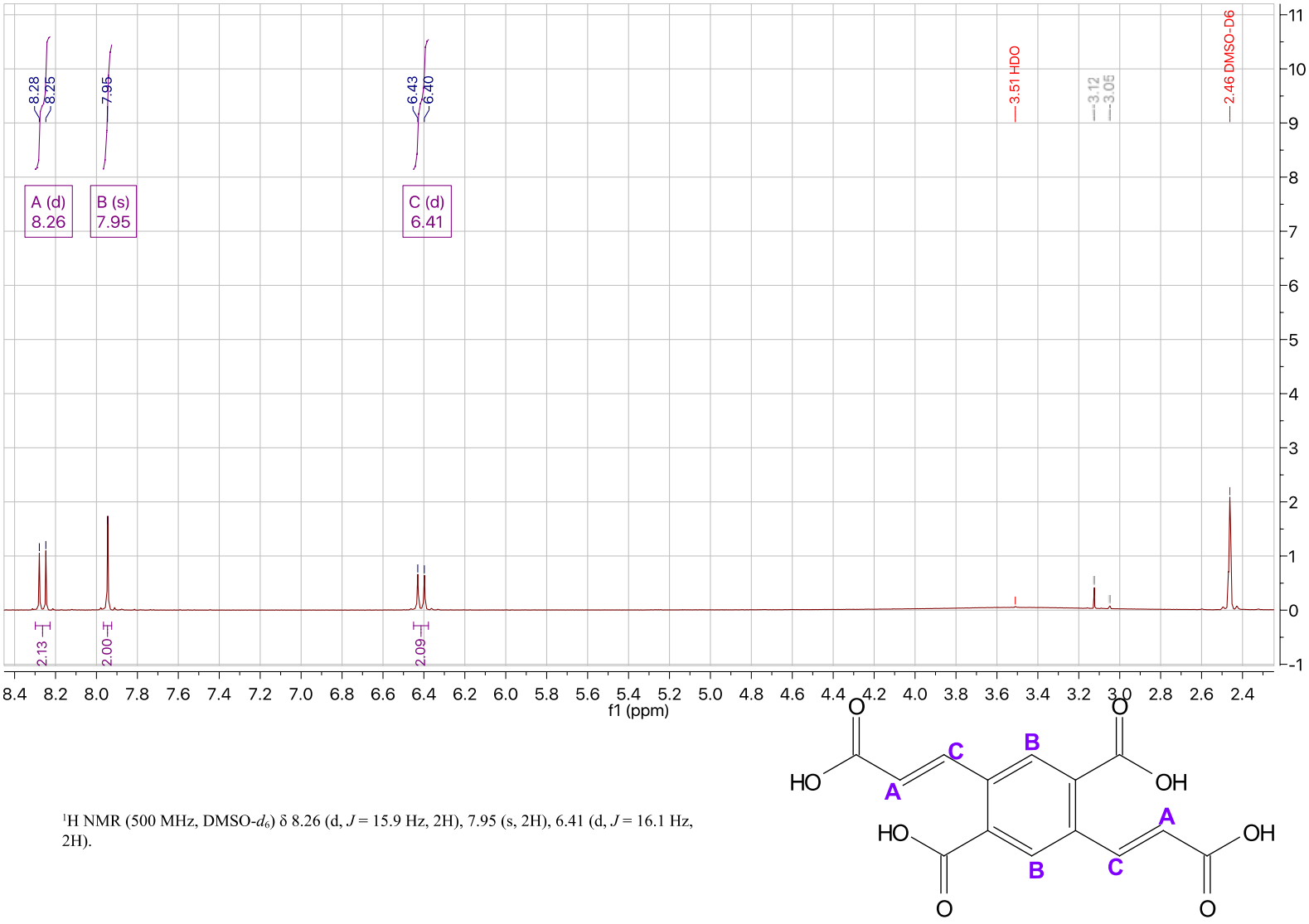

[1]H NMR (500 MHz, DMSO-d_6) δ 8.26 (d, J = 15.9 Hz, 2H), 7.95 (s, 2H), 6.41 (d, J = 16.1 Hz, 2H).

Figure C.23 [1]BM68 - 2,5-bis((*E*)-2-carboxyvinyl) terephthalic acid

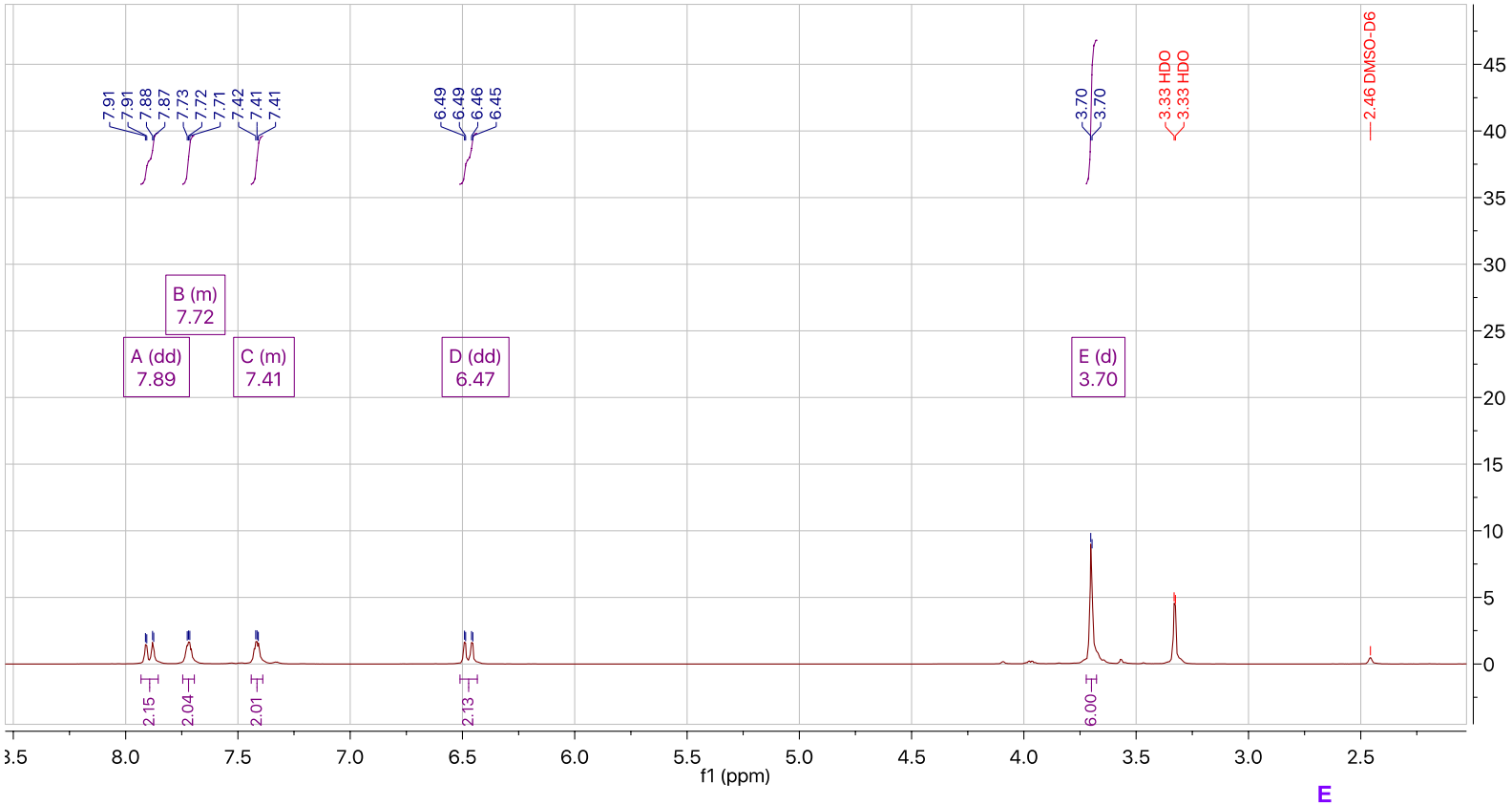

^{1}H NMR (500 MHz, DMSO-d_6) δ 7.89 (dd, J = 15.7, 2.8 Hz, 2H), 7.75 – 7.69 (m, 2H), 7.44 – 7.39 (m, 2H), 6.47 (dd, J = 15.8, 2.9 Hz, 2H), 3.70 (d, J = 2.8 Hz, 6H).

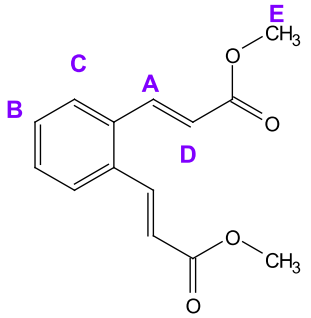

Figure C.24 ^{1}H NMR of BM70 precursor - dimethyl 3,3'-(1,2-phenylene)(2*E*,2'*E*)-diacrylate

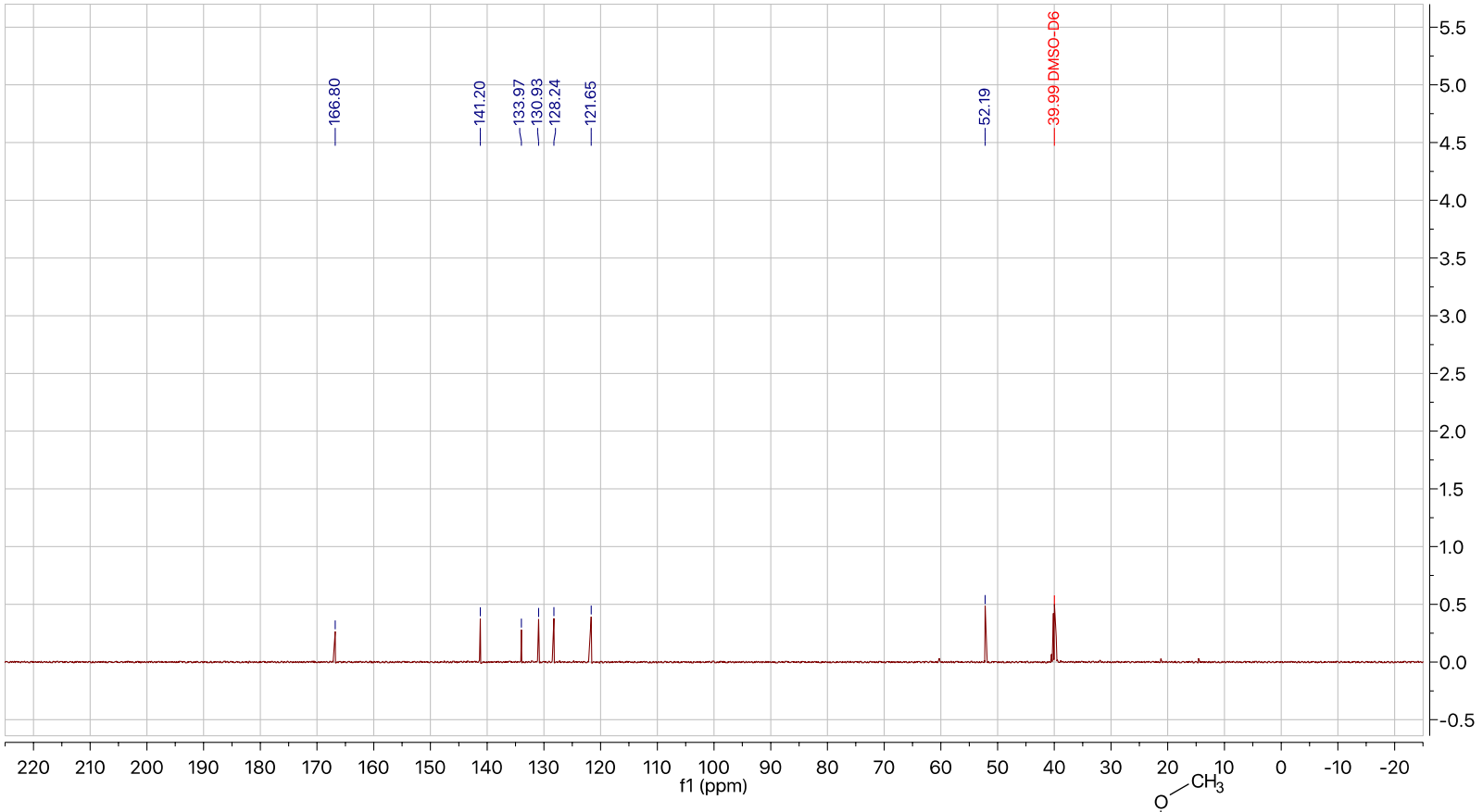

^{13}C NMR (126 MHz, DMSO-D_6) δ 166.80, 141.20, 133.97, 130.93, 128.24, 121.65, 52.19, 39.99.

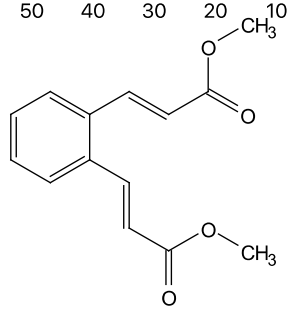

Figure C.25 ^{13}C NMR of BM70 precursor - dimethyl 3,3'-(1,2-phenylene)(2*E*,2'*E*)-diacrylate

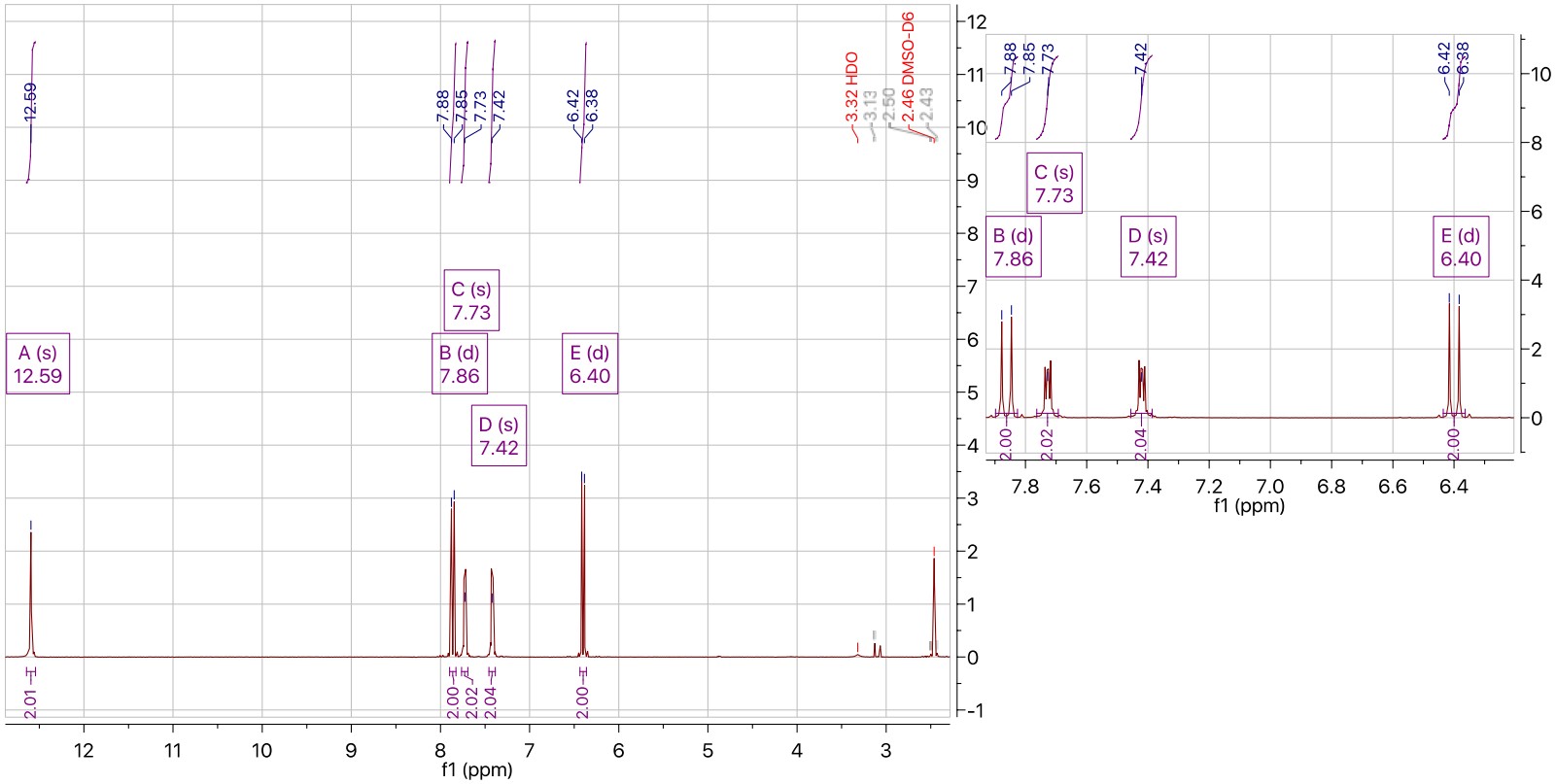

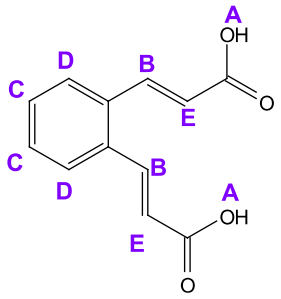

^{1}H NMR (500 MHz, DMSO-d_6) δ 12.59 (s, 2H), 7.86 (d, J = 15.9 Hz, 2H), 7.73 (s, 2H), 7.42 (s, 2H), 6.40 (d, J = 15.9 Hz, 2H).

Figure C.26 ^{1}H NMR of BM70 - (2*E*,2'*E*)-3,3'-(1,2-phenylene) diacrylic acid

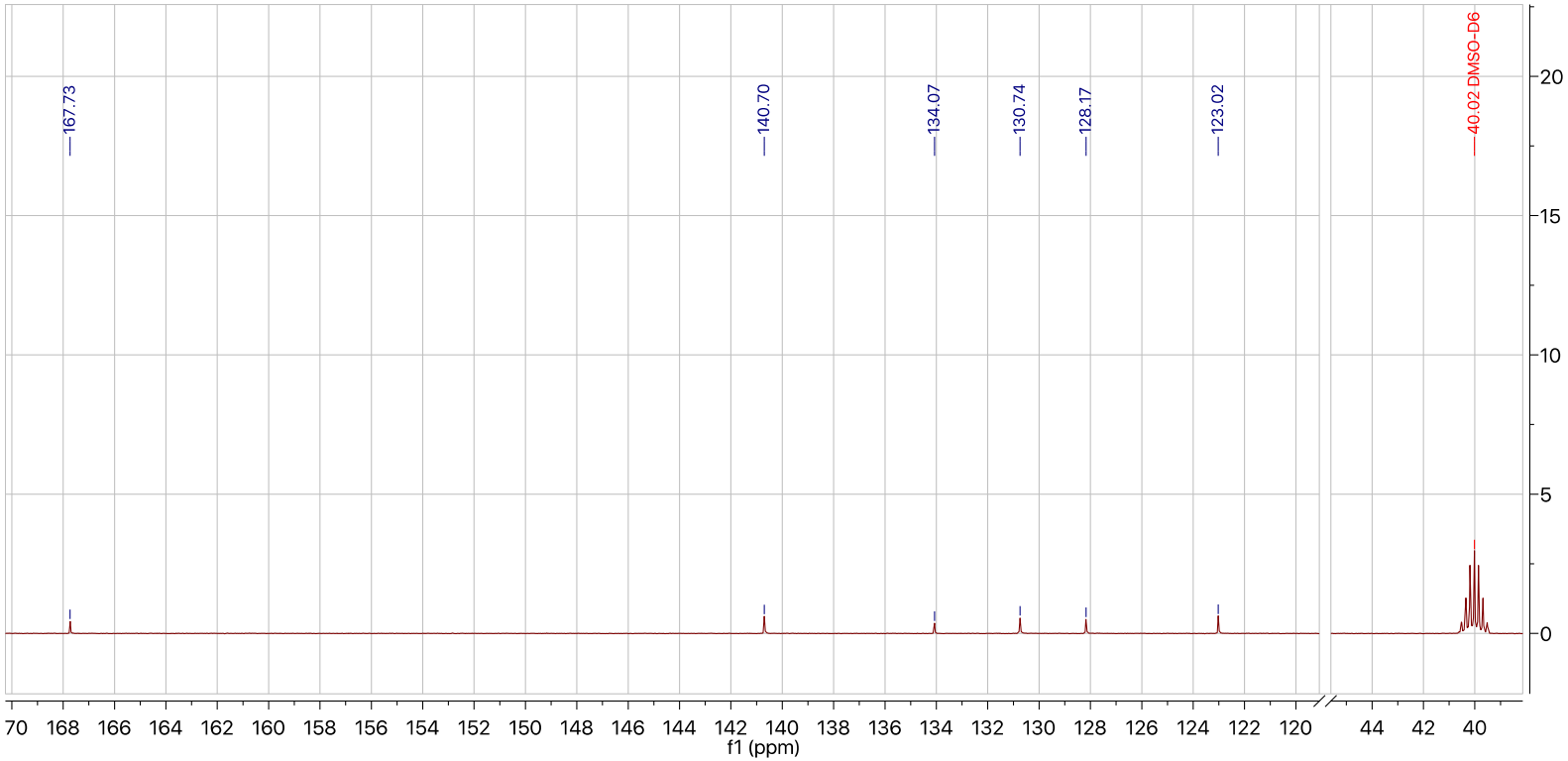

^{13}C NMR (126 MHz, DMSO-D_6) δ 167.73, 140.70, 134.07, 130.74, 128.17, 123.02, 40.02.

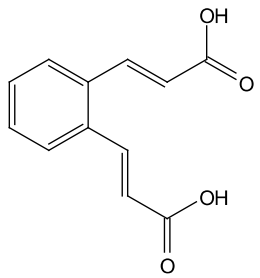

Figure C.27 ^{13}C NMR of BM70 - (2*E*,2'*E*)-3,3'-(1,2-phenylene) diacrylic acid

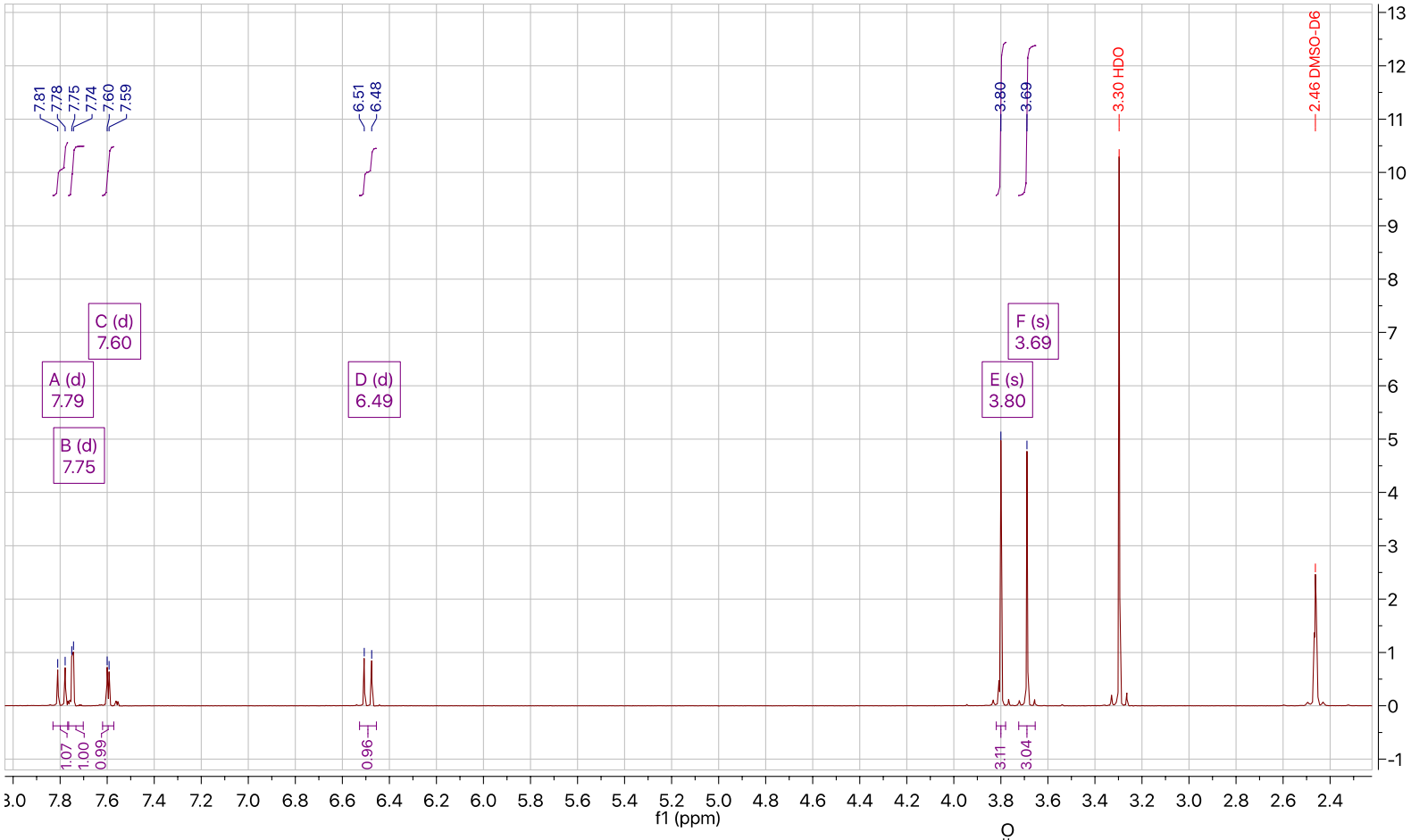

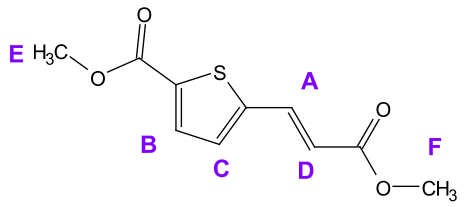

^{1}H NMR (500 MHz, DMSO-d_6) δ 7.79 (d, J = 15.9 Hz, 1H), 7.75 (d, J = 3.9 Hz, 1H), 7.60 (d, J = 4.0 Hz, 1H), 6.49 (d, J = 15.9 Hz, 1H), 3.80 (s, 3H), 3.69 (s, 3H).

Figure C.28 ^{1}H NMR of BM72 - precursor - methyl (*E*)-5-(3-methoxy-3-oxoprop-1-en-1-yl)thiophene-2-carboxylate

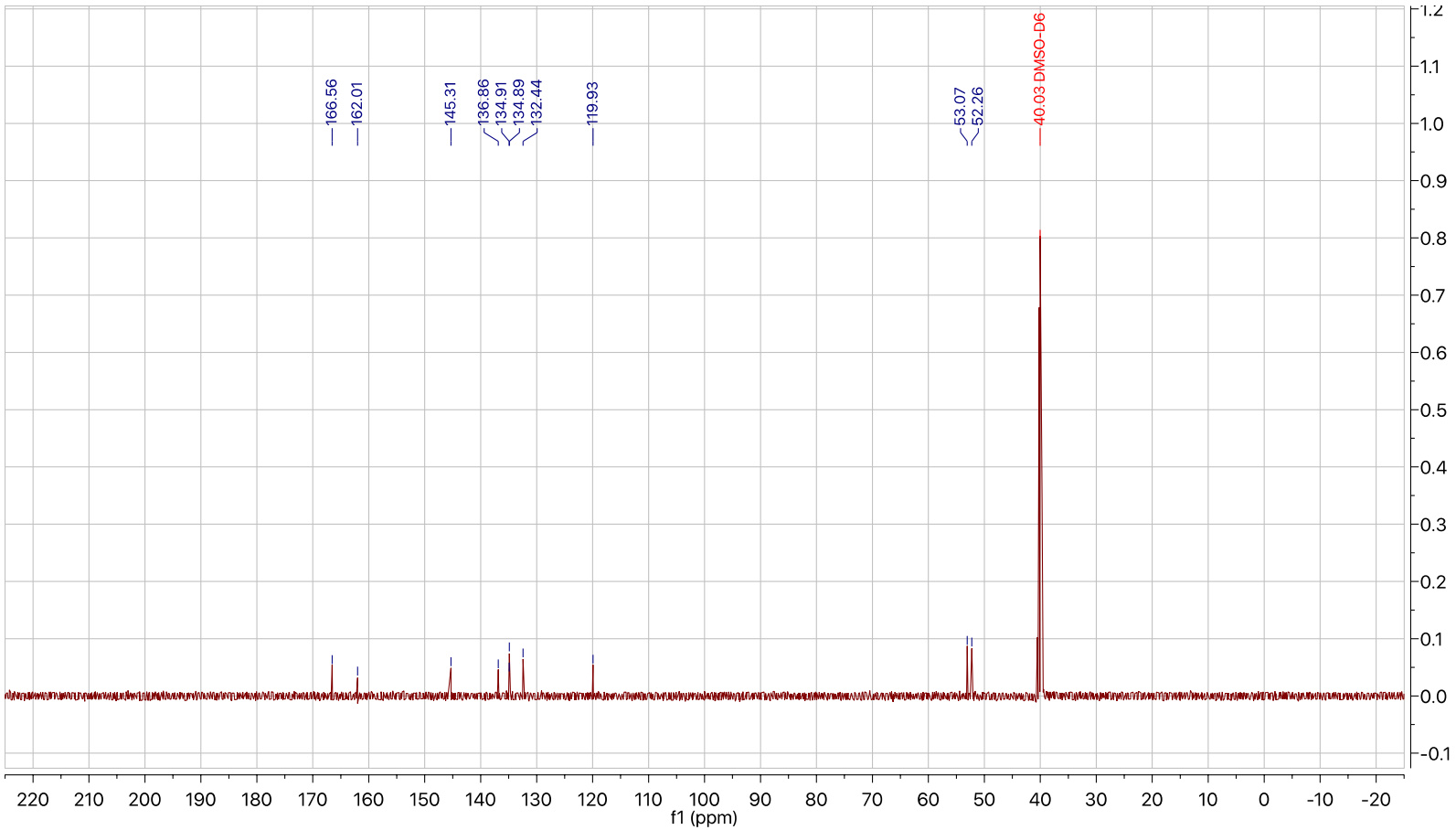

^{13}C NMR (126 MHz, DMSO-D_6) δ 166.56, 162.01, 145.31, 136.86, 134.91, 134.89, 132.44, 119.93, 53.07, 52.26, 40.03.

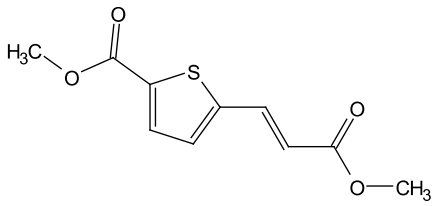

Figure C.29 ^{13}C NMR of BM72 - precursor - methyl (*E*)-5-(3-methoxy-3-oxoprop-1-en-1-yl) thiophene-2-carboxylate

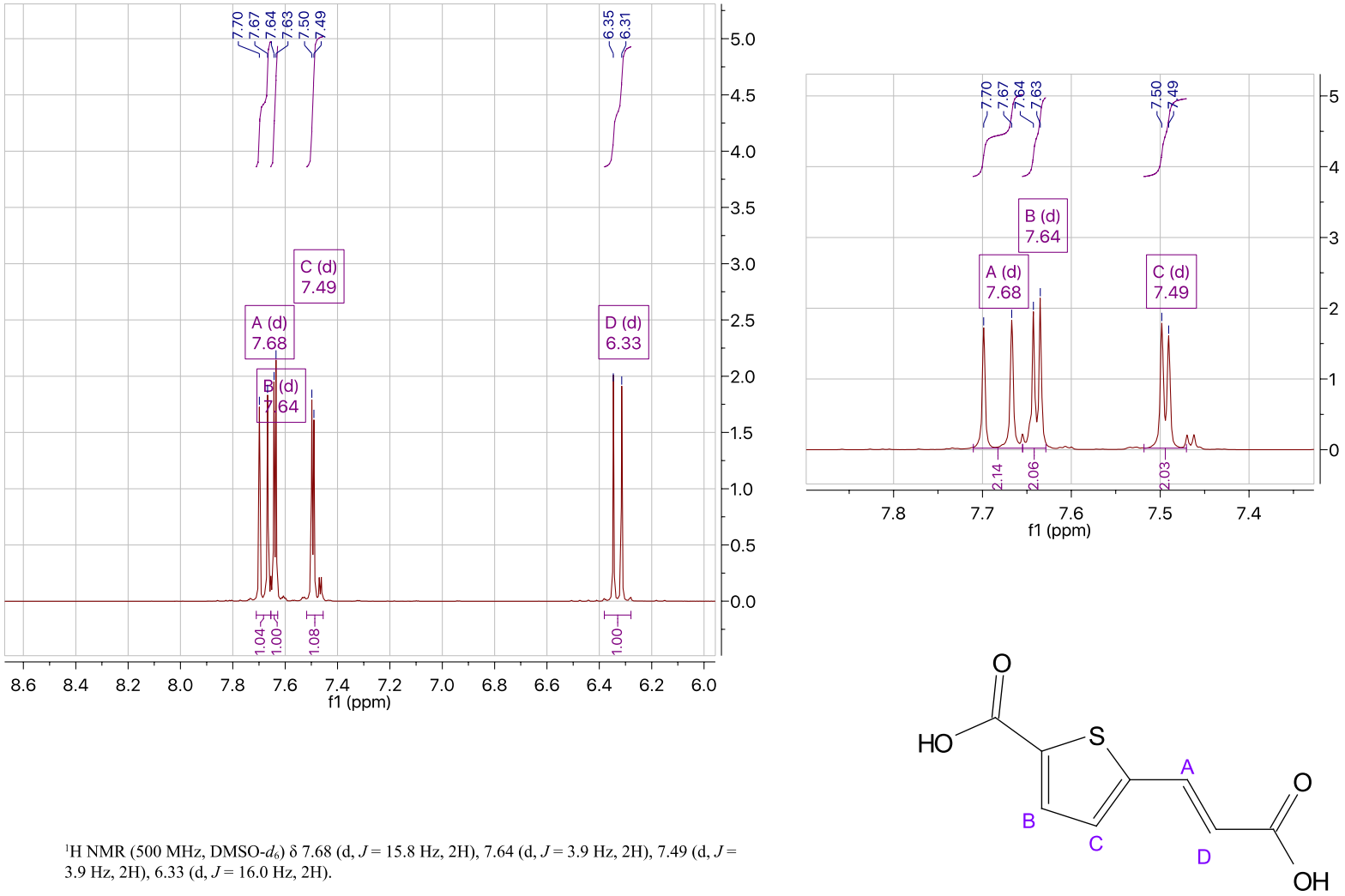

^{1}H NMR (500 MHz, DMSO-d_6) δ 7.68 (d, J = 15.8 Hz, 2H), 7.64 (d, J = 3.9 Hz, 2H), 7.49 (d, J = 3.9 Hz, 2H), 6.33 (d, J = 16.0 Hz, 2H).

Figure C.30 ^{1}H NMR of BM72 - (*E*)-5-(2-carboxyvinyl) thiophene-2-carboxylic acid

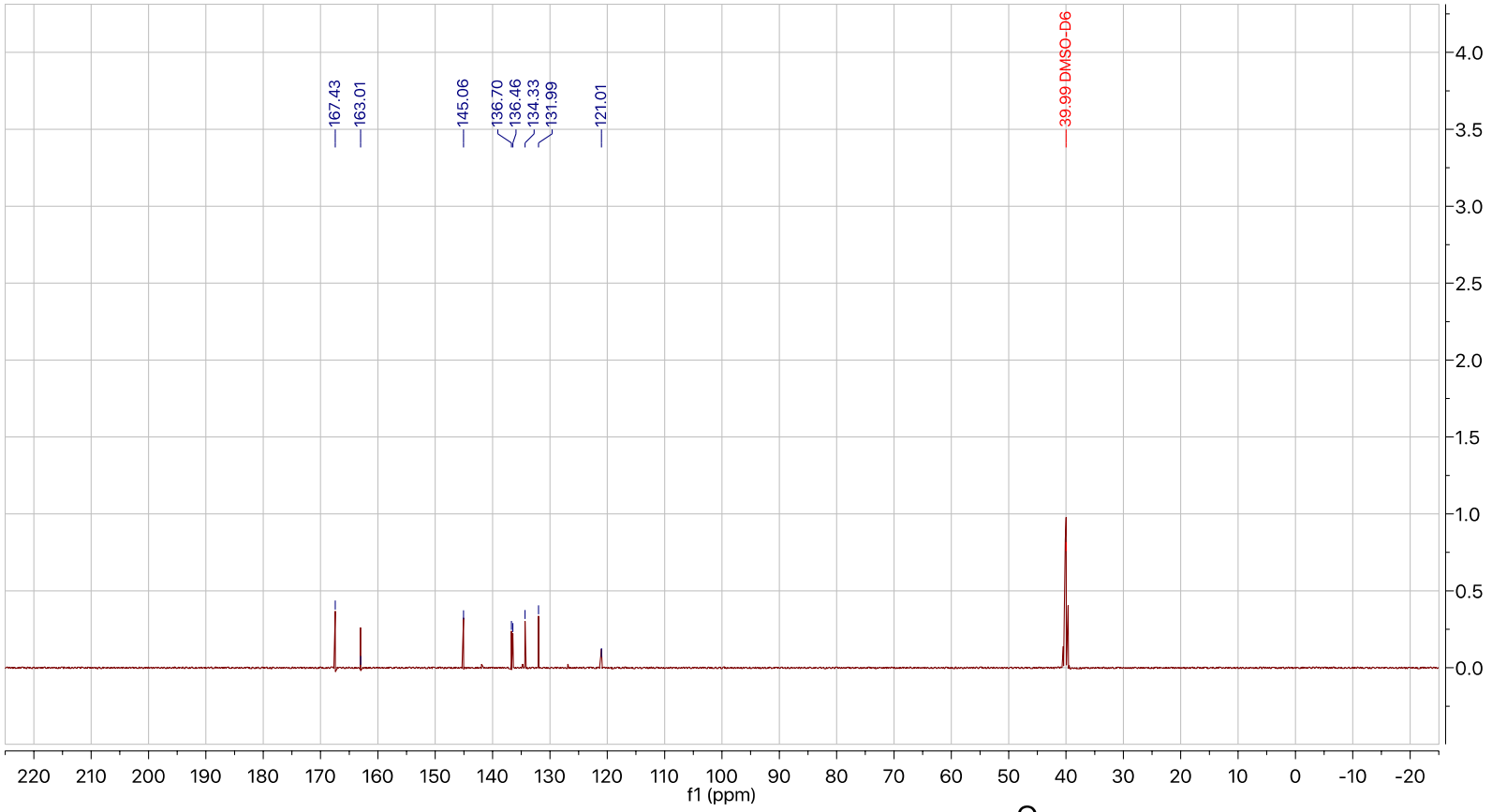

^{13}C NMR (126 MHz, DMSO-D_6) δ 167.43, 163.01, 145.06, 136.70, 136.46, 134.33, 131.99, 121.01, 39.99.

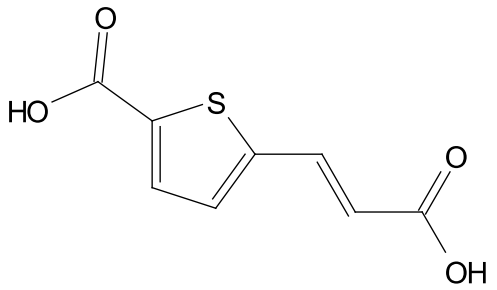

Figure C.31 ^{13}C NMR of BM72 - (*E*)-5-(2-carboxyvinyl) thiophene-2-carboxylic acid

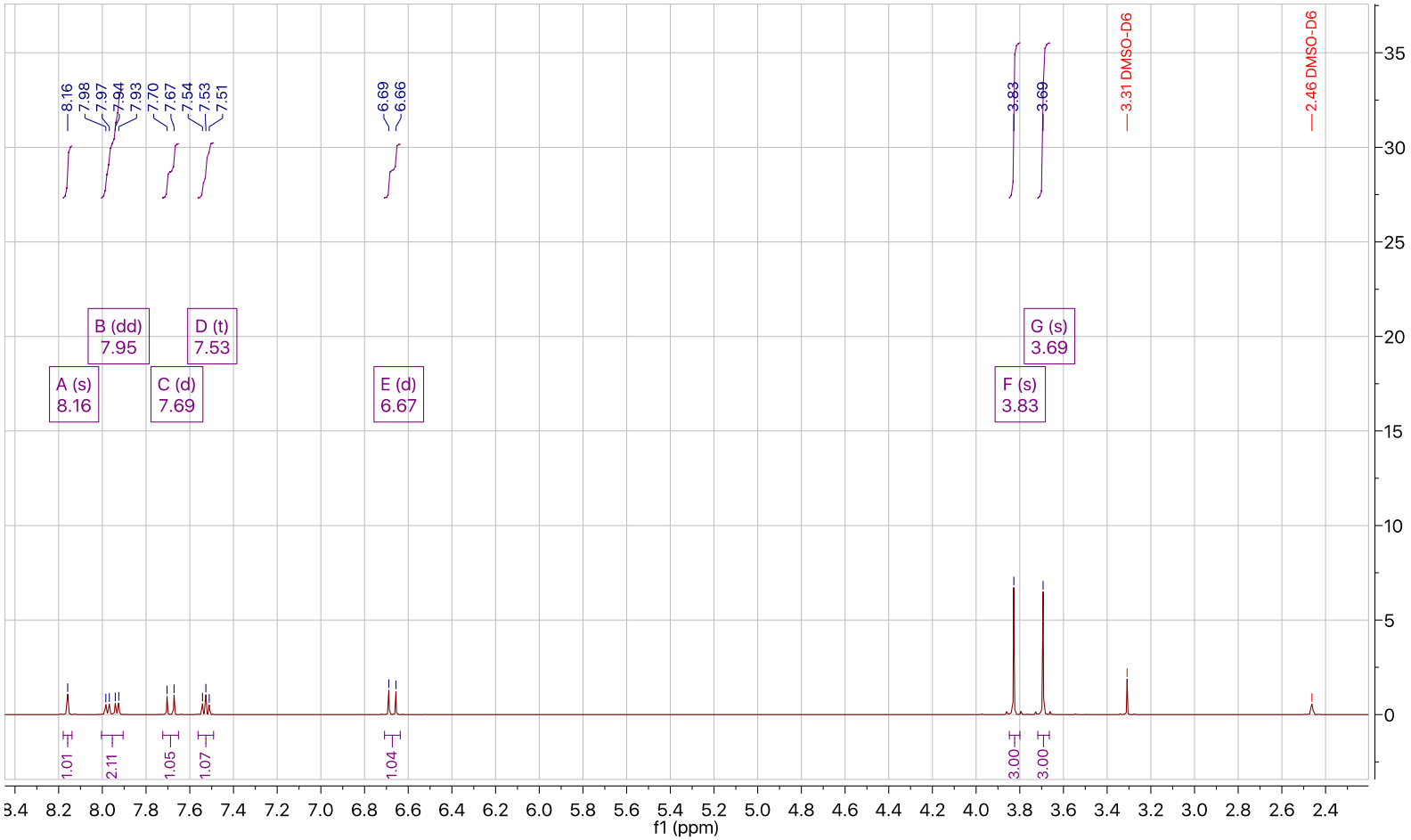

^{1}H NMR (500 MHz, DMSO-d_6) δ 8.16 (s, 1H), 7.95 (dd, J = 21.6, 7.8 Hz, 2H), 7.69 (d, J = 16.1 Hz, 1H), 7.53 (t, J = 7.8 Hz, 1H), 6.67 (d, J = 16.1 Hz, 1H), 3.83 (s, 3H), 3.69 (s, 3H).

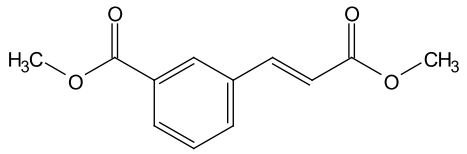

Figure C.32 ^{1}H NMR of BM73 precursor - methyl (*E*)-3-(3-methoxy-3-oxoprop-1-en-1-yl) benzoate

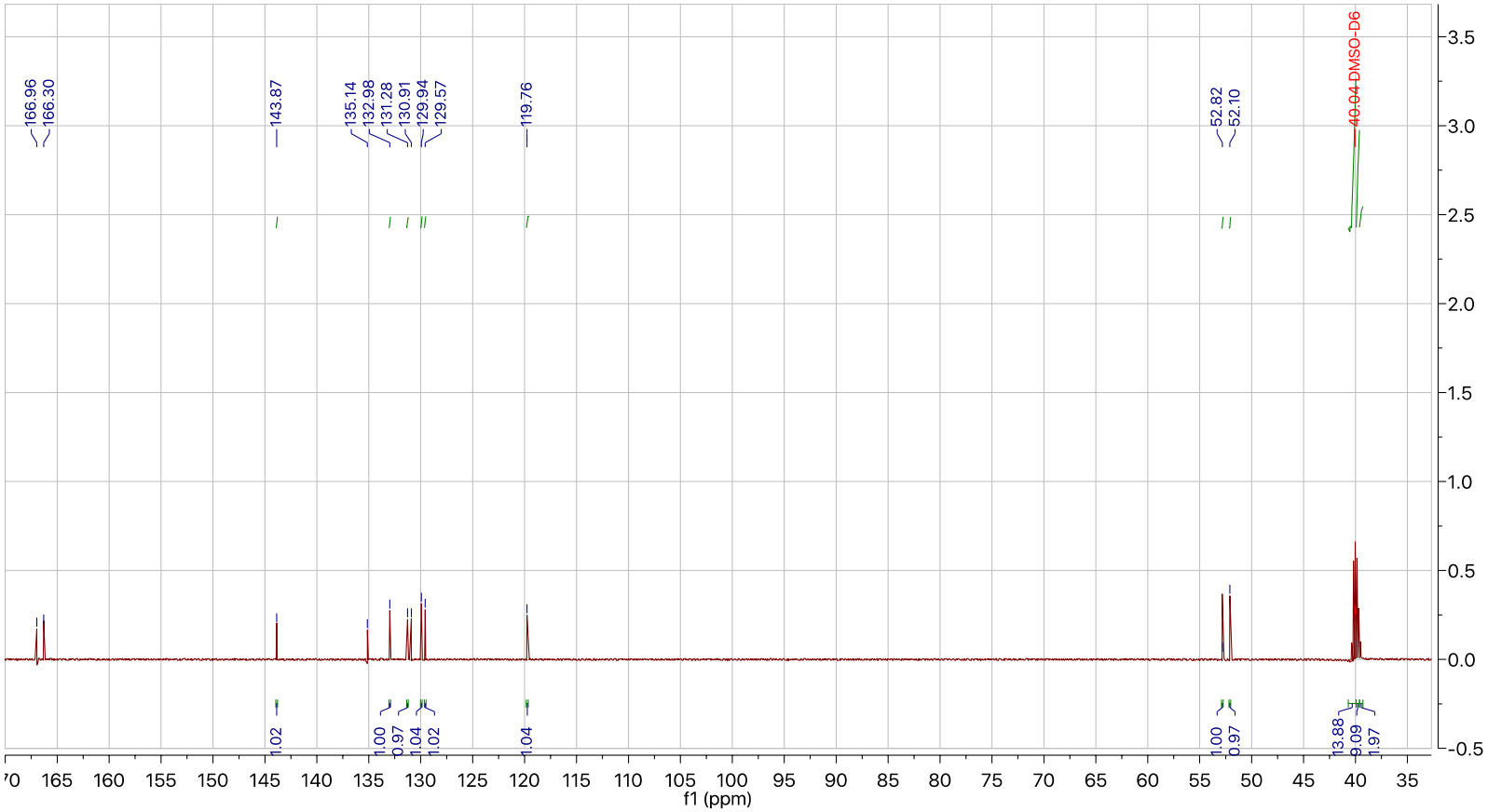

^{13}C NMR (126 MHz, DMSO-D_6) δ 166.96, 166.30, 143.87, 135.14, 132.98, 131.28, 130.91, 129.94, 129.57, 119.76, 52.82, 52.10, 40.04.

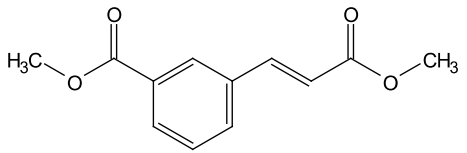

Figure C.33 ^{13}C NMR of BM73 – precursor - methyl (*E*)-3-(3-methoxy-3-oxoprop-1-en-1-yl) benzoate

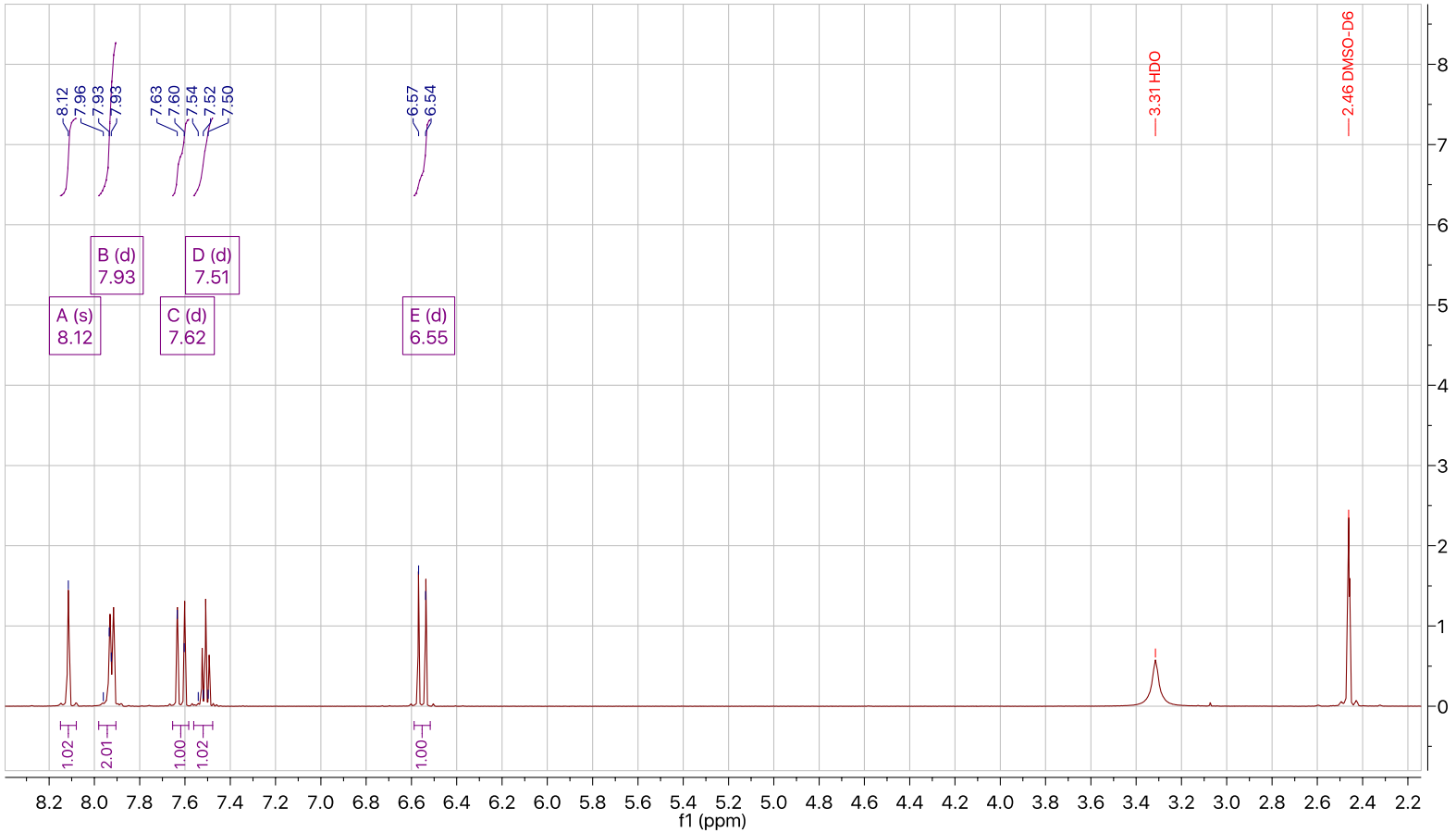

^{1}H NMR (500 MHz, DMSO-d_6) δ 8.12 (s, 1H), 7.93 (d, J = 4.6 Hz, 2H), 7.62 (d, J = 15.5 Hz, 1H), 7.51 (d, J = 10.8 Hz, 1H), 6.55 (d, J = 15.6 Hz, 1H).

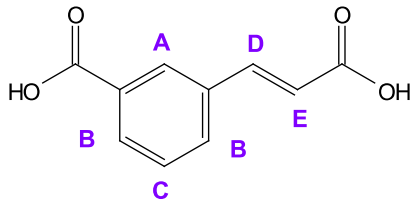

Figure C.34 ^{1}H NMR of BM73 - (*E*)-3-(2-carboxyvinyl) benzoic acid

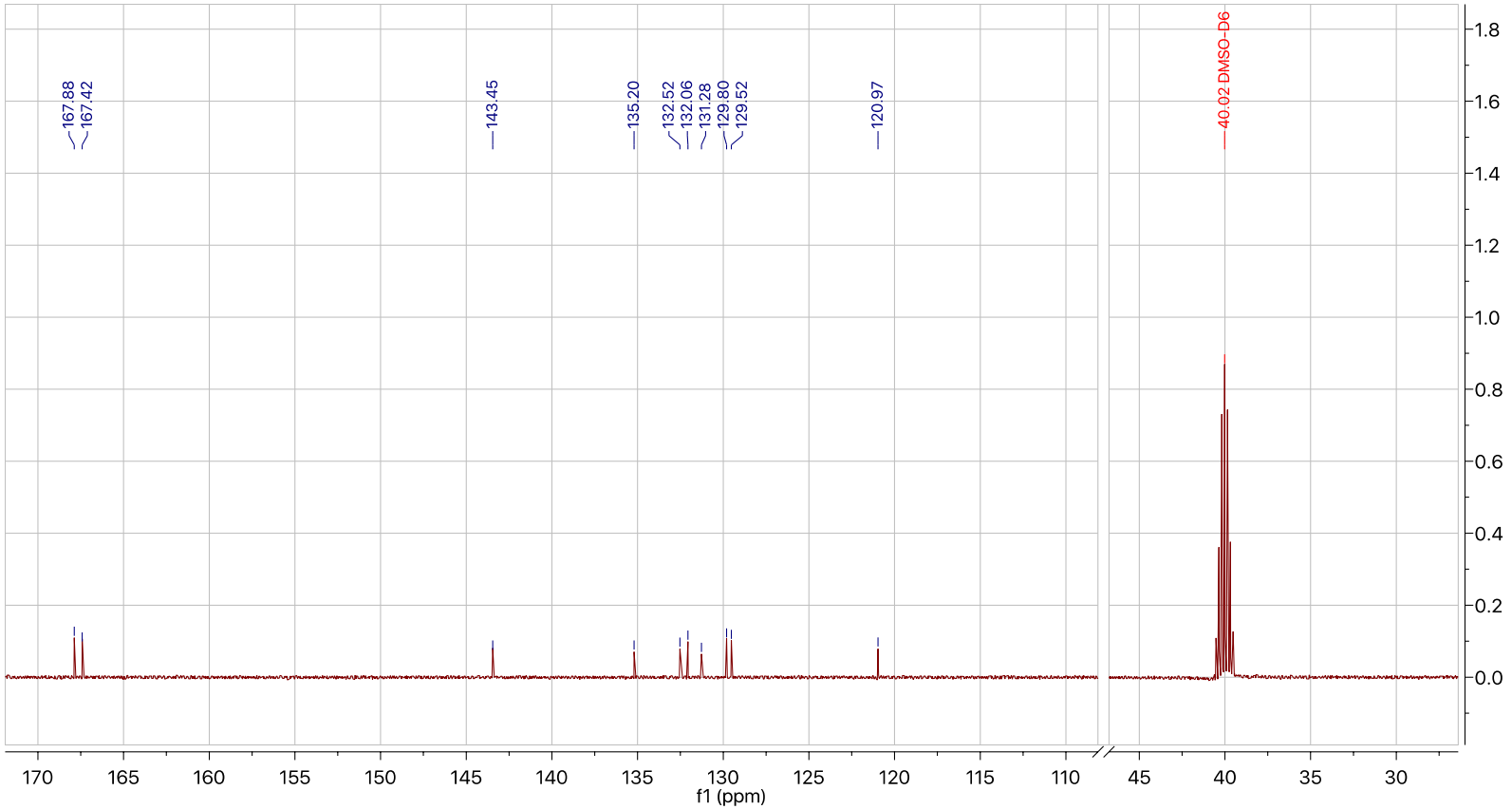

^{13}C NMR (126 MHz, DMSO-D_6) δ 167.88, 167.42, 143.45, 135.20, 132.52, 132.06, 131.28, 129.80, 129.52, 120.97, 40.02.

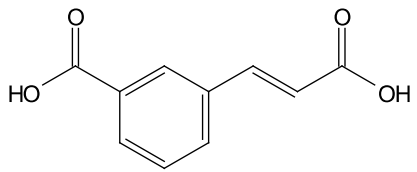

Figure C.35 ^{13}C NMR of BM73 - (*E*)-3-(2-carboxyvinyl) benzoic acid

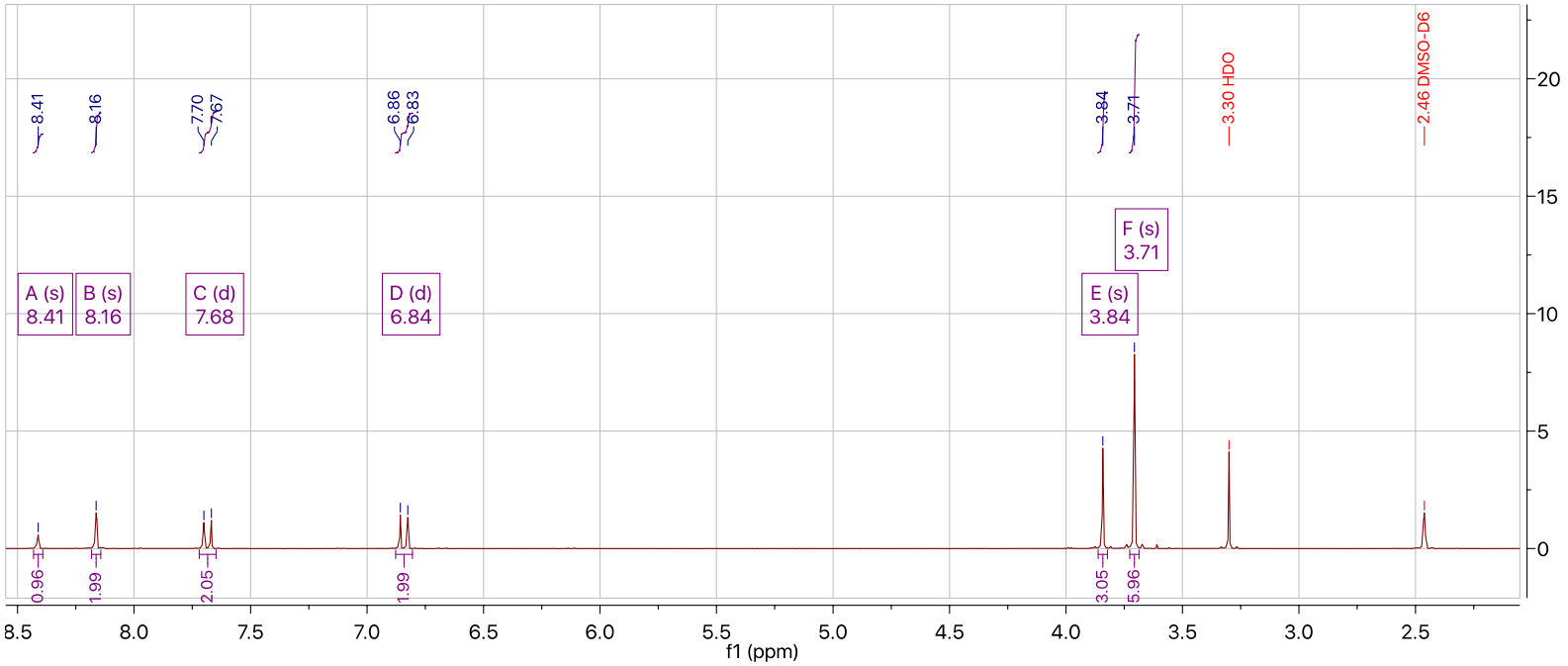

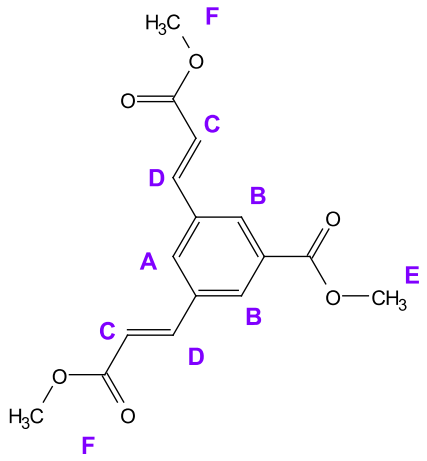

^{1}H NMR (500 MHz, DMSO-d_6) δ 8.41 (s, 1H), 8.16 (s, 2H), 7.68 (d, J = 16.1 Hz, 2H), 6.84 (d, J = 16.1 Hz, 2H), 3.84 (s, 3H), 3.71 (s, 6H).

Figure C.36 ^{1}H NMR of BM74 precursor - dimethyl 3,3'-(5-(methoxycarbonyl)-1,3-phenylene)(2*E*,2'*E*)-diacrylate

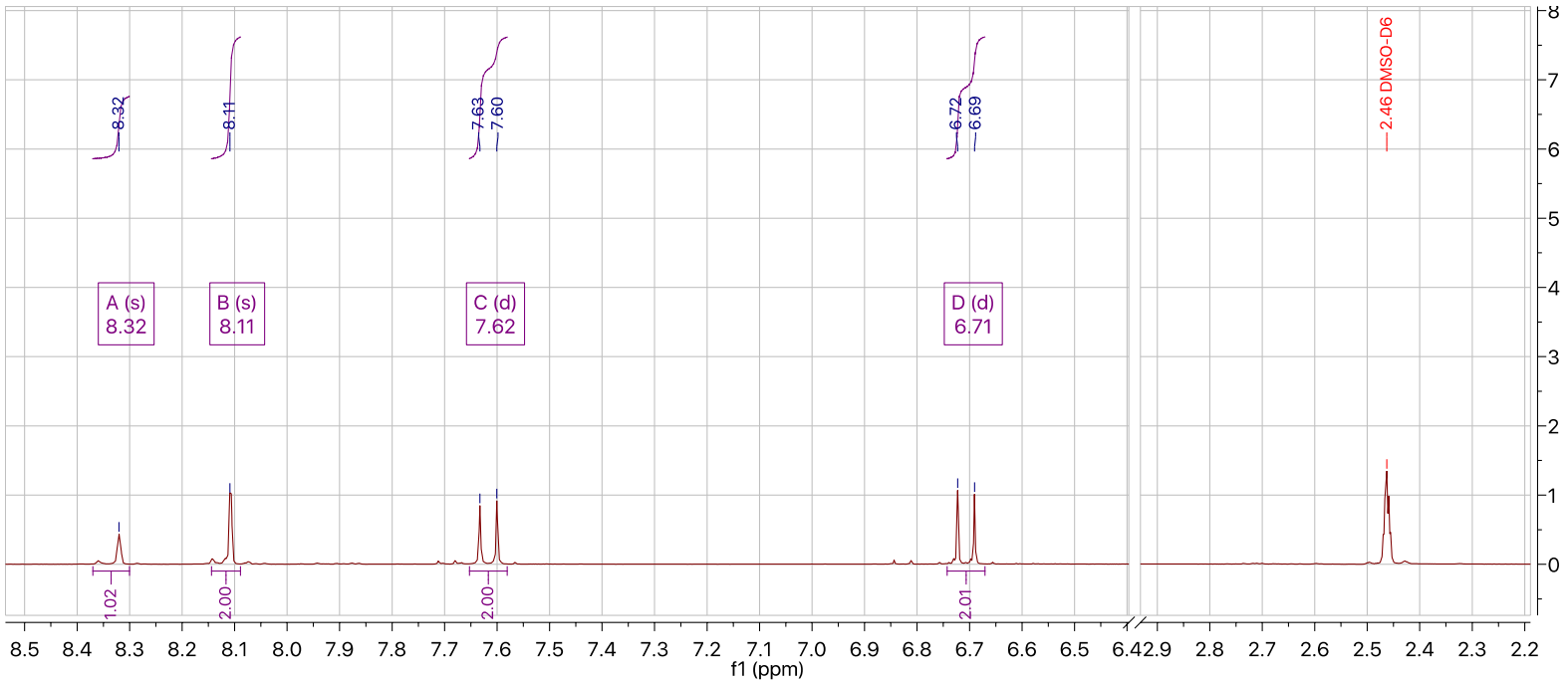

^{1}H NMR (500 MHz, DMSO-d_6) δ 8.32 (s, 1H), 8.11 (s, 2H), 7.62 (d, J = 16.0 Hz, 2H), 6.71 (d, J = 16.1 Hz, 2H).

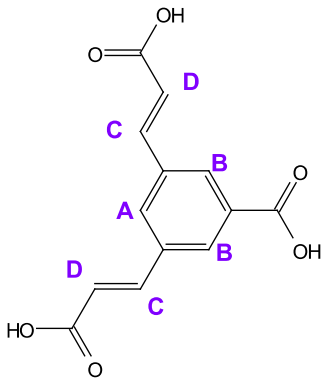

Figure C.37 ^{1}H NMR of BM74 - (2*E*,2'*E*)-3,3'-(5-carboxy-1,3-phenylene) diacrylic acid

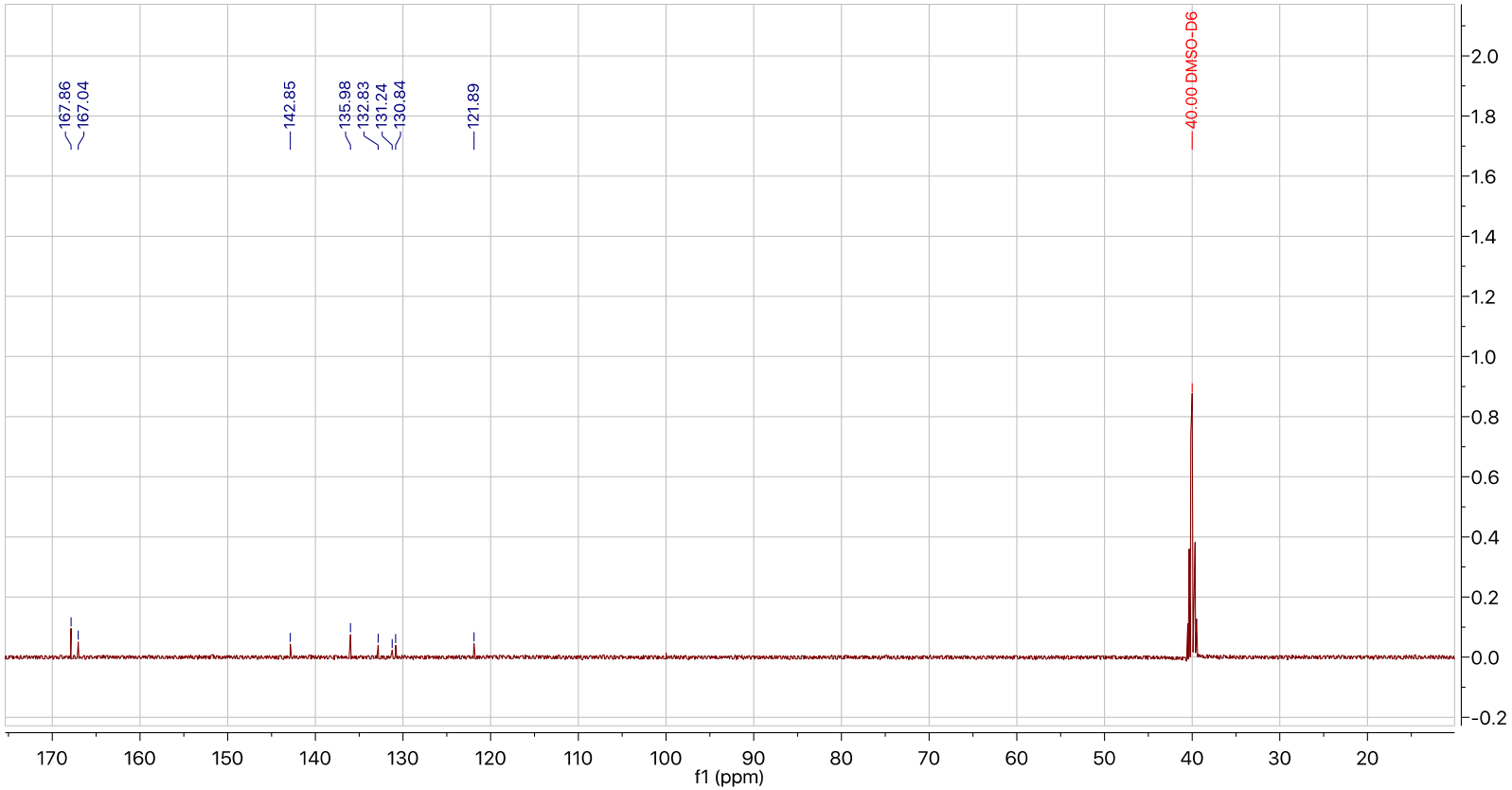

^{13}C NMR (126 MHz, DMSO-D_6) δ 167.86, 167.04, 142.85, 135.98, 132.83, 131.24, 130.84, 121.89, 40.00.

Figure C.38 ^{13}C NMR of BM74 - (2*E*,2'*E*)-3,3'-(5-carboxy-1,3-phenylene) diacrylic acid

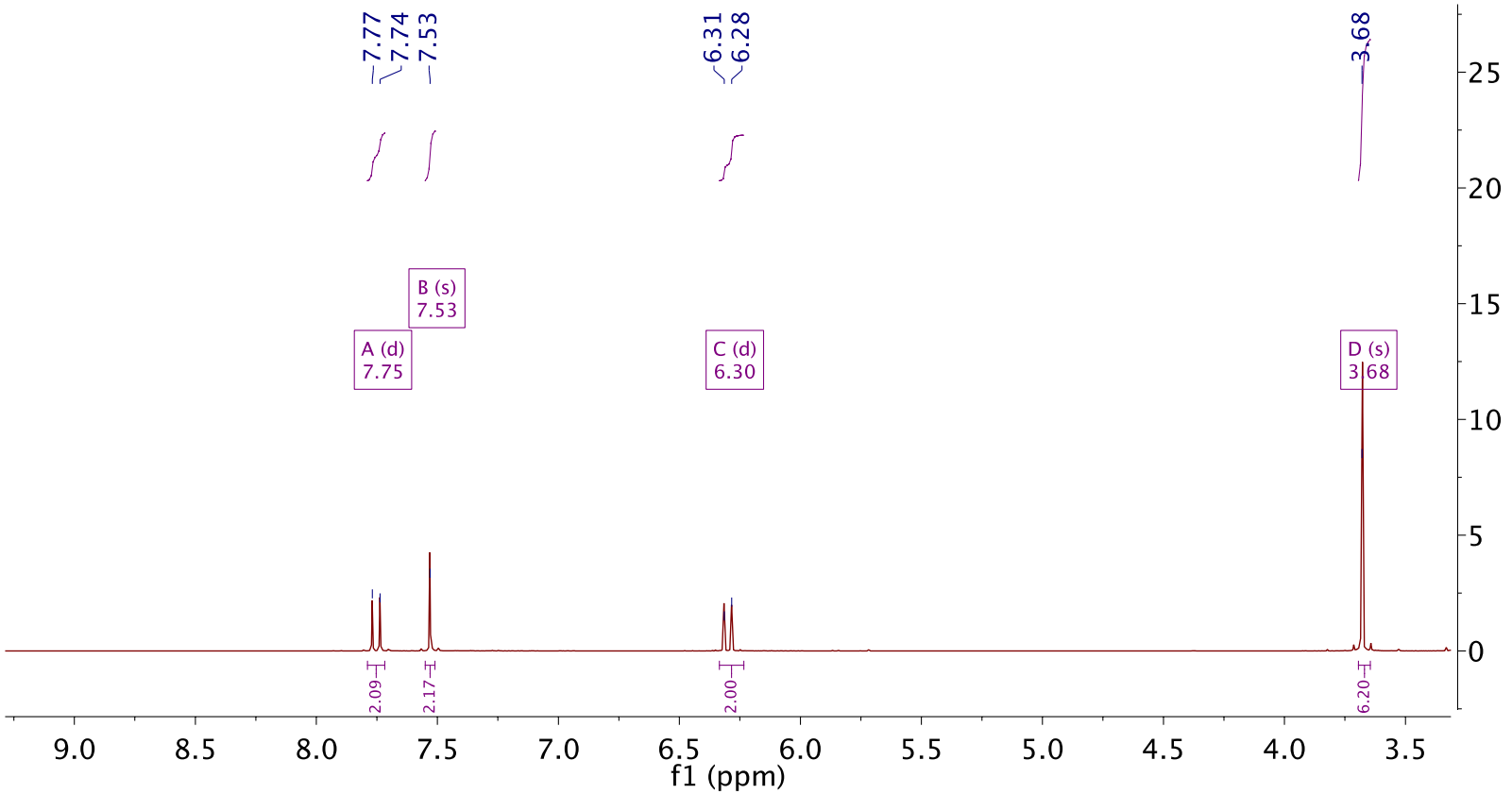

^{1}H NMR (500 MHz, DMSO-d_6) δ 7.75 (d, J = 16.0 Hz, 2H), 7.53 (s, 2H), 6.30 (d, J = 15.4 Hz, 2H), 3.68 (s, 6H).

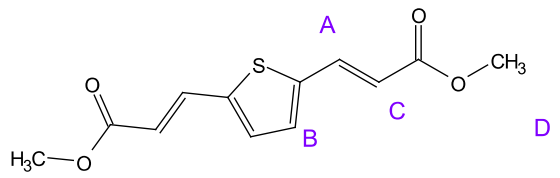

Figure C.39 ^{1}H NMR of JB03- precursor - dimethyl 3,3'-(thiophene-2,5-diyl)(2E,2'E)-diacrylate

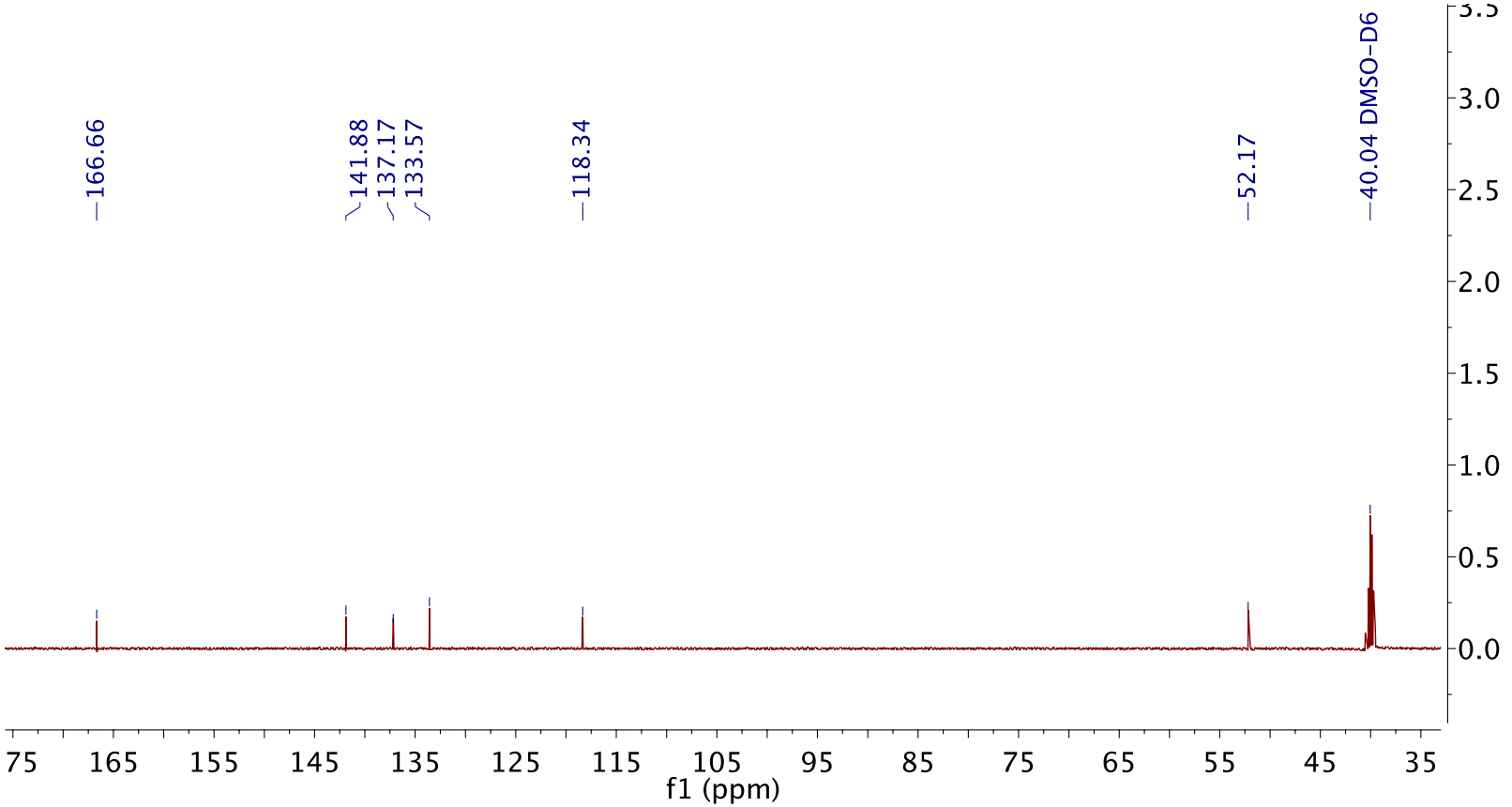

^{13}C NMR (126 MHz, DMSO-D_6) δ 166.66, 141.88, 137.17, 133.57, 118.34, 52.17, 40.04.

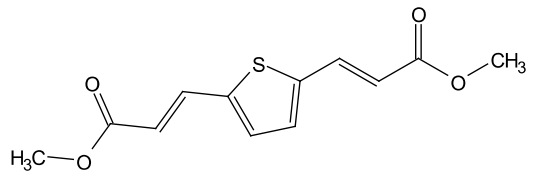

Figure C.40 ^{13}C NMR of JB03- precursor - dimethyl 3,3'-(thiophene-2,5-diyl)(2E,2'E)-diacrylate

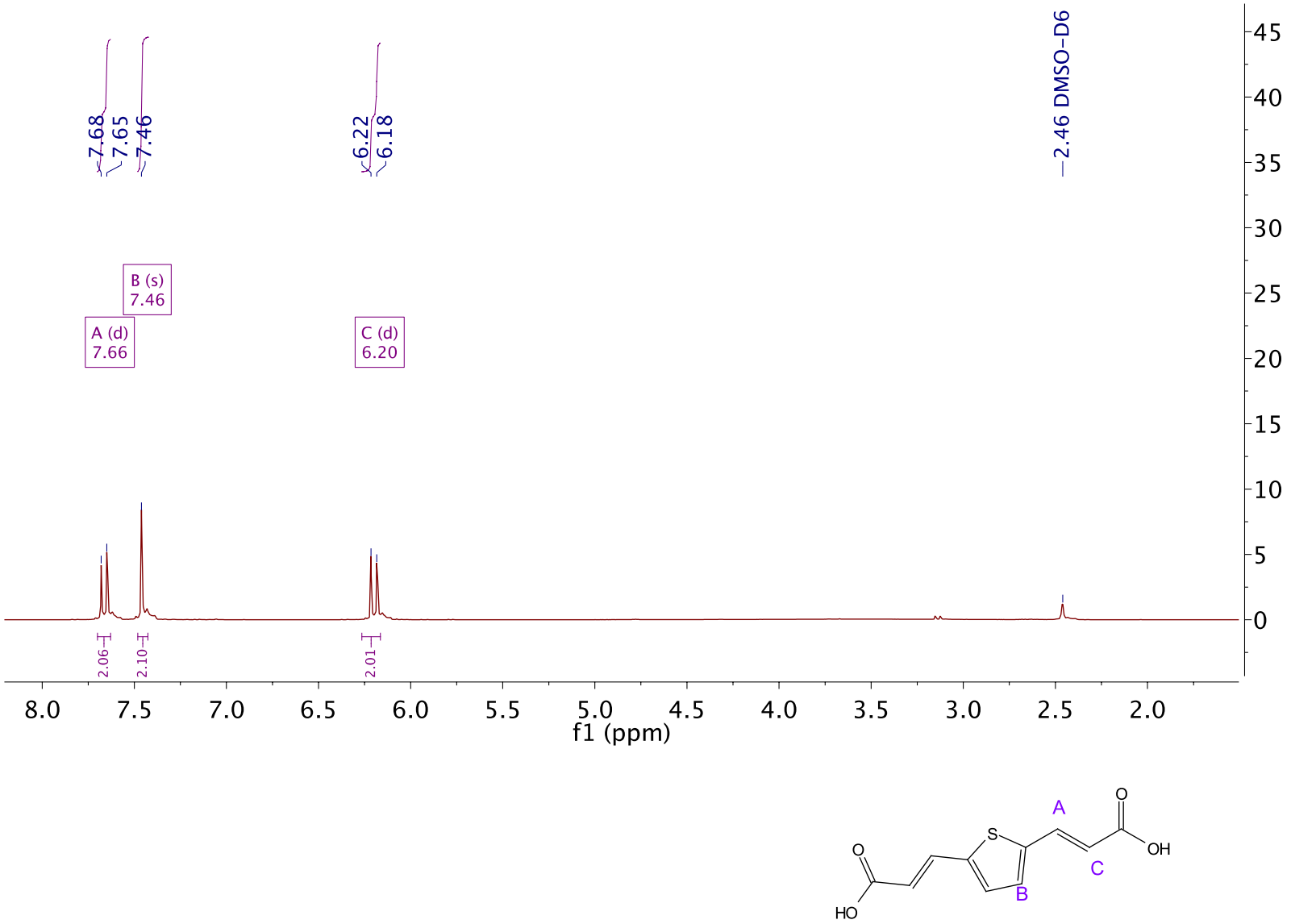

Figure C.41 ^{1}H NMR of JB03 - (2*E*,2'*E*)-3,3'-(thiophene-2,5-diyl) diacrylic acid

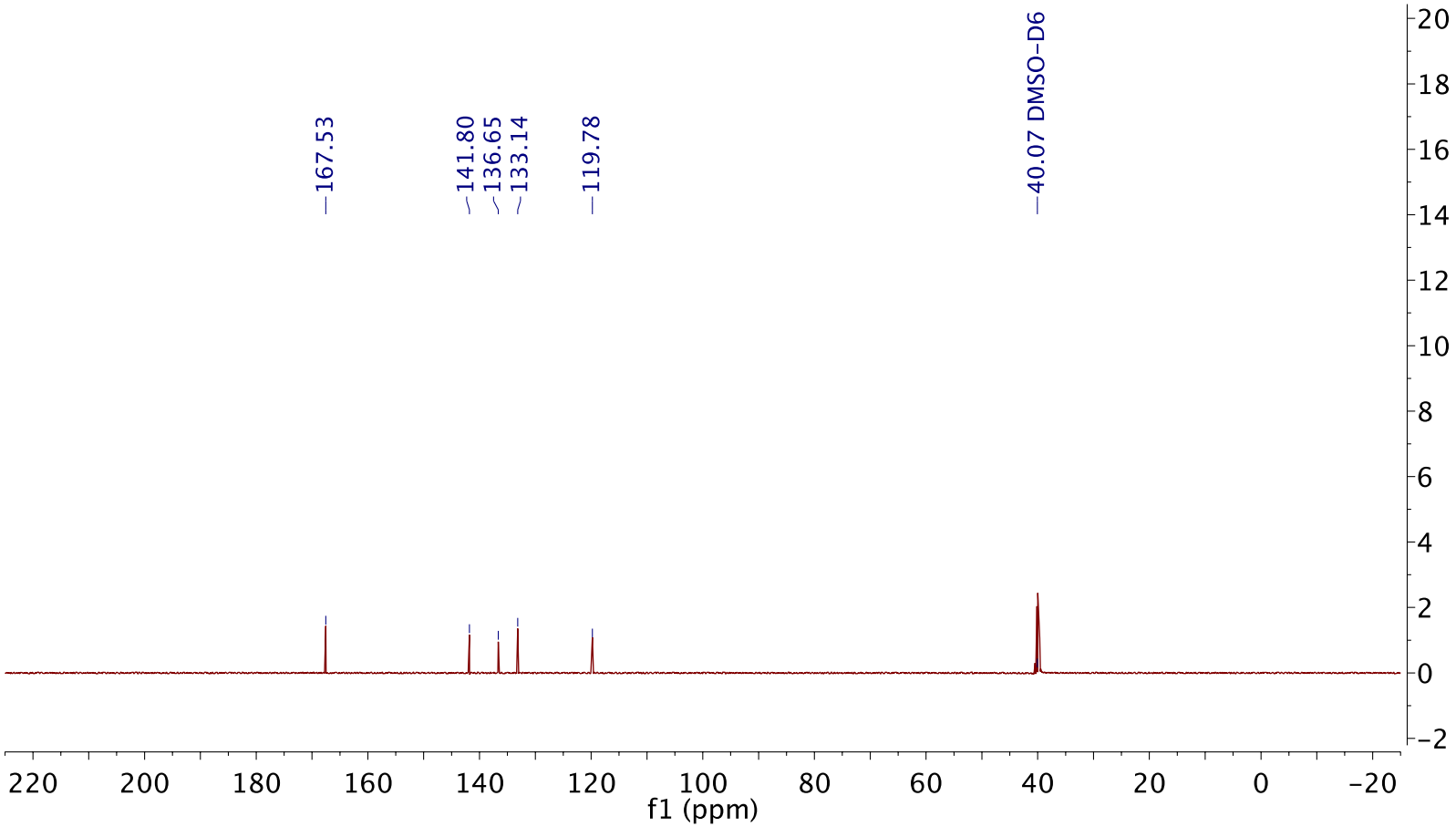

^{13}C NMR (126 MHz, DMSO-D_6) δ 167.53, 141.80, 136.65, 133.14, 119.78, 40.07.

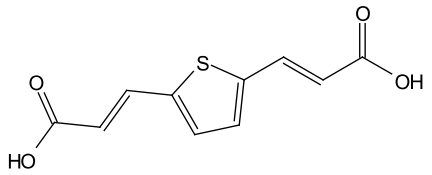

Figure C.42 ^{13}C NMR of JB03 - (2*E*,2'*E*)-3,3'-(thiophene-2,5-diyl) diacrylic acid

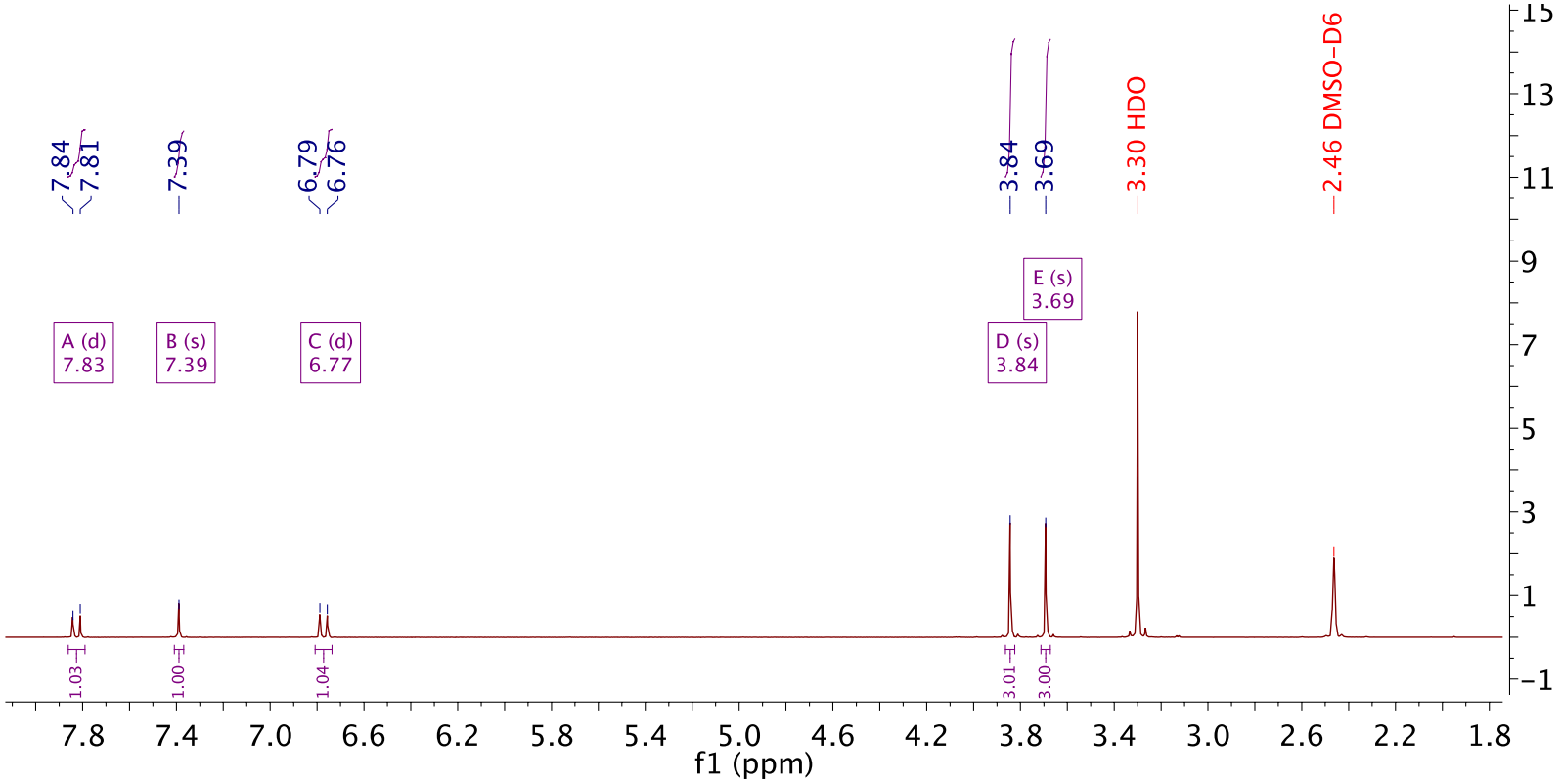

^{1}H NMR (500 MHz, DMSO-d_6) δ 7.83 (d, J = 15.6 Hz, 1H), 7.39 (s, 1H), 6.77 (d, J = 15.9 Hz, 1H), 3.84 (s, 3H), 3.69 (s, 3H).

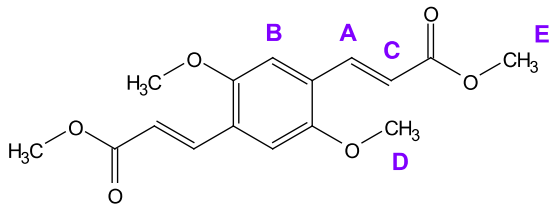

Figure C.43 ^{1}H NMR of JB04 precursor - dimethyl 3,3'-(2,5-dimethoxy-1,4-phenylene)(2*E*,2'*E*)-diacrylate

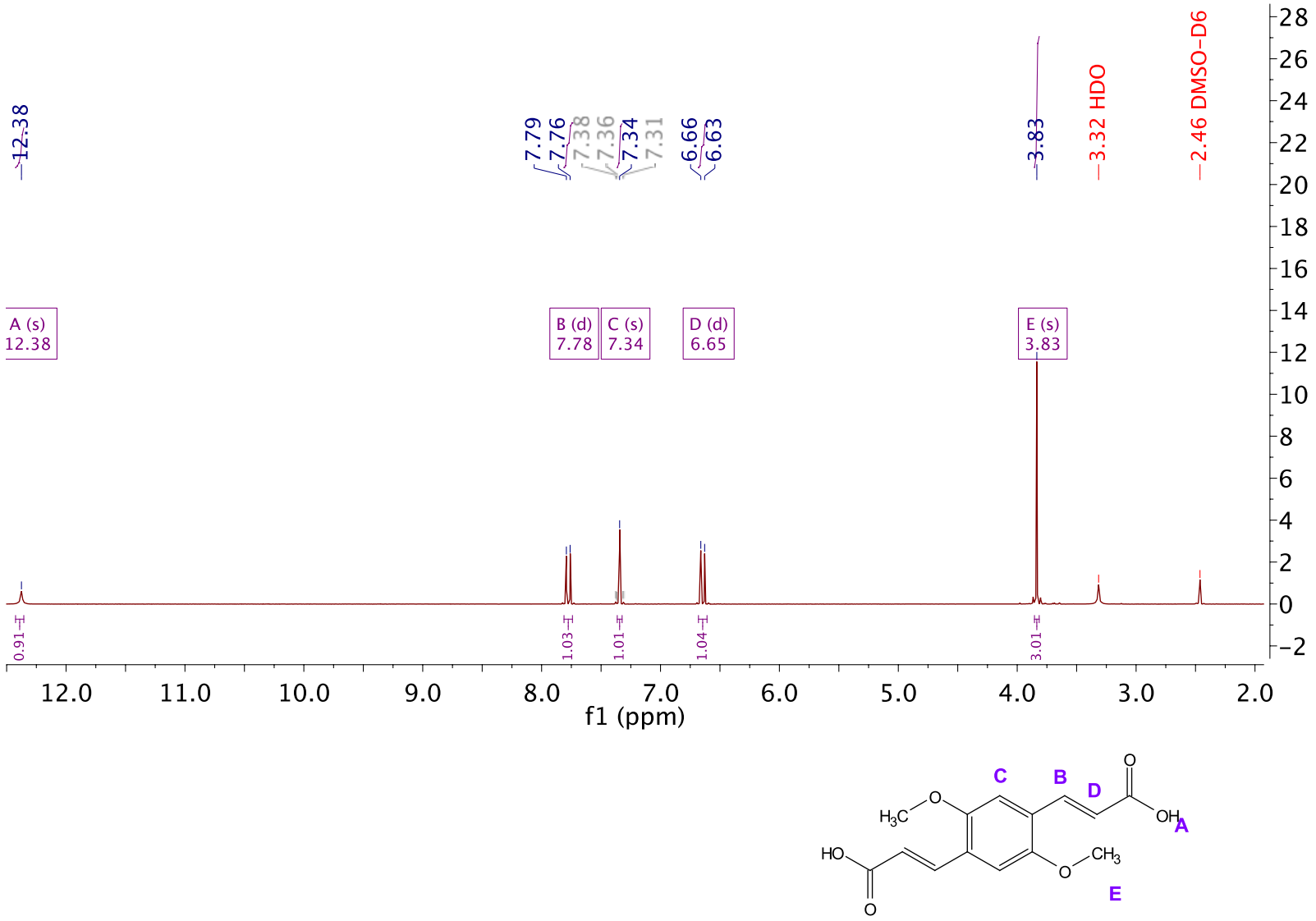

Figure C.44 ^{1}H NMR of JB04 - (2*E*,2'*E*)-3,3'-(2,5-dimethoxy-1,4-phenylene)diacrylic acid

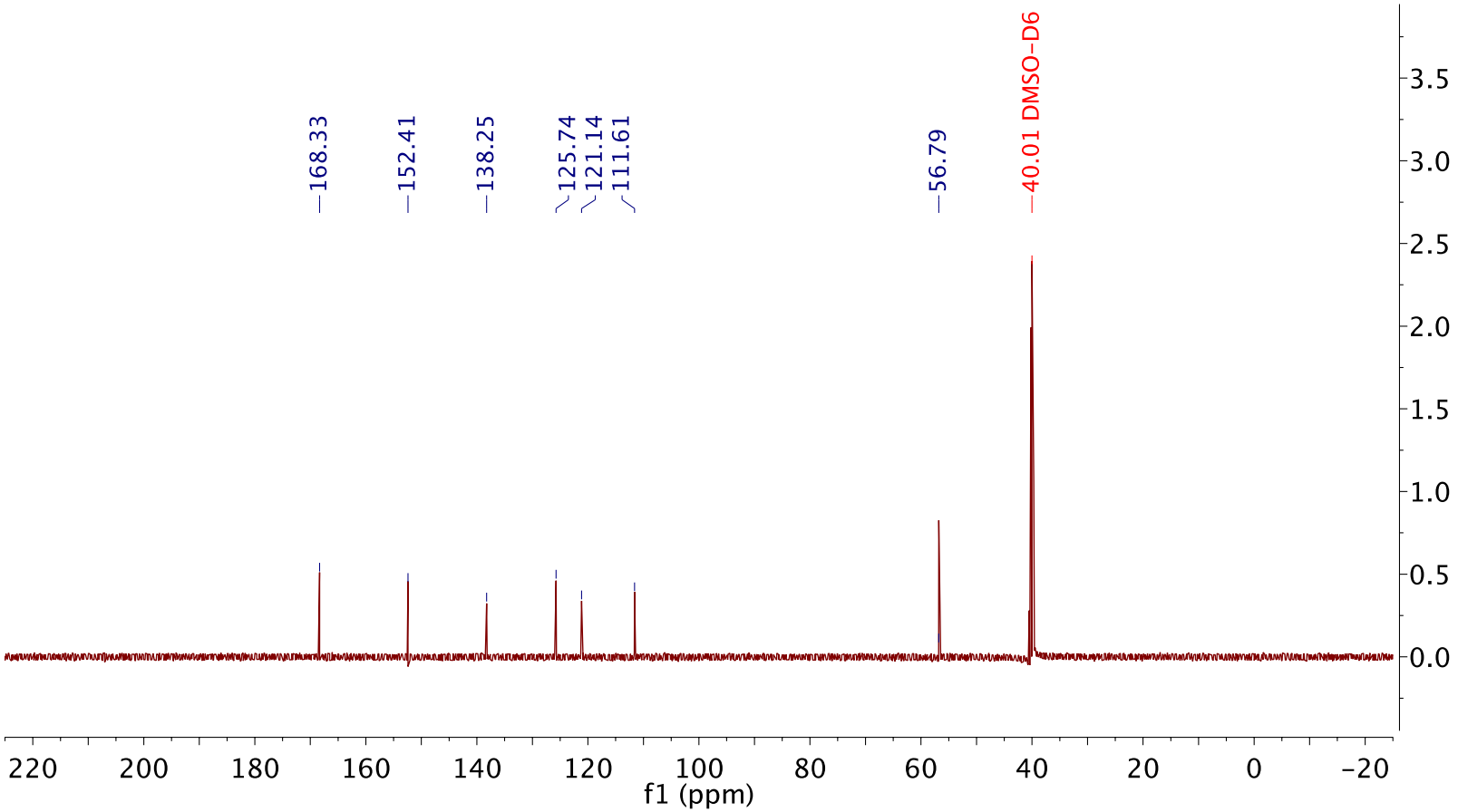

^{13}C NMR (126 MHz, DMSO-D_6) δ 168.33, 152.41, 138.25, 125.74, 121.14, 111.61, 56.79, 40.01.

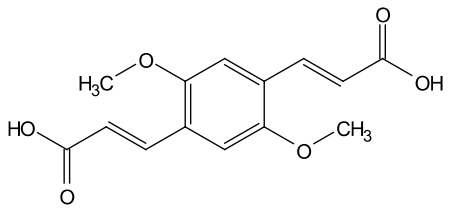

Figure C.45 ^{13}C NMR of JB04 - (2*E*,2'*E*)-3,3'-(2,5-dimethoxy-1,4-phenylene) diacrylic acid

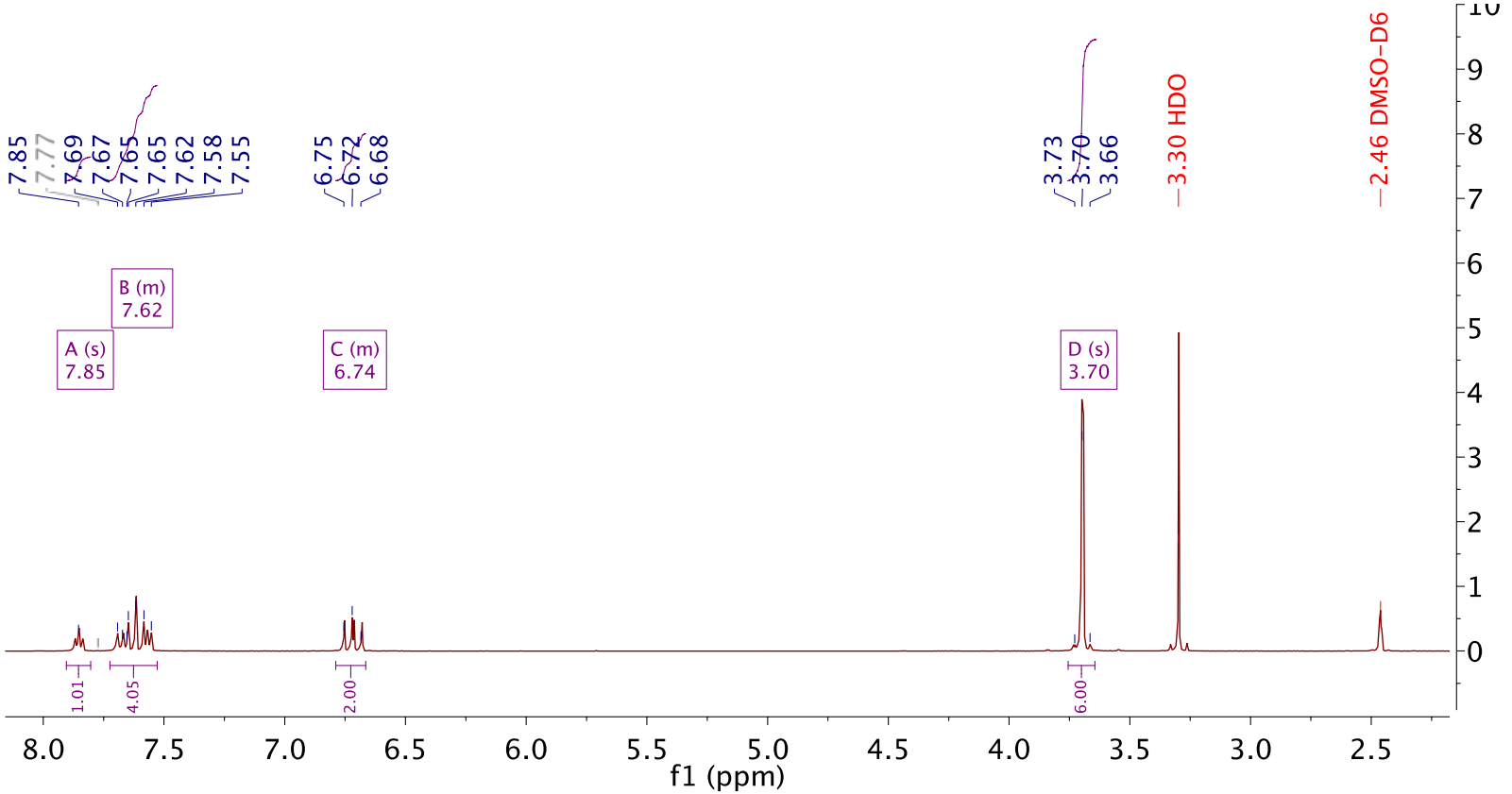

^{1}H NMR (500 MHz, DMSO-d_6) δ 7.85 (s, 1H), 7.72 – 7.53 (m, 4H), 6.79 – 6.66 (m, 2H), 3.70 (s, 6H).

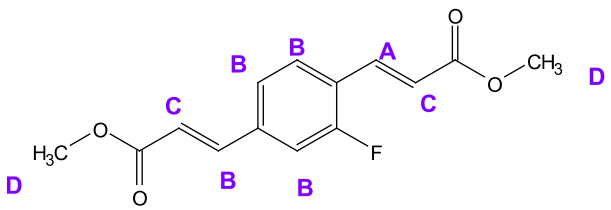

Figure C.46 ^{1}H NMR of JB05 precursor - dimethyl 3,3'-(2-fluoro-1,4-phenylene)(2*E*,2'*E*)-diacrylate

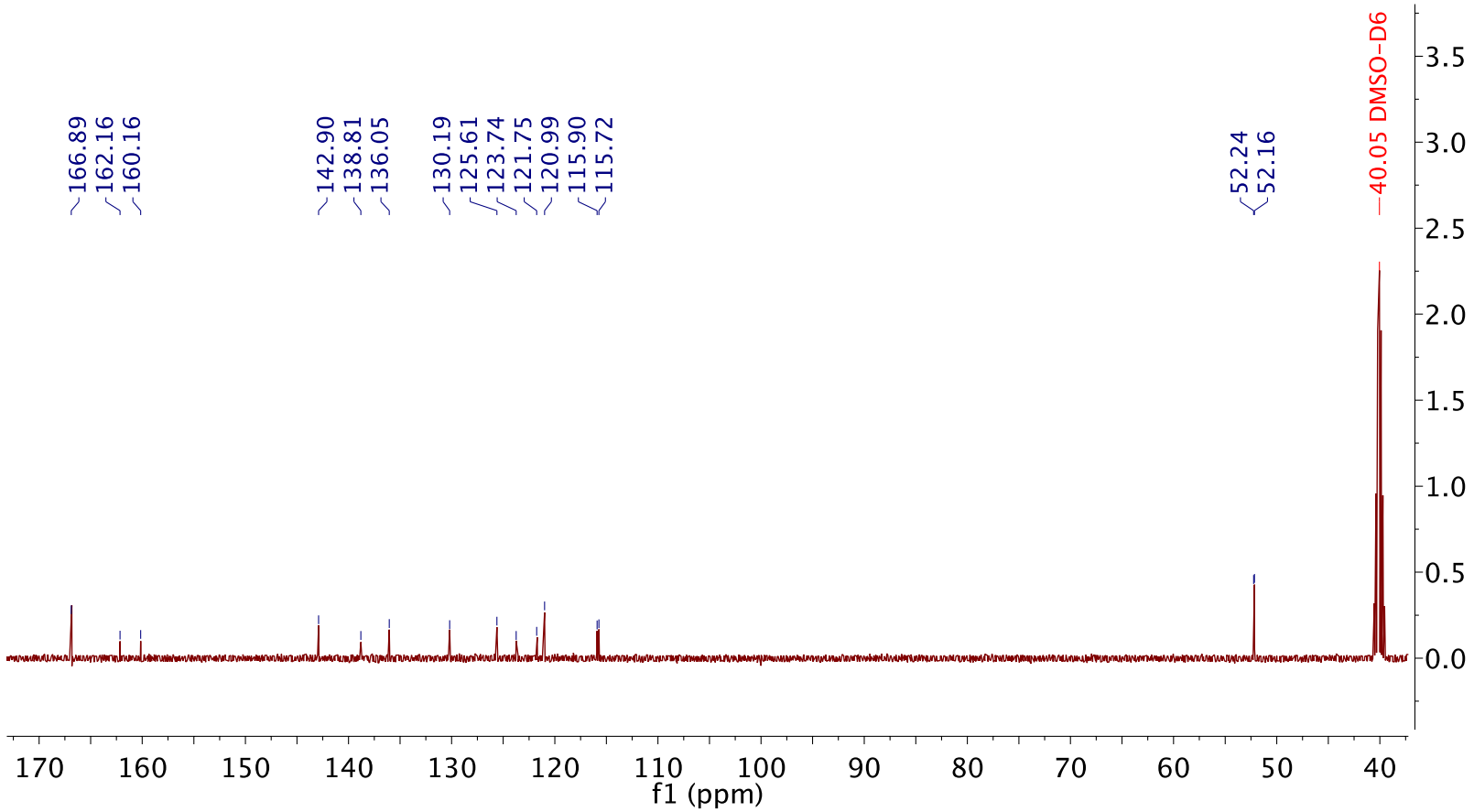

^{13}C NMR (126 MHz, DMSO-D_6) δ 166.89, 162.16, 160.16, 142.90, 138.81, 136.05, 130.19, 125.61, 123.74, 121.75, 120.99, 115.90, 115.72, 52.24, 52.16, 40.05.

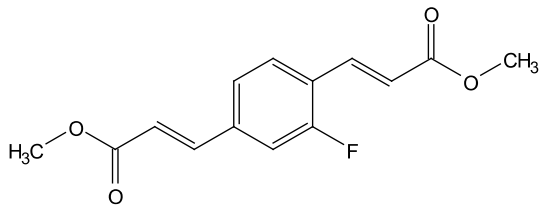

Figure C.47 ^{13}C NMR of JB05 precursor - dimethyl 3,3'-(2-fluoro-1,4-phenylene)(2*E*,2'*E*)-diacrylate

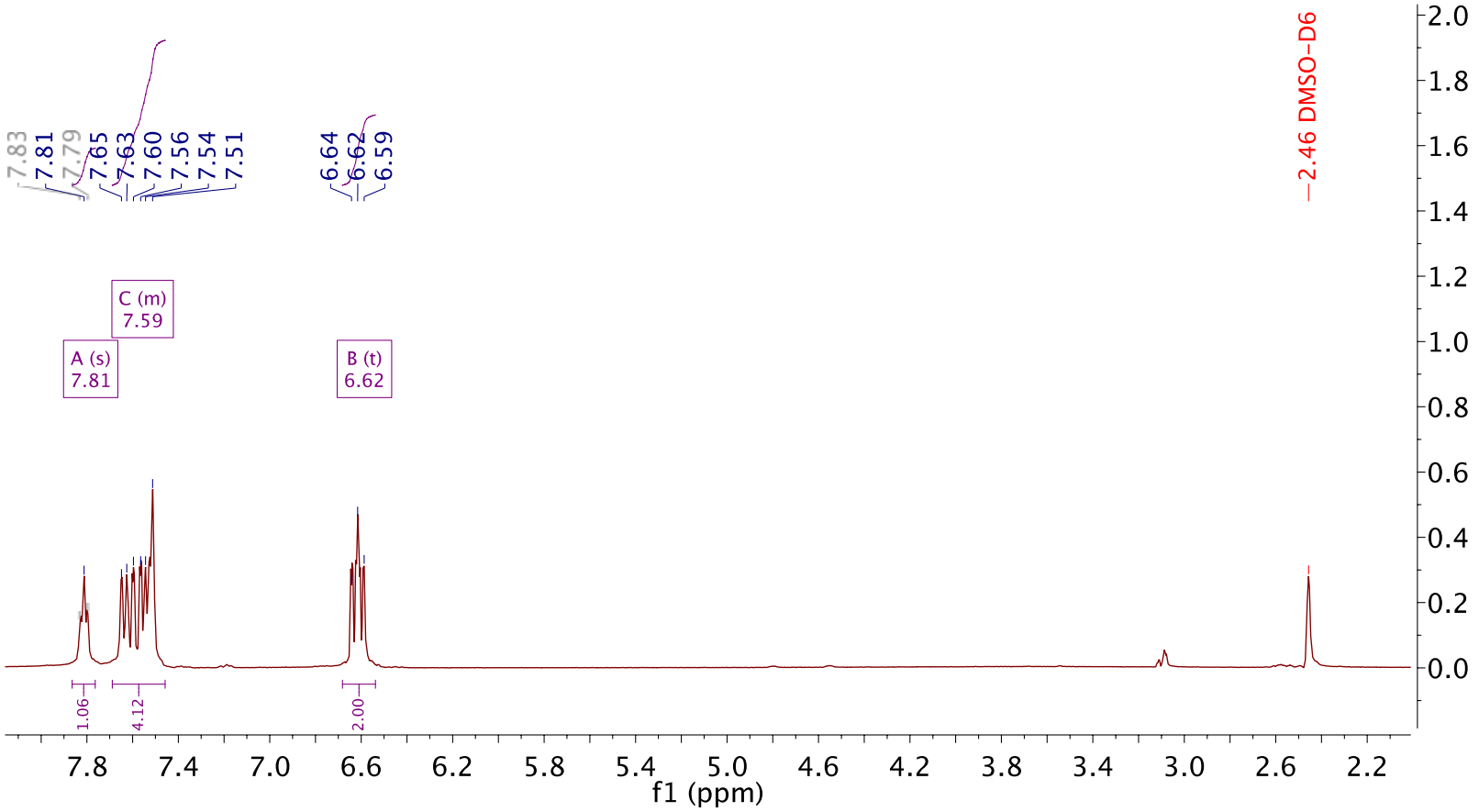

^{1}H NMR (500 MHz, DMSO-d_6) δ 7.81 (s, 1H), 7.69 – 7.46 (m, 4H), 6.62 (t, J = 13.9 Hz, 2H).

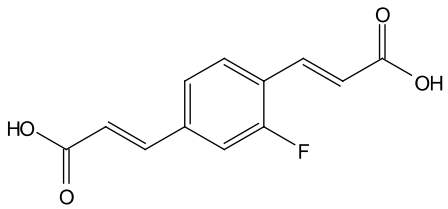

Figure C.48 ^{1}H NMR of JB05 - (2*E*,2'*E*)-3,3'-(2-fluoro-1,4-phenylene) diacrylic acid

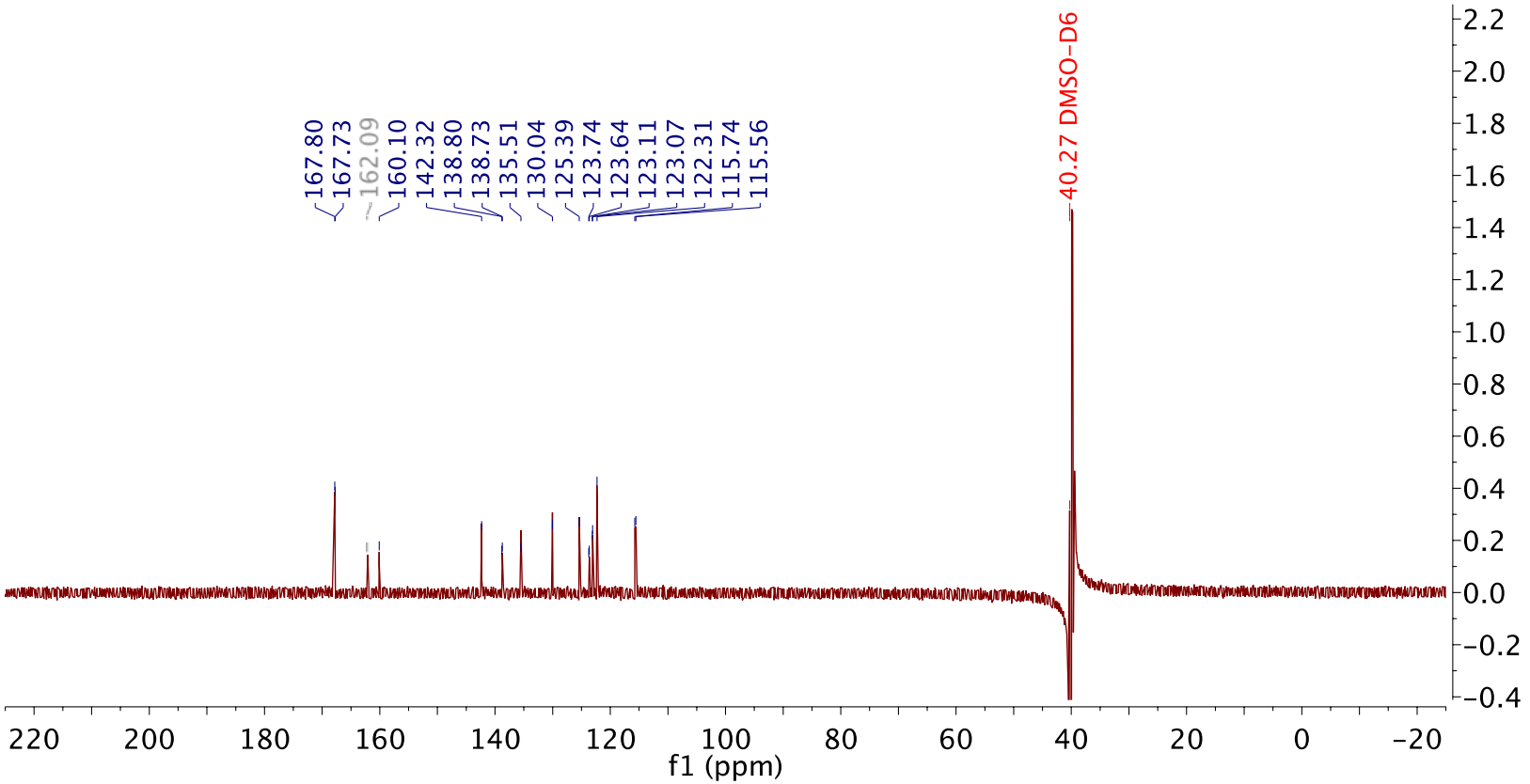

^{13}C NMR (126 MHz, DMSO-D_6) δ 167.80, 167.73, 162.09, 160.10, 142.32, 138.80, 138.73, 135.51, 130.04, 125.39, 123.74, 123.64, 123.11, 123.07, 122.31, 115.74, 115.56, 40.27.

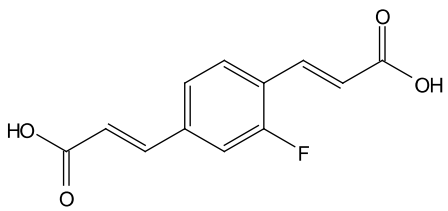

Figure C.49 ^{13}C NMR of JB05 - (2*E*,2'*E*)-3,3'-(2-fluoro-1,4-phenylene) diacrylic acid

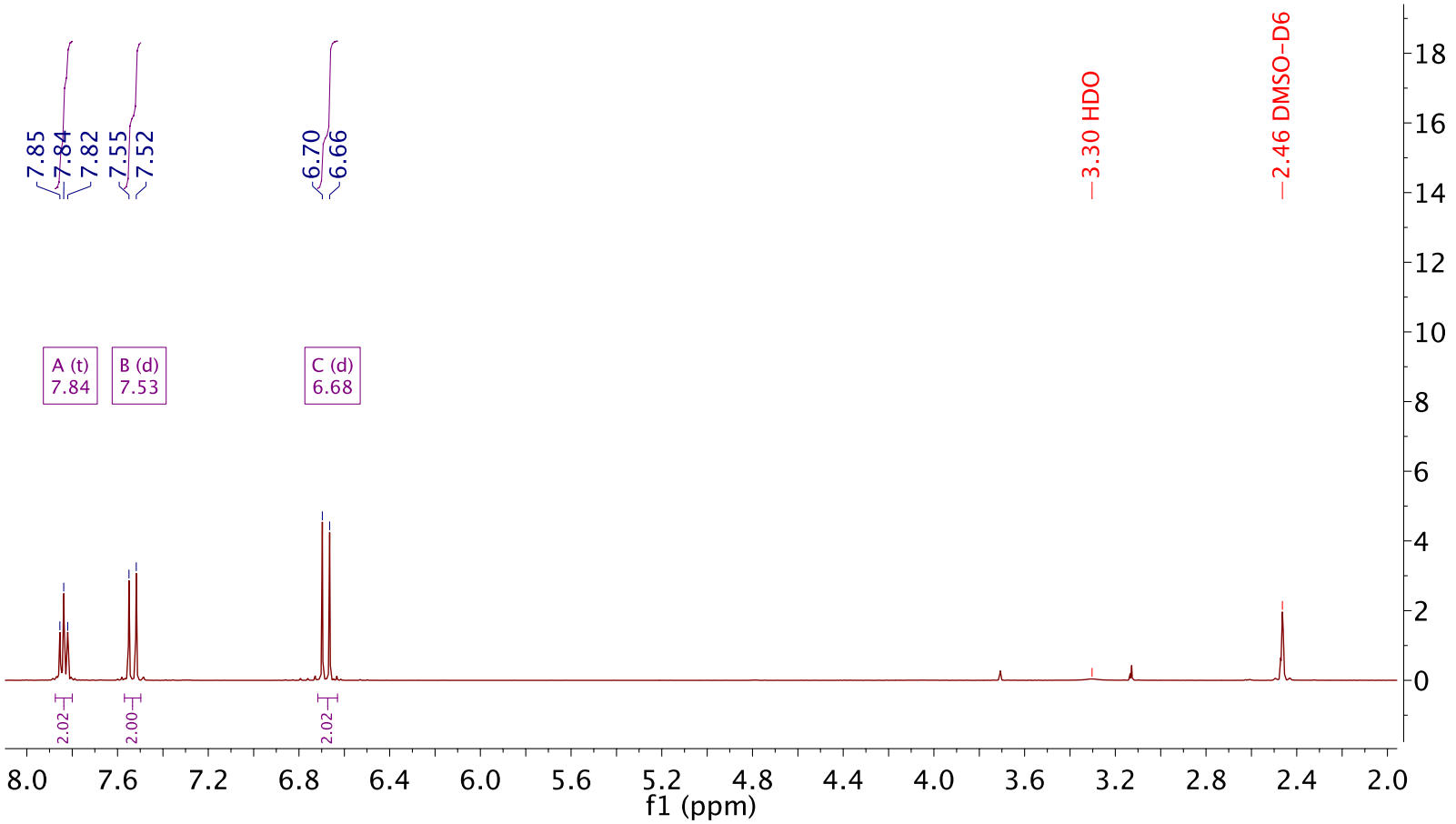

^{1}H NMR (500 MHz, DMSO-d_6) δ 7.84 (t, J = 8.6 Hz, 2H), 7.53 (d, J = 16.1 Hz, 2H), 6.68 (d, J = 16.1 Hz, 2H).

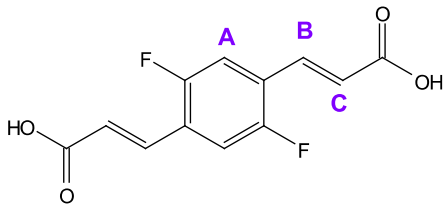

Figure C.50 ^{1}H NMR of JB07 - (2*E*,2'*E*)-3,3'-(2,5-difluoro-1,4-phenylene) diacrylic acid

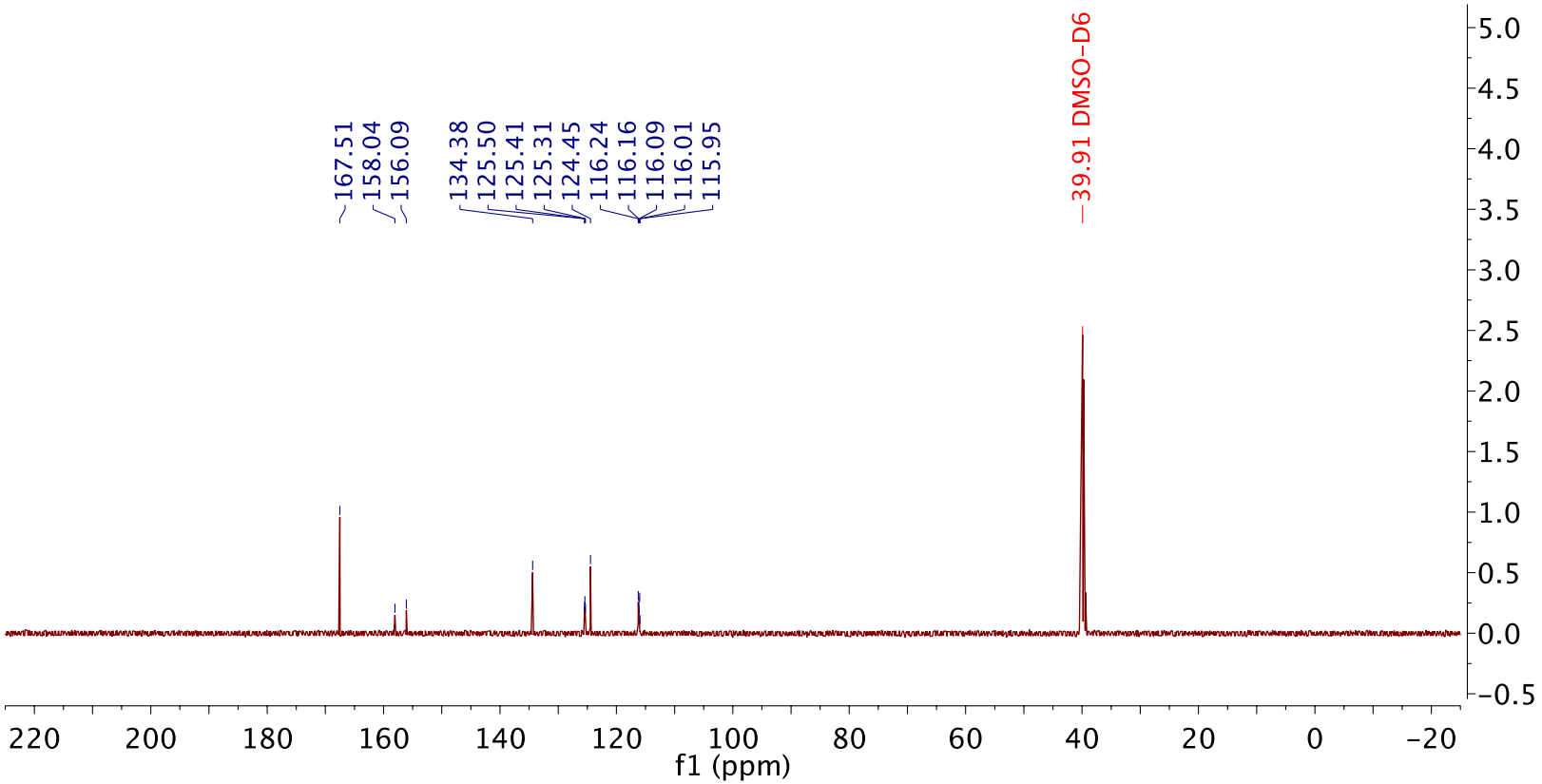

^{13}C NMR (126 MHz, DMSO-D_6) δ 167.51, 158.04, 156.09, 134.38, 125.50, 125.41, 125.31, 124.45, 116.24, 116.16, 116.09, 116.01, 115.95, 39.91.

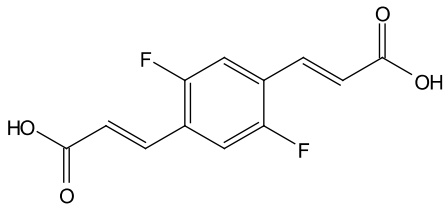

Figure C.51 ^{13}C NMR of JB07 - (2*E*,2'*E*)-3,3'-(2,5-difluoro-1,4-phenylene) diacrylic acid

APPENDIX D

THREE DIMENSIONAL MODELING

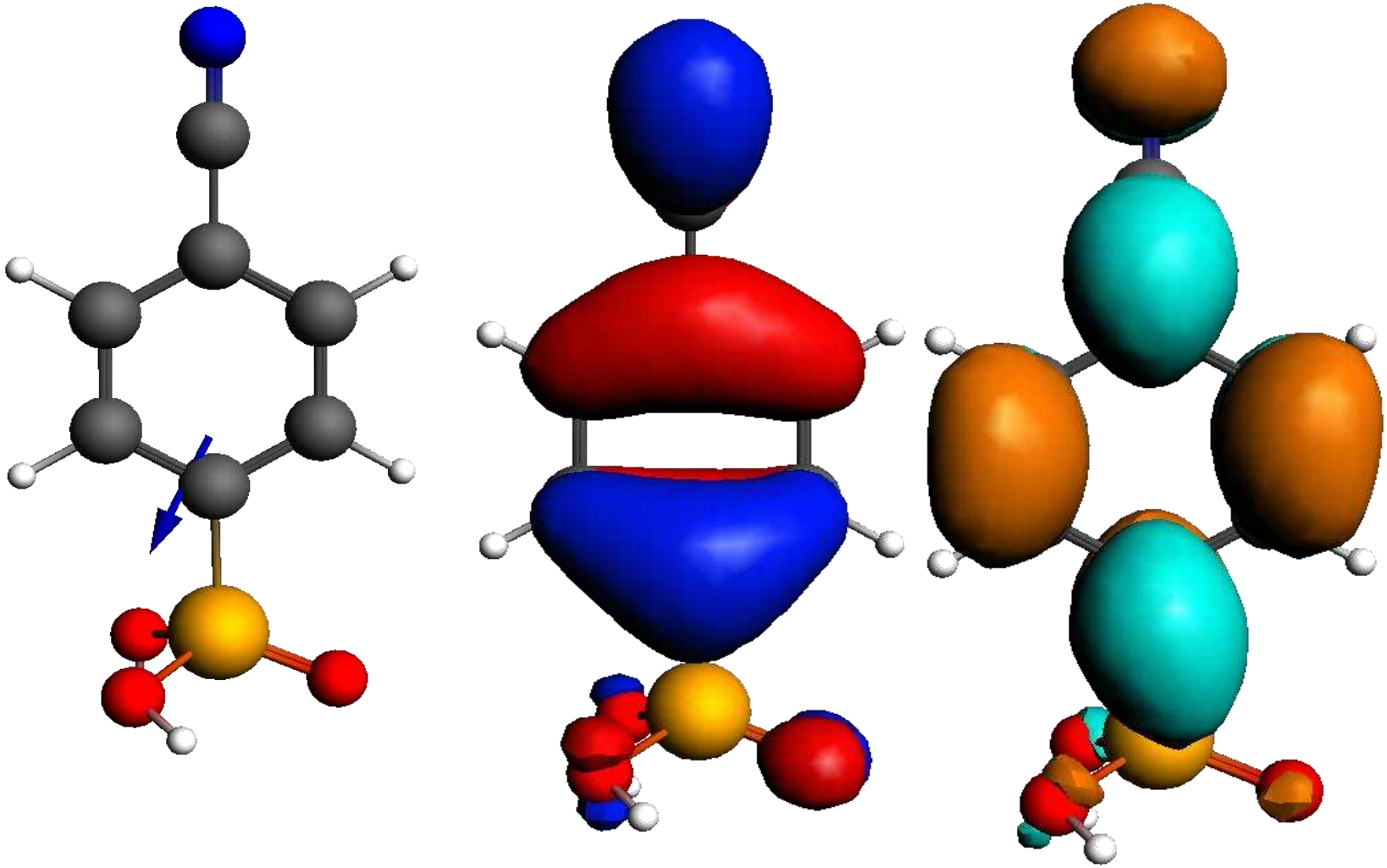

Figure D.1 CNPPA ground state geometry (Left) HOMO orbitals (Middle) LUMO orbitals (right)

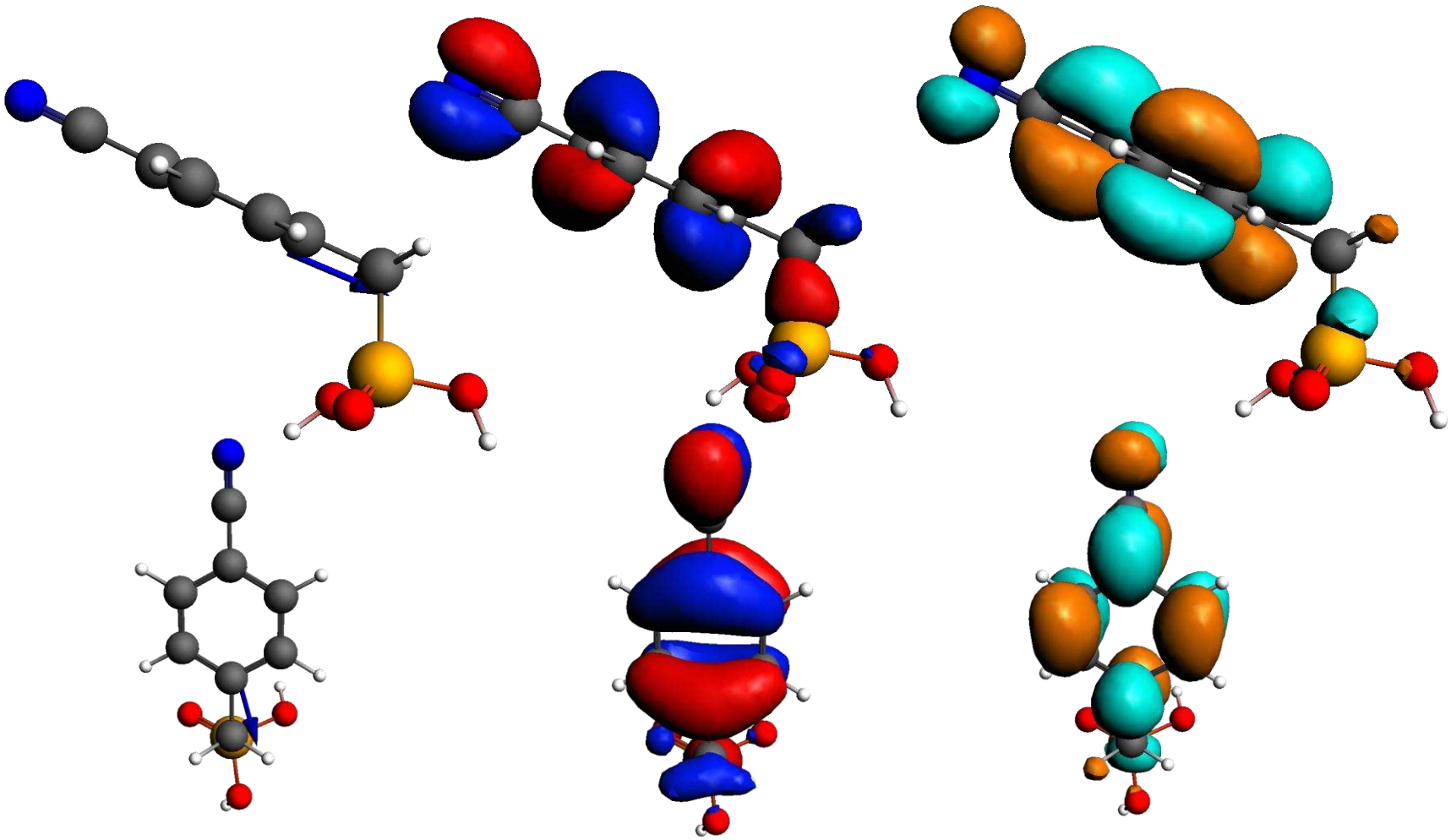

Figure D.2 CNBPA ground state geometry (Left) HOMO orbitals (Middle) LUMO orbitals (right)

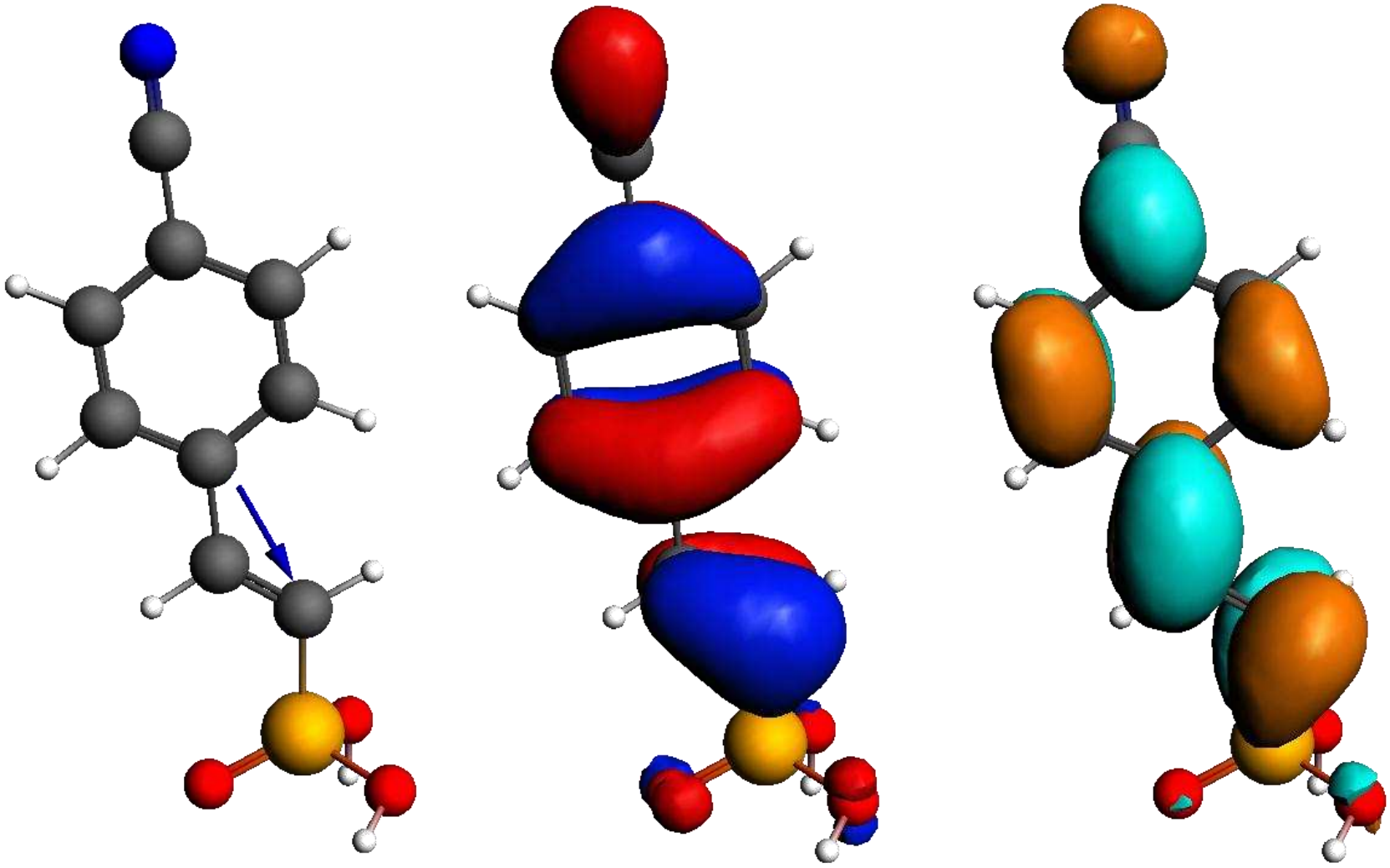

Figure D.3 CNVPA ground state geometry (Left) HOMO orbitals (Middle) LUMO orbitals (right)

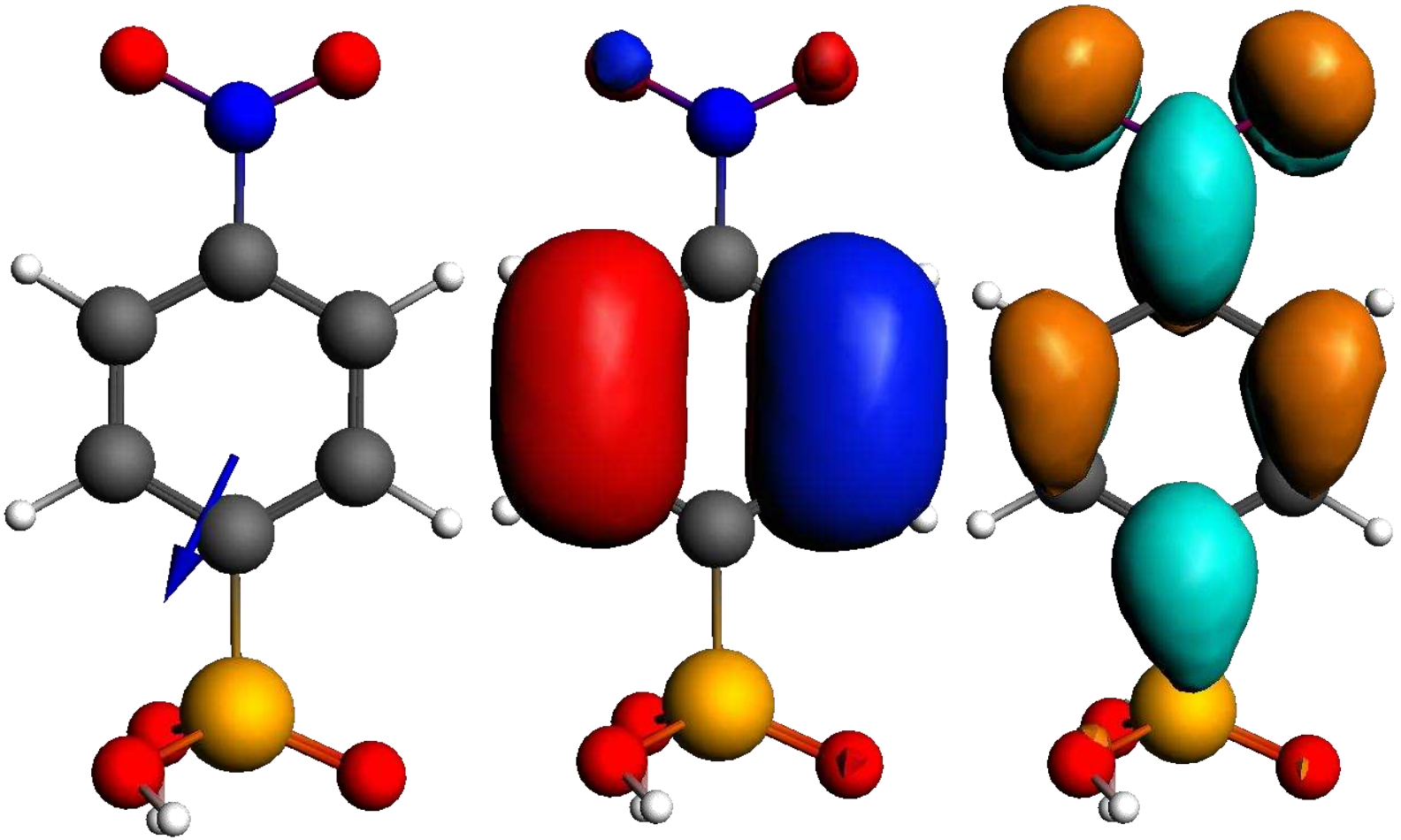

Figure D.4 NO_2PPA ground state geometry (Left) HOMO orbitals (Middle) LUMO orbitals (right)

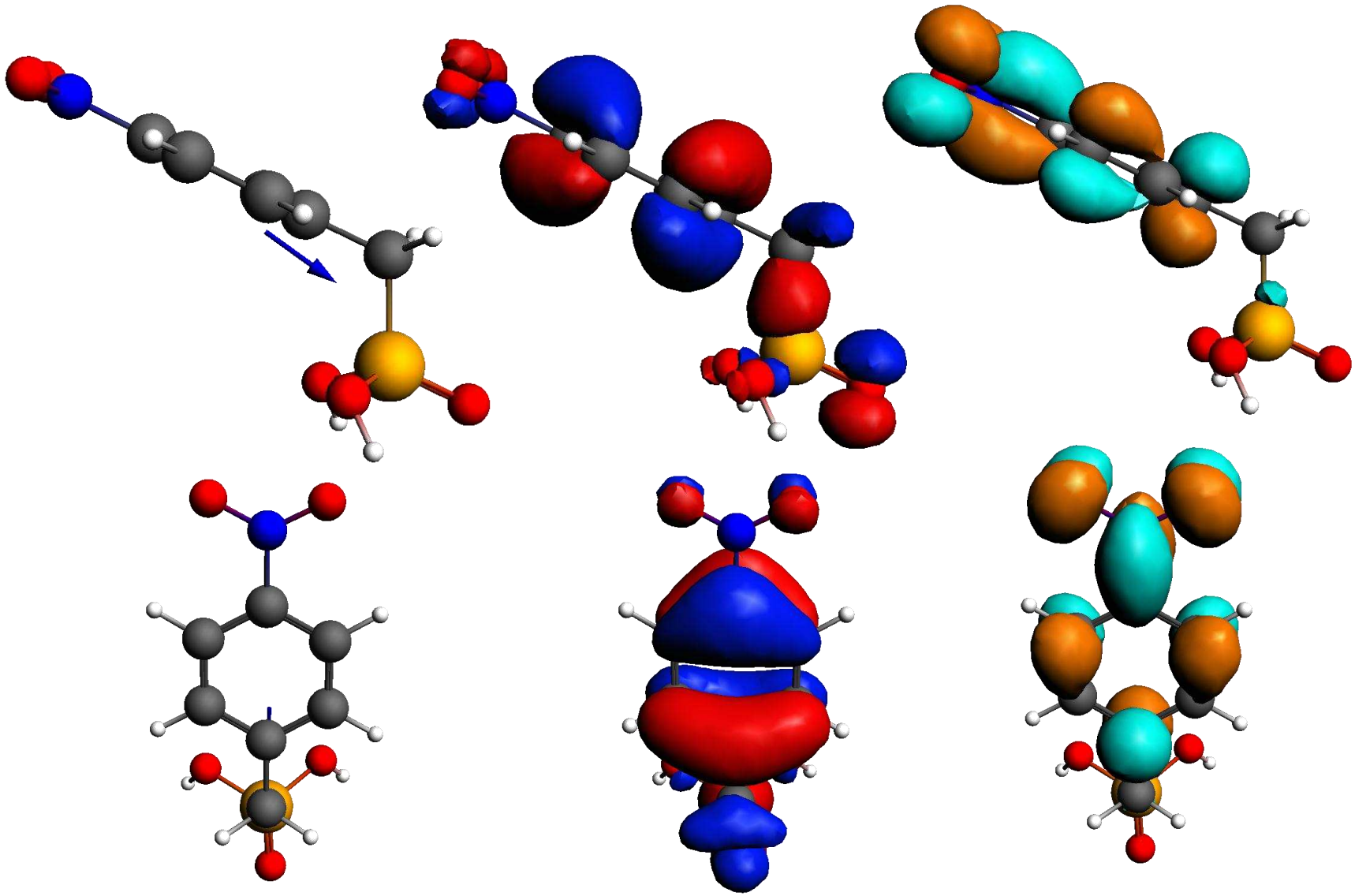

Figure D.5 NO_2BPA ground state geometry (Left) HOMO orbitals (Middle) LUMO orbitals (right)

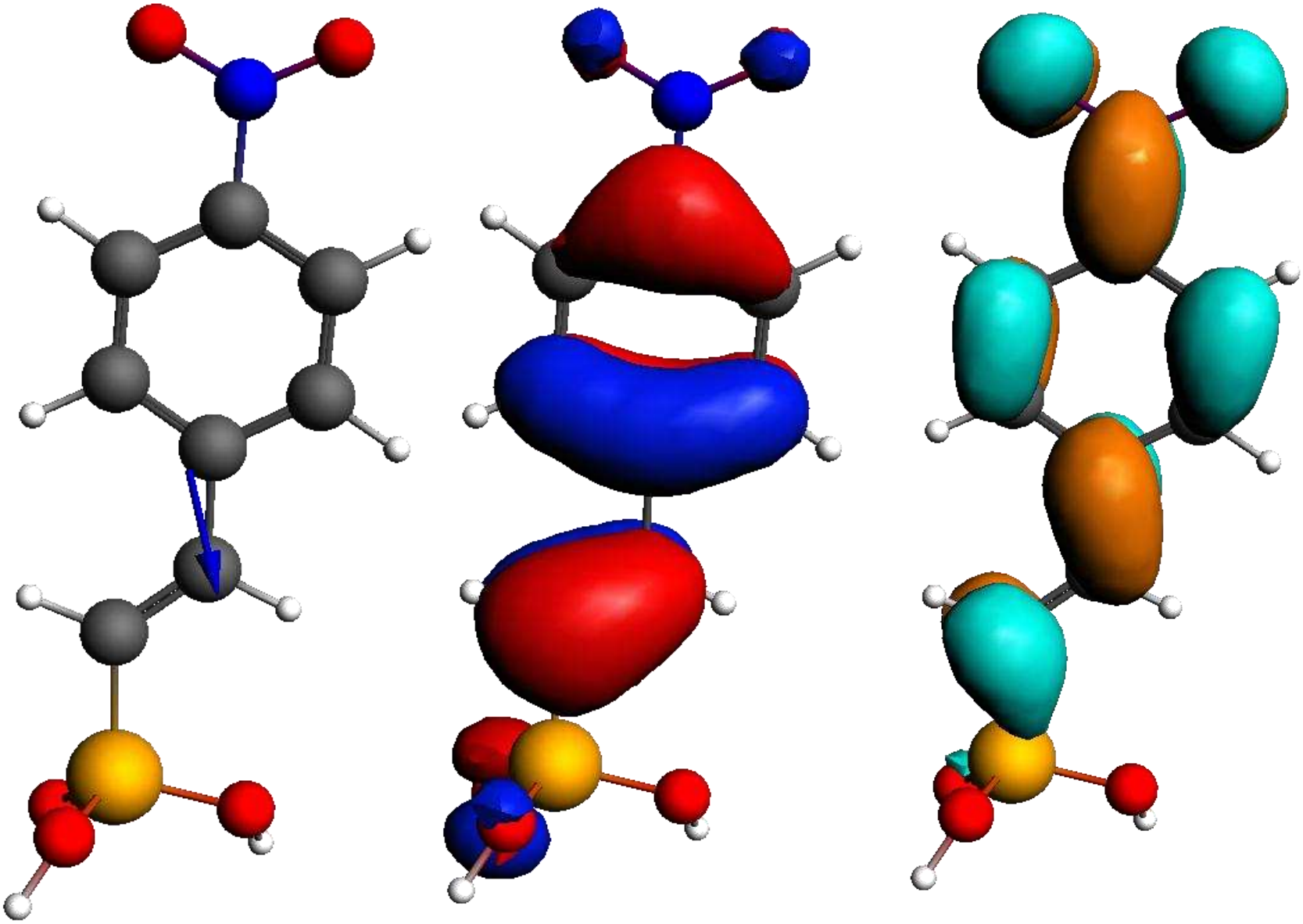

Figure D.6 NO_2VPA ground state geometry (Left) HOMO orbitals (Middle) LUMO orbitals (right)

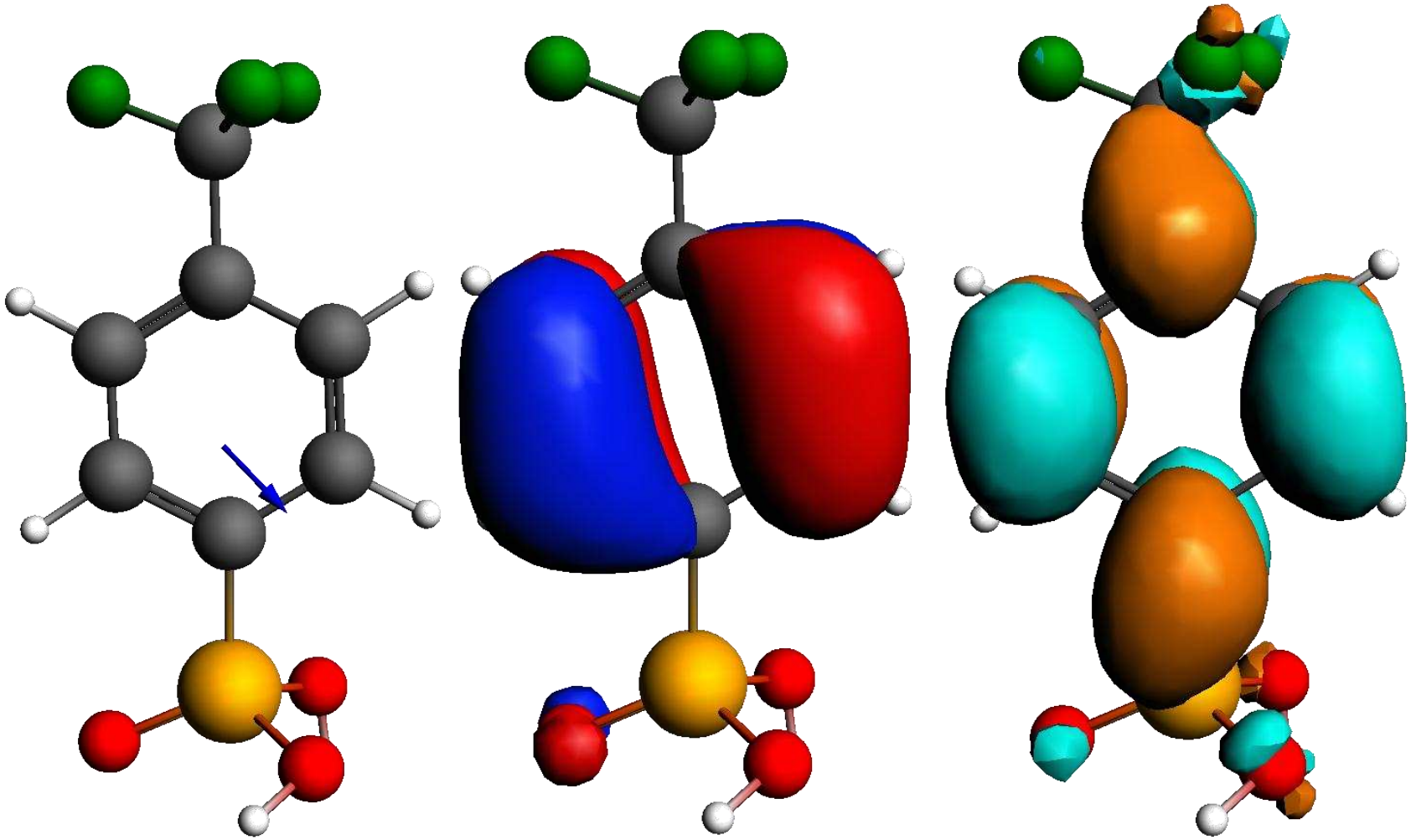

Figure D.7 CF_3PPA ground state geometry (Left) HOMO orbitals (Middle) LUMO orbitals (right)

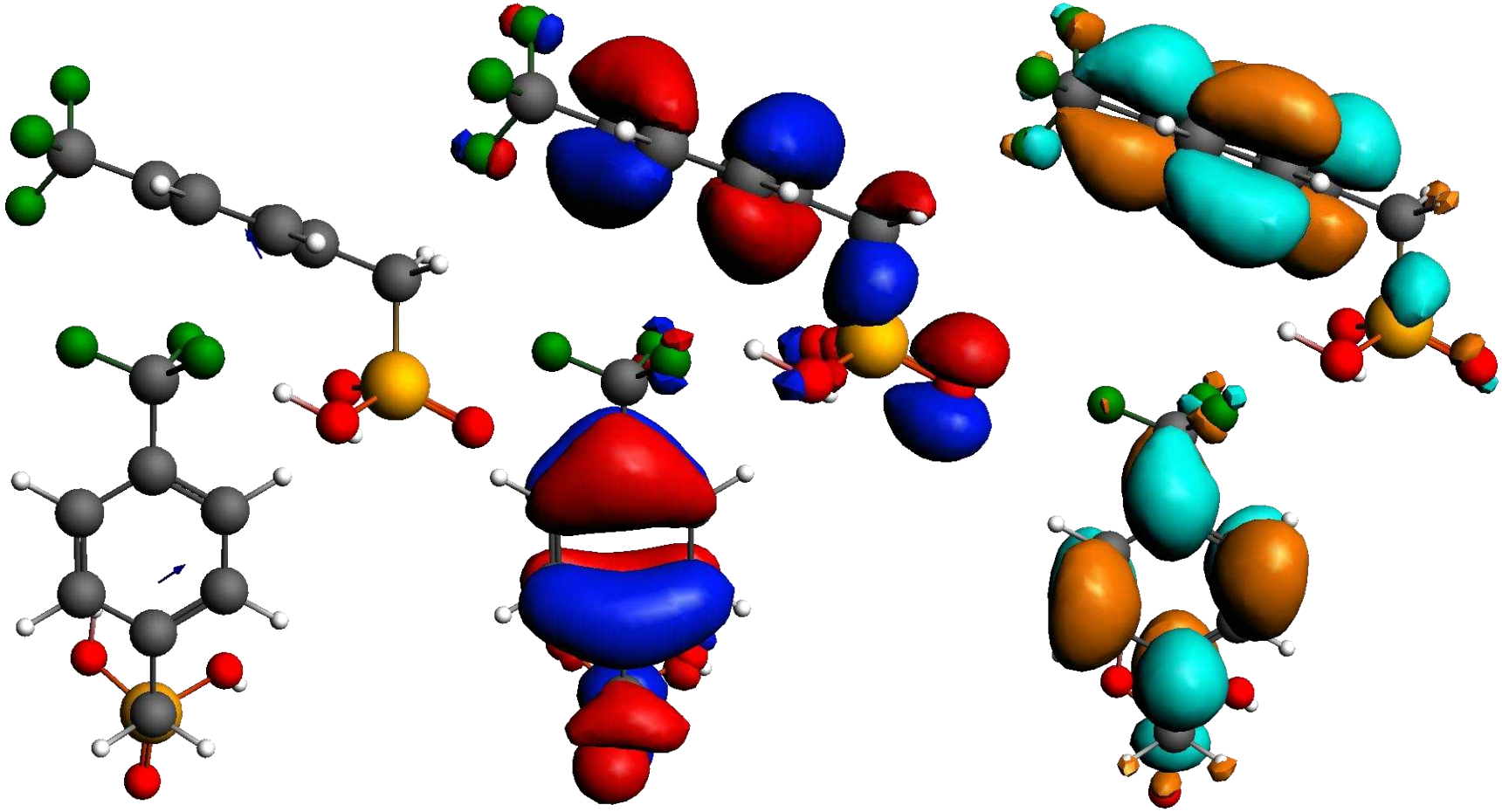

Figure D.8 CF_3BPA ground state geometry (Left) HOMO orbitals (Middle) LUMO orbitals (right)

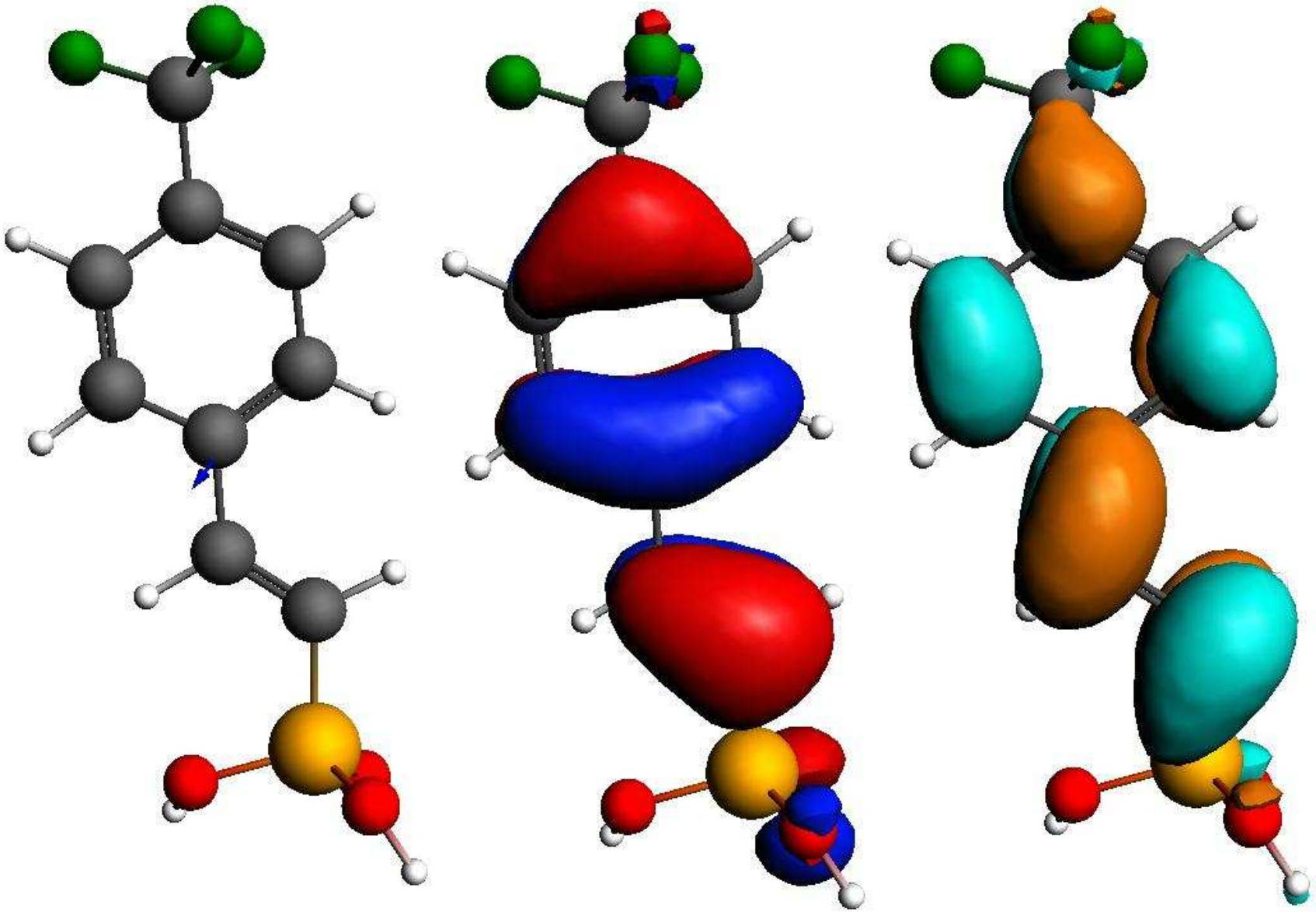

Figure D.9 CF_3VPA ground state geometry (Left) HOMO orbitals (Middle) LUMO orbitals (right)

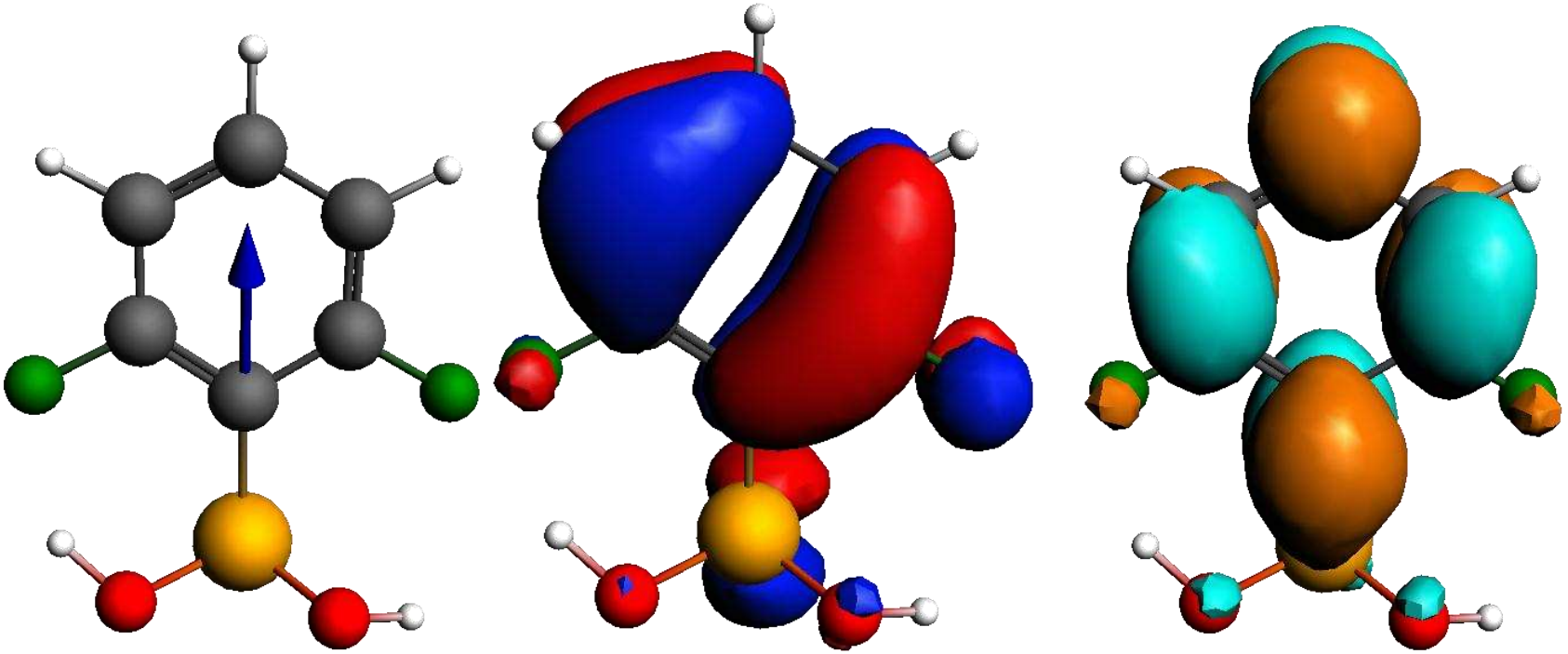

Figure D.10 oF_2PPA ground state geometry (Left) HOMO orbitals (Middle) LUMO orbitals (right)

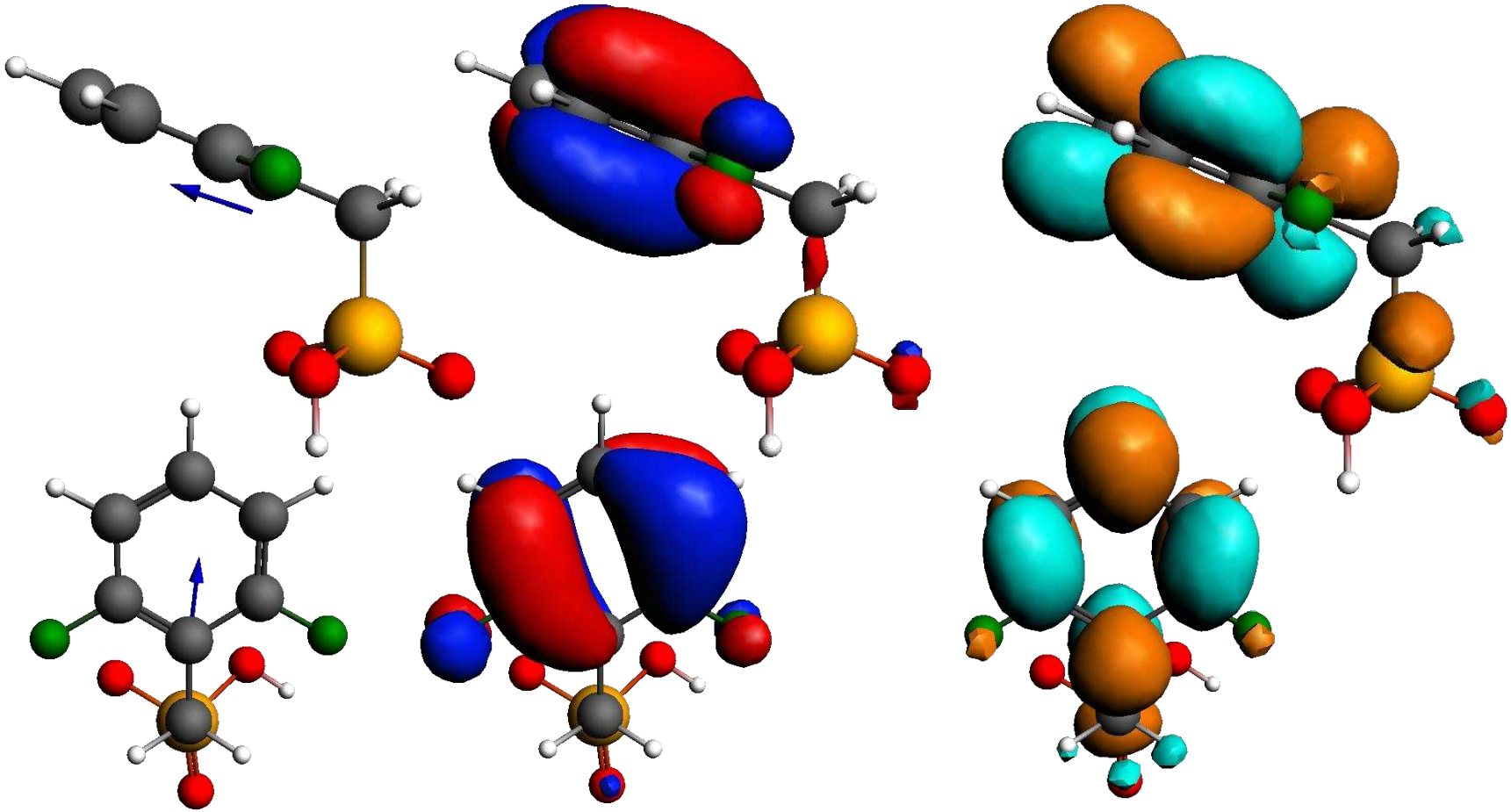

Figure D.11 oF_2BPA ground state geometry (Left) HOMO orbitals (Middle) LUMO orbitals (right)

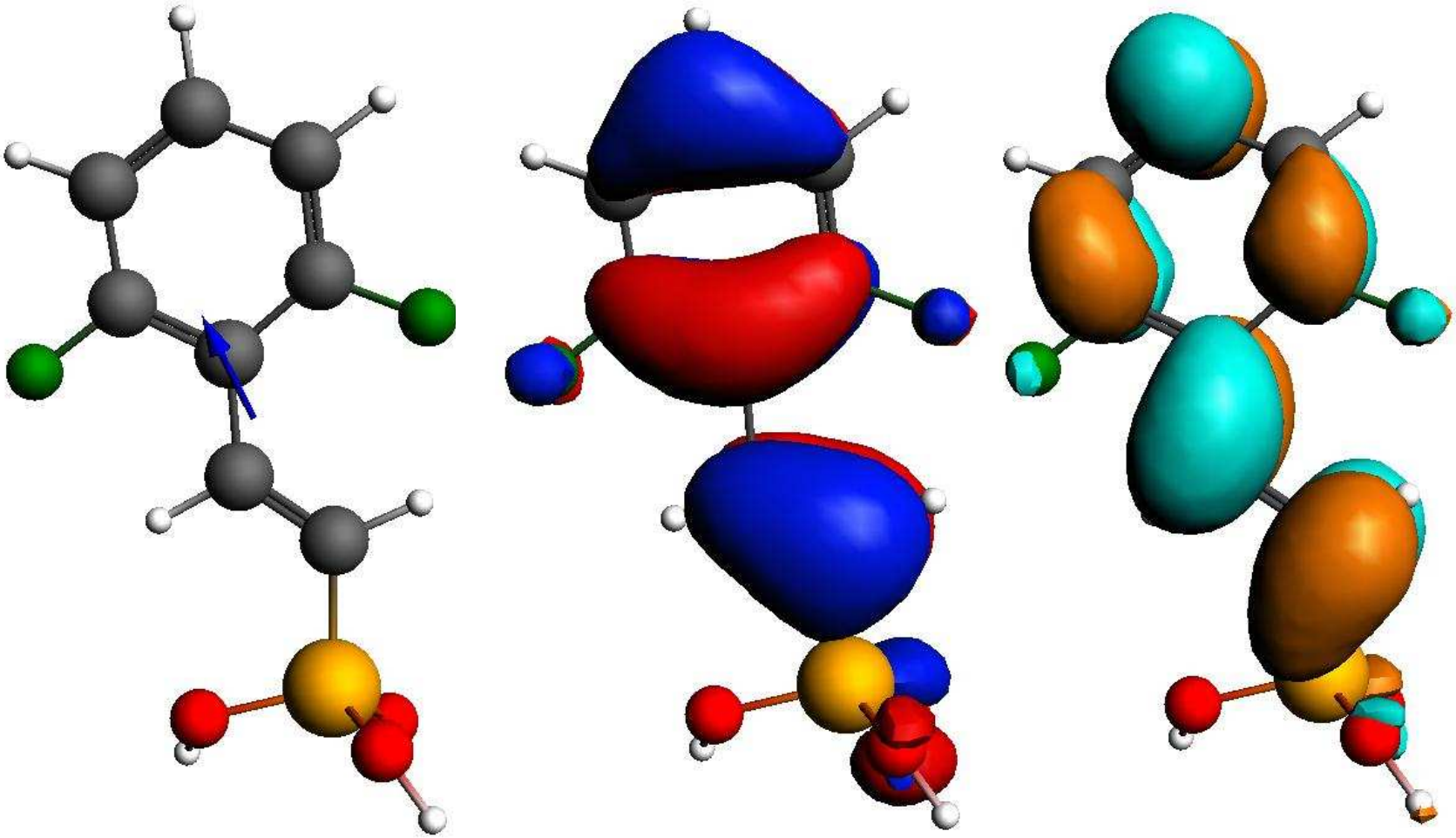

Figure D.12 oF_2VPA ground state geometry (Left) HOMO orbitals (Middle) LUMO orbitals (right)